EMERGING INFECTIOUS DISEASES®

Respiratory Infections

June 2024

J. Potts (details unknown), engraver for Bradbury, Wilkinson & Co. Printer. Fluttering flag and Samoan house on stamp with designation "Samoa," by civil administration of the mandated territory of Western Samoa, 1921. Printed by the Government Printing Office, Wellington, New Zealand. Private collection, Atlanta, Georgia. Photography by Will Breedlove.

EMERGING INFECTIOUS DISEASES®

Emerging Infectious Diseases is published monthly by the Centers for Disease Control and Prevention, 1600 Clifton Rd NE, Mailstop H16-2, Atlanta, GA 30329-4018, USA. Telephone 404-639-1960; email, eideditor@cdc.gov

EMERGING INFECTIOUS DISEASES®

Respiratory Infections **June 2024**

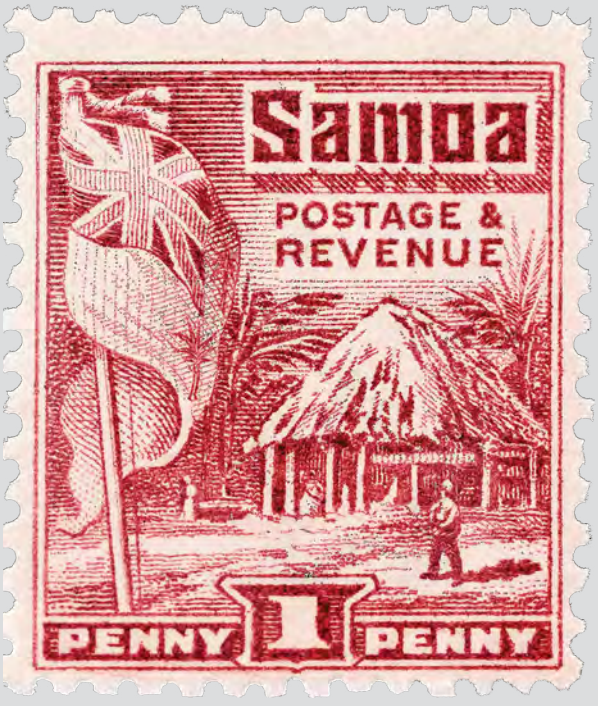

On the Cover

J. Potts (details unknown), engraver for Bradbury, Wilkinson & Co. Printer. Fluttering flag and Samoan house on stamp with designation "Samoa," by civil administration of the mandated territory of Western Samoa, 1921. Printed by the Government Printing Office, Wellington, New Zealand. Private collection, Atlanta, Georgia. Photography by Will Breedlove.

Perspective

Synopses

Research

Medscape EDUCATION ACTIVITY

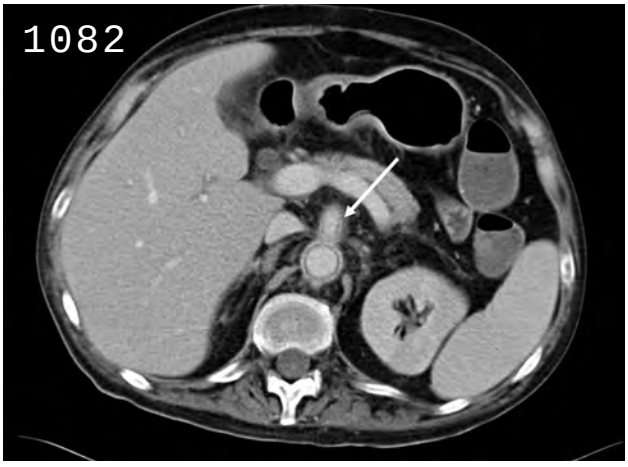

EMERGING INFECTIOUS DISEASES®
June 2024

Dispatches

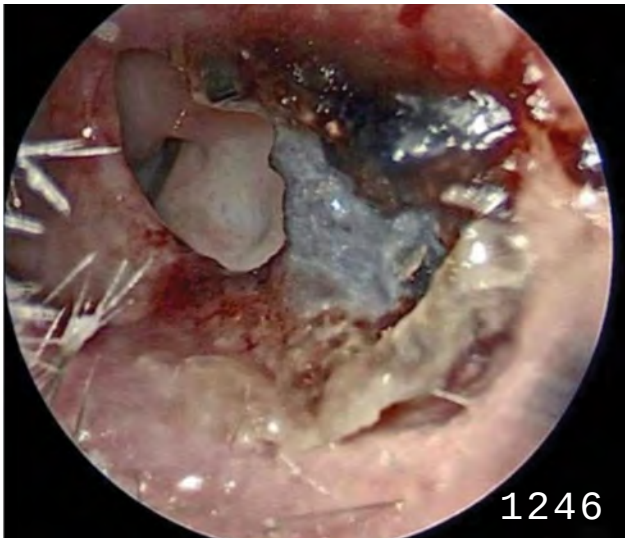

EMERGING INFECTIOUS DISEASES®
June 2024

Research Letters

Comment Letter

Books and Media

About the Cover

Notice to Readers

Emerging Infectious Diseases announces that it is now accepting submissions of articles in a new category, **Letters from the Emerging Infections Network.** The Emerging Infections Network (EIN) is a nationwide United States-based sentinel network of infectious disease physicians and related healthcare professionals that is funded by a 1995 cooperative agreement between the Infectious Disease Society of America and the Centers for Disease Control and Prevention. See page 1304 for more information.

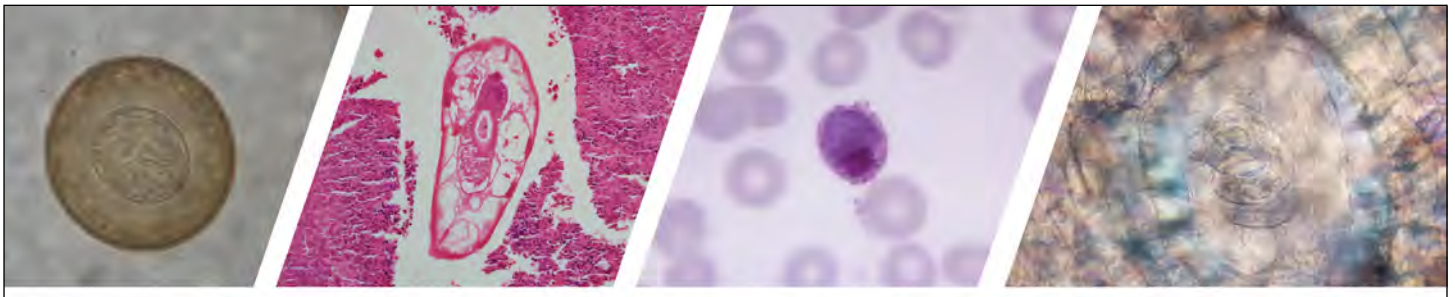

DPDx

Diagnostic Assistance and Training in Laboratory Identification of Parasites

A free service of CDC available to laboratorians, pathologists, and other health professionals in the United States and abroad

- Diagnosis from photographs of worms, histological sections, fecal, blood, and other specimen types
- Expert diagnostic review
- Formal diagnostic laboratory report
- Submission of samples via secure file share

Visit the DPDx website for information on laboratory diagnosis, geographic distribution, clinical features, parasite life cycles, and training via Monthly Case Studies of parasitic diseases.

www.cdc.gov/dpdx
dpdx@cdc.gov

U.S. Department of Health and Human Services
Centers for Disease Control and Prevention

CS272346-DE

Decolonization and Pathogen Reduction Approaches to Prevent Antimicrobial Resistance and Healthcare-Associated Infections

Mihnea R. Mangalea, Alison Laufer Halpin, Melia Haile, Christopher A. Elkins, L. Clifford McDonald

Antimicrobial resistance in healthcare-associated bacterial pathogens and the infections they cause are major public health threats affecting nearly all healthcare facilities. Antimicrobial-resistant bacterial infections can occur when colonizing pathogenic bacteria that normally make up a small fraction of the human microbiota increase in number in response to clinical perturbations. Such infections are especially likely when pathogens are resistant to the collateral effects of antimicrobial agents that disrupt the human microbiome, resulting in loss of colonization resistance, a key host defense. Pathogen reduction is an emerging strategy to prevent transmission of, and infection with, antimicrobial-resistant healthcare-associated pathogens. We describe the basis for pathogen reduction as an overall prevention strategy, the evidence for its effectiveness, and the role of the human microbiome in colonization resistance that also reduces the risk for infection once colonized. In addition, we explore ideal attributes of current and future pathogen-reducing approaches.

Interrupting transmission and infection caused by multidrug-resistant organisms (MDROs) in healthcare settings can help mitigate the global antimicrobial resistance (AMR) crisis, reduce illness and death, increase patient safety, and extend the usefulness of currently available antimicrobial medications. Past progress in this area showed infection prevention and control (IPC) strategies, along with antibiotic stewardship, saved lives and reduced unnecessary antibiotic use. The Centers for Disease Control and Prevention (CDC) reported that, from 2013 to 2019, deaths from AMR infections decreased by 18% overall and by 28% in hospitals (*1*). Despite that progress, during the COVID-19 pandemic, resistant healthcare-associated infections (HAIs) in the United States increased by 15%, possibly because of pandemic-related interruption of comprehensive prevention practices and antibiotic stewardship (*2*). Bacterial AMR remains a leading health issue nationally; >2.8 million persons are infected annually in the United States (*1*), and >4.95 million AMR-associated deaths were reported worldwide in 2019 (*3*).

Many HAIs are preceded by colonization with the infecting pathogen; colonized patients' subsequent infection risk is increased by invasive devices, surgery, and receipt of antibiotics for prophylaxis or treatment for an unrelated infection (*4*–*7*). Pathogens that cause HAIs can be transmitted through direct or indirect contact from both asymptomatically colonized and symptomatically infected patients. Transmission to other persons at risk for colonization, infection, or both is especially notable because many risk factors for colonization overlap with those for infection. Newly colonized or infected persons then become potential secondary reservoirs for transmission. Hence, reducing pathogen burden in colonized patients could reduce not only risk to the original colonized person but also risk to the larger healthcare population. Here, we discuss current strategies for pathogen reduction that decolonize to various extents, evidence for effectiveness in preventing infections, potential future therapies leveraging the colonization resistance afforded by the microbiome, and outstanding needs in this area to promote infection prevention and patient safety.

Role of Colonization in Pathogenesis

The human body is perpetually colonized by microorganisms (i.e., microbiota), along with those organisms'

Author affiliations: Centers for Disease Control and Prevention, Atlanta, Georgia, USA (M.R. Mangalea, A.L. Halpin, M. Haile, C.A. Elkins, L.C. McDonald); United States Public Health Service, Rockville, Maryland, USA (A.L. Halpin)

DOI: https://doi.org/10.3201/eid3006.231338

associated metabolites and immediate environment (i.e., microbiome), which greatly influence human health and well-being. Most abundant in the intestines, mouth, skin, nose, and vagina, bacterial association with a human host can be transient or sequentially develop into life-long colonization (Table). Colonizing bacteria can be integrated as symbionts or pathobionts of the microbiome; pathobionts, in some instances, can be embedded in the commensal landscape and capable of blooming to cause infection in perturbed conditions (*7*,*8*). Because colonization can last for months to years, delineation between endogenous infection, in which a patient is infected with a pathogen from their own microbiota, and exogenous infection, in which they are infected with a pathogen more recently transmitted to them, is not always clear. Of note, pathogenic bacterial colonization in the intestine is normally limited by nonpathogenic commensal bacteria in the human microbiome, known as colonization resistance (*7*). Disruption of the intestinal microbial community with antibiotic prophylaxis before medical procedures or during treatment of unrelated syndromes reduces colonization resistance and opens the door for colonizing pathogens to cause infection, especially when the pathogen is resistant to the antibiotics causing the disruption.

Nasal carriage of *Staphylococcus aureus* has long been considered a major risk factor for wound infections, surgical-site infections (SSIs), or bloodstream infections (BSIs) (*9*). *S. aureus* bacteremia has been shown to be caused by endogenous infections arising from a colonizing *S. aureus* strain; up to 80% of nosocomial bacteremia cases are linked to an endogenous source (*9*,*10*). In a large trial of >14,000 patients screened for *S. aureus* colonization, risk for nosocomial bacteremia was much higher for *S. aureus* nasal carriers than noncarriers (*10*). The HAI burden of *S. aureus* colonization is compounded by methicillin-resistant *S. aureus* (MRSA). MRSA has a higher attributable 30-day mortality risk than multidrug-resistant gram-negative bacteria (MDR-GNB) (*11*) and carries substantial risk for infection after discharge in colonized patients (*12*). One study estimated the pooled global prevalence of MRSA in elderly care centers to be >14%, illustrating the growing need for effective pathogen reduction and decolonization approaches for one of the most prevalent and threatening MDROs for global health (*13*).

In addition to MRSA colonization of the nares, unrecognized colonization with MDROs in the gastrointestinal tract and other body sites poses a risk in vulnerable patient populations (*14*). A recent systematic review and metaregression quantified the pooled cumulative incidence of infection in patients colonized with MDROs; intestinal colonization with MDR-GNB led to 14% incidence of infection at 30 days follow-up and vancomycin-resistant enterococci (VRE) led to 8% incidence (*15*).

Intestinal colonization with extended-spectrum β-lactamase–producing Enterobacterales, a drug-resistant family of bacteria with limited treatment options, is associated with greatly increased incidence of BSIs (*16*). In a longitudinal study, increased relative abundance (i.e., >22%) of carbapenem-resistant Enterobacteriaceae in the microbiota of critically ill patients was associated with increased risk for BSIs (*4*). Likewise, hematopoietic stem cell transplantation patients who had >30% relative abundance of VRE in the microbiota were at a 9-fold higher risk for bloodstream VRE infections (*6*). Therefore, partially or completely reducing the colonizing load of a pathogen, especially during a period of critical illness or for high-risk patients, is a promising approach for HAI prevention.

Evidence for and Current Applications of Pathogen Reduction

Pathogen reduction is central to some forms of currently recommended antibiotic prophylaxis backed

Table. Key definitions used to describe decolonization and pathogen reduction to prevent antimicrobial resistance and healthcare-associated infections

Term	Definition
Colonization	Harboring living, actively dividing, and stable bacterial cell populations that do not cause symptoms of disease or infection.
Decolonization	Removing or reducing the burden of a pathogen, either temporarily or permanently.
Pathogen reduction	Substantial reduction of colonizing pathogen load, inclusive of, but not solely related to, decolonization, and more focused over a short period of increased infection or transmission risk.
Cross-transmission	Transmission of bacterial infection and antimicrobial resistance.
Opportunistic pathogen	Disease-causing microbes that can invade the body and cause disease under conditions of weakened immune defense.
Pathobiont	Opportunistic pathogenic bacteria that can emerge from the human microbiota to cause disease when its microbial ecology is disturbed.
Pathotype	A group of bacteria within the same species that can attack a host in different ways.

by evidence-based guidelines from major public health organizations, specifically for prevention of SSIs (*17*). For example, use of combined oral antimicrobial prophylaxis before elective colorectal surgery and decolonization of surgical patients with antistaphylococcal agents for orthopedic and cardiothoracic procedures received high-quality evidence from a recent practice recommendation to prevent SSIs in acute-care hospitals (*18*). Both examples prevent infections by reducing potentially pathogenic bacterial bioburden and suppressing colonization. In our view, antibiotic selection for prophylaxis should match the expected susceptibility of colonizing pathogens; pathogen reduction in the form of prophylaxis comes at the expense of potentially increasing antimicrobial resistance. Although antibiotic prophylaxis before bowel surgery targets gram-negative and anaerobic bacteria from the gut, mupirocin applied to the anterior nares can decolonize or reduce local numbers of *S. aureus*.

To prevent HAIs more broadly, CDC guidance for preventing MRSA infections includes several core and supplemental strategies to implement decolonization and pathogen reduction, including intranasal mupirocin and chlorhexidine bathing (*19*). Evidence supporting that guidance includes the REDUCE MRSA cluster-randomized trial encompassing 74 intensive care units (ICUs) and nearly 75,000 patients (*20*). That trial reported a 37% reduction in MRSA-positive clinical cultures and a 44% reduction in BSIs from any pathogen by following universal decolonization with chlorhexidine bathing in routine ICU practice (*20*). The benefits of chlorhexidine for routine bathing were also evident after a cluster-randomized trial of 28 nursing homes in which universal decolonization with chlorhexidine and nasal povidone/iodine reduced prevalence of MDRO carriage and need for transfer to a hospital (*21*). An additional benefit of chlorhexidine bathing is a limited potential for unintended microbial consequences because this approach does not greatly disrupt the commensal skin microbiota (*22*). Given its broad-spectrum activity against gram-negative and gram-positive MDROs, chlorhexidine bathing represents an effective and microbiota-sparing pathogen reduction strategy to prevent HAI (*22*). Furthermore, pathogen reduction of the body surface is a widely available, noninvasive solution that, although in some instances challenging to implement, can be used at admission to healthcare settings to reduce general infection risk and increase patient safety facilitywide. The successes of both mupirocin and chlorhexidine as topical decolonization agents cannot be overstated in any discussion on pathogen reduction as a public health intervention for preventing HAIs. A comprehensive review and discussion of those decolonization strategies is available (*23*).

Despite its success, topical decolonization is not simple to implement, but pathogen reduction of the gastrointestinal tract can be even more challenging. One relatively well characterized method is selective decontamination of the digestive tract (SDD), practiced under guidelines in critically ill patients in the Netherlands (*24*). Application of SDD antibacterial suspensions along with short courses of intravenous third-generation cephalosporin has been associated with improved patient outcomes in critically ill hospital patients in the Netherlands, where AMR prevalence is relatively low (*24*). However, SDD effectiveness in settings of moderate to high AMR remains to be verified. The SDD strategy was shown effective at considerably reducing carbapenem-resistant *Klebsiella pneumoniae* in a cohort of colonized patients with severe underlying conditions, suggesting that a pathogen reduction approach might be suitable for critically ill patients colonized with *K. pneumoniae* (*25*). However, the combination of nonabsorbable and intravenous prophylactic antimicrobial drugs during SDD raises concerns for long-term effects on selecting for AMR in patients' gut microbiota once SDD is discontinued (*26*). SDD of critically ill patients colonized with MDR-GNB has been most extensively explored in Europe, including a multiyear trial in Spain that reported marked reduction of MDR-GNB infections after SDD treatment in an ICU with high AR prevalence (*27*). Nevertheless, the European Committee of Infection Control has withheld recommendations for decolonization or pathogen reduction with SDD, citing major limitations in study heterogeneity, colonization pressure, and SDD agents (*28*).

Whether a universal approach to pathogen reduction is more effective than a targeted approach on the basis of screening patients for colonization with specific pathogens is still under scrutiny. Available evidence suggests a universal approach is more effective, for example, in reducing BSIs from any pathogen compared with targeted pathogen reduction of *S. aureus*–colonized patients only (*20*). The potential impact of effective pathogen reduction on illness, death, and costs is greatly influenced by additional indirect benefits that exponentially amplify the direct benefit to the index patient (*29*). Indirect benefits of pathogen reduction have the potential to extend beyond the patient to uncolonized persons through presumed decreases in pathogen shedding from recently decolonized patients, leading to a cascade of (theoretically)

prevented infections and deaths (*29*). One cost-effectiveness analysis measured life-years gained after decolonizing antibiotic treatment compared with infection treatment only and described the cost-effective potential of decolonization in a long-term acute care hospital setting (*30*). Using a compartmental model, those analyses showed up to 40-fold more deaths prevented and up to 30-fold more BSIs prevented, and the cost effectiveness was reflected by negative incremental costs when indirect effects of decolonization were included (*30*). Thus, decolonization can improve not only individual patient safety but also plausibly that of an entire healthcare system by reducing the pathogen burden at the population level.

Leveraging the Human Microbiome in Pathogen Reduction

In addition to the potential long-term AMR risks that could emerge from decolonization strategies that prioritize antibacterial prophylaxis, prophylaxis with broad-spectrum antibiotics including fluoroquinolones (e.g., in neutropenic cancer patients) carries high risk for antibiotic-associated adverse events, including *Clostridioides difficile* infection (CDI) (*31*). Therefore, alternative pathogen reduction approaches are needed. Pathogenic and often drug-resistant bacteria that increase and dominate the gut in clinical settings take advantage of ecologic disturbances in the microbiota during hospitalization. Intestinal domination with drug-resistant pathogens greatly increases risk for bacterial translocation in the gut, leading to bacteremia in vulnerable populations (*4*). To continue to elevate patient safety amid increasing AMR threats, future approaches should focus on microbiome-preserving or microbiome-restorative interventions that enrich beneficial populations of microbes to provide colonization resistance against pathogens. Thus, the functional roles of the human microbiome in colonization resistance should be considered for all decolonization strategies. The loss of microbial diversity in the intestine and the colonization resistance afforded by it resulting from antibiotic exposure, inflammation, or other perturbations, can lead to intestinal domination by pathobionts that produce new or emerging pathotypes (*7*).

Prior antibiotic use is a strong risk factor for healthcare-associated CDI (*31*). Asymptomatic *C. difficile* colonization is common in hospitalized patients and long-term care facility residents, but carriage might be transient depending on the stability of the microbiota. Microbiome disruption and immunosuppression increase CDI risk in colonized patients, and ≈10%–60% of patients colonized with toxigenic *C. difficile* develop symptomatic disease (*32*). High asymptomatic colonization rates of up to 18% in hospitals (*32*), up to 15% in long-term care facilities (*33*), and >50% in 1 reported outbreak setting (*33*) are alarming given the transmission potential of asymptomatic carriers (*32*,*33*). Although prophylactic oral vancomycin for preventing CDI in patients treated with systemic antibiotics is an active area of investigation, considerable long-term impacts of this strategy on the microbiome are possible (*5*). A stable gut microbiome serves as a primary defense from initial *C. difficile* colonization and prevents transition from colonization to symptomatic infection. Even though *C. difficile* colonization can exert toxigenicity at very low relative abundances in human microbiomes, more severe CDI symptoms are positively correlated with lower PCR cycle threshold values, which reflect higher pathogen loads (*34*). Thus, pathogen reduction could be an applicable approach for low abundance toxigenic gut colonizers.

A need for effective gut pathogen reduction strategies for *C. difficile* and other MDROs exists, as does a need for approved and standardized microbiome-based therapeutics aimed at prevention rather than treatment. Fecal microbiota transplantation (FMT) is one strategy to treat patients with recurring CDI who do not respond to standard therapies. A 2013 study reported a successful randomized control trial of FMT to treat recurring CDI (*35*). Since then, continued advancements in safety and efficacy of that treatment have been made through multiple clinical trials with largely favorable outcomes (*36*). Of note, in 2022, the US Food and Drug Administration (FDA) approved a fecal microbiota product under the trade name Rebyota (RBX2660; Ferring Pharmaceuticals, https://www.ferring.com) to treat recurring CDI after antibiotic therapy (*37*). That approval was followed by FDA approval of the oral product Vowst (SER-109; Seres Therapeutics, https://www.serestherapeutics.com) (*38*). Therefore, FMT and related live biotherapeutic products represent a promising microbiome-based therapy for recurring CDI. However, effective prevention and treatment of primary CDI and effective pathogen reduction for asymptomatic carriers are still needed. Challenges in regulation of FMT remain because of sample heterogeneity and other hurdles, but development of more standardized microbiome restoration products through defined bacterial consortia shows positive results after phase 2 clinical trials (*39*).

Fortifying the microbiome with live biotherapeutic products can influence and prevent disease by supplementing essential components of colonization resistance. One study pointed to post-FMT reductions

in hospital stay duration and antibiotic use in addition to overall reduction of bacteremia and illness, despite modest long-term decolonization rates (*40*). FMT-treated recurring CDI patients also have been shown to have lower risk for BSI and reductions in hospitalizations compared with patients treated with antibiotics (*41*). Other clinical and immunologic outcomes that contribute to patient health and safety evidently are also contributing to the holistic benefits of pathogen reduction.

The evidence for decolonization effectiveness and the importance of the human microbiome in colonization resistance still point to pathogen reduction as the primary or preferred mechanism for preventing infection. Another novel approach of preserving the microbiome is demonstrated by a placebo-controlled trial for *S. aureus* decolonization of healthy adults using a probiotic *Bacillus* spp. (i.e., a live biotherapeutic). Oral administration led to a 95% reduction in *S. aureus* total abundance from both the intestines and the nares without adverse effects or altering the microbiome (*42*). The use of live biotherapeutics in pathogen reduction should be further explored for potential clinical impact.

Ideal Attributes of Current and Future Pathogen-Reducing Agents

To devise the best approaches, other ideal attributes of current and future pathogen-reducing agents should be considered (Figure). Given the central role of the microbiome in colonization resistance and the selective pressure that antimicrobial drugs can have on the human microbiota, selectivity is a crucial aspect of pathogen reducing agents, especially agents that directly kill or inhibit bacterial growth. Ideally selectivity would be limited to the pathogen or group in question, for instance, aerobic gram-negative spectrum used in SDD. In addition, the administration routes (e.g., topical chlorhexidine) or drug kinetic factors (e.g., nonabsorbable antibiotics) that limit distribution of the agent to the colonization site would protect the microbiota at other body sites. Chlorhexidine is one beneficial pathogen-reducing agent because it is an antiseptic agent that acts markedly differently from other current therapeutic antimicrobial agents. In addition, chlorhexidine has high potency for gram-positive organisms in relation to levels typically achieved when applied to the skin.

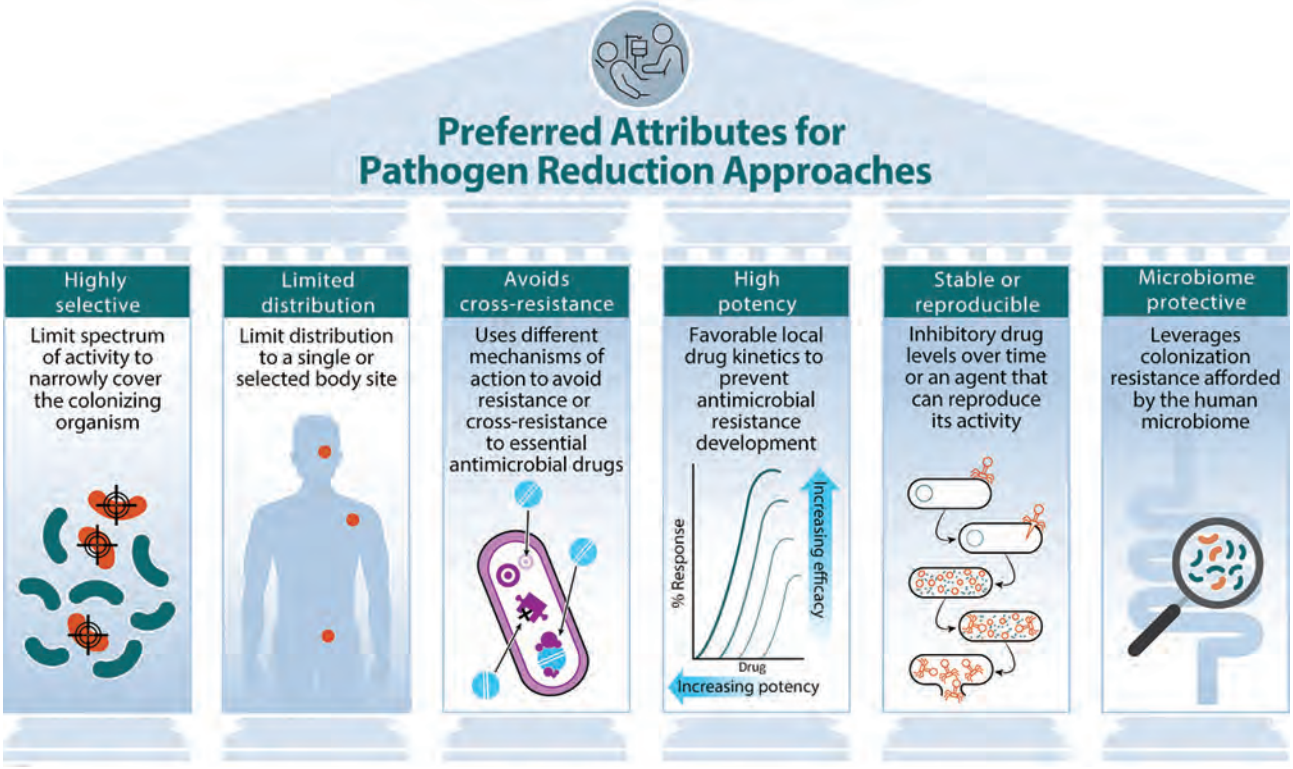

Figure. Preferred attributes for decolonization and pathogen reduction approaches to prevent antimicrobial resistance and healthcare-associated infections. Examples of these approaches include the following: highly selective, e.g., selective digestive decontamination targeting aerobic gram-negative bacilli; limited distribution, e.g., nonabsorbable antimicrobial drugs; avoids cross-resistance, e.g., chlorhexidine biocide; high potency, e.g., preventing selection of resistant mutations; stable or reproducible, e.g., use of phages to decolonize or reduce bacterial burden; and microbiome protective, e.g., using the human microbiome to spare beneficial microbes.

Another example of a potential future agent possessing several ideal attributes is lysostaphin, a bacteriocin with a limited spectrum of activity. Lysostaphin applied nasally is highly active in killing *S. aureus* relative to achievable concentrations (*43*).

Leveraging the microbiome is another ideal attribute of a pathogen-reducing agent. Future strategies that leverage the microbiome in pathogen reduction should expand applications beyond recurrent and primary CDI and capitalize on microbial ecology to achieve MDRO reduction while limiting use of antimicrobial agents. Results from PREMIX, a randomized controlled trial of FMT for MDRO decolonization, reported substantial reductions of colonization and infection, and replacement of extended-spectrum β-lactamase–producing *E. coli* strains by more susceptible strains after FMT (*44*). FMT for pathogen reduction in immunocompromised patients undergoing transplantation for hematologic malignancies is also effective for reconstituting the gut microbiota (*45*).

Another preferred attribute is sustained pathogen reduction activity over time and the ability of an agent to replicate in the human microbiome or the environment. Pathogen reduction could revive interest in the use of bacteriophages, viruses that only infect bacteria, to target specific MDROs. One report highlights the development of an engineered phage combination, SNIPR001, used to reduce *E. coli* gut colonization by targeting *E. coli* strains that cause BSIs among hematology-oncology patients undergoing chemotherapy, similar to current fluoroquinolone prophylaxis (*46*).

Microbiome-complementary therapies, such as FMT, and possible future use of bacteriophages for pathogen reduction represent novel interventions that promote antimicrobial stewardship along with patient well-being. Several ongoing registered clinical trials are using these pathogen reduction approaches and span various trial phases (Appendix Table, https://wwwnc.cdc.gov/EID/article/30/6/23-1338-App1.pdf).

Pathogen Reduction Moving Forward

Pathogen reduction is an essential area for further development. Evidence suggests major benefits for reducing infection risk and improving associated clinical outcomes. Expanding the use of pathogen reduction approaches will require development of new diagnostic tests that can rapidly detect MDROs and quantify MDRO burden at certain anatomic sites. One novel approach applies an engineered reporter phage luminescence assay for swift and accurate point-of-care urinary tract infection diagnostics, which further doubles as rapid phage-patient matching for personalized therapy (*47*). New diagnostic testing will enable well-designed studies of novel agents that assess efficacy in reducing pathogen burden as well as clinical outcomes. A 2022 FDA-CDC public workshop addressed those issues (https://ftp.cdc.gov/pub/ARX-COMMUNICATIONS/pdf/CDC_FDA_Meeting). A primary driver of that workshop was the recognized need for drug development and registration pathways, at least for the regulatory framework in the United States.

The approaches to pathogen reduction will involve drugs and biologics (e.g., live microbials, probiotics and prebiotics, and bacteriophages) that have vastly different regulatory bases and burdens of evidence. In some cases, such as with live microbials marketed as probiotics, avenues exist with current regulation and use as dietary supplements with allowable generalized health claims. Whether those health claims can cover pathogen reduction is unclear because the products are also intended for use in healthy populations and have different expectations than products used for pathogen reduction (*48*). Risks and challenges associated with treatment using live biotherapeutic products include the potential transmission of infectious agents (*49*), and the complex biologic interactions with host microbial communities, including the pharmacokinetics and pharmacodynamics associated with host effects on therapeutic product and vice versa (*50*). Likewise, interplay with microbiome succession and maturation, especially in specialized populations, such as infants, should be considered for analyses of risk in long-term colonizing products (*48*). Regardless, using an underlying mechanistic basis (whether drug or biologic), product development could benefit from focusing on attributes needed for established colonization in or on the human body to avoid the emergence of resistance.

In conclusion, the approaches to pathogen reduction will clearly be multifaceted. Nonetheless, harnessing and applying our understanding of ecologic principles to address the pathogen burden in healthcare might promote enduring success in driving down infections while preserving the lifesaving utility of available therapeutic drugs.

Acknowledgments

We thank Alexander Kallen and John Jernigan for their invaluable review and constructive feedback, which significantly enhanced the quality and impact of this manuscript.

About the Author

Dr. Mangalea is a microbial ecologist and bioinformatician in the Division of Healthcare Quality Promotion, National Center for Emerging and Zoonotic Infectious Diseases, Centers for Disease Control and Prevention, Atlanta, Georgia, USA. His research interests include metagenomic analyses of microbiomes and antimicrobial resistance profiles.

References

1. Centers for Disease Control and Prevention. Antibiotic resistance threats in the United States, 2019 [cited 2023 Jul 20]. https://www.cdc.gov/drugresistance/pdf/threats-report/2019-ar-threats-report-508.pdf
2. Centers for Disease Control and Prevention. COVID-19 U.S. impact on antimicrobial resistance: 2022 special report [cited 2023 Jul 20]. https://www.cdc.gov/drugresistance/pdf/covid19-impact-report-508.pdf
3. Murray CJL, Ikuta KS, Sharara F, Swetschinski L, Robles Aguilar G, Gray A, et al.; Antimicrobial Resistance Collaborators. Global burden of bacterial antimicrobial resistance in 2019: a systematic analysis. Lancet. 2022; 399:629–55. https://doi.org/10.1016/S0140-6736(21)02724-0
4. Shimasaki T, Seekatz A, Bassis C, Rhee Y, Yelin RD, Fogg L, et al.; Centers for Disease Control and Prevention Epicenters Program. Increased relative abundance of *Klebsiella pneumoniae* carbapenemase-producing *Klebsiella pneumoniae* within the gut microbiota is associated with risk of bloodstream infection in long-term acute care hospital patients. Clin Infect Dis. 2019;68:2053–9. https://doi.org/10.1093/cid/ciy796
5. Fishbein SRS, Hink T, Reske KA, Cass C, Struttmann E, Iqbal ZH, et al. Randomized controlled trial of oral vancomycin treatment in *Clostridioides difficile*–colonized patients. MSphere. 2021;6:e00936-20. https://doi.org/10.1128/mSphere.00936-20
6. Taur Y, Xavier JB, Lipuma L, Ubeda C, Goldberg J, Gobourne A, et al. Intestinal domination and the risk of bacteremia in patients undergoing allogeneic hematopoietic stem cell transplantation. Clin Infect Dis. 2012;55:905–14. https://doi.org/10.1093/cid/cis580
7. Tosh PK, McDonald LC. Infection control in the multidrug-resistant era: tending the human microbiome. Clin Infect Dis. 2012;54:707–13. https://doi.org/10.1093/cid/cir899
8. Stecher B, Maier L, Hardt WD. 'Blooming' in the gut: how dysbiosis might contribute to pathogen evolution. Nat Rev Microbiol. 2013;11:277–84. https://doi.org/10.1038/nrmicro2989
9. von Eiff C, Becker K, Machka K, Stammer H, Peters G; Study Group. Nasal carriage as a source of *Staphylococcus aureus* bacteremia. N Engl J Med. 2001;344:11–6. https://doi.org/10.1056/NEJM200101043440102
10. Wertheim HF, Vos MC, Ott A, van Belkum A, Voss A, Kluytmans JA, et al. Risk and outcome of nosocomial *Staphylococcus aureus* bacteraemia in nasal carriers versus non-carriers. Lancet. 2004;364:703–5. https://doi.org/10.1016/S0140-6736(04)16897-9
11. Nelson RE, Slayton RB, Stevens VW, Jones MM, Khader K, Rubin MA, et al. Attributable mortality of healthcare-associated infections due to multidrug-resistant gram-negative bacteria and methicillin-resistant *Staphylococcus aureus*. Infect Control Hosp Epidemiol. 2017;38:848–56. https://doi.org/10.1017/ice.2017.83
12. Nelson RE, Evans ME, Simbartl L, Jones M, Samore MH, Kralovic SM, et al. Methicillin-resistant *Staphylococcus aureus* colonization and pre- and post-hospital discharge infection risk. Clin Infect Dis. 2019;68:545–53. https://doi.org/10.1093/cid/ciy507
13. Hasanpour AH, Sepidarkish M, Mollalo A, Ardekani A, Almukhtar M, Mechaal A, et al. The global prevalence of methicillin-resistant *Staphylococcus aureus* colonization in residents of elderly care centers: a systematic review and meta-analysis. Antimicrob Resist Infect Control. 2023;12:4. https://doi.org/10.1186/s13756-023-01210-6
14. McKinnell JA, Miller LG, Singh RD, Gussin G, Kleinman K, Mendez J, et al. High prevalence of multidrug-resistant organism colonization in 28 nursing homes: an "iceberg effect". J Am Med Dir Assoc. 2020;21:1937–1943.e2. https://doi.org/10.1016/j.jamda.2020.04.007
15. Willems RPJ, van Dijk K, Vehreschild MJGT, Biehl LM, Ket JCF, Remmelzwaal S, et al. Incidence of infection with multidrug-resistant gram-negative bacteria and vancomycin-resistant enterococci in carriers: a systematic review and meta-regression analysis. Lancet Infect Dis. 2023;12:719–31. https://doi.org/10.1016/S1473-3099(22)00811-8
16. Isendahl J, Giske CG, Hammar U, Sparen P, Tegmark Wisell K, Ternhag A, et al. Temporal dynamics and risk factors for bloodstream infection with extended-spectrum β-lactamase-producing bacteria in previously-colonized individuals: national population-based cohort study. Clin Infect Dis. 2019;68:641–9. https://doi.org/10.1093/cid/ciy539
17. Fields AC, Pradarelli JC, Itani KMF. Preventing surgical site infections: looking beyond the current guidelines. JAMA. 2020;323:1087–8. https://doi.org/10.1001/jama.2019.20830
18. Calderwood MS, Anderson DJ, Bratzler DW, Dellinger EP, Garcia-Houchins S, Maragakis LL, et al. Strategies to prevent surgical site infections in acute-care hospitals: 2022 update. Infect Control Hosp Epidemiol. 2023;44:695–720. https://doi.org/10.1017/ice.2023.67
19. Centers for Disease Control and Prevention. Strategies to prevent hospital-onset *Staphylococcus aureus* bloodstream infections in acute care facilities [cited 2023 Dec 4]. https://www.cdc.gov/hai/prevent/staph-prevention-strategies.html
20. Huang SS, Septimus E, Kleinman K, Moody J, Hickok J, Avery TR, et al.; CDC Prevention Epicenters Program; AHRQ DECIDE Network and Healthcare-Associated Infections Program. Targeted versus universal decolonization to prevent ICU infection. N Engl J Med. 2013;368:2255–65. https://doi.org/10.1056/NEJMoa1207290
21. Miller LG, McKinnell JA, Singh RD, Gussin GM, Kleinman K, Saavedra R, et al. Decolonization in nursing homes to prevent infection and hospitalization. N Engl J Med. 2023;389:1766–77. https://doi.org/10.1056/NEJMoa2215254
22. Babiker A, Lutgring JD, Fridkin S, Hayden MK. Assessing the potential for unintended microbial consequences of routine chlorhexidine bathing for prevention of healthcare-associated infections. Clin Infect Dis. 2021;72:891–8. https://doi.org/10.1093/cid/ciaa1103
23. Septimus EJ, Schweizer ML. Decolonization in prevention of health care–associated infections. Clin Microbiol Rev. 2016;29:201–22. https://doi.org/10.1128/CMR.00049-15
24. Wittekamp BHJ, Oostdijk EAN, Cuthbertson BH, Brun-Buisson C, Bonten MJM. Selective decontamination of the digestive tract (SDD) in critically ill patients: a narrative review. Intensive Care Med. 2020;46:343–9. https://doi.org/10.1007/s00134-019-05883-9

25. Saidel-Odes L, Polachek H, Peled N, Riesenberg K, Schlaeffer F, Trabelsi Y, et al. A randomized, double-blind, placebo-controlled trial of selective digestive decontamination using oral gentamicin and oral polymyxin E for eradication of carbapenem-resistant *Klebsiella pneumoniae* carriage. Infect Control Hosp Epidemiol. 2012;33:14–9. https://doi.org/10.1086/663206
26. Buelow E, Gonzalez TB, Versluis D, Oostdijk EAN, Ogilvie LA, van Mourik MSM, et al. Effects of selective digestive decontamination (SDD) on the gut resistome. J Antimicrob Chemother. 2014;69:2215–23. https://doi.org/10.1093/jac/dku092
27. Sánchez-Ramírez C, Hípola-Escalada S, Cabrera-Santana M, Hernández-Viera MA, Caipe-Balcázar L, Saavedra P, et al. Long-term use of selective digestive decontamination in an ICU highly endemic for bacterial resistance. Crit Care. 2018;22:141. https://doi.org/10.1186/s13054-018-2057-2
28. Tacconelli E, Mazzaferri F, de Smet AM, Bragantini D, Eggimann P, Huttner BD, et al. ESCMID-EUCIC clinical guidelines on decolonization of multidrug-resistant gram-negative bacteria carriers. Clin Microbiol Infect. 2019;25:807–17. https://doi.org/10.1016/j.cmi.2019.01.005
29. Jernigan JA. Rationale for decolonization as a strategy for preventing antimicrobial-resistant infections. Presented at: Drug development considerations for the prevention of healthcare-associated infections; virtual public workshop; 2022 Aug 29.
30. Toth DJA, Samore MH, Nelson RE. Economic evaluations of new antibiotics: the high potential value of reducing healthcare transmission through decolonization. Clin Infect Dis. 2021;72:S34–41. https://doi.org/10.1093/cid/ciaa1590
31. Tamma PD, Avdic E, Li DX, Dzintars K, Cosgrove SE. Association of adverse events with antibiotic use in hospitalized patients. JAMA Intern Med. 2017;177:1308–15. https://doi.org/10.1001/jamainternmed.2017.1938
32. Donskey CJ, Kundrapu S, Deshpande A. Colonization versus carriage of *Clostridium difficile*. Infect Dis Clin North Am. 2015;29:13–28. https://doi.org/10.1016/j.idc.2014.11.001
33. Riggs MM, Sethi AK, Zabarsky TF, Eckstein EC, Jump RL, Donskey CJ. Asymptomatic carriers are a potential source for transmission of epidemic and nonepidemic *Clostridium difficile* strains among long-term care facility residents. Clin Infect Dis. 2007;45:992–8. https://doi.org/10.1086/521854
34. Bonacorsi S, Visseaux B, Bouzid D, Pareja J, Rao SN, Manissero D, et al. Systematic review on the correlation of quantitative PCR cycle threshold values of gastrointestinal pathogens with patient clinical presentation and outcomes. Front Med (Lausanne). 2021;8:711809. https://doi.org/10.3389/fmed.2021.711809
35. van Nood E, Vrieze A, Nieuwdorp M, Fuentes S, Zoetendal EG, de Vos WM, et al. Duodenal infusion of donor feces for recurrent *Clostridium difficile*. N Engl J Med. 2013;368:407–15. https://doi.org/10.1056/NEJMoa1205037
36. Tariq R, Syed T, Yadav D, Prokop LJ, Singh S, Loftus EV Jr, et al. Outcomes of fecal microbiota transplantation for *C. difficile* infection in inflammatory bowel disease: a systematic review and meta-analysis. J Clin Gastroenterol. 2023;57:285–93. https://doi.org/10.1097/MCG.0000000000001633
37. US Food and Drug Administration. Rebyota [cited 2023 Jul 20]. https://www.fda.gov/vaccines-blood-biologics/vaccines/rebyota
38. US Food and Drug Administration. Vowst [cited 2023 Dec 15]. https://www.fda.gov/vaccines-blood-biologics/vowst
39. Louie T, Golan Y, Khanna S, Bobilev D, Erpelding N, Fratazzi C, et al. VE303, a defined bacterial consortium, for prevention of recurrent *Clostridioides difficile* infection: a randomized clinical trial. JAMA. 2023;329:1356–66. https://doi.org/10.1001/jama.2023.4314
40. Ghani R, Mullish BH, McDonald JAK, Ghazy A, Williams HRT, Brannigan ET, et al. Disease prevention not decolonization: a model for fecal microbiota transplantation in patients colonized with multidrug-resistant organisms. Clin Infect Dis. 2021;72:1444–7. https://doi.org/10.1093/cid/ciaa948
41. Ianiro G, Murri R, Sciumè GD, Impagnatiello M, Masucci L, Ford AC, et al. Incidence of bloodstream infections, length of hospital stay, and survival in patients with recurrent *Clostridioides difficile* infection treated with fecal microbiota transplantation or antibiotics: a prospective cohort study. Ann Intern Med. 2019;171:695–702. https://doi.org/10.7326/M18-3635
42. Piewngam P, Khongthong S, Roekngam N, Theapparat Y, Sunpaweravong S, Faroongsarng D, et al. Probiotic for pathogen-specific *Staphylococcus aureus* decolonisation in Thailand: a phase 2, double-blind, randomised, placebo-controlled trial. Lancet Microbe. 2023;4:e75–83. https://doi.org/10.1016/S2666-5247(22)00322-6
43. Jayakumar J, Kumar VA, Biswas L, Biswas R. Therapeutic applications of lysostaphin against *Staphylococcus aureus*. J Appl Microbiol. 2021;131:1072–82. https://doi.org/10.1111/jam.14985
44. Woodworth MH, Conrad RE, Haldopoulos M, Pouch SM, Babiker A, Mehta AK, et al. Fecal microbiota transplantation promotes reduction of antimicrobial resistance by strain replacement. Sci Transl Med. 2023;15:eabo2750. https://doi.org/10.1126/scitranslmed.abo2750
45. Taur Y, Coyte K, Schluter J, Robilotti E, Figueroa C, Gjonbalaj M, et al. Reconstitution of the gut microbiota of antibiotic-treated patients by autologous fecal microbiota transplant. Sci Transl Med. 2018;10:eaap9489. https://doi.org/10.1126/scitranslmed.aap9489
46. Gencay YE, Jasinskyte D, Robert C, Semsey S, Martinez V, Petersen AO, et al. Engineered phage with antibacterial CRISPR-Cas selectively reduce *E. coli* burden in mice. Nat Biotechnol. 2024;42:265–74.
47. Meile S, Du J, Staubli S, Grossmann S, Koliwer-Brandl H, Piffaretti P, et al. Engineered reporter phages for detection of *Escherichia coli*, *Enterococcus*, and *Klebsiella* in urine. Nat Commun. 2023;14:4336. https://doi.org/10.1038/s41467-023-39863-x
48. Merenstein D, Pot B, Leyer G, Ouwehand AC, Preidis GA, Elkins CA, et al. Emerging issues in probiotic safety: 2023 perspectives. Gut Microbes. 2023;15:2185034. https://doi.org/10.1080/19490976.2023.2185034
49. Blaser MJ. Fecal microbiota transplantation for dysbiosis–predictable risks. N Engl J Med. 2019;381:2064–6. https://doi.org/10.1056/NEJMe1913807
50. Ducarmon QR, Kuijper EJ, Olle B. Opportunities and challenges in development of live biotherapeutic products to fight infections. J Infect Dis. 2021;223:S283–9. https://doi.org/10.1093/infdis/jiaa779

Address for correspondence: Mihnea R. Mangalea, Centers for Disease Control and Prevention, 1600 Clifton Rd NE, Mailstop H15-SSB, Atlanta, GA 30329-4018, USA; email: mmangalea@cdc.gov

Deciphering Unexpected Vascular Locations of *Scedosporium* spp. and *Lomentospora prolificans* Fungal Infections, France

Carole Vignals, Joseph Emmerich, Hugues Begueret, Dea Garcia-Hermoso, Guillaume Martin-Blondel, Adela Angoulvant, Damien Blez, Patrick Bruneval, Sophie Cassaing, Emilie Catherinot, Pierre Cahen, Cécile Moluçon-Chabrot, Carole Chevenet, Laurence Delhaes, Lélia Escaut, Marie Faruch, Frédéric Grenouillet, Fabrice Larosa, Lucie Limousin, Elisabeth Longchampt, François Mellot, Céline Nourrisson, Marie-Elisabeth Bougnoux, Olivier Lortholary, Antoine Roux, Laura Rozenblum, Mathilde Puges, Fanny Lanternier, Didier Bronnimann

Scedosporium spp. and *Lomentospora prolificans* are emerging non-*Aspergillus* filamentous fungi. The Scedosporiosis/lomentosporiosis Observational Study we previously conducted reported frequent fungal vascular involvement, including aortitis and peripheral arteritis. For this article, we reviewed 7 cases of *Scedosporium* spp. and *L. prolificans* arteritis from the Scedosporiosis/lomentosporiosis Observational Study and 13 cases from published literature. Underlying immunosuppression was reported in 70% (14/20) of case-patients, mainly those who had solid organ transplants (10/14). Osteoarticular localization of infection was observed in 50% (10/20) of cases; infections were frequently (7/10) contiguous with vascular infection sites. *Scedosporium* spp./*Lomentospora prolificans* infections were diagnosed in 9 of 20 patients ≈3 months after completing treatment for nonvascular scedosporiosis/lomentosporiosis. Aneurysms were found in 8/11 aortitis and 6/10 peripheral arteritis cases. Invasive fungal disease–related deaths were high (12/18 [67%]). The vascular tropism of *Scedosporium* spp. and *L. prolificans* indicates vascular imaging, such as computed tomography angiography, is needed to manage infections, especially for osteoarticular locations.

Scedosporium spp. and *Lomentospora prolificans* are non-*Aspergillus* filamentous fungi causing increasingly recognized invasive fungal disease (IFD) in both immunocompromised and immunocompetent patients (*1*,*2*). *Scedosporium* spp. comprise *S. apiospermum* complex species, which includes *S. apiospermum sensu stricto* and *S. boydii*; *L. prolificans* was previously known as *S. prolificans* (*3*). In immunocompetent patients, localized infections have been described, such as mycetomas, osteoarticular infections (*4*), or central nervous system (CNS) infections after near-drownings. In immunocompromised hosts, scedosporiosis and lomentosporiosis mainly affect the lungs and CNS or are disseminated (*5*–*11*). We previously conducted the Scedosporiosis/lomentosporiosis Observational Study (SOS) and reported non-CNS vascular involvement (aorta or peripheral arteries excluding CNS arteries) in 24% of disseminated infections (*12*). Although CNS vascular involvement during invasive scedosporiosis has been described, a scedosporiosis/

Author affiliations: Centre Hospitalier Universitaire de Bordeaux, Bordeaux, France (C. Vignals, H. Begueret, L. Delhaes, M. Puges, D. Bronnimann); Hôpital Saint-Joseph, Paris, France (J. Emmerich); Institut Pasteur, Paris (D. Garcia-Hermoso, M.-E. Bougnoux, O. Lortholary, F. Lanternier); Centre Hospitalier Universitaire de Toulouse, Toulouse, France (G. Martin-Blondel, S. Cassaing, M. Faruch); Hôpital Bicêtre, Le Kremlin-Bicêtre, France (A. Angoulvant, L. Escaut); Hôpital Européen Georges Pompidou, Paris (D. Blez, P. Bruneval); Hôpital Foch, Suresnes, France (E. Catherinot, P. Cahen, L. Limousin, E. Longchampt, F. Mellot, A. Roux); Centre hospitalier universitaire de Clermont-Ferrand, Clermont-Ferrand, France (C. Moluçon-Chabrot, C. Chevenet, C. Nourrisson); Centre hospitalier universitaire de Besançon, Besançon, France (F. Grenouillet); Centre Hospitalier Universitaire de Dijon, Dijon, France (F. Larosa); Hôpital Necker-enfants malades AP-HP, Paris (M.-E. Bougnoux, O. Lortholary, F. Lanternier); Hôpital Pitié-Salpêtrière AP-HP, Paris (L. Rozenblum)

DOI: https://doi.org/10.3201/eid3006.231409

lomentosporiosis case series of non-CNS vascular infections has not been reported (*5*–*11*,*13*–*17*). We describe clinical, imaging, and detailed histopathologic characteristics of all patients with non-CNS vascular scedosporiosis/lomentosporiosis infections identified in the SOS and review cases reported in published literature.

Methods

Ethics Approval

The research was approved by the Institut Pasteur Internal Review Board (approval no. 2009–34/IRB) and by the Commission Nationale de l'Informatique et des Libertés in accordance with the laws of France. All clinical data were recorded anonymously.

Study Design

The SOS included all retrospective cases of proven and probable invasive scedosporiosis/lomentosporiosis (IS) characterized at the National Reference Center for Invasive Mycoses and Antifungals, France, during January 2005–March 2017 (*12*). We performed a medical records review of all patients in the SOS who had non-CNS vascular infections (aortitis or peripheral arteritis) caused by *Scedosporium* spp. or *L. prolificans*. In addition, we performed an electronic literature search for case reports in PubMed on October 10, 2021, by using the following search filter: (Scedospori*[Title/Abstract] OR Pseudallescheri*[Title/Abstract] OR Lomentospori*[Title/Abstract]) AND (invasive[Title/Abstract] OR disseminated[Title/Abstract] OR infection[Title/Abstract]) AND (case[Title/Abstract] OR patient[Title/Abstract] OR report[Title/Abstract]). We selected all articles in English, French, or Spanish that reported proven or probable non-CNS vascular infections caused by *Scedosporium* spp., including *Pseudallescheria* spp., or *L. prolificans*, including *S. prolificans* and *S. inflatum*. We checked reference lists of selected articles for other relevant studies. We only included published case reports or case series with detailed documentation of clinical history, diagnostic methods, treatment, and outcomes. Data from 1 SOS case (patient 5) had been published previously, and we excluded this case from the literature review.

For each case, we reported demographic conditions, underlying diseases/conditions, vascular impairment sites, signs and symptoms, other infected sites, microbiologic results, antifungal treatments, surgical therapy, and clinical outcomes by using a standard anonymous case report form. Each SOS case was reviewed by 4 investigators (C.V., J.E., F.L., and D.B.); each literature review case was reviewed by 2 investigators (C.V. and D.B.).

Definitions

We defined non-CNS vascular infection as either imaging of structural abnormalities of the arterial wall suggestive of aortitis/arteritis (*18*) associated with a concomitant IS diagnosis (Appendix, https://wwwnc.cdc.gov/EID/article/30/6/23-1409-App1.pdf), a positive culture from an intraoperative arterial wall sample, or anatomopathologic evidence of arterial wall fungal infection with a concomitant IS diagnosis. We excluded cases of arterial thrombosis without evidence of parietal impairment. We defined proven and probable IS according to the 2019 European Organization for Research and Treatment of Cancer/Mycoses Study Group criteria (*19*), modified by including trauma and near-drowning as risk factors.

We considered 6 main underlying conditions for IFD, but only 1 condition was assigned to each patient as follows: malignancies; solid organ transplantation; systemic inflammatory disease; contamination by traumatic penetration, injury, surgery, or near-drowning (trauma/inoculation); other, for miscellaneous underlying medical conditions, including neutropenia, chronic renal or respiratory insufficiency, chronic respiratory disease, diabetes mellitus, HIV infection, or corticosteroids administration; and no risk factor in the absence of all previous factors.

We considered infections to be disseminated when they involved ≥2 noncontiguous sites or were associated with fungemia. We defined breakthrough infections as those occurring in patients who received antifungal therapy for ≥7 days within 30 days before IS diagnosis and defined prior colonization as a *Scedosporium/Lomentospora* culture within a nonsterile clinical sample without signs of infection before IS diagnosis. We defined follow-up as the period from IS diagnosis to last patient contact or death if vascular infection was diagnosed at the time of IS diagnosis or within 3 months of diagnosis; otherwise, we defined it as the period from vascular infection diagnosis to last patient contact or death. We considered IFD-related death as death supposedly caused by IFD. We defined radical surgery as complete resection of the vascular infection site, including vascular prothesis removal, whether or not it was associated with vascular reconstruction. For analyses, we described quantitative variables as medians with interquartile ranges and categorical variables as numbers and percentages.

Results

SOS Case-Patients

Case-patient 1 was a 52-year-old man who had liver and kidney transplants because of alcoholic cirrhosis and IgA nephropathy. He had dermohypodermitis of the left lower limb caused by *S. apiospermum* and was treated with voriconazole for 18 months. Despite initial clinical success, *S. apiospermum* oligoarthritis developed 3 months after the patient stopped antifungal therapy; infection was documented in cultures of left knee joint liquid. He received a combination of voriconazole, caspofungin, and terbinafine and reduction of his immunosuppressive regimen. No evidence of endocarditis was found on an echocardiogram. Blood culture results were negative. Because fever persisted during treatment, positron emission tomography (PET)/computed tomography (CT) and abdominal/pelvic CT were performed, which identified multiple osteoarticular localizations (ankles, knees, left sacroiliac joint, left hip, T8 spondylitis, L5–S1 spondylodiscitis), left primitive iliac arteritis (thrombosis with perivascular and soft tissue contrast) (Figure 1) and abdominal bifurcation aortitis (perivascular and soft tissue contrast associated with focal hypermetabolism). The patient died 2 months later from multiorgan failure accompanied by acute left lower limb ischemia and possible mesenteric ischemia.

Case-patient 2 was a 31-year-old woman recovering from a severe road accident in muddy water. She was hospitalized 2 months after the accident for pneumonia and bilateral pulmonary embolisms. She was treated empirically with antimicrobial drugs and anticoagulation therapy, which was stopped a few days later because of massive hemoptysis. She experienced persistent fever and epileptic seizures; an echocardiogram and CT scan revealed tricuspid endocarditis associated with cerebral abscess and bilateral aneurysms of pulmonary arteries rapidly growing and partially thrombosed (Figure 2, panel A). At that time, *S. apiospermum* was identified from blood cultures. She received long-term therapy with voriconazole and caspofungin, which was successful. However, chronic pulmonary arterial hypertension developed, requiring cardiopulmonary transplantation while she was undergoing antifungal treatment for >2 years. She died the day of transplantation because of a pulmonary hilum twist. Postmortem examination showed highly altered pulmonary arteries with major intimal fibrosis and a thrombus containing multiple fungal septate hyphae (Figure 2, panel B).

Case-patient 3 was a 32-year-old man who had macrophage activation syndrome, acute renal failure requiring hemodialysis, and multiple necrotic cutaneous lesions after acute cocaine intoxication. Febrile acute shoulder arthritis and sternal osteochondritis developed for which he underwent surgical debridement; *S. apiospermum* was identified in perioperative shoulder samples, and *L. prolificans* was identified in sternum samples. Thoracic-abdominal-pelvic CT and PET/CT scans revealed pseudonodular pulmonary lesions, abdominal aortitis and primitive iliac arteritis with perivascular contrasts, arterial wall thickenings, and intense vascular hypermetabolism (Figure 2, panels C, D). He was successfully treated with voriconazole, terbinafine, and miltefosine for 3 years, along with γ-interferon in the absence of initial improvement. Follow-up imaging performed 2.5 years after treatment initiation found a clear reduction of periaortic inflammatory thickening and vascular hypermetabolism. Antifungal treatment was stopped after 3 years without any clinical sign of relapse 1 year after interruption.

Case-patient 4 was a 51-year-old woman who had focal segment glomerulosclerosis requiring a kidney transplant, which was complicated by acute graft rejection. Closing surgery of her arteriovenous femoral fistula was complicated by a *Pseudomonas aeruginosa* infection at the surgical site, which was treated by a femoral bypass graft and antimicrobial drugs. Postoperatively, a femoral graft thrombosis and perivascular collection developed and was treated by graft removal, and a 3-month voriconazole course was begun because of positive results for *S. apiospermum*

Figure 1. Abdominal computed tomography scan for case-patient 1 showing arteritis in study of unexpected vascular locations of *Scedosporium* spp. and *Lomentospora prolificans* fungal infections, France. Arrow indicates primitive left iliac artery thrombosis and perivascular soft tissue contrast. Data are from the Scedosporiosis/lomentosporiosis Observational Study (*12*).

from a superficial swab culture. Eight months later, new onset of fever and left limb pain led to discovery of 2 mycotic aneurysms in the left common femoral artery (Figure 3, panels A, B), multiple left thigh abscesses, and left navicular osteitis. The mycotic aneurysms were surgically removed, and vascular reconstruction by arterial allograft bypass was performed. *S. apiospermum* was identified in cultured perioperative samples; histologic analysis revealed vascular invasion, particularly in the tunica media (Figure 3, panels C, D). The patient was successfully treated with voriconazole and caspofungin for 18 months; PET/CT showed no signs of relapse 1 year after stopping antifungal therapy.

Case-patient 5 was a 44-year-old man who had chronic myeloid leukemia and underwent allogeneic hematopoietic stem cell transplant. While he was hospitalized for chronic graft versus host disease, a febrile gingival abscess developed and was treated by dental avulsion. Abscess and blood culture samples tested positive for *L. prolificans*; voriconazole and terbinafine treatments were initiated. Although fungemia persisted during treatment, he complained about abdominal pain; CT revealed abdominal aortitis spreading to the superior mesenteric and left renal arteries manifested by vascular thickenings and perivascular contrast (Figure 4, panels A, B). Within the following month, he had intense abdominal pain and died, likely from mesenteric ischemia.

Case-patient 6 was a 56-year-old man who had diabetes and a lung transplant because of idiopathic chronic pulmonary fibrosis. A thoracotomy scar abscess developed rapidly after his transplantation surgery and was treated by surgical abscess drainage. *S. apiospermum* was documented in a perioperative specimen; therefore, he was treated with voriconazole. Four months later, while still undergoing antifungal treatment, he complained about a nonfebrile thoracic pain; CT revealed a rapidly growing ascending thoracic aortic aneurysm (Figure 5, panels A, B). Surgical aneurysm resection and prosthetic aortic replacement were performed, and he was treated with posaconazole and caspofungin. His perioperative tissue samples confirmed vascular fungal invasion

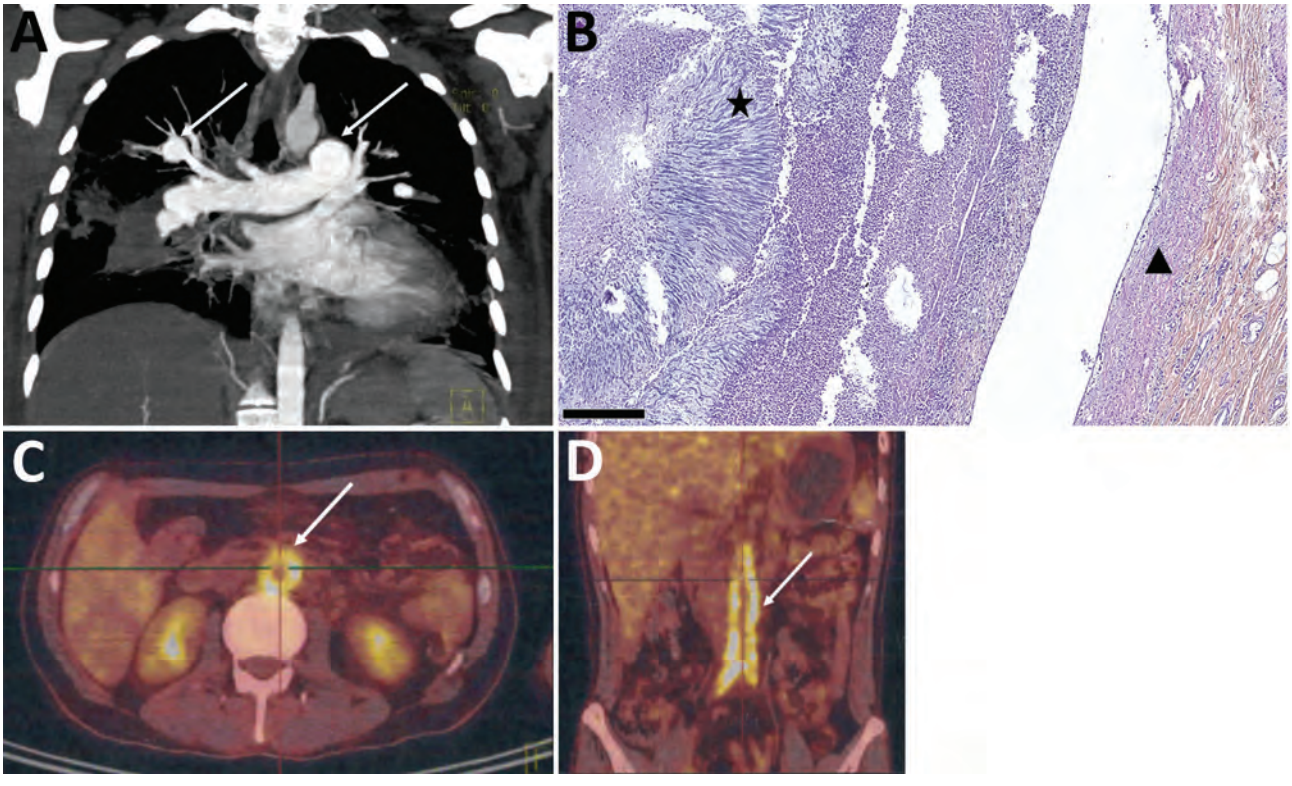

Figure 2. Imaging of pulmonary arteritis and abdominal aortitis for case-patients 2 and 3 in study of unexpected vascular locations of *Scedosporium* spp. and *Lomentospora prolificans* fungal infections, France. A) Thoracic computed tomography scan for case-patient 2. Arrows indicate left pulmonary artery and right lobar pulmonary artery mycotic aneurysms. B) Hematoxylin-eosin-saffron stain of lung tissue from postmortem analysis of case-patient 2. Triangle indicates bronchial artery wall; star indicates bronchial artery thrombus consisting of radially-disposed multiple septate hyphae. Scale bar indicates 250 μm. C, D) Positron emission tomography-computed tomography scans of case-patient 3. C) Arrow indicates intense abdominal aorta hypermetabolism. D) Arrow indicates abdominal aorta and primitive iliac artery hypermetabolisms. Data are from the Scedosporiosis/lomentosporiosis Observational Study (*12*).

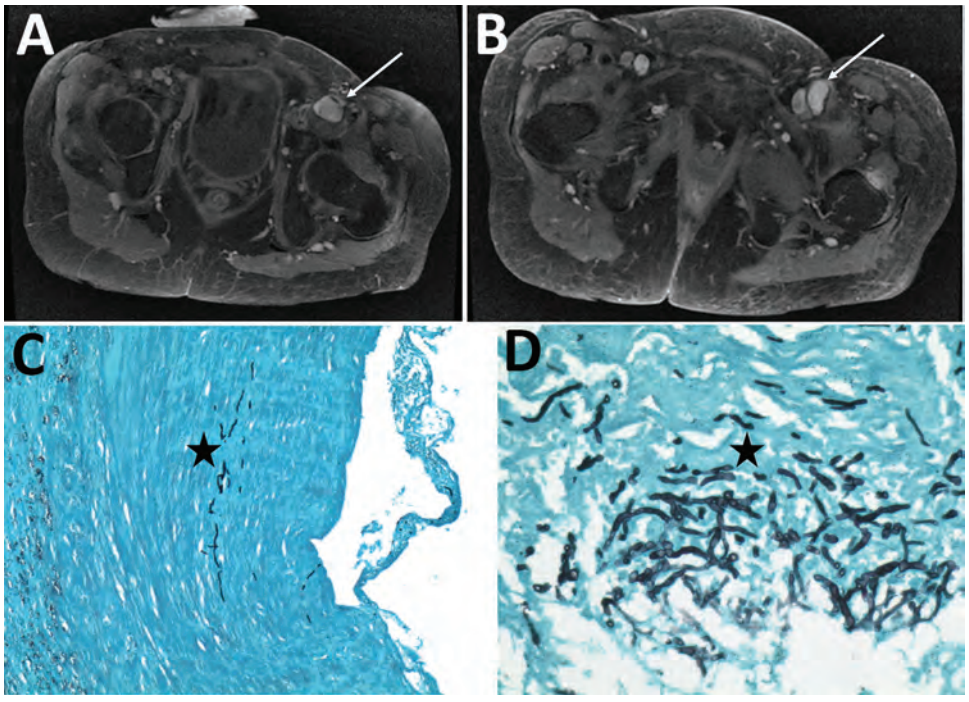

Figure 3. Radiologic and histopathologic analysis of arteritis in case-patient 4 in study of unexpected vascular locations of *Scedosporium* spp. and *Lomentospora prolificans* fungal infections, France. A, B) Pelvic magnetic resonance imaging with T1 gadolinium contrast showing femoral arteritis. A) Arrow shows aneurysms involving the left common femoral artery with posterior mural thrombus. B) Arrow shows left common femoral artery bifurcation. C, D) Grocott-Gomori methenamine silver stain of femoral artery section. C) Star indicates septate fungal hyphae invading the iliofemoral artery tunica media. Original magnification ×100. D) Star indicates septate fungal hyphae invading the iliofemoral artery tunica media. Original magnification ×400. Data are from the Scedosporiosis/lomentosporiosis Observational Study (*12*).

(Figure 5, panels C, D), and cultures tested positive for *S. apiospermum*. After an initial clinical improvement, he died 3 months later; *S. apiospermum* fungemia had developed along with endocarditis complicated by massive ischemic stroke and mycotic aneurysm of the aortic prosthesis anastomosis (Appendix Figure 1). At the time of his death, he also had mycotic intrahepatic and splenic aneurysms.

Case-patient 7 was a 43-year-old woman receiving first-line chemotherapy for acute myeloid leukemia. Four days after chemotherapy initiation, febrile nodular cutaneous lesions developed that persisted despite treatment with wide-spectrum antimicrobial drugs and intravenous liposomal amphotericin B. A blood culture tested positive for *L. prolificans*, and antifungal therapy was switched to voriconazole. She died a few hours later because of refractory sepsis and acute cardiac failure. Postmortem examination revealed massive multiorgan filamentous invasion within blood vessel walls and lumens, particularly in the abdominal aorta, and within the myocardium.

Cohort of SOS and Published Cases

We classified the 7 non-CNS vascular infection cases identified from the SOS as 1 aortitis, 2 peripheral arteritis, and 4 mixed aortitis and peripheral arteritis cases. We identified 26 articles from the published literature search as potential reports of non-CNS vascular scedosporiosis/lomentosporiosis (Appendix Figure 2). We excluded 13 reports, 1 about CNS mycotic aneurysms (n = 11), 1 about ventricular assist device thrombosis (n = 1), and 1 without available full text (n = 1). Thirteen case-reports from the literature search, including 9 aortitis and 4 peripheral arteritis cases, were eligible for analysis (*20*–*32*).

All 20 cases were proven IS (Appendix Table). Vascular infection was confirmed by either histology or vascular sample cultures in 15 cases. For the 5 remaining cases, vascular samples were not available. For those, diagnoses were made on the basis of radiologic imaging compatible with vascular infection and proven IS at another site. All mycologic documentations were obtained from cultures of normally sterile sites.

Host Factors/Underlying Diseases

All but 1 patient had ≥1 risk factor for IS (Table 1). The main underlying condition was solid organ transplant (10/20 [50%]), including lung (n = 5), kidney (n = 3), heart (n = 1), liver/kidney (n = 1) transplants, followed by hematologic malignancy (3/20 [15%]) and solid cancer (1/20 [5%]). IS occurred with a median delay of 165 (interquartile range 25.8–271.3) days after transplantation. Five (25%) cases were associated with trauma or near-drowning, 3 (15%) cases were

breakthrough infections, and 2 (10%) patients had prior *Scedosporium* spp. or *L. prolificans* colonization.

Mycologic and Clinical Manifestations

S. apiospermum complex species were identified in 12 (60%) cases, and *L. prolificans* was identified in 7 (35%) cases. Co-infection with *S. apiospermum* and *L. prolificans* occurred in 1 patient. Fungemia was reported in 8 (44%) cases, more frequently among *L. prolificans* infections (4/5 [80%]) than *S. apiospermum* complex infections (4/12 [33%]). Blood samples were not cultured for 2 patients with *L. prolificans* infection. Disseminated infections occurred in 15 (75%) cases, among which 13 had ≥2 noncontiguous infectious sites.

IS manifested as fever in 9/15 (60%) cases (Table 2). Patients with aortitis frequently (7/14 [50%]) had thoracic or abdominal pain. Vascular impairment was not observed at the time of IS diagnosis in 10/20 (50%) cases. However, impairment was frequently diagnosed months or years after completion of antifungal treatment for nonvascular scedosporiosis/lomentosporiosis (9/20 [45%]) but also while patients were still undergoing antifungal treatment (1/20 [5%]). The median delay between completion of antifungal treatment and diagnosis was 3 (interquartile range 1–13) months (4 years maximum). Moreover, vascular impairment was associated with ≥1 other localization in 18/20 (90%) cases, mostly in osteoarticular (10/20 [50%]) and pulmonary (9/20 [45%]) locations; 5/10 (50%) osteoarticular localizations were spondylodiscitis. Most (7/10 [70%]) osteoarticular localizations were contiguous with the vascular infection site, which included 3 of 5 spondylodiscitis (2 abdominal and 1 thoracic aortitis) and 4 of 5 peripheral osteoarticular localizations (1 femoral arteritis and hip arthritis, 1 iliac arteritis and sacroiliac arthritis, 1 sternal osteomyelitis and thoracic aortitis, and 1 subclavian arteritis and sternoclavicular arthritis).

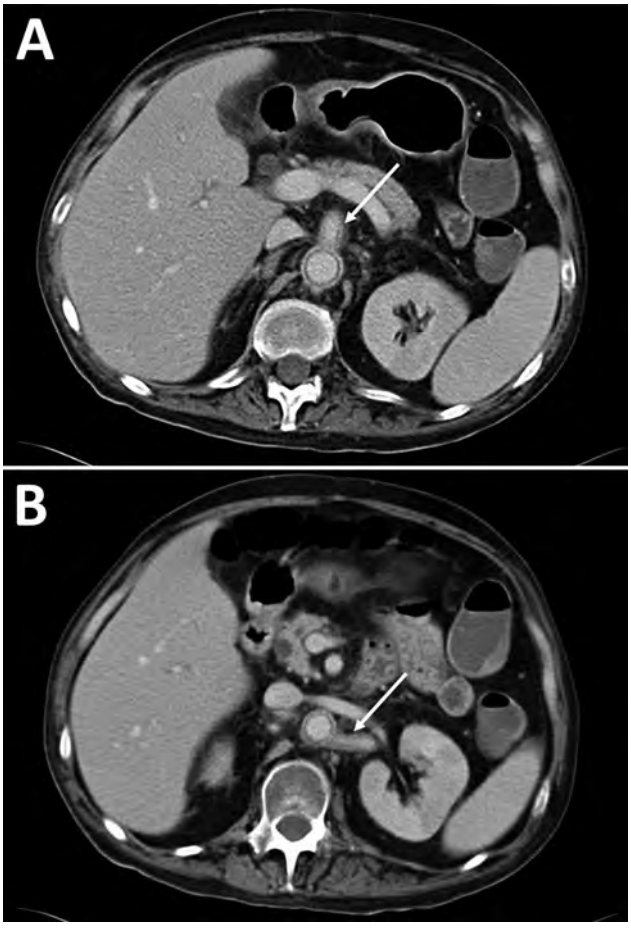

Figure 4. Abdominal computed tomography scans for case-patient 5 showing aortitis in study of unexpected vascular locations of *Scedosporium* spp. and *Lomentospora prolificans* fungal infections, France. A) Arrow indicates abdominal aorta and superior mesenteric artery thickening and perivascular contrast. B) Arrow indicates abdominal aorta and left renal artery thickening and perivascular contrast. Data are from the Scedosporiosis/lomentosporiosis Observational Study (*12*).

Vascular Impairment Type

Aortitis affected the abdominal aorta (8/13 [62%]) more frequently than the thoracic aorta (5/13 [39%]) (Table 2). The location of aortitis was not mentioned for 1 case. Aortitis was mostly identified by the presence of an aneurysmal lesion (8/11 [73%]). Indeed, aneurysmal lesions were noted for all thoracic aortitis and 3 of 6 abdominal aortitis cases. Abdominal aortitis with arterial wall thickening without aneurysms were described for SOS case-patients 1, 3, and 5. The type of imaging anomalies was unknown for 3 patients who had postmortem aortitis diagnoses.

Peripheral arteritis localizations were diverse, affecting the iliac or femoral arteries (4/10 [40%]) and other arteries, such as hepatic (n = 2), pulmonary (n = 1), subclavian (n = 1), renal and mesenteric (n = 1), or arteriovenous fistula (n = 1) arteries. Peripheral arteritis was mainly revealed by the presence of aneurysmal lesions (6/10 [60%]); septic thrombosis was described in 3 cases.

PET/CT consistently showed an elective hypermetabolism of the vascular wall in 3 aneurysmal aortitis, 2 nonaneurysmal aortitis, and 1 peripheral mycotic aneurysm cases. All positive PET/CT scans were associated with concordant CT or magnetic resonance imaging angiography. PET/CT follow-up was available for 3 of 6 patients, and a clear regression of hypermetabolism during IS treatment was reported in all 3 cases, including 1 normalization at the end of treatment.

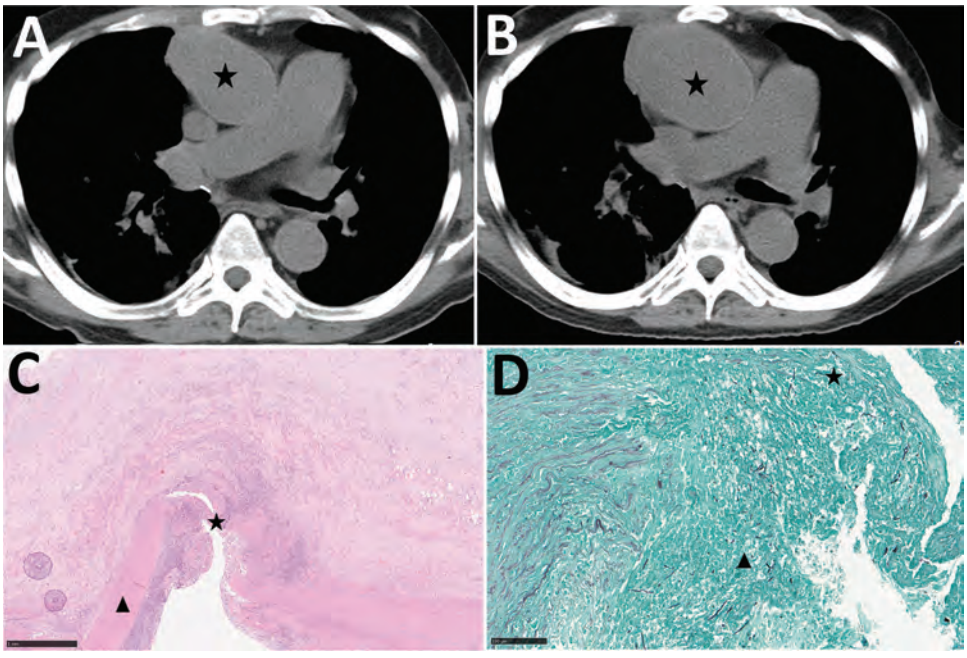

Figure 5. Radiologic and histopathologic analysis of thoracic aortitis in case-patient 6 in study of unexpected vascular locations of *Scedosporium* spp. and *Lomentospora prolificans* fungal infections, France. A) Thoracic computed tomography scan showing sacciform aneurysm of ascending aorta (star). B) Thoracic computed tomography scan 21 days later showing the rapidly growing aneurysm (star). C) Hematoxylin-eosin-saffron stain of thoracic aorta section. Star indicates thoracic aorta wall dissection. Triangle indicates tunica media. Scale bar indicates 1 mm. D) Grocott-Gomori methenamine silver stain of thoracic aorta section. Star indicates septate fungal hyphae invading the thoracic aorta tunica media. Triangle indicates thrombus containing septate fungal hyphae. Scale bar indicates 100 μm. Data are from the Scedosporiosis/lomentosporiosis Observational Study (*12*)

Histopathologic Lesions

Histopathologic analyses were available for 11/20 patients (8 perioperative vascular samples and 3 autopsies) and showed an invasion of the arterial wall by fungal septate hyphae in 10 of 11 samples. Arterial wall necrosis was reported in 6 cases and endoluminal thrombi caused by fungi were reported in 4 cases. Only 1 case showed an arterial granuloma lesion, and 2 cases had arterial wall abscesses. Although rarely specified, fungal invasion affected the tunica media (n = 3) or tunica adventitia (n = 3).

Treatment and Outcomes

After microbiologic identification, voriconazole was the first-line antifungal drug prescribed to all patients (Table 3). A combination of 2 antifungal drugs was frequently (10/16 [63%]) used, mostly voriconazole combined with terbinafine or caspofungin. Four patients did not receive antifungal treatment because the IS diagnosis was made postmortem. Radical surgery was performed in 8 (50%) of 16 patients with an antemortem IS diagnosis, which consisted of 3 biologic vascular reconstructions (2 arterial allografts and 1 arterial homograft), 3 prosthetic vascular reconstructions (Dacron grafts in all cases), and 2 cases without vascular reconstruction. Signs of infection relapse at the vascular sites were reported in the 3 prosthetic vascular reconstruction cases (pseudoaneurysm appearance or prosthetic graft thrombosis).

The IFD-related death rate was 67% (12/18) and 100% (7/7) when fungemia was present. Three IFD-related deaths were attributed to a direct complication of the vascular infection (mesenteric ischemia complicating abdominal aortitis in all cases), but the cause of death was missing for 4 patients. The death rate was higher (11/14 [79%]) for patients with aortitis (whether or not associated with peripheral arteritis) than isolated peripheral arteritis (1/4 [25%]). Patients treated with only antifungal drugs had a higher (7/9 [78%]) death rate than those who underwent radical surgery combined with antifungal drug therapy (2/6 [33%]).

Discussion

We describe non-CNS vascular infections caused by *Scedosporium* spp. and *L. prolificans*, highlighting an underreported localization of clinical significance that affects the management of such infections. Solid organ transplant was the main host risk factor; however, several cases occurred in immunocompetent patients, particularly those who had cutaneous trauma. Vascular invasion was almost always associated with other infectious localizations, such as contiguous osteoarticular localizations. The main radiologic manifestation of infection was a vascular aneurysm, which was observed in all thoracic aortitis and most peripheral arteritis cases. Isolated vascular wall thickening was frequently described for

abdominal aortitis and contiguous aortic branches, constituting overlap between abdominal aortitis and iliofemoral arteritis.

The SOS found that 24% of disseminated scedosporiosis/lomentosporiosis cases involved vascular infections (*5*–*11*,*13*–*17*). No non-CNS vascular infections were reported among 273 IS cases according to the Fungiscope registry (*5*), which gathers rare IFD data from countries around the world. Only 2 cases of mycotic aneurysms were reported among 80 scedosporiosis/lomentosporiosis cases in transplant patients, of which 40 were disseminated (*33*). One possible explanation for this underreporting might be that vascular impairment is rarely at the forefront of IS diagnostic considerations and might not be systematically tracked by imaging checkups or might be insufficiently reported in disseminated cases. All cases from published literature were reported since 2000, which could be partly explained by recent improvements in imaging access. In addition, vascular impairment was diagnosed in many (45%) cases after patients completed antifungal treatment for another IS localization, suggesting that undiagnosed vascular infections might lead to relapse because of insufficient treatment. We found that 50% of IS cases were associated with osteoarticular localization, whereas that localization was usually described in only 18%–26% IS and 14%–17% of disseminated scedosporiosis/lomentosporiosis cases (*5*,*12*,*17*). This finding suggests a potential association between vascular and osteoarticular localizations, especially because most of those were contiguous. In particular, we highlighted a frequent association of peripheral arteritis with aortitis resulting from spondylodiscitis and peripheral osteoarthritis. Finally, we reported high death rates, consistent with previous estimations for overall IS (*5*,*7*).

We focused on non-CNS vascular infections because cerebral mycotic aneurysms caused by *Scedosporium* spp. have already been specifically addressed for near-drowning situations (*34*). The ability of molds to invade vessels is well known; angioinvasion is a key pathogenic characteristic of invasive aspergillosis and mucormycosis. Several reports have described cerebral and pulmonary mycotic aneurysms located contiguously or distant to invasive aspergillosis or mucormycosis (*35*–*39*). However, few studies have reported thoracic aortitis caused by *Aspergillus* spp., which are frequently associated with endocarditis (*40*–*42*).

The strength of this work is that it confirms arterial wall invasion by *Scedosporium* or *Lomentospora* hyphae; histopathologic analyses were available for most cases. Nevertheless, IFD reporting is voluntary in France, and the National Reference Center might not have gathered data for all IFD cases in France during the study period. Moreover, we

Table 1. General patient characteristics in study of unexpected vascular locations of *Scedosporium* spp. and *Lomentospora prolificans* fungal infections, France*

Variables	SOS, n = 7	Literature, n = 13	Total, n = 20
Type of vascular infection			
Aortitis	5 (71)	9 (69)	14 (70)
Peripheral arteritis	6 (86)	4 (31)	10 (50)
Age, y (IQR)	44.0 (37.1–51.5)	55.0 (44.0–64.0)	52.5 (42.0–57.4)
Sex			
M	4 (57)	6 (46)	10 (50)
F	3 (43)	7 (54)	10 (50)
Main underlying disease/condition			
Malignancy	2 (29)	2 (15)	4 (20)
Including hemopathy	2 (29)	1 (8)	3 (15)
Including solid neoplasia	0	1 (8)	1 (5)
Solid organ transplant	3 (43)	7 (54)	10 (50)
Trauma	2 (29)	2 (15)	4 (20)
Near drowning	0	1 (8)	1 (5)
No risk factor	0	1 (8)	1 (5)
Neutropenia	1 (14)	1 (8)	2 (10)
Prior colonization	0	2 (15)	2 (10)
Breakthrough infections	1 (14)	2 (15)	3 (15)
Fungus identification			
S. apiospermum	4 (57)	8 (62)	12 (60)
L. prolificans	2 (29)	5 (39)	7 (35)
S. apiospermum and *L. prolificans*	1 (14)	0	1 (5)
Disseminated infection	7 (100)	8 (62)	15 (75)
Fungemia†	4/7 (57)	4/11 (36)	8/18 (44)

*Values are no. (%) except as indicated. Patients had non–central nervous system vascular infections caused by *Scedosporium* spp. or *Lomentospora prolificans*; cases were obtained from the SOS and from published literature. IQR, interquartile range; SOS, Scedosporiosis/lomentosporiosis Observational Study.
†Blood culture data were not available from published literature for 2 patients. Denominators indicate the total number of patients evaluated.

Table 2. Clinical and radiologic characteristics of patients in study of unexpected vascular locations of *Scedosporium* spp. and *Lomentospora prolificans* fungal infections, France*

Variables	SOS, n = 7	Literature, n = 13	Total, n = 20
Clinical manifestations at diagnosis			
Fever	6/7 (86)	3/8 (38)	9/15 (60)
Sepsis	1/7 (14)	2/13 (15)	3/20 (15)
Thoracic or abdominal pain among aortitis	2/5 (40)	5/9 (56)	7/14 (50)
Local inflammatory sign among peripheral arteritis	0	2/4 (50)	2/10 (20)
Vascular involvement at scedosporiosis/lomentosporiosis diagnosis	5/7 (71)	5/13 (39)	10/20 (50)
Other infection locations			
Pulmonary	4/7 (57)	5/13 (39)	9/20 (45)
Central nervous system	2/7 (29)	3/13 (23)	5/20 (25)
Cutaneous	2/7 (29)	2/13 (15)	4/20 (20)
Osteoarticular	3/7 (43)	7/13 (54)	10/20 (50)
Including spondylodiscitis	1/3 (33)	4/7 (57)	5/10 (50)
Including contiguous localizations	1/3 (33)	6/7 (86)	7/10 (70)
Endocarditis	2/7 (29)	2/13 (15)	4/20 (20)
Localization of vascular infection			
Aortitis	5/7 (71)	9/13 (69)	14/20 (70)
Including thoracic aortitis	1/5 (20)	4/8 (50)	5/13 (39)
Including abdominal aortitis	4/5 (80)	4/8 (50)	8/13 (62)
Peripheral arteritis	6/7 (86)	4/13 (31)	10/20 (50)
Including iliac or femoral arteritis	3/6 (50)	1/4 (25)	4/10 (40)
Type of aortitis vascular impairment			
Aneurysm	1/4 (25)	7/7 (100)	8/11 (73)
With rupture	1/1 (100)	2/7 (29)	3/8 (38)
Perivascular abscess	1/4 (25)	0	1/11 (9)
Isolated vascular thickening	2/4 (50)	0	2/11 (18)
Type of peripheral arteritis vascular impairment			
Aneurysm	3/6 (50)	3/4 (75)	6/10 (60)
With rupture	0	1/3 (33)	1/6 (17)
Perivascular abscess	1/6 (17)	0	1/10 (10)
Septic thrombosis	2/6 (33)	1/4 (25)	3/10 (30)
Isolated vascular thickening	1/6 (17)	0	1/10 (10)
Vascular hypermetabolism on PET/CT	3/3 (100)	3/3 (100)	6/6 (100)

*Values are no./total no. analyzed (%). Denominators are different in some cases because of missing data. Patients had non–central nervous system vascular infections caused by *Scedosporium* spp. or *Lomentospora prolificans*; cases were obtained from the SOS and published literature. PET/CT, positron emission tomography/computed tomography; SOS, Scedosporiosis/lomentosporiosis Observational Study.

could not provide microbiologic identification at the species level for *S. apiospermum* complex species because genotypic analysis was conducted in only 4 of 13 cases reported in published literature, and several diagnoses were made before the last taxonomy classification update. We could not analyze the median duration of antifungal therapy because all but 3 patients were still undergoing treatment at last contact. Also, anticoagulant and antiplatelet drug management could not be assessed because of missing

Table 3. Patient treatment and outcomes in study of unexpected vascular locations of *Scedosporium* spp. and *Lomentospora prolificans* fungal infections, France*

Variables	SOS, n = 7	Literature, n = 13	Total, n = 20
Radical surgery	2/7 (29)	6/13 (46)	8/20 (40)
First-line antifungal treatment after microbiologic identification			
Monotherapy	1/7 (14)	3/9 (33)	4/16 (25)
Combination therapy	5/7 (71)	5/9 (56)	10/16 (63)
Multitherapy, ≥3 antifungal agents	1/7 (14)	1/9 (11)	2/16 (13)
Voriconazole	7/7 (100)	9/9 (100)	16/16 (100)
Terbinafine	2/7 (29)	6/9 (67)	8/16 (50)
Caspofungin	5/7 (71)	1/9 (11)	6/16 (38)
Overall IFD-related deaths	5/7 (71)	7/11 (64)	12/18 (67)
Among patients with fungemia	4/4 (100)	3/3 (100)	7/7 (100)
Among patients with aortitis whether or not associated with arteritis	4/5 (80)	7/9 (78)	11/14 (79)
Among patients with arteritis only	1/2 (50)	0/2 (0)	1/4 (25)
Among patients treated with radical surgery and antifungal	1/2 (50)	1/4 (25)	2/6 (33)
Among patients treated with antifungal only	4/5 (80)	3/4 (75)	7/9 (78)
1-month IFD-related deaths	2/7 (29)	5/11 (46)	7/18 (39)

*Values are no./total no. analyzed (%). Denominators are different in some cases because of missing data. Patients had non–central nervous system vascular infections caused by *Scedosporium* spp. or *Lomentospora prolificans*; cases were obtained from the SOS and published literature. IFD, invasive fungal disease; SOS, Scedosporiosis/lomentosporiosis Observational Study.

data. We were unable to evaluate the effects of vascular impairment on scedosporiosis/lomentosporiosis prognosis because assessing the exact circumstances of death was difficult in many cases; however, ≥3 of the 12 IFD-related deaths seemed to be related to a vascular complication. Finally, we observed that patients who underwent radical surgery seemed to have better prognoses. However, the retrospective study design, small number of cases, and patient population heterogeneity do not permit assessment of the best curative treatment, leading us to interpret the results for radical surgery with caution.

In conclusion, arterial wall infection is observed in 24% of patients with disseminated *Scedosporium*/*Lomentospora* infections and is mainly responsible for arterial aneurysms either by contiguous contamination or systemic dissemination. Our case series and literature review suggest that *Scedosporium* spp. and *L. prolificans* arterial infections might be latent for months after IS diagnosis and treatment, and ad hoc vascular imaging is justified in cases of osteoarticular localization or dissemination. Systematic screening for vascular involvement of *Scedosporium*/*Lomentospora* infections, including aortitis and peripheral arteritis, is needed to improve therapeutic strategies and prognosis.

About the Author

Dr. Vignals is an infectious diseases doctor in the Department of Infectious and Tropical Diseases, Bordeaux University Hospital in France. Her research interests focus on infections occurring in immunocompromised hosts, especially fungal infections, and epidemiology.

References

1. Ramirez-Garcia A, Pellon A, Rementeria A, Buldain I, Barreto-Bergter E, Rollin-Pinheiro R, et al. *Scedosporium* and *Lomentospora*: an updated overview of underrated opportunists. Med Mycol. 2018;56:102–25. https://doi.org/10.1093/mmy/myx113
2. Miceli MH, Lee SA. Emerging moulds: epidemiological trends and antifungal resistance. Mycoses. 2011;54:e666–78. https://doi.org/10.1111/j.1439-0507.2011.02032.x
3. Lackner M, de Hoog GS, Yang L, Ferreira Moreno L, Ahmed SA, Andreas F, et al. Proposed nomenclature for *Pseudallescheria*, *Scedosporium* and related genera. Fungal Divers. 2014;67:1–10. https://doi.org/10.1007/s13225-014-0295-4
4. Blez D, Bronnimann D, Rammaert B, Zeller V, Delhaes L, Hustache L, et al. Invasive bone and joint infections from the French Scedosporiosis/lomentosporiosis Observational Study (SOS) cohort: no mortality with long-term antifungal treatment and surgery. Med Mycol. 2023;61:myad023. https://doi.org/10.1093/mmy/myad023
5. Seidel D, Meißner A, Lackner M, Piepenbrock E, Salmanton-García J, Stecher M, et al. Prognostic factors in 264 adults with invasive *Scedosporium* spp. and *Lomentospora prolificans* infection reported in the literature and FungiScope®.Crit Rev Microbiol. 2019;45:1–21. https://doi.org/10.1080/1040841X.2018.1514366
6. Jenks JD, Seidel D, Cornely OA, Chen S, van Hal S, Kauffman C, et al. Clinical characteristics and outcomes of invasive *Lomentospora prolificans* infections: analysis of patients in the FungiScope® registry. Mycoses. 2020;63:437–42. https://doi.org/10.1111/myc.13067
7. Álvarez-Uría A, Guinea JV, Escribano P, Gómez-Castellá J, Valerio M, Galar A, et al. Invasive *Scedosporium* and *Lomentosora* infections in the era of antifungal prophylaxis: a 20-year experience from a single centre in Spain. Mycoses. 2020;63:1195–202. https://doi.org/10.1111/myc.13154
8. Lamaris GA, Chamilos G, Lewis RE, Safdar A, Raad II, Kontoyiannis DP. *Scedosporium* infection in a tertiary care cancer center: a review of 25 cases from 1989–2006. Clin Infect Dis. 2006;43:1580–4. https://doi.org/10.1086/509579
9. Troke P, Aguirrebengoa K, Arteaga C, Ellis D, Heath CH, Lutsar I, et al.; Global Scedosporium Study Group. Treatment of scedosporiosis with voriconazole: clinical experience with 107 patients. Antimicrob Agents Chemother. 2008;52:1743–50. https://doi.org/10.1128/AAC.01388-07
10. Idigoras P, Pérez-Trallero E, Piñeiro L, Larruskain J, López-Lopategui MC, Rodríguez N, et al. Disseminated infection and colonization by *Scedosporium prolificans*: a review of 18 cases, 1990–1999. Clin Infect Dis. 2001;32:E158–65. https://doi.org/10.1086/320521
11. Heath CH, Slavin MA, Sorrell TC, Handke R, Harun A, Phillips M, et al.; Australian Scedosporium Study Group. Population-based surveillance for scedosporiosis in Australia: epidemiology, disease manifestations and emergence of *Scedosporium aurantiacum* infection. Clin Microbiol Infect. 2009;15:689–93. https://doi.org/10.1111/j.1469-0691.2009.02802.x
12. Bronnimann D, Garcia-Hermoso D, Dromer F, Lanternier F; French Mycoses Study Group; Characterization of the isolates at the NRCMA. Scedosporiosis/lomentosporiosis Observational Study (SOS): clinical significance of *Scedosporium* species identification. Med Mycol. 2021;59:486–97. https://doi.org/10.1093/mmy/myaa086
13. Berenguer J, Rodríguez-Tudela JL, Richard C, Alvarez M, Sanz MA, Gaztelurrutia L, et al.; Scedosporium prolificans Spanish Study Group. Deep infections caused by *Scedosporium prolificans*. A report on 16 cases in Spain and a review of the literature. Medicine (Baltimore). 1997;76:256–65. https://doi.org/10.1097/00005792-199707000-00004
14. Tintelnot K, Just-Nübling G, Horré R, Graf B, Sobottka I, Seibold M, et al. A review of German *Scedosporium prolificans* cases from 1993 to 2007. Med Mycol. 2009;47:351–8. https://doi.org/10.1080/13693780802627440
15. Seidel D, Hassler A, Salmanton-García J, Koehler P, Mellinghoff SC, Carlesse F, et al. Invasive *Scedosporium* spp. and *Lomentospora prolificans* infections in pediatric patients: analysis of 55 cases from FungiScope® and the literature. Int J Infect Dis. 2020;92:114–22. https://doi.org/10.1016/j.ijid.2019.12.017
16. Johnson LS, Shields RK, Clancy CJ. Epidemiology, clinical manifestations, and outcomes of *Scedosporium* infections among solid organ transplant recipients. Transpl Infect Dis. 2014;16:578–87. https://doi.org/10.1111/tid.12244
17. Rodriguez-Tudela JL, Berenguer J, Guarro J, Kantarcioglu AS, Horre R, de Hoog GS, et al. Epidemiology and outcome of *Scedosporium prolificans* infection, a review of 162 cases. Med Mycol. 2009;47:359–70. https://doi.org/10.1080/13693780802524506

18. Carrer M, Vignals C, Berard X, Caradu C, Battut AS, Stenson K, et al. Retrospective multicentric study comparing infectious and noninfectious aortitis. Clin Infect Dis. 2023;76:e1369–78. https://doi.org/10.1093/cid/ciac560
19. Donnelly JP, Chen SC, Kauffman CA, Steinbach WJ, Baddley JW, Verweij PE, et al. Revision and update of the consensus definitions of invasive fungal disease from the European Organization for Research and Treatment of Cancer and the Mycoses Study Group Education and Research Consortium. Clin Infect Dis. 2020;71:1367–76. https://doi.org/10.1093/cid/ciz1008
20. Ong A, Blyth CC, Bency R, Vicaretti M, Harun A, Meyer W, et al. Fatal mycotic aneurysms due to *Scedosporium* and *Pseudallescheria* infection. J Clin Microbiol. 2011;49:2067–71. https://doi.org/10.1128/JCM.02615-10
21. Howden BP, Slavin MA, Schwarer AP, Mijch AM. Successful control of disseminated *Scedosporium prolificans* infection with a combination of voriconazole and terbinafine. Eur J Clin Microbiol Infect Dis. 2003;22:111–3. https://doi.org/10.1007/s10096-002-0877-z
22. Ortmann C, Wüllenweber J, Brinkmann B, Fracasso T. Fatal mycotic aneurysm caused by *Pseudallescheria boydii* after near drowning. Int J Legal Med. 2010;124:243–7. https://doi.org/10.1007/s00414-009-0336-9
23. Malinowski MJ, Halandras P. Arterial reconstruction for atypical mycotic aneurysms. Vasc Endovascular Surg. 2013;47:45–7. https://doi.org/10.1177/1538574412462636
24. Centellas Pérez FJ, Martínez Antolinos C, Piqueras Sánchez S, Lorenzo González I, Llamas Fuentes F, Gómez Roldán C. *Scedosporium apiospermum* infection in a kidney transplant recipient [in Spanish]. Rev Iberoam Micol. 2019;36:48–50. https://doi.org/10.1016/j.riam.2018.10.005
25. Klinken EM, Stevenson BR, Kwok CHR, Hockley JA, Lucas M. Diffuse inflammatory aneurysmal aortitis secondary to *Scedosporium apiospermum* complex in an immunocompetent individual. Pathology. 2019;51:316–8. https://doi.org/10.1016/j.pathol.2018.10.021
26. Blasco-Lucas A, Reyes-Juárez JL, Nazarena Pizzi M, Permanyer E, Evangelista A, Galiñanes M. Aortic arch mycotic aneurysm due to *Scedosporium apiospermum* reconstructed with homografts. Ann Thorac Surg. 2015; 99:2218–20. https://doi.org/10.1016/j.athoracsur.2014.08.067
27. Thomson S, Alibhai K, Winkelaar G, Lien D, Halloran K, Kapasi A, et al. Case report of vertebral osteomyelitis and mycotic abdominal aortic aneurysm caused by *Scedosporium apiospermum* in a lung transplant patient with cystic fibrosis. Transplant Proc. 2015;47:204–9. https://doi.org/10.1016/j.transproceed.2014.07.072
28. Sayah DM, Schwartz BS, Kukreja J, Singer JP, Golden JA, Leard LE. *Scedosporium prolificans* pericarditis and mycotic aortic aneurysm in a lung transplant recipient receiving voriconazole prophylaxis. Transpl Infect Dis. 2013;15:E70–4. https://doi.org/10.1111/tid.12056
29. Wakabayashi Y, Okugawa S, Tatsuno K, Ikeda M, Misawa Y, Koyano S, et al. *Scedosporium prolificans* endocarditis: case report and literature review. Intern Med. 2016;55:79–82. https://doi.org/10.2169/internalmedicine. 55.5592
30. Valerio M, Vásquez V, Álvarez-Uria A, Zatarain-Nicolás E, Pavone P, Martínez-Jiménez MDC, et al. Disseminated lomentosporiosis in a heart transplant recipient: case report and review of the literature. Transpl Infect Dis. 2021;23:e13574. https://doi.org/10.1111/tid.13574
31. Holmes NE, Trevillyan JM, Kidd SE, Leong TYM. Locally extensive angio-invasive *Scedosporium prolificans* infection following resection for squamous cell lung carcinoma. Med Mycol Case Rep. 2013;2:98–102. https://doi.org/10.1016/j.mmcr.2013.04.001
32. Campa-Thompson MM, West JA, Guileyardo JM, Spak CW, Sloan LM, Beal SG. Clinical and morphologic findings in disseminated *Scedosporium apiospermum* infections in immunocompromised patients. Proc (Bayl Univ Med Cent). 2014;27:253–6. https://doi.org/10.1080/08998280.2014.11929129
33. Husain S, Muñoz P, Forrest G, Alexander BD, Somani J, Brennan K, et al. Infections due to *Scedosporium apiospermum* and *Scedosporium prolificans* in transplant recipients: clinical characteristics and impact of antifungal agent therapy on outcome. Clin Infect Dis. 2005;40:89–99. https://doi.org/10.1086/426445
34. Katragkou A, Dotis J, Kotsiou M, Tamiolaki M, Roilides E. *Scedosporium apiospermum* infection after near-drowning. Mycoses. 2007;50:412–21. https://doi.org/10.1111/j.1439-0507.2007.01388.x
35. Hurst RW, Judkins A, Bolger W, Chu A, Loevner LA. Mycotic aneurysm and cerebral infarction resulting from fungal sinusitis: imaging and pathologic correlation. AJNR Am J Neuroradiol. 2001;22:858–63.
36. Kasliwal MK, Reddy VSK, Sinha S, Sharma BS, Das P, Suri V. Bilateral anterior cerebral artery aneurysm due to mucormycosis. J Clin Neurosci. 2009;16:156–9. https://doi.org/10.1016/j.jocn.2008.04.019
37. Sundaram C, Goel D, Uppin SG, Seethajayalakshmi S, Borgohain R. Intracranial mycotic aneurysm due to *Aspergillus* species. J Clin Neurosci. 2007;14:882–6. https://doi.org/10.1016/j.jocn.2006.05.014
38. Coffey MJ, Fantone J 3rd, Stirling MC, Lynch JP 3rd. Pseudoaneurysm of pulmonary artery in mucormycosis. Radiographic characteristics and management. Am Rev Respir Dis. 1992;145:1487–90. https://doi.org/10.1164/ajrccm/145.6.1487
39. Lopez-Pastorini A, Koryllos A, Brockmann M, Windisch W, Stoelben E. Pseudoaneurysm of the pulmonary artery with massive haemoptysis due to an invasive pulmonary mucormycosis. Thorax. 2016;71:199–200. https://doi.org/10.1136/thoraxjnl-2015-207713
40. Silva ME, Malogolowkin MH, Hall TR, Sadeghi AM, Krogstad P. Mycotic aneurysm of the thoracic aorta due to *Aspergillus terreus*: case report and review. Clin Infect Dis. 2000;31:1144–8. https://doi.org/10.1086/317467
41. Rose HD, Stuart JL. Mycotic aneurysm of the thoracic aorta caused by A*spergillus fumigatus*. Chest. 1976;70:81–4. https://doi.org/10.1378/chest.70.1.81
42. Sanchez-Recalde A, Maté I, Merino JL, Simon RS, Sobrino JA. Aspergillus aortitis after cardiac surgery. J Am Coll Cardiol. 2003;41:152–6. https://doi.org/10.1016/s0735-1097(02)02606-2

Address for correspondence: Carole Vignals, service de maladies infectieuses et tropicales, Hôpital Pellegrin, Place Amélie Raba Léon, 33000 Bordeaux, France; email: carole.vignals@chu-bordeaux.fr

Severe Human Parainfluenza Virus Community- and Healthcare-Acquired Pneumonia in Adults at Tertiary Hospital, Seoul, South Korea, 2010–2019

Joung Ha Park,[1] Sang-Bum Hong,[1] Jin Won Huh, Jiwon Jung, Min Jae Kim, Yong Pil Chong, Heungsup Sung, Kyung Hyun Do, Sung-Han Kim, Sang-Oh Lee, Yang Soo Kim, Chae-Man Lim, Younsuck Koh, Sang-Ho Choi

The characteristics of severe human parainfluenza virus (HPIV)–associated pneumonia in adults have not been well evaluated. We investigated epidemiologic and clinical characteristics of 143 patients with severe HPIV-associated pneumonia during 2010–2019. HPIV was the most common cause (25.2%) of severe virus-associated hospital-acquired pneumonia and the third most common cause (15.7%) of severe virus-associated community-acquired pneumonia. Hematologic malignancy (35.0%), diabetes mellitus (23.8%), and structural lung disease (21.0%) were common underlying conditions. Co-infections occurred in 54.5% of patients admitted to an intensive care unit. The 90-day mortality rate for HPIV-associated pneumonia was comparable to that for severe influenza virus–associated pneumonia (55.2% vs. 48.4%; p = 0.22). Ribavirin treatment was not associated with lower mortality rates. Fungal co-infections were associated with 82.4% of deaths. Clinicians should consider the possibility of pathogenic co-infections in patients with HPIV-associated pneumonia. Contact precautions and environmental cleaning are crucial to prevent HPIV transmission in hospital settings.

Human parainfluenza virus (HPIV) is a major cause of acute respiratory tract infections, such as croup in children and pneumonia in immunocompromised patients (*1*). HPIV is a single-stranded, enveloped RNA virus in the Paramyxoviridae family (*2*) and is classified into 4 major serotypes, HPIV-1–4, according to complement fixation and hemagglutinating antigens (*3*). HPIV-1 and HPIV-3 belong to the genus *Respirovirus*, whereas HPIV-2 and HPIV-4 belong to the genus *Rubulavirus*. HPIV-3 is the most common serotype associated with pneumonia and bronchiolitis, and HPIV-1 and HPIV-2 are usually associated with croup in children (*2*).

HPIV infections are generally mild and self-limiting in adults (*4*); however, HPIV-associated pneumonia has been increasingly reported (*5*). HPIV accounts for 2.0%–7.6% of pathogens causing community-acquired pneumonia (CAP) (*6*–*8*) and 3.4%–6.1% of pathogens causing hospital-acquired pneumonia (HAP) (*9*,*10*). Data on the epidemiologic and clinical characteristics of severe HPIV-associated pneumonia in adults are limited. Although a retrospective study described the clinical characteristics of hospitalized adults with HPIV infections, the primary analysis did not focus on patients requiring admission into the intensive care unit (ICU) (*1*). We investigated the epidemiologic and clinical characteristics and outcomes of a large cohort of critically ill adults in South Korea who had severe HPIV-associated pneumonia requiring ICU care during a 10-year period.

Methods

Ethics

This study was approved by the Institutional Review Board of Asan Medical Center, Seoul, South Korea (approval no. 2010–0079). Informed consent was waived because of the observational nature of the study.

Author affiliations: Chung-Ang University Gwangmyeong Hospital, Gwangmyeong, South Korea (J.H. Park); University of Ulsan College of Medicine Asan Medical Center, Seoul, South Korea (S.-B. Hong, J.W. Huh, J. Jung, M.J. Kim, Y.P. Chong, H. Sung, K.H. Do, S.-H. Kim, S-.O. Lee, Y.S. Kim, C.-M. Lim, Y. Koh, S.-H. Choi)

DOI: https://doi.org/10.3201/eid3006.230670

[1]These authors contributed equally to this article.

Study Design

The study was performed as a part of a prospective, observational cohort study of patients with severe virus-associated pneumonia housed within the 28-bed ICU at Asan Medical Center, a 2,700-bed hospital in Seoul (*6*,*9*,*11*). All 3,099 adult patients included in the study were ≥16 years of age and admitted to the ICU with severe pneumonia during January 2010–December 2019; they were prospectively enrolled in the study cohort and monitored until discharge or death. We analyzed clinical data from the patients' electronic medical records, including demographic characteristics, underlying diseases or conditions, clinical manifestations, co-infecting pathogens, and outcomes. To describe clinical outcomes, we compared HPIV-associated pneumonia outcomes with those of severe influenza virus–associated pneumonia. We evaluated outcomes according to the length of hospital stay, duration within the ICU, complications from ventilator-associated pneumonia, and number of deaths.

We performed microbiologic evaluations as previously described (*6*). We identified respiratory viruses from nasopharyngeal swab samples, nasopharyngeal aspirates, bronchial washings, and bronchoalveolar lavage (BAL) fluids by using multiplex reverse transcription PCR (RT-PCR); we used the Anyplex II RV16 Detection Kit during 2010–2017, and the Allplex Respiratory Panel during 2018–2019 (both Seegene Inc., https://www.seegene.com). We tested samples for influenza virus A and B, respiratory syncytial virus A and B, adenovirus, human metapneumovirus, HPIV serotypes 1–4, enterovirus, rhinovirus, and human coronaviruses 229E/NL63, OC43, and HKU1.

Definitions

We defined pneumonia as a case that had new pulmonary infiltrations observed on a chest radiograph and ≥2 of the following symptoms: fever, cough, productive sputum, dyspnea, or prescription of antimicrobial drugs for pneumonia by the attending physician. We defined severe pneumonia as a case requiring invasive mechanical ventilation because of respiratory failure or septic shock requiring vasopressors (*12*). We defined HAP as a case occurring >48 hours after hospital admission (*13*) and HPIV-associated HAP as a case for which a respiratory virus RT-PCR was performed >48 hours after hospital admission and positive HPIV results were obtained. We defined the remaining cases as CAP. We designated immunocompromised patients as those who had undergone solid organ transplants, bone marrow transplants, or cytotoxic chemotherapy within 6 months or those who had received immunosuppressants, including corticosteroids, within 1 month before admission to the ICU. We also defined co-pathogens as pathogenic organisms identified within 3 working days of a severe HPIV-associated pneumonia diagnosis.

Statistical Analyses

We compared categorical variables by using the χ^2 or Fisher exact test and continuous variables by using the Student *t*-test or Mann-Whitney U test, as appropriate. We expressed continuous data as median values and interquartile ranges. We investigated risk factors for 90-day mortality by using univariate and multivariate logistic regression models. We based the final multivariate model on the univariate analysis and clinical relevance of potential risk factors. We included variables with a p value of ≤0.20 in the final multivariate model. All significance tests were 2-tailed, and we considered $p<0.05$ statistically significant. We performed all analyses by using SPSS Statistics 23 (IBM, https://www.ibm.com).

Results

Epidemiology of Severe HPIV-Associated Pneumonia

A total of 2,479 patients with severe pneumonia underwent multiplex RT-PCR testing of their respiratory samples to detect virus infections; pathogenic viruses were identified in 760 patients. Influenza virus was the most common pathogenic virus identified in patients with severe pneumonia; influenza virus was found in 189 (7.6%) patients, followed by rhinovirus in 181 (7.3%) and HPIV in 143 (5.8%) patients. The co-infection rates were 48.7% for influenza virus, 56.9% for rhinovirus, and 54.5% for HPIV among patients with severe virus-associated pneumonia. For severe virus-associated CAP, HPIV was the third most common virus (15.7%), after influenza virus (26.1%) and rhinovirus (25.7%). In contrast, for severe virus-associated HAP, HPIV was the most common virus at 25.2% (Figure 1).

Among the 143 patients with severe HPIV-associated pneumonia, 42 underwent bronchoscopic BAL for etiologic diagnosis. Of those patients, 35 had positive HPIV RT-PCR results from BAL samples, whereas 24 showed positive results from both BAL and nasopharyngeal swab samples. Among the 143 patients, HPIV-3 was the most common serotype (65.7%), followed by HPIV-1 (16.1%), HPIV-4 (14.7%), and HPIV-2 (3.5%). The prevalence of HPIV-1, HPIV-2, and HPIV-4 was higher in the CAP group than in

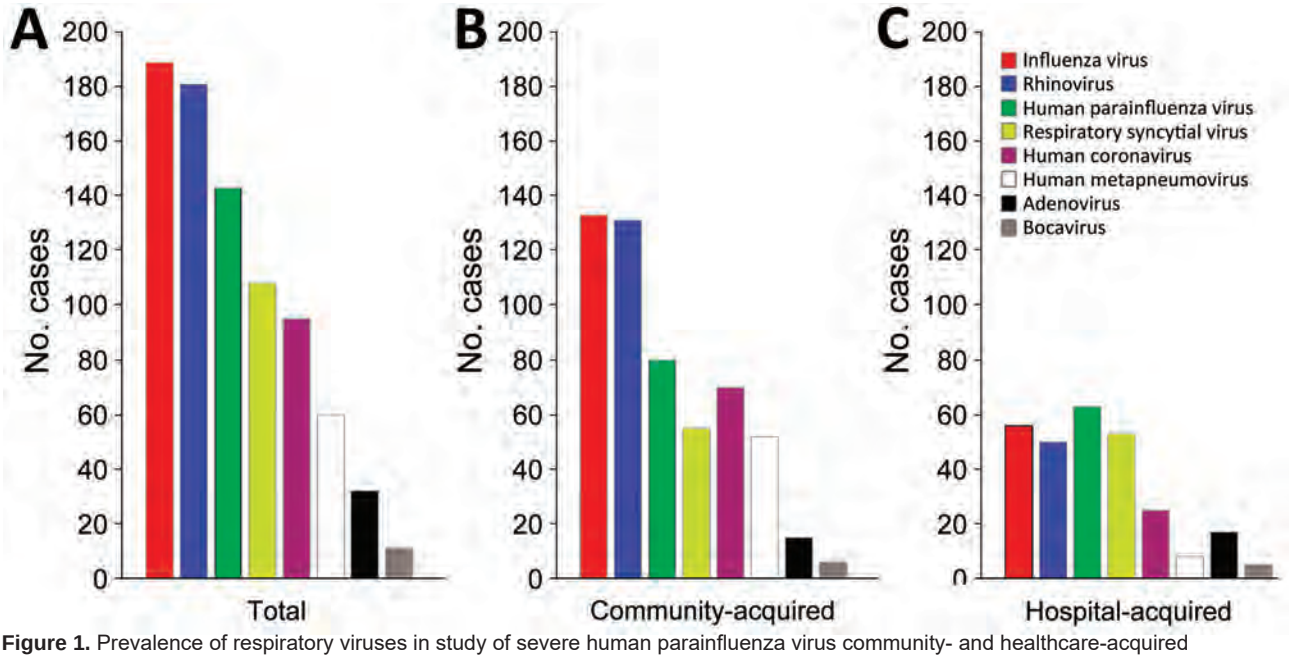

Figure 1. Prevalence of respiratory viruses in study of severe human parainfluenza virus community- and healthcare-acquired pneumonia in adults at a tertiary hospital in Seoul, South Korea, 2010–2019. Number of cases of different respiratory virus infections are given for 760 patients with severe pneumonia admitted to the intensive care unit at Asan Medical Center. A) Total number of patients with indicated virus infections. B) Number of patients with community-acquired virus infections. C) Number of patients with hospital-acquired virus infections.

the HAP group. HPIV-3 was the dominant serotype during all seasons except winter (December–February); HPIV-1 was the dominant serotype during winter (Figure 2).

Demographics and Clinical Characteristics

We analyzed demographic and clinical characteristics of the 143 patients with severe HPIV-associated pneumonia (Table 1). The median age of those patients was 61.6 years; 97.2% had underlying illnesses or conditions. CAP was observed in 80 (55.9%) and HAP in 63 (44.1%) patients. Among the 63 HAP patients, the median hospital stay until HAP diagnosis was 22.0 (interquartile range 13.0–40.0) days. Patients with CAP were older than patients with HAP (median 66.0 vs. 55.9 years; p<0.001).

Hematologic malignancy (35.0%), diabetes mellitus (23.8%), and structural lung disease (21.0%) were the most common underlying illnesses in the total study population. Chronic obstructive pulmonary disease was more common in the CAP group than in the HAP group (16.3% vs. 1.6%; p = 0.003); hematologic

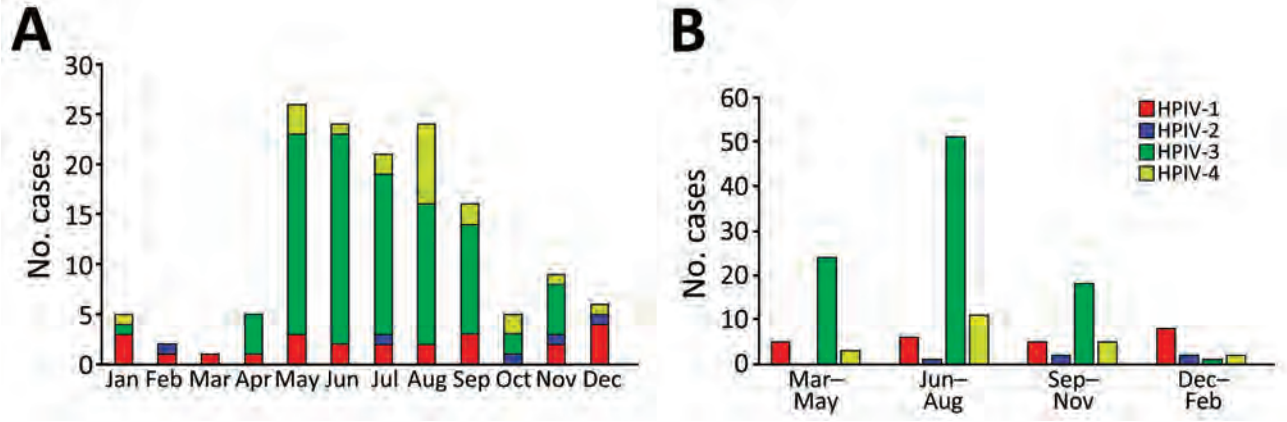

Figure 2. Seasonality of severe HPIV community- and healthcare-acquired pneumonia in adults at a tertiary hospital in Seoul, South Korea, 2010–2019. Colors indicate total number of infection cases caused by 4 parainfluenza virus serotypes during a 10-year period. A) Monthly distribution of severe HPIV-associated pneumonia. B) Seasonal distribution of severe HPIV-associated pneumonia. HPIV, human parainfluenza virus.

malignancies were more common in the HAP group (18.8% vs. 55.6%; p<0.001). Also, immunocompromised conditions were more common in the HAP group (50.0% vs. 76.2%; p = 0.001). The initial sequential organ failure assessment scores were lower in the CAP group than in the HAP group (9.2 vs. 10.8; p = 0.01). Septic shock was observed in 53.8% of patients with CAP and 50.8% of patients with HAP. Oral ribavirin (38.8% vs. 57.1%; p = 0.03) or intravenous immunoglobulin (IVIG) (18.8% vs. 33.3%, p = 0.046) were prescribed less frequently to patients in the CAP group than in the HAP group.

Co-Infection

At the time of ICU admission, 78 (54.5%) of the 143 patients with severe HPIV-associated pneumonia were co-infected with other pathogens; 48 (33.6%) patients were co-infected with bacteria, 21 (14.7%) with viruses, and 17 (11.9%) with fungi (Table 2). Among bacterial pathogens, *Pseudomonas aeruginosa* (9/48) was the most common, followed by *Staphylococcus aureus* (8/48), *Klebsiella pneumoniae* (8/48), and *Acinetobacter baumannii* (8/48). Rhinovirus (6/21) and respiratory syncytial virus (5/21) were the most common co-infecting pathogenic viruses. The rates of bacterial

Table 1. Patient characteristics in study of severe HPIV community- and healthcare-acquired pneumonia in adults at a tertiary hospital in Seoul, South Korea, 2010–2019*

Characteristics	All HPIV infections	Community-acquired HPIV	Hospital-acquired HPIV	p value
No. patients	143	80	63	
Sex				0.27
M	89 (62.2)	53 (66.3)	36 (57.1)	
F	54 (37.8)	27 (33.7)	27 (42.9)	
Mean age, y (±SD)	61.6 (±14.0)	66.0 (±11.6)	55.9 (±14.9)	<0.001
HPIV serotype†				0.25
HPIV-3	94 (65.7)	41 (51.2)	53 (84.1)	
HPIV-1	23 (16.1)	18 (22.5)	5 (7.9)	
HPIV-4	21 (14.7)	16 (20.0)	5 (7.9)	
HPIV-2	5 (3.5)	5 (6.3)	0 (0)	
Underlying disease/condition	139 (97.2)	NA	NA	NA
Structural lung disease	30 (21.0)	23 (28.7)	7 (11.1)	0.01
Chronic obstructive lung disease	14 (9.8)	13 (16.3)	1 (1.6)	0.003
Interstitial lung disease	8 (5.6)	6 (7.5)	2 (3.2)	0.47
Bronchiectasis	7 (4.9)	5 (6.3)	2 (3.2)	0.47
Tuberculosis-destroyed lung	1 (0.7)	0 (0)	1 (1.6)	0.44
Hematologic malignancy	50 (35.0)	15 (18.8)	35 (55.6)	<0.001
Diabetes mellitus	34 (23.8)	22 (27.5)	12 (19.0)	0.24
Solid cancer	22 (15.4)	18 (22.5)	4 (6.3)	0.008
End-stage renal disease	7 (4.9)	6 (7.5)	1 (1.6)	0.10
Chronic renal failure, no hemodialysis	6 (4.2)	3 (3.8)	3 (4.8)	>0.99
Liver cirrhosis	4 (2.8)	2 (2.5)	2 (3.2)	>0.99
Congestive heart failure	4 (2.8)	2 (2.5)	2 (3.2)	>0.99
Cerebrovascular attack	6 (4.2)	4 (5.0)	2 (3.2)	0.69
Solid organ transplant‡	6 (4.2)	4 (5.0)	2 (3.2)	0.69
Hematopoietic stem cell transplant	14 (9.8)	6 (7.5)	8 (12.7)	0.30
Immunocompromised status§	88 (61.5)	40 (50.0)	48 (76.2)	0.001
Receipt of immunosuppressant	42 (29.4)	15 (18.8)	27 (42.9)	0.002
Recent chemotherapy	56 (39.2)	22 (27.5)	34 (54.0)	0.001
Active smoker	11 (7.7)	9 (11.3)	2 (3.2)	0.07
Surgery within 1 mo of ICU admission	11 (7.7)	3 (3.8)	8 (12.7)	0.046
Neutropenia¶	39 (27.3)	14 (17.5)	25 (39.7)	0.003
Clinical manifestations				
Mean APACHE II score (±SD)	25.4 (±7.0)	24.6 (±7.3)	26.4 (±6.5)	0.13
Mean SOFA score (±SD)	9.9 (±4.0)	9.15 (±4.1)	10.8 (± 3.7)	0.01
Septic shock at admission	75 (52.4)	43 (53.8)	32 (50.8)	0.73
Mechanical ventilation	138 (96.5)	75 (93.8)	63 (100.0)	0.07
Treatment				
Oral ribavirin#	67 (46.9)	31 (38.8)	36 (57.1)	0.03
IVIG	36 (25.2)	15 (18.8)	21 (33.3)	0.046

*Values are no. (%) except as indicated. APACHE II, acute physiology and chronic health evaluation II; HPIV, human parainfluenza virus; IQR, interquartile range; IVIG, intravenous immunoglobulin; NA, not applicable; SOFA, sequential organ failure assessment.
†Serotypes are listed according to prevalence.
‡Patients with lung (n = 1) or kidney (n = 5) transplants.
§Defined as either daily receipt of immunosuppressants (including corticosteroids), human immunodeficiency virus infection, solid organ or hematopoietic stem cell transplant recipients, receipt of chemotherapy for underlying malignancy during the previous 6 months, or underlying immune deficiency disorder.
¶Absolute neutrophil count of <500/mm^3.
#Use of oral ribavirin for >2 days.

Table 2. Co-infections of patients in study of severe human parainfluenza virus community- and healthcare-acquired pneumonia in adults at a tertiary hospital in Seoul, South Korea, 2010–2019*

Co-pathogens†	Total, n = 143	Community acquired, n = 80	Hospital acquired, n = 63	p value
Any	78 (54.5)	44 (55.0)	34 (54.0)	0.90
Bacteria	48 (33.6)	32 (40.0)	16 (25.4)	0.07
Gram positive				
Staphylococcus aureus	8	4	4	0.73
Streptococcus pneumoniae	7	6	1	0.13
Streptococcus pyogenes	0	0	0	NA
Streptococcus agalactiae	0	0	0	NA
Corynebacterium striatum	1	0	1	0.44
Gram negative				
Haemophilus influenzae	1	1	0	>0.99
Moraxella catarrhalis	0	0	0	NA
Legionella sp.	1	1	0	>0.99
Enteric gram-negative bacilli				
Klebsiella pneumoniae	8	7	1	0.08
Escherichia coli	2	2	0	0.50
Enterobacter cloacae	2	2	0	0.50
Serratia marcescens	1	1	0	>0.99
Enterobacter aerogenes	1	1	0	>0.99
Nonfermenting gram-negative bacilli				
Pseudomonas aeruginosa	9	5	4	0.98
Acinetobacter baumannii	8	3	5	0.30
Stenotrophomonas maltophilia	1	0	1	0.44
Viruses	21 (14.7)	12 (15.0)	9 (14.3)	0.90
Rhinovirus	6	5	1	0.23
Respiratory syncytial virus	5	2	3	0.65
Adenovirus	3	2	1	>0.99
Human coronavirus	2	2	0	0.50
Human metapneumovirus	2	0	2	0.19
Bocavirus	2	0	2	0.19
Influenza virus	1	1	0	>0.99
Fungi	17 (11.9)	4 (5.0)	13 (20.6)	0.004
Aspergillus species	15	3	12	0.003
Pneumocystis jirovecii	2	1	1	>0.99
Nontuberculous mycobacteria	1 (0.7)	0	1 (1.6)	0.44

*Values are no. (%) except as indicated. NA, not applicable.
†Includes pathogens identified from bronchoalveolar lavage fluid or other specimens, such as nasopharyngeal, sputum, endotracheal aspirate, and blood culture samples during admission to the intensive care unit. Categories of co-infection were not mutually exclusive. Some cases were associated with ≥2 categories of pathogens.

(40.0% vs. 25.4%; p = 0.07) and viral (15.9% vs. 14.3%; p = 0.90) co-infections were not different between the CAP and HAP groups. However, fungal co-infections, mainly *Aspergillus* spp., were less common in the CAP group than in the HAP group (5.0% vs. 20.6%; p = 0.004). *Aspergillus* spp. co-infections were found in 13 of 15 patients who had immunocompromised conditions (7 patients had hematologic malignancy, 3 had hematopoietic stem cell transplants, 2 were taking immunosuppressant medications, and 1 had a solid cancer).

Outcomes and Risk Factors for 90-Day Mortality Rate

The overall 90-day mortality rate was 55.2% for HPIV-associated pneumonia, which was comparable to 48.4% for severe influenza virus–associated pneumonia (p = 0.22) within the same cohort (Table 3). Ventilator-associated pneumonia occurred in 10.5% (15/143) of the study population (Table 3). The mortality rate after oral ribavirin or IVIG treatment was not lower than that for untreated patients (56.7% vs. 53.9%; p = 0.74). Furthermore, mortality rates after oral ribavirin or IVIG treatment were not lower than those for untreated patients in the immunocompromised (65.6% vs. 62.5%; p = 0.77) or nonimmunocompromised (43.6% vs. 37.5%; p = 0.69) patient groups. Patients with a fungal co-infection had a significantly higher 90-day mortality rate than those with no fungal co-infection (82.4% vs. 51.6%; p = 0.02). In multivariate analysis of risk factors, the adjusted odds ratios (aORs) were 2.21 (95% CI 1.00–4.86) for HAP, 1.29 (95% CI 1.15–1.44) for the initial SOFA score, and 4.64 (95% CI 1.05–20.63) for fungal co-infection, which was significantly associated with 90-day mortality rate (p = 0.04) (Table 4).

Discussion

We investigated the epidemiologic and clinical characteristics of severe HPIV-associated pneumonia in adults. HPIV was the leading cause of severe virus-

Table 3. Patient outcomes in study of severe HPIV community- and healthcare-acquired pneumonia in adults at a tertiary hospital in Seoul, South Korea, 2010–2019*

Patient outcomes	HPIV infections			Influenza virus infections			p value†
	Total, n = 143	CAP, n = 80	HAP, n = 63	Total, n = 189	CAP, n = 133	HAP, n = 56	
Mortality rates							
7 d	20 (14.0)	8 (10.0)	12 (19.0)	16/185 (8.6)	11/132 (8.3)	5/53 (9.4)	0.13
30 d	57 (39.9)	22 (27.5)	35 (55.6)	61/185 (33.0)	41/132 (31.1)	20/53 (37.7)	0.21
60 d	73 (51.0)	30 (37.5)	43 (68.3)	81/185 (43.8)	50/132 (37.9)	31/53 (58.5)	0.21
90 d	79 (55.2)	34 (42.5)	45 (71.4)	89/185 (48.1)	53/132 (40.2)	36/53 (67.9)	0.22
In-hospital	73 (51.0)	29 (36.3)	44 (69.8)	78/185 (42.2)	46/132 (34.8)	32/53 (60.4)	0.10
Mean ICU stay, d (±SD)	17.1 (±19.4)	17.4 (±23.0)	16.7 (±13.7)	17.6 (±17.3)	NA	NA	0.82
Mean hospital stay, d (±SD) ‡	50.1 (±47.4)	39.5 (±40.5)	63.6 (±52.2)	53.1 (±71.4)	NA	NA	0.66
Ventilator-associated pneumonia	15 (10.5)	4 (5.0)	11 (17.5)	25 (13.3)	15 (11.3)	10 (17.9)	0.44

*Values are no. (%) except as indicated. Denominators are different in some cases because of missing data. CAP, community-acquired pneumonia; HAP, hospital-acquired pneumonia; HPIV, human parainfluenza virus; ICU, intensive care unit; IQR, interquartile range; NA, not applicable.
†p values were calculated by comparing total numbers of severe HPIV-associated pneumonia and severe influenza virus-associated pneumonia.
‡Defined as the period from hospital admission to discharge from the hospital or death.

associated HAP and the third most common cause of severe virus-associated CAP. Most of the study population comprised elderly patients with underlying illnesses, and ≈50% of patients had co-infections at the time of ICU admission. The 90-day mortality rate for patients with severe HPIV-associated pneumonia was comparable to that of the patients with severe influenza virus-associated pneumonia. Fungal co-infection was strongly correlated with increased death.

HPIV was identified as the leading viral pathogen responsible for severe virus-associated HAP, despite ranking third after influenza and rhinovirus as the most prevalent causes of virus-associated CAP. Those findings might signify a higher risk for HPIV exposure and nosocomial transmission in the hospital environment, especially when compared with influenza and rhinovirus. HPIV generally induces asymptomatic or mild upper respiratory infections in healthy adults (*3*,*14*,*15*), which could result in a delayed or missed diagnosis of HPIV infection in healthcare workers, patient guardians, and patients. Consequently, those asymptomatic carriers might transmit the virus to other patients in the hospital (*16*). Furthermore, HPIV has been shown to survive on experimentally contaminated nonporous surfaces for ≤10 hours (*17*,*18*), suggesting fomites and contaminated environments could act as vehicles for HPIV transmission (*18*–*20*). We have previously reported on environmental contamination during an outbreak of HPIV-3 in a hematology ward; ≈80% of swab samples from an index patient's environment were positive for HPIV-3 RNA, despite the environment being swabbed 5 days after a negative PCR conversion of patient respiratory samples (*16*). This finding suggests that HPIV-3 could potentially spread in hospitals through fomite transmission. In contrast to influenza virus, no effective therapeutic agents or vaccines exist for HPIV.

We found that >50% of patients with severe HPIV-associated pneumonia had co-infections with pathogenic organisms; bacterial co-infections were more common than viral and fungal co-infections. The high rate of co-infection could be linked to the inclusion of a substantial number of HAP cases in the study. Influenza virus–associated pneumonia is often complicated by subsequent pneumonia from *S. aureus* or *S. pneumoniae* (*21*). In contrast, patients with severe HPIV-associated pneumonia are frequently co-infected with gram-negative bacilli, such as *P. aeruginosa* or *K. pneumoniae*. Fungi, especially *Aspergillus* spp., were also major co-pathogens and were significantly associated with a high 90-day mortality rate. Increasing evidence indicates that patients with severe influenza-associated pneumonia (7%–19%) (*22*,*23*) and COVID-19 (5%–30%) are at risk for invasive pulmonary aspergillosis (*24*). However, data on patients with HPIV-associated pneumonia remains scarce. Only a few studies have shown that invasive pulmonary aspergillosis might also occur in patients with

Table 4. Univariate and multivariate analyses of risk factors for severe human parainfluenza virus community- and healthcare-acquired pneumonia in adults at a tertiary hospital in Seoul, South Korea, 2010–2019*

Variable	Univariate analysis		Multivariate analysis	
	Unadjusted odds ratio (95% CI)	p value	Adjusted odds ratio (95% CI)	p value
Hospital-acquired HPIV	3.38 (1.67–6.84)	0.001	2.21 (1.00–4.86)	0.049
SOFA score	1.29 (1.16–1.43)	<0.001	1.29 (1.15–1.44)	<0.001
Hematologic malignancy	3.46 (1.63–7.33)	0.001	1.35 (0.53–3.40)	0.53
Fungal co-infection	4.38 (1.20–15.99)	0.03	4.64 (1.05–20.63)	0.04

*Analyses of risk factors associated with 90-day mortality rates for patients with severe HPIV pneumonia. HPIV, human parainfluenza virus; SOFA, sequential organ failure assessment.

noninfluenza respiratory virus–associated pneumonia, such as respiratory syncytial virus or HPIV, particularly among immunocompromised hosts (*25*,*26*). Because most patients with *Aspergillus* spp. co-infections had immunocompromising conditions in this study, this co-infection can be attributed to host factors rather than an inherent characteristic of HPIV. If the clinical course of a patient with severe HPIV-associated pneumonia continues to deteriorate, clinicians should consider the possibility of co-infection with other pathogens.

Although influenza can be treated with effective antiviral agents, such as oseltamivir and peramivir, no licensed effective therapeutic agents are available to treat HPIV infections. In this study, ribavirin and IVIG did not reduce death, indicating the need for novel therapeutic agents and preventive vaccines for HPIV. A phase III clinical trial of DAS-181 as a novel therapeutic agent for HPIV is ongoing (*27*,*28*). Until novel therapeutic agents or vaccines are developed, it is crucial to maintain contact precautions and environmental cleaning against HPIV in hospital settings.

The strength of this study lies in its comprehensive overview of severe HPIV-associated pneumonia over a decade. We have provided insights into various epidemiologic and clinical characteristics of severe HPIV-associated pneumonia, including the identification of causative serotypes according to the site of pneumonia acquisition. Moreover, our study highlights the relatively frequent incidences of co-infections in patients with severe HPIV-associated pneumonia, particularly focusing on the effects of fungal co-infections on mortality rates.

The first limitation of our study is that it was conducted exclusively at a single tertiary care center and focused on a highly selected subset of HPIV patients. Nonpneumonic patients and those with mild to moderate pneumonia were not included, limiting the generalizability of our findings. Second, HAP cases could have been misclassified according to our definition if patients had upper respiratory infections with asymptomatic or mild symptoms that were not documented upon admission. Third, we did not perform BAL for all patients in this study; therefore, viral pathogens might have been present as bystanders causing asymptomatic, persistent, and prolonged shedding. In addition, HPIV detection might have occurred by chance, possibly stemming from ongoing nosocomial transmission in hospitalized patients who had HAP caused by other pathogens. Fourth, the small numbers of HPIV-1, -2, and -4 infected patients in the study precluded the analyses of differences in clinical characteristics and outcomes among those HPIV serotypes. Finally, we did not perform a molecular study of HPIV. Thus, we could not evaluate the effects of molecular characteristics on clinical features even within the same serotype.

In conclusion, HPIV is the leading viral pathogen of severe HAP in adult patients. In this study, we found that the mortality rate was comparable to that of severe influenza virus–associated pneumonia, and fungal co-infections significantly contributed to the high mortality rate. Clinicians should consider the high likelihood of co-infection with other pathogens in patients with HPIV-associated pneumonia, and contact precautions and environmental cleaning must be used to prevent HPIV transmission in hospital settings.

About the Author

Dr. Park is a physician at Chung-Ang University Gwangmyeong Hospital in Seoul, South Korea. Her research interests focus on infectious diseases and clinical microbiology.

References

1. Russell E, Yang A, Tardrew S, Ison MG. Parainfluenza virus in hospitalized adults: a 7-year retrospective study. Clin Infect Dis. 2019;68:298–305. https://doi.org/10.1093/cid/ciy451
2. Bennett JE, Dolin R, Blaser MJ. Mandell, Douglas, and Bennett's principles and practice of infectious diseases. 9th ed. Amsterdam: Elsevier; 2019.
3. Hall CB. Respiratory syncytial virus and parainfluenza virus. N Engl J Med. 2001;344:1917–28. https://doi.org/10.1056/NEJM200106213442507
4. Kapikian AZ, Chanock RM, Reichelderfer TE, Ward TG, Huebner RJ, Bell JA. Inoculation of human volunteers with parainfluenza virus type 3. JAMA. 1961;178:537–41. https://doi.org/10.1001/jama.1961.03040450001001
5. Russell E, Ison MG. Parainfluenza virus in the hospitalized adult. Clin Infect Dis. 2017;65:1570–6. https://doi.org/10.1093/cid/cix528
6. Choi SH, Hong SB, Ko GB, Lee Y, Park HJ, Park SY, et al. Viral infection in patients with severe pneumonia requiring intensive care unit admission. Am J Respir Crit Care Med. 2012;186:325–32. https://doi.org/10.1164/rccm.201112-2240OC
7. de Roux A, Marcos MA, Garcia E, Mensa J, Ewig S, Lode H, et al. Viral community-acquired pneumonia in nonimmunocompromised adults. Chest. 2004;125:1343–51. https://doi.org/10.1378/chest.125.4.1343
8. Jennings LC, Anderson TP, Beynon KA, Chua A, Laing RTR, Werno AM, et al. Incidence and characteristics of viral community-acquired pneumonia in adults. Thorax. 2008;63:42–8. https://doi.org/10.1136/thx.2006.075077
9. Hong HL, Hong SB, Ko GB, Huh JW, Sung H, Do KH, et al. Viral infection is not uncommon in adult patients with severe hospital-acquired pneumonia. PLoS One. 2014;9:e95865. https://doi.org/10.1371/journal.pone.0095865
10. Shorr AF, Zilberberg MD, Micek ST, Kollef MH. Viruses are prevalent in non-ventilated hospital-acquired pneumonia. Respir Med. 2017;122:76–80. https://doi.org/10.1016/j.rmed.2016.11.023

11. Chung H, Hong SB, Huh JW, Sung H, Do KH, Lee SO, et al. Clinical features and outcomes of severe pneumonia caused by endemic human coronavirus in adults. Am J Respir Crit Care Med. 2022;205:1116–8. https://doi.org/10.1164/rccm.202112-2797LE
12. Metlay JP, Waterer GW, Long AC, Anzueto A, Brozek J, Crothers K, et al. Diagnosis and treatment of adults with community-acquired pneumonia. An official clinical practice guideline of the American Thoracic Society and Infectious Diseases Society of America. Am J Respir Crit Care Med. 2019;200:e45–67. https://doi.org/10.1164/rccm.201908-1581ST
13. Kalil AC, Metersky ML, Klompas M, Muscedere J, Sweeney DA, Palmer LB, et al. Management of adults with hospital-acquired and ventilator-associated pneumonia: 2016 Clinical Practice Guidelines by the Infectious Diseases Society of America and the American Thoracic Society. Clin Infect Dis. 2016;63:e61–111. https://doi.org/10.1093/cid/ciw353
14. Branche AR, Falsey AR. Parainfluenza virus infection. Semin Respir Crit Care Med. 2016;37:538–54. https://doi.org/10.1055/s-0036-1584798
15. Cooney MK, Fox JP, Hall CE. The Seattle Virus Watch. VI. Observations of infections with and illness due to parainfluenza, mumps and respiratory syncytial viruses and *Mycoplasma pneumoniae*. Am J Epidemiol. 1975;101:532–51. https://doi.org/10.1093/oxfordjournals.aje.a112125
16. Kim T, Jin CE, Sung H, Koo B, Park J, Kim SM, et al. Molecular epidemiology and environmental contamination during an outbreak of parainfluenza virus 3 in a haematology ward. J Hosp Infect. 2017;97:403–13. https://doi.org/10.1016/j.jhin.2017.09.003
17. Brady MT, Evans J, Cuartas J. Survival and disinfection of parainfluenza viruses on environmental surfaces. Am J Infect Control. 1990;18:18–23. https://doi.org/10.1016/0196-6553(90)90206-8
18. Boone SA, Gerba CP. Significance of fomites in the spread of respiratory and enteric viral disease. Appl Environ Microbiol. 2007;73:1687–96. https://doi.org/10.1128/AEM.02051-06
19. Henrickson KJ. Parainfluenza viruses. Clin Microbiol Rev. 2003;16:242–64. https://doi.org/10.1128/CMR.16.2.242-264.2003
20. Leung NHL. Transmissibility and transmission of respiratory viruses. Nat Rev Microbiol. 2021;19:528–45. https://doi.org/10.1038/s41579-021-00535-6
21. Mulcahy ME, McLoughlin RM. *Staphylococcus aureus* and influenza A virus: partners in coinfection. mBio. 2016;7:e02068-16. https://doi.org/10.1128/mBio.02068-16
22. Schauwvlieghe AFAD, Rijnders BJA, Philips N, Verwijs R, Vanderbeke L, Van Tienen C, et al.; Dutch-Belgian Mycosis study group. Invasive aspergillosis in patients admitted to the intensive care unit with severe influenza: a retrospective cohort study. Lancet Respir Med. 2018;6:782–92. https://doi.org/10.1016/S2213-2600(18)30274-1
23. Verweij PE, Rijnders BJA, Brüggemann RJM, Azoulay E, Bassetti M, Blot S, et al. Review of influenza-associated pulmonary aspergillosis in ICU patients and proposal for a case definition: an expert opinion. Intensive Care Med. 2020;46:1524–35. https://doi.org/10.1007/s00134-020-06091-6
24. Koehler P, Bassetti M, Chakrabarti A, Chen SCA, Colombo AL, Hoenigl M, et al.; European Confederation of Medical Mycology; International Society for Human Animal Mycology; Asia Fungal Working Group; INFOCUS LATAM/ISHAM Working Group; ISHAM Pan Africa Mycology Working Group; European Society for Clinical Microbiology; Infectious Diseases Fungal Infection Study Group; ESCMID Study Group for Infections in Critically Ill Patients; Interregional Association of Clinical Microbiology and Antimicrobial Chemotherapy; Medical Mycology Society of Nigeria; Medical Mycology Society of China Medicine Education Association; Infectious Diseases Working Party of the German Society for Haematology and Medical Oncology; Association of Medical Microbiology; Infectious Disease Canada. Defining and managing COVID-19–associated pulmonary aspergillosis: the 2020 ECMM/ISHAM consensus criteria for research and clinical guidance. Lancet Infect Dis. 2021;21:e149–62. https://doi.org/10.1016/S1473-3099(20)30847-1
25. Magira EE, Chemaly RF, Jiang Y, Tarrand J, Kontoyiannis DP. Outcomes in invasive pulmonary aspergillosis infections complicated by respiratory viral infections in patients with hematologic malignancies: a case-control study. Open Forum Infect Dis. 2019;6:ofz247. https://doi.org/10.1093/ofid/ofz247
26. Apostolopoulou A, Clancy CJ, Skeel A, Nguyen MH. Invasive pulmonary aspergillosis complicating noninfluenza respiratory viral infections in solid organ transplant recipients. Open Forum Infect Dis. 2021;8:ofab478. https://doi.org/10.1093/ofid/ofab478
27. Boltz DA, Aldridge JR Jr, Webster RG, Govorkova EA. Drugs in development for influenza. Drugs. 2010;70:1349–62. https://doi.org/10.2165/11537960-000000000-00000
28. Chemaly RF, Marty FM, Wolfe CR, Lawrence SJ, Dadwal S, Soave R, et al. DAS181 treatment of severe lower respiratory tract parainfluenza virus infection in immunocompromised patients: a phase 2 randomized, placebo-controlled study. Clin Infect Dis. 2021;73:e773–81. https://doi.org/10.1093/cid/ciab113

Address for correspondence: Sang-Ho Choi, Department of Infectious Diseases, Asan Medical Center, University of Ulsan College of Medicine, Seoul, South Korea; email: sangho@amc.seoul.kr

Electronic Health Record–Based Algorithm for Monitoring Respiratory Virus–Like Illness

Noelle M. Cocoros, Karen Eberhardt, Vu-Thuy Nguyen, Catherine M. Brown, Alfred DeMaria, Lawrence C. Madoff, Liisa M. Randall, Michael Klompas

Viral respiratory illness surveillance has traditionally focused on single pathogens (e.g., influenza) and required fever to identify influenza-like illness (ILI). We developed an automated system applying both laboratory test and syndrome criteria to electronic health records from 3 practice groups in Massachusetts, USA, to monitor trends in respiratory viral–like illness (RAVIOLI) across multiple pathogens. We identified RAVIOLI syndrome using diagnosis codes associated with respiratory viral testing or positive respiratory viral assays or with fever. After retrospectively applying RAVIOLI criteria to electronic health records, we observed annual winter peaks during 2015–2019, predominantly caused by influenza, followed by cyclic peaks corresponding to SARS-CoV-2 surges during 2020–2024, spikes in RSV in mid-2021 and late 2022, and recrudescent influenza in late 2022 and 2023. RAVIOLI rates were higher and fluctuations more pronounced compared with traditional ILI surveillance. RAVIOLI broadens the scope, granularity, sensitivity, and specificity of respiratory viral illness surveillance compared with traditional ILI surveillance.

Respiratory viral illnesses place an enormous burden on human health and the healthcare system (*1*–*3*). Although multiple pathogenic respiratory viruses circulate, often simultaneously, public health has traditionally dedicated most of its attention to monitoring trends in laboratory-confirmed influenza and influenza-like illness (ILI). Illness and death associated with seasonal respiratory syncytial virus (RSV) spikes, the SARS-CoV-2 pandemic, and occasional clusters of infection from other respiratory pathogens, however, illustrate the importance of expanding monitoring to include all respiratory viral–like illness activity. Relying on laboratory testing alone will not accomplish this goal because most persons with respiratory viral illnesses do not seek care, many who do seek care are not tested, and not everyone tested is tested for all respiratory viruses.

Public health agencies have traditionally relied on syndromic surveillance to monitor conditions for which testing rates are low and variable (*4*). The Centers for Disease Control and Prevention's outpatient Influenza-like Illness Surveillance Network and emerging systems designed to monitor COVID-19–like illness are prime examples (*5*–*9*). However, syndromic surveillance systems tend to provide little or no information about which particular pathogens are circulating, and most jurisdictions require fever to define ILI, a requirement that increases specificity but lowers sensitivity (fever occurs in fewer than half of persons with laboratory-confirmed influenza) (*10*). Surveillance focusing on single pathogens (e.g., influenza, SARS-CoV-2), viral testing alone, or syndromic definitions alone provides an incomplete picture of respiratory illness activity and can miss critical trends and developments (*11*,*12*). Extending surveillance to include multiple pathogens, using both laboratory testing and syndromes, and decreasing reliance on fever as a gatekeeper symptom are necessary to provide public health agencies and healthcare institutions with the data needed to improve situational awareness for planning, resource use, internal and external communications, and targeted prevention activities.

To regularly monitor overall respiratory viral illness activity associated with multiple pathogens, we developed an integrated surveillance strategy using a combination of laboratory and syndromic indicators, incorporating logic to identify the relative contributions of different individual pathogens. We describe

Author affiliations: Harvard Pilgrim Health Care Institute, Boston, Massachusetts, USA (N.M. Cocoros, V.-T. Nguyen, M. Klompas); Harvard Medical School, Boston (N.M. Cocoros, M. Klompas); Commonwealth Informatics, Waltham, Massachusetts, USA (K. Eberhardt); Massachusetts Department of Public Health, Boston (C.M. Brown, A. DeMaria, L.C. Madoff, L.M. Randall); Brigham and Women's Hospital, Boston (M. Klompas)

DOI: https://doi.org/10.3201/eid3006.230473

our data-driven approach to developing a routine, automated respiratory virus-like illness (RAVIOLI) algorithm for syndromic surveillance in Massachusetts using live electronic health record (EHR) data drawn from 3 large practice groups. Our work was performed as public health surveillance and therefore not subject to institutional review board oversight.

Methods

We used the Electronic Medical Record Support for Public Health (ESP, https://www.esphealth.org) public health surveillance platform to develop the RAVIOLI algorithm. ESP is open-source software that uses automated daily extracts of EHR data to identify and report conditions of public health interest to health departments (*13*–*17*). ESP maps raw data to common terms and then applies algorithms to identify conditions using diagnosis codes, prescriptions, laboratory tests, and vital signs. In Massachusetts, ESP is used for automated reporting of infectious disease cases to the Massachusetts Department of Public Health, aggregate reporting of chronic diseases, and continuum-of-care assessments (*18*–*21*).

Three multisite clinical practice groups that use ESP for infectious disease reporting, Atrius Health, Cambridge Health Alliance, and Boston Medical Center, contributed data for our project. Atrius Health (https://www.atriushealth.org) is an ambulatory care group with >30 locations in eastern Massachusetts that provides clinical services for a population of ≈700,000. Cambridge Health Alliance (https://www.challiance.org) is a safety-net system that provides ambulatory and inpatient care to >140,000 patients in communities north of Boston. Boston Medical Center (https://www.bmc.org) is a 514-bed academic medical center and safety-net hospital that provides ambulatory and inpatient care to ≈220,000 persons. We combined data from those 3 sites for this analysis.

We sought to develop an evidence-based set of diagnosis codes to identify respiratory virus–like illnesses and assess whether a subset of those codes might be predictive of specific pathogens. To identify codes associated with respiratory viral illness syndrome, we identified all patients tested for respiratory viruses (Table 1) during October 3, 2015–July 30, 2022. Among patients who tested positive for ≥1 virus, we identified all International Classification of Diseases, 10th Revision (ICD-10), diagnosis codes recorded within 2 days before or after the specimen collection date. For patients without a recorded specimen collection date, we used the test order date; if that was unavailable, we used the result date. We manually removed ICD-10 codes unrelated to respiratory viral illness (e.g., trauma, cancer, chronic disease management). The list of >7,000 excluded codes is available upon request from the authors.

Table 1. Respiratory pathogens and test types included in RAVIOLI algorithm for monitoring respiratory virus–like illness*

Pathogen	Test types
Adenovirus	NAAT
Non–SARS-CoV-2 coronaviruses: OC43,229E, HKU1, NL63	NAAT
Human metapneumovirus	NAAT
Influenza	NAAT, antigen/rapid, culture
Parainfluenza	NAAT
Respiratory syncytial virus	NAAT, antigen
Rhinovirus/enterovirus	NAAT
SARS-CoV-2	NAAT, antigen/rapid

*Respiratory virus–like illness is defined as a clinical encounter with a positive laboratory test result for a respiratory virus, as shown in this table; 1 of the International Classification of Diseases, 10th Revision, diagnosis codes shown in Table 1; or a measured fever >100°F. NAAT, nucleic acid amplification test.

We calculated the positive predictive value (PPV) for each ICD-10 code associated with positive respiratory virus test results. We also calculated the PPV for measured temperature >100°F within 2 days before or after a positive respiratory virus test. We calculated the PPV for each ICD-10 code and fever as the number of encounters with the diagnosis code within 2 days of a positive test divided by the total number of times the diagnosis code occurred across all clinical encounters during the study period. We defined a clinical encounter as a patient receiving a relevant diagnosis code, immunization, vital sign measure, laboratory test, or prescription.

We included in the final algorithm diagnosis codes with a PPV ≥10% for any respiratory virus (all viruses combined) or for a specific individual respiratory virus. We also included encounters with positive respiratory virus tests in the total count of respiratory virus encounters as well as in virus-specific categories of RAVIOLI. We counted each viral encounter only 1 time if the patient had both a positive respiratory virus assay result and ≥1 suggestive diagnosis code. We classified measured fever alone and diagnosis codes with a PPV of ≥10% for any positive respiratory virus test but <10% for any specific respiratory virus in a category referred to as nonspecific for respiratory viral illness syndrome. In summary, we categorized positive cases within RAVIOLI as virus-specific (e.g., influenza, adenovirus), based on a positive test or a diagnosis code with a PPV ≥10% for the specific virus, or nonspecific, based on fever or a diagnosis code with a PPV ≥10% for any positive test of interest.

To better understand the underlying data included in the final RAVIOLI algorithm, we examined the proportion of patients in each virus-specific

category of the algorithm with a positive laboratory test and the proportion of patients in the nonspecific category with a fever. We generated weekly counts during October 3, 2015–January 13, 2024, for clinical encounters with patients meeting the RAVIOLI algorithm, overall and stratified by the probable etiology when possible. For comparison, we also identified the proportion of patients that met the definition of ILI: fever and a diagnosis code for any influenza-like symptom or diagnosis; fever was identified by either a measured fever >100°F or diagnosis code for fever (Appendix Table 1, https://wwwnc.cdc.gov/EID/article/30/6/23-0473-App1.pdf).

Results

Forty-two diagnosis codes (Table 2) and measured fever (>100°F) had a PPV ≥10% for either any positive respiratory virus test (nonspecific) or ≥1 virus-specific positive test; those diagnosis codes and fever are included in the RAVIOLI algorithm. We recorded weekly counts of patients with clinical encounters and calculated the proportion that met the definition

Table 2. ICD-10 diagnosis codes that met the positive predictive value threshold for confirmed respiratory viral illnesses and are included in the RAVIOLI algorithm for monitoring respiratory virus–like illness*

Virus	ICD-10 codes†	Description
Adenovirus	A08.2	Adenoviral enteritis
	B34.0	Adenovirus infection, unspecified
	B97.0	Adenovirus as the cause of diseases classified elsewhere
	J12.0	Adenoviral pneumonia
Non–SARS-CoV-2 coronavirus	B34.2	Coronavirus infection, unspecified
SARS-CoV-2	B34.2	Coronavirus infection, unspecified
	B97.29	Other coronavirus as the cause of diseases classified elsewhere
	J12.82	Pneumonia associated with coronavirus disease 2019
	J12.89	Other viral pneumonia
	J80	Acute respiratory distress syndrome
	R05.1	Acute cough
	R48.1	Agnosia
	U07.1	COVID-19
Human metapneumovirus	B97.81	Human metapneumovirus as the cause of diseases classified elsewhere
	J12.3	Human metapneumovirus pneumonia
	J21.1	Acute bronchiolitis associated with human metapneumovirus
Influenza	J09.X1	Influenza from identified novel influenza A virus with pneumonia
	J09.X2	Influenza associated with identified novel influenza A virus with other respiratory manifestations
	J10.00	Influenza associated with other identified influenza virus with unspecified type of pneumonia
	J10.1	Influenza associated with other identified influenza virus with other respiratory manifestations
	J11.00	Influenza associated with unidentified influenza virus with unspecified type of pneumonia
	J11.1	Influenza associated with unidentified influenza virus with other respiratory manifestations
Parainfluenza	B33.8	Other specified viral diseases
	B34.8	Other viral infections of unspecified site
	J20.4	Acute bronchitis associated with parainfluenza virus
Rhinovirus and enterovirus	B34.0	Adenovirus infection, unspecified
	B34.8	Other viral infections of unspecified site
	B97.10	Unspecified enterovirus as the cause of diseases classified elsewhere
	J20.6	Acute bronchitis associated with rhinovirus
	J45.902	Unspecified asthma with status asthmaticus
Respiratory syncytial virus	B97.4	Respiratory syncytial virus as the cause of diseases classified elsewhere
	J12.1	Respiratory syncytial virus pneumonia
	J20.5	Acute bronchitis associated with respiratory syncytial virus
	J21.0	Acute bronchiolitis associated with respiratory syncytial virus
Any respiratory viral test (nonspecific)	J21.8	Acute bronchiolitis associated with other specified organisms
	R06.03	Acute respiratory distress
	P81.9	Disturbance of temperature regulation of newborn, unspecified
	J12.9	Viral pneumonia, unspecified
	R50.81	Fever manifesting with conditions classified elsewhere
	J96.90	Respiratory failure, unspecified, unspecified whether with hypoxia or hypercapnia
	R05.9	Cough, unspecified
	J96.91	Respiratory failure, unspecified with hypoxia
	J96.92	Respiratory failure, unspecified with hypercapnia
	R57.9	Shock, unspecified

*Respiratory virus-like illness is defined as a clinical encounter with a positive laboratory test result for a respiratory virus listed in Table 1; 1 of the ICD-10 diagnosis codes listed in this table; or a measured fever >100°F. ICD-10, International Classification of Diseases, 10th Revision.
†All of the diagnosis codes in the table had a positive predictive value ≥10% PPV for either any positive respiratory virus laboratory test or 1 of the virus-specific positive tests.

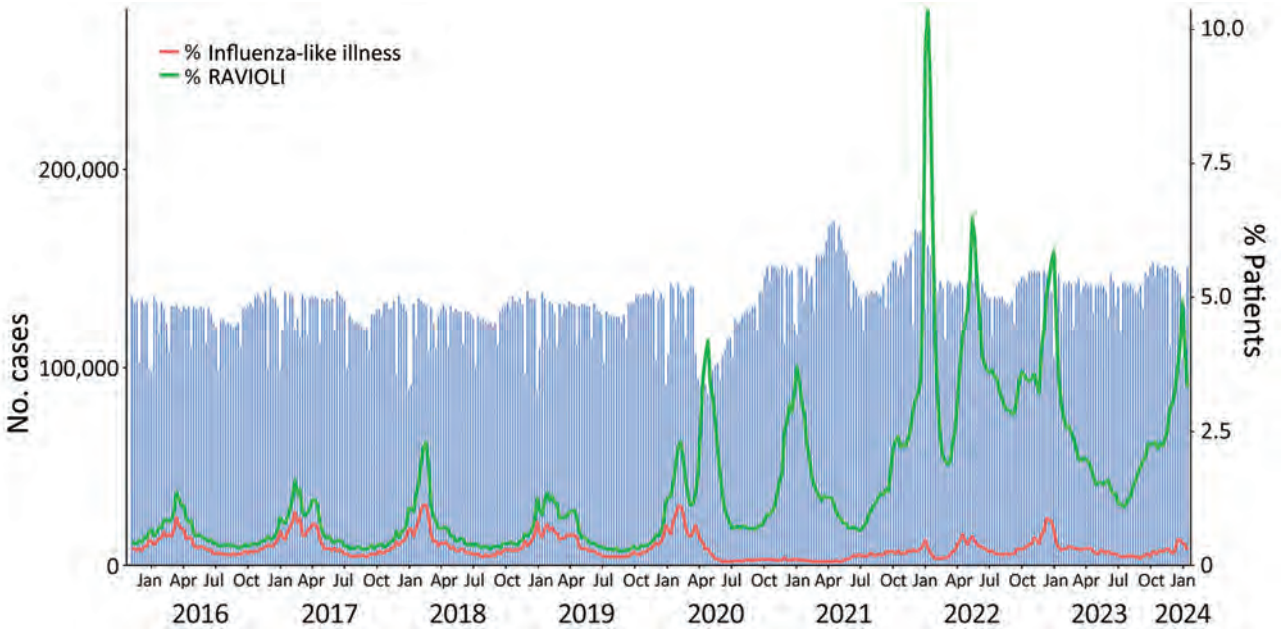

Figure 1. Numbers of patients with a clinical encounter for respiratory virus–like illness and the percentages that met the requirements for influenza-like illness versus those of the RAVIOLI algorithm for monitoring respiratory virus–like illness, by week, Massachusetts, USA, October 2015–January 2024. Patients receiving a diagnosis code, immunization, vital sign measure, laboratory test, or prescription were considered to have a clinical encounter.

for RAVIOLI overall (diagnosis code, fever, or positive respiratory virus test) and, for comparison, the proportion that met the ILI criteria (Figure 1). The percentage of encounters that met the RAVIOLI algorithm showed clear seasonal trends of annual winter spikes during 2015–2019 followed by periodic increases during spring 2020–early 2024, corresponding to emergence or surges of SARS-CoV-2, RSV, and influenza in Massachusetts. RAVIOLI was identified in a much larger proportion of encounters than ILI after March 2020 and, at times (e.g., fall 2021, August–November 2023), ILI did not detect an increase in respiratory virus illness while RAVIOLI did.

We estimated weekly counts of patients with clinical encounters meeting the RAVIOLI algorithm stratified by encounters with virus-specific or nonspecific encounters without a classified virus. We calculated those data for the full study period, October 2015–January 2024 (Figure 2, panel A), and for January 2020–January 2024 (Figure 2, panel B). Before March 2020, most RAVIOLI encounters came from the influenza or nonspecific categories. SARS-CoV-2 subsequently dominated until fall 2021, when the nonspecific category reemerged, along with influenza and RSV. When we examined trends by patient age groups, the highest proportion of encounters that met the RAVIOLI algorithm were among children 0–4 years of age, followed by young persons 5–24 years of age (Figure 3).

Data from January 2023–January 2024 show the proportions of patients in the COVID-19, influenza, and RSV categories with a positive laboratory test versus diagnosis code, as well as the proportion in the nonspecific category with fever (Appendix Table 2). The proportion with a positive test varied by virus and time; patients in the COVID-19 category were least likely and those in the RSV category most likely to have a positive laboratory test. Among patients in the nonspecific category, one third or fewer had evidence of fever, and most were identified by a diagnosis code. We also determined the proportion of RAVIOLI patients identified on the basis of ≥1 positive laboratory test, diagnosis code, or fever during January 2021–January 2024 (Appendix Figure 1); RAVIOLI patients can meet ≥1 criterion (e.g., have both a positive laboratory test and a diagnosis code). Diagnosis codes were the most common element contributing to identification in most weeks, followed by positive laboratory tests and fever.

Discussion

Respiratory viruses continue to impose a high burden on patients, healthcare providers, and society, and multiple pathogens, including SARS-CoV-2, influenza, RSV, and others, contribute to the burden of respiratory illnesses. Both healthcare providers and public health agencies therefore have an interest in having access to timely and granular data on

trends in respiratory viral illnesses and contributing pathogens. We developed an EHR-based algorithm for integrated surveillance of respiratory virus illness syndromes and associated pathogens using historical data to identify diagnosis codes and other characteristics of healthcare visits most predictive of confirmed respiratory viral illnesses. The RAVIOLI algorithm comprises positive laboratory tests, evidence-based diagnosis codes, and measured fever.

We have implemented RAVIOLI surveillance within the ESP automated public health surveillance platform to provide the Massachusetts Department of Public Health and participating practices with weekly reports on RAVIOLI incidence and contributing pathogens. RAVIOLI provides the department

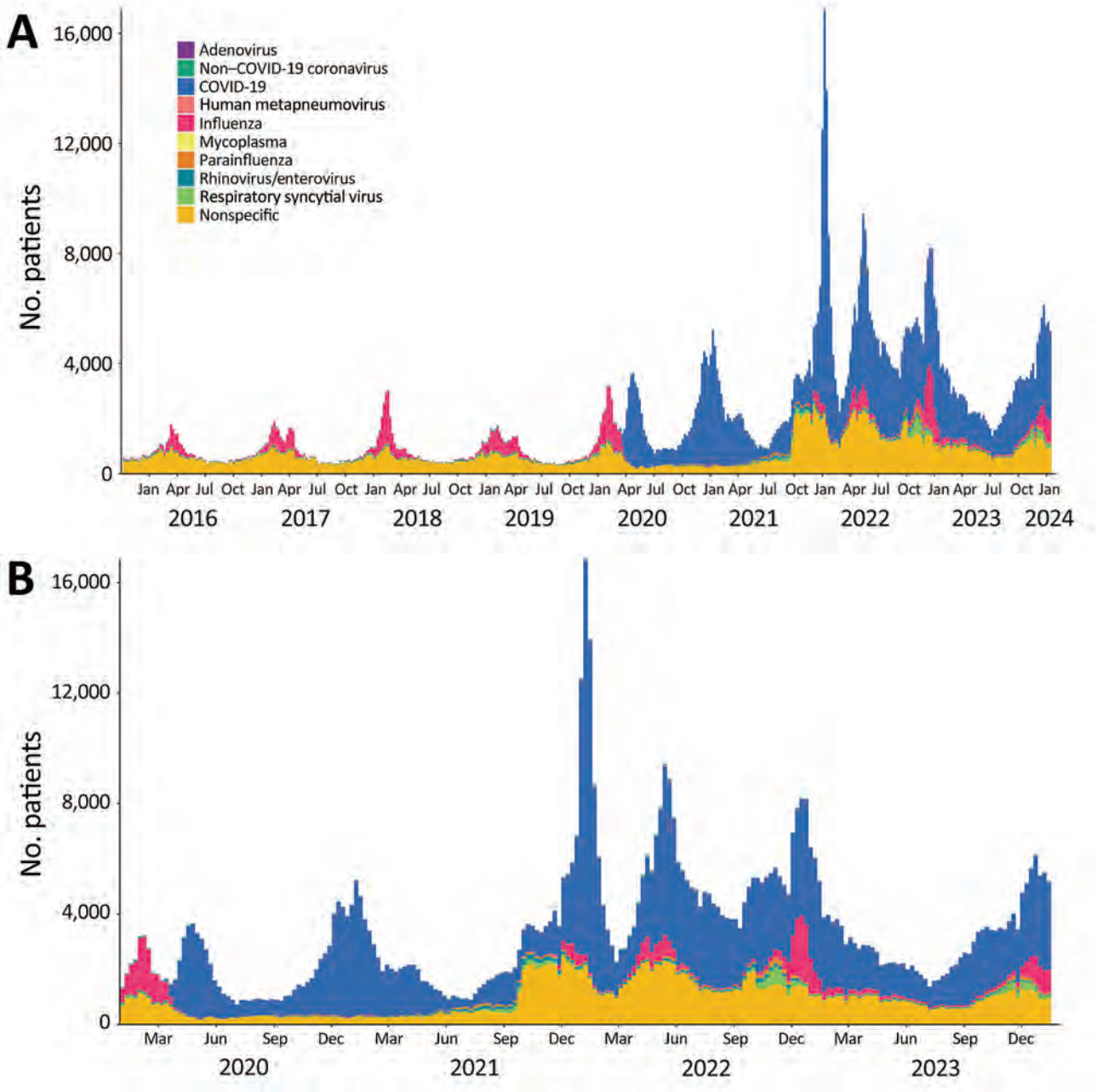

Figure 2. Numbers of patients that met the requirements for the RAVIOLI algorithm for monitoring respiratory virus–like illness, by pathogen category and week, Massachusetts, USA, October 2015–January 2024. A) October 2015–January 2024; B) January 2020–January 2024. Within each virus-specific category are counts of positive test results and diagnosis codes with a positive predictive value (PPV) ≥10% for that specific pathogen. The nonspecific category includes diagnosis codes with a PPV of ≥10% for any positive respiratory viral assay but PPV of <10% for any specific respiratory virus and includes measured fever >100°F.

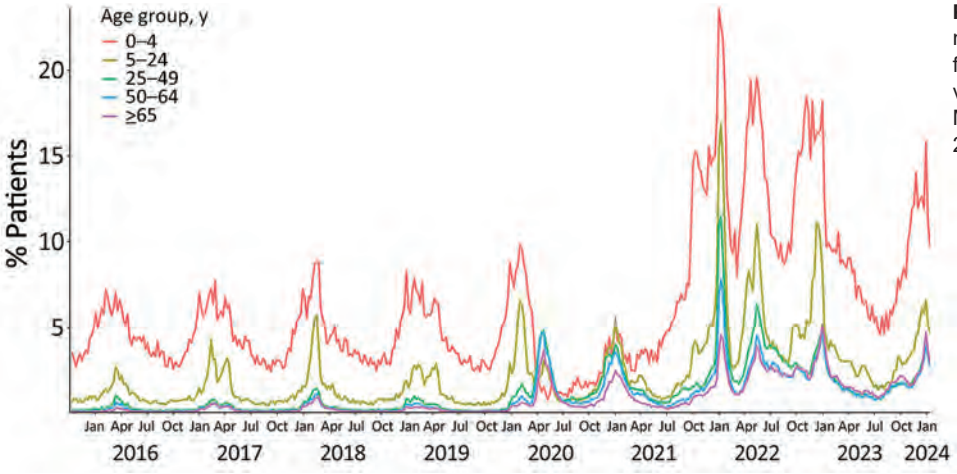

Figure 3. Percentage of patients meeting the RAVIOLI algorithm for monitoring respiratory virus–like illness, by age group, Massachusetts, USA, October 2015–January 2024.

and practices with granular insight into evolving trends in respiratory viral illness rates that both retains the best features of traditional syndromic surveillance (capacity to monitor changes in disease incidence in near real time regardless of whether persons get tested) and simultaneously broadens the scope of surveillance to include multiple pathogens, not just influenza and SARS-CoV-2. The data provide insight into the relative proportions of contributing pathogens across multiple clinical facilities using both test results and diagnosis codes to identify organisms.

When implemented well, syndromic surveillance provides a picture of the frequency, intensity, and trends in indicators of infectious and noninfectious conditions at local and extended scales. Integrating available viral pathogen test results, even if only in a subset of the population under surveillance, as we have done with the RAVIOLI algorithm, can add information about what is or is not contributing to observed increases in respiratory viral activity. Although influenza-like illness and COVID-like illness surveillance have been critical components for monitoring influenza and COVID-19 activity, reliance on fever as a required component of syndromic definitions is problematic because fever occurs only in a minority of laboratory-confirmed influenza and SARS-CoV-2 cases (*22*–*24*). Syndromic surveillance algorithms that require fever can therefore miss critical trends in the incidence of illnesses (*9*). The RAVIOLI algorithm, in contrast, does not require fever as a criterion and uses both laboratory test results and an evidence-based set of diagnosis codes to increase both sensitivity and specificity.

Limitations of RAVIOLI surveillance include its development in a single region of the country using data from just 3 practice groups. Generalizability to other practice groups and regions need to be assessed. Changes in testing practices or coding practices over time and between practices might change the future performance of the RAVIOLI algorithm. The algorithm will require periodic revalidation and possibly modification. Furthermore, the breadth of pathogen capture using the RAVIOLI algorithm depends on the range and frequency of respiratory viral testing by clinicians; greater use of multiplex testing platforms will provide more granular and robust results. RAVIOLI surveillance is limited to patients who seek care, which likely biases the data toward pathogens associated with more severe disease. The PPV of algorithm components may vary by season; whether and how this affects surveillance should be considered. We used a 10% PPV threshold to select diagnosis codes for inclusion. This threshold was arbitrary, but we found using higher thresholds dramatically reduced the number of eligible diagnosis codes. We also found that the terms associated with diagnosis codes with a PPV of ≥10% were specific in their descriptions and not indicative of broad health conditions. However, the PPV threshold for including diagnosis codes should be considered in future revalidation of the algorithm.

The healthcare site data included in developing the algorithm and whose data are part of the weekly reports came from both ambulatory and inpatient care facilities. We observed variation in which RAVIOLI categories (e.g., influenza, RSV) of the algorithm were detected at each site (data not shown). The limited number of sites makes it difficult to know if apparent differences between ambulatory and inpatient sites resulted from differences in catchment populations, illness severity

associated with different viruses, or testing platforms. As the network expands to include a greater number and variety of sites, we plan to examine this question further.

The Massachusetts Department of Public Health has used data from the underlying EHR-based system for infectious disease reporting and surveillance for more than a decade (*18*–*21*,*25*–*28*). This system has been sustained and enhanced over time to meet MDPH needs. As public health agencies consider what they need for the monitoring of current, emerging, and as-yet unidentified pathogens, we have found that a robust EHR data platform is a critical complement to traditional surveillance data.

In conclusion, we developed an integrated, routine, automated EHR-based system for respiratory virus surveillance in Massachusetts. As experience with this approach expands, the hope is that this system will provide early indications of emerging infection trends and prevailing pathogens that render a fuller picture of respiratory viral activity beyond ILI and COVID-like illnesses. A broader view of circulating pathogens will provide public health agencies and healthcare institutions with more precise information useful for informing testing guidance, optimizing health communications; developing more targeted prevention activities, including vaccination; initiating enhanced infection control measures, such as masking and posting of notices in facilities; and generating other policies optimized to minimize the effect on population health of specific circulating pathogens.

Acknowledgments

The authors thank the following colleagues for their contributions: Kelly O'Keefe, Myfanwy Callahan, Dan Flanagan, Jonathan Bress, Brian Herrick, and Michelle Weiss.

This work was supported with funding from the Massachusetts Department of Public Health.

About the Author

Dr. Cocoros is a principal research scientist at the Harvard Pilgrim Health Care Institute and a principal associate in the Department of Population Medicine. Her primary research interests include infectious disease epidemiology, pharmacoepidemiology, and the use of electronic health data for research and surveillance, from pandemic response to pragmatic trials.

References

1. Hansen CL, Chaves SS, Demont C, Viboud C. Mortality associated with influenza and respiratory syncytial virus in the US, 1999–2018. JAMA Netw Open. 2022;5:e220527. https://doi.org/10.1001/jamanetworkopen.2022.0527
2. Ackerson B, Tseng HF, Sy LS, Solano Z, Slezak J, Luo Y, et al. Severe morbidity and mortality associated with respiratory syncytial virus versus influenza infection in hospitalized older adults. Clin Infect Dis. 2019;69:197–203. https://doi.org/10.1093/cid/ciy991
3. Troeger CE, Blacker BF, Khalil IA, Zimsen SRM, Albertson SB, Abate D, et al.; GBD 2017 Influenza Collaborators. Mortality, morbidity, and hospitalisations due to influenza lower respiratory tract infections, 2017: an analysis for the Global Burden of Disease Study 2017. Lancet Respir Med. 2019;7:69–89. https://doi.org/10.1016/S2213-2600(18)30496-X
4. Centers for Disease Control and Prevention. Overview of the National Syndromic Surveillance Program [cited 2022 Aug 9]. https://www.cdc.gov/nssp/documents/NSSP-overview.pdf
5. Boehmer TK, DeVies J, Caruso E, van Santen KL, Tang S, Black CL, et al. Changing age distribution of the COVID-19 pandemic—United States, May–August 2020. MMWR Morb Mortal Wkly Rep. 2020;69:1404–9. https://doi.org/10.15585/mmwr.mm6939e1
6. Elliot AJ, Harcourt SE, Hughes HE, Loveridge P, Morbey RA, Smith S, et al. The COVID-19 pandemic: a new challenge for syndromic surveillance. Epidemiol Infect. 2020;148:e122. https://doi.org/10.1017/S0950268820001314
7. Güemes A, Ray S, Aboumerhi K, Desjardins MR, Kvit A, Corrigan AE, et al. A syndromic surveillance tool to detect anomalous clusters of COVID-19 symptoms in the United States. Sci Rep. 2021;11:4660. https://doi.org/10.1038/s41598-021-84145-5
8. Willis SJ, Eberhardt K, Randall L, DeMaria A, Brown CM, Madoff LC, et al. The evolving nature of syndromic surveillance during the COVID-19 pandemic in Massachusetts. Open Forum Infect Dis. 2021;8(Suppl 1):S695. https://doi.org/10.1093/ofid/ofab466.1401
9. Cocoros NM, Willis SJ, Eberhardt K, Morrison M, Randall LM, DeMaria A, et al. Syndromic surveillance for COVID-19, Massachusetts, February 2020–November 2022: the impact of fever and severity on algorithm performance. Public Health Rep. 2023;138:756–62. https://doi.org/10.1177/00333549231186574
10. Cohen C, Kleynhans J, Moyes J, McMorrow ML, Treurnicht FK, Hellferscee O, et al.; PHIRST group. Asymptomatic transmission and high community burden of seasonal influenza in an urban and a rural community in South Africa, 2017–18 (PHIRST): a population cohort study. Lancet Glob Health. 2021;9:e863–74. https://doi.org/10.1016/S2214-109X(21)00141-8
11. Elson W, Zambon M, de Lusignan S. Integrated respiratory surveillance after the COVID-19 pandemic. Lancet. 2022;400:1924–5. https://doi.org/10.1016/S0140-6736(22)02325-X
12. Ziegler T, Moen A, Zhang W, Cox NJ. Global Influenza Surveillance and Response System: 70 years of responding to the expected and preparing for the unexpected. Lancet. 2022; 400:981–2. https://doi.org/10.1016/S0140-6736(22)01741-X
13. Centers for Disease Control and Prevention. Automated detection and reporting of notifiable diseases using electronic medical records versus passive surveillance—Massachusetts, June 2006–July 2007. MMWR Morb Mortal Wkly Rep. 2008;57:373–6.
14. Klompas M, McVetta J, Lazarus R, Eggleston E, Haney G, Kruskal BA, et al. Integrating clinical practice and public

health surveillance using electronic medical record systems. Am J Public Health. 2012;102(Suppl 3):S325–32. https://doi.org/10.2105/AJPH.2012.300811
15. Klompas M, Cocoros NM, Menchaca JT, Erani D, Hafer E, Herrick B, et al. State and local chronic disease surveillance using electronic health record systems. Am J Public Health. 2017;107:1406–12. https://doi.org/10.2105/AJPH.2017.303874
16. Lazarus R, Klompas M, Campion FX, McNabb SJ, Hou X, Daniel J, et al. Electronic Support for Public Health: validated case finding and reporting for notifiable diseases using electronic medical data. J Am Med Inform Assoc. 2009;16:18–24. https://doi.org/10.1197/jamia.M2848
17. Vogel J, Brown JS, Land T, Platt R, Klompas M. MDPHnet: secure, distributed sharing of electronic health record data for public health surveillance, evaluation, and planning. Am J Public Health. 2014;104:2265–70. https://doi.org/10.2105/AJPH.2014.302103
18. Willis SJ, Cocoros NM, Callahan M, Herrick B, Brown CM, Kruskal BA, et al. Assessment of antibiotic prescriptions for Lyme disease after modification of reporting language for positive screening test results. JAMA Netw Open. 2022;5:e2144928. https://doi.org/10.1001/jamanetworkopen.2021.44928
19. Willis SJ, Elder H, Cocoros NM, Callahan M, Hsu KK, Klompas M. Impact of an electronic medical record best practice alert on expedited partner therapy for chlamydia infection and reinfection. Open Forum Infect Dis. 2022;9:ofab574.
20. Willis SJ, Elder H, Cocoros N, Young J, Marcus JL, Eberhardt K, et al. More screening or more disease? Gonorrhea testing and positivity patterns among men in 3 large clinical practices in Massachusetts, 2010–2017. Clin Infect Dis. 2020;71:e399–405. https://doi.org/10.1093/cid/ciaa066
21. Dee EC, Hsu KK, Kruskal BA, Menchaca JT, Zambarano B, Cocoros N, et al. Temporal patterns in chlamydia repeat testing in Massachusetts. Am J Prev Med. 2019;56:458–63. https://doi.org/10.1016/j.amepre.2018.10.006
22. Sutton D, Fuchs K, D'Alton M, Goffman D. Universal screening for SARS-CoV-2 in women admitted for delivery. N Engl J Med. 2020;382:2163–4. https://doi.org/10.1056/NEJMc2009316
23. Ma Q, Liu J, Liu Q, Kang L, Liu R, Jing W, et al. Global percentage of asymptomatic SARS-CoV-2 infections among the tested population and individuals with confirmed COVID-19 diagnosis: a systematic review and meta-analysis. JAMA Netw Open. 2021;4:e2137257. https://doi.org/10.1001/jamanetworkopen.2021.37257
24. Struyf T, Deeks JJ, Dinnes J, Takwoingi Y, Davenport C, Leeflang MM, et al.; Cochrane COVID-19 Diagnostic Test Accuracy Group. Signs and symptoms to determine if a patient presenting in primary care or hospital outpatient settings has COVID-19 disease. Cochrane Database Syst Rev. 2020;7:CD013665.
25. Elder HR, Gruber S, Willis SJ, Cocoros N, Callahan M, Flagg EW, et al. Can machine learning help identify patients at risk for recurrent sexually transmitted infections? Sex Transm Dis. 2021;48:56–62. https://doi.org/10.1097/OLQ.0000000000001264
26. Gruber S, Krakower D, Menchaca JT, Hsu K, Hawrusik R, Maro JC, et al. Using electronic health records to identify candidates for human immunodeficiency virus pre-exposure prophylaxis: an application of super learning to risk prediction when the outcome is rare. Stat Med. 2020;39:3059–73. https://doi.org/10.1002/sim.8591
27. Yih WK, Cocoros NM, Crockett M, Klompas M, Kruskal BA, Kulldorff M, et al. Automated influenza-like illness reporting—an efficient adjunct to traditional sentinel surveillance. Public Health Rep. 2014;129:55–63. https://doi.org/10.1177/003335491412900109
28. Klompas M, Haney G, Church D, Lazarus R, Hou X, Platt R. Automated identification of acute hepatitis B using electronic medical record data to facilitate public health surveillance. PLoS One. 2008;3:e2626. https://doi.org/10.1371/journal.pone.0002626

Address for correspondence: Noelle M. Cocoros, Harvard Pilgrim Health Care Institute, Department of Population Medicine, 401 Park Dr, Ste 401 East, Boston, MA 02215, USA; email: hphei.harvard.edu

Carbapenem-Resistant and Extended-Spectrum β-Lactamase–Producing Enterobacterales in Children, United States, 2016–2020

Heather N. Grome, Julian E. Grass, Nadezhda Duffy, Sandra N. Bulens, Uzma Ansari, Davina Campbell, Joseph D. Lutgring, Amy S. Gargis, Thao Masters, Alyssa G. Kent, Susannah L. McKay, Gillian Smith, Lucy E. Wilson, Elisabeth Vaeth, Bailey Evenson, Ghinwa Dumyati, Rebecca Tsay, Erin Phipps, Kristina Flores, Christopher D. Wilson, Christopher A. Czaja, Helen Johnston, Sarah J. Janelle, Ruth Lynfield, Sean O'Malley, Paula Snippes Vagnone, Meghan Maloney, Joelle Nadle, Alice Y. Guh

Medscape CME Activity

In support of improving patient care, this activity has been planned and implemented by Medscape, LLC and Emerging Infectious Diseases. Medscape, LLC is jointly accredited with commendation by the Accreditation Council for Continuing Medical Education (ACCME), the Accreditation Council for Pharmacy Education (ACPE), and the American Nurses Credentialing Center (ANCC), to provide continuing education for the healthcare team.

Medscape, LLC designates this Journal-based CME activity for a maximum of 1.00 ***AMA PRA Category 1 Credit(s)™***. Physicians should claim only the credit commensurate with the extent of their participation in the activity.

Successful completion of this CME activity, which includes participation in the evaluation component, enables the participant to earn up to 1.0 MOC points in the American Board of Internal Medicine's (ABIM) Maintenance of Certification (MOC) program. Participants will earn MOC points equivalent to the amount of CME credits claimed for the activity. It is the CME activity provider's responsibility to submit participant completion information to ACCME for the purpose of granting ABIM MOC credit.

All other clinicians completing this activity will be issued a certificate of participation. To participate in this journal CME activity: (1) review the learning objectives and author disclosures; (2) study the education content; (3) take the post-test with a 75% minimum passing score and complete the evaluation at https://www.medscape.org/qna/processor/71771?showStandAlone=true&src=prt_jcme_eid_mscpedu; and (4) view/print certificate. For CME questions, see page 1309.

NOTE: It is the policy of Medscape Education to avoid the mention of brand names or specific manufacturers in accredited educational activities. However, trade and manufacturer names related to treatments and laboratory-related information are provided in this activity in an effort to provide clarity. The use of manufacturer names should not be viewed as an endorsement by Medscape of any specific product or manufacturer.

Release date: May 22, 2024; Expiration date: May 22, 2025

Learning Objectives

Upon completion of this activity, participants will be able to:

- Distinguish the most common bacteria associated with carbapenem-resistant Enterobacterales (CRE) among US children and adolescents
- Distinguish the most common bacteria associated with extended-spectrum β--lactamase-producing Enterobacterales (ESBL-E) among US children and adolescents
- Analyze how age affects the risk for CRE and ESBL-E among children and adolescents
- Evaluate other characteristics of pediatric patients with CRE and ESBL-E in the United States

CME Editor

Amy J. Guinn, BA, MA, Technical Writer/Editor, Emerging Infectious Diseases. *Disclosure: Amy J. Guinn, BA, MA, has no relevant financial relationships.*

CME Author

Charles P. Vega, MD, Health Sciences Clinical Professor of Family Medicine, University of California, Irvine School of Medicine, Irvine, California. *Disclosure: Charles P. Vega, MD, has the following relevant financial relationships: served as a consultant or advisor for Boehringer Ingelheim; GlaxoSmithKline.*

Authors

Heather N. Grome, MD, MPH; Julian E. Grass, MPH; Nadezhda Duffy, MD, MPH; Sandra N. Bulens, MPH; Uzma Ansari, MS; Davina Campbell, MS; Joseph D. Lutgring, MD; Amy S. Gargis, PhD; Thao Masters, PhD; Alyssa G. Kent, PhD; Susannah L. McKay, PhD, MPH; Gillian Smith, MPH; Lucy E. Wilson, MD, ScM; Elisabeth Vaeth, MPH; Bailey Evenson, MHS; Ghinwa Dumyati, MD; Rebecca Tsay, MPH, MLS; Erin Phipps, DVM, MPH; Kristina Flores, PhD; Christopher D. Wilson, MD, MPH; Christopher A. Czaja, MD, DrPH; Helen Johnston, MPH; Sarah J. Janelle, MPH, CIC; Ruth Lynfield, MD; Sean O'Malley, MPH; Paula Snippes Vagnone, MT; Meghan Maloney, MPH; Joelle Nadle, MPH; Alice Y. Guh, MD, MPH.

We conducted surveillance for carbapenem-resistant Enterobacterales (CRE) during 2016–2020 at 10 US sites and extended-spectrum β-lactamase–producing Enterobacterales (ESBL-E) during 2019–2020 at 6 US sites. Among 159 CRE cases in children (median age 5 years), CRE was isolated from urine for 131 (82.4%) and blood from 20 (12.6%). Annual CRE incidence rate (cases/100,000 population) was 0.47–0.87. Among 207 ESBL-E cases in children (median age 6 years), ESBL-E was isolated from urine of 196 (94.7%) and blood of 8 (3.9%). Annual ESBL-E incidence rate was 26.5 in 2019 and 19.63 in 2020. CRE and ESBL-E rates were >2-fold higher among infants than other age groups. Most CRE and ESBL-E cases were healthcare-associated community-onset (68 [43.0%] for CRE vs. 40 [23.7%] for ESBL-E) or community-associated (43 [27.2%] for CRE vs. 109 [64.5%] for ESBL-E). Programs to detect, prevent, and treat multidrug-resistant infections must include pediatric populations (particularly the youngest) and outpatient settings.

Increasing antimicrobial resistance (AMR) remains a critical public health threat (*1*,*2*). Carbapenem-resistant Enterobacterales (CRE) have been identified as an urgent public health threat and extended-spectrum β-lactamase (ESBL)–producing Enterobacterales (ESBL-E) as a serious public health threat (*1*). Both bacteria types remain of concern because of transmissibility of the AMR genes they harbor and limited treatment options. Particularly concerning are plasmid-mediated resistance mechanisms in which genes encoding carbapenemases and ESBLs, as well as other resistance determinants, can disseminate between different organisms, thus furthering the spread of CRE and ESBL-E (*3*). Knowledge of the burden of these infections has implications for public health and the control strategies needed to prevent spread in adult and pediatric populations.

Most US studies have focused on risk factors for infection or colonization of CRE and ESBL-E in adults; national epidemiologic data for children are comparatively lacking (*4*–*9*). Moreover, attention to antimicrobial-resistant bacterial infections in children has perhaps been further disrupted by the COVID-19 pandemic, and trends have potentially worsened over the past 3 years. Few antimicrobial drugs can treat CRE and ESBL-E infections (*10*), and limited pediatric-specific clinical trials of antimicrobial drugs contribute to a scarcity of knowledge with regard to children compared with adults (*11*). A small number of studies have described the continued emergence of AMR mechanisms in US children (*12*–*16*) and identified variations in epidemiology by hospital and bacteria species across multiple pediatric medical centers (*17*–*19*). However, most studies were conducted in earlier years and were not designed to characterize the clinical and molecular features of cases identified from community and hospital settings on a population level.

The Centers for Disease Control and Prevention (CDC) Emerging Infections Program (EIP) conducts laboratory and population-based surveillance for CRE and ESBL-E in diverse US sites through the Multi-site Gram-negative Surveillance Initiative (https://www.cdc.gov/hai/eip/mugsi.html). Using those data, we focused on the descriptive and comparative epidemiology of CRE and ESBL-E, 2 of the most pressing gram-negative bacteria resistance threats, in US children.

Our study activity was reviewed by CDC, deemed not research, and was conducted consistent with applicable federal law and CDC policy (e.g., 45 C.F.R. part 46.102(l)(2), 21 C.F.R. part 56; 42 U.S.C. §241(d); 5 U.S.C. §552a; 44 U.S.C. §3501 et seq.). Similarly, the protocol was reviewed by all participating EIP sites and either was deemed nonresearch or received institutional review board approval with a waiver of informed consent.

Methods

Surveillance Population

As of 2016, county-level CRE surveillance was conducted in selected US metropolitan counties at 8 EIP

Author affiliations: Centers for Disease Control and Prevention, Atlanta, Georgia, USA (H.N. Grome, J.E. Grass, N. Duffy, S.N. Bulens, U. Ansari, D. Campbell, J.D. Lutgring, A.S. Gargis, T. Masters, A.G. Kent, S.L. McKay, A.Y. Guh); Foundation for Atlanta Veterans Education and Research, Decatur, Georgia, USA (G. Smith); Atlanta Veterans Affairs Medical Center, Decatur (G. Smith); Maryland Department of Health, Baltimore, Maryland, USA (L.E. Wilson, E. Vaeth, B. Evenson); New York Rochester Emerging Infections Program at the University of Rochester Medical Center, Rochester, New York, USA (G. Dumyati, R. Tsay); University of New Mexico, Albuquerque, New Mexico, USA (E. Phipps, K. Flores); New Mexico Emerging Infections Program, Santa Fe, New Mexico, USA (E. Phipps, K. Flores); Tennessee Department of Health, Nashville, Tennessee, USA (C.D. Wilson); Colorado Department of Public Health and Environment, Denver, Colorado, USA (C.A. Czaja, H. Johnston, S.J. Janelle); Minnesota Department of Health, St. Paul, Minnesota, USA (R. Lynfield, S. O'Malley, P. Snippes Vagnone); Connecticut Department of Public Health, Hartford, Connecticut, USA (M. Maloney); California Emerging Infections Program, Oakland, California, USA (J. Nadle)

DOI: https://doi.org/10.3201/eid3006.231734

sites (Colorado, Georgia, Maryland, Minnesota, New Mexico, New York, Oregon, Tennessee); surveillance subsequently expanded to 2 additional sites (California in 2017 and Connecticut statewide in 2018) (*20*). The total population of the 10 participating areas under surveillance in 2020 was an estimated 23.2 million, of which an estimated 4.9 million were children (*21*).

County-level ESBL-E surveillance started in July 2019 in selected counties at 6 EIP sites (Colorado, Georgia, Maryland, New Mexico, New York, Tennessee). The total population of the 6 participating areas under surveillance in 2020 was an estimated 3.0 million, of which an estimated 626,000 were children (*21*) (Appendix, https://wwwnc.cdc.gov/EID/article/30/6/23-1734-App1.pdf).

Case Definitions and Data Collection

Beginning in 2016, we defined an incident pediatric CRE case as the first isolation during a 30-day period of *Klebsiella pneumoniae*, *K. oxytoca*, *K. aerogenes*, *Enterobacter cloacae* complex, or *Escherichia coli* resistant to ≥1 carbapenem (imipenem, meropenem, doripenem, ertapenem) from a normally sterile body site (Appendix) or urine specimen from a surveillance area resident <18 years of age. We defined an incident pediatric ESBL-E case as the first isolation during a 30-day period of *E. coli*, *K. pneumoniae*, *K. variicola*, or *K. oxytoca* resistant to ≥1 extended-spectrum cephalosporin (ceftazidime, cefotaxime, or ceftriaxone) and nonresistant (i.e., susceptible or intermediate) to all tested carbapenems from a normally sterile body site or urine specimen from a surveillance area resident <18 years of age. To prevent duplication with CRE surveillance, we excluded ESBL-E isolates that were carbapenem resistant. For both ESBL-E and CRE, if a new specimen meeting the case definition was collected >30 days after the patient's last incident case with the same organism, it was also reported as an incident case. CRE and ESBL-E cases were identified through a query of automated testing instruments based on laboratory protocols (Appendix).

All incident CRE cases, as well as all incident ESBL-E cases from a sterile source, underwent medical record review by using a standardized case report form to collect patient demographics, underlying conditions, healthcare exposures and outcomes, location of specimen collection, associated infection types, and antimicrobial susceptibility testing results (*20*) (Appendix). For ESBL-E cases identified from urine sources, for each year, first incident cases per species in a patient were reviewed.

Cases were considered hospital onset if the incident culture was collected >3 days after hospital admission. All other cases were considered community onset and further classified as either 1) healthcare-associated if the person had hospitalization, surgery, residence in a long-term care facility or long-term care acute care hospital, or chronic dialysis in the year before culture or had an indwelling device in the 2 days before culture; or 2) community-associated if none of those risk factors were identified.

Isolate Collection

We submitted a convenience sample of isolates from all EIP sites to CDC for confirmatory and molecular characterization. CRE and ESBL-E isolates underwent species identification by matrix-assisted laser desorption/ionization time-of-flight mass spectrometry (MALDI-TOF Biotyper 3.1; Bruker Daltronics, https://www.bruker.com). We conducted antimicrobial susceptibility testing of CRE isolates by using reference broth microdilution with a metallo-β-lactamase screen (*22*,*23*), screening for carbapenemases by using the modified carbapenem inactivation method (*24*), and real-time PCR testing for bla_{KPC}, bla_{NDM}, bla_{VIM}, bla_{IMP}, and $bla_{OXA\text{-}48\text{-}like}$ genes (*25*–*28*). If a CRE isolate harbored a carbapenemase-producing gene according to PCR, it was classified as carbapenemase producing (CP). We used real-time PCR to screen all isolates with a colistin MIC ≥2 μg/mL for plasmid-mediated colistin resistance genes (*mcr*-1 and *mcr*-2) (*29*). We conducted antimicrobial susceptibility testing of ESBL-E by using reference broth microdilution and performed phenotypic screening for ESBL production with ceftazidime and cefotaxime alone and in combination with clavulanate (*24*). We conducted whole-genome sequencing on a subset of CRE isolates from 2016–2018 that were confirmed to be carbapenem resistant and on the subset of ESBL isolates received from CDC (Appendix).

Statistical Analyses

We calculated crude incidence rates by using case counts and 2016–2020 US Census estimates of the surveillance area population <18 years of age. For incidence rates presented by region, demographics, or age group, denominators represent the pediatric population also stratified by that subgroup. Analysis was limited to case report forms completed as of November 29, 2022. We performed descriptive and comparative analyses for CRE and ESBL-E cases by using the χ^2 test or the Fisher exact test (where applicable) for categorical variables and the Wilcoxon rank sum test for continuous variables. We used SAS version 9.4 (SAS Institute Inc, https://www.sas.com) to conduct data analyses.

Results

Cases and Incidence Rates

During 2016–2020, a total of 159 incident CRE cases were identified in 142 children across 10 EIP sites. Of the 159 cases, 83 (52.2%) isolates were *E. cloacae* complex, 50 (31.5%) *E. coli*, 17 (10.7%) *K. pneumoniae*, 5 (3.1%) *K. aerogenes*, and 4 (2.5%) *K. oxytoca* (Table 1). The number of CRE cases per EIP site ranged from 3 to 47. *E. coli* comprised half or most of the CRE cases in New Mexico (50.0%), Tennessee (71.4%), and California (85.7%), whereas *E. cloacae* complex were the most common organisms at the other sites (44.4%–71.4%). Of the 142 unique persons with CRE, during the 5-year surveillance period ≥2 incident cultures were obtained from 17 (12.0%) (range 2–6 episodes).

During 2019–2020, a total of 207 incident ESBL-E cases were identified in 184 children across the 6 participating EIP sites. Of the 207 cases, 182 (87.9%) isolates were *E. coli*, 23 (11.1%) *K. pneumoniae*, and 2 (1.0%) *K. oxytoca* (Table 1). The number of ESBL-E cases per EIP site ranged from 14 to 57 cases; at all 6 sites, the predominant organism was *E. coli* (82.5%–100.0%). Of the 184 unique persons with ESBL-E, during the 1.5-year surveillance period, ≥2 incident cultures were obtained from 23 (12.5%) (range 2–4 episodes).

The overall annual CRE incidence rate (cases/100,000 pediatric population) across EIP sites during the 5-year period was 0.70 (range 0.47–0.87). The overall annual ESBL-E incidence rate during the 1.5-year period was 23.08, decreasing from 26.54 in 2019 to 19.63 in 2020. Crude incidence rates for CRE and ESBL-E varied by geographic region and year (Table 2).

During 2016–2020, annual incidence rates for infants (children <1 year of age) were consistently higher than those for other age groups, ranging from 1.95 to 3.82 cases/100,000 pediatric population for CRE and 46.85 to 91.97 cases/100,000 pediatric population for ESBL-E (Figure 1). In addition, crude annual incidence rates for CRE and ESBL-E were nearly always higher for female than male children (Table 2), except in the youngest age group. During 2016–2020, average annual crude incidence rates for CRE cases were higher for male than for female children <1 year of age (3.38 vs. 2.35 cases/100,000 pediatric population).

Demographics and Clinical Characteristics

Of 159 CRE cases, 94 (59.1%) were in girls (Table 3), compared with 49.1% of the overall pediatric population. Median age was 5 (interquartile range [IQR] 1–10) years; 4 (2.5%) children were <1 month of age and 31 (19.5%) were 1–12 months of age (compared with 5.4% of the population <1 year of age). Most children with CRE were White (79 [50.0%]) and non-Hispanic (86 [54.1%]). Similarly, of 207 ESBL-E cases, most were in girls (165 [79.7%] compared with 49.1% of the overall pediatric population), White (92 [44.4%]), and non-Hispanic (96 [46.4%]). The median age was 6 (IQR 2–15) years; 3 (1.5%) children were <1 month of age, and 27 (13.0%) were 1–12 months of age (compared with 5.1% of the population <1 year of age).

Clinical characteristics were available for 158 CRE and 169 ESBL-E cases with completed case report forms (Table 3). Of those, a greater proportion of children with CRE than ESBL-E had a history of premature birth (20 [12.7%] vs. 11 [6.5%] among those with

Table 1. Incident CRE and ESBL-E cases in children, by organism, United States*

	Incident CRE cases, 2016–2020						Incident ESBL-E cases, 2019–2020†		
				No. (%) carbapenemase genes‡					
Organism	No. (%) cases	Isolates submitted for carbapenemase testing, no.	No. (%) CP isolates‡	*bla*$_{KPC}$	*bla*$_{NDM}$	*bla*$_{OXA-48}$-like	No. (%) cases	No. isolates submitted for ESBL testing	No. (%) ESBL-producing organisms§
Escherichia coli	50 (31.5)	26	5 (19.2)	0	2 (7.7)	3 (11.5)	182 (87.9)	16	15 (93.8)
Enterobacter cloacae complex	83 (52.2)	47	1 (2.1)	1 (2.1)	0	0	NA	NA	NA
Klebsiella aerogenes	5 (3.1)	4	1 (25.5)	0	1 (25.0)	0	NA	NA	NA
K. oxytoca	4 (2.5)	1	1 (100.0)	1 (100)	0	0	2 (1.0)	NA	NA
K. pneumoniae	17 (10.7)	8	1 (12.5)	0	1 (12.5)	0	23 (11.1)	3	3 (100.0)
Total	159	86	9 (10.5)	2 (2.3)	4 (4.7)	3 (3.5)	207	19	18 (94.7)

*All incident pediatric cases with available case report form data as of November 28, 2022, were included in this analysis. CP, carbapenemase-producing; CRE, carbapenem-resistant Enterobacterales; ESBL-E, extended-spectrum β-lactamase–producing Enterobacterales; NA, not applicable (no organisms tested; ESBL-E surveillance included *Escherichia coli, Klebsiella oxytoca, Klebsiella pneumoniae*).

†ESBL-E surveillance began in July 2019 at all participating sites. California, Connecticut, Minnesota, and Oregon do not participate in ESBL-E surveillance.

‡Percentages shown are of isolates submitted. Carbapenemases and colistin resistance genes not listed in the table were not detected for any isolates.

§Percentages shown are of isolates submitted. Phenotypic screening for ESBL-E production was performed by using ceftazidime and cefotaxime alone and in combination with clavulanate according to Clinical and Laboratory Standards Institute guidelines (*24*).

Table 2. Incident pediatric CRE and ESBL-E cases with annual crude incidence, by geographic regions and demographic characteristics, United States*

	Crude annual incidence rate						
	Incident CRE cases					Incident ESBL-E cases	
Category	2016	2017	2018	2019	2020	2019‡	2020
EIP sites by geographic region†							
Northeast	0.63	0.00	1.24	0.91	1.38	26.15	24.39
Midwest	1.25	0.74	0.25	0.99	0.99	NA	NA
South	0.82	0.55	0.71	1.05	0.44	26.30	16.57
West	0.86	0.37	0.48	0.64	0.38	27.15	20.15
Total	0.87	0.47	0.68	0.87	0.63	26.54	19.63
Demographic characteristics							
Sex§							
M	0.44	0.32	0.75	0.67	0.52	13.04	6.28
F	1.26	0.62	0.61	1.07	0.74	39.89	33.43
Race							
White	0.68	0.31	0.55	0.78	0.50	23.85	13.96
Black	0.57	0.32	0.57	1.05	0.38	12.79	5.92
Other¶	0.41	0.26	0.35	0.24	0.56	20.26	12.29

*Crude annual incidence rate, cases/100,000 pediatric population. CRE, carbapenem-resistant Enterobacterales; EIP, Emerging Infections Program; ESBL-E, extended-spectrum β-lactamase–producing Enterobacterales; NA, not applicable.
†EIP sites grouped according to the 4 geographic regions defined by the US Census Bureau because of small case counts at some sites. California did not participate in CRE surveillance in 2016. Connecticut did not participate in CRE surveillance in 2016 or 2017. California, Connecticut, Minnesota, and Oregon do not participate in ESBL-E surveillance.
‡ESBL-E surveillance was completed for 6 months during 2019. Crude annual incidence rates estimated as the number of cases multiplied by 2 divided by population based on 2019 US Census for that year.
§One CRE and 1 ESBL-E case had sex reported as unknown.
¶Other represents all reported races not indicated as White or Black, including American Indian or Alaska Native, Asian, Native Hawaiian or other Pacific Islander, or some other race. This combination category was necessary because of small numbers of pediatric cases in persons of races other than White or Black. In addition, 37 CRE cases and 74 ESBL-E cases had race indicated as unknown (not included in this category).

term birth; p = 0.06) and any underlying condition (99 [62.7%] vs. 59 [34.9%] p<0.01).

Culture Sources and Associated Infection Types

For most CRE and ESBL-E cases, including those in children <1 year of age, organisms were isolated from urine (131 [82.4%] from CRE cases and 196 [94.7%] from ESBL-E cases) (Table 4). Accordingly, the most common reported infection type was lower urinary tract infection (89 [56.3%] for CRE and 125 [74.0%] for ESBL-E). For CRE and ESBL-E cases, the greatest number of isolates were collected in an emergency department or outpatient setting (108 [68.4%] for CRE and 154 [91.1%] for ESBL-E), although CRE cases were more likely than ESBL-E cases to be hospital onset (40 [25.3%] vs. 13 [7.7%]; p<0.01) (Table 3). Healthcare-associated community onset (68 [43.0%] CRE vs. 40 [23.7%] ESBL-E) and community-associated (43 [27.2%] CRE vs. 109 [64.5%] ESBL-E) represented most CRE and ESBL-E cases.

Healthcare Exposures and Outcomes

Among cases with available case report form data, a greater proportion of children with CRE than ESBL-E underwent acute care hospitalization (74 [46.8%] CRE vs 38 [22.5%] ESBL-E; p<0.01) or surgery (61 [38.6%] CRE vs. 16 [9.5%] ESBL-E; p<0.01) within 1 year before specimen collection (Table 4). In the 2 days before specimen collection, CRE cases were also more likely than ESBL-E cases to have a central venous catheter (37 [23.4%] CRE vs. 12 [7.1%] ESBL-E; p<0.01) or other indwelling device (excluding urinary catheter) (60 [38.0%] CRE vs. 19 [11.2%] ESBL-E; p<0.01). ESBL-E cases were significantly more likely than CRE cases to have no reported healthcare exposures (110 [65.1%] vs. 43 [27.2%]; p<0.01). Among ESBL-E cases, antimicrobial use was documented in the 30 days before date of incident specimen collection for 52 (31.8%).

Hospitalization at the time of or within 30 days of specimen collection was required for a greater proportion of community-onset CRE (40 [36.0%]) versus ESBL-E (13 [8.7%]) cases (p<0.01). Median duration of admission among all hospitalized community-onset and hospital-onset cases was 18 days (IQR 3–103 days) for those with CRE versus 10 days (IQR 4–43 days) for those with ESBL-E (p = 0.34).

Isolate Testing

The antimicrobial resistance profiles of incident CRE and ESBL-E cases from local clinical laboratories are shown elsewhere (Appendix Table 1). Among the 86 CRE isolates submitted for carbapenemase testing, 9 (10.5%) isolates from 6 of the 10 EIP sites harbored a carbapenemase: 4 bla_{NDM}, 3 bla_{OXA-48}-like, and 2 bla_{KPC} (Table 1). Distribution of CP-CRE varied by organism. The 9 CP-CRE isolates were from 9 children, fewer than half of whom were 1–3 years of age (3 [15.8%]) and 4–9 years of age (3 [13.0%]); 6 (18.8%) were from

children with no reported underlying conditions (Appendix Table 2). The most common source was urine (8 CP-CRE isolates, 11.6% of submitted). Among the 11 CRE isolates from 2016–2018 that were sequenced, identified multilocus sequence types (STs) were diverse (Appendix Table 3); 2 of 11 isolates harbored CP genes. Separately, of the 7 ESBL-E organisms that underwent whole-genome sequencing at CDC, 6 were *E. coli*; ST131 and potential acquired ESBL gene $bla_{\text{CTX-M-15}}$ were most common (Appendix Table 4).

Discussion

Over a 5-year surveillance period, 159 incident pediatric CRE cases were reported across 10 EIP sites (representing >4 million children), resulting in an overall crude incidence of 0.70 cases/100,000 pediatric population. The CRE case estimate is lower than the 207 incident pediatric ESBL-E cases identified over 1.5 years across 6 EIP sites (>600,000 children), which corresponds to an average crude incidence of 23.08 cases/100,000 pediatric population. The burden of infections was higher among girls than boys, more were detected in urine than in sterile site cultures, and incidence was disproportionately high among children <1 year of age. We found variation in rates of infections by year, geographic region, and species and in the percentages of CRE organisms that produced carbapenemases.

Similar to findings of other studies (*17*,*30*), in our study, *E. coli* accounted for many resistant isolates and represented most ESBL-E species identified. Of note, *E. cloacae* complex comprised most of the incident CRE cases. Our finding differs from that of another large, nationally representative pediatric study conducted during 1999–2012 (*30*), in which the most common organisms identified were *E. coli* and *Proteus mirabilis*. It also differs from that of an earlier EIP study of adult CRE cases conducted during 2012–2013, in which *K. pneumoniae* accounted for most CRE cases identified (*5*). The previous EIP study used a different case definition that was more specific for carbapenemase-producing CRE (i.e., excluded ertapenem and required carbapenem nonsusceptibility and third-generation cephalosporin resistance) and thus may have excluded certain species that are less likely to produce carbapenemases, probably affecting the comparison to the cases in our study (*31*). From our sample of 47 pediatric CR–*E. cloacae* complex isolates submitted for carbapenemase testing, only 1 was confirmed to be a carbapenemase producer (bla_{KPC}). Thus, the variability in species predominance and limited number of carbapenemase genes identified in our study may result from differences in case definition.

Most CRE and ESBL-E cases in our study were healthcare-associated infections with community onset or were community-associated infections. Strikingly, nearly 65% of the ESBL-E cases were reported to be community associated, and patients had no reported history of healthcare exposure. In addition, most cases of CRE and ESBL-E were detected from cultures collected outside an acute care hospital, a finding that differs from previous studies reporting pediatric CRE infections more commonly isolated from hospitalized patients (*30*). The most common source of CRE and ESBL-E in this study was urine

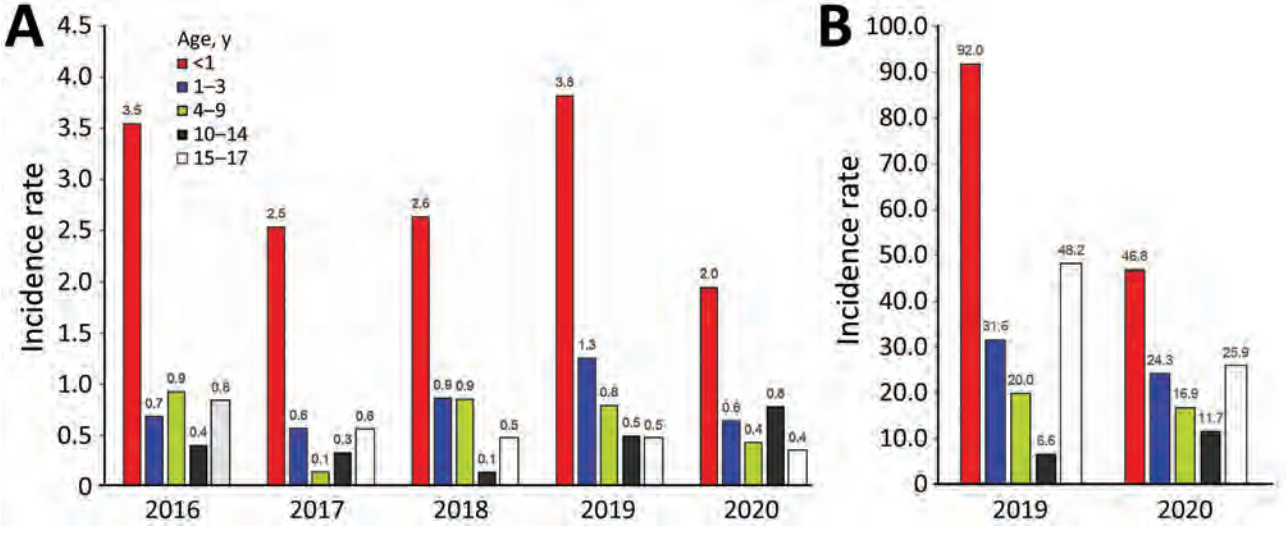

Figure. Annual crude incidence rates (cases/100,000 pediatric population) for incident pediatric carbapenem-resistant Enterobacterales (A) and extended-spectrum β-lactamase–producing Enterobacterales (B) cases, by age group, United States, 2016–2020. Incidence rate denominators are also stratified by age group.

Table 3. Demographic and clinical characteristics of children with incident CRE and ESBL-E cases, United States*

Characteristic	CRE, 2016–2020	ESBL-E, 2019–2020†	p value
Demographic	n = 159	n = 207	
Sex			**<0.01**
F	94 (59.1)	165 (79.7)	
M	64 (40.3)	41 (19.8)	
Unknown	1 (0.6)	1 (0.5)	
Age group, y			**<0.01**
Median, IQR	5 (1–10)	6 (2–15)	
<1	35 (22.0)	30 (14.5)	
1–3	30 (18.9)	40 (19.3)	
4–9	47 (29.6)	56 (27.1)	
10–14	28 (17.6)	27 (13.0)	
15–17	19 (12.0)	54 (26.1)	
Race			0.62
White	79 (50.0)	92 (44.4)	
Black	29 (18.2)	25 (12.1)	
Other	14 (8.8)	16 (7.7)	
Unknown	37 (23.3)	74 (35.8)	
Ethnicity			0.89
Hispanic	43 (27.0)	45 (21.7)	
Non-Hispanic	86 (54.1)	96 (46.4)	
Unknown	30 (18.9)	66 (31.9)	
Clinical‡			
Underlying conditions§	n = 158	n = 169	
Premature birth	20 (12.7)	11 (6.5)	0.06
Diabetes mellitus	0	2 (1.2)	0.27
Neurologic condition, any	34 (21.5)	20 (11.8)	**0.02**
Urinary tract problems/abnormalities	42 (26.6)	22 (13.0)	**<0.01**
Cardiovascular disease	13 (8.2)	3 (1.8)	**<0.01**
Chronic pulmonary disease	25 (15.8)	21 (12.4)	0.38
Chronic renal disease	24 (15.2)	3 (1.8)	**<0.01**
Gastrointestinal disease	3 (1.9)	1 (0.6)	0.23
Skin condition	12 (7.6)	8 (4.3)	0.28
Malignancy (hematologic or solid organ)	10 (6.3)	2 (1.2)	**<0.01**
Transplant (hematopoietic stem cell or solid organ)	15 (9.5)	1 (0.6)	**<0.01**
None	59 (37.3)	110 (65.1)	**<0.01**
Any condition	99 (62.7)	59 (34.9)	**<0.01**
Epidemiologic classification of incident cases			
Hospital onset	40 (25.3)	13 (7.7)	**<0.01**
Community-associated	43 (27.2)	109 (64.5)	**<0.01**
Healthcare-associated community onset	68 (43.0)	40 (23.7)	**<0.01**
Unknown	7 (4.4)	7 (4.1)	0.90

*Values are no. (%) except as indicated. Fisher exact test used for comparative statistics when >20% of expected cell counts were <5. Boldface indicates p<0.05. CRE, carbapenem-resistant Enterobacterales; ESBL-E, extended-spectrum β-lactamase–producing Enterobacterales.
†ESBL-E surveillance was completed for 6 months during 2019.
‡Clinical characteristics were available for cases with completed case report forms only.
§Cases could have >1 underlying condition associated with culture. Underlying conditions are further defined as follows: premature birth, birth before the week 37 of pregnancy, selected if medical record indicated premature birth and patient was <2 y of age; diabetes mellitus, includes both type I and type II; neurologic condition, any, includes cerebral palsy, chronic cognitive deficits, epilepsy/seizure/seizure disorders, multiple sclerosis, neuropathy, and others; urinary tract problems/abnormalities, a structural or functional urinary tract abnormality leading to obstruction or retention of urine as documented in the medical record; cardiovascular disease, includes congenital heart disease, congestive heart failure, prior cerebrovascular accident/stroke, peripheral vascular disease; chronic pulmonary disease, includes cystic fibrosis and any chronic respiratory condition resulting in chronic symptomatic dyspnea in medical record; chronic renal disease, includes chronic kidney disease (all stages), end-stage renal disease with or without dialysis; gastrointestinal disease, includes inflammatory bowel disease, liver disease, peptic ulcer disease, and short gut syndrome; skin condition, includes pressure ulcers, surgical wounds, other skin conditions such as eczema, psoriasis; malignancy, includes hematologic, metastatic and nonmetastatic solid organ; transplant, includes hematopoietic stem cell and solid organ.

(and lower urinary tract infections), which probably contributed to the high proportion of cases collected in outpatient settings. Increasing prevalence of community-associated ESBL-E urinary tract infections has been noted across patients of all ages (*32*,*33*). Our findings highlight a similar shift in the clinical epidemiology of multidrug-resistant infections in children, supported by a rising trend in community-acquired ESBL-E causing urinary tract infections in children (*34*). Continued implementation of national programs to detect, prevent, and treat multidrug-resistant infections must increasingly include pediatric populations and outpatient settings.

Although incidence of CRE was lower than that of ESBL-E, children with CRE infection were generally hospitalized for longer durations, and rates of intensive care unit admission were higher. Children with CRE infection were also more likely to have ≥1 underlying

condition and prior healthcare exposure. Meropol et al. (*19*) and Logan et al. (*30*) also reported higher proportions of underlying conditions in children with multidrug-resistant gram-negative infections. However, our direct comparison of CRE and ESBL-E epidemiology revealed statistically significant clinical differences even among children with multidrug-resistant gram-negative infections. We also observed the proportion of CRE and ESBL-E in patients with no underlying conditions to be markedly higher than that found in previous studies focused on adult populations with those infections (*5*,*9*).

CRE incidence rates fluctuated by region throughout the study period, partly reflecting variation in the small number of cases occurring on a yearly basis. Separately, the overall incidence of ESBL-E clearly decreased during 2020. That finding contrasts with reports of increased rates of ESBL-E infections among hospitalized patients, primarily adults, in 2020 (*2*). Our data were unadjusted and included nonhospitalized

Table 4. Isolate culture source, collection location, and infection types among incident pediatric CRE and ESBL-E cases, United States*

Category	CRE, 2016–2020	ESBL-E, 2019–2020†	p value
Culture source	n = 159	n = 207	
Urine‡	131 (82.4)	196 (94.7)	**<0.01**
Blood	20 (12.6)	8 (3.9)	**<0.01**
Other normally sterile site	8 (5.0)	3 (1.5)	**0.05**
Isolate collection location§	n = 158	n = 169	
Acute care hospital	49 (31.0)	15 (8.9)	**<0.01**
Outside acute care hospital	108 (68.4)	154 (91.1)	**<0.01**
Emergency department	16/108 (14.8)	0	**<0.01**
Outpatient setting	92/108 (85.2)	154/154 (100.0)	**<0.01**
Long-term care facility	0	0	NA
Long-term acute care facility	0	0	NA
Unknown	1 (0.6)	0	0.48
Infection types¶			
Lower urinary tract infection#	89 (56.3)	125 (74.0)	**<0.01**
Pyelonephritis	9 (5.7)	9 (5.3)	0.88
Bacteremia**	20 (12.7)	9 (5.3)	**0.02**
Other infection types	27 (17.1)	14 (8.3)	**0.02**
None	21 (13.3)	19 (11.2)	0.57
Unknown	9 (5.7)	8 (4.7)	0.70
Healthcare exposures in prior year			
Acute care hospitalization	74 (46.8)	38 (22.5)	**<0.01**
Resident of long-term care facility	0	2 (1.2)	0.27
Admission to long-term acute care hospital	0	0	NA
Inpatient or outpatient surgery††	61 (38.6)	16 (9.5)	**<0.01**
Chronic dialysis	5 (3.2)	0	**0.03**
Indwelling device in the 2 d before DISC			
Urinary catheter	29 (18.4)	20 (11.8)	0.10
Central venous catheter	37 (23.4)	12 (7.1)	**<0.01**
Any other device	60 (38.0)	19 (11.2)	**<0.01**
IV or oral antimicrobial use 30 d before DISC‡‡	N/A	52 (30.8)	N/A
None of the above healthcare exposures	43 (27.2)	110 (65.1)	**<0.01**
Outcomes, no. patients			
Hospitalization among community-onset cases§§	40/111 (36.0)	13/149 (8.7)	**<0.01**
ICU admission ≤6 d after DISC	10 (6.3)	5 (3.0)	0.15
30-d mortality			
Cases with an incident blood or sterile site specimen	4/27 (14.8)	2/9 (22.2)	0.29
Cases with an incident urine specimen	2/131 (1.5)	0	0.23

*Values are no. (%) except as indicated. Denominators are indicated when different from total number. Fisher exact test used for comparative statistics when >20% of expected cell counts were <5. Boldface indicates p<0.05. CRE, carbapenem-resistant Enterobacterales; DISC, date of incident specimen collection; ESBL-E, extended-spectrum β-lactamase–producing Enterobacterales; IV, intravenous.
†ESBL-E surveillance was completed for 6 mo during 2019.
‡Two incident urine CRE cases with subsequent nonincident blood cultures were identified. One incident urine ESBL-E case with subsequent nonincident blood culture was identified. Nonincident blood cultures are not counted here.
§Isolate collection location, epidemiologic class, infection types available for cases with completed case report forms only.
¶Cases could have >1 type of associated infection reported.
#Lower urinary tract infection includes cases involving infection of the bladder or urethra. Pyelonephritis, or infections involving the kidney(s), were counted separately.
**Bacteremia includes cases with a positive blood specimen or a documented diagnosis of sepsis, septicemia, bacteremia, or blood stream infection. 3 CRE cases of sepsis and 2 ESBL-E cases of sepsis (with or without blood cultures) are included in the bacteremia classification above.
††Surgery defined as procedures occurring in an operating room where a surgeon makes ≥1 incision through skin or mucous membrane, including laparoscopic approach. Ambulatory surgery centers may be included.
‡‡Antimicrobial use (intravenous or oral) in 30 d before DISC collected for ESBL-E cases only.
§§Hospitalization at time of or within 30 d after DISC.

patients, and it is possible that declines in outpatient healthcare use during the pandemic may have affected rates of ESBL-E among children. In addition, our data represent only mid-2019 through 2020, making the decline more difficult to interpret.

We also found annual CRE and ESBL-E incidence rates to be higher for female children and infants (most >1 month of age) compared with other age groups. We suspect that rates of antimicrobial-resistant infections were higher among girls in part because of increased testing in those populations resulting from a higher number of baseline urinary tract infections. The epidemiology among infants may differ from that among the overall pediatric population because of risk factors associated with infection acquired in neonatal intensive care units (*35*–*37*), vertical transmission (*38*,*39*), and higher rates of fecal colonization with antimicrobial-resistant *Enterobacteriaceae* (*40*). Recent evidence highlights how the human microbiome undergoes marked developmental progression over the first 2 years of life (*41*). Consistent with such a maturation process, Darda et al. observed spontaneous decolonization within 12 months among all neonates colonized with carbapenem-resistant gram-negative bacteria (*42*). Nonetheless, even when limited to prenatal and intrapartum exposures, antimicrobial drugs can profoundly affect the infant microbiome, involving expansion of gram-negative populations (proteobacteria) and supporting our observation of differences in the epidemiology among infants (*43*). A more focused look at that age group may be noteworthy for future studies.

Among the several limitations inherent in the use of surveillance systems, the case definitions for CRE and ESBL-E relied on susceptibility testing performed locally, and methods varied across laboratories. In addition, automated testing instruments at clinical laboratories may be more likely than other test methods to overdiagnose CRE. Second, data were retrospectively abstracted from medical records, and the quality of medical record documentation can vary between healthcare system and facility types, resulting in differences in reporting for some data elements. In addition, medical records were reviewed for the child only, and no maternal information was included in chart review, which may have limited identification of household risk factors (e.g., international travel by family, previously established as a risk factor for CRE and ESBL-E). Separately, because ≈97% of the incident ESBL-E cases from 1 site in 2020 did not have a case report form completed, no data beyond the clinical laboratory report were available. Third, isolate collection represents a convenience sample and may not be representative of all cases. In addition, we have limited data on STs because not all isolates submitted to CDC were sequenced. Fourth, we acknowledge that data for ESBL-E in our study are limited to 1.5 years and collected from fewer sites than surveillance data for CRE. Last, although the surveillance system includes geographically diverse catchment areas, it is not designed to be representative of the entire US pediatric population.

In summary, we found that CRE infections occurred less frequently than ESBL-E infections among US children but were more often associated with healthcare risk factors and hospitalization. Despite annual and geographic variation in the incidence of CRE and ESBL-E, the rate of infection for both pathogens was consistently highest among infants. Our descriptive data about major antimicrobial-resistant pathogens among children support continued infection prevention and control practices and antimicrobial stewardship in pediatric healthcare settings, particularly for patients in the youngest age group.

Acknowledgments

We thank Medora Witwer, Annastasia Gross, Laura Tourdot, Melissa Anacker, Jennifer Dale, and the Genomic Sequencing Laboratory of the Biotechnology Core Facility Branch, Division of Scientific Resources, National Center for Emerging and Zoonotic Infectious Diseases, CDC, for their contributions to this work.

This work was supported by the CDC EIP, CDC-RFA-CK17-1701.

R.L. is an associate editor for the American Academy of Pediatrics Red Book. All other authors report no conflicts of interest.

About the Author

Dr. Grome is an infectious diseases physician and medical officer in the Division of Healthcare Quality Promotion, National Center for Emerging and Zoonotic Infectious Diseases, CDC. Her current research includes work through CDC Healthcare-Associated Infections–Community Interface activities within EIP.

References

1. Centers for Disease Control and Prevention. Antibiotic resistance threats in the United States, 2019 [cited 2024 Apr 22]. https://www.cdc.gov/drugresistance/pdf/threats-report/2019-ar-threats-report-508.pdf
2. Centers for Disease Control and Prevention. COVID-19: US impact on antimicrobial resistance [cited 2024 Apr 22]. https://www.cdc.gov/drugresistance/pdf/covid19-impact-report-508.pdf
3. Logan LK, Weinstein RA. The epidemiology of carbapenem-resistant Enterobacteriaceae: the impact and evolution of

a global menace. J Infect Dis. 2017;215(suppl_1):S28–36. https://doi.org/10.1093/infdis/jiw282
4. Braykov NP, Eber MR, Klein EY, Morgan DJ, Laxminarayan R. Trends in resistance to carbapenems and third-generation cephalosporins among clinical isolates of *Klebsiella pneumoniae* in the United States, 1999–2010. Infect Control Hosp Epidemiol. 2013;34:259–68. https://doi.org/10.1086/669523
5. Guh AY, Bulens SN, Mu Y, Jacob JT, Reno J, Scott J, et al. Epidemiology of carbapenem-resistant Enterobacteriaceae in 7 US communities, 2012–2013. JAMA. 2015;314:1479–87. https://doi.org/10.1001/jama.2015.12480
6. Kritsotakis EI, Tsioutis C, Roumbelaki M, Christidou A, Gikas A. Antibiotic use and the risk of carbapenem-resistant extended-spectrum-β-lactamase-producing *Klebsiella pneumoniae* infection in hospitalized patients: results of a double case-control study. J Antimicrob Chemother. 2011;66:1383–91. https://doi.org/10.1093/jac/dkr116
7. Swaminathan M, Sharma S, Poliansky Blash S, Patel G, Banach DB, Phillips M, et al. Prevalence and risk factors for acquisition of carbapenem-resistant *Enterobacteriaceae* in the setting of endemicity. Infect Control Hosp Epidemiol. 2013;34:809–17. https://doi.org/10.1086/671270
8. Marchaim D, Chopra T, Bhargava A, Bogan C, Dhar S, Hayakawa K, et al. Recent exposure to antimicrobials and carbapenem-resistant Enterobacteriaceae: the role of antimicrobial stewardship. Infect Control Hosp Epidemiol. 2012;33:817–30. https://doi.org/10.1086/666642
9. Duffy N, Karlsson M, Reses HE, Campbell D, Daniels J, Stanton RA, et al. Epidemiology of extended-spectrum β-lactamase-producing Enterobacterales in five US sites participating in the Emerging Infections Program, 2017. Infect Control Hosp Epidemiol. 2022;43:1586–94.
10. Tamma PD, Aitken SL, Bonomo RA, Mathers AJ, van Duin D, Clancy CJ. Infectious Diseases Society of America 2023 guidance on the treatment of antimicrobial resistant gram-negative infections. Clin Infect Dis. 2023; ciad428
11. Romandini A, Pani A, Schenardi PA, Pattarino GAC, De Giacomo C, Scaglione F. Antibiotic resistance in pediatric infections: global emerging threats, predicting the near future. Antibiotics (Basel). 2021;10:393. https://doi.org/10.3390/antibiotics10040393
12. Logan LK, Bonomo RA. Metallo-β-lactamase (MBL)-producing *Enterobacteriaceae* in United States children. Open Forum Infect Dis. 2016;3:ofw090. https://doi.org/10.1093/ofid/ofw090
13. Logan LK, Medernach RL, Domitrovic TN, Rispens JR, Hujer AM, Qureshi NK, et al. The clinical and molecular epidemiology of CTX-M-9 group producing Enterobacteriaceae infections in children. Infect Dis Ther. 2019;8:243–54. https://doi.org/10.1007/s40121-019-0237-2
14. Logan LK, Hujer AM, Marshall SH, Domitrovic TN, Rudin SD, Zheng X, et al. Analysis of beta-lactamase resistance determinants in *Enterobacteriaceae* from Chicago children: a multicenter survey. Antimicrob Agents Chemother. 2016;60:3462–9. https://doi.org/10.1128/AAC.00098-16
15. Logan LK, Rispens JR, Medernach RL, Domitrovic TN, Hujer AM, Marshall SH, et al. A multicentered study of the clinical and molecular epidemiology of TEM- and SHV-type extended-spectrum beta-lactamase producing Enterobacterales infections in children. Pediatr Infect Dis J. 2021;40:39–43. https://doi.org/10.1097/INF.0000000000002916
16. Logan LK, Medernach RL, Rispens JR, Marshall SH, Hujer AM, Domitrovic TN, et al. Community origins and regional differences highlight risk of plasmid-mediated fluoroquinolone resistant Enterobacteriaceae infections in children. Pediatr Infect Dis J. 2019;38:595–9. https://doi.org/10.1097/INF.0000000000002205
17. Zerr DM, Weissman SJ, Zhou C, Kronman MP, Adler AL, Berry JE, et al. The molecular and clinical epidemiology of extended-spectrum cephalosporin- and carbapenem-resistant *Enterobacteriaceae* at 4 US pediatric hospitals. J Pediatric Infect Dis Soc. 2017;6:366–75. https://doi.org/10.1093/jpids/piw076
18. Chiotos K, Tamma PD, Flett KB, Naumann M, Karandikar MV, Bilker WB, et al. Multicenter study of the risk factors for colonization or infection with carbapenem-resistant Enterobacteriaceae in children. Antimicrob Agents Chemother. 2017;61:e01440-17. https://doi.org/10.1128/AAC.01440-17
19. Meropol SB, Haupt AA, Debanne SM. Incidence and outcomes of infections caused by multidrug-resistant *Enterobacteriaceae* in children, 2007–2015. J Pediatric Infect Dis Soc. 2018;7:36–45. https://doi.org/10.1093/jpids/piw093
20. Centers for Disease Control and Prevention. Multi-site Gram-negative Surveillance Initiative [cited 2023 Apr 24]. https://www.cdc.gov/hai/eip/mugsi.html#anchor_46658
21. US Census Bureau. 2020 Population estimates 2020 [cited 2023 Jan 19]. https://www.census.gov/quickfacts/fact/faq/US/PST045221
22. Migliavacca R, Docquier JD, Mugnaioli C, Amicosante G, Daturi R, Lee K, et al. Simple microdilution test for detection of metallo-β-lactamase production in *Pseudomonas aeruginosa.* J Clin Microbiol. 2002;40:4388–90. https://doi.org/10.1128/JCM.40.11.4388-4390.2002
23. Karlsson M, Lutgring JD, Ansari U, Lawsin A, Albrecht V, McAllister G, et al. Molecular characterization of carbapenem-resistant Enterobacterales collected in the United States. Microb Drug Resist. 2022;28:389–97. https://doi.org/10.1089/mdr.2021.0106
24 Clinical and Laboratory Standards Institute. Performance standards for antimicrobial susceptibility testing; 33rd edition. Supplement M100. Wayne (PA): The Institute; 2023.
25. Rasheed JK, Kitchel B, Zhu W, Anderson KF, Clark NC, Ferraro MJ, et al. New Delhi metallo-β-lactamase-producing *Enterobacteriaceae*, United States. Emerg Infect Dis. 2013;19:870–8. https://doi.org/10.3201/eid1906.121515
26. Lutgring JD, Zhu W, de Man TJB, Avillan JJ, Anderson KF, Lonsway DR, et al. Phenotypic and genotypic characterization of *Enterobacteriaceae* producing oxacillinase-48-like carbapenemases, United States. Emerg Infect Dis. 2018;24:700–9. https://doi.org/10.3201/eid2404.171377
27. Campbell D, Daniels J, Rasheed JK, Karlsson M. Development of a multiplex TaqMan probe-based real-time PCR assay for detection of blaIMP variants. Poster presented at: ASM Microbe 2017; New Orleans, LA, USA; 2017 June 1–5.
28. Prussing C, Canulla T, Singh N, McAuley P, Gosciminski M, King E, et al. Characterization of the first carbapenem-resistant *Pseudomonas aeruginosa* clinical isolate harboring bla_{SIM-1} from the United States. Antimicrob Agents Chemother. 2021;65:e0106621. https://doi.org/10.1128/AAC.01066-21
29. Daniels JB, Campbell D, Boyd S, Ansari U, Lutgring J, Rasheed JK, et al. Development and validation of a Clinical Laboratory Improvement Amendments-compliant multiplex real-time PCR assay for detection of *mcr* genes. Microb Drug Resist. 2019;25:991–6. https://doi.org/10.1089/mdr.2018.0417
30. Logan LK, Renschler JP, Gandra S, Weinstein RA, Laxminarayan R; Centers for Disease Control; Prevention

Epicenters Program. Carbapenem-resistant *Enterobacteriaceae* in children, United States, 1999–2012. Emerg Infect Dis. 2015;21:2014–21. https://doi.org/10.3201/eid2111.150548
31. Chea N, Bulens SN, Kongphet-Tran T, Lynfield R, Shaw KM, Vagnone PS, et al. Improved phenotype-based definition for identifying carbapenemase producers among carbapenem-resistant *Enterobacteriaceae*. Emerg Infect Dis. 2015;21:1611–6. https://doi.org/10.3201/eid2109.150198
32. Thaden JT, Fowler VG Jr, Sexton DJ, Anderson DJ. Increasing incidence of extended-spectrum beta-lactamase-producing *Escherichia coli* in community hospitals throughout the southeastern United States. Infect Control Hosp Epidemiol. 2016;37:49–54. https://doi.org/10.1017/ice.2015.239
33. Horie A, Nariai A, Katou F, Abe Y, Saito Y, Koike D, et al. Increased community-acquired upper urinary tract infections caused by extended-spectrum beta-lactamase-producing *Escherichia coli* in children and the efficacy of flomoxef and cefmetazole. Clin Exp Nephrol. 2019;23:1306–14. https://doi.org/10.1007/s10157-019-01775-w
34. Collingwood JD, Yarbrough AH, Boppana SB, Dangle PP. Increasing prevalence of pediatric community-acquired UTI by extended spectrum β-lactamase-producing *E. coli*: cause for concern. Pediatr Infect Dis J. 2023;42:106–9. https://doi.org/10.1097/INF.0000000000003777
35. Yin L, He L, Miao J, Yang W, Wang X, Ma J, et al. Carbapenem-resistant Enterobacterales colonization and subsequent infection in a neonatal intensive care unit in Shanghai, China. Infect Prev Pract. 2021;3:100147. https://doi.org/10.1016/j.infpip.2021.100147
36. Flannery DD, Chiotos K, Gerber JS, Puopolo KM. Neonatal multidrug-resistant gram-negative infection: epidemiology, mechanisms of resistance, and management. Pediatr Res. 2022;91:380–91. https://doi.org/10.1038/s41390-021-01745-7
37. Yaffee AQ, Roser L, Daniels K, Humbaugh K, Brawley R, Thoroughman D, et al. Notes from the field: Verona integron-encoded metallo-beta-lactamase-producing carbapenem-resistant Enterobacteriaceae in a neonatal and adult intensive care unit—Kentucky, 2015. MMWR Morb Mortal Wkly Rep. 2016;65:190. https://doi.org/10.15585/mmwr.mm6507a5
38. Principe L, Meroni E, Conte V, Mauri C, Di Pilato V, Giani T, et al. Mother-to-child transmission of KPC-producing *Klebsiella pneumoniae*: potential relevance of a low microbial urinary load for screening purposes. J Hosp Infect. 2018;98:314–6. https://doi.org/10.1016/j.jhin.2017.10.008
39. Sotgiu G, Are BM, Pesapane L, Palmieri A, Muresu N, Cossu A, et al. Nosocomial transmission of carbapenem-resistant *Klebsiella pneumoniae* in an Italian university hospital: a molecular epidemiological study. J Hosp Infect. 2018;99:413–8. https://doi.org/10.1016/j.jhin.2018.03.033
40. Islam S, Selvarangan R, Kanwar N, McHenry R, Chappell JD, Halasa N, et al. Intestinal carriage of third-generation cephalosporin-resistant and extended-spectrum β-lactamase-producing *Enterobacteriaceae* in healthy US children. J Pediatric Infect Dis Soc. 2018;7:234–40. https://doi.org/10.1093/jpids/pix045
41. Wernroth ML, Peura S, Hedman AM, Hetty S, Vicenzi S, Kennedy B, et al. Development of gut microbiota during the first 2 years of life. Sci Rep. 2022;12:9080. https://doi.org/10.1038/s41598-022-13009-3
42. Darda VM, Iosifidis E, Antachopoulos C, Kirvasilis F, Zarras C, Simitsopoulou M, et al. A longitudinal study of spontaneous gut decolonization of carbapenem-resistant gram-negative bacteria in neonatal and pediatric patients. Pediatr Infect Dis J. 2022;41:648–53. https://doi.org/10.1097/INF.0000000000003562
43. Dierikx TH, Visser DH, Benninga MA, van Kaam AHLC, de Boer NKH, de Vries R, et al. The influence of prenatal and intrapartum antibiotics on intestinal microbiota colonisation in infants: a systematic review. J Infect. 2020;81:190–204. https://doi.org/10.1016/j.jinf.2020.05.002

Address for correspondence: Heather N. Grome, Centers for Disease Control and Prevention, 1600 Clifton Rd NE, Mailstop H16-3, Atlanta, GA 30329-4018, USA; email: qds9@cdc.gov

Chest Radiograph Screening for Detecting Subclinical Tuberculosis in Asymptomatic Household Contacts, Peru

Qi Tan,[1] Chuan-Chin Huang,[1] Mercedes C. Becerra, Roger Calderon, Carmen Contreras, Leonid Lecca, Judith Jimenez, Rosa Yataco, Jerome T. Galea, Jia-Yih Feng, Sheng-Wei Pan, Yen-Han Tseng, Jhong-Ru Huang, Zibiao Zhang, Megan B. Murray

The World Health Organization's end TB strategy promotes the use of symptom and chest radiograph screening for tuberculosis (TB) disease. However, asymptomatic early states of TB beyond latent TB infection and active disease can go unrecognized using current screening criteria. We conducted a longitudinal cohort study enrolling household contacts initially free of TB disease and followed them for the occurrence of incident TB over 1 year. Among 1,747 screened contacts, 27 (52%) of the 52 persons in whom TB subsequently developed during follow-up had a baseline abnormal radiograph. Of contacts without TB symptoms, persons with an abnormal radiograph were at higher risk for subsequent TB than persons with an unremarkable radiograph (adjusted hazard ratio 15.62 [95% CI 7.74–31.54]). In young adults, we found a strong linear relationship between radiograph severity and time to TB diagnosis. Our findings suggest chest radiograph screening can extend to detecting early TB states, thereby enabling timely intervention.

Recognizing the key role early detection plays in interrupting further tuberculosis (TB) transmission, the World Health Organization (WHO) has emphasized the need for global investment in that area. In line with that objective, the end TB strategy promotes the use of TB symptom and chest radiograph screening for active case finding (*1*).

Chest radiography has been widely used as a diagnostic and screening tool for TB (*2*,*3*). Currently, the impact of chest radiograph screening largely depends on its ability to detect patients with clinically apparent TB disease (*4*–*6*). Recent understanding of TB has revealed a heterogeneous period of pathophysiological transition with a spectrum of early TB states, ranging from the time of exposure to *Mycobacterium tuberculosis* to the onset of symptomatic active disease (*7*–*10*). However, asymptomatic early states of TB beyond latent and active disease can be potentially unrecognized using current diagnostic or screening criteria for TB (*11*–*14*).

Accessing chest radiograph screening in low-resource settings, particularly in low- and middle-income countries, has been challenging and has hindered early detection of disease. However, WHO recommended chest radiography with computer-aided detection as a screening tool for TB in its 2021 guidelines (*15*), holding promise for the early detection and triage of TB.

In this study, we used data from a longitudinal cohort of household contacts of TB patients in Lima, Peru, to examine the frequency of baseline abnormal chest radiographs (defined as the presence of any intrathoracic abnormalities compatible with TB disease) in adult contacts who were initially classified

Author affiliations: Harvard Medical School, Boston, Massachusetts, USA (Q. Tan, C.-C. Huang, M.C. Becerra, M.B. Murray); Brigham and Women's Hospital, Boston (C.-C. Huang, M.C. Becerra, Z. Zhang, M.B. Murray); Partners In Health—Socios En Salud Sucursal Peru, Lima, Peru (R. Calderon, C. Contreras, L. Lecca, J. Jimenez, R. Yataco); University of South Florida, Tampa, Florida, USA (J.T. Galea); Taipei Veterans General Hospital, Taipei, Taiwan (J.-Y. Feng, S.-W. Pan, Y.-H. Tseng, J.-R. Huang); National Yang Ming Chiao Tung University, Taipei (J.-Y. Feng, S.-W. Pan, Y.-H. Tseng, J.-R. Huang); Harvard T.H. Chan School of Public Health, Boston (M.B. Murray)

DOI: https://doi.org/10.3201/eid3006.231699

[1]These authors contributed equally to this article.

as free from TB disease and in whom incident disease subsequently developed. We further evaluated the association between severity of radiograph abnormalities and time to occurrence of TB disease. Our objective was to assess whether baseline chest radiograph screening can identify early TB states among asymptomatic household contacts beyond active case finding.

Methods

Study Design and Participants

During September 1, 2009–August 29, 2012, we conducted a prospective longitudinal cohort study of household contacts of index TB patients in Lima, encompassing 20 districts and ≈3.3 million residents of urban areas and peri-urban, informal shantytown settlements. Peru is a middle-income country with TB services concentrated in district health centers. Chest radiograph was not recommended by Peru's National TB Program Guidelines for community screening during the cohort study period. In the parent study, we enrolled 4,500 index patients >15 years of age with newly diagnosed pulmonary TB from 106 district health centers in Lima (*16*). The study was approved by the Institutional Review Board of Harvard School of Public Health and the Research Ethics Committee of the National Institute of Health of Peru. All study participants provided informed consent.

Procedures

In the parent study, health center clinicians diagnosed pulmonary TB according to Peru's National TB program guidelines (*17*), which required ≥1 of 2 sputum smears to be positive for acid-fast bacilli by Ziehl-Neelsen staining or, in the absence of positive sputum smears, a chest radiograph consistent with TB. We then visited patient households to enroll all household contacts. We gave contacts with no history of TB infection or disease a tuberculin skin test (TST). Health center clinicians made the decision to request a baseline radiograph in symptomatic household contacts. To elucidate why clinicians ordered those radiographs, we compared baseline clinical characteristics in contacts who received a radiograph and those who did not. We screened all enrolled contacts for TB symptoms (cough for >14 days, coughing blood or phlegm, fever, shortness of breath, or night sweats). We used a standardized case report form to collect symptoms; that information was obtained by Spanish or Quechua speakers in private in health clinics or in persons' homes. Household contacts chosen for evaluation by health center clinicians provided 2 sputum samples for smear microscopy and culture on solid media and were referred for a routine work-up that included a chest radiograph. Persons who did not receive a TB diagnosis at enrollment were then followed for the occurrence of TB disease over a 12-month period. Those in whom incident disease developed were given TB treatment according to Peru's National TB guidelines (*17*). We collected demographic and health data for each enrolled contact consisting of height and weight; previous TB history; smoking or drinking addiction status; and any comorbidity of HIV infection, diabetes, hypertension, cardiovascular disease, kidney disease, or asthma. We limited our analysis to persons >15 years of age who were TST-positive (Table 1) and who did not receive a diagnosis of TB disease within the first 30 days after enrollment (Figure 1).

Table 1. Baseline characteristics of adult tuberculin skin test–positive household contacts of TB patients, Peru*

Characteristic	No. (%)
Age group. y	
16–24	985 (22)
25–44	1,879 (42)
≥45	1,642 (36)
Total	4,506 (100)
Sex	
F	2,624 (58)
M	1,882 (42)
BCG-vaccinated	4,070 (90)
History of TB	1,017 (22)
HIV-positive	27 (1)
Diabetes mellitus	131 (3)
With no TB symptoms	3,610 (80)
Baseline chest radiograph performed	1,848 (41)
TB diagnosis received at baseline	252 (6)

*BCG, Bacillus Calmette–Guérin; TB, tuberculosis.

Radiograph Evaluation and Study Outcomes

We retrospectively evaluated chest radiographs of participants who received a radiograph within 10 days of enrollment. The digitalized anteroposterior films were reevaluated by 3 readers. The first and second readers were both senior pulmonologists with 10–15 years of experience in TB care and TB-related radiographic evaluation. The third reader was a senior radiologist specializing in TB with 20 years' experience in chest radiologic evaluation for TB diagnosis. Radiologic findings and scoring were assessed following a well-established radiologic protocol (*4*,*17*–*20*) (Appendix, https://wwwnc.cdc.gov/EID/article/30/6/23-1699-App1.pdf). That protocol outlines 3 parameters: whether the radiograph is abnormal, whether abnormalities are suggestive of TB, and the extent of abnormalities (Appendix Table 2). The first reader was blinded to

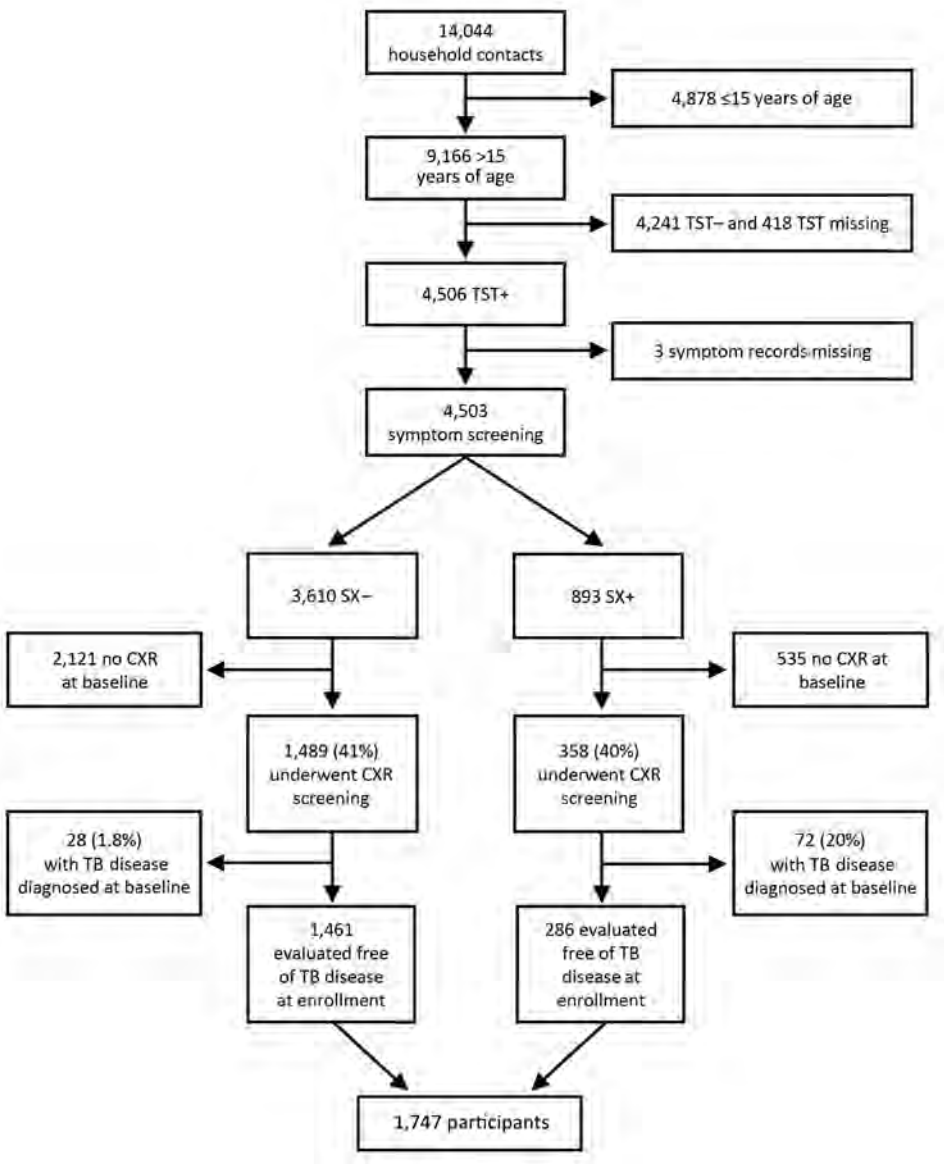

Figure 1. Flowchart of enrollment in study of chest radiograph screening for detection of subclinical TB in asymptomatic household contacts, Peru. CXR, chest radiograph; SX–, no symptoms; SX+, symptoms; TB, tuberculosis; TST–, tuberculin skin test negative; TST+, tuberculin skin test positive.

symptoms, TST results, and clinical outcomes. The second reader reviewed chest radiographs deemed abnormal by the first reader to validate those readings. Discrepant interpretations were resolved by a third reader who adjudicated on the basis of the protocol. The final scores for each radiograph were calculated by averaging the results from the 2 readers. Final decisions were reached by consensus. We considered a radiograph to be abnormal at enrollment if any intrathoracic abnormalities were present including cavitation, noncavitary lung lesions, hilar lymphadenopathy, and pleural disorders (Appendix). We classified a parenchymal lesion as noncavitary if we found patchy or confluent consolidation, ground glass opacity, noncalcified nodules, calcified nodules (Ghon focus), diffuse micronodules (miliary pattern), fibrosis, bronchiectasis, collapse (atelectasis), and hyperinflation (*18*,*19*). We further categorized those abnormal findings as TB-suggestive or TB-nonsuggestive (Appendix). To grade the extent of abnormalities, we reported the percentage of lung affected by any pathological abnormality for each of 3 zones (upper, middle, and lower) in each lung. We estimated the total percentage of lung affected by summing the percentages of the 6 zones (0–6) (Appendix) (*18*). We defined the study outcome as incident TB disease detected during a 12-month follow-up period in participants in whom TB disease had been ruled out at baseline.

Statistical Analyses

Associations between Baseline Abnormalities and Incident TB Disease

We used a Cox proportional hazards model to investigate the association between baseline chest radiograph abnormalities and the occurrence of incident TB disease. We categorized participants into 4 groups: those with no TB symptoms and normal chest radiograph (SX–CXR– group); those with TB symptoms and normal radiograph (SX+CXR– group); those with no TB symptoms and abnormal radiograph (SX–CXR+ group); and those with TB symptoms and abnormal radiograph (SX+CXR+ group). We first performed a univariate analysis, followed by a multivariate model that adjusted for potential confounders: age, sex, alcohol use, tobacco use, diabetes, TB history, hypertension, cardiovascular disease, kidney disease, asthma, and body mass index (BMI). We considered that older household contacts and those with a history of TB might be more likely to have residual abnormalities on radiographs that were unrelated to recent TB exposure (*21*,*22*). We therefore repeated our analyses in 3 age subgroups: persons 16–24 years of age, 25–44 years of age, and ≥45 years of age. In a second sensitivity analysis, we restricted our analyses to contacts with no known previous TB history.

Association between Severity of Radiograph Abnormality and TB Progression Trajectory

We used linear regression to evaluate the association between the extent of abnormality on baseline radiograph and the trajectory of TB progression, indicated by the time to the occurrence of TB disease, among household contacts in whom incident TB disease developed during the 1-year follow-up period. Similar to the process discussed previously, we repeated the analyses in 3 age groups and among persons with no known previous TB history, conducting those analyses separately.

To determine whether consistent baseline radiograph readings could serve as an indicator of the risk for incident TB, we compared the risk for incident TB among household contacts with concordant versus discordant radiograph readings. We conducted an analysis using the Pearson χ^2 test to identify any association between the risk for incident TB and radiograph concordance. We performed all statistical analyses using R version 4.2.2 (The R Foundation for Statistical Computing, https://www.r-project.org).

Results

Among 9,166 adult household contacts, 4,506 (49%) were TST-positive at baseline; of those, 4,503 (99%) underwent symptom screening. Of the 3,610 persons with TB symptoms and 893 without symptoms at baseline, 1,489 (41%) persons with symptoms and 358 (40%) without symptoms underwent a chest radiograph at baseline. Those referred for chest radiograph were less likely to be male (37% vs. 45%; p = 0.001), HIV-positive (0.4% vs. 0.8%; p = 0.02), or have a previous history of TB disease (17% vs. 26%; p<0.001) (Appendix Table 1). The presence of TB symptoms was similar among those referred for radiograph and those not referred (19% vs. 20%; p = 0.54). Of the 1,847 subjects with a baseline radiograph, TB disease developed in 100 (5%) persons within 30 days after enrollment; we considered those to be coprevalent cases and excluded them from analysis (Figure 1).

Associations between Baseline Radiograph Abnormalities and Incident TB Disease

Subsequent TB in All Screened Participants

Among the 1,747 persons who were determined to be TB-negative at baseline and who had a baseline radiograph, 52 (3%) received a diagnosis of incident TB disease within the next 12 months. Among those 52 persons, 25 (48%) of the diagnoses were confirmed through microbiological tests and 8% through chest radiograph and symptoms; the remaining 44% lacked diagnostic information. Of the 52 persons, 38 (73%) were asymptomatic at baseline and 27 (52%) had an abnormal chest radiograph result at baseline (Appendix Figure 1). Of the 27 with abnormal radiographs, 2 (7%) had cavities, 18 (67%) had noncavitary parenchymal lesions, 6 (22%) had hilar lymphadenopathy, and 4 (15%) had pleural disorders; 3 (11%) of the 27 radiographs were agreed upon by 2 readers to have >1 abnormality. (Appendix Table 3, Figure 2). The risk for TB disease in those with an abnormal radiograph was higher both among those with initial symptoms and those without symptoms than for persons with normal x-ray and no symptoms at baseline (adjusted hazard ratio [aHR] of SX+CXR– vs. SX–CXR– was 2.24 [95% CI 0.92–5.74]; aHR of SX–CXR+ vs. SX–CXR– was 15.62 [95% CI 7.74–31.54]; aHR of SX+CXR+ vs. SX–CXR– was 26.50 [95% CI 9.98–70.36]) (Table 2; Figure 2). Among the 135 abnormal radiographs evaluated by 2 readers, readers agreed on the presence or absence of abnormalities in 133 (99%) films. The risk for TB disease was higher in contacts in whom readers disagreed on the presence of noncavitary parenchymal lesions (Appendix Table 4).

Table 2. Chest radiograph and symptom screening results and their association with risk for subsequent TB in tuberculin skin test–positive adults, Peru*

Result†	No. household contacts	No. (%) incident TB cases	Univariate analysis Hazard ratio (95% CI), n = 1,747, events = 52§	p value	Multivariate analysis‡ Hazard ratio (95% CI), n = 1,630, events = 49§	p value
CXR–SX–	1,349	18 (1)	Referent		Referent	
CXR–SX+	263	7 (3)	2.01 (0.84–4.82)	0.12	2.24 (0.92–5.47)	0.08
CXR+SX–	112	20 (18)	14.64 (7.74–27.67)	<0.001	15.62(7.74–31.54)	<0.001
CXR+SX+	23	7 (30)	26.85 (11.21–64.31)	<0.001	26.50 (9.98–70.36)	<0.001

*In both analyses, n indicates number of analyzed participants and event indicates number of participants in whom incident TB developed. CXR–, unremarkable chest radiograph, CXR+, abnormal chest radiograph; SX–, no symptoms; SX+, symptoms; TB, tuberculosis.
†Household contacts were categorized into 4 groups by screening results: CXR–SX–, n = 1,349; CXR–SX+, n = 263; CXR+SX–, n = 112; CXR+SX+, n = 23. Symptoms were defined as any of the following: cough>14 d, cough with blood or phlegm, fever, shortness of breath, night sweats. Abnormal chest radiograph was defined as a radiograph with any intra-thorax abnormalities compatible with TB.
‡Adjusted for age, sex, alcohol use, tobacco use, diabetes, hypertension, cardiovascular disease, kidney disease, asthma, previous TB history, and body mass index. HIV-positive participants (n = 4) were excluded.

Subsequent TB by Age Groups

The risk for incident TB disease fell from 7% in participants 16–24 years of age to 2% in persons 25–44 years of age and 2% in those ≥45 years of age (Appendix Table 5, Figure 3). A similar pattern was observed in participants with an abnormal radiograph at enrollment (Appendix Table 6, Figure 3). Among participants 16–24 years of age with abnormal radiographs at baseline, incident TB developed in 12 (50%) persons; 9 of those (75%) were asymptomatic at enrollment. In contrast, among those with an abnormal radiograph, TB developed in only 6 (13%) of those 25–44 years of age and 9 (14%) of those ≥45 years of age; of those, 3 (50%) persons 25–44 years of age and 8 (89%) persons ≥45 years of age were asymptomatic (Appendix Figure 6). The risk for subsequent TB disease was higher in both initially asymptomatic and symptomatic persons of all subgroups who had an abnormal baseline radiograph than in persons with a normal radiograph (Table 3; Figure 3).

Subsequent TB in Participants with No TB History

When we restricted our analysis to the 1,440 persons with no known TB history, the effect sizes for the associations between radiograph status and subsequent incident TB increased by 30% compared with the analysis that included adult contacts with a TB history. aHRs were 23.11 (95% CI 10.35–51.57) for SX–CXR+ versus SX–CXR– and 34.24 (95% CI 9.65–124.54) for SX+CXR+ versus SX–CXR– (Table 4).

Associations between Severity of Radiograph Abnormality and TB Progression Trajectory

The severity grade of the baseline radiograph was not significantly associated with time from enrollment to TB diagnosis (mean difference of −0.002 [95% CI –0.005 to 0.001] days; n = 27) among all adults in whom incident TB developed (Appendix Figure 5). However, we found a strong linear relationship between the radiograph severity grade and time to TB diagnosis among participants 16–24 years of age (mean difference of −0.004 [95% CI –0.007 to −0.001]; n = 12) but not among older persons (Figure 4). We also did not find an association between severity grade and time to incident TB among persons with no known TB history (mean difference of 0.002 [95% CI –0.006 to 0.001]; n = 19) (Appendix Figure 6).

Discussion

In this study, we found that among persons ≥15 years of age who were exposed to TB at home, those who were initially deemed TB-free but had an abnormal baseline chest radiograph had a 15-fold higher risk for incident TB developing during 12 months of follow-up than did persons with an unremarkable radiograph. That finding was more pronounced in household contacts with no TB history and in younger participants, who were less likely to have residual abnormalities on radiograph from past TB or other comorbidities. Our findings remained unaltered in

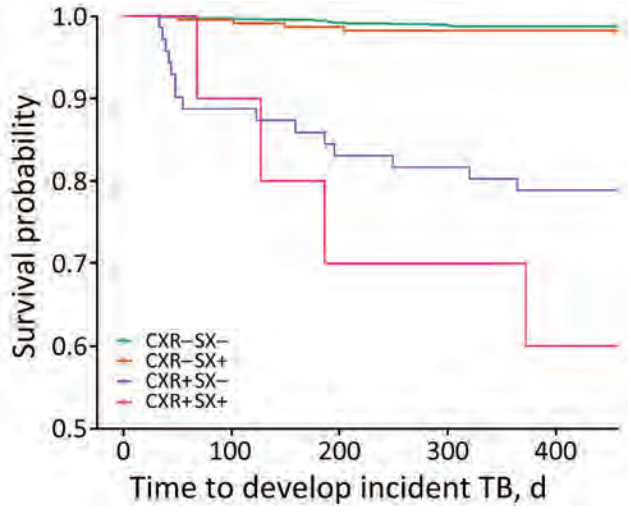

Figure 2. Associations between chest radiograph and symptom screening results and time to incident TB among tuberculin skin test–positive adults, Peru. N = 1,747, incident events = 52. CXR–, unremarkable chest radiograph; CXR+, abnormal chest radiograph; SX–, no symptoms; SX+, symptoms; TB, tuberculosis.

Table 3. Chest radiograph and symptom screening results and association with risk for subsequent TB, by age group, Peru*

Age group, y†	No. (%) incident TB cases	Univariate analysis		Multivariate analysis	
		Hazard ratio (95% CI)	p value	Hazard ratio (95% CI)	p value
16–24		n = 370, events = 25		n = 360, events = 24‡	
CXR–SX–	9 (0.3)	Referent		Referent	
CXR–SX+	4 (7)	2.25 (0.69–7.31)	0.18	2.12(0.59–7.55)	0.25
CXR+SX–	9 (50)	20.47 (8.11–51.64)	<0.001	19.12 (7.19–50.79)	<0.001
CXR+SX+	3 (50)	24.26 (6.53–90.12)	<0.001	21.03 (5.12–86.30)	<0.001
25–45		n = 709, events = 13		n = 664, events = 13§	
CXR–SX–	6 (1)	Referent		Referent	
CXR–SX+	1 (1)	0.93 (0.11–7.73)	0.95	0.89 (0.11–7.57)	0.92
CXR+SX–	3 (8)	8.38 (2.09–33.51)	<0.01	8.85 (2.09–37.44)	<0.01
CXR+SX+	3 (33)	33.21 (8.29–132.97)	<0.001	28.89 (6.07–137.67)	<0.001
≥45		n = 668, events = 14		n = 630, events = 14¶	
CXR–SX–	3 (0.6)	Referent		Referent	
CXR–SX+	2 (2)	3.23 (0.53–19.32)	0.19	3.01 (0.49–18.44)	0.23
CXR+SX–	8 (14)	24.21 (6.42–91.26)	<0.001	18.32 (4.37–76.87)	<0.001
CXR+SX+	1 (12)	22.98 (2.39–220.96)	<0.01	29.22 (2.42–352.91)	<0.001

*In both analyses, n indicates number of analyzed participants and event indicates number of participants in whom incident TB developed. CXR–, unremarkable chest radiograph, CXR+, abnormal chest radiograph; SX–, no symptoms; SX+, symptoms; TB, tuberculosis.
†Symptoms were defined as any of the following: cough >14 d, cough with blood or phlegm, fever, shortness of breath, night sweats. Abnormal chest radiograph was defined as a radiograph with any intra-thorax abnormalities compatible with TB. Abnormal CXR was defined as a CXR with any intra-thorax abnormalities compatible with TB.
‡Adjusted for sex, cardiovascular disease, kidney disease, asthma, TB history, and body mass index. All persons in this age group were HIV negative.
§Adjusted for sex, alcohol use, hypertension, kidney disease, asthma, TB history, and body mass index. HIV-positive persons (n = 4) were excluded.
¶Adjusted for sex, alcohol use, tobacco use, diabetes, hypertension, TB history, and body mass index. All persons in this age group were HIV negative.

multivariate models when we further adjusted for demographic and clinical variables, as well as history of comorbidity. Among young persons with abnormal radiograph who were initially deemed TB-free at baseline, incident TB developed in 50% during follow-up. The severity grade of radiograph abnormalities was a strong indicator of an early-state TB trajectory in young persons.

Although numerous investigators have examined the use of chest radiography in screening for clinically apparent TB, few have evaluated whether abnormal radiographs could help identify early TB. The idea of using chest radiograph examination for incipient pulmonary TB was first proposed by Dr. Francis Williams, the father of chest radiology in the United States, in 1899 (*23*). Chest radiography for mass screening and active case-finding for pulmonary TB was recommended by the New York City Health Department in the United States as early as the 1920s–1930s (*24*,*25*) and was widely implemented in industrialized countries in the 1940s–1960s, contributing to the success of TB control in developed countries (*3*,*26*). However, by the late 1960s, WHO no longer recommended active case finding through mass radiograph screening for developing countries because of financial constraints (*27*). Not until 2015 was chest radiograph screening re-recommended by WHO as part of the end TB strategy (*1*,*27*). Even today, radiograph screening remains inaccessible in resource-limited areas in many low- and

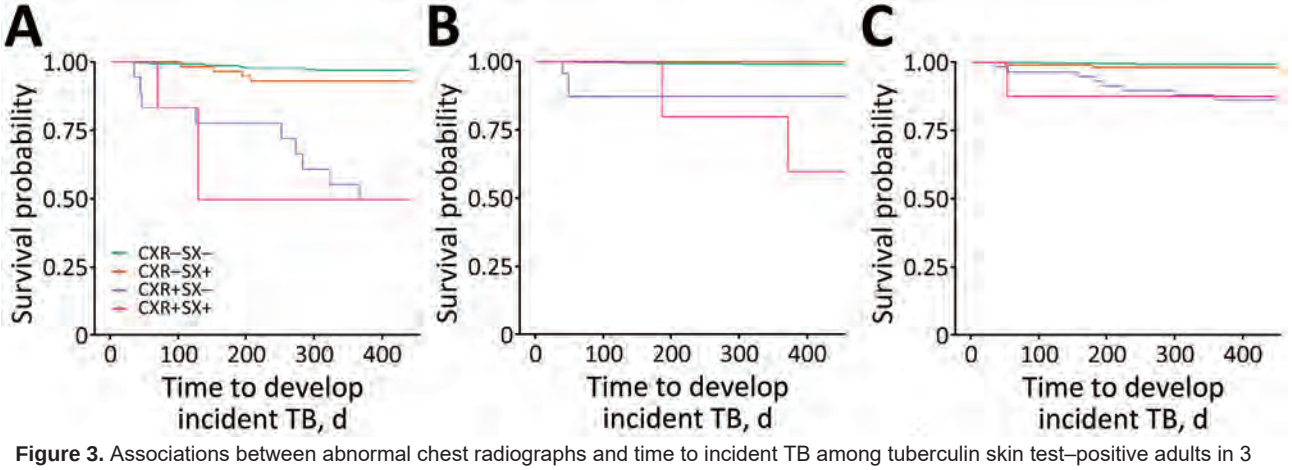

Figure 3. Associations between abnormal chest radiographs and time to incident TB among tuberculin skin test–positive adults in 3 age groups, Peru. A) 16–24-year age group (N = 370, incident events = 25); B) 25–44-year age group (N = 709, incident events = 13); C) ≥45-year age group (N = 668, incident events = 14). CXR–, unremarkable chest radiograph, CXR+, abnormal chest radiograph; SX–, no symptoms; SX+, symptoms; TB, tuberculosis.

Table 4. Chest radiograph and symptom screening results and their association with risk for subsequent TB in adults with no known TB history*

Result†	No. (%) incident TB cases	Univariate analysis: Hazard ratio (95% CI), n = 1,440, event = 37	Univariate analysis: p value	Multivariate analysis‡: Hazard ratio (95% CI), n = 1,347, event = 34	Multivariate analysis‡: p value
CXR–SX–	14 (1)	Referent		Referent	
CXR–SX+	4 (3)	1.45 (0.48–4.39)	0.51	1.64 (0.53–5.11)	0.39
CXR+SX–	15 (21)	19.46 (9.39–40.33)	<0.001	23.11 (10.35–51.57)	<0.001
CXR+SX+	4 (40)	38.53 (12.67–117.18)	<0.001	34.24 (9.65–121.54)	<0.001

*In both analyses, n indicates number of analyzed participants and event indicates number of participants in whom incident TB developed. CXR–, unremarkable chest radiograph, CXR+, abnormal chest radiograph; SX–, no symptoms; SX+, symptoms; TB, tuberculosis.
†Symptoms were defined as any of the following: cough>14 d, cough with blood or phlegm, fever, shortness of breath, night sweats. Abnormal chest radiograph was defined as a radiograph with any intra-thorax abnormalities compatible with TB. Abnormal CXR was defined as a CXR with any intra-thorax abnormalities compatible with TB.
‡Adjusted for age, sex, alcohol use, tobacco use, diabetes, hypertension, cardiovascular disease, kidney disease, asthma, TB history and BMI. HIV-positive persons (n = 3) were excluded.

middle-income countries. Screening criteria typically focus on previously underdiagnosed TB disease, which is known as the late stage of TB disease (*26*). As a consequence, the very early stage of TB, known as subclinical TB, which is characterized by minimal or atypical presentations on chest radiograph, could still be underrecognized.

Nonetheless, our findings are consistent with several previous studies. In a study conducted in Czechoslovakia among a district-level cohort of 7,800 adults followed during 1961–1964 (*28*), 44% of persons in whom incident TB developed during follow-up had a previous abnormal chest radiograph indicating inactive TB or a fibrotic lesion. In a cohort study conducted during 1950–1952 in Denmark, persons with fibrotic lesions and shadows suspicious of TB on chest radiograph had a >10-fold higher annual rate of subsequent TB during the follow-up period (*29*). Similarly, in cohort studies conducted in 1988 among Southeast Asian refugees in Seattle (*30*) and in the early 1980s among recent Asian immigrants to northern Canada (*31*), persons with radiograph abnormalities indicative of or interpreted as inactive TB had 6-fold higher and 19-fold higher risk for subsequent TB. Those studies demonstrate that different types of lesions on baseline radiograph are associated with varying risks of subsequent TB in different mass screening settings. In a 1981 study from Hong Kong, 176 smear- and culture-negative adults with TB-compatible lesions were monitored for up to 30

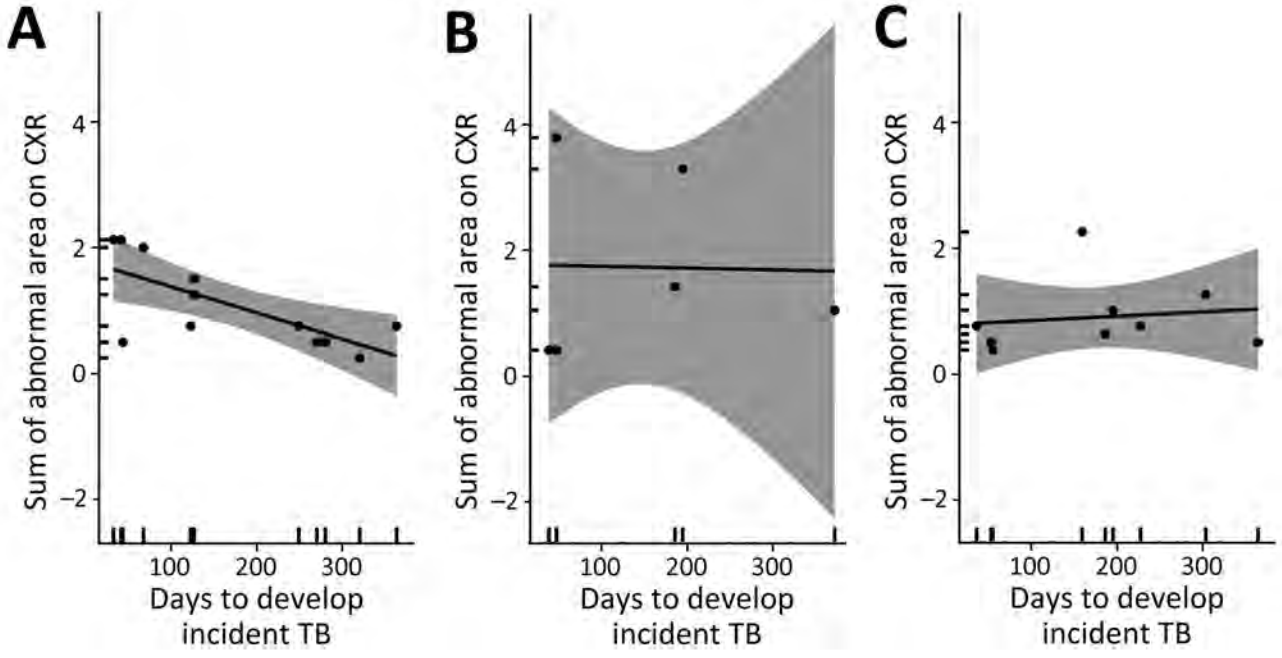

Figure 4. Association between degree of baseline chest radiograph severity and time to developing incident TB among persons with abnormal radiograph findings by age group, Peru. Gray shading indicates 95% CIs. A) 16–24-year age group (n = 12). Mean difference −0.004 (95% CI −0.007 to −0.001); p≤0.001, ρ = −0.71; B) 25–44-year age group (n = 6). Mean difference −0.0002 (95% CI −0.015 to 0.015); p = 0.96, ρ = −0.025; C) ≥45-year age group (n = 9). Mean difference 0.0006 (95% CI −0.004 to 0.005); p = 0.73, ρ = 0.14. ρ, Pearson correlation coefficient.

months (*32*). Of those, TB was eventually diagnosed in 30%; most cases occurred within the first 12 months of follow-up. Similarly, a 1985 study conducted in South Africa found that among 152 TST-positive gold miners with evolving apical lung lesions on baseline radiograph who were smear- and culture-negative, bacteriologically confirmed pulmonary TB developed in 58% during a 58-month follow-up period (*33*). In a recent systematic review and meta-analysis of studies of 34 cohorts observed in the prechemotherapy era of persons with untreated TB who underwent follow-up, progression from microbiologically negative to positive disease was observed at an annualized rate of 10% in those with initial radiographs suggestive of active TB and at a rate of 1% in those initially suggestive of inactive TB (*12*). Although the incidence rate in this systemic review is lower than in our study, only 1 of the studies cited previously focused on a cohort of household contacts with known exposure to TB. The higher incidence in our study might be because we did not require microbiological confirmation to classify incident disease.

The finding that chest radiography might help identify pathological changes before the onset of TB symptoms aligns with recent evidence from South Africa. Esmail et al. (*34*) followed 250 HIV-negative adults exposed to TB at home for >4.7 years. Among 14 persons in whom active disease developed during follow-up, 6 exhibited baseline abnormalities on computed tomography/positron emission tomography (*34*). The TB research community now widely acknowledges that TB follows a dynamic continuum, encompassing TB infection, asymptomatic incipient or subclinical TB, and symptomatic clinically manifested disease (*7*–*10*). A 1982 study by the International Union Against Tuberculosis Committee on Prophylaxis revealed that among 28,000 adults with radiograph-identified fibrotic pulmonary lesions compatible with TB, a 24-week regimen of isoniazid preventive treatment decreased tuberculosis incidence by 65% compared with the placebo group over a 5-year follow-up period (*35*). Those findings suggest that lung changes can be observed in the asymptomatic phase of TB. Given that the cost of computed tomography/positron emission tomography makes it impractical for many screening programs, radiography could play a pivotal role in early TB detection, enabling early interventions such as close follow-up, preventive therapy, or full-dose combination therapy in populations at risk.

Our study revealed that young persons 16–24 years of age with abnormal baseline chest radiograph had a 3-fold higher risk for TB than older adults with abnormal radiograph. The observed association between the severity of baseline radiograph abnormalities and the trajectory of early TB disease within this young age group further supports the notion that an abnormal radiograph might serve as an indicator of undiagnosed or subclinical TB in this specific population, whereas older adults are more likely to have abnormal radiographs caused by non-TB lung diseases. That notion is supported by 2 cross-sectional studies conducted in Malawi during 2018–2020 (*36*) and the 2016 Kenya national TB prevalence survey (*37*). Both those studies reported a high prevalence of non-TB abnormalities on chest radiographs among older adults, with the proportion increasing with age.

The first limitation of this study is that only 40% of TST-positive adults received a baseline radiograph independent of symptoms; the decision to request a radiograph was made by local health center clinicians. Second, we lacked lateral positioning radiographs, which might have led to misclassifications of abnormalities. Third, readings were initially blinded for the first reader, and only abnormal radiographs were subsequently validated by a second reader who was not blinded. Therefore, misclassification of findings could have occurred. The fact that the second reader only read the films initially deemed to be abnormal and was not blinded to this classification might have resulted in overidentifying abnormalities in keeping with the first reader's interpretations, leading to inflated measures of inter-rater agreement and consequently overestimating the effect size of the association between abnormalities and subsequent TB disease. Because the radiographs initially read as unremarkable were not read by a second reader, some of those might have been classified as abnormal if all radiographs had been read. Fourth, the relatively high prevalence of previous TB history among household contacts raises the possibility that some abnormal baseline radiographs were a result of inadequately treated previous TB or residual, minimally active TB. We did not have previous treatment or drug sensitivity information for those contacts and so cannot rule out the possibility that a history of TB might contribute to the elevated risk for incident TB among those persons. However, we also observed that persons with TB history were less likely to undergo baseline examinations. Moreover, when we excluded those with TB history from the 1,747 contacts who underwent radiograph screening, we found that the effect size increased by 30%. Finally, health center clinicians were expected to follow the clinical diagnosis guidelines outlined by Peru's National TB Program, but different clinicians might have applied varying criteria for TB diagnosis. The absence of a standardized set of

criteria for TB diagnosis might have resulted in nondifferential misclassification, potentially influencing the results toward a null effect.

Overall, our study revealed a significant association between abnormal baseline chest radiograph results and subsequent diagnosis of TB among asymptomatic adults with recent TB exposure. The severity of baseline radiograph results also reflected the early TB progression trajectory. Our findings strongly support the wide use of chest radiography with computer-aided detection as a screening tool in exposed adults and prompt the development of accurate criteria and algorithms for human and artificial intelligence readers to effectively identify early TB states beyond active TB disease, leading to timely intervention and proper management.

Acknowledgments

We thank the patients and their families, the healthcare personnel at the 106 participating health centers in Lima, and Guoqing Zhang for the third reader contribution to inter-reader validation of the chest radiograph.

This work was supported by the National Institutes of Health and the National Institute of Allergy and Infectious Diseases grants U01AI057786, U19AI076217, U19AI111224, and U19AI142793

Q.T., M.B.M., and C.-C.H led the study design. M.B.M., L.L., M.B.C., J.T.G., J.J., and R.Y. designed and implemented the parent study. R.C. managed laboratory work. Q.T., J.-Y.F., S.-W.P., Y.-H.T. and J.-R.H. read and evaluated all radiography films. Z.Z. led data management. Q.T. and C.-C.H. analyzed the data. Q.T., C.-C.H., and M.B.M. wrote the first draft of the manuscript. All authors contributed to the paper writing.

About the Author

Dr. Tan was previously a physician specialist in lung disease and tuberculosis at Jiangsu Province Hospital in China and is currently a research fellow of Global Health and Social Medicine at Harvard Medical School. Her primary research interests are the epidemiology of TB, diagnostic tools for subclinical TB, and feasible approaches for infection control and management in source-limited setting.

References

1. World Health Organization. Implementing the end TB strategy: the essentials [cited 2023 Mar 6]. https://www.who.int/publications/i/item/WHO-HTM-TB-2015.19
2. World Health Organization. Systematic screening for active tuberculosis: principles and recommendations [cited 2023 Mar 6]. https://apps.who.int/iris/bitstream/handle/10665/84971/9789241548601_eng.pdf
3. Miller C, Lonnroth K, Sotgiu G, Migliori GB. The long and winding road of chest radiography for tuberculosis detection. Eur Respir J. 2017;49:1700364. https://doi.org/10.1183/13993003.00364-2017
4. World Health Organization. The WHO manual of diagnostic imaging: radiographic anatomy and interpretation of the chest and the pulmonary system 2012 [cited 2023 Mar 6]. https://www.who.int/publications/i/item/9241546778
5. Law I, Floyd K; African TB Prevalence Survey Group. National tuberculosis prevalence surveys in Africa, 2008–2016: an overview of results and lessons learned. Trop Med Int Health. 2020;25:1308–27. https://doi.org/10.1111/tmi.13485
6. Wetscherek MTA, Sadler TJ, Lee JYJ, Karia S, Babar JL. Active pulmonary tuberculosis: something old, something new, something borrowed, something blue. Insights Imaging. 2022;13:3. https://doi.org/10.1186/s13244-021-01138-8
7. Drain PK, Bajema KL, Dowdy D, Dheda K, Naidoo K, Schumacher SG, et al. Incipient and subclinical tuberculosis: a clinical review of early stages and progression of infection. Clin Microbiol Rev. 2018;31:e00021-18. https://doi.org/10.1128/CMR.00021-18
8. Migliori GB, Ong CWM, Petrone L, D'Ambrosio L, Centis R, Goletti D. The definition of tuberculosis infection based on the spectrum of tuberculosis disease. Breathe (Sheff). 2021;17:210079. https://doi.org/10.1183/20734735.0079-2021
9. Kendall EA, Shrestha S, Dowdy DW. The epidemiological importance of subclinical tuberculosis. a critical reappraisal. Am J Respir Crit Care Med. 2021;203:168–74. https://doi.org/10.1164/rccm.202006-2394PP
10. Achkar JM, Jenny-Avital ER. Incipient and subclinical tuberculosis: defining early disease states in the context of host immune response. J Infect Dis. 2011;204:1179–86.
11. Huang CC, Tan Q, Becerra MC, Calderon R, Chiang SS, Contreras C, et al. The contribution of chest radiography to the clinical management of children exposed to tuberculosis. Am J Respir Crit Care Med. 2022;206:892–900. https://doi.org/10.1164/rccm.202202-0259OC
12. Sossen B, Richards AS, Heinsohn T, Frascella B, Balzarini F, Oradini-Alacreu A, et al. The natural history of untreated pulmonary tuberculosis in adults: a systematic review and meta-analysis. Lancet Respir Med. 2023;11:367–79. https://doi.org/10.1016/S2213-2600(23)00097-8
13. Kendall EA, Wong EB. Do chest x-ray–positive, sputum-negative individuals warrant more attention during tuberculosis screening? Lancet Respir Med. 2023;11:304–6. https://doi.org/10.1016/S2213-2600(23)00085-1
14. Richards AS, Sossen B, Emery JC, Horton KC, Heinsohn T, Frascella B, et al. Quantifying progression and regression across the spectrum of pulmonary tuberculosis: a data synthesis study. Lancet Glob Health. 2023;11:e684–92. https://doi.org/10.1016/S2214-109X(23)00082-7
15. World Health Organization. WHO consolidated guidelines on tuberculosis: module 2: screening: systematic screening for tuberculosis disease. 2021 [cited 2023 Mar 6]. https://www.who.int/publications/i/item/9789240022676
16. Becerra MC, Huang CC, Lecca L, Bayona J, Contreras C, Calderon R, et al. Transmissibility and potential for disease progression of drug resistant *Mycobacterium tuberculosis*: prospective cohort study. BMJ. 2019;367:l5894. https://doi.org/10.1136/bmj.l5894
17. Ministry of Health Peru. General Directorate of People's Health—national health prevention strategy and technical health standard for the control of tuberculosis [in Spanish].

2006 [cited 2023 Mar 7]. http://bvs.minsa.gob.pe/local/MINSA/3731.pdf
18. Ralph AP, Ardian M, Wiguna A, Maguire GP, Becker NG, Drogumuller G, et al. A simple, valid, numerical score for grading chest x-ray severity in adult smear-positive pulmonary tuberculosis. Thorax. 2010;65:863–9. https://doi.org/10.1136/thx.2010.136242
19. Lau A, Lin C, Barrie J, Winter C, Armstrong G, Egedahl ML, et al. The radiographic and mycobacteriologic correlates of subclinical pulmonary TB in Canada: a retrospective cohort study. Chest. 2022;162:309–20. https://doi.org/10.1016/j.chest.2022.01.047
20. US Department of Health and Human Services. Technical instructions for civil surgeons; tuberculosis medical examination. 2008 May [cited 2023 Mar 7]. https://stacks.cdc.gov/view/cdc/22142
21. Meghji J, Simpson H, Squire SB, Mortimer K. A systematic review of the prevalence and pattern of imaging defined post-TB lung disease. PLoS One. 2016;11:e0161176. https://doi.org/10.1371/journal.pone.0161176
22. van Kampen SC, Wanner A, Edwards M, Harries AD, Kirenga BJ, Chakaya J, et al. International research and guidelines on post-tuberculosis chronic lung disorders: a systematic scoping review. BMJ Glob Health. 2018;3:e000745. https://doi.org/10.1136/bmjgh-2018-000745
23. Williams FH. Röntgen ray examinations in incipient pulmonary tuberculosis. Trans Am Climatol Assoc. 1899;15:68–86.
24. Lerner BH. New York City's tuberculosis control efforts: the historical limitations of the "war on consumption". Am J Public Health. 1993;83:758–66. https://doi.org/10.2105/AJPH.83.5.758
25. Edwards HR. Administration of a Bureau of Tuberculosis in a City Department of Health. Am J Public Health Nations Health. 1933;23:591–9. https://doi.org/10.2105/AJPH.23.6.591
26. Golub JE, Mohan CI, Comstock GW, Chaisson RE. Active case finding of tuberculosis: historical perspective and future prospects. Int J Tuberc Lung Dis. 2005;9:1183–203.
27. Raviglione MC, Pio A. Evolution of WHO policies for tuberculosis control, 1948–2001. Lancet. 2002;359:775–80. https://doi.org/10.1016/S0140-6736(02)07880-7
28. Stýblo K, Danková D, Drápela J, Galliová J, Jezek Z, Krivánek J, et al. Epidemiological and clinical study of tuberculosis in the district of Kolin, Czechoslovakia. Report for the first 4 years of the study (1961–64). Bull World Health Organ. 1967;37:819–74.
29. Groth-Petersen E, Knudsen J, Wilbek E. Epidemiological basis of tuberculosis eradication in an advanced country. Bull World Health Organ. 1959;21:5–49.
30. Nolan CM, Elarth AM. Tuberculosis in a cohort of Southeast Asian Refugees. A five-year surveillance study. Am Rev Respir Dis. 1988;137:805–9. https://doi.org/10.1164/ajrccm/137.4.805
31. Wang JS, Allen EA, Enarson DA, Grzybowski S. Tuberculosis in recent Asian immigrants to British Columbia, Canada: 1982–1985. Tubercle. 1991;72:277–83. https://doi.org/10.1016/0041-3879(91)90054-V
32. Hong Kong Chest Service; Tuberculosis Research Centre, Mad; British Medical Research Council. A study of the characteristics and course of sputum smear-negative pulmonary tuberculosis. Tubercle. 1981;62:155–67. https://doi.org/10.1016/0041-3879(81)90001-5
33. Cowie RL, Langton ME, Escreet BC. Diagnosis of sputum smear- and sputum culture-negative pulmonary tuberculosis. S Afr Med J. 1985;68:878.
34. Esmail H, Coussens AK, Thienemann F, Sossen B, Mukasa SL, Warwick J, et al. High resolution imaging and five-year tuberculosis contact outcomes. medRxiv. 2023. https://doi.org/10.1101/2023.07.03.23292111
35. International Union Against Tuberculosis Committee on Prophylaxis. Efficacy of various durations of isoniazid preventive therapy for tuberculosis: five years of follow-up in the IUAT trial. Bull World Health Organ. 1982;60:555–64.
36. Twabi HH, Semphere R, Mukoka M, Chiume L, Nzawa R, Feasey HRA, et al. Pattern of abnormalities amongst chest X-rays of adults undergoing computer-assisted digital chest x-ray screening for tuberculosis in Peri-Urban Blantyre, Malawi: a cross-sectional study. Trop Med Int Health. 2021;26:1427–37. https://doi.org/10.1111/tmi.13658
37. Mungai BN, Joekes E, Masini E, Obasi A, Manduku V, Mugi B, et al.; IMPALA Consortium. 'If not TB, what could it be?' Chest x-ray findings from the 2016 Kenya Tuberculosis Prevalence Survey. Thorax. 2021;76:607–14. https://doi.org/10.1136/thoraxjnl-2020-216123

Address for correspondence: Megan B. Murray, Department of Global Health and Social Medicine, Harvard Medical School, 641 Huntington Ave, 4th Fl, Rm 4A07, Boston, MA 02115, USA; email: megan_murray@hms.harvard.edu

Yersinia ruckeri Infection and Enteric Redmouth Disease among Endangered Chinese Sturgeons, China, 2022

Yibin Yang, Shijian Xu, Hao He, Xia Zhu, Yongtao Liu, Mou Hu, Bobin Jiang, Yuqiang Li, Xiaohui Ai, Guihong Fu, Hongyu Zhang

During October 2022, enteric redmouth disease (ERM) affected Chinese sturgeons at a farm in Hubei, China, causing mass mortality. Affected fish exhibited characteristic red mouth and intestinal inflammation. Investigation led to isolation of a prominent bacterial strain, zhx1, from the internal organs and intestines of affected fish. Artificial infection experiments confirmed the role of zhx1 as the pathogen responsible for the deaths. The primary pathologic manifestations consisted of degeneration, necrosis, and inflammatory reactions, resulting in multiple organ dysfunction and death. Whole-genome sequencing of the bacteria identified zhx1 as *Yersinia ruckeri*, which possesses 135 drug-resistance genes and 443 virulence factor-related genes. Drug-susceptibility testing of zhx1 demonstrated high sensitivity to chloramphenicol and florfenicol but varying degrees of resistance to 18 other antimicrobial drugs. Identifying the pathogenic bacteria associated with ERM in Chinese sturgeons establishes a theoretical foundation for the effective prevention and control of this disease.

Chinese sturgeons (*Acipenser sinensis*) are large migratory fish that are native to the Yangtze River and coastal areas of China (*1*). However, human activities (e.g., water-related engineering projects, fishing, pollution, and shipping) have degraded or destroyed much of the Chinese sturgeon natural habitat (*2*–*4*), limiting the suitable area for their reproduction (*5*) and resulting in a sharp decrease in natural population. Consequently, the Chinese sturgeon has been designated as a first-class protected animal in China (*2*). Since 2012, the Yangtze River Fisheries Research Institute has been conducting artificial breeding of Chinese sturgeons (*1*), establishing an artificial population, which is relevant to implementing large-scale reproduction and release activities of Chinese sturgeons and continuation of the species. However, artificial breeding poses some challenges to species preservation because of degradation of genetic resources, intensive cultivation practices, and the imbalance in nutritional requirements. Disease resistance among artificially reared Chinese sturgeons is low, and the fish are highly susceptible to pathogenic microorganisms such as *Aeromonas* (*6*), *Mycobacterium* (*7*), and *Pseudomonas* (*8*). Infections frequently result in large-scale mortality of Chinese sturgeons, imposing obstacles to their conservation.

In October 2022, a farm in Hubei, China, experienced a mass mortality event among artificially bred Chinese sturgeon offspring. To investigate the cause, we used pathogen isolation, pathology assessment, artificial infection, drug sensitivity testing, and bacterial whole-genome analysis.

All animal experiments were approved and conducted in compliance with the experimental practices and standards developed by the Animal Welfare and Research Ethics Committee of Yangtze River Fisheries Research Institute (YFI2022YYB019). The animals used in this study were derived from commercial

Author affiliations: Yangtze River Fisheries Research Institute, Chinese Academy of Fishery Sciences, Wuhan, China (Y. Yang, H. He, X. Zhu, Y. Liu, X. Ai); Key Laboratory of Sturgeon Genetics and Breeding, Ministry of Agriculture and Rural Affairs, Hangzhou Qiandao Lake Sturgeon Technology Co., Ltd., Hangzhou, China (Y. Yang, S. Xu, M. Hu, B. Jiang, Y. Li); Yangtze River Fisheries Research Institute, Chinese Academy of Fishery Sciences, Wuhan, China (Y. Yang, H. He, X. Zhu, Y. Liu, X. Ai); College of Animal Science and Technology, Hunan Agricultural University, Changsha, China (G. Fu); Fishery Resource and Environment Research Center, Chinese Academy of Fishery Sciences, Beijing, China (H. Zhang)

DOI: https://doi.org/10.3201/eid3006.231354

sources, and owners' consent was not required. All surviving fish continue to be cultured in the laboratory in accordance with standard breeding procedures.

Materials and Methods

Fish

We collected Chinese sturgeons displaying clinical signs and transported them to our laboratory (Yangtze River Fisheries Research Institute, Chinese Academy of Fishery Sciences, Wuhan, China) for disease diagnosis and isolation of pathogens. For infection experiments, we obtained healthy hybrid sturgeons (*Acipenser baeri* [male] × *Acipenser schrenckii* [female]) from farms without any history of such diseases. The hybrid sturgeons selected were energetic, showed no visible scars, and weighed 100 ±10 g. The hybrid sturgeons were temporarily housed in buckets for 7 days to confirm their health before infection testing.

Pathogen Confirmation

We investigated the breeding environment and water source of the Chinese sturgeon farm to determine the temperature and water quality conditions during the onset of disease as well as the disease history and drug use at the farm. To identify the key characteristics of the disease, we examined the body surface and anatomy of Chinese sturgeons displaying typical signs and those in critical condition. Fish showing typical signs were brought back to the laboratory, where we examined the internal organs and gills under an optical microscope to look for parasites and fungi (*9*).

Initially, we anesthetized the Chinese sturgeons and placed them on ice and disinfected their entire body with 75% ethanol. Using an inoculation ring, we sampled blood, kidneys, and intestines of each fish and inoculated the samples onto brain–heart infusion agar plates, incubated at 28°C for 24 hours. We selected the dominant strain on the plate for further purification, resulting in a dominant strain temporarily named zhx1. To preserve the purified strain, we added 15% glycerol, mixed well, and then stored it at –80°C for future use (*10*,*11*).

We fixed intestines, spleen, liver, kidneys, and gills of the Chinese sturgeons that had displayed clinical signs with 10% neutral formalin fixative. We then prepared slides of the tissues and performed histologic examination according to standard methods (*12*,*13*). We inoculated the isolated strain zhx1 onto brain–heart infusion agar plates and cultured them at 28°C for 18 hours. We then washed the bacterial moss with sterile phosphate-buffered saline (PBS) and adjusted the bacterial suspension to different concentrations.

For the experiment with healthy fish, we randomly divided 150 healthy hybrid sturgeons into 5 group of 30 each: A, B, C, D, and E. Each sturgeon in groups A–D was injected with 0.1 mL of bacterial suspension at the base of the ventral fin, at concentrations of 10^9 CFU/mL for group A, 10^8 CFU/mL for group B, 10^7 CFU/mL for group C, and 10^6 CFU/mL for group D. The sturgeons in the control group (group E) were injected with an equal dose of sterile PBS at the same site. During the experiment, the fish were not fed, dissolved oxygen was maintained between 7.5 and 8.5 mg/L, the water temperature was controlled at 21°C to 22°C, and the fully aerated tap water was changed daily. We collected visceral tissues of dying sturgeons for bacterial isolation and purification and monitored the condition of the experimental hybrid sturgeons until deaths ceased. We recorded our observations of the experimental sturgeons daily and calculated the mortality rate.

Antimicrobial Susceptibility of the Pathogen

We analyzed drug sensitivity of the zhx1 isolate by using the disk-diffusion method according to the Clinical and Laboratory Standards Institute antimicrobial drug sensitivity experimental standard (*14*). We inoculated the zhx1 isolate into brain–heart infusion and maintained the culture at 28°C with constant temperature oscillation (200 r/min) for 24 hours. Subsequently, we diluted the bacterial suspension with PBS to a concentration of 10^7 CFU/mL. Next, we spread 100 μL of the bacterial suspension onto Mueller-Hinton agar plates, placed the drug-sensitive disks on the plates, incubated them at 28°C for 24 hours, and measured the diameter of the inhibition rings.

Whole-Genome Sequencing

We extracted genomic DNA from bacterial cultures of zhx1 in brain–heart infusion by using a genomic DNA extraction kit (TaKaRa, https://www.takarabiomed.com). We used the PacBio Sequel platform (https://www.pacb.com) to sequence the entire genome. We used the hierarchical genome-assembly process version 2.3.0, single-molecular real-time analysis, for read assembly (*15*). We conducted predictions of coding DNA sequences by using Glimmer 3.02 (*16*). We generated the circular map of the genome by using Circos version 0.64 (*17*) and predicted genome islands by using the IslandPath-DIOMB genomic island prediction method (*18*). We predicted transfer RNA by using tRNAscan-Sev1.3.1 and ribosomal RNA by using Barrnap 0.7 software (*19*). We identified clusters

of regularly interspaced short palindromic repeats by using MinCED (*20*). We performed functional annotation through a BLASTP search (BLAST 2.2.28+, https://blast.ncbi.nlm.nih.gov/Blast.cgi) against the National Center for Biotechnology Information nonredundant database, gene database, string database, and gene ontology (GO) database. Protein function classifications were based on clustering of protein homology group (clusters of orthologous genes) annotations by using the string database and BLASTP comparisons (*21*). We compared predicted genes with the Kyoto Encyclopedia of Genes and Genomes database by using the BLAST algorithm to identify corresponding genes involved in specific biologic pathways, based on the Kyoto Encyclopedia of Genes and Genomes orthogonal number obtained from the comparison (*22*). GO annotations were performed by using Blast2GO.

Results

We identified pathologic changes in the intestines, spleen, liver, kidneys, and gills of infected Chinese sturgeons (Figure 1). Laboratory examination under microscopy did not reveal any parasitic or fungal infections. However, after bacteriological study, we isolated and identified a dominant bacterial strain, zhx.

During the artificial infection and pathogenicity study, hybrid sturgeons in the experimental groups exhibited varying degrees of mortality (Figure 2). The mortality rate in groups A and B reached 100%, and the fish displayed signs similar to those that occur with

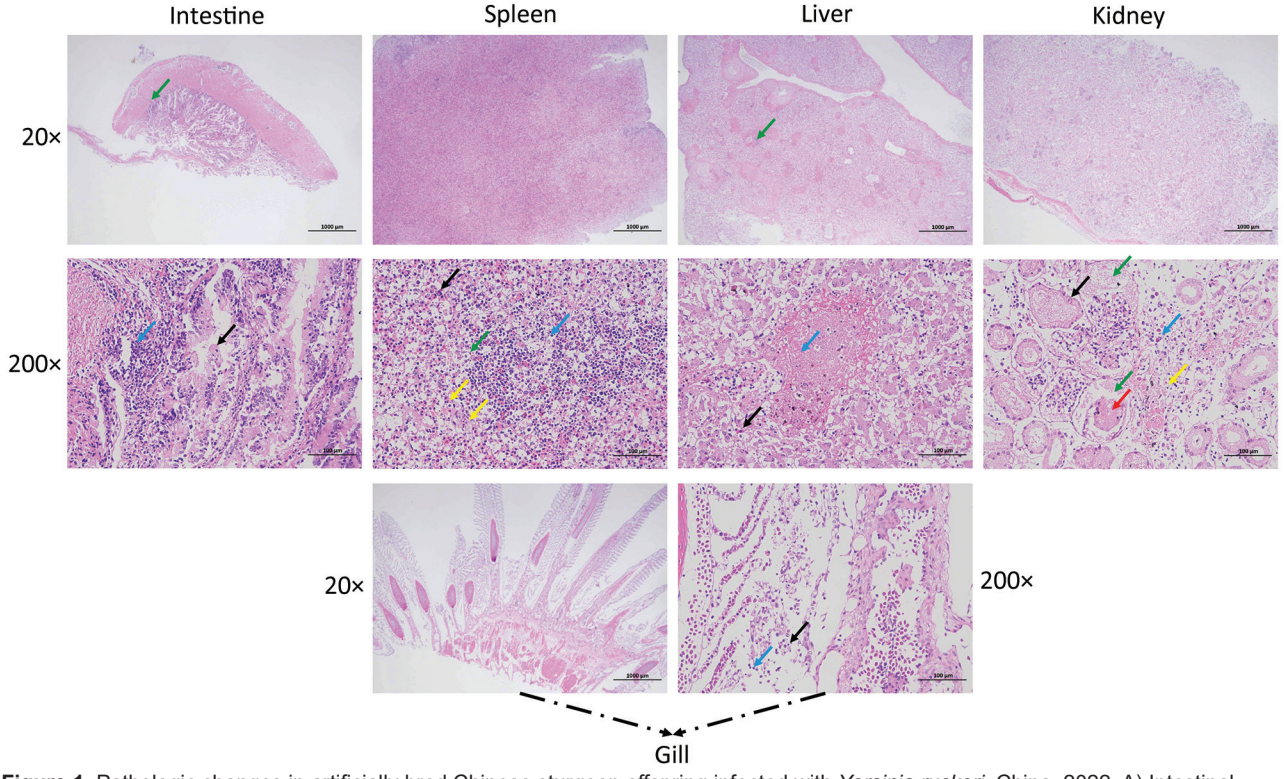

Figure 1. Pathologic changes in artificially bred Chinese sturgeon offspring infected with *Yersinia ruckeri*, China, 2022. A) Intestinal tissue showing mass intestinal villus necrosis and disordered structure; a large amount of mucosal epithelial cell necrosis and shedding (black arrow); extensive intestinal gland necrosis and connective tissue hyperplasia, with multiple lymphocyte infiltration (blue arrow); thick muscularis propria layer with small amount of connective tissue hyperplasia and small amount of lymphocyte infiltration (green arrow). B) Spleen tissue showing no obvious white pulp and unclear boundary between red pulp and white pulp; large area of red pulp congestion (black arrow); excessive lymphocyte necrosis and nuclear fragmentation (blue arrow); large number of lymphocytes with ballooning degeneration and vacuolization of the cytoplasm (green arrow); excessive infiltration of neutrophils (yellow arrows). C) Liver tissue showing diffuse balloon-like cell degeneration with vacuolization of cytoplasm (black arrow), dilation of liver sinuses, and irregular cell arrangement; multiple necrotic foci with a small amount of liver cell necrosis, nuclear lysis, and enhanced eosinophilia (blue arrow); small amount of focal infiltration of lymphocytes around the central vein (green arrow). D) Renal tissue showing diffuse watery degeneration of renal tubular epithelial cells with loose cytoplasm and light staining (black arrow) and loose arrangement of renal tubules; renal tubular epithelial cell necrosis, nuclear fragmentation (blue arrow), renal tubular structure disorder, accompanied by a small amount of lymphocyte infiltration (yellow arrow); excessive glomerular dilation with eosinophilic substances visible in the renal capsule (green arrow), cell necrosis and dissolution in the lumen, and disappearance of capillary loop structure (red arrow). E) Gill tissue showing small necrotic and detached pieces (black arrow) accompanied by a small amount of lymphocyte infiltration (blue arrow).

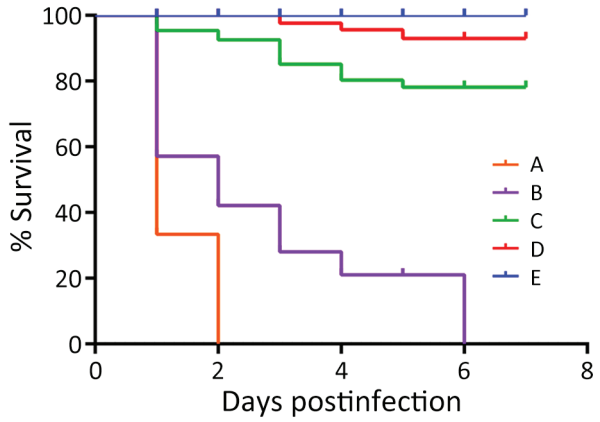

Figure 2. Survival rates for Chinese sturgeon experimentally inoculated with *Yersinia ruckeri* strain zhx1 isolated from artificially bred Chinese sturgeon offspring, China, 2022. Fish were injected with 0.1 mL of bacterial suspension at the base of the ventral fin at concentrations of 10^8 (group A), 10^7 (group B), 10^6 (group C), or 10^5 CFU/mL (group D) or with 0.1 mL phosphate-buffered saline as control (group E).

natural onset (e.g., red mouth and enteritis), but red mouth appeared very late. In contrast, we observed no disease or death among fish in control group E. The same bacteria with morphologic characteristics similar to zhx1 were isolated from the dying hybrid sturgeons, and subsequent identification confirmed the bacteria to be the same: zhx1. The infection experiment followed Koch's postulates, indicating that zhx1 was the pathogenic bacteria causing Chinese sturgeon disease.

Pathogen Confirmation

A phylogenetic tree based on bacterial whole-genome sequencing results (Figure 3, panel A) revealed clustering of zhx1 with *Y. ruckeri*, confirming that the isolated strain zhx1 is *Y. ruckeri*. The whole genome of zhx1 consists of a circular chromosome spanning 3,772,850 bp with an average guanine-cytosine content of 47.61% (Figure 3, panel B). Genome DNA sequencing generated 855,183 reads totaling 8,513,300,630 bp; sequencing depth was 1990×, and coverage rate was 100%. We identified 3,475 coding sequence genes, 22 ribosomal RNA genes, and 80 transfer RNA genes. Using the genomic island prediction method, we found 8 putative genomic islands in zhx1. In zhx1, we also identified 2 clustered regularly interspaced short palindromic repeats containing multiple short and repetitive sequences, 21-47–bp long. The sequencing reads are available in the National Center for Biotechnology Information Sequence Read Archive database (accession no. PRJNA1007872).

The zhx1 genome consisted of 443 virulence factor-related genes (e.g., which affect hemolysin, flagella, enterobactin, and outer membrane protein A), 135 drug-resistance-related genes (e.g., which affect macrolide, fluoroquinolones, aminoglycosides, cephalosporins, tetracyclines, and phenicol), 109 carbohydrate enzyme-associated genes, and 514 host–pathogen interaction–associated genes.

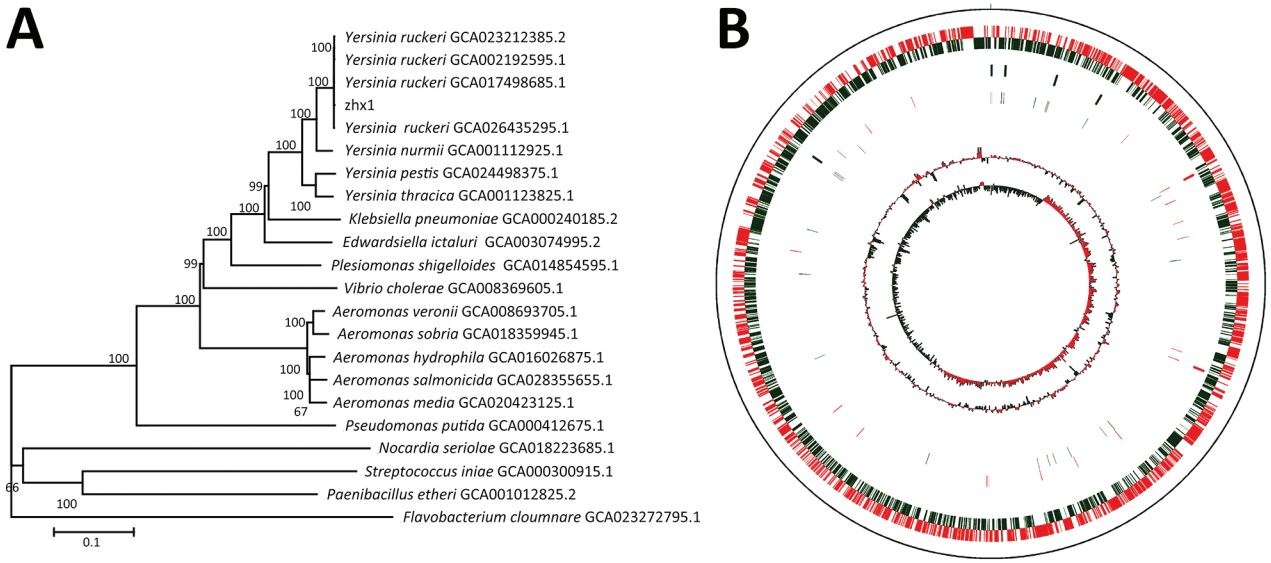

Figure 3. Genome characteristics of *Yersinia ruckeri* strain zhx1 isolated from artificially bred Chinese sturgeon offspring, China. A) Phylogenetic tree based on the whole genome of zhx1 and other pathogenic bacteria. B) Genome map of zhx1. The distribution of the circle from the outside indicates the genome size, forward coding DNA sequence (CDS), reverse CDS, repeat sequence, transfer RNA (black), ribosomal RNA (blue), and guanine-cytosine (GC) ratio. Colors indicate regions where the GC ratio is higher than average (red) and lower than average (green), and GC skewed either positive (red) or negative (green).

Pathogen Antimicrobial Susceptibility

We determined the sensitivity of the zhx1 isolate to 20 antimicrobial agents. zhx1 was highly sensitive to chloramphenicol and florfenicol and exhibited varying degrees of resistance to other drugs, especially those commonly used in aquaculture (e.g., doxycycline, neomycin) (Table 1).

Discussion

Chinese sturgeon farms have been experiencing disease outbreaks of enteric redmouth disease (ERM) for many years; incidence rates are high. In some ponds, the incidence rate has reached 80% and the mortality rate 50%. The disease is observed in sturgeons weighing 1–2 kg, with no noticeable individual differences. Disease onset occurs at water temperature <22°C. Diseased Chinese sturgeons exhibit signs such as red mouth and severe enteritis (Figure 4).

Y. ruckeri is classified as family *Enterobacteriaceae*, genus *Yersinia*, and is the pathogen responsible for ERM in cold-water salmonid fish (*23*,*24*). ERM was first detected in rainbow trout in the United States in 1952; subsequently, the pathogen was isolated from infected rainbow trout by Ross et al. in 1965 (*23*). During the 1970s and 1980s, *Y. ruckeri* spread from the United States to Europe, primarily between the United Kingdom and the European continent, infecting wild and farmed salmon in freshwater and seawater (*25*,*26*). However, since ERM was initially reported, its host range and geographic distribution have gradually expanded. Of note, channel catfish (*Ictalurus punctatus*) have become a major target of *Y. ruckeri* infection, especially in China (*27*,*28*), resulting in considerable economic losses for the global aquaculture industry.

Although local fish farmers have noted ERM in Chinese sturgeons in the past, infections with *Y. ruckeri* were not investigated or reported, but Shaowu et al. reported it in Amur sturgeons (*Acipenser schrencki*) (*29*). In various species of infected fish, the main clinical signs of ERM are subcutaneous hemorrhage around the mouth, varying degrees of hemorrhage in multiple visceral organs, intestinal inflammation accompanied by yellow mucus, and similar signs (*24*,*28*). In our study, the diseased Chinese sturgeons showed clinical signs and pathologic changes consistent with signs characteristic of ERM (*24*,*28*). Disease coincided with water temperatures <22°C, consistent with the environmental requirements of *Y. ruckeri* (*30*). Furthermore, our histopathologic results confirmed that the disease in Chinese sturgeons

Table. Antimicrobial susceptibility of *Yersinia ruckeri* strain zhx1 causing enteric redmouth disease in Chinese sturgeon, China, 2022*

Drug	Approximate judgment standard of inhibition zone, diameter, mm			Dose, μg	Inhibition zone diameter, mm, mean ± SD (susceptibility)
	R	I	S		
β-lactams					
Penicillin	≤17	18–20	≥21	10	0 (R)
Amoxicillin	≤13	14–17	≥18	20	0 (R)
Cephalosporins					
Ceftizoxime	≤14	15–19	≥20	30	0 (R)
Cefradine	≤14	15–17	≥18	30	0 (R)
Cefotaxime	≤14	15–22	≥23	30	0 (R)
Aminoglycosides					
Gentamicin	≤12	13–14	≥15	10	10.50 ± 0.50 (R)
Streptomycin	≤11	12–14	≥15	10	0 (R)
Netilmicin	≤12	13–14	≥15	30	9.00 ± 0.71(R)
Kanamycin	≤13	14–17	≥18	30	11.00 ± 1.41 (R)
Tobramycin	≤12	13–14	≥15	10	12.75 ± 0.83 (I)
Neomycin†	≤12	13–16	≥17	30	13.50 ±1.12 (I)
Macrolides					
Azithromycin	≤13	14–17	≥18	15	9.75 ± 1.09 (R)
Erythromycin	≤13	14–22	≥23	15	12.25 ± 0.83 (R)
Tetracyclines					
Tetracycline	≤18	19–22	≥23	30	18.00 ± 1.58 (I)
Doxycycline†	≤12	13–15	≥16	30	14.25 ± 1.48 (I)
Quinolones					
Enoxacin	≤14	15–17	≥18	10	14.75 ± 1.64 (I)
Norfloxacin	≤12	13–16	≥17	10	15.50 ± 1.12 (I)
Amphenicols					
Chloramphenicol	≤12	13–17	≥18	300	22.75 ± 0.83 (S)
Florfenicol†	≤12	13–17	≥18	75	20.75 ± 1.30 (S)
Sulfonamides					
Sulfisoxazole	≤12	13–16	≥17	300	11.25 ± 0.43 (R)

*I, intermediately sensitive; R, resistant; S, sensitive.
†Veterinary antibiotics used in aquaculture.

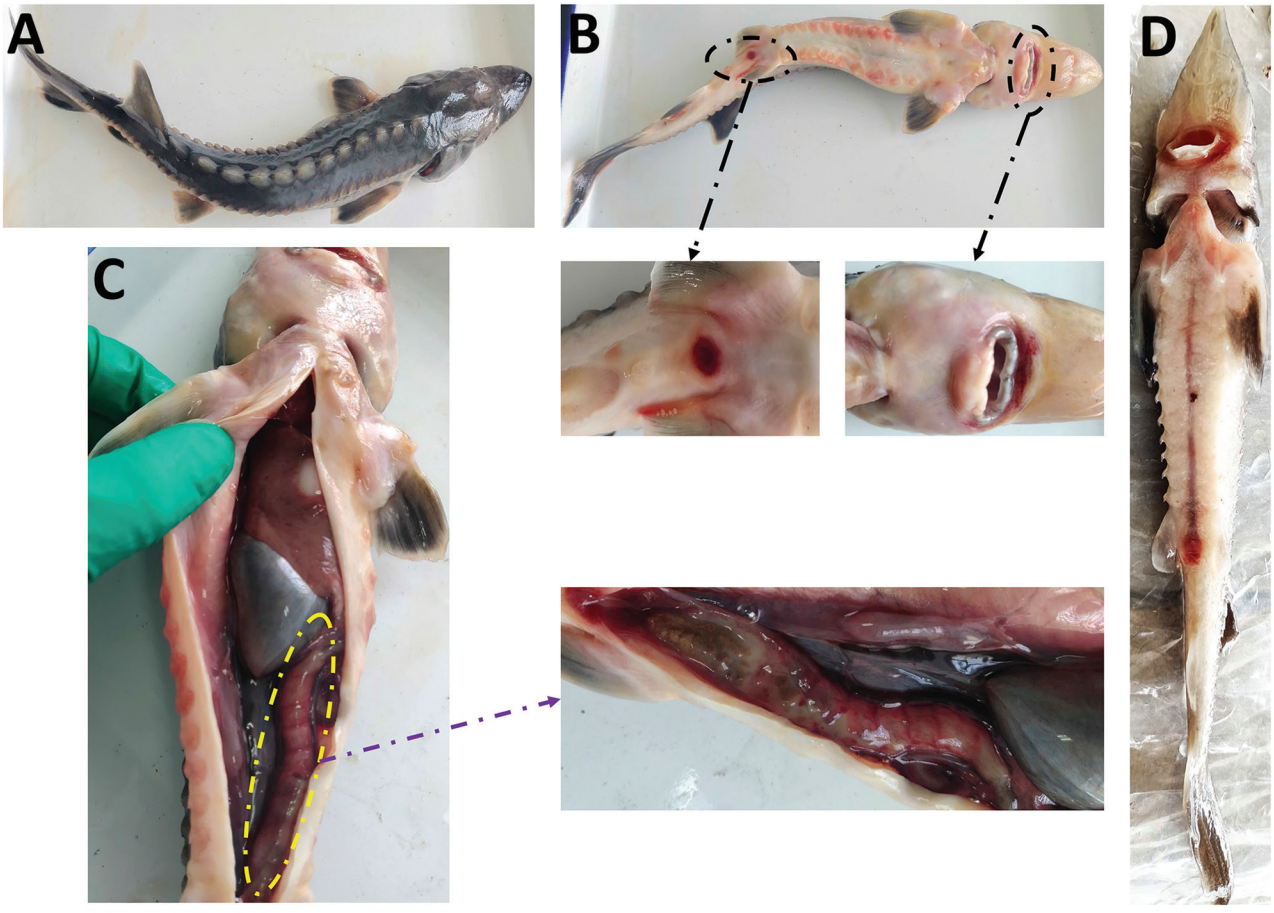

Figure 4. Clinical signs of Chinese sturgeons infected with *Yersinia ruckeri*, China. A–C) Naturally infected artificially bred Chinese sturgeon offspring: A) back; B) anal redness and swelling, red mouth; C) severe intestinal inflammation. D) Fish experimentally infected with *Y. ruckeri*.

followed the general pattern of *Y. ruckeri* infection (i.e., the pathogen invades the body through the circulatory system after entering either the gills or intestine) (*28*). Our results indicate expanded host range of *Y. ruckeri* infection. Other research has isolated *Y. ruckeri* pathogens from human infected wounds, suggesting its potential as a pathogenic bacterium for humans and other animals (*31*) and raising concerns regarding public health.

As first-class protected animals in China, Chinese sturgeons have been endangered, and their protection is of great value (*1*). The large-scale mortality caused by the infection of *Y. ruckeri* in Chinese sturgeons poses a threat to survival of the species, which may be catastrophic for the fish, creating significant challenges for species protection. Current prevention and control of bacterial diseases in fish rely mainly on antibacterial drugs (*32*). However, antibacterial drug use has resulted in bacterial drug resistance, which has induced numerous problems and garnered more attention (*33*). Our results indicate that zhx1 is a strain of severely drug-resistant *Y. ruckeri* bacteria. Genomewide analysis also revealed the presence of 133 drug-resistant genes in the chromosomal region of zhx1 (e.g., affecting macrolides, fluoroquinolones, aminoglycosides, cephalosporins, tetracyclines, and phenicol). However, carrying drug-resistance genes did not necessarily result in corresponding drug-resistant phenotypes (*34*). For example, zhx1 carried phenicol-resistant genes but demonstrated high sensitivity to chloramphenicol. Therefore, the mechanism of bacterial drug resistance is complex (*35*).

In conclusion, our findings contribute valuable insight for promoting healthy breeding, preventing disease, and protecting Chinese sturgeons. Selecting appropriate antimicrobial agents for treating ERM in Chinese sturgeons is challenging. Thus, the preferred approach has become using vaccines to prevent ERM. The formalin-inactivated vaccine of *Y. ruckeri* has shown promising results for preventing and treating salmonid fish diseases (*36*). Consequently, vaccination has become a practical method for

preventing *Y. ruckeri* disease in fish (*37*). However, in China, because of strict restrictions on the use of biological products and rigorous reviews, no *Y. ruckeri* vaccine is currently available, which brings about substantial difficulties for prevention and control of ERM in Chinese sturgeons and becomes a bottleneck problem for protecting the species. Therefore, in-depth research on the mechanism of ERM in Chinese sturgeons focuses on the development of an inactivated vaccine against *Y. ruckeri*, and breakthroughs in administrative approval are crucial. Those actions will help overcome challenges associated with the prevention and control of ERM in Chinese sturgeons, safeguard the Chinese sturgeon species, and contribute to biodiversity.

Acknowledgments

We sincerely thank anonymous reviewers for their constructive comments which lead to an improved manuscript.

This work was supported by Central Public-Interest Scientific Institution Basal Research Fund, CAFS (2023TD12 and 2023TD47), and China Postdoctoral Fund (2023M733700). The authors declare that they have no conflict of interest.

About the Author

Dr. Yang is an associate researcher at Yangtze River Fisheries Research Institute, Chinese Academy of Fishery Sciences. His main research interest is infectious diseases of aquatic animals, particularly the use of human drugs, veterinary drugs, or aquatic animal specific drugs for disease prevention and control in the protection of endangered aquatic animals.

References

1. Leng X, Luo J, Du H, Xiong W, Qiao X, Wei Q. Alterations in the gut microbiota in Chinese sturgeon (*Acipenser sinensis*) suffering from haemorrhagic septicaemia. Aquaculture Research. 2021;52:6410–9. https://doi.org/10.1111/are.15506
2. Wang JH, Wei QW, Zou YC. Conservation strategies for the Chinese sturgeon, *Acipenser sinensis*: an overview on 30 years of practices and future needs. Journal of Applied Ichthyology. 2011;27:176–80. https://doi.org/10.1111/j.1439-0426.2011.01716.x
3. Qiao Y, Tang X, Brosse S, Chang J. Chinese sturgeon (*Acipenser sinensis*) in the Yangtze River: a hydroacoustic assessment of fish location and abundance on the last spawning ground. Journal of Applied Ichthyology. 2006;22(s1):140–4. https://doi.org/10.1111/j.1439-0426.2007.00942.x
4. Zhuang P, Zhao F, Zhang T, Chen Y, Liu J, Zhang L, et al. New evidence may support the persistence and adaptability of the near-extinct Chinese sturgeon. Biological Conservation. 2016;193:66–9. https://doi.org/10.1016/j.biocon.2015.11.006
5. Yang D, Kynard B, Wei Q, Chen X, Zheng W, Du H. Distribution and movement of Chinese sturgeon, *Acipenser sinensis*, on the spawning ground located below the Gezhouba Dam during spawning seasons. Journal of Applied Ichthyology. 2006;22(s1):145–51. https://doi.org/10.1111/j.1439-0426.2007.00943.x
6. Di J, Zhang S, Huang J, Du H, Zhou Y, Zhou Q, et al. Isolation and identification of pathogens causing haemorrhagic septicaemia in cultured Chinese sturgeon (*Acipenser sinensis*). Aquaculture Research. 2018;49:3624–33. https://doi.org/10.1111/are.13830
7. Zhang DF, Ji C, Zhang XJ, Li TT, Li AH, Gong XN. Mixed mycobacterial infections in farmed sturgeon. Aquaculture Research. 2015;46:1914–23. https://doi.org/10.1111/are.12346
8. Xu J, Zeng X, Jiang N, Zhou Y, Zeng L. *Pseudomonas alcaligenes* infection and mortality in cultured Chinese sturgeon, *Acipenser sinensis.* Aquaculture. 2015;446:37–41. https://doi.org/10.1016/j.aquaculture.2015.04.014
9. Qin GX, Xu J, Ai XH, Yang YB. Isolation, identification, and pathogenicity of *Aeromonas veronii*, the causal agent of hemorrhagic septicemia in channel catfish (*Ictalurus punctatus*) in China. Fishes. 2022;7:394. https://doi.org/10.3390/fishes7060394
10. Yang YB, Zhang HX, Liu YT, Dong J, Xu N, Yang QH, et al. Identification of *Vibrio cholerae* as a bacterial pathogen of bluegill sunfish. Aquaculture Reports. 2022;23:101092. https://doi.org/10.1016/j.aqrep.2022.101092
11. Yang Y, Zhu X, Zhang H, Chen Y, Liu Y, Song Y, et al. *Vibrio cholerae* was found in cultured bullfrog. Epidemiol Infect. 2022;150:e30. https://doi.org/10.1017/S0950268822000164
12. Hofmann I, Kemter E, Fiedler S, Theobalt N, Fonteyne L, Wolf E, et al. A new method for physical disector analyses of numbers and mean volumes of immunohistoc hemically labeled cells in paraffin sections. J Neurosci Methods. 2021;361:109272. https://doi.org/10.1016/j.jneumeth.2021.109272
13. Zhu W, Zhang Y, Zhang J, Yuan G, Liu X, Ai T, et al. *Astragalus polysaccharides*, chitosan and poly(I:C) obviously enhance inactivated *Edwardsiella ictaluri* vaccine potency in yellow catfish *Pelteobagrus fulvidraco*. Fish Shellfish Immunol. 2019;87:379–85. https://doi.org/10.1016/j.fsi.2019.01.033
14. Humphries R, Bobenchik AM, Hindler JA, Schuetz AN. Overview of changes to the Clinical and Laboratory Standards Institute performance standards for antimicrobial susceptibility testing, M100, 31st edition. J Clin Microbiol. 2021;59:e0021321.
15. Chin C-S, Alexander DH, Marks P, Klammer AA, Drake J, Heiner C, et al. Nonhybrid, finished microbial genome assemblies from long-read SMRT sequencing data. Nat Methods. 2013;10:563–9. https://doi.org/10.1038/nmeth.2474
16. Delcher AL, Kasif S, Fleischmann RD, Peterson J, White O, Salzberg SL. Alignment of whole genomes. Nucleic Acids Res. 1999;27:2369–76. https://doi.org/10.1093/nar/27.11.2369
17. Krzywinski M, Schein J, Birol I, Connors J, Gascoyne R, Horsman D, et al. Circos: an information aesthetic for comparative genomics. Genome Res. 2009;19:1639–45. https://doi.org/10.1101/gr.092759.109
18. Dhillon BK, Laird MR, Shay JA, Winsor GL, Lo R, Nizam F, et al. IslandViewer 3: more flexible, interactive genomic island discovery, visualization and analysis. Nucleic Acids Res. 2015;43:W104-8. https://doi.org/10.1093/nar/gkv401
19. Lowe TM, Eddy SR. tRNAscan-SE: a program for improved detection of transfer RNA genes in genomic sequence.

Nucleic Acids Res. 1997;25:955–64. https://doi.org/10.1093/nar/25.5.955
20. Grissa I, Vergnaud G, Pourcel C. CRISPRFinder: a web tool to identify clustered regularly interspaced short palindromic repeats. Nucleic Acids Res. 2007;35:W52–57.
21. Tatusov RL, Natale DA, Garkavtsev IV, Tatusova TA, Shankavaram UT, Rao BS, et al. The COG database: new developments in phylogenetic classification of proteins from complete genomes. Nucleic Acids Res. 2001;29:22–8. https://doi.org/10.1093/nar/29.1.22
22. Kanehisa M, Goto S. KEGG: kyoto encyclopedia of genes and genomes. Nucleic Acids Res. 2000;28:27–30. https://doi.org/10.1093/nar/28.1.27
23. Ross AJ, Rucker RR, Ewing WH. Description of a bacterium associated with redmouth disease of rainbow trout (*Salmo gairdneri*). Can J Microbiol. 1966;12:763–70. https://doi.org/10.1139/m66-103
24. Kumar G, Menanteau-Ledouble S, Saleh M, El-Matbouli M. *Yersinia ruckeri*, the causative agent of enteric redmouth disease in fish. Vet Res (Faisalabad). 2015;46:103. https://doi.org/10.1186/s13567-015-0238-4
25. Huang Y, Runge M, Michael GB, Schwarz S, Jung A, Steinhagen D. Biochemical and molecular heterogeneity among isolates of *Yersinia ruckeri* from rainbow trout (*Oncorhynchus mykiss*, Walbaum) in North West Germany. BMC Vet Res. 2013;9:215. https://doi.org/10.1186/1746-6148-9-215
26. Calvez S, Fournel C, Douet DG, Daniel P. Pulsed-field gel electrophoresis and multi locus sequence typing for characterizing genotype variability of *Yersinia ruckeri* isolated from farmed fish in France. Vet Res (Faisalabad). 2015;46:73. https://doi.org/10.1186/s13567-015-0200-5
27. Yang Y, Zhu X, Zhang H, Chen Y, Song Y, Ai X. Dual RNA-Seq of trunk kidneys extracted from channel catfish infected with *Yersinia ruckeri* reveals novel insights into host-pathogen interactions. Front Immunol. 2021;12:775708. https://doi.org/10.3389/fimmu.2021.775708
28. Liu T, Wang KY, Wang J, Chen DF, Huang XL, Ouyang P, et al. Genome sequence of the fish pathogen *Yersinia ruckeri* sc09 provides insights into niche adaptation and pathogenic mechanism. Int J Mol Sci. 2016;17:557. https://doi.org/10.3390/ijms17040557
29. Shaowu L, Di W, Hongbai L, Tongyan L. Isolation of *Yersinia ruckeri* strain H01 from farm-raised Amur sturgeon *Acipenser schrencki* in China. J Aquat Anim Health. 2013;25:9–14. https://doi.org/10.1080/08997659.2012.728169
30. Danley ML, Goodwin AE, Killian HS. Killian HS. Epizootics in farm–raised channel catfish, *Ictalurus punctatus* (Rafinesque), caused by the enteric redmouth bacterium *Yersinia ruckeri*. Journal of Fish Diseases. 1999;22:451–6. https://doi.org/10.1046/j.1365-2761.1999.00196.x
31. De Keukeleire S, De Bel A, Jansen Y, Janssens M, Wauters G, Piérard D. *Yersinia ruckeri*, an unusual microorganism isolated from a human wound infection. New Microbes New Infect. 2014;2:134–5. https://doi.org/10.1002/nmi2.56
32. Liu X, Steele JC, Meng X-Z. Usage, residue, and human health risk of antibiotics in Chinese aquaculture: a review. Environ Pollut. 2017;223:161–9. https://doi.org/10.1016/j.envpol.2017.01.003
33. Cabello FC. Heavy use of prophylactic antibiotics in aquaculture: a growing problem for human and animal health and for the environment. Environ Microbiol. 2006;8:1137–44. https://doi.org/10.1111/j.1462-2920.2006.01054.x
34. Christaki E, Marcou M, Tofarides A. Antimicrobial resistance in bacteria: mechanisms, evolution, and persistence. J Mol Evol. 2020;88:26–40. https://doi.org/10.1007/s00239-019-09914-3
35. Munita JM, Arias CA. Mechanisms of antibiotic resistance. Microbiol Spectr. 2016;4:4.2.15. https://doi.org/10.1128/microbiolspec.VMBF-0016-2015
36. Ellis AE. Immunity to bacteria in fish. Fish & Shellfish Immunology. 1999;9:291–308. https://doi.org/10.1006/fsim.1998.0192
37. Raida MK, Buchmann K. Innate immune response in rainbow trout (*Oncorhynchus mykiss*) against primary and secondary infections with *Yersinia ruckeri* O1. Dev Comp Immunol. 2009;33:35–45. https://doi.org/10.1016/ j.dci.2008.07.001

Address for correspondence: Hongyu Zhang, Fishery Resource and Environment Research Center, Chinese Academy of Fishery Sciences, 150 Nanqingta Village, Yongding Rd, Fengtai District, Beijing, 100141, China, China; email: zhanghy@cafs.ac.cn; Guihong Fu, College of Animal Science and Technology, Hunan Agricultural University, No. 1 Nongda Rd, Furong District, Changsha City, Hunan Province, 410128, China; email: snow03221@163.com; Shijian Xu, Key Laboratory of Sturgeon Genetics and Breeding, Ministry of Agriculture and Rural Affairs, Hangzhou Qiandao Lake Sturgeon Technology Co., Ltd., 55 Pailing South Rd, Qiandao Lake Town, Chun'an County, Hangzhou City, Zhejiang Province, 311799; email: xsj@kalugaqueen.com

Outbreak of Highly Pathogenic Avian Influenza A(H5N1) Virus in Seals, St. Lawrence Estuary, Quebec, Canada[1]

Stéphane Lair, Louise Quesnel, Anthony V. Signore, Pauline Delnatte, Carissa Embury-Hyatt, Marie-Soleil Nadeau, Oliver Lung, Shannon T. Ferrell, Robert Michaud, Yohannes Berhane

We describe an unusual mortality event caused by a highly pathogenic avian influenza (HPAI) A(H5N1) virus clade 2.3.4.4b involving harbor (*Phoca vitulina*) and gray (*Halichoerus grypus*) seals in the St. Lawrence Estuary, Quebec, Canada, in 2022. Fifteen (56%) of the seals submitted for necropsy were considered to be fatally infected by HPAI H5N1 containing fully Eurasian or Eurasian/North American genome constellations. Concurrently, presence of large numbers of bird carcasses infected with HPAI H5N1 at seal haul-out sites most likely contributed to the spillover of infection to the seals. Histologic changes included meningoencephalitis (100%), fibrinosuppurative alveolitis, and multiorgan acute necrotizing inflammation. This report of fatal HPAI H5N1 infection in pinnipeds in Canada raises concerns about the expanding host of this virus, the potential for the establishment of a marine mammal reservoir, and the public health risks associated with spillover to mammals.

Nous décrivons un événement de mortalité inhabituelle causé par un virus de l'influenza aviaire hautement pathogène A(H5N1) clade 2.3.4.4b chez des phoques communs (*Phoca vitulina*) et gris (*Halichoerus grypus*) dans l'estuaire du Saint-Laurent au Québec, Canada, en 2022. Quinze (56%) des phoques soumis pour nécropsie ont été considérés comme étant fatalement infectés par le virus H5N1 de lignées eurasiennes ou de réassortiment eurasiennes/nord-américaines. Un grand nombre simultané de carcasses d'oiseaux infectés par le H5N1 sur les sites d'échouement a probablement contribué à la contamination de ces phoques. Les changements histologiques associés à cette infection incluaien: méningo-encéphalite (100%), alvéolite fibrino-suppurée et inflammation nécrosante aiguë multi-organique. Cette documentation soulève des préoccupations quant à l'émergence de virus mortels, à la possibilité d'établissement de réservoirs chez les mammifères marins, et aux risques pour la santé publique associés aux propagations du virus chez les mammifères.

Sporadic outbreaks of influenza A virus (IAV) infections have been reported in pinnipeds in the United States and Europe, most commonly in harbor (*Phoca vitulina*) and gray (*Halichoerus grypus*) seals (*1*–*3*). Characterization of the IAV-associated subtypes has suggested an avian-variant origin, thought to occur through cross-species transmission or spillover from wild aquatic birds (*4*,*5*). The reported IAV outbreaks in pinnipeds have mainly caused fatal respiratory diseases (*6*,*7*). Harbor seals seem to be particularly susceptible to IAV infections, and factors such as close contact with wild birds and mammalian adaptations of the virus subtypes have been suggested as drivers in establishing a potential reservoir of IAV in marine mammals (*5*,*8*).

Although epidemics of IAV have been reported since the late 1970s in seals on the North American Atlantic coast, fatal influenza virus infections have not been documented in marine mammals from the St. Lawrence Estuary and Gulf, Quebec, Canada.

Author affiliations: Université de Montréal, St. Hyacinthe, Quebec, Canada (S. Lair, L. Quesnel, P. Delnatte, S.T. Ferrell); Canadian Food Inspection Agency, Winnipeg, Manitoba, Canada (A.V. Signore, C. Embury-Hyatt, O.Lung, Y. Berhane); Ministère de l'Agriculture, des Pêcheries et de l'Alimentation du Quebec, St. Hyacinthe (M.-S. Nadeau); Groupe de recherche et d'éducation sur les mammifères marins, Tadoussac, Quebec, Canada (R. Michaud).

DOI: https://doi.org/10.3201/eid3006.231033

[1]Preliminary results from this study were presented at the International Association for Aquatic Animal Medicine Conference, May 24, 2023, Salt Lake City, Utah, USA.

Moreover, despite the documented high seroprevalence of influenza virus A and B in Canada seal populations (*9*), seal deaths caused by an influenza infection were initially reported in Canada when a novel low-pathogenicity avian IAV (H10N7) caused fatal bronchointerstitial pneumonia in a harbor seal in British Columbia (*10*).

A wild gull found dead in eastern Canada in November 2021 was confirmed to be infected by HPAI H5N1 clade 2.3.4.4b A/goose/Guangdong/1/1996 (Gs/GD) lineage (*11*). That novel virus subtype was likely introduced by wild birds that carried it across the Atlantic Ocean through pelagic routes or during direct winter migration (*11*). The virus spread rapidly across North America and reassorted with North American lineage IAVs, causing unprecedented outbreaks in many species of wild birds and commercial and backyard poultry flocks and spillover to several species of wild terrestrial mammals (*12*–*16*).

During summer 2022, deaths of harbor and gray seals caused by H5N1 clade 2.3.4.4b virus infection were confirmed in eastern Quebec and on the coast of Maine, USA, prompting the US National Oceanic and Atmospheric Administration to declare an unusual mortality event for Maine harbor and gray seals (*17*). HPAI infections have also recently been reported as the cause of death of harbor seals in the North Sea (H5N8 virus) (*18*), gray seals in the Baltic Sea (H5N8 virus) (*19*), South American sea lions (*Otaria flavescens*) in Peru (*20*) and Chile (*21*), and other marine mammals in Peru (*22*). Given the emergence of this virus in marine mammals in the St. Lawrence Estuary and public health concerns associated with mammalian spillover of avian IAV, we aimed to describe the 2022 outbreak of HPAI H5N1 affecting pinniped species, emphasizing epidemiologic data and pathology findings.

Material and Methods

Stranding Data Analysis

We obtained stranding data from the archives of the Quebec Marine Mammal Emergency Response Network, which monitors mortality and morbidity of marine mammals in the St. Lawrence River, Estuary and Gulf (48°23′N, 69°07′W). We compared the number of stranded (dead, ill, or injured) harbor seals, gray seals, and seals of unspecified species during the second and third quarters of 2022 (April 1–September 30) with the average of the 10 previous years for the same period using a 1-sample *t*-test. We evaluated goodness-of-fit of the stranding distribution of 2012 to 2021 with a Shapiro-Wilk test for both groups of seals. We considered distribution normal if $p>0.05$. We combined seals of unidentified species with harbor seals for this comparison to control for the differences in species identification rates in 2022 compared with previous years (data not shown).

Postmortem Examination

We based our selection of carcasses to be examined on the state of decomposition (*23*) and field access. All carcasses were submitted frozen and, after thawing, were examined by veterinary pathologists with experience in marine mammal pathology. Animals were classified into 2 age groups, <1 year old or adult, on the basis of total length (*24*). Animals with no evidence of muscular or fat depletion were considered to be in good nutritional condition. Tissue samples of major organs (lung, heart, kidney, brain, intestines, lymph nodes, liver, spleen, pancreas, tongue, adrenal gland, esophagus, bladder, stomach, thyroid gland, mammary gland, and thymus) were processed for histopathologic evaluation by light microscopy using standard laboratory procedures. For each necropsy case, separate nasal and rectal swab samples were collected using a sterile polyester-tipped plastic applicator (UltiDent Scientific, https://www.ultident.com) placed in UT medium (Micronostyx, https://micronostyx.com). In addition, rectal and nasal swab samples were collected from seals found stranded for which the carcass could not be examined either because of poor preservation state or logistical limitations. All samples were first tested for IAV by PCR at the provincial Animal Health Laboratory (Laboratoire de santé animale, Ministère de l'Agriculture, des Pêcheries et de l'Alimentation du Québec; MAPAQ). All IAV H5–positive samples were subsequently sent to the National Centre for Foreign Animal Disease (NCFAD) laboratory (Winnipeg, MB, Canada) for confirmatory testing. Samples of brain or lung were also submitted for PCR for cases that had lesions suggestive of IAV but tested negative on swab samples.

RNA Extraction, Reverse Transcription PCR, and Virus Isolation

Both laboratories (MAPAQ and NCFAD) used the same methods for RNA extraction and PCR. Total RNA was extracted from clinical specimens (swabs and tissues) and virus isolates using the MagMax AM1836 96 Viral RNA Isolation Kit (ThermoFisher Scientific, https://www.thermofisher.com) according to manufacturer recommendations, using the KingFisher Duo Prime, KingFisher Flex, or Apex platforms (ThermoFisher Scientific). Spiked enteroviral armored RNA (Asuragen, https://asuragen.com)

was used as an exogenous extraction and reaction control. The extracted RNA samples were tested for IAV genomic material by using matrix gene–specific real-time reverse transcription PCR. Samples positive with the matrix primer set underwent repeat PCR with H5- and H7-specific primer sets, as described previously (*25*,*26*). Cycle threshold values <36.00 were considered positive and values 36.00–40.00 suspicious. For virus isolation, PCR-positive samples were inoculated into 9-day-old embryonated specific pathogen-free chicken eggs via the allantoic route.

Nanopore Sequencing and Genome Assembly

To determine the clade, lineage, and clusters of each positive sample, the full genome segments of IAVs were amplified directly from clinical specimens or isolates using reverse transcription PCR, as described previously (*27*). Nanopore sequencing was performed on a GridION sequencer (Oxford Nanopore, https://nanoporetech.com) with an R9.4.1 flowcell after library construction using the rapid barcoding kit (SQKRBK004 or SQK-RBK110.96). The raw nanopore signal data was basecalled and demultiplexed with Guppy version 5.1.12 (Oxford Nanopore) using the high accuracy or super-accurate basecalling model on each run. Basecalled nanopore reads were analyzed and assembled with a BLAST search (https://blast.ncbi.nlm.nih.gov) of Iterative Refinement Meta-Assembler assembled genome segment sequences against all sequences from the National Center for Biotechnology Information Influenza Virus Sequence Database (n = 959,847) (https://www.ncbi.nlm.nih.gov/genomes/FLU/Database/nph-select.cgi) and influenza virus sequences from the 2021–2022 HPAI H5N1 outbreaks. We deposited whole-genome sequences of the HPAI H5N1 viruses from seals into the GISAID database (https://www.gisaid.org; accession nos. EPI_ISL_18916928–37).

Phylogenetic Analyses

We combined the HPAI H5N1 genomes sequenced from seals (10 samples) with 40 closely related sequences (as determined by BLAST similarity search) collected from wild birds during April–September 2022. We trimmed individual viral segments (polymerase basic 1 and 2, polymerase acidic, hemagglutinin, nucleoprotein, neuraminidase, matrix, nonstructural) of regions flanking the open reading frames and concatenated. We removed duplicate sequences from the dataset, leaving 43 complete viral genomes, totaling 13,112 nt in length, which we aligned using MAFFT version 7.49 (https://mafft.cbrc.jp). We used that alignment to estimate a time-scaled phylogenetic tree using BEAST version 1.10.4 (*28*). We performed tree estimations under the best fitting model of nucleotide substitution as determined by ModelFinder (generalized time-reversible model, empirical base frequencies, invariant sites, 4-category gamma distribution of rate heterogeneity) (*29*), a relaxed molecular clock with log-normal distribution, and a Gaussian Markov Random Field Bayesian skyride tree prior (*30*). We also ran 2 independent Markov chain Monte Carlo chains (200 million steps, sampled every 20,000 steps), discarding the first 10% of samples from each chain as burn-in, and assessed the chains for convergence (based on effective sample size >200) using Tracer version 1.7.2 (*31*). We combined post–burn-in samples using LogCombiner version 1.10.4 and produced maximum clade credibility (MCC) trees by using TreeAnnotator version 1.10.4 (*28*).

Immunohistochemistry

For immunohistochemistry (IHC), we quenched paraffin tissue sections for 10 minutes in aqueous 3% hydrogen peroxide. We then retrieved epitopes using proteinase K for 15 minutes and rinsed. The primary antibody applied to the sections was a mouse monoclonal antibody specific for IAV nucleoprotein (F26NP9, produced in-house) used at a 1:5,000 dilution for 30 minutes. We visualized the primary antibody binding by using a horseradish peroxidase labeled polymer, the Dako EnVision+ system (anti-mouse) (Agilent, https://www.agilent.com), reacted with chromogen diaminobenzidine. We then counterstained the section with Gill hematoxylin.

Results

Stranding Data

During April 1–September 30, 2022, a total of 209 dead or sick seals were reported in the waters bordering Quebec: 127 harbor seals, 47 gray seals, 6 harp seals (*Pagophilus groenlandicus*), 1 hooded seal (*Cystophora cristata*), and 28 seals of undetermined species. The number of dead or sick stranded harbor seals and seals of unknown species combined during that period of time (n = 55) was 3.7 times higher than the average annual number in the previous 10 years for the same period (n = 41.6), representing a statistically significant increase in number of strandings (t = 5.55, d.f. = 9; p<0.001) (Figure 1, panel A). A statistically significant increase of similar magnitude was noted for the number of gray seals found dead or sick during the second and third quarters of 2022 (47 in 2022 compared with an average of 12 in 2012–2021; t = 4.35, d.f. = 9; p = 0.002) (Figure 1, panel B). We

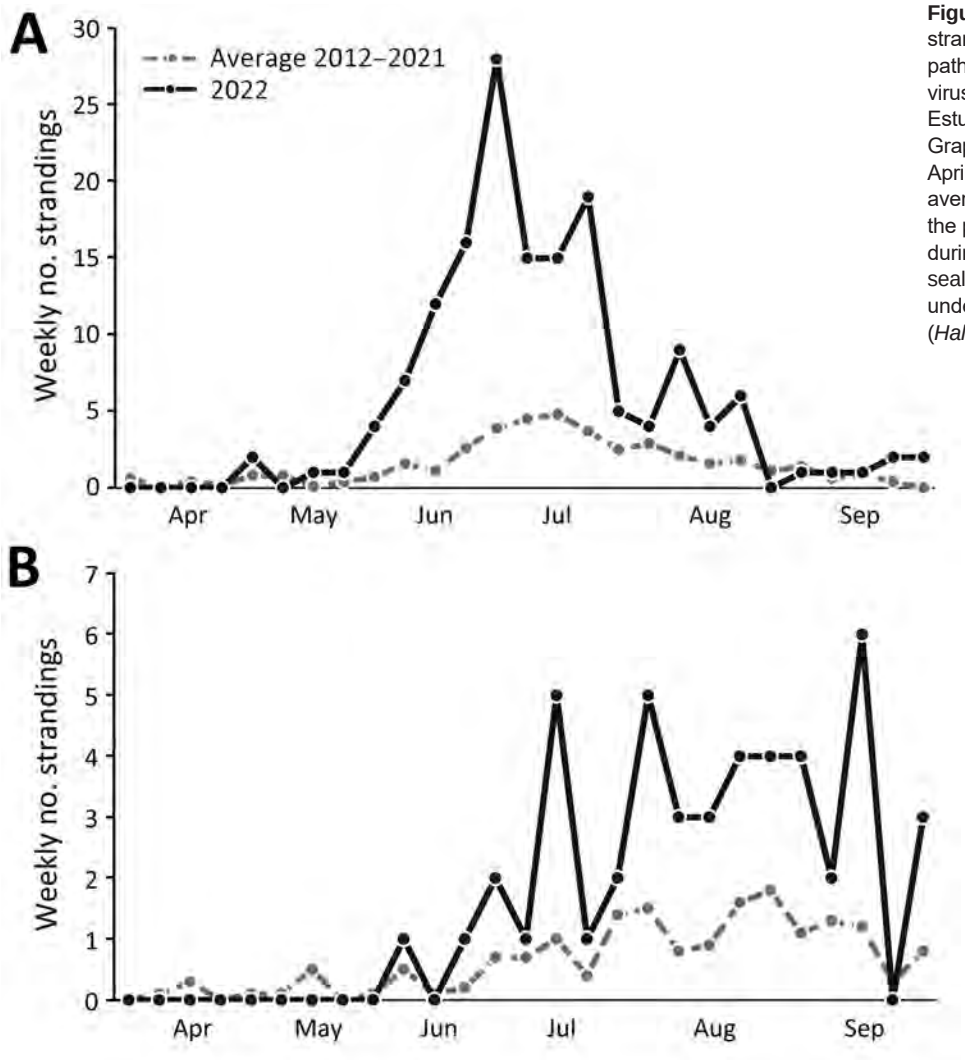

Figure 1. Weekly occurrences of stranded seals in an outbreak of highly pathogenic avian influenza A(H5N1) virus in seals, the St. Lawrence Estuary and Gulf, Quebec, Canada. Graphs compare strandings during April 1–September 30, 2022, with the average number of strandings over the previous 10 years (2012–2021) during the same quarters. A) Harbor seals (*Phoca vitulina*) and seals of undetermined species; B) gray seals (*Halichoerus grypus*).

observed no increase in mortality or morbidity for the other species of pinnipeds compared with the previous 10 years.

Descriptive Epidemiology and Necropsy Findings

Carcasses of 22 harbor seals, 3 gray seals, 1 harp seal, and 1 hooded seal found during April 22–October 6, 2022, were submitted for postmortem examination. On the basis of molecular detection of H5 and presence of lesions suggestive of IAV infection, HPAI H5N1 was identified as cause of death of 14 harbor seals and 1 gray seal (56%) (Table 1). Combined nasal and rectal swab samples were obtained on the shore from an additional 11 harbor seal and 1 gray seal carcasses, and HPAI H5N1 was identified in 6 of the harbor seals (50% of those sampled) (Table 1).

All 21 infected seals were found during May 30–July 8, 2022, in the estuarine segment of the St. Lawrence waterway, mainly on the south shore, between the towns of Baie-Comeau (49.2213°N, 68.1504°W) and Notre-Dame-du-Portage (47.7630°N, 69.6096°W) (Figure 2). Infections were detected in both <1 year old and adult seals with no age predilection. All the infected adult harbor seals (n = 9) were female, and 6 had evidence of recent parturition (active lactation, asymmetric uterine horns without the presence of a fetus, or both). The infected adult gray seal was male. There were 3 male and 7 female (and 1 nondetermined) infected <1 year old seals (Table 2). One of the infected seals was found alive with profound lethargy and neurologic signs. In addition, anecdotal observations of weak and dyspneic harbor seals were reported during the outbreak.

Carcasses were attributed decomposition scores (*21*), varying from code 2–2.5 (fresh to mild decomposition) in 12 cases to code 3 (moderate decomposition) for 3 cases. Twelve seals were in excellent nutritional condition, 2 were thin, and 1 was emaciated.

Postmortem findings (Table 3) showed notable gross lesions limited to lymphadenomegaly (submandibular and mesenteric lymph nodes), red-tinged foam in the tracheal lumen, and pulmonary congestion. Relevant histologic lesions (Table 3) included acute multifocal to diffuse mixed meningoencephalitis (Figure 3, panel A), characterized by a predominantly neutrophilic infiltrate with lymphocytes in Virchow-Robin spaces, the meninges, the submeningeal neuropil. Neuronal necrosis, satellitosis, and gliosis were also regularly observed. Acute fibrinosuppurative alveolitis, consisting of neutrophils with fibrinous aggregates in the alveolar lumen (Figure 3, panel B), was observed in 9/15 seals. Interstitial pneumonia, characterized by a mild to moderate mixed inflammatory infiltrate within the alveolar septa, was seen either concurrently or distinctively from the alveolitis. In addition to the inflammatory changes, alveolar emphysema, mild acute alveolar damage with hyaline membranes, and necrotic type 1 pneumocytes were sometimes present. Six animals presented multifocal necrotic foci of the adrenal cortex with infiltrates of degenerate neutrophils (Figure 3, panel C). Acute necrotizing thymitis, lymphadenitis, and splenitis were also observed and consisted of multifocal to coalescing zones of necrosis, mainly centered on cortical lymphoid follicles along with extensive lymphoid depletion (Figure 3, panel D). Lymph nodes were often

Table 1. Percentages of stranded seals tested that were infected by HPAI A(H5N1) in the St. Lawrence Estuary, Quebec, Canada, April 22–October 6, 2022*

Species and sampling	% Infected (no. infected†/no. tested)
Harbor seal (*Phoca vitulina*)	
Full postmortem examination	64 (14/22)
Nasal/rectal field swab	55 (6/11)
Total	61 (20/33)
Grey seal (*Halichoerus grypus*)	
Full postmortem examination	33 (1/3)
Nasal/rectal field swab	0 (0/1)
Total	25 (1/4)
Hooded seal (*Cystophora cristata*)	
Full postmortem examination	0 (0/1)
Harp seal (*Pagophilus groenlandicus*)	
Full postmortem examination	0 (0/1)
Total pinnipeds	
Full postmortem examination	56 (15/27)
Nasal/rectal field swab	50 (6/12)
Total	54 (21/39)

*Postmortem and field swab samples were from different individual strandings. HPAI, highly pathogenic avian influenza.
†Infections were determined on the basis of epidemiologic data, presence of suggestive lesions, and PCR testing using H5-specific primers.

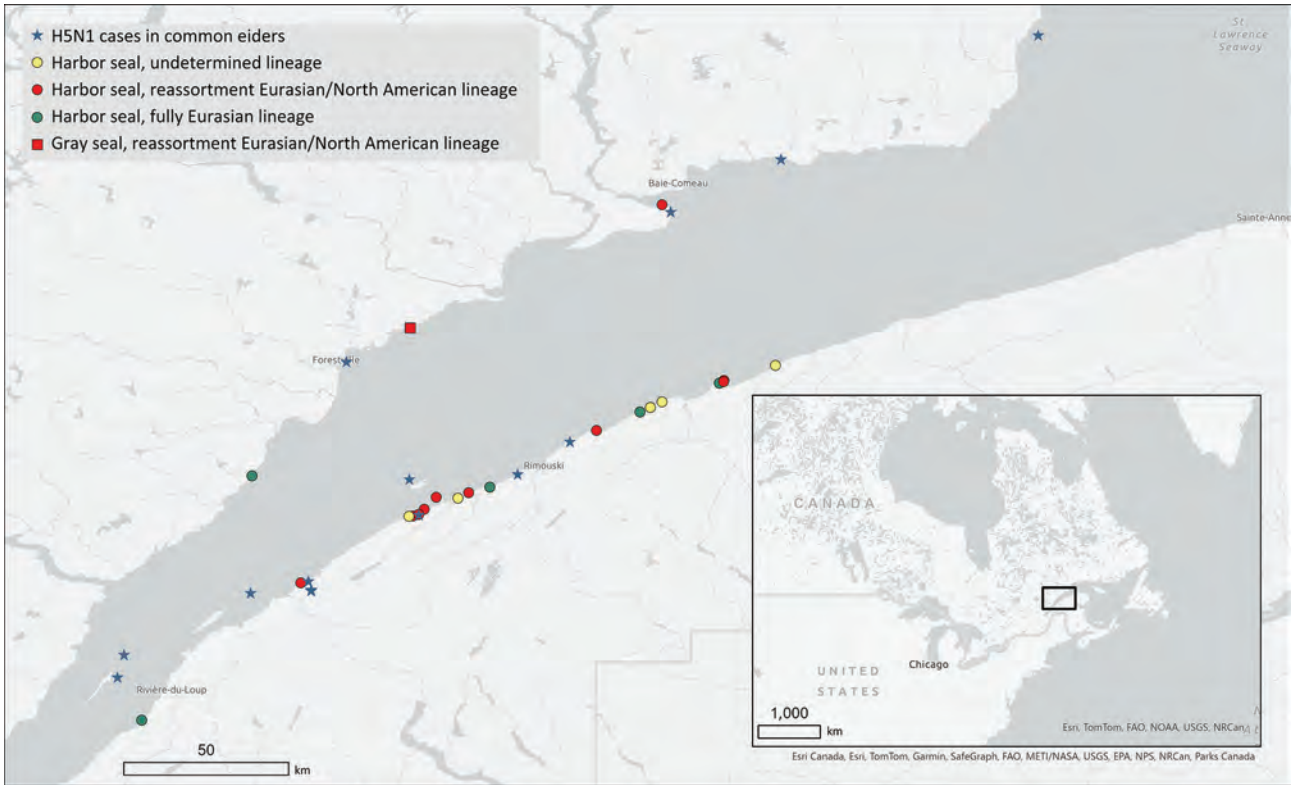

Figure 2. Geographic locations of stranded, dead, or sick seals infected by highly pathogenic avian influenza A(H5N1) virus during the 2022 outbreak in the St. Lawrence Estuary, Quebec, Canada. The locations of harbor seals (*Phoca vitulina*) gray seals (*Halichoerus grypus*) and detected H5N1 lineages are marked as are the documented outbreaks in common eider (*Somateria mollissima*) colonies. Inset shows study location in a map of eastern Canada and US Midwest and Northeast.

reactive with an accumulation of histiocytic cells in the lymphatic trabeculae and medullary sinus, macrophages in the germinal centers, and an infiltration of the subcapsular sinus with granulocytes and macrophages. Other microscopic changes were seen in 6 cases with mild membranous glomerulonephritis, 4 cases with necrotizing fibrinous hepatitis of variable severity, 1 case of mild multifocal myocarditis with degenerate myofibers, and 1 animal with mild neutrophilic perivascular infiltration in the perimysium.

Immunoreactivity for IAV antigen was observed in tissues from 12 of the 13 cases that were tested (Table 2). Variable abundance of antigens, from mild to extensive, was detected in different tissues, including the neuropils and neurons (Figure 4, panel A), pulmonary alveolar septa and glandular bronchial cells (Figure 4, panel B), renal glomeruli, spleen, pancreas, liver, vascular walls of skeletal muscle, lymph nodes, tracheal vessels, and adrenal glands. Those antigens were often associated with, but not limited to, necrotic foci.

Virology Assessment

The presence of IAV H5 RNA was confirmed by PCR in 15 necropsied seals and in 6 seals that were swabbed in the field (n = 21) (Table 2). All samples were negative for H7. All 15 necropsied seals had lesions suggestive of IAV on histology. In 4 cases, NCFAD confirmatory PCRs for H5 performed on combined rectal/nasal swab samples were negative but H5 RNA was detected by subsequent PCR on frozen lung or brain tissues. Virus isolation (using embryonated specific pathogen-free chicken eggs) was successful in 16 of those 21 cases. The 16 isolates were sequenced to determine the subtype and lineage of the H5 virus. All isolates belonged to Gs/GD lineage H5N1 clade 2.3.4.4b. Five isolates had fully Eurasian gene segments similar to the Newfoundland-like clade 2.3.4.4b H5N1 viruses that emerged in Canada in late 2021. The other 11 isolates were reassortant H5N1 viruses containing gene segments polymerase basic 1 and 2, polymerase acidic, and nucleoprotein, belonging to the North American lineage IAVs and hemagglutinin, neuraminidase, matrix, and nonstructural gene segments belonging to the Newfoundland-like clade 2.3.4.4b H5N1 viruses. Accordingly, the phylogenetic tree estimated from those sequences is bifurcated at the root between fully Eurasian and reassortant viruses (Figure 5). In both the fully Eurasian and reassortant lineages, sequences derived from wild birds are ancestral to the (well-supported and monophyletic) clades that include seals. That finding provides strong support for independent bird-to-seal spillover events for each viral lineage, rather than a single spillover and subsequent reassortment event in seals.

Table 2. Demographic data and results of immunohistochemistry and molecular testing performed in seals infected by HPAI A(H5N1) during the 2022 outbreak in the St. Lawrence Estuary, Quebec, Canada*

Case no.	Date found	Species†	Age group/sex	AIV IHC	Initial PCR at MAPAQ		Confirmatory PCR at NCFAD		Sample type‡	Lineage	IAV histologic lesions
					Matrix	H5	Matrix	H5			
217719	May 30	Harbor seal	Adult/F	+	+	+	+	+	Swab	EU/NA	Yes
216969	June 7	Harbor seal	<1 y	+	+	+	+	+	Swab	EU	Yes
216970	June 7	Harbor seal	Adult/F	+	+	+	+	+	Swab	EU	Yes
216971	June 8	Harbor seal	Adult/F	-	+/−	+	+	+	Swab	EU	Yes
216947	June 10	Harbor seal	Adult/F	+	+	+	+	+	Brain	EU/NA	Yes
216983	June 11	Harbor seal	Adult/F	NP	+	+	+	+	Swab	EU/NA	NP§
216985	June 13	Harbor seal	<1 y/F	NP	+	+	+	+	Swab	NP	NP§
216972	June 14	Harbor seal	<1 y/F	+	+	+	+	+	Swab	EU	Yes
217671	June 14	Harbor seal	Adult/F	+	+	+	+	+	Swab	EU	Yes
216987	June 19	Harbor seal	Adult/F	NP	+	+	+	+	Swab	EU/NA	NP§
216988	June 20	Harbor seal	<1 y/F	+	+	+	+	+	Swab	EU/NA	Yes
216989	June 20	Harbor seal	Adult/F	NP	+	+	+	+	Swab	NP	NP§
217670	June 20	Harbor seal	<1 y/F	+	+	+	+	+	Swab	EU/NA	Yes
216973	June 22	Harbor seal	Adult/F	NP	+	+/−	+	+	Brain	NP	Yes
216974	June 22	Harbor seal	<1 y/F	+	+/−	+	+	+	Brain	EU/NA	Yes
217794	June 24	Gray seal	Adult/F	+	+	+	+	+	Swab	EU/NA	Yes
217642	June 26	Harbor seal	<1 y/F	+	+	+	+	+	Swab	EU/NA	Yes
217665	June 26	Harbor seal	<1 y/F	+	+/−	+	+	+	Swab	EU/NA	Yes
217667	June 26	Harbor seal	<1 y/F	NP	+	+	+	-	Lung	NP	Yes
217611	July 7	Harbor seal	<1 y/F	NP	+	+	+	+	Swab	EU/NA	NP§
217612	July 8	Harbor seal	<1 y/ND	NP	+/−	+/−	+	+	Swab	NP	NP§

*EU, fully Eurasian lineage; EU/NA, reassortment between Eurasian and North American lineages; HPAI, highly pathogenic avian influenza; IAV, influenza virus; IHC, immunohistochemistry; MAPAQ, Ministère de l'Agriculture, des Pêcheries et de l'Alimentation du Québec; NCFAD, National Center for Foreign Animal Disease; ND, not determined; NP, not performed. –, negative; +, positive; +/−, suspicious.
†Harbor seal, *Phoca vitulina*; gray seal, *Halichoerus grypus*.
‡Swab indicates combined nasal and rectal swab samples. Frozen lung or brain were submitted when swab testing results were negative.
§Cases for which only swabs collected in the fields were available; no necropsy performed.

Table 3. Microscopic lesions documented in harbor (*Phoca vitulina*) and gray (*Halichoerus grypus*) seals infected by HPAI A(H5N1) during the 2022 outbreak in the St. Lawrence Estuary, Quebec, Canada

Microscopic lesions	% Seals affected (no. with lesions/no. examined)
Brain	
Meningoencephalitis	100 (15/15)
Predominantly neutrophilic	80 (12/15)
Predominantly lymphoplasmacytic	20 (3/15)
Lung	
Pulmonary inflammatory changes	73 (11/15)
Acute multifocal fibrinosuppurative alveolitis	60 (9/15)
Acute interstitial pneumonia	53 (8/15)
Acute alveolar damage	40 (6/15)
Alveolar emphysema	27 (4/15)
Adrenal gland	
Adrenocortical necrosis	60 (6/10)
Thymus	
Acute multifocal necrotizing thymitis	50 (2/4)
Lymph nodes	
Reactional lymph nodes	43 (6/14)
Acute multifocal necrotizing lymphadenitis	36 (5/14)
Kidney	
Multifocal membranous glomerulonephritis	40 (6/15)
Liver	
Necrotizing hepatitis	29 (4/14)
Spleen	
Necrotizing splenitis	21 (3/14)
Muscle	
Neutrophilic infiltration of the perimysium	9 (1/11)
Heart	
Multifocal myocarditis	7 (1/14)

Discussion

Investigation of increased deaths among the pinniped populations of the St. Lawrence Estuary and Gulf during the summer of 2022 detected HPAI H5N1 infections in harbor and gray seals. All necropsied seals that were positive for H5 by PCR also manifested histologic lesions consistent with IAV infection. The demonstration by IHC that IAV antigens were often associated with necrotic and inflammatory lesions further supports a causal relationship between this virus, the observed lesions, and the animal deaths. The almost 4-fold increase in summer deaths among harbor and gray seals compared with historic data could reasonably be explained, at least in part, by an HPAI H5N1 outbreak affecting those populations of seals.

Even though we observed good agreement between the different diagnostic modalities, a few discrepancies between the results are worth noting (Table 2): IHC failed to detect 1 infected seal; 4 cases that were considered only suspected based on an initial matrix or H5 PCRs by MAPAQ were later confirmed positive by NCFAD; and PCR results for combined nasal/rectal swab samples had a false-negative rate of 27% (4/15). Such differences in diagnostic results highlight the importance of a multistep diagnostic methodology to confirm avian IAV cases and demonstrate that surveillance efforts solely based on nasal/rectal swab sample PCR results likely grossly underestimate the actual prevalence of infection.

Most of the examined animals were in good nutritional condition with only minor macroscopic changes, except for noticeable lymphadenomegaly. However, some macroscopic changes possibly were overlooked because of postmortem and freezing artifacts. Inflammatory and necrotic changes were detected in several organs, including brain, lungs, adrenal glands, liver, and lymph. The central nervous system (100%) and the lungs (73%) were the most commonly affected organs. That neurotropism and respirotropism are similar to what has been reported in birds (*32*) and in mesocarnivores infected with HPAI H5N1 (*12*,*15*), as well as in 3 harbor seals from the North Sea near Germany infected with HPAI H5N8 (*18*). The predominantly neutrophilic nature of the meningoencephalitis is unusual for a viral infection and indicative of a very acute infection.

The route of transmission and the viral pathogenesis for HPAI infection have not been established in pinnipeds. In most mammals, including humans, IAVs are transmitted through inhaling aerosols or respiratory fomites from an infected individual and replicate primarily in respiratory epithelium. Previous reports of infections with low-pathogenicity avian influenza in pinnipeds are consistent with the same pathophysiology as with stranded sick seals

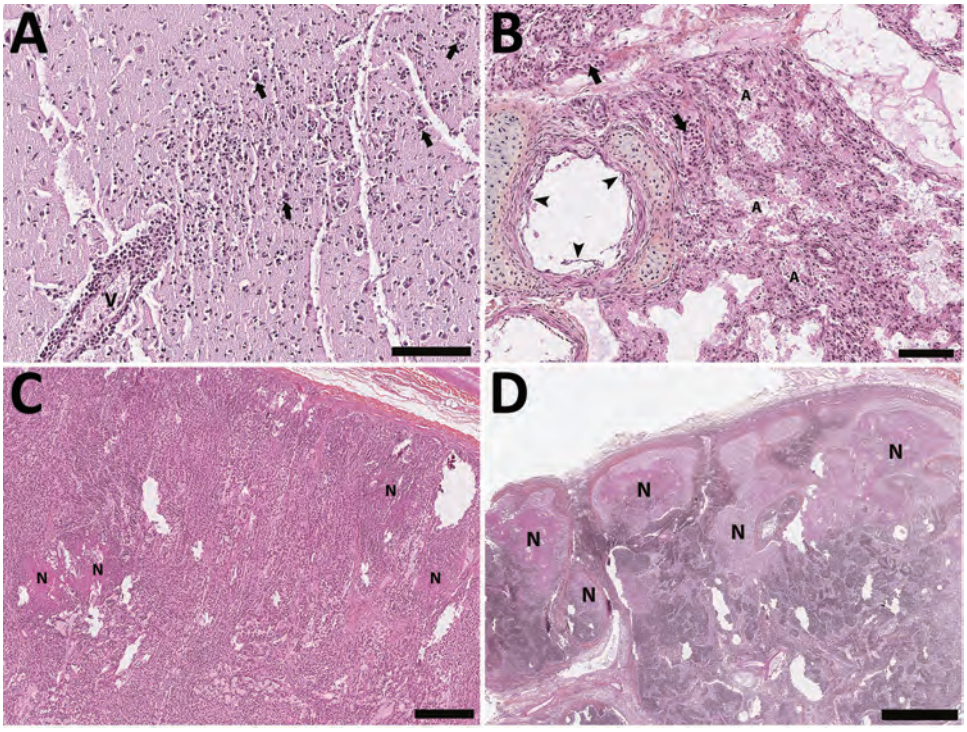

Figure 3. Histology section of thawed, formalin-fixed tissues from harbor seals (*Phoca vitulina*) infected by highly pathogenic avian influenza A(H5N1) virus in the St. Lawrence Estuary, Quebec, Canada, 2022. Hematoxylin phloxine saffron stain. A) Brain tissue from a young (<1 year old) female seal. The Virchow-Robin space around a vessel (V) is infiltrated by numerous layers of polymorphonuclear cells. Several neurons have a condensed hyperacidophilic cytoplasm indicative of necrosis and are often associated with satellitosis (arrows). A focally extensive infiltration of the neuropil by neutrophils and glial cells is also present. Scale bar indicates 100 µm. B) Lung from a young (<1 year old) female seal. The alveolar (A) and vascular (arrow) lumens contain numerous, often degenerate, polymorphonuclear cells. The alveolar walls are infiltrated by numerous inflammatory cells composed of neutrophils and mononuclear cells. The epithelial cells bordering the small bronchi are often necrotic. Scale bar indicates 100 µm. C) Adrenal gland of an adult female seal. Multifocal foci of necrosis are present in the cortical zone (N). Scale bar indicates 300 µm. D) Lymph node from an adult female seal. Marked multifocal to coalescing necrosis of the lymphoid tissues in the cortical region are noted (N). Scale bar indicates 1 mm.

displaying respiratory signs, whereas dead seals showed necrotizing hemorrhagic bronchitis and alveolitis (*6*,*7*). However, the clinical manifestations and postmortem lesions seen in various mammal species affected by HPAI H5N1, including the seals from this study, indicate a clear neurotropism (*12*,*15*,*16*). Neurologic signs, encephalitis, and a high load of viral antigens and RNA in the brain all point toward a different pathogenesis and possibly a different route of inoculation.

Most mammal species that have been reported to be infected by HPAI H5N1 are carnivores that are likely to prey or scavenge on wild birds. Consequently, ingestion of birds infected with HPAI is presumed to be the most likely source of infection in free-ranging wild mesocarnivores (*12*,*15*) and in sporadic cases of infected domestic or captive wild carnivores (*33*,*34*). That route of transmission, which has been proven successful by red foxes being experimentally infected with HPAI H5N1 clade 2.2 after eating infected bird carcasses (*35*), is also plausible in gray seals because this species is known to prey on sea birds, making a weakened bird or infected carcass a potential source of infection. However, that pathway of infection is

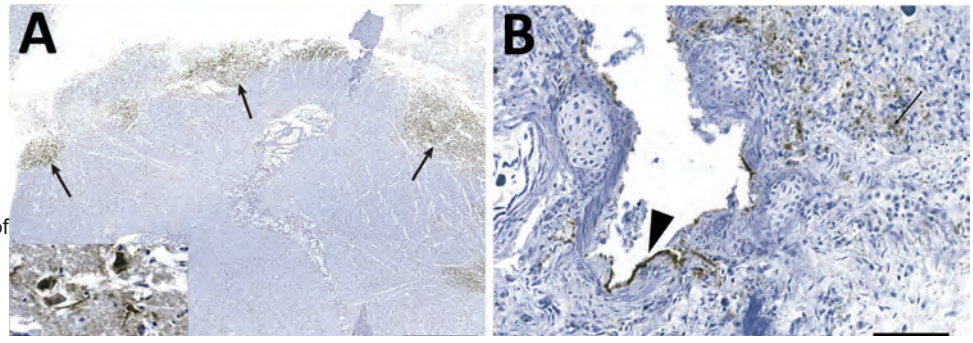

Figure 4. Detection of influenza virus antigen by immunohistochemistry in brain (A) and lung (B) of harbor seals (*Phoca vitulina*) infected by highly pathogenic avian influenza A(H5N1) virus, St. Lawrence Estuary, Quebec, Canada, 2022. A) Brain tissue. Multifocal areas of intense immunostaining (arrows) with staining of all structures are seen in the affected area, including neurons and neuropil (inset). Scale bar indicates 2 mm. B) Lung tissue. Positive immunostaining can be observed within alveolar septae (arrow) and in bronchiolar epithelial cells (arrowhead). Scale bar indicates 80 µm.

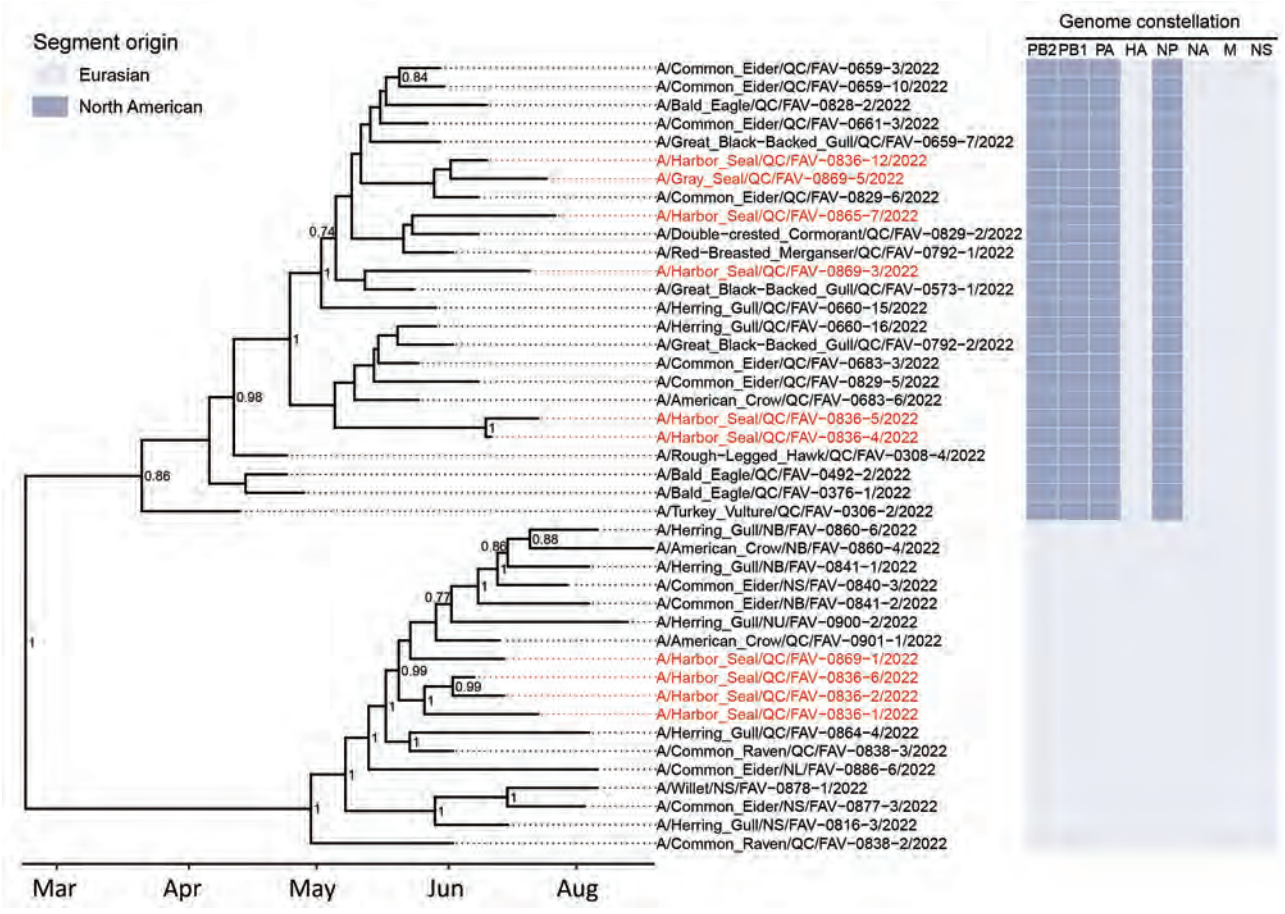

Figure 5. Time-scaled phylogenetic tree of 43 highly pathogenic avian influenza A(H5N1) virus clade 2.3.4.4b complete viral genomes from seals and wild birds in the St. Lawrence Estuary, Quebec, Canada, 2022. Tree was inferred by Bayesian analysis. Red text indicates seal-derived sequences and black text indicates wild bird–derived sequences. Posterior probability values >0.70 are displayed at the tree nodes. The genome constellation for each sequence (i.e., the compliment of Eurasian and North American derived genome segments) is presented to the right of the tree tips. HA, hemagglutinin; M, matrix; NA, neuraminidase; NP, nucleoprotein; NS, nonstructural; PA, polymerase acidic; PB, polymerase basic.

unlikely for harbor seals because they are not known to predate or scavenge on birds. Consequently, transmission through environmental exposure, such as accidentally ingesting feces or feathers from infected birds, drinking fecal-contaminated water, or inhaling aerosols or respiratory fomites from infected avian carcasses, should be considered for harbor seals. All harbor seals that died of HPAI H5N1 in this population were found in relatively close proximity to islands used as pupping grounds. Some of those islands also harbor breeding colonies of marine birds, such as the common eiders (*Somateria mollissima*). Numerous cases of death caused by HPAI H5N1 were documented in those marine bird colonies during the same time period (Canadian Wildlife Health Cooperative database, unpub. data). Anecdotal observations of seals hauling out on sites where carcasses of eiders were present were reported during the outbreak. Those observations would support the hypothesis that harbor seals were exposed to HPAI H5N1 by close contact with infected marine birds. The infected harbor seals were also either newborn or female and in breeding age, supporting the link between the infections and contact with marine birds at pupping sites.

The fact that infections by HPAI H5N1 was documented in only 1 gray seal, even if that species was abundant in the St. Lawrence Estuary during the period of the outbreak (*36*), suggests either that gray seals are less sensitive to this virus or that they were less exposed to the virus compared with harbor seals. Indeed, in contrast to harbor seals that give birth to their pups in the spring/summer, the gray seal pupping season is in the winter. Therefore, that species is less likely to be in contact with potentially infected nestling colonial birds. The absence of documentation of cases of infections in seals in the

St. Lawrence Gulf, where both species of seals are abundant (*36*), might be because nestling colonies of eiders are smaller in number and size and limited to the northern shore of the gulf, an area with a low density of potential observers.

The presence of HPAI H5N1 clade 2.3.4.4b viruses with 2 different genome constellations and the temporo-geographic distribution of the seals indicates that this outbreak was associated with >1 source of infection, an assertion supported by phylogenetic analyses. Some seal-derived sequences form monophyletic clades that exclude those from wild birds (e.g., samples FAV-0836-1, FAV-0836-2, and FAV-0836-6; Figure 5), suggesting a common source of infection for those seals. However, with the data currently available, we cannot determine if direct seal-to-seal transmission occurred. In addition, the absence of cases of HPAI H5N1 in seals from the St. Lawrence Estuary since the original outbreak (Canadian Wildlife Health Cooperative database, unpub. data) suggests that this condition has not become endemic in this population of marine mammals.

In conclusion, the infection of mammal species such as seals by HPAI H5N1 viruses raises concern about recent viral mutations making possible entry and replication within mammalian cells. From a human health perspective, such changes in viral host range warrant continued vigilance to detect a potentially deadly epidemic before its emergence. In addition, marine mammals, such as seals or other pinnipeds, might act as reservoirs for this virus, which could contribute to increasing risk for mutations and viral reassortment, favoring the infection of new mammal hosts. Therefore, monitoring the occurrence and molecular characteristics of this HPAI virus in populations of wild marine mammals is essential for assessing the public health risk associated with this emerging pathogen–host dynamic.

Acknowledgments

We thank the staff and volunteers of the Réseau québécois d'urgences pour les mammifères marins and the staff of Canadian Wildlife Health Cooperative in Quebec for their help with carcass retrieval and necropsy. Thanks also to the professional and technical staff of the Complexe de Diagnostic et d'Epidemiosurveillance vétérinaire du Québec for their help with sample analysis and to Estella Moffat for the technical assistance with immunohistochemistry. Finally, the authors acknowledge Tristan Juette for his assistance with statistics, Jean-Francois Giroux and Matthieu Beaumont for their contribution regarding the unusual mortality event in common eiders, and Matthew Fisher and Daniel Sullivan for nanopore sequencing, data processing, and reporting.

Funding was provided to O.L. by the Canadian Safety and Security Program (CSSP-2018-TA-2362) for the Oxford Nanopore GridION sequencer. The scientific conclusions and opinions expressed herein are those of the authors and do not necessarily reflect the views or policies of the Canadian Government, its agencies, or any of the included organizations.

About the Author

Dr. Lair is a professor in Wildlife Health at the Faculté de médecine vétérinaire of the Université de Montréal, where he serves as the Canadian Wildlife Health Cooperative regional director for the province of Quebec.

References

1. Fereidouni S, Munoz O, Von Dobschuetz S, De Nardi M. Influenza virus infection of marine mammals. EcoHealth. 2016;13:161–70. https://doi.org/10.1007/s10393-014-0968-1
2. Anthony SJ, St Leger JA, Pugliares K, Ip HS, Chan JM, Carpenter ZW, et al. Emergence of fatal avian influenza in New England harbor seals. MBio. 2012;3:e00166–12. https://doi.org/10.1128/mBio.00166-12
3. Bodewes R, Bestebroer TM, van der Vries E, Verhagen JH, Herfst S, Koopmans MP, et al. Avian influenza A(H10N7) virus–associated mass deaths among harbor seals. Emerg Infect Dis. 2015;21:720–2. https://doi.org/10.3201/eid2104.141675
4. Groth M, Lange J, Kanrai P, Pleschka S, Scholtissek C, Krumbholz A, et al. The genome of an influenza virus from a pilot whale: relation to influenza viruses of gulls and marine mammals. Infect Genet Evol. 2014;24:183–6. https://doi.org/10.1016/j.meegid.2014.03.026
5. Reperant LA, Rimmelzwaan GF, Kuiken T. Avian influenza viruses in mammals. Rev Sci Tech. 2009;28:137–59. https://doi.org/10.20506/rst.28.1.1876
6. van den Brand JMA, Wohlsein P, Herfst S, Bodewes R, Pfankuche VM, van de Bildt MWG, et al. Influenza A (H10N7) virus causes respiratory tract disease in harbor seals and ferrets. PLoS One. 2016;11:e0159625. https://doi.org/10.1371/journal.pone.0159625
7. Duignan PJ, Van Bressem MF, Cortés-Hinojosa G, Kennedy-Stoskopf S. Viruses. In: Gulland FMD, Dierauf LA, Whitman KL, editors. CRC handbook of marine mammal medicine. 3rd edition. Boca Raton (FL): CRC Press; 2018. p. 331–66.
8. Shin DL, Siebert U, Haas L, Valentin-Weigand P, Herrler G, Wu NH. Primary harbour seal (*Phoca vitulina*) airway epithelial cells show high susceptibility to infection by a seal-derived influenza A virus (H5N8). Transbound Emerg Dis. 2022;69:e2378–88. https://doi.org/10.1111/tbed.14580
9. Measures LN, Fouchier RAM. Antibodies against influenza virus types A and B in Canadian seals. J Wildl Dis. 2021;57:808–19. https://doi.org/10.7589/JWD-D-20-00175
10. Berhane Y, Joseph T, Lung O, Embury-Hyatt C, Xu W, Cottrell P, et al. Isolation and characterization of novel reassortant influenza A(H10N7) virus in a harbor seal, British Columbia, Canada. Emerg Infect Dis. 2022;28:1480–4. https://doi.org/10.3201/eid2807.212302
11. Caliendo V, Lewis NS, Pohlmann A, Baillie SR, Banyard AC, Beer M, et al. Transatlantic spread of highly pathogenic avian influenza H5N1 by wild birds from Europe to North America

in 2021. Sci Rep. 2022;12:11729. https://doi.org/10.1038/s41598-022-13447-z
12. Alkie TN, Cox S, Embury-Hyatt C, Stevens B, Pople N, Pybus MJ, et al. Characterization of neurotropic HPAI H5N1 viruses with novel genome constellations and mammalian adaptive mutations in free-living mesocarnivores in Canada. Emerg Microbes Infec. 2023;12:2186608.
13. Bevins SN, Shriner SA, Cumbee JC Jr, Dilione KE, Douglass KE, Ellis JW, et al. Intercontinental movement of highly pathogenic avian influenza A(H5N1) clade 2.3.4.4 virus to the United States, 2021. Emerg Infect Dis. 2022;28:1006–11. https://doi.org/10.3201/eid2805.220318
14. Canadian Food Inspection Agency. Highly pathogenic avian influenza in wildlife [cited 2023 May 16]. https://cfia-ncr.maps.arcgis.com/apps/dashboards/89c779e98cdf492c899df23e1c38fdbc
15. Elsmo EJ, Wünschmann A, Beckmen KB, Broughton-Neiswanger LE, Buckles EL, Ellis J, et al. Highly pathogenic avian influenza A(H5N1) virus clade 2.3.4.4b infections in wild terrestrial mammals, United States, 2022. Emerg Infect Dis. 2023;29:2451–60. https://doi.org/10.3201/eid2912.230464
16. Vreman S, Kik M, Germeraad E, Heutink R, Harders F, Spierenburg M, et al. Zoonotic mutation of highly pathogenic avian influenza H5N1 virus identified in the brain of multiple wild carnivore species. Pathogens. 2023;12:168. https://doi.org/10.3390/pathogens12020168
17. Puryear W, Sawatzki K, Hill N, Foss A, Stone JJ, Doughty L, et al. Highly pathogenic avian influenza A(H5N1) virus outbreak in New England seals, United States. Emerg Infect Dis. 2023;29:786–91. https://doi.org/10.3201/eid2904.221538
18. Postel A, King J, Kaiser FK, Kennedy J, Lombardo MS, Reineking W, et al. Infections with highly pathogenic avian influenza A virus (HPAIV) H5N8 in harbor seals at the German North Sea coast, 2021. Emerg Microbes Infect. 2022;11:725–9. https://doi.org/10.1080/22221751.2022.2043726
19. Shin DL, Siebert U, Lakemeyer J, Grilo M, Pawliczka I, Wu NH, et al. Highly pathogenic avian influenza A(H5N8) virus in gray seals, Baltic Sea. Emerg Infect Dis. 2019;25:2295–8. https://doi.org/10.3201/eid2512.181472
20. Gamarra-Toledo V, Plaza PI, Gutiérrez R, Inga-Diaz G, Saravia-Guevara P, Pereyra-Meza O, et al. Mass mortality of sea lions caused by highly pathogenic avian influenza A(H5N1) virus. Emerg Infect Dis. 2023;29:2553–6. https://doi.org/10.3201/eid2912.230192
21. Ulloa M, Fernández A, Ariyama N, Colom-Rivero A, Rivera C, Nuñez P, et al. Mass mortality event in South American sea lions (*Otaria flavescens*) correlated to highly pathogenic avian influenza (HPAI) H5N1 outbreak in Chile. Vet Q. 2023;43:1–10. https://doi.org/10.1080/01652176.2023.2265173
22. Leguia M, Garcia-Glaessner A, Muñoz-Saavedra B, Juarez D, Barrera P, Calvo-Mac C, et al. Highly pathogenic avian influenza A (H5N1) in marine mammals and seabirds in Peru. Nat Commun. 2023;14:5489. https://doi.org/10.1038/s41467-023-41182-0
23. Geraci JR, Lounsbury V. Marine mammals ashore. A field guide for strandings. Galveston (TX, USA): Texas A&M Sea Grant Publications; 1993.
24. Wilson DE, Mittermeier RA. Handbook of the mammals of the world, vol. 4: sea mammals. Barcelona (Spain): Lynx Edicions; 2014.
25. Weingartl HM, Berhane Y, Hisanaga T, Neufeld J, Kehler H, Emburry-Hyatt C, et al. Genetic and pathobiologic characterization of pandemic H1N1 2009 influenza viruses from a naturally infected swine herd. J Virol. 2010;84:2245–56. https://doi.org/10.1128/JVI.02118-09
26. Spackman E, Senne DA, Myers TJ, Bulaga LL, Garber LP, Perdue ML, et al. Development of a real-time reverse transcriptase PCR assay for type A influenza virus and the avian H5 and H7 hemagglutinin subtypes. J Clin Microbiol. 2002;40:3256–60. https://doi.org/10.1128/JCM.40.9.3256-3260.2002
27. Chrzastek K, Lee DH, Smith D, Sharma P, Suarez DL, Pantin-Jackwood M, et al. Use of Sequence-Independent, Single-Primer-Amplification (SISPA) for rapid detection, identification, and characterization of avian RNA viruses. Virology. 2017;509:159–66. https://doi.org/10.1016/j.virol.2017.06.019
28. Suchard MA, Lemey P, Baele G, Ayres DL, Drummond AJ, Rambaut A. Bayesian phylogenetic and phylodynamic data integration using BEAST 1.10. Virus Evol. 2018;4:vey016. https://doi.org/10.1093/ve/vey016
29. Kalyaanamoorthy S, Minh BQ, Wong TKF, von Haeseler A, Jermiin LS. ModelFinder: fast model selection for accurate phylogenetic estimates. Nat Methods. 2017;14:587–9. https://doi.org/10.1038/nmeth.4285
30. Minin VN, Bloomquist EW, Suchard MA. Smooth skyride through a rough skyline: Bayesian coalescent-based inference of population dynamics. Mol Biol Evol. 2008;25:1459–71. https://doi.org/10.1093/molbev/msn090
31. Rambaut A, Drummond AJ, Xie D, Baele G, Suchard MA. Posterior summarization in Bayesian phylogenetics using tracer 1.7. Syst Biol. 2018;67:901–4. https://doi.org/10.1093/sysbio/syy032
32. Caliendo V, Leijten L, van de Bildt M, Germeraad E, Fouchier RAM, Beerens N, et al. Tropism of highly pathogenic avian influenza H5 viruses from the 2020/2021 epizootic in wild ducks and geese. Viruses. 2022;14:280. https://doi.org/10.3390/v14020280
33. Klopfleisch R, Wolf PU, Uhl W, Gerst S, Harder T, Starick E, et al. Distribution of lesions and antigen of highly pathogenic avian influenza virus A/Swan/Germany/R65/06 (H5N1) in domestic cats after presumptive infection by wild birds. Vet Pathol. 2007;44:261–8. https://doi.org/10.1354/vp.44-3-261
34. Keawcharoen J, Oraveerakul K, Kuiken T, Fouchier RA, Amonsin A, Payungporn S, et al. Avian influenza H5N1 in tigers and leopards. Emerg Infect Dis. 2004;10:2189–91. https://doi.org/10.3201/eid1012.040759
35. Reperant LA, van Amerongen G, van de Bildt MW, Rimmelzwaan GF, Dobson AP, Osterhaus AD, et al. Highly pathogenic avian influenza virus (H5N1) infection in red foxes fed infected bird carcasses. Emerg Infect Dis. 2008;14:1835–41. https://doi.org/10.3201/eid1412.080470
36. Mosnier A, Dispas A, Hammill MO. Spatial distribution and count of harbour seals (*Phoca vitulina*) and grey seals (*Halichoerus grypus*) in the Estuary and Gulf of St. Lawrence from an aerial survey conducted in June 2019. Can Tech Rep Fish Aquat Sci. 2023;3541:v–60.

Address for correspondence: Stéphane Lair, Université de Montréal, 3200 Sicotte, Saint-Hyacinthe, QB, J2S 2M2, Canada; email: stephane.lair@umontreal.ca

Estimates of SARS-CoV-2 Hospitalization and Fatality Rates in the Prevaccination Period, United States

Isabel Griffin, Jessica King,[1] B. Casey Lyons,[1] Alyson L. Singleton,[1] Xidong Deng, Beau B. Bruce, Patricia M. Griffin

Few precise estimates of hospitalization and fatality rates from COVID-19 exist for naive populations, especially within demographic subgroups. We estimated rates among persons with SARS-CoV-2 infection in the United States during May 1–December 1, 2020, before vaccines became available. Both rates generally increased with age; fatality rates were highest for persons ≥85 years of age (24%) and lowest for children 1–14 years of age (0.01%). Age-adjusted case hospitalization rates were highest for African American or Black, not Hispanic persons (14%), and case-fatality rates were highest for Asian or Pacific Islander, not Hispanic persons (4.4%). Eighteen percent of hospitalized patients and 44.2% of those admitted to an intensive care unit died. Male patients had higher hospitalization (6.2% vs. 5.2%) and fatality rates (1.9% vs. 1.5%) than female patients. These findings highlight the importance of collecting surveillance data to devise appropriate control measures for persons in underserved racial/ethnic groups and older adults.

The COVID-19 pandemic caused by the novel coronavirus SARS-CoV-2 resulted in >20 million reported cases, 480,000 hospitalizations, and 350,000 deaths in the United States through December 2020 (*1*). SARS-CoV-2 self-testing was not widely available at the time, which likely resulted in underreporting of infections (*2*,*3*). Beginning in mid-December 2020, COVID-19 case detection was affected by the availability of commercial testing and the introduction of at-home antigen-based diagnostic tests (*2*). The development of effective vaccines against SARS-CoV-2 after mid-December 2020 had notable effects on reducing hospitalization and fatality rates (*4*–*6*). Analyses in the United States and other countries have found higher case fatality rates associated with certain person-level (e.g., vaccination status, older age, race and ethnicity, and presence of underlying conditions), clinical (hospitalization and admission to critical care units), and country-level infrastructure (e.g., healthcare capacity) characteristics (*7*–*12*). Few precise estimates of hospitalization and mortality rates exist in the COVID-19–naive population in the United States, especially among demographic and clinical subgroups. We estimated US case hospitalization and fatality rates by demographic and clinical characteristics during May 1–December 1, 2020, before vaccine availability, among persons with reported SARS-CoV-2 infections. These estimates are unique because most populations worldwide now have some vaccine- or natural-induced immunity (*13*).

Methods

State and territorial epidemiologists from 56 US jurisdictions submitted COVID-19 case reports to the Centers for Disease Control and Prevention (CDC) using a standard COVID-19 case report form; submissions were through direct data entry or comma separated value (CSV) files upload into CDC's Data Collation and Integration for Public Health Event Response HHS Protect platform or through the National Notifiable Diseases Surveillance System (*14*–*16*). Jurisdictions included all 50 states, New York

Author affiliations: Centers for Disease Control and Prevention, Atlanta, Georgia, USA (I. Griffin, J. King, B.C. Lyons, X. Deng, B.B. Bruce, P.M. Griffin); Oak Ridge Institute for Science and Education, Oak Ridge, Tennessee, USA (A.L. Singleton)

DOI: https://doi.org/10.3201/eid3006.231285

[1]These authors contributed equally to this article.

City (reporting separately from New York state), the District of Columbia (DC), and 4 territories (Guam, Northern Mariana Islands, Puerto Rico, and the US Virgin Islands). Jurisdictions voluntarily reported confirmed and probable COVID-19 cases based on the case definition promulgated by the Council of State and Territorial Epidemiologists (CSTE) at the time of reporting (*15*,*16*) (Appendix, https://wwwnc.cdc.gov/EID/article/30/6/23-1285-App1.pdf). Health officials in each jurisdiction determine the manner in which they obtain race and ethnicity information; common methods include interviews with patients and their families and reviews of medical records.

To create the hospitalization dataset, we identified jurisdictions in which ≥80% of case reports had the CDC hospitalization query not missing (i.e., answered yes, no, or unknown) for illnesses during May 1–December 1, 2020. If the date of illness onset was not provided or the person had no symptoms, the earliest date provided was used; this date was typically either the date the positive specimen was collected or the date of the case report. We used the same restriction to create the deaths dataset, requiring ≥80% of case reports with the CDC death query not missing for illnesses during May 1–December 1, 2020. This approach resulted in some variation in jurisdictions included in the hospitalization and death datasets. We then excluded from the hospitalization database any case record with missing information on hospitalization and excluded from the death database any case record with missing information on death.

For the hospitalization rate calculations, all numerators included confirmed and probable COVID-19 cases according to the CSTE definition at the time of reporting (Appendix). We calculated a lower bound for the rate by including in the denominator as not hospitalized those cases with unknown checked for hospitalization on the reporting form (N1 = 2,479,423). We calculated an upper bound for the rate by excluding from the denominator cases with unknown checked for hospitalization (n1 = 687,527 [27.7% of N1]). For the death rate calculations, all numerators included confirmed and probable COVID-19 cases according to the CSTE definition at the time of reporting (Appendix). We calculated a lower bound for the rate by including in the denominator as alive those cases with unknown checked for death on the reporting form (N2 = 4,708,444). We calculated an upper bound for the rate by excluding from the denominator cases with unknown checked for death (n2 = 756,133 [16.1% of N2]).

We chose a study period that reduced possible biases from variability in testing availability and data completeness. For each jurisdiction in the hospitalization analysis, we examined 2 metrics by week: the proportion of CDC's COVID Electronic Lab Reporting (CELR) weekly testing volume reported as positive, and the proportion of cases reported to CDC that had symptoms using COVID-19 case report data. Those metrics had stabilized by May 1 and remained stable until December 1, 2020, which we chose as the last date included to eliminate any effects from vaccination. A brief survey was sent to health officials in jurisdictions included in the analysis to assess how data were being collected and reported.

We calculated case-hospitalization and case-fatality rates by sex (male, female), age group (<1, 1–4, 5–14, 15–24, 25–34, 35–44, 45–54, 55–64, 65–74, 75–84, and ≥85 years), race and ethnicity (American Indian or Alaska Native, not Hispanic or Latino; Asian or Pacific Islander, not Hispanic or Latino; African American or Black, not Hispanic or Latino; Hispanic; other or multiple races, not Hispanic or Latino; White, not Hispanic or Latino; and unknown), hospitalization and intensive care unit (ICU) admission (admitted to ICU; hospitalized but not admitted to ICU; and not hospitalized), and presence of any symptoms. We show race and ethnicity data in a combined variable; the other or multiple races category includes not Hispanic or Latino persons whose race was reported as other or for whom more than one race was reported, and persons whose record had both a racial designation and racial information unknown selected. The unknown category includes cases who have a known ethnicity of not Hispanic or Latino but either unknown or missing race; have a known race but either unknown or missing ethnicity; or have both unknown or missing race and unknown or missing ethnicity. Although included in the unknown category in the main analysis, we excluded persons from the race and ethnicity subanalysis if ethnicity was unknown, regardless of race.

To account for differences in age distribution by race and ethnicity, so rates among the groups can be compared, we adjusted hospitalization and fatality rates for race and ethnicity to the age distribution of the largest group in the 2019 national census of the US population: White, not Hispanic or Latino (*17*). We compared the census population distributions by sex, age group, and race and ethnicity for our subset populations to the full 2019 US census to determine whether our subsets were representative of the United States (Appendix Table 1) (*17*). We also describe demographic characteristics of all COVID-19 cases reported to CDC during May 1–

December 1, 2020, by sex, age group, race and ethnicity, hospitalization and ICU admission status, presence of any symptoms, and deaths (Appendix Table 2). We used the 2019 US Census midyear estimates because they were the most recent data available at time of analysis.

Ethics

This activity was deemed not to be research as defined in 45 CFR 46.102(l), and institutional review board review was not required. This activity was reviewed by CDC and was conducted consistent with applicable federal law and CDC policy (Appendix).

Results

Study Population and Comparison with Cases in the Entire United States

A total of 10,332,323 COVID-19 cases were reported to CDC during May 1, 2020–December 1, 2020. Only 58.8.% of those had valid, nonmissing information for hospitalization and 63.5% for death during the study period (Appendix Table 2), compared with ≥80% of records in the populations from which our datasets were drawn. After deleting records with hospitalization information missing, 2,479,423 cases from 21 jurisdictions were included in the hospitalization dataset (Table 1). After deleting records with death information missing, 4,708,444 cases from 22 jurisdictions were included in the deaths dataset (Table 2). The underlying populations of the study jurisdictions closely matched the US Census total population distribution in 2019 by sex and age group but varied by race and ethnicity (Appendix Table 1). The case-hospitalization dataset covers 25.5% of the US population, and the case-fatality dataset covers 43.7% of the US population.

Case-Hospitalization Rates

Twenty-one jurisdictions met the inclusion criteria for the case-hospitalization rate calculation. The overall case hospitalization rate among case-patients was 5.7%. The rate was <8.3% for every age group for persons up to 64 years of age. The rate was 5.0% for infants (defined as <1 year of age), 1.2% for children 1–4 years of age, and 0.6% for children 5–14 years of age. Among persons ≥15 years of age, the rate steadily increased for each older age group; it was 16.3% in persons 65–74 years of age and 25.9% in persons 75–84 and ≥85 years of age. Overall, the case hospitalization rate by sex was 6.2% for male and 5.2% for female. Female persons had lower case-hospitalization rates in every age group except those 15–24 and 25–34 years of age (Table 3). The case-hospitalization rate was 6.3% for persons whose report indicated they had symptoms and 3.3% for persons whose report indicated they were asymptomatic (Table 1).

The crude case-hospitalization rate was highest among persons who were African American or Black, not Hispanic or Latino (11.4%). After age adjustment, the highest case-hospitalization rates were among persons who were African American or Black, not Hispanic or Latino (14.0%), and Asian or Pacific Islander, not Hispanic or Latino (11.2%); persons who were White, not Hispanic or Latino, had the lowest rate (6.8%) (Table 4).

Case-Fatality Rates

Twenty-two jurisdictions met the inclusion criteria for the fatality rate calculation. The overall case-fatality rate was 1.7%. The rate was <1.6% for all age groups up to persons 64 years of age. The rate was 0.05% for infants and 0.01% for children 1–4 and 5–14 years of age. The 10 infants who died (6 girls) had laboratory-confirmed SARS-CoV-2 infection. Among persons >15 years of age, the rate steadily increased for each older age group; it was 4.7% in persons 65–74 years of age, 12.0% in persons 75–84 years of age, and 23.6% in persons ≥85 years of age (Table 2; Figure). Overall, the case-fatality rate was 1.9% for male sex and 1.5% for female sex (Table 2). Case-fatality rates for female sex were lower than or equal to those for male sex in every age group except infants (Table 5). The fatality rate was 1.7% both for persons whose report indicated they had symptoms and for persons whose report indicated they were asymptomatic (Table 2).

The crude case-fatality rate was highest among persons who were Asian or Pacific Islander, not Hispanic or Latino (3.0%), followed by African American or Black, not Hispanic or Latino (2.8%), and White, not Hispanic or Latino (2.7%) (Table 2). After age adjustment, fatality rates among all racial and ethnic groups except White, not Hispanic or Latino, increased (Table 4): 4.4% for Asian or Pacific Islander, not Hispanic or Latino; 4.0% for African American or Black, not Hispanic or Latino; 3.4% for American Indian or Alaska Native, not Hispanic or Latino; 2.5% for Hispanic or Latino; and 2.1% for other or multiple races, not Hispanic or Latino. The rate decreased to 1.5% for persons who were White, not Hispanic or Latino. The fatality rate was 0.6% in persons who were not hospitalized, 17.6% among all persons who were hospitalized, and 44.2% in those admitted to an ICU (Table 2). Hospitalization and fatality rates by age group showed a steady increase, with highest rates among older age groups (Figure).

Table 1. Demographic and clinical characteristics of SARS-CoV-2 infections that met inclusion criteria for case hospitalization rate analysis, United States, 2020*

Characteristic	Includes cases for which hospitalization status was unknown, counted as not hospitalized			Includes only cases for which hospitalization status was known		
	No. hospitalizations	No. cases	Case-hospitalization rate, %	No. hospitalizations	No. cases	Case-hospitalization rate, %
Overall	140,644	2,479,423	5.7	140,644	1,791,896	7.9
Sex						
M	72,372	1,164,257	6.2	72,372	834,733	8.7
F	67,894	1,300,788	5.2	67,894	946,921	7.2
Other	2	18	11.1	2	12	16.7
Missing†	134	4,006	3.3	134	2,657	5.0
Unknown	242	10,354	2.3	242	7,573	3.2
Age group, y						
<1	564	11,208	5.0	564	8,478	6.7
1–4	386	32,180	1.2	386	24,791	1.6
5–14	823	137,646	0.6	823	104,483	0.8
15–24	4,228	470,395	0.9	4,228	337,187	1.3
25–34	8,035	429,855	1.9	8,035	305,416	2.6
35–44	10,391	373,602	2.8	10,391	270,249	3.8
45–54	16,723	357,683	4.7	16,723	257,484	6.5
55–64	25,361	309,488	8.2	25,361	221,684	11.4
65–74	31,181	190,946	16.3	31,181	141,469	22.0
75–84	26,967	103,990	25.9	26,967	77,281	34.9
≥85	15,973	61,604	25.9	15,973	42,872	37.3
Missing†	12	826	1.5	12	502	2.4
Race and ethnicity†§						
AI or AN, NH	1,974	26,745	7.4	1,974	21,821	9.1
Asian or PI, NH	3,468	49,774	7.0	3,468	43,118	8.0
AA or Black, NH	18,470	161,642	11.4	18,470	133,485	13.8
Hispanic	17,159	365,476	4.7	17,159	304,239	5.6
Other or multiple races, NH	4,705	60,408	7.8	4,705	47,583	9.9
White, NH	69,165	1,068,295	6.5	69,165	870,193	8.0
Unknown	25,703	747,083	3.4	25,703	371,457	6.9
Symptom status						
Symptomatic	105,131	1,664,240	6.3	105,131	1,484,676	7.1
Asymptomatic	1,870	55,987	3.3	1,870	50,657	3.7
Missing†	11,423	168,365	6.8	11,423	82,936	13.8
Unknown	22,220	590,831	3.8	22,220	173,627	12.8

*Data from 21 jurisdictions that met the study inclusion criteria, Case Only Epi Task Force dataset, accessed March 17, 2021, based on responses to the CDC 2019 Novel Coronavirus Case Report Form during May 1–December 1, 2020 (Figure). Reports in which no response was provided about hospitalization were excluded from the rate calculation. AA, African American; AI, American Indian; AN, Alaska Native; NH, not Hispanic or Latino; PI, Pacific Islander.
†Missing indicates that the field was left blank.
‡Other or multiple races category includes NH persons whose race was reported as other or for whom >1 race was reported and persons whose record had both a racial designation and "racial information unknown" selected. The unknown category includes cases who have a known ethnicity of NH but either unknown or missing race; have a known race but either unknown or missing ethnicity; or have both unknown or missing race and unknown or missing ethnicity.
§The jurisdictions used for the hospitalization calculation had a smaller percentage of AA or Black, NH; Asian or PI, NH; and Hispanic persons, and a larger percentage of White, NH; and AI or AN, NH, persons than the US 2019 population.

Survey of Surveillance Practices

Health officials in 17 (65%) of the 26 jurisdictions included in either or both of the hospitalization and deaths final datasets responded to the survey. Officials in 6 jurisdictions commented that default values chosen for death reporting may be "no" or "alive" when the outcome is unknown. The methods used to determine if a death was COVID-19–related varied by jurisdiction; 7 reported using the CSTE COVID-19 case definition, and 10 reported using guidance unique to their state (e.g., designating death as COVID-19–related if a positive COVID-19 laboratory result was recorded in temporal proximity to the death).

Discussion

We describe hospitalization and fatality rates of persons with COVID-19 reported through CDC surveillance, by age group, sex, race and ethnicity, and hospital and intensive care, during May 1–December 1, 2020, before the availability of COVID-19 vaccines and widespread commercial at-home testing. This study estimated rates in large US populations that included 2.4 million COVID-19 cases for measuring hospitalization rates and 4.7 million cases for fatality rates.

Age was a primary driver of SARS-CoV-2 hospitalization and death; rates had a U-shaped curve, be-

ing higher in infants, lowest in children 5 to 14 years of age, and highest among persons ≥65 years of age, confirming previous reports (*3*,*17*,*18*). Other studies have identified older age and underlying medical conditions as risk factors for severe COVID-19 outcomes, including hospitalization, admission to an ICU, requiring mechanical ventilation, and death (*3*,*18*). Those findings highlight the importance of

Table 2. Demographic and clinical characteristics of SARS-CoV-2 infections that met inclusion criteria for case fatality rate analysis, United States, 2020*

	Includes cases for which death status was not known, counted as live			Includes only cases for which death status was known		
Characteristic	No. deaths	No. cases	Case-fatality rate, %	No. deaths	No. cases	Case-fatality rate, %
Overall	78,663	4,708,444	1.7	78,663	3,952,311	2.0
Sex						
M	42,184	2,230,579	1.9	42,184	1,871,418	2.3
F	36,330	2,452,617	1.5	36,330	2,058,984	1.8
Other	0	45	0	0	42	0
Missing†	54	4,822	1.1	54	4,444	1.2
Unknown	95	20,381	0.5	95	17,423	0.6
Age group, y						
<1	10	21,331	0.05	10	18,694	0.05
1–4‡	7	66,098	0.01	7	58,590	0.01
5–14‡	15	270,467	0.01	15	233,021	0.01
15–24	175	864,837	0.02	175	717,778	0.02
25–34	571	849,838	0.06	571	717,833	0.08
35–44	1,290	717,446	0.2	1,290	605,432	0.2
45–54	3,390	687,837	0.5	3,390	576,674	0.6
55–64	8,701	589,496	1.5	8,701	488,624	1.8
65–74	16,197	341,936	4.7	16,197	283,996	5.7
75–84	21,689	180,869	12.0	21,689	150,871	14.4
≥85	26,614	112,566	23.6	26,614	95,515	27.9
Missing†	4	5,723	0.06	4	5,283	0.08
Race and ethnicity§¶						
AI or AN, NH	591	30,312	2.0	591	24,687	2.4
Asian or PI, NH	2,847	96,073	3.0	2,847	86,842	3.3
AA or Black, NH	6,529	230,117	2.8	6,529	204,784	3.2
Hispanic	2,694	347,365	0.8	2,694	282,684	1.0
Other or multiple races, NH	2,270	148,408	1.5	2,270	133,038	1.7
White, NH	41,451	1,512,389	2.7	41,451	1,207,934	3.4
Unknown	22,281	2,343,780	1.0	22,281	2,012,342	1.1
Hospitalized#						
Yes	45,328	257,208	17.6	45,328	235,206	19.3
No	13,133	2,182,361	0.6	13,133	1,982,656	0.7
Unknown	9,809	1,116,549	0.9	9,809	652,037	1.5
Missing	10,393	1,152,326	0.9	10,393	1,082,412	1.0
Hospitalized or ICU**						
Hospitalized in ICU	13,906	31,461	44.2	13,906	30,122	46.2
Hospitalized, not ICU	31,497	226,235	13.9	31,497	205,428	15.3
Not hospitalized	13,058	2,181,873	0.6	13,058	1,982,312	0.7
Unknown	20,202	2,268,875	0.9	20,202	1,734,449	1.2
Symptom status						
Symptomatic	43,395	2,537,903	1.7	43,395	2,212,265	2.0
Asymptomatic	1,850	110,446	1.7	1,850	109,243	1.7
Missing†	12,504	814,456	1.5	12,504	672,665	1.9
Unknown	20,914	1,245,639	1.7	20,914	958,138	2.2

*Data from 22 jurisdictions that met the study inclusion criteria, Case Only Epi Task Force dataset, accessed March 17, 2021, based on responses to the CDC 2019 Novel Coronavirus Case Report Form during May 1–December 1, 2020 (Figure). Reports in which no response was provided about death were excluded from the rate calculation. AA, African American; AI, American Indian; AN, Alaska Native; NH, not Hispanic or Latino; ICU, intensive care unit; PI, Pacific Islander.

†Missing indicates that the field was left blank.

‡Case-fatality rate was 0.0105%–0.0119% for 1–4 years age group and 0.0055%–0.0064% for 5–14 years age group.

§Other or multiple races category includes NH persons whose race was reported as other or for whom >1 race was reported and persons whose record had both a racial designation and "racial information unknown" selected. The unknown category includes cases who have a known ethnicity of NH, but either unknown or missing race; have a known race but either unknown or missing ethnicity; or have both unknown or missing race and unknown or missing ethnicity.

¶The jurisdictions used for the fatality calculation had a greater percentage of Asian or PI, NH, persons and a smaller percentage of AA or Black, NH, persons than the US 2019 population.

#Hospitalized status (yes or no) collected in a separate variable from "hospitalized or ICU" and numbers of hospitalized patients may not match.

**Known to have been admitted to an ICU. The dataset contained separate variables for "hospitalized" and for "hospitalized in an ICU." The 2 variables differed in the number not hospitalized and number hospitalized not in an ICU by <100 persons.

Table 3. Case-hospitalization rates by age group and sex of patients with SARS-CoV-2 infections that met inclusion criteria for case hospitalization rate analysis, United States, 2020*

	Case-hospitalization rate including cases for which hospitalization status was not known, counted as not hospitalized, %		Case-hospitalization rate among cases for which hospitalization status was known, %	
Age group, y	Male sex	Female sex	Male sex	Female sex
<1	5.2	4.9	6.9	6.4
1–4	1.3	1.1	1.7	1.4
5–14	0.6	0.6	0.8	0.8
15–24	0.7	1.1	1.0	1.5
25–34	1.6	2.2	2.2	3.0
35–44	3.0	2.6	4.2	3.6
45–54	5.3	4.1	7.5	5.6
55–64	9.4	7.1	13.2	9.9
65–74	18.5	14.3	24.9	19.3
75–84	30.1	22.5	39.7	30.8
≥85	35.4	21.4	47.8	31.7
Missing†	1.4	1.6	2.5	2.4

*Data from 21 jurisdictions that met the study inclusion criteria, CDC line level surveillance dataset, accessed March 17, 2021, based on responses to the CDC 2019 Novel Coronavirus Case Report Form during May 1–December 1, 2020. Reports in which no response was provided about hospitalization were excluded from the rate calculation.
†Missing indicates that the field was left blank.

vaccination and other mitigation methods to prevent SARS-CoV-2 infection in high-risk age groups.

Fatality rates were lowest for children 1–14 years of age (0.01%), in keeping with previous reports (*19*). We found fatality rates among infants to be slightly higher (0.05%). We have not found comparable data for infants in other studies. Higher fatality and hospitalization rates in infants may be attributable to other factors, including maternal COVID-19 infection or medical problems that may arise during the first year of life. Hospitalization rates and mortality rates are generally higher among infants than older children, primarily from complications of prematurity and birth defects (*20*,*21*). Our findings among infants should be interpreted with caution because only 10 deaths were reported among the 21,331 infant cases.

We found that male persons had higher hospitalization rates than female persons except in the 15–24- and 25–34-year age groups, and that male persons, except infants, had higher fatality rates than female persons. The reason for the disparity by sex is unknown; biologic, behavioral, and psychosocial factors could be involved (*22*–*26*). The 2 female age groups with higher hospitalization rates than the male group include female persons of childbearing age. Pregnancy and recent pregnancy may be associated with severe COVID-19 outcomes, including hospitalization and admission to ICUs (*27*,*28*).

Both unadjusted and age-adjusted hospitalization and fatality rates showed differences by race and ethnicity; the highest hospitalization rate was for the African American or Black, not Hispanic category, and the highest fatality rates were for the Asian or

Table 4. Race- and ethnicity-specific unadjusted and age-adjusted case hospitalization and fatality rates of patients with SARS-CoV-2 infections that met inclusion criteria for fatality rate analysis, United States, 2020*

	Case hospitalization rate including cases for which hospitalization status was not known, counted as not hospitalized		Case fatality rate including cases for which death status was not known, counted as live	
Race and ethnicity†	Unadjusted	Age-adjusted‡	Unadjusted	Age-adjusted‡
AI or AN, NH	7.4	10.1	2.0	3.4
Asian or PI, NH	7.0	11.2	3.0	4.4
AA or Black, NH	11.4	14.0	2.8	4.0
Hispanic	4.7	9.0	0.8	2.5
Other or multiple races, NH	7.8	9.8	1.5	2.1
White, NH	6.5	6.8	2.7	1.5
Unknown	3.4	4.2	1.0	2.6

*Data from 21 (hospitalization) and 22 (fatality) jurisdictions that met the study inclusion criteria, CDC line level surveillance dataset, accessed March 17, 2021, based on responses to the CDC 2019 Novel Coronavirus Case Report Form during May 1–December 1, 2020. Reports in which no response was provided about death or hospitalization were excluded from the rate calculation. AA, African American; AI, American Indian; AN, Alaska Native; ICU, intensive care unit; NH, not Hispanic or Latino; PI, Pacific Islander..
†Other or multiple races category includes not Hispanic or Latino persons whose race was reported as other or for whom >1 race was reported and persons whose record had both a racial designation and "racial information unknown" selected. The unknown category includes cases who have a known ethnicity of NH, but either unknown or missing race; have a known race but either unknown or missing ethnicity; or have both unknown or missing race and unknown or missing ethnicity.
‡Hospitalization and fatality rates by race and ethnicity adjusted to the age distribution of the White, NH, population based on 2019 US Census population.

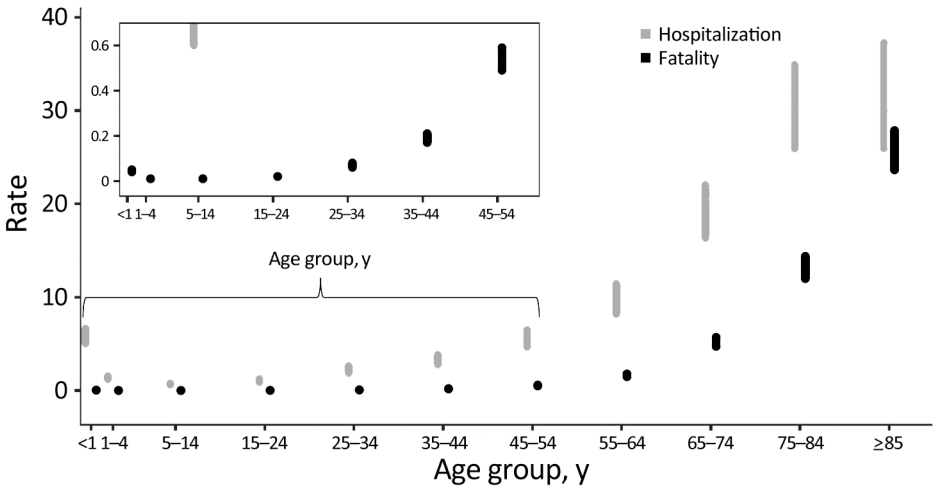

Figure. Upper and lower estimates of case-hospitalization (gray) and case-fatality (black) rates by age group of patients with SARS-CoV-2 infection, United States, 2020. Graphical representation of upper and lower estimates of rates in Tables 1 and 2. For case-hospitalization, lower bound was calculated by including cases with unknown hospitalization information as not hospitalized and upper bound by excluding cases with unknown hospitalization information. For case-fatality, lower bound was calculated by including cases with unknown death status as alive and upper bound by excluding cases with unknown death status information. Reports in which no response was provided about death or hospitalization were excluded from the respective rate calculation. Inset graph provides greater detail for younger age groups by using smaller y-axis values.

Pacific Islander and African American or Black, not Hispanic categories. Similar disparities in SARS-CoV-2 infections have been reported in other studies. Data in our analysis did not include information (e.g., socioeconomic status and occupation) to enable further examination of the reasons for these disparities (*7*). One study found no association between race and ethnicity category and severe COVID-19 outcomes after primary COVID-19 vaccination series (receipt of 2 doses), which suggests that access to COVID-19 vaccines can help mitigate racial and ethnic disparities (*18*).

We found that almost half of persons admitted to an ICU died, similar to studies of <400 persons conducted in Seattle (50%), Washington (52%), and New York City (78%) (*22*,*29*,*30*). This finding emphasizes the importance of early diagnosis and treatment of SARS-CoV-2 infection. Mechanical ventilation is often associated with high fatality rates (*22*,*26*,*31*).

One limitation of this analysis is the use of data from only 21 jurisdictions for hospitalization rate calculations and 22 for fatality rate calculations of the 56 jurisdictions that reported case information to CDC. However, the inclusion of only those jurisdictions is also a strength of the analysis because a relatively high percentage of case reports had valid, nonmissing hospitalization or death data. A high percentage of case reports were for persons with unknown race and ethnicity, in large part because reports without ethnicity were classified as unknown even if race was recorded (*32*); a smaller percentage were categorized as having other or multiple races. Had ethnicity been known, the hospitalization rate for racial and ethnic groups with

Table 5. Case-fatality rates by age group and sex of patients with SARS-CoV-2 infections, United States, 2020*

	Case-fatality rates including cases for which death status was not known, counted as live, %		Case-fatality rates among cases for which death status was known, %	
Age group, y	Male	Female	Male	Female
<1	0.04	0.06	0.04	0.07
1–4	0.01	0.01	0.01	0.01
5–14	0.00	0.01	0.01	0.01
15–24	0.03	0.01	0.03	0.02
25–34	0.09	0.05	0.11	0.06
35–44	0.2	0.1	0.3	0.2
45–54	0.7	0.3	0.8	0.4
55–64	2.0	1.0	2.4	1.2
65–74	6.0	3.6	7.2	4.3
75–84	14.7	9.8	17.5	11.8
≥85	29.4	20.9	34.0	24.9
Missing†	0.1	0.0	0.1	0.0

*Data from 22 jurisdictions that met the study inclusion criteria, CDC line level surveillance dataset, accessed March 17, 2021, based on responses to the CDC 2019 Novel Coronavirus Case Report Form during May 1–December 1, 2020. Reports in which no response was provided about death were excluded from the rate calculation.
†Missing indicates that the field was left blank.

added cases would be lower, and the effect on death rate would vary by group. Public health authorities have made recommendations to improve race and ethnicity reporting in surveillance data (*33*,*34*). Our comparisons of age-adjusted rates among racial and ethnic groups do not adjust for differences in prevalence of underlying diseases. Tests were performed only on persons who sought testing or medical care; therefore, cases in persons with no or mild symptoms were less likely to be identified and reported. Differences in the application of death definitions across jurisdictions highlight the need for standardized definitions during a pandemic; in December 2021, CSTE released a definition of COVID-19–associated deaths, developed with input from jurisdictional health departments (*35*). Limitations of using surveillance data to estimate fatality rates include preferential ascertainment of severe infections that may lead to overestimation of fatality rates, and the effect of specific interventions (e.g., hospitalization or hospitalization at a particular hospital) on survival (*36*). Although the National Center for Health Statistics has provisional data on COVID-19–related deaths, it does not have information on ill persons who did not die, so rates cannot be calculated from these data. We used surveillance data, which commonly, and in this study, have quality issues, including missing key variables such as race, ethnicity, and symptoms. Because of those limitations, we bounded our primary results by different assumptions on which outcome those with missing data had and we avoided statistical approaches, which, because of our large sample size, would have led to misleadingly narrow confidence bounds. Furthermore, the large sample size ensures that many differences would be statistically significant even if those differences may be of little practical significance.

Caution is needed before drawing conclusions from our study population. One might expect concerns with the quality of data collected during an emergency response above those in other surveillance data. Yet, such surveillance data can provide information that would not otherwise be available (*37*). Despite the limitations of our study dataset, the inclusion of data from most of the country, including many persons of all ages, races, and ethnicities, and our method of accounting for missing information in the analyses make these estimates valuable to the public health community.

This analysis presents case-hospitalization and case-fatality rates by age group, sex, and racial and ethnic groups before the introduction of vaccinations targeting SARS-CoV-2. The introduction of vaccinations and the presence of new strains of SARS-CoV-2 altered those rates. Moreover, the wide availability of at-home tests for detecting infection and the lack of national reporting for home testing results make it more likely that only severe infections will be reported. Our results document the severity of SARS-CoV-2 infections early in the pandemic, provide a baseline for future comparisons, and highlight the importance of preventing severe illness in high-risk populations (e.g., through vaccination, early identification of symptoms, testing, and isolation to prevent transmission). Devising appropriate control measures, with community input, for persons in historically underserved racial and ethnic groups and among adults ≥65 years of age is especially important (*18*).

Acknowledgments

We thank state, local, and territorial health department personnel; healthcare community caring for patients; and the CDC COVID-19 Data, Analytics, and Visualization Task Force (Roger Mir, William Duck, Diba Khan, Amanda Jones, Tory Seffren, and Matthew Ritchey).

About the Author

Dr. Griffin is an Epidemic Intelligence Service fellow for the Centers for Disease Control and Prevention in Atlanta, Georgia, United States.

References

1. Centers for Disease Control and Prevention. COVID data tracker. 2020 [cited 2021 Dec 22]. https://covid.cdc.gov/covid-data-tracker/#datatracker-home
2. US Food and Drug. Coronavirus (COVID-19) update: FDA authorizes antigen test as first over-the-counter fully at-home diagnostic test for COVID-19. 2020 Dec 15 [cited 2022 Mar 5]. https://www.fda.gov/news-events/press-announcements/coronavirus-covid-19-update-fda-authorizes-antigen-test-first-over-counter-fully-home-diagnostic
3. Bialek S, Bowen V, Chow N, Curns A, Gierke R, Hall A, et al.; CDC COVID-19 Response Team. Geographic differences in COVID-19 cases, deaths, and incidence—United States, February 12–April 7, 2020. MMWR Morb Mortal Wkly Rep. 2020;69:465–71. https://doi.org/10.15585/mmwr.mm6915e4
4. Johnson AG, Amin AB, Ali AR, Hoots B, Cadwell BL, Arora S, et al. COVID-19 incidence and death rates among unvaccinated and fully vaccinated adults with and without booster doses during periods of delta and omicron variant emergence—25 U.S. jurisdictions, April 4–December 25, 2021. MMWR Morb Mortal Wkly Rep. 2022;71:132–8. https://doi.org/10.15585/mmwr.mm7104e2
5. BBC. First COVID vaccine is administered in the US. 2020 Dec 14 [cited 2022 Mar 5]. https://www.bbc.com/news/av/world-us-canada-55307642
6. Ergönül Ö, Akyol M, Tanrıöver C, Tiemeier H, Petersen E, Petrosillo N, et al. National case fatality rates of the

COVID-19 pandemic. Clin Microbiol Infect. 2021;27:118–24. https://doi.org/10.1016/j.cmi.2020.09.024
7. Golestaneh L, Neugarten J, Fisher M, Billett HH, Gil MR, Johns T, et al. The association of race and COVID-19 mortality. EClinicalMedicine. 2020;25:100455. https://doi.org/10.1016/j.eclinm.2020.100455
8. Ge Y, Sun S, Shen Y. Estimation of case-fatality rate in COVID-19 patients with hypertension and diabetes mellitus in the New York state: a preliminary report. Epidemiol Infect. 2021;149:e14. https://doi.org/10.1017/S0950268821000066
9. Perone G. The determinants of COVID-19 case fatality rate (CFR) in the Italian regions and provinces: an analysis of environmental, demographic, and healthcare factors. Sci Total Environ. 2021;755:142523. https://doi.org/10.1016/j.scitotenv.2020.142523
10. Macedo A, Gonçalves N, Febra C. COVID-19 fatality rates in hospitalized patients: systematic review and meta-analysis. Ann Epidemiol. 2021;57:14–21. https://doi.org/10.1016/j.annepidem.2021.02.012
11. Scobie HM, Johnson AG, Suthar AB, Severson R, Alden NB, Balter S, et al. Monitoring incidence of COVID-19 cases, hospitalizations, and death by vaccination status—13 U.S. jurisdictions, April 4–July 17, 2021. MMWR Morb Mortal Wkly Rep. 2021;70:1284–90. https://doi.org/10.15585/mmwr.mm7037e1
12. Centers for Disease Control and Prevention. Rates of COVID-19 cases and deaths by vaccination status. 2021 [cited 2022 Aug 25]. https://covid.cdc.gov/covid-data-tracker/#rates-by-vaccine-status
13. Stein C, Nassereldine H, Sorensen RJD, Amlag JO, Bisignano C, Byrne S, et al.; COVID-19 Forecasting Team. Past SARS-CoV-2 infection protection against re-infection: a systematic review and meta-analysis. Lancet. 2023;401:833–42. https://doi.org/10.1016/S0140-6736(22)02465-5
14. Centers for Disease Control and Prevention. COVID-19 case report form. 2020 [cited 2021 Jan 21]. https://www.cdc.gov/coronavirus/2019-ncov/downloads/pui-form.pdf
15. Centers for Disease Control and Prevention. Coronavirus disease 2019 (COVID-19) 2020 interim case definition, approved August 5, 2020. 2020 Aug 5 [cited 2021 Apr 22]. https://ndc.services.cdc.gov/case-definitions/coronavirus-disease-2019-2020
16. Council of State and Territorial Epidemiologists. Coronavirus disease 2019 (COVID-19) 21-ID-01 update to the standardized surveillance case definition and national notification for 2019 novel coronavirus disease (COVID-19), approved June 17, 2021. 2021 Jun 17 [cited 2021 Aug 12]. https://cdn.ymaws.com/www.cste.org/resource/resmgr/ps/ps2021/21-ID-01_COVID-19.pdf
17. Sudharsanan N, Didzun O, Bärnighausen T, Geldsetzer P. The contribution of the age distribution of cases to COVID-19 case fatality across counties: a nine-country demographic study. Ann Intern Med. 2020;173:714–20. https://doi.org/10.7326/M20-2973
18. Yek C, Warner S, Wiltz JL, Sun J, Adjei S, Mancera A, et al. Risk factors for severe COVID-19 outcomes among persons aged ≥18 years who completed a primary COVID-19 vaccination series—465 health care facilities, United States, December 2020–October 2021. MMWR Morb Mortal Wkly Rep. 2022;71:19–25. https://doi.org/10.15585/mmwr.mm7101a4
19. Leidman E, Duca LM, Omura JD, Proia K, Stephens JW, Sauber-Schatz EK. COVID-19 trends among persons aged 0–24 years—United States, March 1–December 12, 2020. MMWR Morb Mortal Wkly Rep. 2021;70:88–94. https://doi.org/10.15585/mmwr.mm7003e1
20. Centers for Disease Control and Prevention. Reproductive health: infant mortality. 2021 [cited 2021 Feb 14]. https://www.cdc.gov/reproductivehealth/maternalinfanthealth/infantmortality.htm
21. Hobbs CV, Woodworth K, Young CC, Jackson AM, Newhams MM, Dapul H, et al.; for the Overcoming COVID-19 Investigators. Frequency, characteristics and complications of COVID-19 in hospitalized infants. Pediatr Infect Dis J. 2022;41:e81–6. https://doi.org/10.1097/INF.0000000000003435
22. Richardson S, Hirsch JS, Narasimhan M, Crawford JM, McGinn T, Davidson KW, et al.; the Northwell COVID-19 Research Consortium. Presenting characteristics, comorbidities, and outcomes among 5700 patients hospitalized with COVID-19 in the New York City Area. JAMA. 2020;323:2052–9. https://doi.org/10.1001/jama.2020.6775
23. Green MS, Nitzan D, Schwartz N, Niv Y, Peer V. Sex differences in the case-fatality rates for COVID-19—a comparison of the age-related differences and consistency over seven countries. PLoS One. 2021;16:e0250523. https://doi.org/10.1371/journal.pone.0250523
24. Danielsen AC, Lee KM, Boulicault M, Rushovich T, Gompers A, Tarrant A, et al. Sex disparities in COVID-19 outcomes in the United States: quantifying and contextualizing variation. Soc Sci Med. 2022;294:114716. https://doi.org/10.1016/j.socscimed.2022.114716
25. Griffith DM, Sharma G, Holliday CS, Enyia OK, Valliere M, Semlow AR, et al. Men and COVID-19: a biopsychosocial approach to understanding sex differences in mortality and recommendations for practice and policy interventions. Prev Chronic Dis. 2020;17:E63. https://doi.org/10.5888/pcd17.200247
26. Lim ZJ, Subramaniam A, Ponnapa Reddy M, Blecher G, Kadam U, Afroz A, et al. Case fatality rates for patients with COVID-19 requiring invasive mechanical ventilation. A meta-analysis. Am J Respir Crit Care Med. 2021;203:54–66. https://doi.org/10.1164/rccm.202006-2405OC
27. Collin J, Byström E, Carnahan A, Ahrne M. Public Health Agency of Sweden's brief report: pregnant and postpartum women with severe acute respiratory syndrome coronavirus 2 infection in intensive care in Sweden. Acta Obstet Gynecol Scand. 2020;99:819–22. https://doi.org/10.1111/aogs.13901
28. Zambrano LD, Ellington S, Strid P, Galang RR, Oduyebo T, Tong VT, et al.; CDC COVID-19 Response Pregnancy and Infant Linked Outcomes Team. Update: characteristics of symptomatic women of reproductive age with laboratory-confirmed SARS-CoV-2 infection by pregnancy status—United States, January 22–October 3, 2020. MMWR Morb Mortal Wkly Rep. 2020;69:1641–7. https://doi.org/10.15585/mmwr.mm6944e3
29. Bhatraju PK, Ghassemieh BJ, Nichols M, Kim R, Jerome KR, Nalla AK, et al. COVID-19 in critically ill patients in the Seattle region—case series. N Engl J Med. 2020;382:2012–22. https://doi.org/10.1056/NEJMoa2004500
30. Arentz M, Yim E, Klaff L, Lokhandwala S, Riedo FX, Chong M, et al. Characteristics and outcomes of 21 critically ill patients with COVID-19 in Washington State. JAMA. 2020;323:1612–4. https://doi.org/10.1001/jama.2020.4326
31. Oliveira E, Parikh A, Lopez-Ruiz A, Carrilo M, Goldberg J, Cearras M, et al. ICU outcomes and survival in patients with severe COVID-19 in the largest health care system in central Florida. PLoS One. 2021;16:e0249038. https://doi.org/10.1371/journal.pone.0249038
32. Yoon P, Hall J, Fuld J, Mattocks SL, Lyons BC, Bhatkoti R, et al. Alternative methods for grouping race and ethnicity

to monitor COVID-19 outcomes and vaccination coverage. MMWR Morb Mortal Wkly Rep. 2021;70:1075–80. https://doi.org/10.15585/mmwr.mm7032a2
33. Council of State and Territorial Epidemiologists (CSTE). Addressing gaps in public health reporting of race and ethnicity data for COVID-19: findings and recommendations among 45 state & local health departments. 2022 Apr 20 [cited 2022 Nov 10]. https://preparedness.cste.org/wp-content/uploads/2022/04/RaceEthnicityData_FINAL.pdf
34. US Department of Health and Human Services. Office of the Inspector General (OIG). CDC found ways to use data to understand and address COVID-19 health disparities, despite challenges with existing data (OEI-05–20–00540). 2022 Jul [cited 2022 Nov 10]. https://oig.hhs.gov/oei/reports/OEI-05-20-00540.pdf
35. Council of State and Territorial Epidemiologists. Interim guidance for public health surveillance programs for classification of COVID-19 associated deaths among COVID-19 cases. Version 1. 2021 Dec 22 [cited 2021 Dec 23]. https://cdn.ymaws.com/www.cste.org/resource/resmgr/pdfs/pdfs2/20211222_interim-guidance.pdf
36. Lipsitch M, Donnelly CA, Fraser C, Blake IM, Cori A, Dorigatti I, et al. Potential biases in estimating absolute and relative case-fatality during outbreaks. PLoS Negl Trop Dis. 2015;9:e0003846. https://doi.org/10.1371/journal.pntd.0003846
37. German RR, Lee LM, Horan JM, Milstein RL, Pertowski CA, Waller MN; Guidelines Working Group Centers for Disease Control and Prevention (CDC). Updated guidelines for evaluating public health surveillance systems: recommendations from the Guidelines Working Group. MMWR Recomm Rep. 2001;50(RR-13):1–35.

Address for correspondence: Isabel Griffin, Centers for Disease Control and Prevention, 1600 Clifton Rd NE, Mailstop H16-3, Atlanta, GA 30329-4018, USA; email: pli7@cdc.gov

Trends in Nationally Notifiable Infectious Diseases in Humans and Animals during COVID-19 Pandemic, South Korea

Taehee Chang, Sung-il Cho, Dae sung Yoo, Kyung-Duk Min

We investigated trends in notifiable infectious diseases in both humans and animals during the COVID-19 pandemic in South Korea and compared those data against expected trends had nonpharmaceutical interventions (NPIs) not been implemented. We found that human respiratory infectious diseases other than COVID-19 decreased by an average of 54.7% after NPIs were introduced. On the basis of that trend, we estimated that annual medical expenses associated with respiratory infections other than COVID-19 also decreased by 3.8% in 2020 and 18.9% in 2021. However, human gastrointestinal infectious diseases and livestock diseases exhibited similar or even higher incidence rates after NPIs were instituted. Our investigation revealed that the preventive effect of NPIs varied among diseases and that NPIs might have had limited effectiveness in reducing the spread of certain types of infectious diseases. These findings suggest the need for future, novel public health interventions to compensate for such limitations.

The global COVID-19 pandemic, caused by SARS-CoV-2, dramatically disrupted the lives of persons around the world, resulting in record numbers of cases and deaths (*1*). In the early stages of the pandemic, public health measures primarily consisted of nonpharmaceutical interventions (NPIs), such as social distancing, mask wearing, and contact tracing. NPIs are effective in mitigating the epidemic curves in various contexts, even without vaccines or specific treatments targeting the pathogen (*2*–*4*). Since March 2020, stringent public health measures have been implemented nationwide in South Korea, effectively suppressing the spread of COVID-19 (*5*–*7*).

The effects of NPIs are not necessarily limited to COVID-19. Because NPIs reduce effective contacts within a population, such measures can also mitigate other respiratory infectious diseases (*5*,*8*,*9*). Likewise, implementation of social distancing measures (e.g., restrictions on social gatherings in restaurants) and improved personal hygiene practices can reduce occurrence rates of gastrointestinal diseases (*9*,*10*). Mitigation measures targeting COVID-19 might even extend beyond human diseases, potentially reducing risks for infectious diseases in animals (*11*–*13*). Human movement restrictions and the global economic crisis have greatly disrupted farming operations, veterinary services, wildlife surveillance, and zoonotic disease control, broadly influencing animal health and welfare (*11*,*12*). Those effects could contribute to outbreaks of major zoonotic diseases, such as brucellosis and bovine tuberculosis in animal populations, increasing the risk for zoonotic spillover (*13*).

Research on the effects of NPIs implemented during the COVID-19 pandemic on other infectious diseases in South Korea has found that reductions in respiratory infections coincided with social distancing interventions (*14*–*20*). However, the effects of NPIs on gastrointestinal diseases were inconsistent. Studies revealed a notable reduction in viral gastrointestinal infections but no marked decrease in bacterial infections, such as those caused by *Campylobacter* spp., *Clostridium perfringens*, and *Salmonella* spp. (*10*,*18*,*20*). Decreases in viral gastrointestinal diseases were attributed to the primary transmission route being fecal–oral contamination or direct contact between persons. In contrast, bacterial gastrointestinal infections

Author affiliations: Seoul National University, Seoul, South Korea (T. Chang, S. Cho); Institute of Health and Environment, Seoul (S. Cho); Chonnam National University, Gwangju, South Korea (D. Yoo); Chungbuk National University, Cheongju, South Korea (K.-D. Min)

DOI: http://doi.org/10.3201/eid3006.231422

are mainly foodborne illnesses attributable to consuming contaminated food or water (*21*).

We focused on nationally notifiable infectious diseases in humans and livestock, using data collected after 2020. We sought to quantify the effect of nationally implemented NPIs in South Korea on the trends of infectious diseases other than COVID-19, to evaluate the benefits and drawbacks of NPIs, and to provide scientific evidence informing future health policy decisions aimed at mitigating various types of infectious diseases. We focused our study on the period from 2016 through the end of 2021, a period of social distancing in South Korea instituted in response to the COVID-19 pandemic. In the first half of 2022, NPIs were tapered back, as were their potential attenuation effects. To quantify the effect of NPIs in South Korea, we built time series models (*22*) for 6 respiratory human infectious diseases, 4 human gastrointestinal diseases, and 2 livestock diseases.

Methods

Study Design

We retrospectively analyzed the effect of COVID-19–associated NPIs on incidence of infectious diseases in South Korea. We used the following criteria in selecting target infectious diseases from among the nationally notifiable diseases: human infectious diseases with a principal mode of transmission that is respiratory (airborne or droplets) or gastrointestinal (foodborne or via fecal–oral route); animal infectious diseases with a risk for zoonotic transmission; and diseases with an annual average incidence >100 cases. Acknowledging that the effects of NPIs might not be fully applicable to certain infectious diseases that require isolation after diagnosis or symptom onset, we nonetheless theorized that implementation of NPIs in a population can potentially suppress the spread caused by asymptomatic carriers or infectious persons before isolation. We therefore included such diseases as target infectious diseases in this study. We defined the preintervention period as January 2016–February 2020 and the intervention period as March 2020–December 2021. From May 2022 onward, the outdoor mask mandate was conditionally lifted.

We used autoregressive integrated moving average (ARIMA) models to forecast disease incidence during the intervention period on the basis of patterns in the preintervention period and compared predicted values with observed values in the intervention period. The time-dependent reproduction number (R_t) affords an optimal understanding of the transmission dynamics of respiratory infectious diseases (*23*). Therefore, we calculated R_t values for respiratory infectious diseases during time series forecasting.

Previous studies investigating the effects of COVID-19 and NPIs on other diseases suggest that the reduced burden of target diseases during the early stages of the COVID-19 pandemic could be attributed to pandemic-related decreases in healthcare utilization and disease diagnoses (*19*). To adjust for the effect of decreased healthcare utilization, we collected information on annual hospital visits (*24*) and annual health insurance claims (*25*) (Appendix 1 Table 1, https://wwwnc.cdc.gov/EID/article/30/6/23-1422-App1.pdf), and used those numbers as denominators when calculating disease incidence. When calculating incidence rates per population, we collected annual midyear population data for each year in South Korea (*26*). We also obtained total annual medical expenses associated with each infectious disease to evaluate how changes in disease occurrence after NPI implementation might have affected the overall disease burden (*27*). We calculated annual medical expenses per case using Health Insurance Review and Assessment Service data from 2018–2021 (*27*). Then, we multiplied expenses per case by the estimated and observed cases of each disease to determine the model-based medical costs and observation-based values for each disease. We compared those values when assessing changes in the overall disease burden.

Social Distancing Measures

In February 2020, in response to the COVID-19 outbreak in China, South Korea implemented a universal mask mandate and recommended physical distancing (Table 1). After the increase in COVID-19 cases in South Korea, nationwide social distancing requirements were implemented with various restrictions starting in March 2020 (*28*). During the initial phase of the COVID-19 pandemic, the Distancing in Daily Life strategy was put into practice in South Korea (*29*). After multiple outbreaks occurred near metropolitan areas, the Distancing in Daily Life strategy was restructured on June 28, 2020, into a 3-tier social distancing system that consisted of levels 1, 2, and 3 (Appendix 1 Table 2) (*1*). In November 2020, the social distancing system was reorganized into a 5-tier structure that consisted of levels 1, 1.5, 2, 2.5, and 3 (Appendix 1 Table 3). Subsequently, in July 2021, the system was modified to a 4-tier structure that consisted of levels 1, 2, 3, and 4 (Appendix 1 Table 4) (*29*). In this study, we documented the policy changes based on the 4-tier structure; we did not consider any rapid changes within short periods (e.g., 1–2 weeks or 1 month) because they might not have been adequately effective (Figure 1).

Table 1. Changes in social distancing policies used in a study of trends in nationally notifiable infectious diseases in humans and animals during COVID-19 pandemic, South Korea

Time period and social distancing level	General description of terms
June 2020–November 2020	
1	Distancing in daily life
2	Moderate social distancing
3	Intensive social distancing
November 2020–July 2021	
1	Distancing in daily life
1.5	Local outbreak initiation
2	Rapid local spread, nationwide spread initiation
2.5	Nationwide outbreak intensification
3	Nationwide major epidemic
July 27, 2021 onward	
1	Sustained suppression phase
2	Regional outbreak
3	Regional epidemic
4	Nationwide epidemic

Data Acquisition

We collected data on the weekly and monthly domestic cases of nationally notifiable infectious diseases from the Infectious Disease Portal of the Korea Disease Control and Prevention Agency (*30*). To minimize sampling bias and ensure that our analysis was robust despite the COVID-19–related decrease in healthcare utilization, we focused on only infectious diseases listed in the mandatory surveillance system. We collected records on cases of 6 respiratory infectious diseases (varicella, pertussis, mumps, invasive pneumococcal disease [IPD], scarlet fever, and tuberculosis [TB]); 4 gastrointestinal diseases (typhoid fever, shigellosis, hepatitis A, and enterohemorrhagic Escherichia coli [EHEC]) that occurred during January 2016–December 2021 (Appendix 1 Table 5).

We collected data from the Korea Animal Health Integrated System in investigating animal diseases with zoonotic potential (*31*). The Korea Animal Health Integrated System is a comprehensive system operated by the Animal and Plant Quarantine Agency that integrates and provides nationwide information on livestock diseases. We selected 2 livestock diseases (cattle TB and cattle brucellosis) and collected occurrence data for January 2016–December 2021 (Appendix 1 Table 5). We focused on cattle TB and cattle brucellosis because those diseases pose risks for human infection and annual cases are numerous. We then investigated the effects of NPIs. We also collected data relating to the annual number of livestock and the annual scale of livestock farming (*32*) when calculating incidence rates relative to the livestock population.

R_t Estimation

R_t represents the average number of new infections generated by an infected person during the infectious period. This time- and context-specific measure is frequently used to assess the transmissibility of a pathogen during an outbreak. Therefore, in this study, we used R_t to reflect the dynamics of respiratory infectious diseases accurately when estimating the effectiveness of NPIs. We estimated the incidence levels of infectious diseases within the population and assessed trends in disease occurrence, except for TB, on the basis of R_t. Although TB is a respiratory infectious disease, we did not calculate R_t because of the complex transmission routes and long latent period; rather, we used reported cases for time series forecasting of tuberculosis. The calculation of R_t was based on examples from previous studies (*23*,*33*–*35*) (Appendix 2, https://wwwnc.cdc.gov/EID/article/30/6/23-1422-App2.pdf).

Time Series Analysis

The ARIMA model is a time series forecasting technique that incorporates elements of an autoregressive moving average when making predictions (*22*). Autoregression of time series data shows how past values influence the current value. The moving average

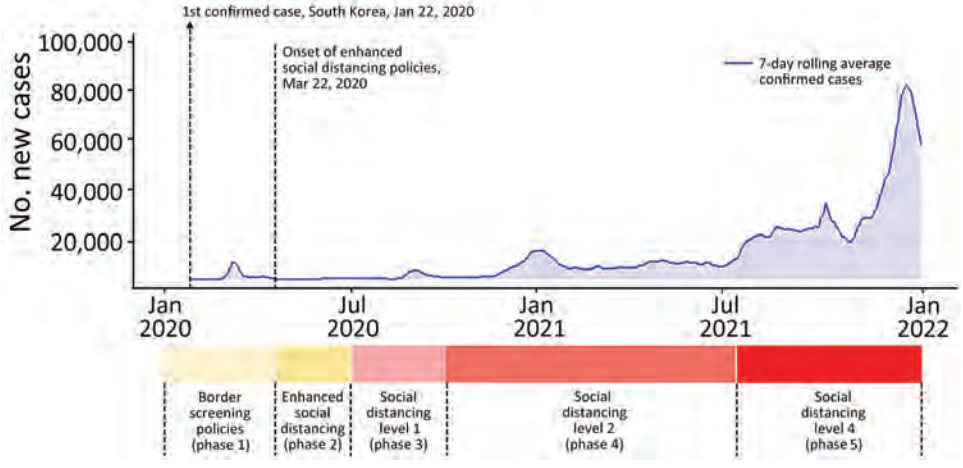

Figure 1. Daily numbers of confirmed cases and 7-day rolling average numbers of COVID-19 cases in a study of trends in nationally notifiable infectious diseases in humans and animals during the COVID-19 pandemic, South Korea. Phase and level information is provided in Tables 2 and 3. The levels of nonpharmaceutical interventions depicted in this figure are those of the 4-tier system implemented in July 2021.

Table 2. Weekly average incidences of diseases included in study of trends in nationally notifiable infectious diseases in humans and animals during COVID-19 pandemic, South Korea*

Disease	2016–2019	2020–2021					
		Overall	Phase 1	Phase 2	Phase 3	Phase 4	Phase 5
Human, cases/1 million population							
Respiratory diseases							
Varicella	30.11	12.09	25.76	9.29	9.31	8.27	7.81
Pertussis	0.18	0.05	0.17	0.03	0.01	0.01	0.01
Mumps	6.95	4.00	3.89	4.28	4.34	3.29	4.21
Invasive pneumococcal disease	0.21	0.13	0.28	0.11	0.08	0.1	0.1
Scarlet fever	5.57	0.80	2.12	0.76	0.59	0.34	0.21
Tuberculosis	13.13	9.16	10.02	9.17	9.31	8.94	8.34
Gastrointestinal or enteroviral diseases							
Typhoid	0.04	0.03	0.03	0.05	0.04	0.02	0.03
Shigellosis	0.02	0.02	0.03	0.04	0.01	0.01	0.01
Hepatitis A	3.02	1.91	1.37	1.58	1.59	2.48	2.53
Enterohemorrhagic *Escherichia coli*	0.05	0.12	0.04	0.23	0.21	0.06	0.06
Veterinary, cases/100,000 animals							
Bovine tuberculosis	2.19	1.29	1.04	1.82	1.43	1.27	0.91
Bovine brucellosis	0.49	0.61	0.41	0.51	0.55	0.83	0.74

*Detailed information on social distancing policies is provided in Appendix 1 Tables 2–4 (https://wwwnc.cdc.gov/EID/article/30/6/23-1422-App1.pdf). Phase 1, border screening policies, February 20–March 21, 2020; phase 2, enhanced social distancing, March 22–June 27, 2020; phase 3, social distancing level 1, June 28–August 22, 2020; phase 4, social distancing level 2, August 23, 2020–July 26, 2021; phase 5, social distancing level 4, July 27–December 31, 2021.

indicates how prediction errors affect the current value. This component adjusts for irregularities in the time series by using past prediction errors to correct the current value. The model is commonly used to predict the short-term impacts and trends of acute infectious diseases (*9*,*22*). Time series forecasting based on the Box-Jenkins method features 4 steps: identification, estimation, diagnostic checking, and forecasting (*36*). We used those steps when making predictions. In addition, we conducted out-of-sample validation to confirm the predictive performance of the model and ensure that the model had not overfitted the training data. In the validation process, we used data from 2015–2018 as training data and predicted and compared the trends for 2019 with the observed values (Appendix 2). We performed all data processing and analyses using R version 4.2.2 (The R Foundation for Statistical Computing, https://www.r-project.org).

Results

Incidences of Human Respiratory Diseases

After nationwide social distancing measures were put in place in South Korea in March 2020 (Figure 1), considerable decreases in the weekly reported case numbers for human respiratory diseases were observed (Table 2). The mean weekly incidence levels (cases/1 million population) for 2016–2019 varied for each disease: varicella, 30.11; pertussis, 0.18; mumps, 6.95; IPD, 0.21; scarlet fever, 5.57; and TB, 13.13. However, after implementation of NPIs, the mean weekly incidence levels for 2020–2021 substantially decreased, and showed slight variations among the phases: varicella, 12.09; pertussis, 0.05; mumps, 4.00; IPD, 0.13; scarlet fever, 0.80; and TB, 9.16. The annual medical expenses associated with respiratory infectious diseases decreased by 3.77% in 2020, compared with the value calculated using the average estimated incidence; the value decreased by an additional 18.91% in 2021 (Table 3). Whereas medical expenses related to respiratory infectious diseases exhibited an overall decreasing trend, TB-related expenses showed a slight increase in 2020; scarlet fever–related expenses also exhibited a slight increase in 2021.

ARIMA models (Appendix 1 Tables 7–19, Figures 1–12) showed that, except for TB, the actual incidence of diseases examined during the intervention period were substantially lower than the predicted incidence (Figure 2, panels A–J, http://wwwnc.cdc.gov/EID/article/30/6/23-1422-F2.htm). The incidence levels of TB were lower than the predicted values, but the average predicted values were within 25.6% of the numbers of reported cases. Although the average predicted values decreased, compared with predicted values, after the implementation of social distancing measures, the observed incidence remained at levels similar to the predicted values from the second half of 2020 (Figure 2, panels K, L).

Incidence of Human Gastrointestinal Diseases

Unlike for respiratory infectious diseases, the incidence of the 4 gastrointestinal diseases did not exhibit remarkable decreases after the implementation of NPIs (Table 2). The mean weekly incidence levels (cases/1 million population) for 2016–2019 varied among the diseases: typhoid, 0.04; shigellosis, 0.02; hepatitis A, 3.02; and EHEC, 0.05. Although we

Table 3. Annual medical expenses due to infectious diseases in a study of trends in nationally notifiable infectious diseases in humans and animals during COVID-19 pandemic, South Korea*

	Expenses, in million USD									
			Estimated, 2020			Observed,	Estimated, 2021			Observed,
Diseases	Observed, 2018	Observed, 2019	Lower 95%	Average	Upper 95%	2020 (% difference)†	Lower 95%	Average	Upper 95%	2021 (% difference)‡
Respiratory										
Varicella	5,399	5,590	3,704	7,153	13,548	2,675 (−62.61)	2,692	6,559	16,001	1,971 (−69.95)
Pertussis	544	298	44	380	1,171	42 (−88.98)	13	409	1,900	6 (−98.65)
Mumps	1,283	1,445	1,203	1,552	2,189	790 (−49.08)	1,066	1,532	2,203	775 (−49.42)
IPD	1,988	1,686	1,305	2,920	6,437	1,360 (−53.41)	1,305	3,370	8,717	1,116 (−66.87)
Scarlet fever	1,283	691	182	465	947	317 (−31.80)	28	124	567	154 (24.27)
Tuberculosis	61,241	63,535	42,695	48,705	55,593	53,681 (10.21)	48,536	59,956	74,117	54,324 (−9.39)
Subtotal	71,738	73,244	49,134	61,174	79,886	58,864 (−3.77)	53,640	71,951	103,505	58,345 (−18.91)
Gastrointestinal										
Typhoid	153	41	6	17	62	27 (89.81)	5	22	102	41 (90.625)
Shigellosis	36	49	6	22	40	12 (−46.86)	3	21	126	15 (−28.06)
Hepatitis A	2,248	27,297	1,477	6,193	22,857	4,820 (−22.17)	1,466	9,407	60,328	9,769 (3.85)
EHEC	120	157	94	176	275	364 (106.61)	86	184	388	244 (33.06)
Subtotal	2,557	27,544	1,583	6,408	23,234	5,223 (−18.49)	1,560	9,633	60,945	10,070 (4.53)
Total	74,295	100,788	50,717	67,582	103,120	64,087 (−5.17)	55,201	81,584	164,450	68,415 (−16.14)

*EHEC, enterohemorrhagic *Escherichia coli*; IPD, invasive pneumococcal disease; USD, US dollars.
†Difference from average estimates for 2020.
‡Difference from average estimates for 2021.

observed slight variations among the phases, the mean weekly incidence levels for 2020–2021 after implementation of social distancing measures were as follows: typhoid, 0.03; shigellosis, 0.02; hepatitis A, 1.91; and EHEC, 0.12. Annual medical expenses associated with gastrointestinal infectious diseases decreased by 18.49% in 2020, compared with the value calculated by using the average estimated incidence; the value increased by 4.53% in 2021 (Table 3). The trend in medical expenses associated with gastrointestinal infectious diseases varied depending on the specific condition; different trends were observed for each disease.

ARIMA models (Appendix 1 Tables 7, 20–27, Figures 13–20) Showed that the observed incidence levels of gastrointestinal diseases were generally close to the average predicted values (Figure 3). However, unexpected outbreaks of typhoid and EHEC occurred, resulting in higher observed incidence levels than predicted (Figure 3, panels A, B, G, H).

Incidence of Zoonotic Diseases in Animals

Comparisons of the periods before and after implementation of NPIs revealed contrasting patterns for bovine TB and bovine brucellosis (Table 2). The mean weekly incidence (cases/100,000 cattle) for 2016–2019 varied between the diseases: bovine TB, 2.19; and bovine brucellosis, 0.49. Although slight variations were observed among the phases, the mean weekly incidence levels for 2020–2021 after implementation of social distancing measures were as follows: bovine TB, 1.29; bovine brucellosis, 0.61.

ARIMA models (Appendix 1 Tables 7, 28–31, Figures 21–24) showed that incidence levels of bovine TB were noticeably lower than expected from the end of 2020 (Figure 4, panels A, B). In contrast, the incidence of bovine brucellosis rapidly increased and reached a record high in June 2021 (Figure 4, panels C, D).

Discussion

We used national surveillance data on notifiable infectious diseases in South Korea from 2016–2021 to examine how NPI implementation to control the COVID-19 pandemic affected patterns of various other diseases. We used data from 2016–2019 to develop a reliable time series model and then predicted the incidence of communicable diseases for 2020–2021 under the assumption that NPIs had not been implemented. By comparing the model-predicted values with observed values, we found that the incidence of respiratory infectious diseases decreased considerably after the implementation of NPIs. However, the incidence of human gastrointestinal infectious diseases and livestock diseases remained comparable or even increased after NPIs were implemented. The overall medical expenses associated with infectious diseases other than COVID-19 decreased by 5.17% in 2020 and 16.14% in 2021 compared with the predicted values (Table 3). Our findings offer valuable insights for implementing appropriate control measures during future epidemics.

The reductions in and the continuously low incidence levels of respiratory infectious diseases in South Korea during the COVID-19 pandemic can be attributed principally to the extensive adoption of NPIs. Regardless of whether the infectious agent was a bacterium (pertussis, scarlet fever, IPD, and TB) or

a virus (varicella and mumps), respiratory infectious diseases transmitted via droplets, fomites, or direct contact generally exhibited lower incidence levels after implementation of NPIs; most of those trends persisted until the end of 2021. The sharp decline in the respiratory infectious disease incidence after implementation of NPIs was consistent with the findings of previous studies on the occurrence trends of respiratory infectious diseases in South Korea (*5*,*15*–*17*,*37*,*38*) and the findings of studies that focused on respiratory infectious disease patterns in other countries, such as China and the United States (*9*,*39*–*41*).

After NPI implementation, the number of mumps cases remained lower than predicted. However, beginning in October 2021, the number of cases increased above the expected value. That change can be attributed to the nationwide relaxation of school attendance criteria in the fall semester of 2021, which led to more outbreaks in schools. Mumps is commonly observed among adolescents 13–18 years of age and frequently spreads in settings where persons engage in group activities (e.g., schools) (*42*). Therefore, precautions are needed to prevent a mumps resurgence after cessation of NPIs.

TB exhibited a slightly different pattern from those of other respiratory infectious diseases. In the early stages of NPI implementation, the number of cases noticeably decreased. However, beginning in

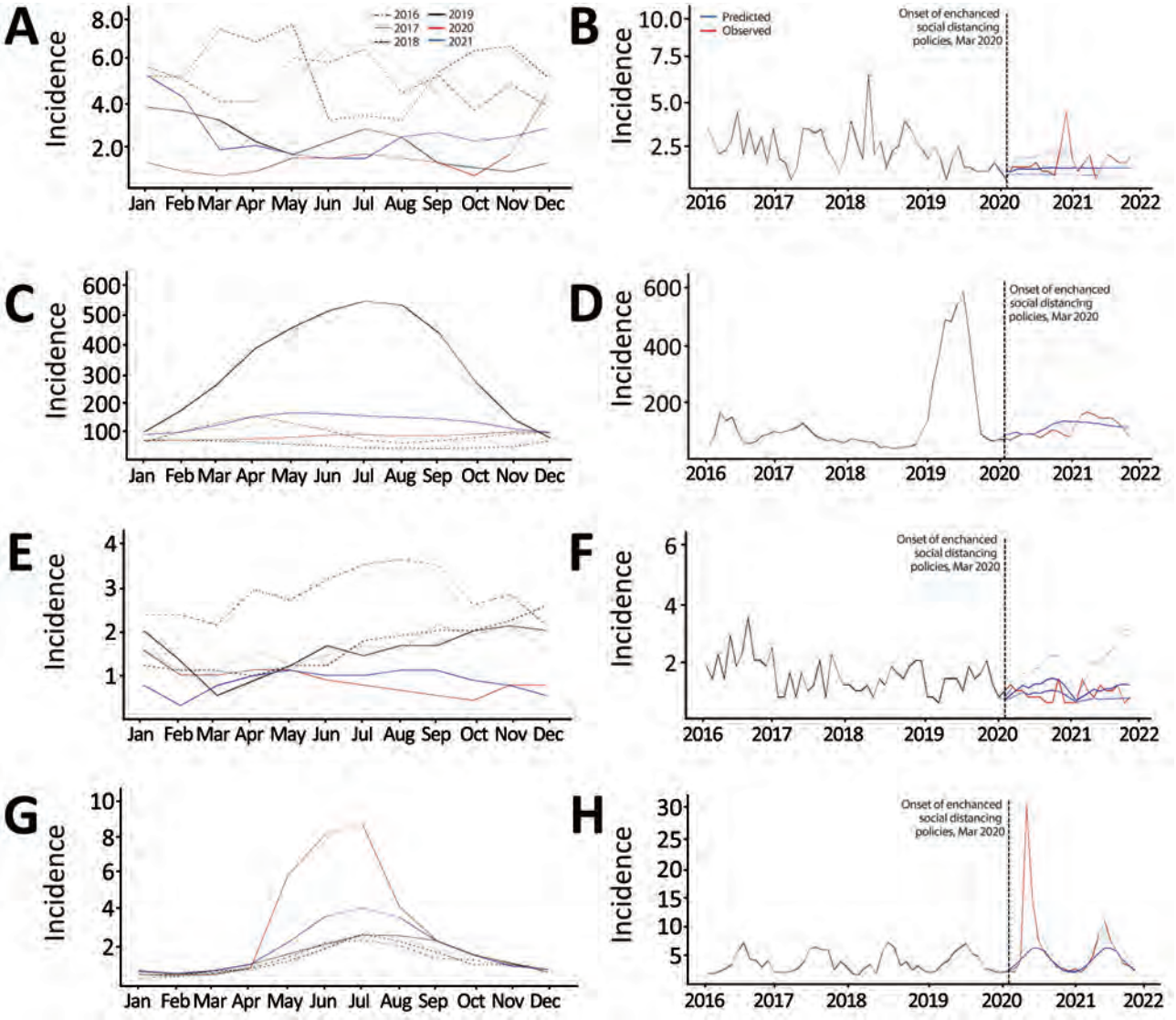

Figure 3. Incidence trends (cases/1 million population) in 4 nationally notifiable gastrointestinal infectious diseases in humans before and during the COVID-19 pandemic, South Korea. A, C, E, G) Monthly incidence levels retrieved from the national surveillance system for 2016–2019 versus 2020–2021; B, D, F, H) observed and predicted monthly incidence levels during 2016–2021. A, B) typhoid; C, D) hepatitis A; E, F) shigellosis; and G, H) *Escherichia coli*.

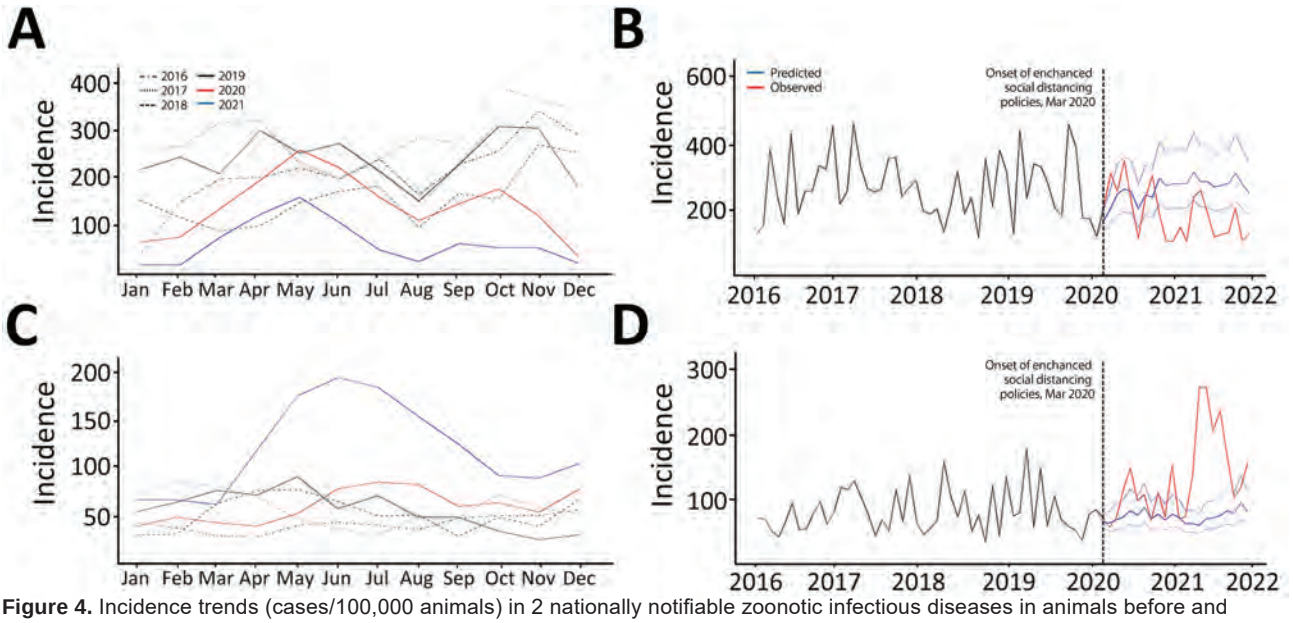

Figure 4. Incidence trends (cases/100,000 animals) in 2 nationally notifiable zoonotic infectious diseases in animals before and during the COVID-19 pandemic, South Korea. A, C) Monthly incidence levels retrieved from the national surveillance system for 2016–2019 versus 2020–2021; B, D) observed and predicted monthly incidence levels during 2016–2021. A, B) Bovine tuberculosis; C, D) bovine brucellosis.

the second half of 2020, we saw little or no difference between the observed and the predicted values. Reductions in TB notifications in early 2020, because of complex factors affecting disease diagnosis, have been reported in several countries, including South Korea (*19*,*43*). However, the effects of NPIs known to prevent acute infections were limited in suppressing TB cases in South Korea in the medium- to long-term because a many cases are presumed to arise when latent infections progress to active TB disease (*19*,*44*). Thus, even if NPIs are implemented, the existing strategies focusing on prophylactic treatment to prevent new infections and treating latent infections to prevent active TB onset still need to be incorporated.

The incidence of gastrointestinal diseases did not decrease after implementation of NPIs. Studies using data from countries such as China (*9*) and the United States (*45*) revealed notable decreases in most gastrointestinal infectious diseases after NPI implementation. Although the dissimilar contexts hinder direct comparisons, differences in the extent of NPIs and accessibility to medical services might explain the discrepancies. In the early stages of the COVID-19 pandemic, China and the United States put in place strict social distancing measures and emphasized stay-at-home orders. In contrast, South Korea used less strict policies that focused on personal hygiene measures. Therefore, the effectiveness of NPIs in terms of controlling infectious diseases might have varied among countries, and the decrease in healthcare facility utilization may have been smaller in South Korea (*18*,*19*,*45*). In addition, the gastrointestinal diseases included in this study were primarily foodborne diseases that commence after consumption of contaminated food or water (*20*). Therefore, the occurrence of the foodborne diseases included might not have been greatly affected by personal hygiene enhancement or social distancing measures.

This study revealed inconsistent temporal trends between the 2 target zoonotic diseases in industrial animals: bovine TB and brucellosis. The increased incidence of brucellosis was consistent with the prior predictions. Social distancing is likely to compromise appropriate veterinary care and restrict the logistical activities necessary for good livestock management (*11*). Moreover, in South Korea, the number of cattle farms increased during social distancing, possibly because of the increased profit to be made from beef (*46*). The sudden increases in disease incidence could indicate an increased number of inexperienced cattle owners, which would influence management quality. Because the primary route of brucellosis transmission is associated with the mass movement of infected cattle (*47*), inexperienced owners might need to require better brucellosis screening skills. However, accurate indicators of livestock movement during the COVID-19 period could not be collected. In contrast, the decreased incidence of bovine TB differed from our expectations. One possible explanation is that

bovine TB surveillance increased in South Korea; the number of cattle screened for bovine tuberculosis infection has risen since 2017, as has the relevant budget (Appendix 1 Table 32) (*48*). Because early detection via effective surveillance plays a key role in controlling chronic diseases with long latent periods, the decreased incidence might be explained by effective surveillance efforts.

The first limitation of this study is that the incidence levels of infectious diseases are influenced by various factors, including population immunity, seasonal changes, climatic features, and human mobility patterns. Thus, drawing causal inferences regarding the effects of social distancing measures and changes on disease patterns is challenging. We can only interpret and analyze potential influencing factors. Second, the observed decreases in the incidence of certain infectious diseases might not solely reflect the effects of NPIs on incidence rates. The decreases also could be influenced by other pandemic-related factors, including healthcare utilization. Thus, we examined annual hospital visits and health insurance claims to adjust for any changes in healthcare utilization. However, biases might have persisted in terms of altered healthcare-seeking behaviors and surveillance capacities. Moreover, given the strict infection control regulations, healthcare utilization by symptomatic patients was particularly restricted. Therefore, the data on healthcare utilization among all patients considered in this study might not fully reflect the reduction in healthcare use by those with symptoms. Third, although ARIMA is a well-established and practical technology for infectious disease forecasting (*22*,*41*), the method has limitations in distinguishing various factors that affect transmission, such as genetic strain and latent infections. Furthermore, ARIMA might not be the most appropriate method for long-term predictions. However, the infectious diseases targeted in this study generally exhibit stable trends, with clear seasonal variabilities, and the fitted models indeed exhibited relatively good fits with the training data and reasonably good predictive performances, as confirmed by out-of-sample validation. In addition, the time-series forecasting models were used in previous studies to predict influenza virus activity for 2020–2022 (*49*), or to estimate excess mortality during the COVID-19 period, 2020–2021 (*50*). Therefore, we believe that the reliability of long-term predictions of the incidence of the chosen diseases remains robust. Thus, we used the ARIMA approach (a descriptive method) to present our results. Finally, this study did not consider demographic information, such as age and sex.

In conclusion, the implementation of NPIs considerably reduced the incidence of infectious diseases transmitted via respiratory routes or direct person-to-person contact in South Korea, a trend that continued until late 2021. Although identifying a single factor that explains changes in the incidence of all infectious diseases is difficult, the concurrent implementation of NPIs at various levels (individual, community, environmental, and national), along with behavioral changes, likely played a key role in reducing community transmission and alleviating the associated healthcare burden. Therefore, comprehensive NPI strategies are critical public health considerations for controlling infectious diseases and preparing for future pandemics.

The R code used in this study is publicly available (https://github.com/TaeHChang/For-the-Paper-4). The complete dataset is available upon request from the authors.

Acknowledgments

This research was supported by the Bio & Medical Technology Development Program of the National Research Foundation, funded by the Korean government (grant no. 2021M3E5E3081366). However, the funders played no role in the design and conduct of the study; data collection, management, analysis, or interpretation; preparation, review, or approval of the paper; or the decision to submit the article for publication.

About the Author

Mr. Chang is a PhD candidate in the Graduate School of Public Health, Seoul National University. His research interests focus on the association between environmental factors and the dynamics of infectious diseases.

References

1. Wang H, Paulson KR, Pease SA, Watson S, Comfort H, Zheng P, et al.; COVID-19 Excess Mortality Collaborators. Estimating excess mortality due to the COVID-19 pandemic: a systematic analysis of COVID-19-related mortality, 2020–21. Lancet. 2022;399:1513–36. https://doi.org/10.1016/S0140-6736(21)02796-3
2. Bielecki M, Züst R, Siegrist D, Meyerhofer D, Crameri GAG, Stanga Z, et al. Social distancing alters the clinical course of COVID-19 in young adults: a comparative cohort study. Clin Infect Dis. 2021;72:598–603. https://doi.org/10.1093/cid/ciaa889
3. Giles ML, Wallace EM, Alpren C, Brady N, Crouch S, Romanes F, et al. Suppression of severe acute respiratory syndrome coronavirus 2 (SARS-CoV-2) after a second wave in Victoria, Australia. Clin Infect Dis. 2021;73:e808–10. https://doi.org/10.1093/cid/ciaa1882
4. Tsai AC, Harling G, Reynolds Z, Gilbert RF, Siedner MJ. Coronavirus disease 2019 (COVID-19) transmission in the United States before versus after relaxation of statewide social distancing measures. Clin Infect Dis. 2021;73(Suppl 2):S120–6. https://doi.org/10.1093/cid/ciaa1502

5. Ahn JG. Epidemiological changes in infectious diseases during the coronavirus disease 2019 pandemic in Korea: a systematic review. Clin Exp Pediatr. 2022;65:167–71. https://doi.org/10.3345/cep.2021.01515
6. Min KD, Kang H, Lee JY, Jeon S, Cho SI. Estimating the effectiveness of non-pharmaceutical interventions on COVID-19 control in Korea. J Korean Med Sci. 2020;35:e321. https://doi.org/10.3346/jkms.2020.35.e321
7. Choi JH. Effects of nonpharmaceutical interventions for coronavirus disease 2019. Clin Exp Pediatr. 2022;65:250–1. https://doi.org/10.3345/cep.2021.01830
8. Chow EJ, Uyeki TM, Chu HY. The effects of the COVID-19 pandemic on community respiratory virus activity. Nat Rev Microbiol. 2023;21:195–210.
9. Geng MJ, Zhang HY, Yu LJ, Lv CL, Wang T, Che TL, et al. Changes in notifiable infectious disease incidence in China during the COVID-19 pandemic. Nat Commun. 2021;12:6923. https://doi.org/10.1038/s41467-021-27292-7
10. Ahn SY, Park JY, Lim IS, Chae SA, Yun SW, Lee NM, et al. Changes in the occurrence of gastrointestinal infections after COVID-19 in Korea. J Korean Med Sci. 2021;36:e180. https://doi.org/10.3346/jkms.2021.36.e180
11. Rahman MT, Islam MS, Shehata AA, Basiouni S, Hafez HM, Azhar EI, et al. Influence of COVID-19 on the sustainability of livestock performance and welfare on a global scale. Trop Anim Health Prod. 2022;54:309. https://doi.org/10.1007/s11250-022-03256-x
12. Hashem NM, González-Bulnes A, Rodriguez-Morales AJ. Animal welfare and livestock supply chain sustainability under the COVID-19 outbreak: an overview. Front Vet Sci. 2020;7:582528. https://doi.org/10.3389/fvets.2020.582528
13. Raihan A, Himu HA. Global impact of COVID-19 on the sustainability of livestock production. Global Sustainability Research. 2023;2:1–11. https://doi.org/10.56556/gssr.v2i2.447
14. Huh K, Kim YE, Ji W, Kim DW, Lee EJ, Kim JH, et al. Decrease in hospital admissions for respiratory diseases during the COVID-19 pandemic: a nationwide claims study. Thorax. 2021;76:939–41. https://doi.org/10.1136/thoraxjnl-2020-216526
15. Kim JH, Roh YH, Ahn JG, Kim MY, Huh K, Jung J, et al. Respiratory syncytial virus and influenza epidemics disappearance in Korea during the 2020–2021 season of COVID-19. Int J Infect Dis. 2021;110:29–35. https://doi.org/10.1016/j.ijid.2021.07.005
16. Lee H, Lee H, Song K-H, Kim ES, Park JS, Jung J, et al. Impact of public health interventions on seasonal influenza activity during the COVID-19 outbreak in Korea. Clin Infect Dis. 2021;73:e132–40. https://doi.org/10.1093/cid/ciaa672
17. Park S, Michelow IC, Choe YJ. Shifting patterns of respiratory virus activity following social distancing measures for coronavirus disease 2019 in South Korea. J Infect Dis. 2021;224:1900–6. https://doi.org/10.1093/infdis/jiab231
18. Yun HE, Ryu BY, Choe YJ. Impact of social distancing on incidence of vaccine-preventable diseases, South Korea. J Med Virol. 2021;93:1814–6. https://doi.org/10.1002/jmv.26614
19. Kwak N, Hwang S-S, Yim J-J. Effect of COVID-19 on tuberculosis notification, South Korea. Emerg Infect Dis. 2020;26:2506–8. https://doi.org/10.3201/eid2610.202782
20. Park S, Michelow IC, Choe YJ. Trend of gastrointestinal infections following nonpharmaceutical interventions, South Korea, 2020. J Infect Dis. 2021;224:368–71. https://doi.org/10.1093/infdis/jiab244
21. Scallan E, Mahon BE, Hoekstra RM, Griffin PM. Estimates of illnesses, hospitalizations and deaths caused by major bacterial enteric pathogens in young children in the United States. Pediatr Infect Dis J. 2013;32:217–21. https://doi.org/10.1097/INF.0b013e31827ca763
22. Benvenuto D, Giovanetti M, Vassallo L, Angeletti S, Ciccozzi M. Application of the ARIMA model on the COVID-2019 epidemic dataset. Data Brief. 2020;29:105340. https://doi.org/10.1016/j.dib.2020.105340
23. Cori A, Ferguson NM, Fraser C, Cauchemez S. A new framework and software to estimate time-varying reproduction numbers during epidemics. Am J Epidemiol. 2013;178:1505–12. https://doi.org/10.1093/aje/kwt133
24. National Health Insurance Service. Status of medical treatment by region 2006–2021 [in Korean] [cited 2023 Jan 11]. https://kosis.kr/statHtml/statHtml.do?orgId=350&tblId=TX_35003_A004&vw_cd=MT_ZTITLE&list_id=350_35003_1&scrId=&seqNo=&lang_mode=ko&obj_var_id=&itm_id=&conn_path=MT_ZTITLE&path=%252FstatisticsList%252FstatisticsListIndex.do
25. Health Insurance Review and Assessment Service. Total medical expenses status [in Korean] [cited 2023 Jan 11]. http://opendata.hira.or.kr/op/opc/olapHthInsRvStatInfo.do
26. Korea Statistics. Total population of South Korea [in Korean] [cited 2023 Jan 13]. https://kosis.kr/visual/populationKorea/PopulationDashBoardDetail.do
27. Health Insurance Review and Assessment Service. Infectious disease treatment expenses statistics [in Korean] [cited 2023 Jan 14]. https://www.data.go.kr/data/15085952/fileData.do
28. Song JY, Peck KR; Korean Society of Infectious Diseases. A debate on public health responses to COVID-19: focused protection versus sustained suppression. J Korean Med Sci. 2020;35:e433–0. https://doi.org/10.3346/jkms.2020.35.e433
29. Central Disaster and Safety Countermeasure Headquarters/Central Disaster and Safety Countermeasure Headquarters of the Republic of Korea. Rules and guidelines for distancing in daily life to control coronavirus disease 2019 in Korea: 3rd version, announced on July 3, 2020. J Educ Eval Health Prof. 2020:17:20.
30. Korea Disease Control and Prevention Agency. Infectious disease portal. 2023 [in Korean] [cited 2023 Jan 21]. https://www.mohw.go.kr/react/al/sal0301vw.jsp
31. Animal and Plant Quarantine Agency. Korea Animal Health integrated system [in Korean] [cited 2023 Jan 21]. https://home.kahis.go.kr/home/lkntscrinfo/selectLkntsOccrrncList.do
32. Ministry of Agriculture, Food and Rural Affairs. Regional livestock farming status [in Korean] [cited 2023 Jan 26]. https://uni.agrix.go.kr/docs7/biOlap/fixType.do
33. Campbell F, Strang C, Ferguson N, Cori A, Jombart T. When are pathogen genome sequences informative of transmission events? PLoS Pathog. 2018;14:e1006885. https://doi.org/10.1371/journal.ppat.1006885
34. Lau EHY, Nishiura H, Cowling BJ, Ip DKM, Wu JT. Scarlet fever outbreak, Hong Kong, 2011. Emerg Infect Dis. 2012;18:1700–2. https://doi.org/10.3201/eid1810.120062
35. Vink MA, Bootsma MCJ, Wallinga J. Serial intervals of respiratory infectious diseases: a systematic review and analysis. Am J Epidemiol. 2014;180:865–75. https://doi.org/10.1093/aje/kwu209
36. Dritsakis N, Klazoglou P. Forecasting unemployment rates in USA using Box-Jenkins methodology. Int J Econ Financial Issues. 2018;8:9–20.
37. Shi HJ, Kim NY, Eom SA, Kim-Jeon MD, Oh SS, Moon BS, et al. Effects of non-pharmacological interventions on respiratory viruses other than SARS-CoV-2: analysis of laboratory surveillance and literature review from 2018 to 2021. J Korean Med Sci. 2022;37:e172. https://doi.org/10.3346/jkms.2022.37.e172

38. Yum S, Hong K, Sohn S, Kim J, Chun BC. Trends in viral respiratory infections during COVID-19 pandemic, South Korea. Emerg Infect Dis. 2021;27:1685–8. https://doi.org/10.3201/eid2706.210135
39 Li ZJ, Yu LJ, Zhang HY, Shan CX, Lu QB, Zhang XA, et al.; Chinese Centers for Disease Control and Prevention (CDC) Etiology Surveillance Study Team of Acute Respiratory Infections. Broad impacts of coronavirus disease 2019 (COVID-19) pandemic on acute respiratory infections in China: an observational study. Clin Infect Dis. 2022;75:e1054–62. https://doi.org/10.1093/cid/ciab942
40. Fricke LM, Glöckner S, Dreier M, Lange B. Impact of non-pharmaceutical interventions targeted at COVID-19 pandemic on influenza burden—a systematic review. J Infect. 2021;82:1–35. https://doi.org/10.1016/j.jinf.2020.11.039
41 Feng L, Zhang T, Wang Q, Xie Y, Peng Z, Zheng J, et al. Impact of COVID-19 outbreaks and interventions on influenza in China and the United States. Nat Commun. 2021;12:3249. https://doi.org/10.1038/s41467-021-23440-1
42. Park SH. Resurgence of mumps in Korea. Infect Chemother. 2015;47:1–11. https://doi.org/10.3947/ic.2015.47.1.1
43. Cilloni L, Fu H, Vesga JF, Dowdy D, Pretorius C, Ahmedov S, et al. The potential impact of the COVID-19 pandemic on the tuberculosis epidemic a modelling analysis. EClinicalMedicine. 2020;28:100603. https://doi.org/10.1016/j.eclinm.2020.100603
44. Jeong D, Kang HY, Kim J, Lee H, Yoo BN, Kim HS, et al. Cohort rpofile: Korean tuberculosis and post-tuberculosis cohort constructed by linking the Korean National Tuberculosis Surveillance System and National Health Information Database. J Prev Med Public Health. 2022;55:253–62. https://doi.org/10.3961/jpmph.21.635
45. Kim S, Kim J, Choi BY, Park B. Trends in gastrointestinal infections before and during non-pharmaceutical interventions in Korea in comparison with the United States. Epidemiol Health. 2022;44:e2022011. https://doi.org/10.4178/epih.e2022011
46. Lee HW, Ji SW, Lee Y, Kim HJ, Song WJ. Recent reasons for the decline in Hanwoo (Korean native cattle) prices and outlook [in Korean]. Naju; Republic of Korea: Korea Rural Economic Institute; 2022.
47. Yoon H, Moon O-K, Lee S-H, Lee W-C, Her M, Jeong W, et al. Epidemiology of brucellosis among cattle in Korea from 2001 to 2011. J Vet Sci. 2014;15:537–43. https://doi.org/10.4142/jvs.2014.15.4.537
48. Ministry of Agriculture, Food and Rural Affairs. Guidelines for livestock epidemic prevention and control, 2022 [in Korean] [cited 2023 Jan 21]. https://www.mafra.go.kr/bbs/mafra/71/419654/artclView.do
49. Kim HK, Min KD, Cho SI. Analysis of the effectiveness of non-pharmaceutical interventions on influenza during the Coronavirus disease 2019 pandemic by time-series forecasting. BMC Infect Dis. 2023;23:717. https://doi.org/10.1186/s12879-023-08640-y
50. Wang H, Paulson KR, Pease SA, Watson S, Comfort H, Zheng P, et al.; COVID-19 Excess Mortality Collaborators. Estimating excess mortality due to the COVID-19 pandemic: a systematic analysis of COVID-19-related mortality, 2020-21. Lancet. 2022;399:1513–36. https://doi.org/10.1016/S0140-6736(21)02796-3

Address for correspondence: Kyung-Duk Min, Chungbuk National University, Chungdae-ro, Seowon-gu, Cheongju-si 311, South Korea; email: kdmin@chungbuk.ac.kr

Follow-Up Study of Effectiveness of 23-Valent Pneumococcal Polysaccharide Vaccine Against All-Type and Serotype-Specific Invasive Pneumococcal Disease, Denmark

Katrine Finderup Nielsen,[1] Lise Birk Nielsen,[1] Tine Dalby, Frederikke Kristensen Lomholt, Hans-Christian Slotved, Kurt Fuursted, Zitta Barrella Harboe, Charlotte Sværke Jørgensen, Palle Valentiner-Branth

As a follow-up to a previous study, we investigated vaccine effectiveness (VE) of 23-valent pneumococcal polysaccharide vaccine (PPSV23) against invasive pneumococcal disease (IPD) among 1,254,498 persons ≥65 years of age as part of a vaccination program in Denmark during April 2020–January 2023. We assessed VE by using a Cox regression model and adjusted for age, sex, and underlying conditions. Using nationwide data, we estimated a VE of PPSV23 against all-type IPD of 32% and against PPSV23-serotype IPD of 41%. Because this follow-up study had more statistical power than the original study, we also estimated VE against IPD caused by PPSV23-serotypes excluding serotype 3; serotype 3; serotype 8; serotype 22F; PPSV23 non-PCV15 serotypes; PPSV23 non-PCV20 serotypes; and IPD over time. Our findings suggest PPSV23 vaccination can protect persons ≥65 years of age against IPD caused by all serotypes or serotype groupings, except serotype 3.

Invasive *Streptococcus pneumoniae* infections can cause deadly diseases such as meningitis and bacteremia. In Denmark, children ≤2 years of age have been routinely vaccinated against pneumococcal disease with pneumococcal conjugate vaccine (PCV): a 7-valent PCV (PCV7) since October 2007 and a 13-valent PCV (PCV13) since 2010 (*1*,*2*). For adults, pneumococcal vaccination has only been recommended for those at increased risk for pneumococcal disease; whereas childhood vaccinations were free, adults had to pay. After PCV vaccines were added to the childhood vaccination program, the rate of invasive pneumococcal disease (IPD) declined drastically in children ≤2 years of age, and a simultaneus but less pronounced decline was detected in those ≥65 years of age due to herd immunity (*1*). The serotype distribution also changed in the oldest age group; whereas non-PCV13 serotypes accounted for 30% of IPD cases before the introduction of PCV in the childhood vaccination program, they accounted for 59% during 2011–2013 (*1*).

During the COVID-19 pandemic, there was a focus on preventing hospitalizations in those ≥65 years of age, who are at increased risk for both IPD (*3*,*4*) and severe COVID-19 (*5*,*6*). Therefore, the government of Denmark initiated a vaccination program to prevent IPD, using the 23-valent pneumococcal polysaccharide vaccine (PPSV23), aimed at persons ≥65 years of age (*7*). The program started on April 22, 2020, and was first aimed at persons ≥65 years of age who had an increased risk for IPD (e.g., those with chronic lung or heart disease). On June 15, 2020, the program was expanded to include all persons ≥65 years of age and ran until January 15, 2023. During the first year of the program, 61% of Denmark residents ≥65 years of age were vaccinated with PPSV23 (*8*). The most common IPD-causing serotypes in persons ≥65 years of age in Denmark during the study period were 3 (19%),

Author affiliations: Statens Serum Institut, Copenhagen, Denmark (K. Finderup Nielsen, L.B. Nielsen, T. Dalby, F.K. Lomholt, H.-C. Slotved, K. Fuursted, Z.B. Harboe, C.S. Jørgensen, P. Valentiner-Branth); Copenhagen University Hospital, North Zealand, Copenhagen (Z.B. Harboe); University of Copenhagen, Copenhagen (Z.B. Harboe)

DOI: https://doi.org/10.3201/eid3006.230975

[1]These authors contributed equally to this article.

8 (12%) and 22F (7%). All 3 serotypes are included in PPSV23. PPSV23 has previously been shown to have an effect against IPD caused by the included serotypes in persons ≥60 years of age, although the effectiveness levels covered a wide range, from 24% (95% CI 10%–36%) to 72% (95% CI 46%–85%) (*9*–*15*).

We previously estimated the vaccine effectiveness (VE) of PPV23 for part of the vaccination program (June 15, 2020–September 18, 2021) (*9*). In this new study, we aimed to evaluate the real-life effectiveness of PPSV23 against IPD in persons ≥65 years of age in Denmark after a widely accepted vaccination program that ran during the period April 22, 2020–March 15, 2023. The longer study period and the inclusion of persons who turned 65 years of age during the study period enabled us to estimate VE for specific serotypes and for serotypes included in different types of pneumococcal vaccines, thereby adding new knowledge to the previous study. The primary outcomes were VE against all-type IPD and PPSV23-vaccine type IPD. Exploratory outcomes were VE against PPSV23-vaccine type IPD excluding serotype 3, VE against the most common IPD-causing serotypes in Denmark during the study period (3, 8, and 22F), and VE against serotypes present in PPSV23 but not in the now available 15-valent pneumococcal conjugate vaccine (PCV15) (i.e., serotypes 8, 10A, 11A, 12F, 15B, 2, 9N, 17F, and 20) or in the 20-valent pneumococcal conjugate vaccine (PVC20) (i.e., serotypes 2, 9N, 17F, and 20). In addition, we estimated VE over time, where statistical power allowed. The aim of this study was to explore the unique context of widespread PPSV23 vaccination directed at an entire population ≥65 years of age in a high-income country. We sought to gain insights into the effectiveness of PPSV23 vaccination 2 years after its introduction. The investigation includes extensive nationwide data within a high vaccination coverage setting, incorporating serotype-specific analyses.

We used administrative register data for the study. According to Danish law, ethics approval is exempt for such research, and the Danish Data Protection Agency thus waives ethical approval for our study of administrative register data, when no individual contact of participants is necessary and only aggregate results are included as findings. The study is therefore fully compliant with all legal and ethical requirements.

Methods

All residents of Denmark are assigned a unique personal identification number known as a CPR number. The CPR number enables person-level linkage among a variety of nationwide registries (*16*). This study used 4 registries: The Danish Civil Registration System (CPR register), The Danish Vaccination Register (DVR), the Danish Microbiology Database (MiBa), and the Danish National Patient Registry (DNPR).

We retrieved information on age, sex, and migration from the CPR register. Using Anatomic Therapeutic Chemical (ATC) classification codes (Appendix Table 1, https://wwwnc.cdc.gov/EID/article/30/6/23-0975-App1.pdf), we retrieved information on vaccine type and date of administration from the DVR, in which all administered vaccines have been recorded by law since 2015 (*17*). We obtained information on comorbidities within 5 years of study entry and exit from the DNPR, which holds information on all hospital admissions (except to psychiatric wards) with diagnoses coded according to the International Classification of Diseases, 10th Revision (ICD-10; Appendix Table 4) (*16*). We only considered the primary diagnosis. Selected comorbidities were based on the Charlson Comorbidity score (*18*,*19*) but counted as individual comorbidities and not given a score. We retrieved microbiological data from MiBa, which holds information on all microbiological test results in Denmark (*20*). In this study, an IPD case was defined as a positive diagnostic test for *S. pneumoniae* from cerebrospinal fluid, blood, or other normally sterile sites (e.g., pleura). All registries are updated regularly and contain near–real-time information.

The study period started on April 22, 2020, and ended on March 15, 2023. We chose the end date to allow time for potential cases of IPD to develop in persons vaccinated at the end of the program, and extracted data on IPD on March 29, 2023, to allow for a delay in registration. We collected data on previously administered vaccines for all persons in the cohort: influenza vaccine within 2 years before study entry, and PCV7 or PCV13 at any time before study entry. The data covering the period from June 15, 2020–September 18, 2021, was also presented in the previous study (*1*).

We included all residents in Denmark who were ≥65 years of age or turned 65 years of age during the study period. We excluded persons who had evidence of previous laboratory-confirmed IPD because they are at increased risk for another IPD episode (*21*,*22*). We also excluded persons who received a PPSV23 vaccine within 6 years before study entry so that we could assess VE for persons vaccinated within the vaccination program. Previous studies have shown a waning effect of PPSV23 VE over time (*23*–*26*), resulting in a recommendation of re-vaccination every

6th year in Denmark (*27*). We followed all persons in the study until the date of IPD diagnosis, emigration, death, or the end of the study period.

Because the immune response to vaccination is delayed by 2–3 weeks (*28*,*29*), persons were censored from the unvaccinated group at date of vaccination and entered the vaccinated group 14 days after vaccination; that is, they were censored from the study during the 14 days in between. Hence, persons accrued person-time in each group when appropriate. For the analyses regarding specific serotypes or groups of specific serotypes, persons were censored with an event at date of IPD if the disease was caused by the serotype(s) of interest, otherwise they were considered to be without an event.

We conducted 2 sensitivity analyses. The first analysis assessed whether there was any effect of censoring 0–14 days after vaccination. In the main analyses, participants were censored from day 0–14 after vaccination, and in the first sensitivity analysis, they were included as unvaccinated until 14 days after vaccination. The second analysis assessed whether there was any effect of including persons previously vaccinated with PCV. In the main analyses, participants were included regardless of previous vaccination with PCV. In the second sensitivity analysis, participants who had received PCV at any time before the study were excluded, and those who received PCV during the study period were censored at date of vaccination.

We calculated VE estimates by using a Cox regression model to estimate hazard ratios (HRs) with calendar time as the underlying timescale. We adjusted the estimates for age (restricted cubic spline), sex (male/female), and comorbidities (restricted cubic spline). We estimated VE using the formula 1 – HR × 100% with 95% CIs. We estimated waning VE by considering time intervals since vaccination: 14 days to 1 year, 1–2 years, and 2–3 years. Hence, some persons might contribute to risk time in all periods moving from group to group as time passes. We made all analyses by using R version 4.2.2 (The R Foundation for Statistical Computing, https://www.r-project.org).

Results

During the study period, approximately 6,221,398 persons resided in Denmark; approximately 1,358,914 were ≥65 years of age or turned 65 years of age during the study period. We excluded 100,448 persons vaccinated with PPSV23 within 6 years before study entry, and 3,952 persons who had prior IPD. Because of censoring 14 days after vaccination, 16 persons vaccinated on April 22, 2020, who died within 14 days of vaccination, did not contribute person-time in the study. The final study cohort consisted of 1,254,498 persons (Figure), corresponding to 3,196,988 person-years of follow-up.

We stratified the characteristics of included persons at entry date and at the end of follow-up by vaccination status (Table 1). The median age at entry was 72 years (interquartile range [IQR] 67–78 years), 74 years (IQR 68–81 years) for those unvaccinated at exit, and 75 years (IQR 70–81 years) for those vaccinated with PPSV23 at exit. Most (77%) of the persons in the study subjects were vaccinated with PPSV23 during the study period. Persons in the PPSV23 vaccinated group were more likely than those in the PPSV23 unvaccinated group to have been vaccinated against influenza within 2 years before study entry (55% vs. 21%) and during the study period (97% vs. 34%).

A total of 513 persons (200 in the unvaccinated group and 313 in the vaccinated group) had IPD caused by any serotype during the study period (Table 2). For PPSV23-serotype IPD, 134 events occurred in the unvaccinated group and 186 in the vaccinated group, whereas when serotype 3 was excluded, 105 events occurred in the unvaccinated group and 102 in the vaccinated group. For specific serotypes analyzed in the unvaccinated versus vaccinated groups, there were 29 versus 84 serotype 3 events, 32 versus 27 serotype 8 events, and 25 versus 9 serotype 22F events.

The estimated VE against all-type IPD was 32% (95% CI 18%–44%), and VE against PPSV23-serotype IPD was 41% (95% CI 25%–53%) (Table 2). When estimating VE for PPSV23-serotype IPD but not considering serotype 3 as an event, we found a higher VE of 58% (95% CI 43%–68%). VE against serotype 3 was −17% (95% CI −83% to 25%). We found the highest VE estimates for serotype 8 (62% [95% CI 36%–77%]) and serotype 22F (88% [95% CI 75%–95%]). VE for PPSV23 non-PCV15 serotype IPD (8, 10A, 11A, 12F, 15B, 2, 9N, 17F, and 20) was 50% (95% CI 28%–65%). VE for PPSV23 non-PCV20 serotype IPD (2, 9N, 17F, and 20) was 61% (95% CI 10%–83%), largely powered by IPD caused by serotype 9N (21/32 events; data not shown). We were unable to assess VE against the PCV15/PCV20 non-PPSV23 serotype 6A because only 3 cases of IPD were caused by this serotype.

The sensitivity analysis excluding persons who received PCV before study entry and censoring those who received PCV during the study period showed only minor changes in the point estimates compared with the estimates calculated when those persons were included. Most estimates increased slightly except against all-type IPD or IPD caused by serotype

22F (Appendix Table 2). The sensitivity analysis including persons as unvaccinated day 0–14 after vaccination showed no difference in the VE estimates compared with the estimates calculated when persons in that time period were excluded (Appendix Table 3).

When estimating VE over time (Table 3), we found that VE remained stable but declined slightly 2 years after vaccination. For all-type IPD, the VE was reduced from 39% to 27%. VE against PPSV23-serotype IPD declined from 52% to 43% and from 65% to 57% when excluding serotype 3. Protection against serotype 8 was high the first year after vaccination (86% [95% CI 54%–96%]), but estimates after 1–2 years were not significant (46% [95% CI −35% to 80%]). VE against serotype 22F remained very high, at 92% to 86%, but few events occurred (*34*).

Discussion

Using nationwide data, this cohort study shows that PPSV23 vaccination in persons ≥65 years old is associated with protection against all-type IPD, IPD caused by PPSV23 vaccine serotypes, and IPD caused by serotypes 8 and 22F, specifically, but not IPD caused by serotype 3. Studies from Spain, Israel, Taiwan, England, and Wales, as well as our previous study from Denmark, have shown PPSV23 VE against all-type IPD ranging from 42% (95% CI 19%–59%) to 70% (95% CI 48%–82%) (*1*,*10*,*30*–*32*) and against PPSV23-serotype IPD ranging from 24% (95% CI 10%–36%) to 72% (95% CI 46%–85%) in persons ≥60 years of age (*1*,*10*–*15*). In this study, we found a lower estimate against all-type IPD (VE 32%), which could be the result of the higher age of our study population because the effect of PPSV23 lessens with age (*33*). The difference could also be because of differences in serotype distribution or comorbidities in the study populations, but unfortunately, not all studies have provided this level of detail or include the same comorbidities. Our estimate against PPSV23-serotype IPD (VE 41%) falls within the range of the VE found in previous studies. Compared with our previous study on PPSV23 in Denmark (*1*), this follow-up study finds a lower VE against all-type IPD (42% vs. 32%) and PPSV23-vaccine type IPD (58% vs. 41%). This study covers the entire vaccination program and includes persons offered PPSV23 at the beginning of the program; that is, more vulnerable groups where the vaccine might not have the same effect. In this study, persons who received a vaccination were censored for 14 days after vaccination. In contrast, they were included in the unvaccinated group in the previous study. In this study, we performed a sensitivity analysis investigating the effect of censoring persons 0–14 days after vaccination, which did not affect the VE estimates (Appendix Table 3).

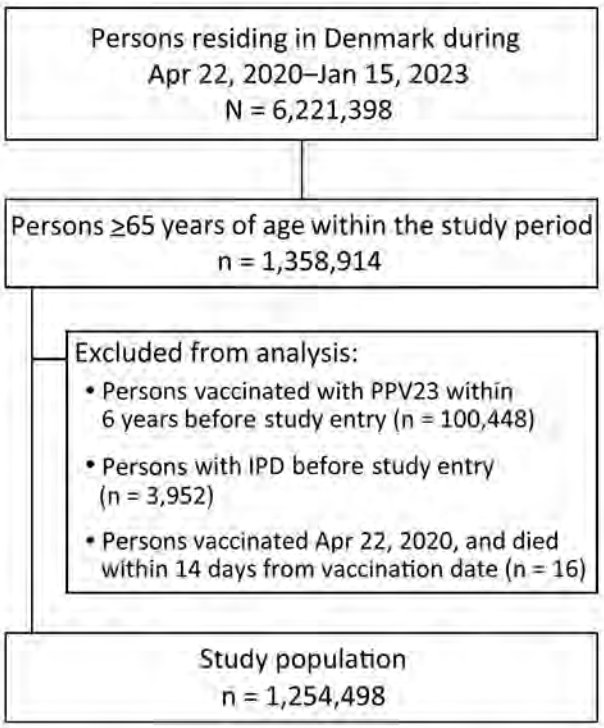

Figure. Flowchart of cohort development for follow-up study of effectiveness of 23-valent pneumococcal polysaccharide vaccine against invasive pneumococcal disease, Denmark.

Previous research has shown that the VE against IPD caused by serotype 3 is low to nonexistent, whereas the VE against IPD caused by serotype 8 or 22F varies from low to moderate (*11*,*13*,*34*–*36*). Our study also showed no effect against IPD caused by serotype 3; therefore, we estimated VE against PPSV23-vaccine type IPD excluding serotype 3. As expected, and seen before for overall VE against IPD (*34*), this estimate yields an increased VE of 58%, compared with 41%, and indicates that a VE including all PPSV23 vaccine serotypes might underestimate the effectiveness of the vaccine against the other 22 serotypes because of the poor effect against serotype 3. Because serotype 3 continues to cause the most IPD cases of any serotype in those ≥65 years of age in Denmark, comparing studies including all PPSV23 vaccine serotypes shows the effectiveness of the vaccine on all the IPD cases that could potentially be prevented by PPSV23. However, that the effectiveness against serotype 3 clearly is very low. Estimating VE against PPSV23-serotype IPD excluding serotype 3 provides a better idea of how the vaccine works against the rest of the serotypes grouped together and of how many cases we can actually hope to prevent by using this vaccine.

Table 1. Patient characteristics according to vaccination status in follow-up study of effectiveness of PPSV23 vaccine against invasive pneumococcal disease, Denmark*

Characteristic	Study population at entry	Study population at exit	
		Unvaccinated	Vaccinated with PPSV23 during the study period
Total	1,254,498 (100)	288,383	966,115
Sex			
F	668,726 (53)	157,590 (55)	511,136 (53)
M	585,772 (47)	130,793 (45)	454,979 (47)
Age, y			
Median (IQR)	72 (67–78)	74 (68–81)	75 (70–81)
<75	760,980 (61)	150,620 (52)	436,070 (45)
75–84	373,294 (30)	91,009 (32)	391,251 (41)
≥85	120,224 (9)	46,754 (16)	138,794 (14)
Vaccination status			
Received PCV7 or PCV13 before study entry	19,035 (2)	2,494 (1)	16,541 (2)
Received PCV7 or PCV13 during follow-up	NA	1,500 (1)	15,558 (2)
Received influenza vaccine within 2 y before study entry	645,980 (52)	59,105 (21)	530,467 (55)
Received of influenza vaccine during follow-up	NA	97,400 (34)	937,489 (97)
No. underlying conditions†			
0	1,017,954 (81)	204,788 (71)	652,863 (68)
1	198,611 (16)	60,364 (21)	231,957 (24)
2	32,047 (3)	17,334 (6)	61,742 (6)
≥3	5,886 (0)	5,897 (2)	19,553 (2)
Individual underlying conditions†			
Myocardial infarction	18,684 (1)	4,433 (2)	16,507 (2)
Congestive heart failure	15,256 (1)	7,624 (3)	26,295 (3)
Peripheral vascular disease	23,780 (2)	8,761 (3)	35,072 (4)
Cerebrovascular disease	50,748 (4)	16,028 (6)	55,803 (6)
Dementia	16,044 (1)	7,354 (3)	25,564 (3)
Chronic pulmonary disease	24,074 (2)	7,948 (3)	36,996 (4)
Connective tissue disease	10,765 (1)	4,955 (2)	23,406 (2)
Ulcer disease	8,893 (1)	2,693 (1)	8,755 (1)
Mild liver disease	3,512 (0)	2,277 (1)	6,328 (1)
Diabetes mellitus	15,130 (1)	3,699 (1)	14,362 (1)
Hemiplegia	621 (0)	347 (0)	1,407 (0)
Moderate/severe renal disease	11,104 (1)	6,404 (2)	20,725 (2)
Diabetes with chronic complications	7,301 (1)	4,806 (2)	16,603 (2)
Any tumor	67,451 (5)	29,878 (10)	109,912 (11)
Leukemia	715 (0)	1,087 (0)	4,157 (0)
Lymphoma	1,471 (0)	1,969 (1)	7,998 (1)
Moderate/severe liver disease	1,120 (0)	823 (0)	1,681 (0)
Metastatic solid tumor	4,785 (0)	3,271 (1)	7,573 (1)
AIDS	37 (0)	159 (0)	539 (0)

*Values are no. (%) except as indicated. Persons vaccinated with PPSV23 during follow-up contributed to the analysis for both unvaccinated and vaccinated. IQR, interquartile range; NA, not applicable; PCV7, 7-valent pneumococcal conjugate vaccine; PCV13, 13-valent pneumococcal conjugate vaccine; PPSV23, 23-valent polysaccharide pneumococcal vaccine.
†Within 5 y before study entry (1st column) or within 5 y from end of follow-up (2nd and 3rd columns).

In Denmark, serotype replacement is taking place, similar to what has been seen in other countries, and policy makers have to consider the indirect effect of pediatric vaccination against pneumococcal disease on the adult population (*37*). The incidence of IPD caused by serotype 8 increased after the introduction of PCVs into the childhood vaccination program (*38*,*39*); those vaccines do not include serotype 8 (*40*), leaving room for that serotype to advance. In Denmark, such an increase occurred in age groups ≥15 years, and especially for persons ≥65 years of age (*38*). Our study shows that PPSV23 is effective against serotypes 8 and 22F and that a vaccination program might be an important factor in protecting persons ≥65 years of age against IPD caused by those serotypes. On the other hand, PCV13 vaccination in children in Denmark has not reduced the incidence of serotype 3 (*41*) in the population, and in our study, we still see serotype 3 causing most IPD cases among older adults. Unfortunately, vaccination with PPSV23 is unlikely to reduce this burden because of the lack of effect on IPD caused by serotype 3. Other conjugated vaccines, such as PCV15 and PCV20, offer a broader serotype coverage than PCV13. Both contain 1 serotype that is not included in PPSV23 (serotype 6A) (*42*), whereas PPSV23 contains 9 serotypes not included in PCV15 and 4 serotypes not included in PCV20 (*28*). Of 513 cases of IPD included in this study, 138 cases were caused by the PPSV23 non-PCV15 serotypes, 32 by the PPSV23 non-PCV20 serotypes, and 3

Table 2. Effectiveness of PPSV23 vaccine against IPD compared with no vaccination in follow-up study, Denmark, April 22, 2020–March 15, 2023*

IPD type	Vaccination status	No. events	Person-years	VE, % (95% CI)	
				Unadjusted	Adjusted†
All	Unvaccinated	200	1,277,147	Referent	
	Vaccinated	313	1,919,841	26 (11–39)	32 (18–44)
PPSV23 serotype	Unvaccinated	134	1,277,147	Referent	
	Vaccinated	186	1,919,841	36 (19–49)	41 (25–53)
PPSV23 serotype excluding serotype 3	Unvaccinated	105	1,277,147	Referent	
	Vaccinated	102	1,919,841	54 (38–65)	58 (43–68)
Serotype 3	Unvaccinated	29	1,277,147	Referent	
	Vaccinated	84	1,919,841	−25 (−95 to 20)	−17 (−83 to 25)
Serotype 8	Unvaccinated	32	1,277,147	Referent	
	Vaccinated	27	1,919,841	56 (27–74)	62 (36–77)
Serotype 22F	Unvaccinated	25	1,277,147	Referent	
	Vaccinated	9	1,919,841	86 (70–94)	88 (75–95)
PPSV23 non-PCV15 serotype‡	Unvaccinated	67	1,277,147	Referent	
	Vaccinated	71	1,919,841	45 (21–61)	50 (28–65)
PPSV23 non-PCV20 serotype§	Unvaccinated	18	1,277,147	Referent	
	Vaccinated	14	1,919,841	57 (2–81)	61 (10–83)

*IPD, invasive pneumococcal disease; PCV15, 15-valent pneumococcal conjugate vaccine; PCV20, 20-valent pneumococcal conjugate vaccine; PPSV23, 23-valent polysaccharide pneumococcal vaccine; VE, vaccine effectiveness.
†Adjusted for age and comorbidities as a restricted cubic spline and sex as a categorical variable.
‡Serotypes 8, 10A, 11A, 12F, 15B, 2, 9N, 17F, and 20.
§Serotypes 2, 9N, 17F, and 20.

by the PCV15/PCV20 non-PPSV23 serotype 6A. Our findings indicate that persons ≥65 of age still suffer from IPD caused by PPSV23 non-PCV15/PCV20 serotypes, and that PPSV23 offers protection, having a VE of 50% for PPSV23 non-PCV15 serotypes and 61% for PPSV23 non-PCV20 serotypes.

The first limitation of this study is that, for some analyses, few events occurred, which decreases the statistical power and results in wide 95% CIs when estimating VE. That finding was especially true for the PPSV23 non-PCV20 estimate. In this study, we also did not have enough follow-up time to evaluate a waning effect beyond 3 years. However, we can conclude that only minor waning was seen during the study period. To detect the long-term durability of protection, a follow-up study should be conducted.

Table 3. Hazard ratios and effectiveness of PPSV23 vaccine against IPD in follow-up study, comparing time since vaccination with PPSV23 with no vaccination, Denmark, April 22, 2020–March 15, 2023*

IPD type	Vaccination status	No. events	Person-years	VE, % (95% CI)	
				Unadjusted	Adjusted†
All	Unvaccinated	200	1,277,147	Referent	
	0–1 y after vaccination	74	838,041	38 (18–53)	39 (19–53)
	1–2 y after vaccination	131	728,480	24 (3–40)	30 (10–45)
	2–3 y after vaccination	108	353,319	14 (−15 to 36)	27 (2–46)
PPSV23 serotype	Unvaccinated	134	1,277,147	Referent	
	0–1 y after vaccination	38	838,041	51 (29–66)	52 (30–67)
	1–2 y after vaccination	85	728,480	25 (−2 to 44)	30 (5–48)
	2–3 y after vaccination	63	353,319	34 (5–54)	43 (19–61)
PPSV23 serotype excluding serotype 3	Unvaccinated	105	1,277,147	Referent	
	0–1 y after vaccination	23	838,041	64 (43–78)	65 (44–78)
	1–2 y after vaccination	44	728,480	47 (22–64)	52 (29–67)
	2–3 y after vaccination	35	353,319	49 (20–68)	57 (32–73)
Serotype 3	Unvaccinated	29	1,277,147	Referent	
	0–1 y after vaccination	15	838,041	−2 (−95 to 46)	−2 (−94 to 47)
	1–2 y after vaccination	41	728,480	−47 (−148 to 13)	−39 (−135 to 18)
	2–3 y after vaccination	28	353,319	−14 (−110 to 38)	−1 (−87 to 46)
Serotype 8	Unvaccinated	32	1,277,147	Referent	
	0–1 y after vaccination	3	838,041	86 (52–96)	86 (54–96)
	1–2 y after vaccination	15	728,480	37 (−24 to 68)	46 (−8 to 73)
	2–3 y after vaccination	9	353,319	34 (−71 to 74)	48 (−35 to 80)
Serotype 22F	Unvaccinated	25	1,277,147	Referent	
	0–1 y after vaccination	1	838,041	92 (40–99)	92 (39–99)
	1–2 y after vaccination	3	728,480	88 (59–96)	89 (64–97)
	2–3 y after vaccination	5	353,319	82 (47–94)	86 (60–95)

*IPD, invasive pneumococcal disease; PCV15, 15-valent pneumococcal conjugate vaccine; PCV20, 20-valent pneumococcal conjugate vaccine; PPSV23, 23-valent polysaccharide pneumococcal vaccine; VE, vaccine effectiveness.
†Adjusted for age and comorbidities as a restricted cubic spline and sex as a categorical variable.

Healthy vaccinee bias cannot be ruled out. In this study, 21% of unvaccinated persons received influenza vaccination before the study, compared with 55% among the vaccinated persons (Table 1). That finding indicates that persons who accept 1 vaccination are more likely to accept another and that those vaccinated in general are more adherent to the recommendations from public health authorities. However, the vaccinated persons are approximately the same age and have the same distribution of comorbidities as the unvaccinated persons, which speaks against a healthy vaccinee bias. The similar distribution of comorbidities between the groups speaks against the opposite bias, confounding by indication, where those who are more at risk might be more likely to get vaccinated. To account for both those biases, we adjusted our results for comorbidities. Another limitation to this study is that the difference in influenza vaccination coverage between the groups of PPSV23 vaccinated (97%) and nonvaccinated (34%) persons increased during the study period because influenza vaccination might also reduce the risk for IPD (*43*), which could lead to an overestimation of the PPSV23 VE.

This study is strengthened by the comprehensiveness of the Denmark registries, enabling inclusion of all residents ≥65 years of age. Similar to our previous study on PPSV23 VE in Denmark (*1*), the study period spans a time in which nonpharmacologic restrictions were in place due to COVID-19. However, our study covers a longer period after those restrictions were lifted, when Denmark experienced a return to more normal levels of IPD cases. Thus, we believe that the VE found in this study reflects the VE in a setting without extraordinary restrictions.

In conclusion, this study shows that persons ≥65 years of age who are vaccinated with PPSV23 are protected against all-type IPD, PPSV23-serotype IPD, IPD caused by serotypes 8 and 22F, and IPD caused by PPSV23 non-PCV15/PCV20 serotypes, but not against IPD caused by serotype 3. In addition, the protection persists; VE only wanes marginally and insignificantly over almost 3 years. These findings support a vaccination program with PPSV23 against IPD to protect those ≥65 years of age.

The data included in this research are part of the Danish national vaccination surveillance system at Statens Serum Institut. The data are available for research upon reasonable request and with permission from the Danish Data Protection Agency and Danish Health and Medicines Authority.

H.C.S. reports involvement with MSD seminars and is part of a Pfizer supported pneumococcal carriage project. Z.B.H. received a grant from Independent Research Fund (grant no. 0134-00257B), Lundbeck Foundation (grant no. R349-2020-835), Helen Rudes Foundation, and the Danish Cancer Society (grant no. KBVU-MS R327-A19137).

K.F.N., L.B.N., F.K.L., and P.V.B. designed the study. K.F.N. and L.B.N. drafted the article; K.F.N. finalized it. L.B.N. led the statistical and data analyses, with contributions from K.F.N. All authors commented, revised, and approved the final manuscript. K.F.N. attests that all listed authors meet authorship criteria and that no others meeting the criteria have been omitted.

About the Author

Ms. Finderup Nielsen is an epidemiologist at Statens Serum Institut, Copenhagen, with a background in biomedical science and vaccine research. Her research interests focus on vaccine surveillance and effectiveness for *Streptococcus pneumoniae*, human papillomavirus, and COVID-19.

References

1. Harboe ZB, Dalby T, Weinberger DM, Benfield T, Mølbak K, Slotved HC, et al. Impact of 13-valent pneumococcal conjugate vaccination in invasive pneumococcal disease incidence and mortality. Clin Infect Dis. 2014;59:1066–73. https://doi.org/10.1093/cid/ciu524
2. Statens Serum Institut. PCV coverage and invasive pneumococcal disease 2011. EPI-NEWS No. 21—2012 [cited 20 Nov 2023]. https://en.ssi.dk/news/epi-news/2012/no-21---2012
3. Centers for Disease Control and Prevention. Pneumococcal disease: risk factors and how it spreads. 2022 Jul 28 [cited 2023 Apr 26]. https://www.cdc.gov/pneumococcal/about/risk-transmission.html
4. Statens Serum Institut. Pneumococcal disease—risk groups [in Norwegian] [cited 2022 Mar 11]. https://www.ssi.dk/vaccinationer/risikogrupper/invasiv-pneumokoksygdom/pneumokok-risikogrupper
5. Centers for Disease Control and Prevention. COVID-19 risks and information for older adults. 2023 Feb 22 [cited 2023 Apr 26]. https://www.cdc.gov/aging/covid19/index.html
6. Holler JG, Eriksson R, Jensen TØ, van Wijhe M, Fischer TK, Søgaard OS, et al. First wave of COVID-19 hospital admissions in Denmark: a nationwide population-based cohort study. BMC Infect Dis. 2021;21:39. https://doi.org/10.1186/s12879-020-05717-w
7. Indenrigs- og Sundhedsministeriet. Bekendtgørelse om gratis vaccination mod influenza, pneumokokker og COVID-19 til visse persongrupper. 2022 Sep 9 [cited 2024 Feb 17]. https://www.retsinformation.dk/eli/lta/2022/1260
8. Statens Serum Institut. Extension of the invasive pneumococcal disease vaccination programme. Tuberculosis in 2019–20. 2022 Feb 4 [cited 2024 Apr 29]. https://en.ssi.dk/news/epi-news/2021/no-49-50---2021
9. Nielsen KF, Nielsen LB, Lomholt FK, Nørgaard SK, Slotved H-C, Dalby T, et al. Effectiveness of the 23-valent

pneumococcal polysaccharide vaccine against invasive pneumococcal disease among 948,263 individuals ≥65 years of age: a Danish cohort study. Eur J Clin Microbiol Infect Dis. 2022;41:1473–7.
10. Dominguez A, Salleras L, Fedson DS, Izquierdo C, Ruiz L, Ciruela P, et al. Effectiveness of pneumococcal vaccination for elderly people in Catalonia, Spain: a case-control study. Clin Infect Dis. 2005;40:1250–7. https://doi.org/10.1086/429236
11. Andrews NJ, Waight PA, George RC, Slack MPE, Miller E. Impact and effectiveness of 23-valent pneumococcal polysaccharide vaccine against invasive pneumococcal disease in the elderly in England and Wales. Vaccine. 2012; 30:6802–8. https://doi.org/10.1016/j.vaccine.2012.09.019
12. Djennad A, Ramsay ME, Pebody R, Fry NK, Sheppard C, Ladhani SN, et al. Effectiveness of 23-valent polysaccharide pneumococcal vaccine and changes in invasive pneumococcal disease incidence from 2000 to 2017 in those aged 65 and over in England and Wales. EClinicalMedicine. 2019;6:42–50.
13. Gutierrez Rodriguez MA, Ordobas Gavin MA, Garcia-Comas L, Sanz Moreno JC, Cordoba Deorador E, Lasheras Carbajo MD, et al. Effectiveness of 23-valent pneumococcal polysaccharide vaccine in adults aged 60 years and over in the Region of Madrid, Spain, 2008–2011. Euro Surveill. 2014;19:20922. https://doi.org/10.2807/1560-7917.ES2014.19.40.20922
14. Wright LB, Hughes GJ, Chapman KE, Gorton R, Wilson D. Effectiveness of the 23-valent pneumococcal polysaccharide vaccine against invasive pneumococcal disease in people aged 65 years and over in the North East of England, April 2006–July 2012. Trials Vaccinol. 2013;2:45–8. https://doi.org/10.1016/j.trivac.2013.09.004
15. Su W-J, Chuang P-H, Chang L-Y, Lo H-Y, Chiang C-S, Wang E-T, et al. Application of the screening and indirect cohort methods to evaluate the effectiveness of pneumococcal vaccination program in adults 75 years and older in Taiwan. BMC Infect Dis. 2021;21:45. https://doi.org/10.1186/s12879-020-05721-0
16. Schmidt M, Schmidt SAJ, Adelborg K, Sundbøll J, Laugesen K, Ehrenstein V, et al. The Danish health care system and epidemiological research: from health care contacts to database records. Clin Epidemiol. 2019;11:563–91. https://doi.org/10.2147/CLEP.S179083
17. Grove Krause T, Jakobsen S, Haarh M, Mølbak K. The Danish vaccination register. Euro Surveill. 2012;17:20155. https://doi.org/10.2807/ese.17.17.20155-en
18. Charlson ME, Pompei P, Ales KL, MacKenzie CR. A new method of classifying prognostic comorbidity in longitudinal studies: development and validation. J Chronic Dis. 1987;40:373–83. https://doi.org/10.1016/0021-9681(87)90171-8
19. Thygesen SK, Christiansen CF, Christensen S, Lash TL, Sørensen HT. The predictive value of ICD-10 diagnostic coding used to assess Charlson comorbidity index conditions in the population-based Danish National Registry of Patients. BMC Med Res Methodol. 2011;11:83. https://doi.org/10.1186/1471-2288-11-83
20. Voldstedlund M, Haarh M, Mølbak K; MiBa Board of Representatives. The Danish Microbiology Database (MiBa) 2010 to 2013. Euro Surveill. 2014;19:20667. https://doi.org/10.2807/1560-7917.ES2014.19.1.20667
21. Norwegian Institute of Public Health. Recommendations for the use of pneumococcal vaccine outside the child vaccination program in Norway [in Norwegian] [cited 2022 Oct 3]. https://www.fhi.no/publ/2015/anbefalinger-for-bruk-av-pneumokokk
22. King MD, Whitney CG, Parekh F, Farley MM; Active Bacterial Core Surveillance Team/Emerging Infections Program Network. Recurrent invasive pneumococcal disease: a population-based assessment. Clin Infect Dis. 2003;37:1029–36. https://doi.org/10.1086/377736
23. Shapiro ED, Berg AT, Austrian R, Schroeder D, Parcells V, Margolis A, et al. The protective efficacy of polyvalent pneumococcal polysaccharide vaccine. N Engl J Med. 1991;325:1453–60. https://doi.org/10.1056/NEJM199111213252101
24. MacIntyre CR, Ridda I, Trent MJ, McIntyre P. Persistence of immunity to conjugate and polysaccharide pneumococcal vaccines in frail, hospitalised older adults in long-term follow up. Vaccine. 2019;37:5016–24. https://doi.org/10.1016/j.vaccine.2019.07.005
25. Lawrence H, Pick H, Baskaran V, Daniel P, Rodrigo C, Ashton D, et al. Effectiveness of the 23-valent pneumococcal polysaccharide vaccine against vaccine serotype pneumococcal pneumonia in adults: a case-control test-negative design study. PLoS Med. 2020;17:e1003326. https://doi.org/10.1371/journal.pmed.1003326
26. Falkenhorst G, Remschmidt C, Harder T, Hummers-Pradier E, Wichmann O, Bogdan C. Effectiveness of the 23-valent pneumococcal polysaccharide vaccine (PPV23) against pneumococcal disease in the elderly: systematic review and meta-analysis. PLoS One. 2017;12:e0169368. https://doi.org/10.1371/journal.pone.0169368
27. Statens Serum Institut. Pneumococci [cited 2022 Sep 28]. https://en.ssi.dk/vaccination/vaccination-of-risk-groups/pneumococci
28. Danish Medicines Agency. Pneumovax. Summary of product characteristics [cited 2023 Jul 4]. http://produktresume.dk/AppBuilder/search?utf8=%E2%9C%93&id=&type=&q=pneumovax&button=S%C3%B8g
29. Centers for Disease Control and Prevention. About pneumococcal vaccine: for poviders. 2022 Sep 8 [cited 2022 Oct 6]. https://www.cdc.gov/vaccines/vpd/pneumo/hcp/about-vaccine.html
30. Vila-Corcoles A, Ochoa-Gondar O, Guzmán JA, Rodriguez-Blanco T, Salsench E, Fuentes CM; EPIVAC Study Group. Effectiveness of the 23-valent polysaccharide pneumococcal vaccine against invasive pneumococcal disease in people 60 years or older. BMC Infect Dis. 2010;10:73. https://doi.org/10.1186/1471-2334-10-73
31. Jackson LA, Neuzil KM, Yu O, Benson P, Barlow WE, Adams AL, et al.; Vaccine Safety Datalink. Effectiveness of pneumococcal polysaccharide vaccine in older adults. N Engl J Med. 2003;348:1747–55. https://doi.org/10.1056/NEJMoa022678
32. Leventer-Roberts M, Feldman BS, Brufman I, Cohen-Stavi CJ, Hoshen M, Balicer RD. Effectiveness of 23-valent pneumococcal polysaccharide vaccine against invasive disease and hospital-treated pneumonia among people aged ≥65 years: a retrospective case-control study. Clin Infect Dis. 2015;60:1472–80. https://doi.org/10.1093/cid/civ096
33. Sikjær MG, Pedersen AA, Wik MS, Stensholt SS, Hilberg O, Løkke A. Vaccine effectiveness of the pneumococcal polysaccharide and conjugated vaccines in elderly and high-risk populations in preventing invasive pneumococcal disease: a systematic search and meta-analysis. Eur Clin Respir J. 2023;10:2168354. https://doi.org/10.1080/20018525.2023.2168354
34. Perniciaro S, van der Linden M. Pneumococcal vaccine uptake and vaccine effectiveness in older adults with invasive pneumococcal disease in Germany: a retrospective cohort study. Lancet Reg Health Eur. 2021;7:100126.

35. Shimbashi R, Suzuki M, Chang B, Watanabe H, Tanabe Y, Kuronuma K, et al.; Adult IPD Study Group. Effectiveness of 23-valent pneumococcal polysaccharide vaccine against invasive pneumococcal disease in adults, Japan, 2013–2017. Emerg Infect Dis. 2020;26:2378–86. https://doi.org/10.3201/eid2610.191531
36. Suzuki M, Dhoubhadel BG, Ishifuji T, Yasunami M, Yaegashi M, Asoh N, et al.; Adult Pneumonia Study Group-Japan (APSG-J). Serotype-specific effectiveness of 23-valent pneumococcal polysaccharide vaccine against pneumococcal pneumonia in adults aged 65 years or older: a multicentre, prospective, test-negative design study. Lancet Infect Dis. 2017;17:313–21. https://doi.org/10.1016/S1473-3099(17)30049-X
37. Statens Serum Institut. EPI-NEWS No. 14/16—2020. [cited 2023 Jul 18]. https://en.ssi.dk/news/epi-news/2020/no-14---2020
38. Hansen CB, Fuursted K, Valentiner-Branth P, Dalby T, Jørgensen CS, Slotved H-C. Molecular characterization and epidemiology of *Streptococcus pneumoniae* serotype 8 in Denmark. BMC Infect Dis. 2021;21:421. https://doi.org/10.1186/s12879-021-06103-w
39. Amin-Chowdhury Z, Collins S, Sheppard C, Litt D, Fry NK, Andrews N, et al. Characteristics of invasive pneumococcal disease caused by emerging serotypes after the introduction of the 13-valent pneumococcal conjugate vaccine in England: a prospective observational cohort study, 2014–2018. Clin Infect Dis. 2020;71:e235–43. https://doi.org/10.1093/cid/ciaa043
40. European Medicines Agency. Prevenar 13. 2018 Sep 17 [cited 2023 Jun 16]. https://www.ema.europa.eu/en/medicines/human/EPAR/prevenar-13
41. Slotved H-C, Dalby T, Harboe ZB, Valentiner-Branth P, Casadevante VF, Espenhain L, et al. The incidence of invasive pneumococcal serotype 3 disease in the Danish population is not reduced by PCV-13 vaccination. Heliyon. 2016;2:e00198. https://doi.org/10.1016/j.heliyon.2016.e00198
42. European Medicines Agency. Vaxneuvance. 2021 Oct 12 [cited 2023 Jul 5]. https://www.ema.europa.eu/en/medicines/human/EPAR/vaxneuvance
43. Christenson B, Hedlund J, Lundbergh P, Örtqvist A. Additive preventive effect of influenza and pneumococcal vaccines in elderly persons. Eur Respir J. 2004;23:363–8. https://doi.org/10.1183/09031936.04.00063504

Address for correspondence: Katrine Finderup Nielsen, Statens Serum Institut, Artillerivej 5, 2300 Copenhagen S, Denmark; email: kafn@ssi.dk

Incubation Period and Serial Interval of Mpox in 2022 Global Outbreak Compared with Historical Estimates

Luis Ponce, Natalie M. Linton, Wu Han Toh, Hao-Yuan Cheng, Robin N. Thompson, Andrei R. Akhmetzhanov, Jonathan Dushoff

Understanding changes in the transmission dynamics of mpox requires comparing recent estimates of key epidemiologic parameters with historical data. We derived historical estimates for the incubation period and serial interval for mpox and contrasted them with pooled estimates from the 2022 outbreak. Our findings show the pooled mean infection-to-onset incubation period was 8.1 days for the 2022 outbreak and 8.2 days historically, indicating the incubation periods remained relatively consistent over time, despite a shift in the major mode of transmission. However, we estimated the onset-to-onset serial interval at 8.7 days using 2022 data, compared with 14.2 days using historical data. Although the reason for this shortening of the serial interval is unclear, it may be because of increased public health interventions or a shift in the mode of transmission. Recognizing such temporal shifts is essential for informed response strategies, and public health measures remain crucial for controlling mpox and similar future outbreaks.

Mpox, caused by monkeypox virus (MPXV), is a viral illness characterized by rash, influenza-like symptoms, and fever. A global outbreak of mpox attracted increased public attention in 2022 and became recognized as a public health event of international concern (PHEIC). Historical estimates of the case-fatality ratio (CFR) associated with mpox infection vary by clade; clade I exhibits a CFR of ≈10%, whereas clade II the CFR is ≤1% (*1*). Although mpox historically experienced limited transmission (*2*,*3*), the 2022 outbreak, originating in nonendemic countries in Europe and North America, resulted in ≈90,000 cases by mid-April 2023 and demonstrated enhanced transmissibility (*4*). The outbreak was driven primarily by sexually associated transmission, which altered the clinical manifestations and epidemiology of the infections when compared with historical reports (*5*). Clade II was dominant; its case-fatality ratio was ≈0.1% (*6*). Although certain epidemiologic parameters, such as the incubation period and serial interval, have been estimated using case records from 2022 (*7*–*13*), comprehensive analysis of historical estimates and assessment of their relationship to the recent outbreak is limited (*14*).

After MPXV was identified in imported monkeys in Denmark in 1958, reported mpox infections were frequently associated with contact with monkeys (*15*–*17*). However, subsequent findings revealed that primates are not the only reservoir hosts (*18*). Before the eradication of smallpox in 1980, mpox was rarely observed in humans, in part because mpox is unlikely to have been widespread but also because of cross-immunity between the 2 viruses. The mpox outbreaks in the 1970s–1990s were relatively small in scale, typically involving ≤5 cases, and predominantly affected children because most adults possessed some level of immunity from smallpox infection or vaccination (*18*). However, as herd immunity waned, outbreaks in the 2000s caused dozens of cases (*19*,*20*); mpox became endemic in some regions of Africa, and Nigeria reporting the largest outbreaks (*21*,*22*).

Author affiliations: National Taiwan University, Taipei, Taiwan (L. Ponce, A.R. Akhmetzhanov); California Department of Public Health, Richmond, California, USA (N.M. Linton); Johns Hopkins University, Baltimore, Maryland, USA (W.H. Toh); Taiwan Centers for Disease Control, Taipei (H. Cheng); University of Oxford, Oxford, UK (R.N. Thompson); McMaster University, Hamilton, Ontario, Canada (J. Dushoff)

DOI: http://doi.org/10.3201/eid3006.231095

The first major outbreak reported beyond the borders of Africa occurred in the United States in 2003; there were 81 confirmed cases linked to imported wild animals (*23*). The global outbreak in 2022 caught many by surprise as mpox spread rapidly in countries across Western Europe and North America in which it was not endemic, before expanding worldwide. The World Health Organization (WHO) declared the 2022 mpox outbreak a PHEIC on July 23, 2022 (*24*). By early 2023, case numbers had begun to decline, likely because there were fewer highly connected susceptible persons within sexual networks (*25*). In addition to the depletion of susceptible persons, general behavioral changes in high-risk populations resulting from increased awareness of risk and vaccination of at-risk persons played an important role in the decline in mpox cases (*26*). Modeling of infections caused by sexual interactions among men who have sex with men (MSM) has shown that having fewer 1-time partnerships can significantly reduce mpox transmission (*27*). Furthermore, members of higher-risk populations proactively altered their behaviors in response to the outbreak; many were vaccinated. In August 2022, a survey of MSM in the United States revealed that ≈50% had reduced their use of dating apps, number of sexual partners, and number of 1-time partnerships (*28*).

The clinical manifestation of mpox has historically been similar to that of smallpox or chickenpox, characterized by fever, rash, and lymphadenopathy (*1*). Its distinctive rash initiates as macules and progresses through papules, vesicles, pustules, and crusts before resolving. Lymphadenopathy, reported in 85% of mpox cases (*29*), distinguishes mpox from smallpox and chickenpox. Some mpox patients also exhibit respiratory symptoms such as sore throat, nasal congestion, or cough.

Since 2022, some changes in the clinical manifestations of mpox have been observed (*5*), including a tendency for skin lesions to localize to specific body regions associated with sexual transmission, such as the genital, anorectal, or oral areas. Rectal symptoms such as purulent or bloody stools, rectal pain, or bleeding were frequently reported (*30*). Some patients exhibited only a few cutaneous formations near affected areas, whereas others experienced disseminated body rashes complicating their infection. Although the localized rash may appear almost concurrently with other initial symptoms, the disseminated rash usually appeared several days after symptom onset.

Some estimates of the incubation period and serial interval for the global mpox outbreak in 2022 have been affected by right-truncation bias. This bias arises when only persons who have experienced the event (e.g., symptom onset or rash appearance) and were confirmed by testing at the time of data collection are included in the sample. By accounting for right truncation, we can estimate the length of the incubation period and serial interval more accurately and include cases with symptoms who have not yet been reported. Ignoring right truncation leads to underestimation of such epidemiologic parameters, because cases with longer incubation periods or serial intervals are overlooked in the analysis. Earlier studies reported short mean incubation period estimates of 9.0 days (*7*) and 7.6 days (95% credible interval [CrI] 6.5–9.9 days) (*10*), extended to 9.5 days (95% CrI 7.4–12.3 days) when accounting for right truncation (*10*).

Estimation of the incubation period of mpox presents several difficulties. One challenge arises from the absence of definitive information on times of exposure. The exposure time window for much recorded data was often >1 day, complicating estimation. Excluding records with longer windows may yield biased estimates, as we saw in lower estimates from the exclusion-based approach (*31*) compared with other studies (*32*,*33*). Furthermore, some studies calculated the incubation period from the last known time of contact (*5*) instead of considering the entire exposure period, which also led to underestimation of the true incubation period.

Estimating generation time or serial intervals (time intervals from an event in an infector to the same event in an infectee) for the historical period before 2022 presents even greater uncertainty. As of April 2024, we are aware of no published formal estimates of such intervals from historical data, although estimates for the global 2022 outbreak exist; 34 transmission (infector–infectee) pairs studied in the Netherlands yielded a mean onset-to-onset serial interval estimate of 10.1 days (95% CrI 6.6–14.7 days) (*9*), and another estimate of 9.5 days (95% CrI 7.4–12.3 days) was based on 79 transmission pairs notified in the United Kingdom (*10*). In contrast, limited information on transmission pairs is available for the pre-2022 period; researchers observed onset-to-onset intervals of 8–11 days (*34*,*35*). We analyzed additional published data from before 2022 for rash-to-rash (*2*) and onset-to-onset serial intervals (*19*,*20*,*35*). The aim of our research is to provide historical estimates of the epidemiologic parameters associated with mpox by aggregating available historical data and to compare those estimates with pooled estimates for the global 2022 outbreak. In our analysis, we corrected previous

estimates as appropriate to account for right truncation, enabling systematic comparison of incubation periods and serial intervals across the 2 time periods. Our work did not require the approval of an ethics committee because it was based on a literature search and the analysis of publicly available data.

Despite successful containment of mpox in 2022–2023, monkeypox virus has continued to spread via human-to-human transmission worldwide. Investment in mpox surveillance and prevention methods, including vaccination, are critical to prevent the virus from causing future outbreaks and reaching PHEIC status again. As emphasized by WHO (*24*), it is necessary to remain vigilant and implement preventive measures to stop mpox from becoming endemic worldwide. Improving available knowledge of the epidemiologic parameters characterizing transmission, such as the incubation period and serial interval, represents a fundamental aspect of this global effort.

Methods

Epidemiologic Data

We conducted a comprehensive literature search without language restriction using the electronic databases PubMed, Embase, and Web of Science through January 4, 2024. We searched for the terms monkeypox, mpox, or mpx, and ≥1 occurrence of the terms incubation, serial, symptoms, onset, or rash. We extracted individual case records of infections from the studies published before 2022 and extracted estimates of the incubation period and serial interval from the studies published after 2022. The search yielded a total of 2,384 references after deduplication (Figure 1).

We deemed a total of 101 references published before 2022 relevant for collection of historical data after manual examination. We found specific information on dates of exposure and symptom onset in 21 references. We excluded 6 studies containing duplicate data. Ultimately, we selected 15 studies with a total of 42 case records. Of those, 16 records were associated with clade I MPXV, and all contained information on rash and symptom onset date; 26 records were associated with clade II, and 12 had information on rash and symptom onset date.

Among manuscripts published after 2022, we deemed 42 relevant after manual inspection. We retrieved 12 estimates of the incubation period and 5 estimates of the serial interval from studies providing data from Colombia (*36*), Italy (*8*), the Netherlands (*7*,*9*), Nigeria (*37*), Spain (*5*,*38*), the United Kingdom (*10*,*39*), and the United States (*11*), as well as studies providing data from multiple countries (*12*,*13*,*40*). Three of those publications included estimates that adjusted for right truncation of the data. To account for right truncation in estimates from the other studies, we extracted individual case data from published materials or obtained the data from the authors. We also compared the extracted list of publications with the literature search conducted by WHO as of December 29, 2022 (*41*). Some references listed by WHO were not identified in our search because they were posted on a preprint server and not peer reviewed by the time of our assessment. (Appendix Table 1, https://wwwnc.cdc.gov/EID/article/30/6/23-1095-App1.pdf).

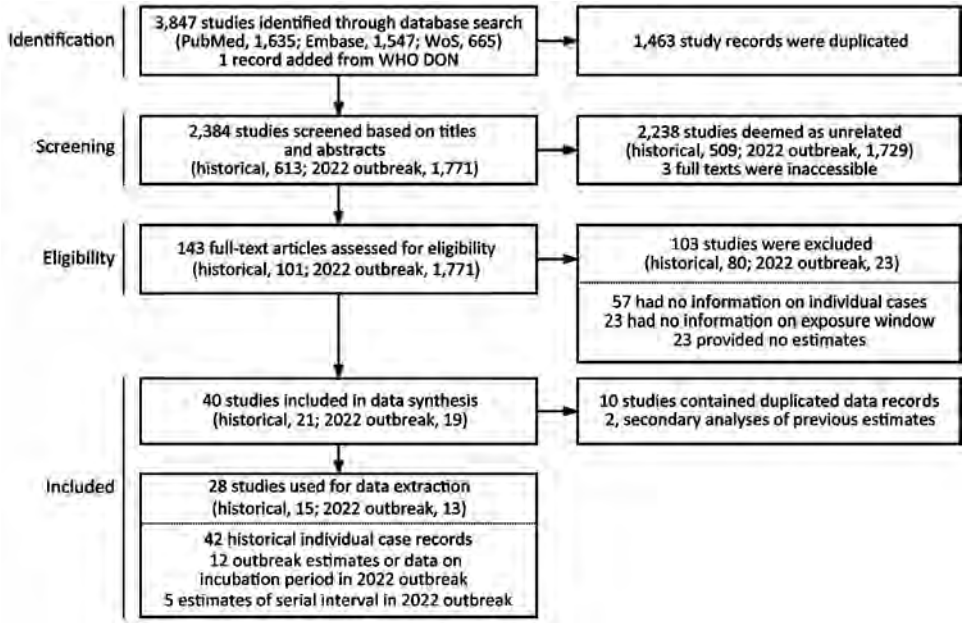

Figure 1. Flow diagram describing identification of historical case records from before the 2022 mpox outbreak eligible for estimation of the incubation period and studies reporting estimates of the incubation period and serial interval during the 2022 outbreak. WoS, Web of Science.

Statistical Analysis

We estimated the incubation period and serial interval distributions using a Bayesian model with Markov chain Monte Carlo implemented in Stan version 2.34.0 (https://mc-stan.org). We used the generalized gamma distribution to determine the incubation period and serial interval because it encompasses 3 commonly used distributions (gamma, Weibull, and log-normal) (*42*). We considered alternative formulations using standalone gamma, Weibull, or log-normal distributions or their mixture and saw no clear differences in the results (Appendix Figure 2).

For identified studies from the 2022 outbreak that did not account for right truncation (*7*,*8*,*11*), we extracted case data. In 2 of those studies (*7*,*8*), the authors provided the truncation date (the final day that case data were available)—day 38 (*7*) and 68 (*8*). With those dates, we could re-estimate the incubation period and serial interval accounting for right truncation. However, in 2 studies (*11*,*39*), no information about truncation date was available, so we were unable to conduct a re-analysis to account for right truncation. The authors of those studies stated that they observed no significant difference between nontruncated and right-truncated likelihoods. We obtained a pooled estimate of the mean incubation period from the meta-analysis using a random-effects model (*43*).

To estimate historical serial intervals, we used data from published studies (*2*,*19*,*20*,*35*). We extracted rash-to-rash time intervals from the dataset provided by Ježěk et al. (*2*) and onset-to-onset intervals (based on generalized symptoms) from other sources (*19*,*20*,*35*); the result was available data from 28 transmission pairs. Consistent with the discussion in Jezek et al., we omitted rash-to-rash intervals of <8 days, which likely resulted from co-primary infections.

To ensure the robustness of our estimates, we conducted a sensitivity analysis (Appendix). First, we considered different cutoff values (2, 4, 6, or 10 days), below which the rash-to-rash intervals were omitted. Second, we fitted the observed distribution to a composition of 2 distributions to allow for the possibility that cases with serial intervals longer than the cutoff value could still be co-primary infections. The first component was modeled either by an exponential distribution or by a scaled standard normal distribution, normal(0, σ), in line with previous studies. The second component was the rash-to-rash serial interval of interest, which was modeled by the generalized gamma distribution.

Results

We report estimates of the mean and SD of the incubation period for mpox based on recent literature (Figure 2, panel A; Appendix Table 2). We obtained those estimates in various ways. For 2 previous studies, we re-derived the estimates in the original articles to account for right truncation (*7*,*8*). We obtained other estimates by either fitting our model to data from the original publications (*5*,*36*,*38*) or reporting the findings from the original studies directly (*10*,*11*). The pooled mean incubation period was estimated to be 8.1 days (95% CrI 7.0–9.2 days); here, we reported all estimates as the posterior median and 95% CrI. The mean between-study variance was 1.8 days^2. Analysis of historical data (before the 2022 outbreak) suggested a mean incubation period of 8.2 days (95% CrI 6.7–10.0 days). Considering only cases associated with clade I resulted in a slightly lower mean of 7.3 days (95% CrI 5.0–10.2 days), whereas clade II infections were characterized by longer mean of 8.9 days (95% CrI 6.6–11.7 days). The 95th percentile of the incubation period distribution, commonly used to determine the quarantine period, was 16–20 days across all studies of the global 2022 outbreak and was 17 days for the historical data.

We also assessed the infection-to-rash incubation period, which tracks the time from infection to the manifestation of a cutaneous rash (Figure 2, panel B; Appendix Table 3). We estimated the pooled mean as 8.7 days (95% CrI 6.5–11.0 days), whereas the between-study variance was 6.4 days^2. Historical data gave a larger estimate of 10.3 days (95% CrI 8.5–12.3 days). We reviewed 3 studies for the 2022 outbreak; Madewell et al. (*11*) estimated a mean incubation period substantially lower than 2 other studies that looked at infection-to-rash time intervals (*5*,*38*), which resulted in a larger discrepancy between the pooled mean and historical estimate compared with the infection-to-onset incubation period estimates. Rash emergence was delayed by a mean of 0.6 days, compared with the infection-to-onset incubation period. Analyzing the data from Viedma-Martinez et al. (*38*), we first calculated the time from infection to the appearance of any cutaneous formations to have a mean value of 9.8 days (95% CrI 8.5–11.2 days). We then calculated the time from infection to the appearance of a disseminated rash, excluding the rash around or at the site of infection. We estimated a mean time period of 11.5 days (95% CrI 10.0–12.8 days). The difference between initial onset of symptoms and rash onset was 1.7 days (95% CrI 0.2–3.7 days) when considering a localized rash and 3.4 days (95% CrI 1.4–5.3 days) when considering a disseminated rash.

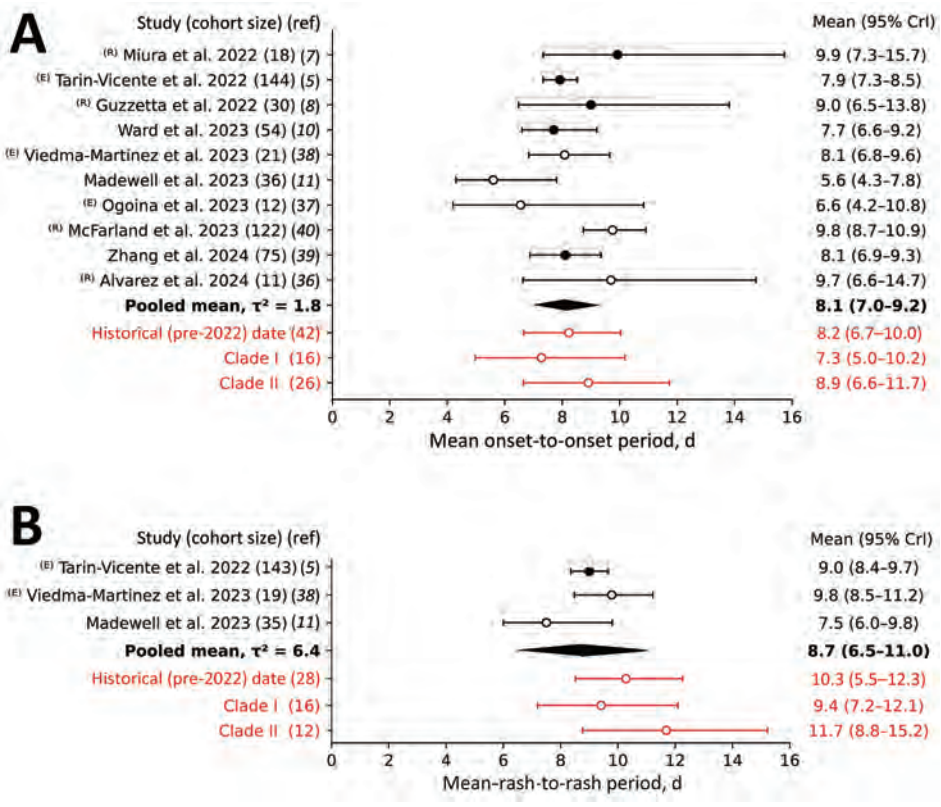

Figure 2. Forest plot of the mean infection-to-onset (A) and infection-to-rash (B) incubation periods for studies conducted during the 2022–2023 global mpox outbreak and analyses of the historical case records. Open circles indicate analyses performed without adjusting for right truncation (ICC); solid circles indicate analysis when an adjustment was made (ICRTC). Whiskers indicate 95% CrIs. Studies are denoted by the leading author and year of publication and ordered by their date of publication; the numbers in parentheses indicate the number of case records used for estimation. (E) indicates that we evaluated the estimates using the data provided in our study; (R) indicates that we re-evaluated estimates for consistency of the methods used. Gray indicates estimates not used for deriving the pooled mean, which is in bold text. Red indicates estimates for historical (pre–2022 outbreak) data, indicating that they were not used for deriving the pooled mean. CrI, credible interval; ICC, interval censoring corrected model; ICRTC, interval censoring and right truncation corrected model; τ^2 = -squared statistics indicating the between-study variance measured in days^2; ref, reference.

As for incubation period estimates, serial interval estimates varied substantially across studies. We estimated the pooled mean for onset-to-onset serial intervals as 8.7 days (95% CrI 6.5–11.0 days) and between-study variance as 6.4 days^2. We estimated the historical mean onset-to-onset serial interval at a much longer 14.2 days (95% CrI 12.5–16.2 days) (Figure 3, panel A; Appendix Table 4, Figure 1, panel A). Madewell et al. (*11*) reported rash-to-rash serial intervals for the 2022 outbreak; they reported a mean of 7.0 days (95% CrI 5.8–8.4 days). That value is much shorter than the historical estimate of the mean rash-to-rash serial interval, which was 14.3 days (95% CrI 13.2–15.3 days) (Figure 3, panel B; Appendix Table 5, Figure 1, panel B). Although Madewell et al. suggested that serial intervals might be shorter than incubation periods for the 2022 outbreak, we found that serial intervals were substantially longer for historical data. Specifically, our analyses suggested that onset-to-onset serial intervals were on average 6.0 days longer than for infection-to-onset incubation periods, and rash-to-rash serial intervals were on average 4.0 days longer than for infection-to-rash incubation periods.

Discussion

In this study, we undertook a systematic literature search and meta-analysis to provide estimates of the incubation period and serial interval of mpox. We compared estimates from the 2022 outbreak with pre-2022 estimates. We found a strong similarity in estimates of infection-to-onset and infection-to-rash incubation periods between studies for the 2022 outbreak and historical case records. However, the serial interval estimates based on historical data were longer than the incubation period estimates based on historical data, which suggests a lower risk of presymptomatic transmission during the pre-2022 period. The shorter serial interval observed in the 2022 outbreak might also be partially attributable to nonpharmaceutical interventions such as contact tracing, active case finding, and behavioral changes, as noted during the COVID-19 pandemic (*44*). A shift toward a sexually associated mode of transmission as the dominant route may also have influenced the serial interval, perhaps by increasing transmission efficiency. All of those theories merit further investigation.

The estimated incubation period in this study remains similar to historical estimates (*45*), suggesting

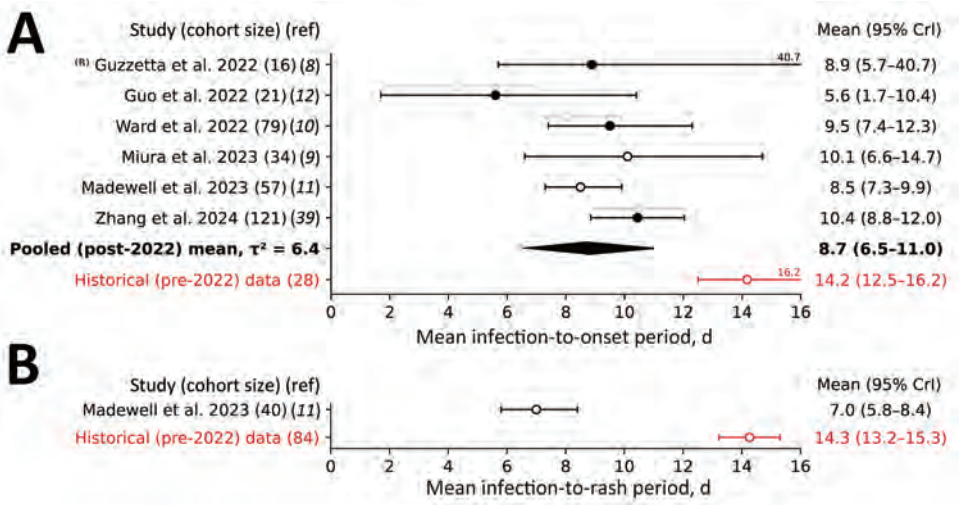

Figure 3. Forest plot of the estimated mean serial interval based on the date of symptom onset (A) and the date of rash onset (B) for studies conducted during the 2022–2023 global mpox outbreak and analyses of the historical case records. Open circles indicate analyses performed without adjusting for right truncation (ICC); solid circles indicate analyses when an adjustment was made (ICRTC). Whiskers indicate 95% CrI. Studies are denoted by the leading author and year of publication and ordered by their date of publication; the numbers in parentheses indicate the number of case records used for estimation. R) indicates that we re-evaluated estimates for consistency of the methods used. Gray indicates estimates not used for deriving the pooled mean, which is in bold text. Red indicates estimates for historical (pre–2022 outbreak) data, indicating that they were not used for deriving the pooled mean. CrI, credible interval; ICC, interval censoring corrected model; ICRTC, interval censoring and right truncation corrected model; ref, reference; τ^2, -squared statistics indicating the between-study variance measured in days^2.

that the recommended quarantine period of 21 days after contact with a potential infector is still appropriate. However, the possible increase in presymptomatic transmission, as suggested by a shortened serial interval, presents challenges for successful containment of future outbreaks (*9*,*11*). Moreover, underascertainment of cases further reduces the chances of efficient case finding and contact tracing. Vaccination is regarded as the most reliable measure to prevent future waves of infections, but vaccine availability and uptake have been limited. Some countries that observed a spike in cases in 2022 saw their outbreaks fade in 2023, but other countries in the Western Pacific region, such as Japan, South Korea, and Taiwan, observed a rise in cases at the beginning of 2023 (*46*).

The 2022 global mpox outbreak shares some similarities with a previous outbreak in Taiwan involving a sexually transmitted pathogen that also affected a vulnerable group. In 2015–2016, hepatitis A virus (HAV) infections spread progressively among the MSM population. The Taiwan Centers for Disease Control (CDC) reported an increase in HAV cases in 2015. A free HAV vaccination campaign was initiated in October 2016, several months after the peak of disease incidence, targeting at-risk populations. Because it was difficult to quantify the direct impact of vaccination after the peak on the course of the outbreak, many attributed the decline in cases to the promotion of both HAV screening and vaccination by physicians earlier in the outbreak (*47*). In the 2022 global mpox outbreak, there has been much debate about the key factors behind the decline in incidence observed in all hard-hit countries in mid-to-late 2022. Some suggested depletion of susceptible persons within sexual networks of MSM was the key factor (*25*); others argued that a synergetic effect of behavioral change and vaccination was crucial (*48*). Going forward, proactive vaccination campaigns are advised to reduce transmission; such a campaign was implemented in Taiwan at the beginning of 2023 after reports of locally acquired mpox infections.

The first limitation of this study is that we derived the pooled estimates of the mean incubation period and serial interval from various sources, each with their own potential biases and limitations. For example, the study by Ward et al. (*10*) did not consider the possibility of co-primary cases; however, it used personally identifiable information to establish linked pairs. Second, the aggregated historical data could also be prone to selection and recall biases; many studies were conducted retrospectively, and mild cases may have been missed. Third, most cases in the historical datasets involved children and teenagers, whereas in the 2022 outbreak the group that was infected the most was adult males. Such a shift in the age distribution of mpox cases (before and after 2022) may have affected the time delays and introduced bias into our comparison of their estimates. Fourth, the differences in epidemiology of mpox infections respective to their clades remain uncertain. Although our estimated mean incubation period for clade I was shorter than the mean for clade II, the difference was not statistically clear and could simply caused by sampling variability (the samples were

also relatively small). Overall, the studies aggregated in our meta-analysis were conducted during different time periods and in different geographic locations involving diverse social groups. This variation could introduce variability in public health interventions, diagnostic methods, and reporting practices, potentially affecting estimates of epidemiologic parameters such as the incubation period and serial interval. A cohort-based comparison taking account of observed severity, social status, and other factors could help to address potential biases.

Despite those limitations, our study provides evidence that the incubation period for mpox was similar in 2022 to that of historical outbreaks, whereas the serial interval was shorter. This finding likely reflects both the result of interventions and a shift toward a sexually associated mode of transmission in the 2022 outbreak. Because estimated values of epidemiologic parameters are often used to inform interventions against a range of pathogens, our study highlights the importance of monitoring temporal changes in transmission and disease progression. Effective public health interventions that are tailored to the characteristics of future mpox outbreaks could be crucial for mitigating transmission in the future. Overall, our findings provide useful information to inform evidence-based control strategies to curtail the spread of mpox and other directly transmitted infectious diseases.

Study data are available at https://github.com/aakhmetz/Mpox-IncubationPeriodSerialInterval-Meta2023/blob/main/SupplementaryFile1.xlsx.

Acknowledgments

We thank A. Alemany, K. Charniga, and J.M.E. Alvarez for providing the datasets underlying their studies (*5*,*11*,*36*) on behalf of their co-authors. A.R.A. is thankful to F. Miura and S. Merler for communicating details about the datasets used in the studies in which they were involved (*7*–*9*).

The work was supported by the National Science and Technology Council, Taiwan (NSTC #111-2314-B-002-289).

The findings and conclusions in this article are those of the authors and do not necessarily represent the views or opinions of the California Department of Public Health (USA) or the Taiwan Centers for Disease Control (Taiwan).

About the Author

Mr. Ponce is a graduate of the master's program in global health at the National Taiwan University College of Public Health. His primary research interest is the epidemiology of infectious diseases and mathematical modeling.

References

1. Centers for Disease Control and Prevention. About mpox. 2023 [cited 2003 Feb 3]. https://www.cdc.gov/poxvirus/monkeypox/about/index.html
2. Jezek Z, Grab B, Dixon H. Stochastic model for interhuman spread of monkeypox. Am J Epidemiol. 1987;126:1082–92. https://doi.org/10.1093/oxfordjournals.aje.a114747
3. Fine PE, Jezek Z, Grab B, Dixon H. The transmission potential of monkeypox virus in human populations. Int J Epidemiol. 1988;17:643–50. https://doi.org/10.1093/ije/17.3.643
4. Endo A, Murayama H, Abbott S, Ratnayake R, Pearson CAB, Edmunds WJ, et al. Heavy-tailed sexual contact networks and monkeypox epidemiology in the global outbreak, 2022. Science. 2022;378:90–4. https://doi.org/10.1126/science.add4507
5. Tarín-Vicente EJ, Alemany A, Agud-Dios M, Ubals M, Suñer C, Antón A, et al. Clinical presentation and virological assessment of confirmed human monkeypox virus cases in Spain: a prospective observational cohort study. Lancet. 2022;400:661–9. https://doi.org/10.1016/S0140-6736(22)01436-2
6. Laurenson-Schafer H, Sklenovská N, Hoxha A, Kerr SM, Ndumbi P, Fitzner J, et al.; WHO mpox Surveillance and Analytics team. Description of the first global outbreak of mpox: an analysis of global surveillance data. Lancet Glob Health. 2023;11:e1012–23. https://doi.org/10.1016/S2214-109X(23)00198-5
7. Miura F, van Ewijk CE, Backer JA, Xiridou M, Franz E, Op de Coul E, et al. Estimated incubation period for monkeypox cases confirmed in the Netherlands, May 2022. Euro Surveill. 2022;27:2200448. https://doi.org/10.2807/1560-7917.ES.2022.27.24.2200448
8. Guzzetta G, Mammone A, Ferraro F, Caraglia A, Rapiti A, Marziano V, et al. Early estimates of monkeypox incubation period, generation time, and reproduction number, Italy, May–June 2022. Emerg Infect Dis. 2022;28:2078–81. https://doi.org/10.3201/eid2810.221126
9. Miura F, Backer JA, van Rijckevorsel G, Bavalia R, Raven S, Petrignani M, et al. Time scales of human mpox transmission in the Netherlands. J Infect Dis. 2023;229:800–4. https://doi.org/10.1093/infdis/jiad091
10. Ward T, Christie R, Paton RS, Cumming F, Overton CE. Transmission dynamics of monkeypox in the United Kingdom: contact tracing study. BMJ. 2022;379:e073153. https://doi.org/10.1136/bmj-2022-073153
11. Madewell ZJ, Charniga K, Masters NB, Asher J, Fahrenwald L, Still W, et al.; 2022 Mpox Outbreak Response Team. Serial interval and incubation period estimates of monkeypox virus infection in 12 jurisdictions, United States, May–August 2022. Emerg Infect Dis. 2023;29:818–21. https://doi.org/10.3201/eid2904.221622
12. Guo Z, Zhao S, Sun S, He D, Chong KC, Yeoh EK. Estimation of the serial interval of monkeypox during the early outbreak in 2022. J Med Virol. 2023;95:e28248. https://doi.org/10.1002/jmv.28248
13. Thornhill JP, Barkati S, Walmsley S, Rockstroh J, Antinori A, Harrison LB, et al.; SHARE-net Clinical Group. Monkeypox virus infection in humans across 16 countries—April–June 2022. N Engl J Med. 2022;387:679–91. https://doi.org/10.1056/NEJMoa2207323
14. Lim EY, Whitehorn J, Rivett L. Monkeypox: a review of the 2022 outbreak. Br Med Bull. 2023;145:17–29. https://doi.org/10.1093/bmb/ldad002
15. Ladnyj ID, Ziegler P, Kima E. A human infection caused by monkeypox virus in Basankusu territory, Democratic

Republic of the Congo. Bull World Health Organ. 1972;46:593–7.
16. Arita I, Henderson DA. Monkeypox and whitepox viruses in West and Central Africa. Bull World Health Organ. 1976;53:347–53.
17. Mutombo M, Arita I, Jezek Z. Human monkeypox transmitted by a chimpanzee in a tropical rain-forest area of Zaire. Lancet. 1983;321:735–7. https://doi.org/10.1016/S0140-6736(83)92027-5
18. Khodakevich L, Jezek Z, Messinger D. Monkeypox virus: ecology and public health significance. Bull World Health Organ. 1988;66:747–52.
19. Learned LA, Reynolds MG, Wassa DW, Li Y, Olson VA, Karem K, et al. Extended interhuman transmission of monkeypox in a hospital community in the Republic of the Congo, 2003. Am J Trop Med Hyg. 2005;73:428–34. https://doi.org/10.4269/ajtmh.2005.73.428
20. Formenty P, Muntasir MO, Damon I, Chowdhary V, Opoka ML, Monimart C, et al. Human monkeypox outbreak caused by novel virus belonging to Congo Basin clade, Sudan, 2005. Emerg Infect Dis. 2010;16:1539–45. https://doi.org/10.3201/eid1610.100713
21. Yinka-Ogunleye A, Aruna O, Ogoina D, Aworabhi N, Eteng W, Badaru S, et al. Reemergence of human monkeypox in Nigeria, 2017. Emerg Infect Dis. 2018;24:1149–51. https://doi.org/10.3201/eid2406.180017
22. Durski KN, McCollum AM, Nakazawa Y, Petersen BW, Reynolds MG, Briand S, et al. Emergence of monkeypox—west and central Africa, 1970–2017. MMWR Morb Mortal Wkly Rep. 2018;67:306–10. https://doi.org/10.15585/mmwr.mm6710a5
23. Reynolds MG, Yorita KL, Kuehnert MJ, Davidson WB, Huhn GD, Holman RC, et al. Clinical manifestations of human monkeypox influenced by route of infection. J Infect Dis. 2006;194:773–80. https://doi.org/10.1086/505880
24. World Health Organization. WHO Director-General's statement at the press conference following IHR Emergency Committee regarding the multi-country outbreak of monkeypox—23 July 2022. 2022 [cited 2023 Sep 18]; https://www.who.int/director-general/speeches/detail/who-director-general-s-statement-on-the-press-conference-following-IHR-emergency-committee-regarding-the-multi–country-outbreak-of-monkeypox–23-july-2022
25. Murayama H, Pearson CAB, Abbott S, Miura F, Jung S, Fearon E, et al. Accumulation of immunity in heavy-tailed sexual contact networks shapes mpox outbreak sizes. J Infect Dis. 2024;229:59–63. https://doi.org/10.1093/infdis/jiad254
26. Brand SPC, Cavallaro M, Cumming F, Turner C, Florence I, Blomquist P, et al. The role of vaccination and public awareness in forecasts of mpox incidence in the United Kingdom. Nat Commun. 2023;14:4100. https://doi.org/10.1038/s41467-023-38816-8
27. Spicknall IH, Pollock ED, Clay PA, Oster AM, Charniga K, Masters N, et al. Modeling the impact of sexual networks in the transmission of monkeypox virus among gay, bisexual, and other men who have sex with men—United States, 2022. MMWR Morb Mortal Wkly Rep. 2022;71:1131–5. https://doi.org/10.15585/mmwr.mm7135e2
28. Delaney KP, Sanchez T, Hannah M, Edwards OW, Carpino T, Agnew-Brune C, et al. Strategies adopted by gay, bisexual, and other men who have sex with men to prevent monkeypox virus transmission—United States, August 2022. MMWR Morb Mortal Wkly Rep. 2022;71:1126–30. https://doi.org/10.15585/mmwr.mm7135e1
29. Jezek Z, Gromyko AI, Szczeniowski MV. Human monkeypox. J Hyg Epidemiol Microbiol Immunol. 1983;27:13–28.
30. Sihuincha Maldonado M, Lucchetti AJ, Paredes Pacheco RA, Martínez Cevallos LC, Zumaeta Saavedra EU, Ponce Zapata LR, et al. Epidemiologic characteristics and clinical features of patients with monkeypox virus infection from a hospital in Peru between July and September 2022. Int J Infect Dis. 2023;129:175–80. https://doi.org/10.1016/j.ijid.2023.01.045
31. Ogata T, Tanaka H. SARS-CoV-2 incubation period during the Omicron BA.5–dominant period in Japan. Emerg Infect Dis. 2023;29:595–8. https://doi.org/10.3201/eid2903.221360
32. Wu Y, Kang L, Guo Z, Liu J, Liu M, Liang W. Incubation period of COVID-19 caused by unique SARS-CoV-2 strains: a systematic review and meta-analysis. JAMA Network Open. 2022;5:e2228008-e. https://doi.org/10.1001/jamanetworkopen.2022.28008
33. Cheng HY, Akhmetzhanov AR, Dushoff J. SARS-CoV-2 incubation period during Omicron BA.5–dominant period, Japan. Emerg Infect Dis. 2024;30:206–7. https://doi.org/10.3201/eid3001.230208
34. Jezek Z, Grab B, Paluku KM, Szczeniowski MV. Human monkeypox: disease pattern, incidence, and attack rates in a rural area of northern Zaire. Trop Geogr Med. 1988;40:73–83.
35. Nolen LD, Osadebe L, Katomba J, Likofata J, Mukadi D, Monroe B, et al. Extended human-to-human transmission during a monkeypox outbreak in the Democratic Republic of the Congo. Emerg Infect Dis. 2016;22:1014–21. https://doi.org/10.3201/eid2206.150579
36. Estrada Alvarez JM, Acuña MH, García Arias HF, Alvarado FEP, Ospina Ramírez JJ. Estimation of incubation period of mpox during 2022 outbreak in Pereira, Colombia. Emerg Infect Dis. 2024;30:180–2. https://doi.org/10.3201/eid3001.221663
37. Ogoina D, James HI. Mpox among linked heterosexual casual partners in Bayelsa, Nigeria. N Engl J Med. 2023;388:2101–4. https://doi.org/10.1056/NEJMc2300866
38. Viedma-Martinez M, Dominguez-Tosso FR, Jimenez-Gallo D, Garcia-Palacios J, Riera-Tur L, Montiel-Quezel N, et al. MPXV transmission at a tattoo parlor. N Engl J Med. 2023;388:92–4. https://doi.org/10.1056/NEJMc2210823
39 Zhang XS, Mandal S, Mohammed H, Turner C, Florence I, Walker J, et al. Transmission dynamics and effect of control measures on the 2022 outbreak of mpox among gay, bisexual, and other men who have sex with men in England: a mathematical modelling study. Lancet Infect Dis. 2024;24:65–74. https://doi.org/10.1016/S1473-3099(23)00451-6
40. McFarland SE, Marcus U, Hemmers L, Miura F, Iñigo Martínez J, Martínez FM, et al. Estimated incubation period distributions of mpox using cases from two international European festivals and outbreaks in a club in Berlin, May to June 2022. Euro Surveill. 2023;28:2200806. https://doi.org/10.2807/1560-7917.ES.2023.28.27.2200806
41. World Health Organization (WHO). 2022–23 Mpox (monkeypox) outbreak: global trends. Produced 2023 Mar 8 [cited 2023 Mar 10]. https://worldhealthorg.shinyapps.io/mpx_global
42. Hoffmann T, Alsing J. Faecal shedding models for SARS-CoV-2 RNA among hospitalised patients and implications for wastewater-based epidemiology. J R Stat Soc Ser C Appl Stat. 2023;72:330–45. https://doi.org/10.1093/jrsssc/qlad011
43. Serghiou S, Goodman SN. Random-effects meta-analysis: summarizing evidence with caveats. JAMA. 2019;321:301–2. https://doi.org/10.1001/jama.2018.19684
44. Ali ST, Wang L, Lau EHY, Xu XK, Du Z, Wu Y, et al. Serial interval of SARS-CoV-2 was shortened over time by nonpharmaceutical interventions. Science. 2020;369:1106–9. https://doi.org/10.1126/science.abc9004

45. Grant R, Nguyen LL, Breban R. Modelling human-to-human transmission of monkeypox. Bull World Health Organ. 2020;98:638–40. https://doi.org/10.2471/BLT.19.242347
46. Endo A, Jung SM, Miura F. Mpox emergence in Japan: ongoing risk of establishment in Asia. Lancet. 2023;401:1923–4. https://doi.org/10.1016/S0140-6736(23)00766-3
47. Chen WC, Chiang PH, Liao YH, Huang LC, Hsieh YJ, Chiu CM, et al. Outbreak of hepatitis A virus infection in Taiwan, June 2015 to September 2017. Euro Surveill. 2019;24:1800133. https://doi.org/10.2807/1560-7917.ES.2019.24.14.1800133
48. Clay PA, Asher JM, Carnes N, Copen CE, Delaney KP, Payne DC, et al. Modelling the impact of vaccination and sexual behaviour adaptations on mpox cases in the USA during the 2022 outbreak. Sex Transm Infect. 2024;100:70–6. https://doi.org/10.1136/sextrans-2023-055922
49. Akhmetzhanov AR, Jung S, Cheng H-Y, Thompson RN. A hospital-related outbreak of SARS-CoV-2 associated with variant Epsilon (B.1.429) in Taiwan: transmission potential and outbreak containment under intensified contact tracing, January–February 2021. Int J Infect Dis. 2021;110:15–20. https://doi.org/https://doi.org/10.1016/j.ijid.2021.06.028

Address for correspondence: Andrei R. Akhmetzhanov, College of Public Health, National Taiwan University, No. 17 Xuzhou Rd, Zhongzheng District, Taipei 10055, Taiwan; email: akhmetzhanov@ntu.edu.tw

SARS-CoV-2 Disease Severity and Cycle Threshold Values in Children Infected during Pre-Delta, Delta, and Omicron Periods, Colorado, USA, 2021–2022

Laura Bankers, Shannon C. O'Brien, Diana M. Tapay, Erin Ho, Isaac Armistead, Alexis Burakoff, Samuel R. Dominguez, Shannon R. Matzinger

In adults, viral load and disease severity can differ by SARS-CoV-2 variant, patterns less understood in children. We evaluated symptomatology, cycle threshold (Ct) values, and SARS-CoV-2 variants among 2,299 pediatric SARS-CoV-2 patients (0–21 years of age) in Colorado, USA, to determine whether children infected with Delta or Omicron had different symptom severity or Ct values than during earlier variants. Children infected during the Delta and Omicron periods had lower Ct values than those infected during pre-Delta, and children <1 year of age had lower Ct values than older children. Hospitalized symptomatic children had lower Ct values than asymptomatic patients. Compared with pre-Delta, more children infected during Delta and Omicron were symptomatic (75.4% pre-Delta, 95.3% Delta, 99.5% Omicron), admitted to intensive care (18.8% pre-Delta, 39.5% Delta, 22.9% Omicron), or received oxygen support (42.0% pre-Delta, 66.3% Delta, 62.3% Omicron). Our data reinforce the need to include children, especially younger children, in pathogen surveillance efforts.

SARS-CoV-2 is characterized by diverse variants (*1*) with differing transmissibility and disease severity (*2*). The rapid evolution and spread of new variants has required a nimble public health response to understand dynamics and clinical implications (*3*), but most work thus far has focused on adults.

Author affiliations: Colorado Department of Public Health and Environment, Denver, Colorado, USA (L. Bankers, S.C. O'Brien, D.M. Tapay, I. Armistead, A. Burakoff, S.R. Matzinger); University of Colorado, Aurora, Colorado, USA (E. Ho, S.R. Dominguez); Children's Hospital Colorado, Aurora (E. Ho, S.R. Dominguez)

DOI: https://doi.org/10.3201/eid3006.231427

The highly transmissible SARS-CoV-2 Delta variant (B.1.617.2) was detected and became the predominant variant in the United States over an 8-week period during May–June 2021 (*4*,*5*). Adults infected by Delta exhibited higher viral loads (*6*) and potentially increased disease severity than those infected by previous variants (*3*,*5*). Taylor et al. (*5*) found a significantly higher proportion of hospitalized patients after Delta became predominant than in earlier pandemic phases. However, in-hospital outcomes did not differ between Delta and pre-Delta variants. Similarly, Twohig et al. (*3*) observed higher risk for hospitalization and emergency care for those infected by Delta than by Alpha (B.1.1.7).

During December 2021, Delta was swiftly overtaken by the more transmissible Omicron (B.1.1.529), which became predominant in the United States over a 2-week period (*4*). Adults infected by Omicron tended to exhibit similar viral loads but lower disease severity compared with Delta-infected adults (*7*). Ulloa et al. (*7*) found reduced risk for hospitalization, intensive care unit (ICU) admission, and death among persons infected by Omicron compared with Delta. Taylor et al. (*8*) observed smaller proportions of hospitalized patients admitted to the ICU or requiring invasive mechanical ventilation and lower rates of in-hospital death with Omicron than Delta. In addition, some studies found that vaccine effectiveness against hospitalization and visits to emergency department or urgent care was lower against Omicron than against Delta (*9*).

Less is known about symptom severity among pediatric patients infected with different variants. Some work suggests little or no difference in disease

severity among children infected by Delta compared with previous variants (*10*). However, much of that work has been limited to hospitalized patients. In addition, although the incidence rate of detected infections with Omicron was higher for young children compared with Delta, some studies showed that clinical outcomes of infections with Omicron tended to be less severe than Delta (*11*). However, the large increase in the number of infections during Omicron's predominance might increase the number of severe outcomes (*12*).

The relationship between cycle threshold (Ct) values and quantitative viral load is tightly inversely correlated (*13*), such that relatively lower Ct values are indicative of higher viral loads. Similar to adults, children who have symptomatic SARS-CoV-2 infections might have lower Ct values (suggesting higher viral loads) compared with those who have asymptomatic infections (*14*), and those infected with Delta or Omicron might have lower Ct values than those infected with other variants (*15*). However, the interplay between SARS-CoV-2 variant, Ct, and symptom severity has not been well studied among pediatric cases, especially among nonhospitalized children.

We evaluated hospitalized and nonhospitalized SARS-CoV-2 pediatric cases in Colorado, USA, during January 2021–January 2022. We used clinical surveillance data, Ct values, and whole-genome sequencing (WGS) to determine whether children infected with either Delta or early Omicron variants had different symptom severity or Ct values from children infected with earlier SARS-CoV-2 variants.

Methods

Ethics Statement

The data used in this study were generated for public health surveillance purposes. This activity was determined to be consistent with enhanced disease surveillance activities, not human subjects research, by the Colorado Department of Public Health and Environment's (CDPHE) Communicable Disease branch. Institutional review board approval was provided by the Colorado Multiple Institutional Review Board. Informed consent was waived.

Study Population

The study population consisted of hospitalized (hereafter inpatient) and nonhospitalized (hereafter outpatient) cases from the Children's Hospital Colorado (CHCO) hospitals and outpatient clinics who were Colorado residents <21 years of age and tested positive for SARS-CoV-2 by PCR during January 1, 2021–January 31, 2022. We collected demographic and clinical information including age, race/ethnicity, symptomatology, number of days between symptom onset and positive test (hereafter symptom onset date), and vaccination status. Data were extracted from a state communicable disease database (Colorado Electronic Disease Reporting System), in which communicable diseases are entered as part of public health surveillance and investigation activities.

We performed inpatient chart abstraction to collect data about comorbidities, admission and discharge dates, whether patients were admitted to the hospital because of COVID-19 as opposed to with COVID-19, whether patients were symptomatic because of COVID-19, whether they were admitted to the pediatric ICU (PICU) because of COVID-19, whether they received oxygen support (and type of support) because of COVID-19, and vaccination status. We limited comparisons among inpatients and between inpatients and outpatients to those hospitalized because of COVID-19. We classified patients as admitted because of COVID-19 if their primary complaint symptoms at time of admission to CHCO were consistent with COVID-19 and a COVID-19 test was positive at admission, or if symptoms consistent with COVID-19 developed during hospitalization (with positive test upon admission or later during hospitalization) that would have resulted in admission if they were not already hospitalized. We classified patients as admitted with COVID-19 if they sought care at CHCO with a non–COVID-19 primary diagnosis (e.g., trauma, psychiatry, social reasons, surgery, non–COVID-19 medical diagnoses) and tested positive upon admission on routine surveillance testing. Those persons might also have had ≥1 symptoms consistent with COVID-19 that did not require admission solely for those symptoms. We determined classification by reviewing clinical provider documentation of assessments and medical decision-making, because International Classification of Diseases, 10th Revision, codes were not consistently available. We considered all common symptoms of COVID-19, including fever, congestion/rhinorrhea, cough, shortness of breath, vomiting/diarrhea, fatigue, headache, and loss of sense of taste/smell.

RNA Extraction and Quantitative Reverse Transcription PCR

SARS-CoV-2–positive nasopharyngeal swab specimens collected at CHCO hospitals (inpatient) and outpatient clinics (outpatients) were sent to the CDPHE Laboratory. We extracted RNA using the Applied

Biosystems MagMAX Viral/Pathogen II Nucleic Acid Isolation Kit on the KingFisher Flex System for automated extraction (ThermoFisher Scientific, https://www.thermofisher.com). We used the Applied Biosystems TaqPath COVID-19 Combo Kit multiplexed reverse transcription PCR (RT-PCR) (ThermoFisher Scientific) to obtain Ct values for open reading frame 1ab (ORF1ab), spike (S), and nucleocapsid (N) gene targets. We used N gene Ct values as a correlate of viral load (*13*).

Library Preparation and WGS

We performed WGS on either GridION (Oxford Nanopore Technologies, https://www.nanoporetech.com) or NextSeq550 (Illumina, https://www.illumina.com) on all samples that met sequencing criteria (N gene Ct ≤28). For samples sequenced on GridION, we performed library preparation following the ARTIC tiled PCR amplicon sequencing protocol (*16*,*17*), and for samples sequenced on the NextSeq550, we performed library preparation and single-end Illumina sequencing following the Illumina COVID-Seq assay (*18*) (Appendix, https://wwwnc.cdc.gov/EID/article/30/6/23-1427-App1.pdf).

Bioinformatic Analysis of WGS Data

We performed assembly and analysis of WGS data on the terra.bio platform (*19*), using our custom, publicly available workflows for SARS-CoV-2 (*20*,*21*) (Appendix). Sequenced samples with ≥50% coverage are publicly available in the GISAID (https://www.gisaid.org) database and the National Center for Biotechnology Information Sequence Read Archive (BioProject accession no. PRJNA686984) (Appendix Table 1).

Data Analysis and Statistics

We merged WGS results and deidentified patient data using internal identifiers in Tableau version 2021.4 (*22*). To include data for samples that were not successfully sequenced, we performed analyses in 2 ways.

Our first approach mitigates the risk that Ct value analyses could be biased toward lower Ct values because of ability to sequence. We generated a lineage distribution over the course of the study and assigned all samples with Ct values to variant periods. We defined 3 periods on the basis of when Delta or Omicron were at a prevalence of ≥80% among sequenced Colorado pediatric samples: pre-Delta during January 1–May 1, 2021; Delta during June 15–September 29, 2021; and Omicron during December 26, 2021–January 31, 2022. We excluded samples collected between the pre-Delta and Delta periods and between the Delta and Omicron periods (in which variants were mixed) to improve the accuracy of variant period assignments (Figure 1). Second, to evaluate sensitivity, we performed analyses only on samples that were successfully sequenced and assigned a lineage.

We visualized analyses of Ct values, variant period and lineage, and patient data using Tableau. We performed statistical analyses (analysis of covariance, 1- or 2-way analysis of variance with Tukey test, or χ^2 test, as appropriate) in Rstudio base packages version 1.4.1106 (RStudio, http://www.rstudio.com). We calculated descriptive characteristics of inpatients including counts and proportions with 95% CI using R version 4.1.1 (The R Foundation for Statistical Computing, https://www.r-project.org). We considered a p value ≤0.05 statistically significant.

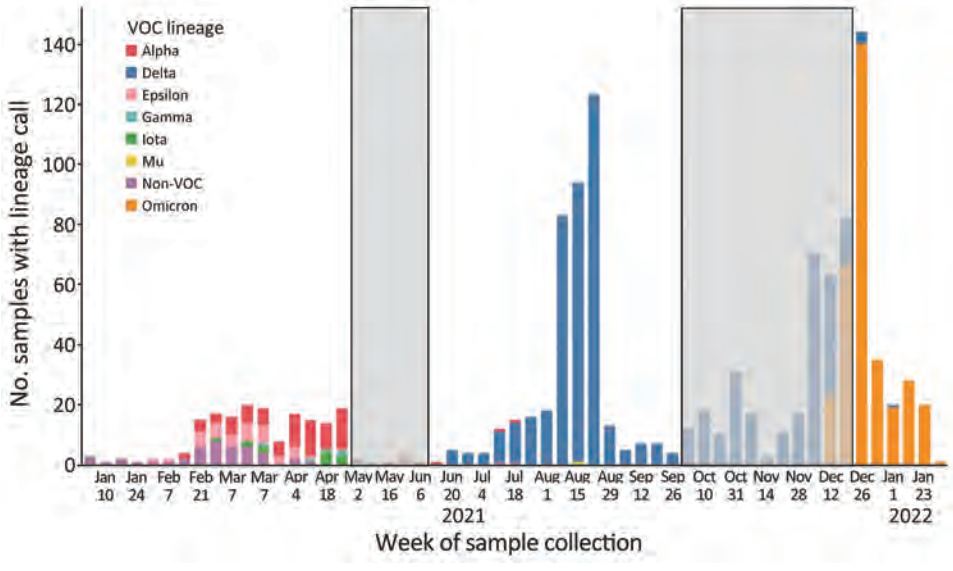

Figure 1. Variant counts of sequencing-confirmed lineages by week of sample collection in study of SARS-CoV-2 disease severity in children during pre-Delta, Delta, and Omicron periods, Colorado, USA, January 2021–January 2022. Gray boxes indicate time periods of potentially mixed lineage that were excluded from time period analyses.

Table 1. Descriptive characteristics of 2,299 children with positive SARS-CoV-2 tests during pre-Delta, Delta, and Omicron periods, Colorado, USA, January 2021–January 2022*

Characteristic	Total	Pre-Delta period	Delta period	Omicron period	p value†
Total population	2,299	429 (18.7, 17.1–20.3)	752 (32.7, 30.8–34.7)	543 (23.6, 21.9–25.4)	
Sex					
F	923 (40.1, 38.1–42.2)	215 (50.1, 45.3–55.0)	352 (46.8, 43.2–50.5)	185 (34.1, 30.1–38.2)	0.44
M	945 (41.1, 39.1–43.2)	198 (46.2, 41.4–51.0)	373 (49.6, 46.0–53.2)	200 (36.8, 32.8–41.0)	
Median age, y (range)	6.5 (0–21)	6.5 (0–20.2)	6.0 (0–21)	6.3 (0–20.9)	
Racial/ethnic group					
Hispanic	560 (24.4, 22.6–26.2)	131 (30.5, 26.2–35.1)	212 (28.2, 25.0–31.6)	127 (23.4, 19.9–27.2)	
Non-Hispanic White	750 (32.6, 30.7–34.6)	203 (47.3, 42.5–52.2)	307 (40.8, 37.3–44.4)	134 (24.7, 21.1–28.5)	<0.0001
Non-Hispanic Black	135 (5.9, 5.0–6.9)	19 (4.4, 2.7–6.8)	58 (7.7, 5.9–9.9)	32 (5.9, 4.1–8.2)	
Non-Hispanic Asian	43 (1.9, 1.4–2.5)	9 (2.1, 1.0–3.9)	17 (2.3, 1.3–3.6)	10 (1.8, 0.9–3.4)	
Unknown‡	673 (29.3, 27.4–31.2)	40 (9.3, 6.7–12.5)	97 (12.9, 10.6–15.5)	213 (39.2, 35.1–43.5)	
Hospitalization status					
Outpatient	1,629 (70.9, 69.0–72.7)	261 (60.8, 56.0–65.5)	619 (82.3, 79.4–85.0)	233 (42.9, 38.7–47.2)	<0.0001
Inpatient	670 (29.1, 27.3–31.1)	168 (39.2, 34.5–44.0)	133 (17.7, 15.0–20.6)	310 (57.1, 52.8–61.3)	
Any comorbidity, inpatient only§	383 (57.2, 53.3–61.0)	101 (60.1, 52.3–67.6)	74 (55.6, 46.8–64.3)	173 (55.8, 50.1–61.4)	0.62
Median time from symptom onset to testing, d (range)	2 (–29 to 320)	2 (–1 to 57)	2 (–2 to 320)	2 (–29 to 44)	
Patients with confirmed sequence	1,177 (51.2, 49.1–53.3)	189 (16.1, 14.0–18.3)	654 (55.6, 52.7–58.4)	334 (28.4, 25.8–31.1)	

*Values are no. (%, 95% CI) except as indicated. p values are indicated as appropriate.
†p values were obtained from χ^2 test of patient characteristics across the 3 variant periods.
‡Unknown racial/ethnic group includes persons with unknown, unknown or not reported, or missing race or ethnicity variables.
§Any comorbidity includes history of cardiac, respiratory, gastrointestinal/liver, neurologic, oncologic, obesity, chronic kidney disease, diabetes, or other comorbid condition.

Results

Characteristics of Patient Population

The study population included 2,299 persons, 1,629 (70.9%) outpatients and 670 inpatients (29.1%). Of the 670 inpatients, 395 were hospitalized because of COVID-19 and 275 were hospitalized with COVID-19) (Table 1; Appendix Tables 2, 3). Among the entire population, 40.1% were female, 32.6% were non-Hispanic White, 24.4% were Hispanic, and the median age was 6.5 years. A total of 1,724 cases occurred during the pre-Delta (n = 429), Delta (n = 752), and Omicron (n = 543) periods. Proportions of male versus female patients and those with ≥1 known comorbidity did not differ by variant period (p = 0.44 by χ^2 test for sex and p = 0.62 by χ^2 test for comorbidities). However, proportions of racial/ethnic groups differed significantly across variant periods (p<0.0001 by χ^2 test).

Among inpatients, a larger proportion infected during the Delta or Omicron periods were symptomatic (p<0.0001 by χ^2 test), admitted to the PICU (p = 0.002 by χ^2 test), or received oxygen support (p = 0.04 by χ^2 test) because of COVID-19 compared with persons infected during the pre-Delta period (Table 2; Appendix Tables 4, 5). Mean hospital stay durations were 5.72 (SD ±8.30) days for the pre-Delta period, 7.84 (SD ±20.6) days for the Delta period, and 3.32 (SD ±5.79) days for the Omicron period and were not significantly different (p = 0.1).

We obtained Ct values for 1,796 (78.1%) of 2,299 persons; of those, 362 were inpatients and 1,434 were outpatients. Of those 1,796 persons, 1,240 were collected during the 3 variant periods: pre-Delta period (n = 307), Delta period (n = 582), and Omicron period (n = 351). We successfully sequenced 1,276 (55.5%) of 2,299 samples (219 inpatients and 1,057 outpatients) to ≥50% coverage and obtained lineage calls for 1,177

Table 2. Number of pediatric COVID-19 inpatients by SARS-CoV-2 variant period and potential indicator of disease severity during pre-Delta, Delta, and Omicron periods, Colorado, USA, January 2021–January 2022*

Indicator of disease severity†	No. (%, 95% CI]				
	Total, n = 395	Pre-Delta, n = 69	Delta, n = 86	Omicron, n = 210	p value‡
Symptomatic	343 (86.8, 83.1–90.0)	52 (75.4, 63.5–84.9)	82 (95.3, 88.5–98.7)	209 (99.5, 97.4–99.9)	<0.0001
Hospitalized	395 (100, 99.1–100)	69 (100, 94.8–100)	86 (100, 95.8–100)	210 (100, 98.3–100)	1.0
PICU admission	94 (23.8, 19.7–28.3)	12 (18.8, 9.3–28.4)	34 (39.5, 29.2–50.7)	48 (22.9, 17.4–29.1)	0.002
Received any oxygen support	217 (54.9, 49.9–59.9)	29 (42.0, 30.2–54.5)	57 (66.3, 55.3–76.1)	131 (62.4, 55.5–69.0)	0.04

*PICU, pediatric intensive care unit.
†All indicators of disease severity included here were considered to be a result of COVID-19 illness.
‡p values were obtained from χ^2 test of patient characteristics across the 3 variant periods.

(51.2%) samples (183 inpatients and 1,053 outpatients; 654 Delta, 334 Omicron, and 189 other).

Ct Value Patterns across All Variants

We first evaluated overall patterns of Ct values among our dataset categories. Patients <1 year of age had significantly lower Ct values than the other age groups (adjusted p<0.0001 for 1–4 years, 5–11 years, and ≥12 years) (Table 3; Figure 2). We observed the same pattern among patients <1 year of age when limited to sequenced samples (adjusted p = 0.0003 for patients 1–4 years of age, adjusted p = 0.0002 for 5–11 years, and adjusted p = 0.0002 for ≥12 years) (Appendix Tables 6–8, Figure 1). Patients who received any number of vaccine doses had significantly higher Ct values than unvaccinated patients (adjusted p = 0.003). In addition, patients who had received a booster had significantly higher Ct values than unvaccinated patients (adjusted p = 0.0081).

Regarding potential disease severity indicators, we found that inpatients hospitalized with COVID-19 had significantly higher Ct values than both inpatients hospitalized because of COVID-19 (adjusted p<0.0001) and outpatients (adjusted p<0.0001). Ct values for inpatients hospitalized because of COVID-19 and outpatients did not differ significantly from each other (Table 3; Figure 2). Symptomatic patients had significantly lower Ct values than asymptomatic patients (adjusted p = 0.0081). Those tested soon after symptom onset had lower Ct values than patients tested 8–14 days after symptom onset (adjusted p<0.0001 for 0–3 days and 4–7 days after symptom onset). Similarly, Ct values were significantly lower in the groups tested 0–3 days and 4–7 days after symptom onset than in the 8–14 days group when limited to sequenced samples (adjusted p<0.0001 for 0–3 days, adjusted p = 0.0055 for 4–7 days) (Appendix Tables 6–8, Figure 1).

Among inpatients, we did not observe a significant difference in Ct values according to PICU admission status. However, those who received any type of supplemental oxygen support (invasive or noninvasive) and those who received noninvasive supplemental oxygen had lower Ct values than those who did not receive any form of supplemental oxygen (adjusted p = 0.0002 for any type of supplemental oxygen and adjusted p = 0.0012 for noninvasive supplemental oxygen).

Ct Value Patterns by Variant Period

We analyzed Ct value patterns for each dataset category across variant periods (Table 3; Figures 3, 4) as

Table 3. Mean nucleocapsid gene cycle threshold values by category in study of SARS-CoV-2 disease severity in children during pre-Delta, Delta, and Omicron periods, Colorado, USA, January 2021–January 2022*

Characteristic	Cycle threshold (±SD)			
	All	Pre-Delta period	Delta period	Omicron period
All	22.4 (6.79)	26.5 (6.96)	22.8 (7.81)	22.9 (5.51)
Age group, y				
<1	19.5 (6.54)	22.0 (7.49)	17.2 (6.64)	21.4 (5.79)
1–4	22.6 (6.74)	24.7 (6.53)	21.4 (7.61)	21.9 (4.82)
5–11	23.2 (6.61)	23.1 (7.07)	23.1 (6.85)	23.0 (5.44)
≥12	23.3 (6.73)	24.1 (7.28)	22.2 (6.77)	24.7 (5.39)
Time from symptom onset, d				
0–3	20.7 (6.32)	21.5 (6.36)	20.5 (6.95)	20.4 (4.71)
4–7	21.9 (5.85)	20.1 (5.02)	22.1 (6.49)	22.3 (4.47)
8–14	25.8 (5.58)	29.0 (6.22)	24.7 (5.79)	26.7 (3.48)
Vaccination status				
Unvaccinated	22.2 (6.53)	23.6 (7.17)	21.2 (7.31)	22.2 (5.53)
Vaccinated (any doses)	23.2 (6.76)	24.1 (6.99)	22.9 (6.87)	22.8 (4.67)
Partially vaccinated (1 dose)	23.4 (7.45)	28.5 (7.33)	21.0 (6.43)	23.7 (5.16)
Fully vaccinated (2 doses)	23.0 (6.59)	22.5 (6.51)	23.0 (6.91)	22.8 (4.80)
Fully vaccinated + booster	25.3 (6.81)	25.9 (6.92)	24.5 (7.26)	20.7 (3.04)
Disease severity				
Outpatient	22.1 (6.47)	22.4 (6.79)	21.4 (7.07)	21.9 (5.40)
Inpatient, hospitalized with COVID-19	26.2 (6.92)	27.9 (6.93)	24.3 (8.25)	25.5 (5.70)
Inpatient, hospitalized because of COVID-19	22.1 (6.31)	24.6 (6.62)	22.1 (7.53)	21.3 (4.75)
Symptomatic	21.5 (6.37)	21.6 (6.24)	21.7 (7.02)	21.4 (5.24)
Asymptomatic	22.5 (6.80)	23.7 (6.99)	21.6 (7.29)	22.4 (5.43)
Admitted to PICU because of COVID-19	21.9 (5.84)	22.5 (5.95)	22.3 (6.88)	21.0 (4.17)
Hospitalized but not admitted to PICU	22.1 (6.50)	25.3 (6.76)	21.9 (8.04)	21.3 (4.97)
No supplemental oxygen	24.3 (7.16)	27.8 (7.62)	22.3 (8.35)	23.5 (5.12)
Any supplemental oxygen	21.3 (5.82)	22.1 (6.55)	22.1 (6.60)	20.7 (4.79)
Noninvasive supplemental oxygen	21.4 (5.67)	22.2 (5.59)	22.7 (6.66)	20.4 (4.72)
Invasive supplemental oxygen	20.9 (6.82)	22.0 (10.2)	18.7 (5.40)	22.7 (5.35)

*PICU, pediatric intensive care unit.

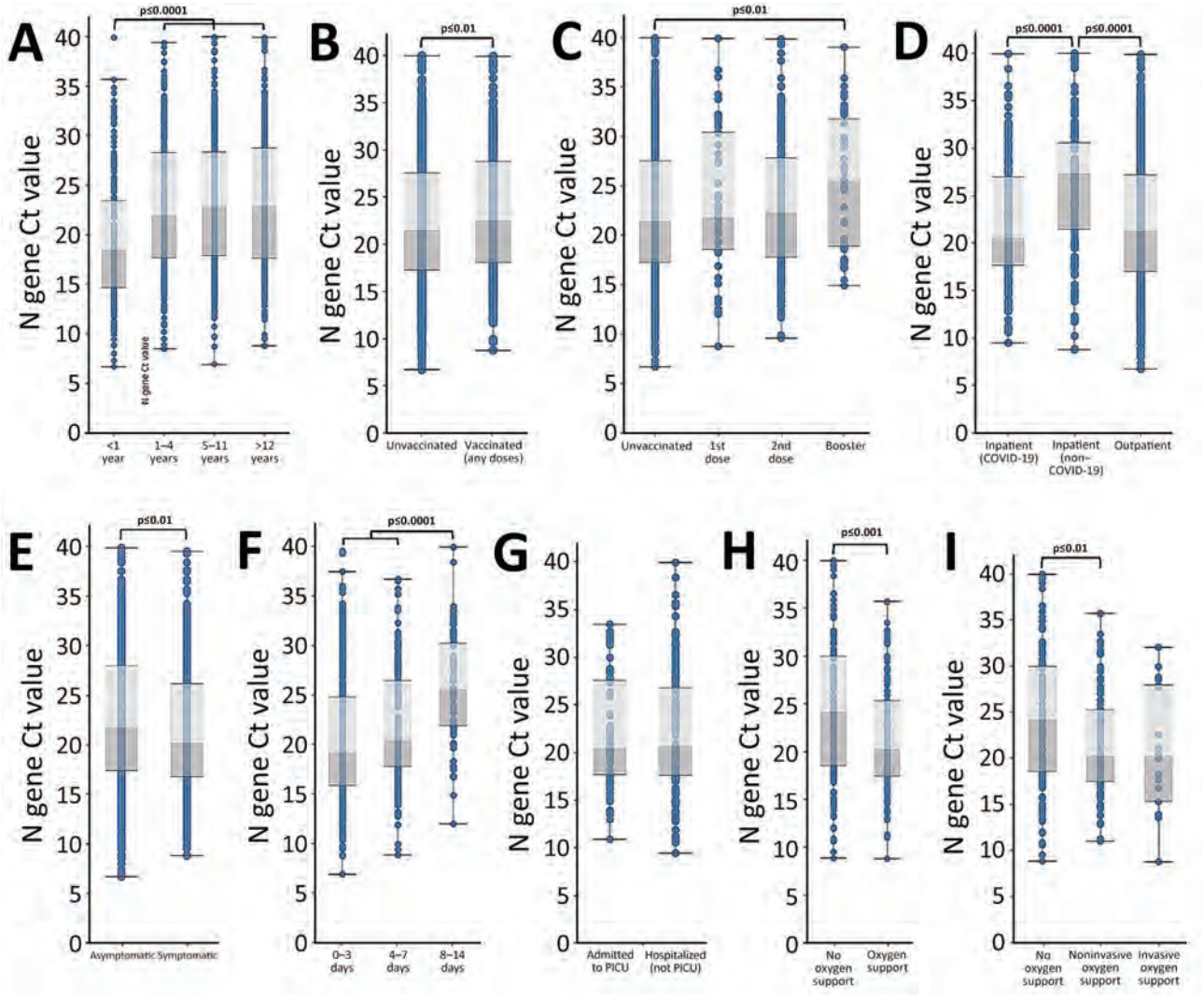

Figure 2. Ct value patterns across all variants in study of SARS-CoV-2 disease severity in children during pre-Delta, Delta, and Omicron periods, Colorado, USA, January 2021–January 2022. Boxplots indicate overall Ct value patterns across categories of patient characteristics, regardless of variant period. A) Age group; B) vaccination status (unvaccinated vs. vaccinated with any number of doses); C) vaccination status (unvaccinated versus vaccinated by number of doses); D) patient type (outpatient/not hospitalized, hospitalized because of COVID-19, hospitalized but not because of COVID-19); E) symptomatic versus asymptomatic; F) number of days between symptom onset and positive test (symptom onset groups); G) hospitalized but not admitted to PICU versus admitted to PICU; H) any type of supplemental oxygen support versus no oxygen support received; I) highest level of supplemental oxygen support received (none, noninvasive oxygen support, invasive oxygen support). Significance was determined using 1-way analysis of variance with Tukey test. Brackets indicate which comparisons correspond to the significance codes, and connected brackets indicate comparisons that have the same significance code. Ct, cycle threshold; PICU, pediatric intensive care unit.

well as among lineages for sequenced samples (Appendix Tables 6–8, Figures 2 and 3). Ct values were significantly lower during the Delta and Omicron periods than in the pre-Delta period (adjusted p value = 0.0004 for Delta period and adjusted p = 0.0003 for Omicron period) but did not differ significantly between Delta and Omicron (Table 3; Figure 3). We did not observe this pattern in the subset of sequenced samples (Appendix Tables 6–8, Figure 2). We observed a significant interaction between variant period and patient age (adjusted p = 0.001). Among patients infected during the Delta period, children <1 year of age had significantly lower Ct values than those ≥1 year of age (adjusted p = 0.0021 for children 1–4 years of age, adjusted p<0.0001 for 5–11 years, and adjusted p<0.0001 for ≥12 years) (Table 3; Figure 3). In addition, patients <1 year of age infected during Delta had significantly lower Ct values than children of the same age group infected during the Omicron period (adjusted p = 0.0156). Patients infected

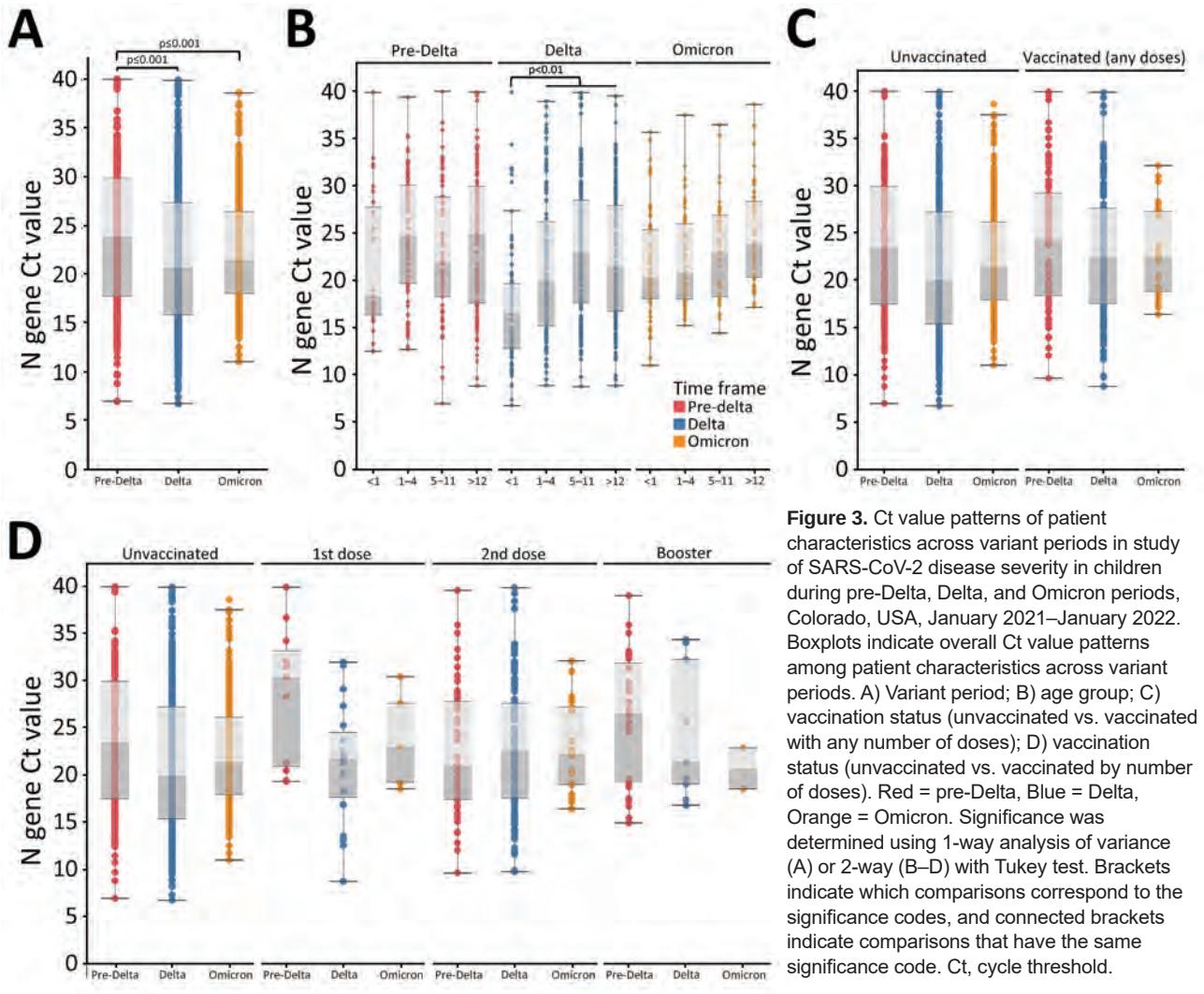

Figure 3. Ct value patterns of patient characteristics across variant periods in study of SARS-CoV-2 disease severity in children during pre-Delta, Delta, and Omicron periods, Colorado, USA, January 2021–January 2022. Boxplots indicate overall Ct value patterns among patient characteristics across variant periods. A) Variant period; B) age group; C) vaccination status (unvaccinated vs. vaccinated with any number of doses); D) vaccination status (unvaccinated vs. vaccinated by number of doses). Red = pre-Delta, Blue = Delta, Orange = Omicron. Significance was determined using 1-way analysis of variance (A) or 2-way (B–D) with Tukey test. Brackets indicate which comparisons correspond to the significance codes, and connected brackets indicate comparisons that have the same significance code. Ct, cycle threshold.

during the Delta period who were 1–4 years of age had lower Ct values than children in the same age group who were infected during the pre-Delta period (adjusted p = 0.031). We did not observe a significant interaction between lineage and patient age among sequenced samples (Appendix Tables 6–8, Figure 2). Furthermore, we did not observe a significant interaction between either variant period or sequenced lineage and vaccination status (Table 3; Figure 3; Appendix Tables 6–8, Figure 2).

When we evaluated potential indicators of disease severity across variant periods, we did not observe a statistically significant interaction between the variant period and patient type (inpatient because of COVID-19 vs. outpatient), the presence or absence of symptoms, days from symptom onset, or whether inpatients were admitted to the PICU (Table 3; Figure 4). Among patients who did not receive supplemental oxygen, those infected during the pre-Delta period had higher Ct values than those infected during the Delta (adjusted p = 0.0017) or Omicron (adjusted p = 0.0238) periods, in addition to having higher Ct values than children infected during pre-Delta who received supplemental oxygen (adjusted p = 0.0121). However, when compared by the highest level of supplemental oxygen support received (none, invasive, or noninvasive), results were not statistically significant. Among sequenced samples, we did not observe any statistically significant interactions between lineage and disease severity indicators, likely because of Ct value bias and smaller sample sizes (Appendix Tables 6–8, Figure 3).

Discussion

We found that children infected with SARS-CoV-2 during the Delta and Omicron periods had lower Ct values (suggesting higher viral load) than children infected during the pre-Delta period. Patients who

were <1 year of age had lower Ct values than children in other age groups, a pattern potentially driven by Delta. In addition, inpatients with symptomatic infections had lower Ct values than asymptomatic inpatients, but we did not observe significant differences in Ct values among disease severity markers among variant periods. Therefore, Ct value might not be a strong correlate of disease severity outcomes across variant periods in children. During the Delta and Omicron periods, a greater proportion of inpatients were symptomatic, hospitalized in the PICU, or received oxygen support because of COVID-19 than during the pre-Delta period, but those proportions did not differ significantly between Delta and Omicron. This finding suggests that, for hospitalized children, Delta and Omicron infections might be more severe than earlier variants, regardless of Ct value.

Although many studies have evaluated relationships between SARS-CoV-2 variants and Ct values or viral load (*6*,*7*), transmission (*23*), and symptom severity (*3*,*5*,*7*) in adults, fewer studies have focused on children. Therefore, the effects of SARS-CoV-2 variant on Ct values or viral load and symptom severity in this population remain poorly understood.

Previous studies in adults observed that those infected by Delta exhibit higher viral loads (*6*) than those infected by previous variants and those infected by Omicron exhibit similar viral loads to those infected by Delta (*7*). Consistent with our results, previous studies in children observed lower Ct values in hospitalized children infected with Delta and Omicron than for previous variants (*15*). On the other hand, studies regarding the relationship between viral load and patient age yielded mixed results (*24*). Consistent with our results, others have found that infants (*25*) and young children (*26*,*27*) exhibit higher viral loads

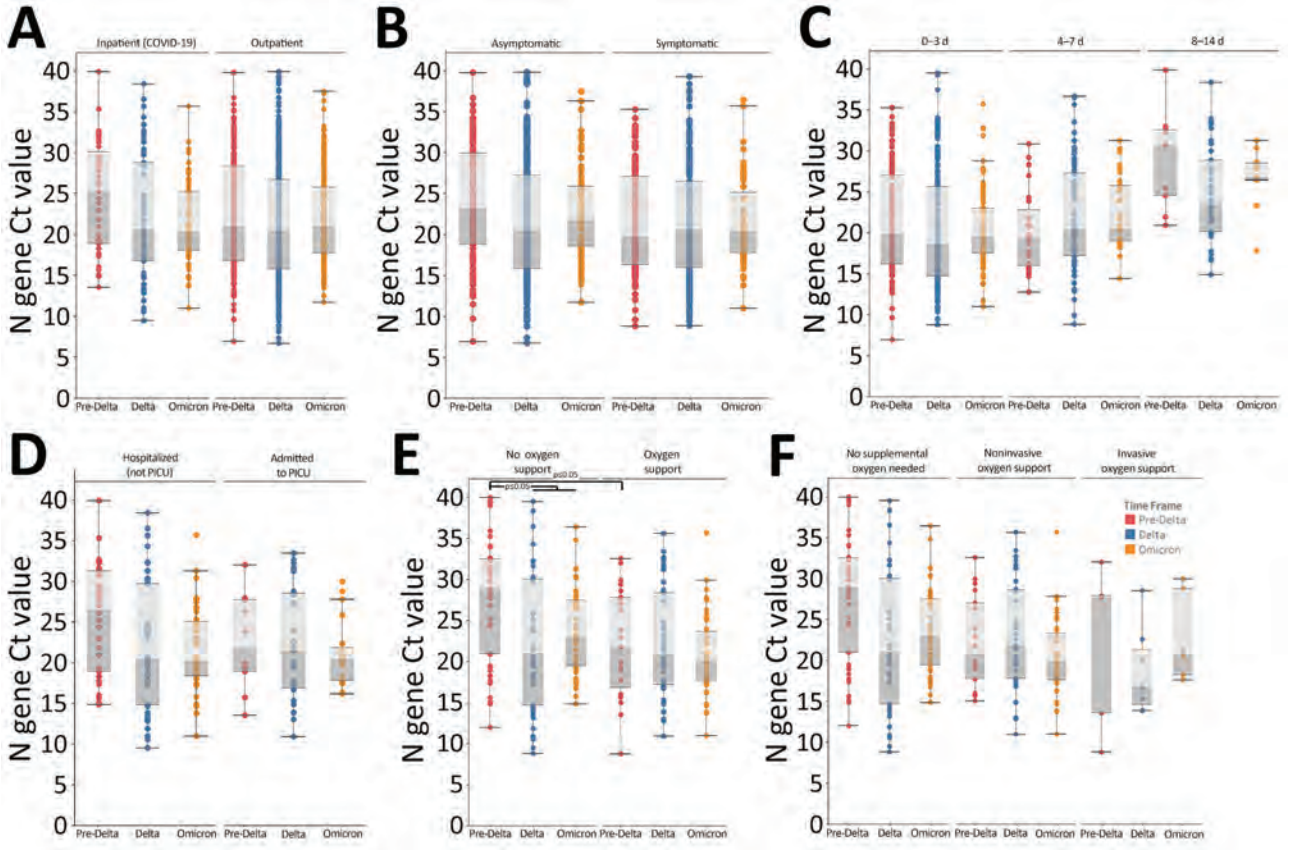

Figure 4. Ct value patterns among markers of disease severity across variant periods in study of SARS-CoV-2 disease severity in children during pre-Delta, Delta, and Omicron periods, Colorado, USA, January 2021–January 2022. Boxplots indicate overall Ct value patterns across disease severity markers by variant period. A) Patient type (outpatient/not hospitalized, hospitalized because of COVID-19); B) symptomatic versus asymptomatic; C) number of days between symptom onset and positive test (symptom onset groups); D) hospitalized but not admitted to PICU versus admitted to PICU; E) any type of supplemental oxygen support versus no oxygen support received; F) highest level of supplemental oxygen support received (none, noninvasive oxygen support, invasive oxygen support). Red = pre-Delta, Blue = Delta, Orange = Omicron. Significance was determined using 2-way analysis of variance with Tukey test. Brackets indicate which comparisons correspond to the significance codes, and connected brackets indicate comparisons that have the same significance code. Ct, cycle threshold; PICU, pediatric intensive care unit.

than older children. One study observed that older children exhibit similar viral loads to adults (*25*), whereas others found no significant effect of age on viral load (*28*–*30*). Therefore, more work with larger sample sizes or meta-analyses will be required to describe the relationship between age and Ct values or viral load in pediatric cases.

Although not directly addressed in this study, differences in viral loads among age groups or among SARS-CoV-2 variants have the potential to influence SARS-CoV-2 transmission dynamics. Early household transmission studies found that children transmit SARS-CoV-2 at lower rates than adults (*23*,*31*). However, more recent studies showed increased transmission by children in schools (*32*) and athletic facilities (*33*) during Delta compared with earlier variants. In addition, Omicron is more contagious than previous variants, including Delta (*34*). Finally, Costa et al. (*29*) found faster RNA clearance in children than in adults, suggesting a shorter viral shedding period, which might contribute to differing transmission dynamics between adults and children. This finding suggests that children might have a more significant effect on SARS-CoV-2 transmission dynamics than previously thought.

Consistent with our study, Chung et al. (*28*) found lower Ct values in symptomatic children than asymptomatic children. However, we did not observe a significant relationship between Ct values and markers of disease severity across variant periods among hospitalized children. Instead, higher proportions of hospitalized children exhibited disease severity markers during the Delta and Omicron periods than during pre-Delta, regardless of Ct values. Similarly, Quintero et al. (*15*) found that children infected by Delta were more likely to be symptomatic than those infected by earlier variants, and Mitchell et al. (*35*) found the highest proportion of PICU admissions after the emergence of Omicron. A review by Khemiri et al. (*36*) observed similar clinical manifestations in children and adults infected by Delta and Omicron. Furthermore, children, particularly those <5 years of age, were at higher risk for hospitalization (*8*,*37*–*39*) and had a higher incidence of croup (*40*) during Omicron than during earlier variants. In sum, those studies suggest that Delta and Omicron infections might be more severe in children than previous variants.

The first limitation of our study is that analyses of the relationship between WGS-based SARS-CoV-2 lineage calls and Ct values might be biased toward lower Ct values because the CDPHE Laboratory uses a cutoff of <28 Ct for WGS. As such, we performed our analyses using variant periods to include all samples for which we had Ct data, regardless of whether they were successfully sequenced, with the understanding that a small number of samples might be assigned to the incorrect variant period. We found that our analysis lost some power when only looking at samples that were successfully sequenced, but the results largely agree with the full dataset that used variant periods. Second, although the relationship between Ct values and quantitative viral load are not exact, they are tightly inversely correlated (*13*). Because we used a single quantitative RT-PCR protocol and platform for all samples, we expect the Ct patterns, as they relate to viral load, to be consistent. Third, whether samples with high Ct values represent the beginning or end of infection is unclear. However, it is assumed that most patients are tested early in the course of infection. Fourth, because we concluded data collection in January 2022, our analyses of Omicron only include the sublineages BA.1.1.529, BA.1, and BA.1.1. Because of the rapid evolution of SARS-CoV-2, numerous Omicron sublineages have emerged since and are not included here. Those other sublineages could exhibit different characteristics, such as different Ct values and altered transmissibility or virulence (*34*). Future work could address those differences among Omicron sublineages. Finally, our analyses only included Colorado residents and therefore might not be generalizable to other jurisdictions or geographic locations.

Our study provides insight into the relationship between Ct values, the presence of symptoms, and disease severity markers across variant periods. A strength of our study is the inclusion of in-depth data for both inpatient and outpatient populations. Similar studies are limited to performing in-depth analyses on Ct values to inpatient populations (*37*). In addition, our study is unique in its integration of clinical and laboratory data. Furthermore, rather than relying on RT-PCR of a small number of mutations to delineate variant periods, we were able to use entire genomes, enabling more accurate lineage determination.

In conclusion, our results suggest that children infected with either Delta or Omicron had lower Ct values (suggesting higher viral load) and potentially greater disease severity than children infected with earlier variants. Those patterns were particularly pronounced in the youngest children (<1 year of age). Our data highlight the importance of monitoring children, particularly in younger age groups, as new variants emerge and including pediatric cases in surveillance efforts for current and future SARS-CoV-2 variants to understand the potential differences in Ct values and viral loads, transmission, and disease severity across the age spectrum.

Acknowledgments

We thank the Microbiology Laboratory at CHCO for submitting samples to the CDPHE Lab, the accessioning team at the CDPHE lab for logging in all samples, and the sequencing team for sample processing. We thank Brian Erly for helpful comments and edits on an earlier draft.

The data included in this work were generated for public health surveillance purposes and was funded by 6 NU50CK000552-02-01 Epidemiology and Laboratory Capacity for Infectious Diseases (ELC) and NU-50CK000483 Emerging Infections Program (EIP) Cooperative Agreements from the Centers for Disease Control and Prevention.

About the Author

Dr. Bankers is the Bioinformatics and Genomic Analysis supervisor at the Colorado Department of Public Health and Environment Laboratory in Denver. Her research interests focus on the intersection of evolutionary genomics, pathogen genomic surveillance, and public health.

References

1. Harvey WT, Carabelli AM, Jackson B, Gupta RK, Thomson EC, Harrison EM, et al.; COVID-19 Genomics UK (COG-UK) Consortium. SARS-CoV-2 variants, spike mutations and immune escape. Nat Rev Microbiol. 2021;19:409–24. https://doi.org/10.1038/s41579-021-00573-0
2. Telenti A, Hodcroft EB, Robertson DL. The evolution and biology of SARS-CoV-2 variants. Cold Spring Harb Perspect Med. 2022;12:a041390. https://doi.org/10.1101/cshperspect.a041390
3. Twohig KA, Nyberg T, Zaidi A, Thelwall S, Sinnathamby MA, Aliabadi S, et al.; COVID-19 Genomics UK (COG-UK) consortium. Hospital admission and emergency care attendance risk for SARS-CoV-2 delta (B.1.617.2) compared with alpha (B.1.1.7) variants of concern: a cohort study. Lancet Infect Dis. 2022;22:35–42. https://doi.org/10.1016/S1473-3099(21)00475-8
4. Lambrou AS, Shirk P, Steele MK, Paul P, Paden CR, Cadwell B, et al.; Strain Surveillance and Emerging Variants Bioinformatic Working Group; Strain Surveillance and Emerging Variants NS3 Working Group. Genomic surveillance for SARS-CoV-2 variants: predominance of the Delta (B.1.617.2) and Omicron (B.1.1.529) variants—United States, June 2021–January 2022. MMWR Morb Mortal Wkly Rep. 2022;71:206–11. https://doi.org/10.15585/mmwr.mm7106a4
5. Taylor CA, Patel K, Pham H, Whitaker M, Anglin O, Kambhampati AK, et al.; COVID-NET Surveillance Team. Severity of disease among adults hospitalized with laboratory-confirmed COVID-19 before and during the period of SARS-CoV-2 B.1.617.2 (Delta) predominance—COVID-NET, 14 states, January–August 2021. MMWR Morb Mortal Wkly Rep. 2021;70:1513–9. https://doi.org/10.15585/mmwr.mm7043e1
6. Wang Y, Chen R, Hu F, Lan Y, Yang Z, Zhan C, et al. Transmission, viral kinetics and clinical characteristics of the emergent SARS-CoV-2 Delta VOC in Guangzhou, China. EClinicalMedicine. 2021;40:101129. https://doi.org/10.1016/j.eclinm.2021.101129
7. Ulloa AC, Buchan SA, Daneman N, Brown KA. Estimates of SARS-CoV-2 Omicron variant severity in Ontario, Canada. JAMA. 2022;327:1286–8. https://doi.org/10.1001/jama.2022.2274
8. Taylor CA, Whitaker M, Anglin O, Milucky J, Patel K, Pham H, et al.; COVID-NET Surveillance Team. COVID-19–associated hospitalizations among adults during SARS-CoV-2 Delta and Omicron variant predominance, by race/ethnicity and vaccination status—COVID-NET, 14 states, July 2021–January 2022. MMWR Morb Mortal Wkly Rep. 2022;71:466–73. https://doi.org/10.15585/mmwr.mm7112e2
9. Ferdinands JM, Rao S, Dixon BE, Mitchell PK, DeSilva MB, Irving SA, et al. Waning 2-dose and 3-dose effectiveness of mRNA vaccines against COVID-19–associated emergency department and urgent care encounters and hospitalizations among adults during periods of Delta and Omicron variant predominance—VISION Network, 10 states, August 2021–January 2022. MMWR Morb Mortal Wkly Rep. 2022;71:255–63. https://doi.org/10.15585/mmwr.mm7107e2
10. Delahoy MJ, Ujamaa D, Whitaker M, O'Halloran A, Anglin O, Burns E, et al.; COVID-NET Surveillance Team. Hospitalizations associated with COVID-19 among children and adolescents—COVID-NET, 14 states, March 1, 2020–August 14, 2021. MMWR Morb Mortal Wkly Rep. 2021;70:1255–60. https://doi.org/10.15585/mmwr.mm7036e2
11. Wang L, Berger NA, Kaelber DC, Davis PB, Volkow ND, Xu R. Incidence rates and clinical outcomes of SARS-CoV-2 infection with the Omicron and Delta variants in children younger than 5 years in the US. JAMA Pediatr. 2022;176:811–3. https://doi.org/10.1001/jamapediatrics.2022.0945
12. Belay ED, Godfred-Cato S. SARS-CoV-2 spread and hospitalisations in paediatric patients during the Omicron surge. Lancet Child Adolesc Health. 2022;6:280–1. https://doi.org/10.1016/S2352-4642(22)00060-8
13. Walker AS, Pritchard E, House T, Robotham JV, Birrell PJ, Bell I, et al. Ct threshold values, a proxy for viral load in community SARS-CoV-2 cases, demonstrate wide variation across populations and over time. eLife. 2021;10:e64683.
14. Rostad CA, Kamidani S, Anderson EJ. Implications of SARS-CoV-2 viral load in children: getting back to school and normal. JAMA Pediatr. 2021;175:e212022. https://doi.org/10.1001/jamapediatrics.2021.2022
15. Quintero AM, Eisner M, Sayegh R, Wright T, Ramilo O, Leber AL, et al. Differences in SARS-CoV-2 clinical manifestations and disease severity in children and adolescents by infecting variant. Emerg Infect Dis. 2022;28:2270–80. https://doi.org/10.3201/eid2811.220577
16. DNA Pipelines R&D, Farr B, Rajan D, Betteridge E, Shirley L, Quail M, et al. COVID-19 ARTIC v3 Illumina library construction and sequencing protocol. 2020 Nov 4 [cited 2022 Feb 15]. https://www.protocols.io/view/covid-19-artic-v3-illumina-library-construction-an-j8nlke665l5r/v5
17. Quick J. nCoV-2019 sequencing protocol v3 (LoCost). 2020 Aug 25 [cited 2022 Feb 15]. https://www.protocols.io/view/ncov-2019-sequencing-protocol-v3-locost-bp2l6n26rgqe/v3
18. Illumina CovidSeq Test. Instructions for use [cited 2022 Feb 15]. https://support.illumina.com/content/dam/illumina-support/documents/documentation/chemistry_documentation/Illumina-COVIDSeq-Test/illumina-covidseq-test-instructions-for-use-1000000128490-03.PDF
19. The Broad Institute. Terra [cited 2022 Feb 22]. https://app.terra.bio
20. Colorado Department of Public Health and Environment. CDPHE-bioinformatics/CDPHE-SARS-CoV-2 [cited 2022

Feb 22]. https://github.com/CDPHE-bioinformatics/CDPHE-SARS-CoV-2
21. Colorado Department of Public Health and Environment. CDPHEsarscov2 [cited 2022 Feb 22]. https://dockstore.org/organizations/CDPHE/collections/CDPHEsarscov2
22. Tableau (version. 9.1). J Med Libr Assoc. 2016;104:182–3. https://doi.org/10.3163/1536-5050.104.2.022
23. Silverberg SL, Zhang BY, Li SNJ, Burgert C, Shulha HP, Kitchin V, et al. Child transmission of SARS-CoV-2: a systematic review and meta-analysis. BMC Pediatr. 2022;22:172. https://doi.org/10.1186/s12887-022-03175-8
24. Bayhan Gİ, Özkubat Korkmaz I, Şahiner ES, Tekeli N, Akdağ AG, Uyan Erten AZ, et al. Are SARS-CoV-2 viral loads in children lower than in adults? J Infect. 2023;86:e13–4. https://doi.org/10.1016/j.jinf.2022.08.025
25. Ochoa V, Díaz FE, Ramirez E, Fentini MC, Carobene M, Geffner J, et al.; INBIRS COVID-19 Study Group. Infants younger than 6 months infected with SARS-CoV-2 show the highest respiratory viral loads. J Infect Dis. 2022;225:392–5. https://doi.org/10.1093/infdis/jiab577
26. Cendejas-Bueno E, Romero-Gómez MP, Escosa-García L, Jiménez-Rodríguez S, Mingorance J, García-Rodríguez J; SARS-CoV-2 Working Group. Lower nasopharyngeal viral loads in pediatric population. The missing piece to understand SARS-CoV-2 infection in children? J Infect. 2021;83:e18–9. https://doi.org/10.1016/j.jinf.2021.06.009
27. Heald-Sargent T, Muller WJ, Zheng X, Rippe J, Patel AB, Kociolek LK. Age-related differences in nasopharyngeal severe acute respiratory syndrome coronavirus 2 (SARS-CoV-2) levels in patients with mild to moderate coronavirus disease 2019 (COVID-19). JAMA Pediatr. 2020; 174:902–3. https://doi.org/10.1001/jamapediatrics.2020.3651
28. Chung E, Chow EJ, Wilcox NC, Burstein R, Brandstetter E, Han PD, et al. Comparison of symptoms and RNA levels in children and adults with SARS-CoV-2 infection in the community setting. JAMA Pediatr. 2021;175:e212025–212025. https://doi.org/10.1001/jamapediatrics.2021.2025
29. Costa R, Bueno F, Albert E, Torres I, Carbonell-Sahuquillo S, Barrés-Fernández A, et al. Upper respiratory tract SARS-CoV-2 RNA loads in symptomatic and asymptomatic children and adults. Clin Microbiol Infect. 2021;27:1858.e1–7. https://doi.org/10.1016/j.cmi.2021.08.001
30. Yonker LM, Boucau J, Regan J, Choudhary MC, Burns MD, Young N, et al. Virologic features of severe acute respiratory syndrome coronavirus 2 infection in children. J Infect Dis. 2021;224:1821–9. https://doi.org/10.1093/infdis/jiab509
31. Maltezou HC, Vorou R, Papadima K, Kossyvakis A, Spanakis N, Gioula G, et al. Transmission dynamics of SARS-CoV-2 within families with children in Greece: a study of 23 clusters. J Med Virol. 2021;93:1414–20. https://doi.org/10.1002/jmv.26394
32. Torjesen I. Covid-19: Delta variant is now UK's most dominant strain and spreading through schools. BMJ. 2021;373:n1445. https://doi.org/10.1136/bmj.n1445
33. Sheikh A, McMenamin J, Taylor B, Robertson C; Public Health Scotland and the EAVE II Collaborators. SARS-CoV-2 Delta VOC in Scotland: demographics, risk of hospital admission, and vaccine effectiveness. Lancet. 2021;397:2461–2. https://doi.org/10.1016/S0140-6736(21)01358-1
34. Setiabudi D, Sribudiani Y, Hermawan K, Andriyoko B, Nataprawira HM. The Omicron variant of concern: the genomics, diagnostics, and clinical characteristics in children. Front Pediatr. 2022;10:898463. https://doi.org/10.3389/fped.2022.898463
35. Mitchell R, Cayen J, Thampi N, Frenette C, Bartoszko J, Choi KB, et al. Trends in severe outcomes among adult and pediatric patients hospitalized with COVID-19 in the Canadian Nosocomial Infection Surveillance Program, March 2020 to May 2022. JAMA Netw Open. 2023;6:e239050. https://doi.org/10.1001/jamanetworkopen.2023.9050
36. Khemiri H, Ayouni K, Triki H, Haddad-Boubaker S. SARS-CoV-2 infection in pediatric population before and during the Delta (B.1.617.2) and Omicron (B.1.1.529) variants era. Virol J. 2022;19:144. https://doi.org/10.1186/s12985-022-01873-4
37. Acker KP, Levine DA, Varghese M, Nash KA, RoyChoudhury A, Abramson EL, et al. Indications for hospitalization in children with SARS-CoV-2 infection during the Omicron wave in New York City. Children (Basel). 2022;9:1043. https://doi.org/10.3390/children9071043
38. Iuliano AD, Brunkard JM, Boehmer TK, Peterson E, Adjei S, Binder AM, et al. Trends in disease severity and health care utilization during the early Omicron variant period compared with previous SARS-CoV-2 high transmission periods—United States, December 2020–January 2022. MMWR Morb Mortal Wkly Rep. 2022;71:146–52. https://doi.org/10.15585/mmwr.mm7104e4
39. Marks KJ, Whitaker M, Agathis NT, Anglin O, Milucky J, Patel K, et al.; COVID-NET Surveillance Team. Hospitalization of infants and children aged 0–4 years with laboratory-confirmed COVID-19—COVID-NET, 14 states, March 2020–February 2022. MMWR Morb Mortal Wkly Rep. 2022;71:429–36. https://doi.org/10.15585/mmwr.mm7111e2
40. Iijima H, Kubota M, Ogimi C. Clinical characteristics of pediatric patients with COVID-19 between Omicron era vs. pre-Omicron era. J Infect Chemother. 2022;28:1501–5. https://doi.org/10.1016/j.jiac.2022.07.016

Address for correspondence: Laura Bankers, Colorado Department of Public Health and Environment, 8100 E Lowry Blvd, Denver, CO 80230, USA; email: laura.bankers@state.co.us

Lack of Transmission of Chronic Wasting Disease Prions to Human Cerebral Organoids

Bradley R. Groveman,[1] Katie Williams,[1] Brent Race, Simote Foliaki, Tina Thomas, Andrew G. Hughson, Ryan O. Walters, Wenquan Zou, Cathryn L. Haigh

Chronic wasting disease (CWD) is a cervid prion disease with unknown zoonotic potential that might pose a risk to humans who are exposed. To assess the potential of CWD to infect human neural tissue, we used human cerebral organoids with 2 different prion genotypes, 1 of which has previously been associated with susceptibility to zoonotic prion disease. We exposed organoids from both genotypes to high concentrations of CWD inocula from 3 different sources for 7 days, then screened for infection periodically for up to 180 days. No de novo CWD propagation or deposition of protease-resistant forms of human prions was evident in CWD-exposed organoids. Some persistence of the original inoculum was detected, which was equivalent in prion gene knockout organoids and thus not attributable to human prion propagation. Overall, the unsuccessful propagation of CWD in cerebral organoids supports a strong species barrier to transmission of CWD prions to humans.

Chronic wasting disease (CWD) is a member of the prion family of fatal, infectious neurodegenerative diseases. CWD affects cervids, such as moose, elk, and several species of deer, across much of North America, South Korea, and certain countries in northern Europe, including Norway, Finland, and Sweden (*1*). CWD is the most transmissible of the prion disease family; transmission between cervids is highly efficient. Another member of the prion disease family, bovine spongiform encephalopathy (BSE), has transmitted to humans and caused the emergence of variant Creutzfeldt-Jakob disease (vCJD). That transmission is widely believed to have occurred through ingestion of contaminated food. Subsequently, concern is ongoing as to whether CWD prions could likewise infect humans because of the high likelihood of CWD-tainted meat entering the human food chain.

Prions are formed by the conversion of the normal cellular prion protein (PrP) into abnormally folded isoforms. The current understanding is that, once formed, prions continue to propagate themselves by recruiting normally folded PrP molecules, which then undergo templated conversion into new prions (*2*,*3*). In humans, the amino acid sequence of PrP influences disease susceptibility, manifestation, and clinical course. A single amino acid polymorphism at codon 129 has been shown to influence susceptibility to prion disease, disease duration, phenotype, and the propensity of PrP to form amyloid (*4*,*5*). Persons can be homozygous for methionine (MM) or valine (VV) at codon 129 or heterozygous (MV), with the prevalence of each allele varying by geographic location (*5*). Worldwide, the 129 MM and MV genotypes comprise ≈80%–100% of the population (*5*). When BSE crossed the species barrier and transmitted to humans, the MM polymorphism was present in most symptomatic patients; only 1 possible and 1 confirmed case in patients carrying the MV polymorphism were identified (*6*–*8*). After the BSE epidemic, histological screening of appendices was used to attempt an approximation of the prevalence of preclinical or subclinical vCJD. This screening found abnormal PrP in all 3 genotypes in the ratio of 2:1:1 (MM:MV:VV), which indicated BSE infection might be possible in persons of all 3 genotypes (*9*). That finding is, however, confounded by the finding of the follow-up appendix-3 survey that abnormal PrP was present in 2 appendices

Author affiliations: Rocky Mountain Laboratories, National Institute of Allergy and Infectious Diseases, Hamilton, Montana, USA (B.R. Groveman, K. Williams, B. Race, S. Foliaki, T. Tomas, A.G. Hughson, R.O. Walters, C.L. Haigh); Jiangxi Academy of Clinical Medical Sciences, The First Affiliated Hospital of Nanchang University, Nanchang, China (W. Zou)

DOI: https://doi.org/10.3201/eid3006.231568

[1]These authors contributed equally to this article.

removed before the known BSE exposure period (*10*). Therefore, although the onset of BSE exposures might have begun sooner than originally realized, resulting in earlier silent infections, a low background of abnormal (but not necessarily pathogenic) PrP could possibly be present in lymphoid tissue of the wider population, independent of BSE exposure (*10*). Despite this possibility, most patients who contracted vCJD from BSE-infected meat had methionine homozygosity at codon 129, supporting increased susceptibility of this genotype to infection.

In attempts to ascertain the risk to humans posed by CWD-tainted meat or other cervid-derived products, various studies have looked at the propensity of cervid prions to cross the species barrier, seed the conversion of human prions, and by inference determine the likelihood of causing human disease. In vitro studies have demonstrated that CWD prions can seed human PrP substrates (*11*,*12*), although conversion of human PrP was less efficient than for cervid PrP (*12*). Transmission studies in mice have principally shown that CWD prions do not readily infect transgenic mice expressing either normal or very high levels of human PrP (*13*–*17*). However, using the highly sensitive real-time quaking-induced conversion (RT-QuIC) assay, low levels of PrP seeding activity could be detected in 4/50 *tg66* mice inoculated with either elk or whitetail deer CWD, in the absence of any other indicators of disease (*18*). The *tg66* mice express levels of human PrP 8–16-fold above normal; when the same inocula were tested in mice expressing only 2–4-fold higher levels, no seeding activity was detected. Follow-up experiments passaging brain material from those 4 mice demonstrated a lack of prion infectivity in the brain, suggesting that what was detected was likely residual inoculum, or false-positive reactions, and not transmissible disease (*19*). Conversely, a different study indicated putative transmission, finding RT-QuIC activity in 77.7% of CWD-inoculated *tg650* mice (6-fold overexpression of human PrP); 44.4% displayed progressive clinical signs (myoclonus) although only 1 mouse had histochemical abnormalities (*20*). Any potential transmission is cause for concern; thus, models that more closely represent humans are required.

The need for models that are more closely related to humans has been partially addressed using nonhuman primates. Transmission of CWD to squirrel monkeys has been readily demonstrated but, to date, transmission studies in cynomolgus macaques (a closer laboratory animal model to humans than squirrel monkeys) have not shown evidence of prion disease (*21*,*22*). In those studies, no markers of prion infection were found in macaques euthanized as many as 13 years after inoculation with CWD (*22*). In contrast, BSE readily transmitted to macaques, causing behavioral and cerebellar signs and progressing to extremely severe ataxia within a few weeks of initial clinical signs (*23*). For adult animals, euthanasia was required at ≈160 weeks after inoculation. This encouraging difference between BSE and CWD supports a strong species barrier against CWD infecting humans.

To further address those questions of susceptibility, we used human cerebral organoids (hCOs) to model CWD infection in human neural tissue. hCOs are spheres of self-structuring brain tissue grown in a dish and are the closest model to human brain currently available. They are susceptible to infection with human prions and faithfully propagate the infecting prion strain (*24*,*25*). Using the predominant codon 129 genotypes, including the most susceptible to BSE (129MM) and the most common codon 129 genotype in many countries (129MV), we sought to determine whether CWD infection could be established in human cerebral organoid cultures by direct exposure to high titers of CWD prions.

Methods

Human-Induced Pluripotent Stem Cells and Culture

The production and routine maintenance of the human-induced pluripotent stem cells (hu-iPSCs) used in this study have been described in detail previously (*25*). In brief, codon 129MV (ACS-1023; ATCC) and 129MM hu-iPSCs (RAH019A) (*26*) were routinely cultured on low growth factor Matrigel in mTeSR1 Plus medium with 5% CO_2 in a humidified incubator and passaged before colonies started to contact each other.

CRISPR/Cas9 Knockout of PRNP

Knockout (KO) of PRNP by CRISPR/Cas9 cloning was performed by Applied StemCell (https://www.appliedstemcell.com). The guide RNAs G1 GCTTCGGGCGCTTCTTGCAG and G2 CTGGGGGCAGCCGATACCCG were used to introduce a frameshift mutation around aa 21 (within the N terminal signal sequence) (Appendix, https://wwwnc.cdc.gov/EID/article/30/6/23-1568-App1.pdf).

Human Cerebral Organoid Generation and Routine Culture

We generated cerebral organoids using the cerebral organoid differentiation kit (StemCell Technologies, https://www.stemcell.com), which follows the protocol described in Lancaster et al. (*27*). After

differentiation, cultures were maintained in conical flasks on an orbital shaker at 80 rpm in complete maintenance medium: 1 × glutamax, 1 × penicillin/streptomycin solution, 0.5% vol/vol N2, 1% vol/vol B12 with retinoic acid (all ThermoFisher Scientific, https://www.thermofisher.com) and 0.5 × nonessential amino acids, 0.025% vol/vol insulin, and 0.00035% vol/vol 2-Merceptoethanol (all Sigma-Aldrich, https://www.sigmaaldrich.com) in 1:1 Neurobasal:DME-F12 medium (ThermoFisher Scientific), under standard incubator conditions (5% CO_2, 37°C, humidified).

Prion Infections of Human Cerebral Organoids

We cultured hCOs for 5 months before infection to enable the development of astrocytes and maturation of neurons (*28*). We diluted previously characterized brain homogenates (*29*) from an uninfected deer, a pool of 6 CWD-infected mule deer, a pool of 7 CWD-infected white-tailed deer, an uninfected elk, a pool of 6 CWD-infected elk, and sporadic CJD (sCJD) (MV2) into organoid maintenance media to a final concentration of 0.1% (tissue wet) wt/vol (Table). Control sCJD brain homogenate was a kind gift from Gianluigi Zanusso (University of Verona, Italy). At the start of infection, existing media were removed from the organoids and replaced with the inoculated media. At 24 hours after inoculation, we added an equivalent volume of fresh media to the cultures (diluting the original inoculum 1:1). We performed a full media and vessel exchange 7 days after initial exposure.

RT-QuIC Analysis

We performed RT-QuIC assays as previously described (*25*). We homogenized organoids to 10% wt/vol in phosphate-buffered saline by motorized pestle and cleared by centrifugation at 2,000 × *g* for 2 minutes. We serially diluted organoid homogenates diluted in 0.1% sodium dodecyl sulfate/phosphate-buffered saline/N2 solution to 0.1% wt/vol, a 10^{-3} dilution, and loaded 1 µL into each well of a black 384-well plate with a clear bottom (Nunc) containing 49 µL of reaction mixture. RT-QuIC reaction mix contained 10 mM phosphate buffer (pH 7.4), 300 mM NaCl, 0.1 mg/ml of truncated hamster recombinant PrP (amino acids 90–231), 10 µM thioflavin T (ThT), 0.002% SDS (contributed by homogenate dilution), and 1 mM ethylenediaminetetraacetic acid tetrasodium salt (EDTA). We sealed plates using a Nalgene Nunc International sealer (ThermoFisher Scientific) and incubated in a FLUOstar Omega plate reader (BMG LabTech, https://www.bmglabtech.com) at 50°C with cycles of 60 seconds of shaking (700 rpm, double-orbital) and 60 seconds of rest throughout the 50-hour incubation time. We took ThT fluorescence measurements (excitation, 450 ± 10 nm; emission, 480 ± 10 nm [bottom read]) every 45 minutes. We ran quadruplicate reactions for each sample. We considered an individual reaction positive if its maximum fluorescence reading within 50 hours was >10% of the maximum fluorescence reading in the experiment. We considered a sample positive if >25% of the replicate reactions were scored as positive. We performed estimates of the concentrations of seeding activity using endpoint dilution analysis and calculated with Spearman-Kärber analyses as previously described (*25*) and provided as 50% seeding dose.

Immunohistochemistry

We submitted 2–6 organoids from each experimental group for histologic studies. Organoids were immersed in 3.7% neutral buffered formalin for ≈24 hours before standard embedding in paraffin. We performed immunohistochemical (IHC) staining specifically for PrP using 3 different PrP antibodies: SAF32 (Cayman Chemical, https://www.caymanchem.com) (*30*), F89/160.1.5 (F89) (GeneTex, https://www.genetex.com) (*31*) and F99/97.6.1 (F99) (VMRD, Inc., https://vmrd.com) (*31*). We sectioned organoids into 5-µm slices and performed deparaffinization,

Table. Inoculum details used in study of attempted CWD prion transmission to human cerebral organoids*

Sample	Name	log LD_{50}/mg brain†	log SD_{50}/mg brain‡
Human normal brain homogenate	hNBH	Negative	Negative
Human sporadic CJD MV2	CJD	ND	6.9
Deer normal brain homogenate	dNBH	Negative	Negative
Whitetail deer CWD§ (pool of 7)	dCWD1	5.6 (WTD)	6
Mule deer CWD¶ (pool of 6)	dCWD2	5.7 (MD)	6.2
Elk normal brain homogenate	eNBH	Negative	Negative
Elk CWD# (pool of 6)	eCWD	5.3	6.5

*CJD, Creutzfeldt-Jakob disease; CWD, chronic wasting disease; LD_{50}, 50% lethal dose; negative, negative control; ND, not done; SD_{50}, 50% seeding dose.
†Adapted from Race et al. (*29*).
‡Inocula.
§WTD-1 in nomenclature as found in (*29*).
¶MD-1 in nomenclature as found in (*29*)
#Elk-2 in nomenclature as found in (*29*).

antigen retrieval and staining using the Discovery Ultra Staining Module (Roche, https://www.roche.com). We retrieved antigens for all PrP IHC staining by using extended cell conditioning with CC1 buffer (Roche) containing Tris-Borate-EDTA, pH 8.0 for 100 minutes at 95°C. Before staining, we applied a horse serum blocker (Vector #136021) at 37°C for 20 minutes. To stain PrP, we applied either SAF32 at a dilution of 1:2,000, F89 at 1:250, or F99 at 1:25 for 1 hour at 37°C. We performed all antibody dilutions using antibody dilution buffer (Roche). The secondary antibody for all 3 primary PrP antibodies was horse anti-mouse IgG (Vector #30129), applied undiluted for 32 minutes at 37°C, followed by detection with ChromoMap DAB (Roche). We digitized and analyzed all histopathology slides using Aperio Imagescope software (https://www.leicabiosystems.com/us/digital-pathology/manage/aperio-imagescope).

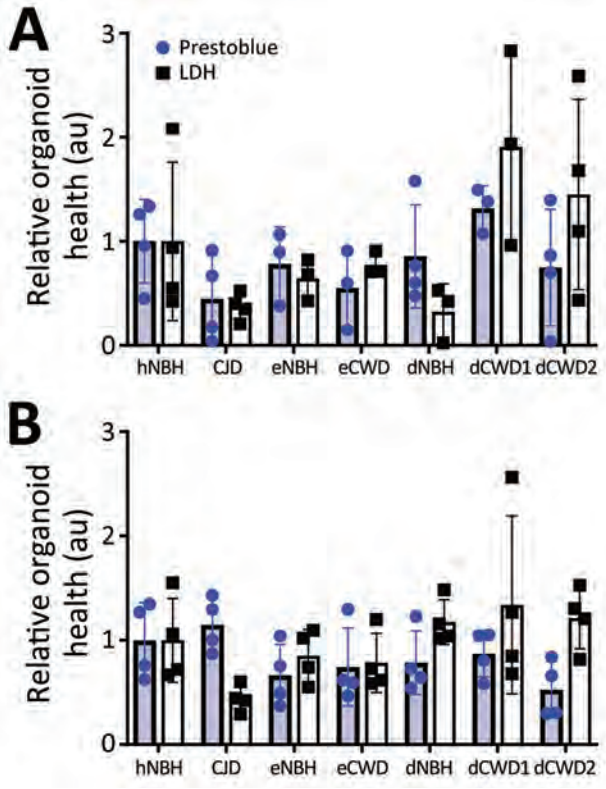

Figure 1. PrestoBlue viability and LDH release assays for the 129MM (A) and 129MV (B) representative organoids measured before harvest at 180 days post innoculation in study of lack of transmission of CWD prions to human cerebral organoids. Results indicate CWD exposure does not reduce organoid viability. Individual dots represent a single organoid, bars indicate the mean response, and error bars show SDs. No condition was statistically changed from controls as determined by 1-way analysis of variance with Welch's correction. au, arbitrary units; CJD, Creutzfeldt-Jakob disease; CWD, chronic wasting disease; dCWD1, whitetail deer CWD; dCWD2, mule deer CWD; dNBH, deer normal brain homogenate; eCWD, elk CWD; eNBH, elk normal brain homogenate; hNBH, human normal brain homogenate; LDH, lactate dehydrogenase.

Proteinase K Digests and Western Blot Analysis

We performed proteinase K digests and Western blot analysis as described previously (*25*). In brief, we treated 10% organoid homogenates with 5 μg/mL proteinase K in 1% Sarkosyl for 1 hour at 37°C with 400 rpm shaking. We ran equal volumes of the digested 10% homogenates on Bolt 4%–12% Bis-Tris gels and transferred to PVDF membranes using the iBlot 2 transfer system (ThermoFisher Scientific). We detected PrP by using the 3F4 antibody (Millipore Sigma, https://www.emdmillipore.com) at a 1:10,000 dilution, visualized using ECL Select (Cytiva, https://www.cytivalifesciences.com), and imaged on the iBright imaging system (ThermoFisher Scientific). We visualized total protein with Coomassie blue staining.

PrestoBlue and Lactate Dehydrogenase

We assessed relative organoid health using PrestoBlue metabolism and lactate dehydrogenase (LDH) release assays, per the manufacturer's instructions. In brief, we plated 3–6 random representative organoids from each group in 24-well plates with 0.5 mL of fresh media. Approximately 24 hours later, we mixed 50 μL media with 50 μL LDH catalyst and dye in a 96-well plate, then incubated the plate for 15 minutes at 37°C before adding 25 μL of stop solution. We measured absorbance on the ClarioStar plate reader (BMG LabTech) at 460 nm, subtracting reference wavelength 690 nm from the reading. Once LDH was measured, we used the same organoids for PrestoBlue metabolism. We diluted PrestoBlue reagent in organoid maintenance media at a 1:10 ratio. We then removed the organoids' existing media, added 0.5 mL of the PrestoBlue media, and incubated at 37°C for 30 minutes before transferring the media to a black 96-well plate for analysis. We measured fluorescence at 560 nm excitation and 590 nm emission in the ClarioStar plate reader. Values are presented as relative change from the normal brain homogenate (NBH) controls.

Results

Organoid Viability after CWD Exposure

We immersed hCOs for 7 days in media containing negative control normal brain inocula either from humans (hNBH), deer (dNBH), or elk (eNBH) or infectious prions from sCJD human brain homogenate (CJD; positive control), 2 species of deer (dCWD1,

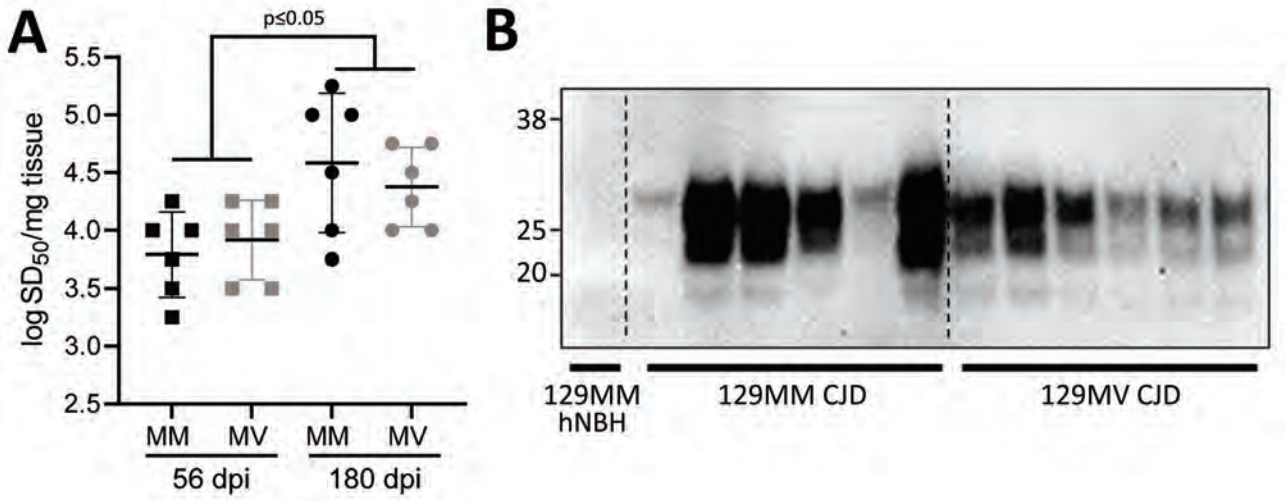

Figure 2. Demonstration of infection and accumulation of MV2 sporadic CJD prions in human cerebral organoids in study of lack of transmission of chronic wasting disease prions to human cerebral organoids. Both the 129MM and MV organoids were infected with MV2 sporadic CJD prions to ensure uptake and accumulation could be measured in both lines. A) Real-time quaking-induced conversion seeding activity; B) accumulation of protease resistant prion protein were assayed at 56 and 180 dpi. Each marker in panel A represents the organoid from an individual with the means and SDs of all organoids per condition indicated. Panel B indicates Western blots using prion 3F4 antibody following protease digest of lysates from 2 representative MM and 2 representative MV organoids that received the same starting inoculum (MV2 CJD) along with a 129MM 180dpi organoid that received hNBH. CJD, Creutzfeldt-Jakob disease; dpi, days postinoculation; hNBH, human normal brain homogenate.

dCWD2), or elk (eCWD), as previously described (Table). We monitored hCOs for 180 days after infection for visible signs of distress, including changes in appearance and metabolizing of the media. Before the final harvest, we assessed 3 or 4 organoids from each treatment group for differences in metabolism by PrestoBlue viability assay or cellular integrity by LDH release. Although there was wide variability in the organoid responses, no signs of decreased health were evident in any condition (Figure 1). Thus, exposure to the homogenates had no influence on organoid viability.

Propagation of MV2 sCJD Prions in 129MM and 129MV Organoids

We have previously demonstrated that 129MV hCOs are susceptible to infection with human 129MV prions (*25*,*32*) and that 129MM hCOs are susceptible to infection with human 129MM prions (*33*). As a positive control, and to ensure that 129MM organoids were also susceptible to 129MV prions, we inoculated both organoid lines (129MV and 129MM) with 129MV2 human sCJD prions and assessed RT-QuIC seeding activity and protease-resistant PrP (a biochemical marker of disease associated prion deposition) at 56 and 180 days postinoculation (dpi). RT-QuIC seeding activity was present at 56 dpi and showed a significant increase after incubation to 180 dpi (Figure 2, panel A). No protease-resistant PrP could be detected within the organoids at 56 dpi, but significant accumulation had occurred by 180 dpi (Figure 2, panel B). Therefore, the CJD control organoids did take up infection and propagate it, with accumulation over time.

No Propagation of PrP Seeding Activity in CWD-Exposed Organoids

RT-QuIC analysis of the organoids collected at 180 dpi showed that, with the exception of the CJD-positive controls, no inoculum in either the codon 129MM or 129MV organoids resulted in the production of significant seeding activity (Figure 3). In the case of the 129MM hCOs, some weak positive signals were observed (Figure 3; Appendix Figure 2). However, similar observations were made in genetically matched PrP KO organoids (Figure 3; Appendix Figure 2, gray markers), which have no PrP substrate for propagation of misfolding. Coupled with a decline in seeding activity over the course of the experiment (Appendix Figure 2), this finding suggests that the observed signals are a likely result of residual inocula persisting in the organoids for a prolonged period, producing false-positive reactions. Altogether, RT-QuIC analysis for prion seeding activity indicated that none of the CWD-inoculated organoids contained seeding activity indicative of actively propagating infection, such as is seen with CJD-infected hCOs.

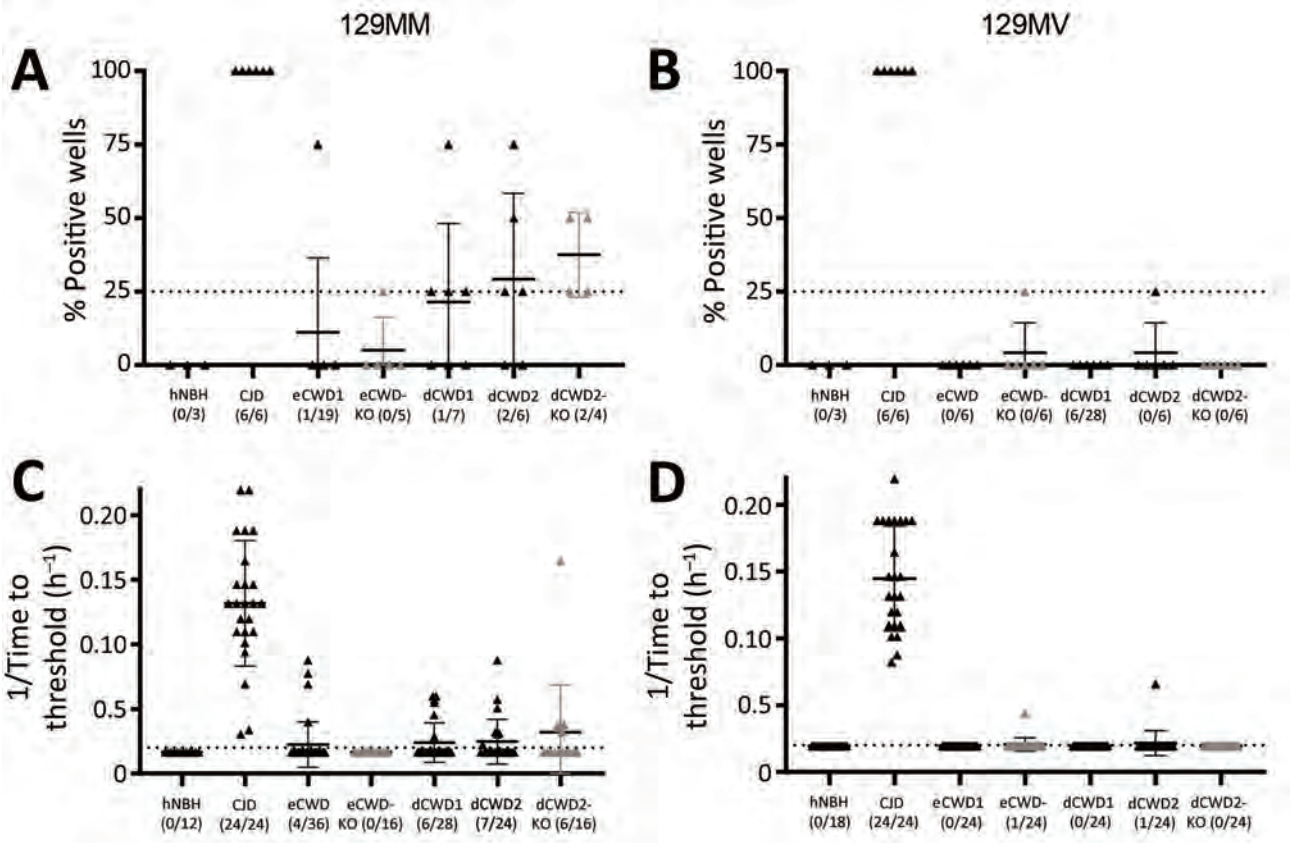

Figure 3. Real-time quaking-induced conversion (RT-QuIC) seeding activity of CWD-exposed organoids in study of lack of transmission of chronic wasting disease prions to human cerebral organoids. RT-QuIC seeding activity in organoids harvested at 180 days postinoculation is shown as either % positive wells (A, B) or the reciprocal of time-to-significance threshold (C, D) for the 129MM (A, C) and 129MV (B, D) organoids. Dotted lines indicate the threshold above which a sample would be classified as positive. Individual dots show single organoids with the means and SDs indicated. Gray symbols are indicative of knockout organoids. No significant differences were observed between the CWD-inoculated wild type organoids and their corresponding knockout organoids by Welch's t-test. CJD, Creutzfeldt-Jakob disease; CWD, chronic wasting disease; dCWD1, whitetail deer CWD; dCWD2, mule deer CWD; dNBH, deer normal brain homogenate; eCWD, elk CWD; eNBH, elk normal brain homogenate; hNBH, human normal brain homogenate.

No Protease-Resistant PrP in CWD-Exposed Organoids

Accumulation of disease-associated, protease-resistant PrP is also a hallmark of prion disease. Therefore, we probed organoid homogenates from the CWD infections for PrP levels with and without proteinase K digestion. Protease-resistant PrP was only observed in the CJD-infected control organoids and not in any of the CWD-exposed organoids (Figure 4), and none of the CWD conditions showed a significant increase in total PrP levels (Figure 4).

No Human Prion Deposition in CWD-Exposed Organoids

Histologic examination of the tissues at the conclusion of the experiment (180 dpi) showed no evidence of pathology or plaques within the CWD-inoculated organoids. However, several dCWD2 and eCWD organoids contained scattered regions of abnormal PrP deposition. Although the PrP KO organoids showed no native PrP staining compared with the background hue of normal PrP expression seen in the wild type organoids, further examination revealed abnormal PrP deposits similar to those seen in the wild type organoids using the SAF32 PrP antibody. This finding indicates that the deposits are likely residual CWD inoculum and not de novo deposition of human PrP (Figure 5, panel A). To verify that those deposits were indeed residual inocula, we further analyzed the tissue slices using F89 and F99 PrP antibodies. F89 is a PrP antibody that detects both cervid and human PrP, similar to SAF32, whereas F99 is a PrP antibody that detects only cervid PrP and not human PrP. Staining with F89 demonstrated similar results for both CJD- and CWD-exposed organoids, similar to that of SAF32. However, when stained with the F99 cervid PrP antibody, only the CWD-exposed hCOs showed PrP staining, confirming that the positive staining

material was cervid in origin and not converted human PrP (Figure 5, panel B; Appendix Figure 4). Altogether, despite clear accumulation of pathogenic (seeding positive, protease-resistant) PrP in the sCJD-infected organoids, prolonged, high-dose exposure of hCOs to CWD prions was not sufficient to cause conversion of human PrP or disease propagation.

Discussion

The data presented in this study show that, despite weeklong exposure to CWD prions with high infectivity and the capacity to readily become infected with CJD prions, hCOs were not capable of propagating CWD prions. This finding indicates that, even after direct exposure of human central nervous system tissues to CWD prions, a substantial resistance or barrier to the propagation of infection exists.

Although we tested the 2 most common PrP genotypes (129MM and 129MV), our results do not preclude the possibility that homozygosity for the valine allele at codon 129 would result in increased susceptibility to CWD. There is precedent for that possibility. Wang et al. (*34*) were able to generate human CWD prions by using the protein misfolding cyclic amplification (PMCA) assay. Using that approach, the authors found that elk CWD prions could trigger conversion and amplification of human 129VV PrP in brain homogenate that was subsequently transmissible to mice. Conversely, 129MM human brain homogenate would not amplify CWD, and 129 MV brain homogenate was not tested. Other studies, however, have demonstrated CWD codon 129 susceptibility similar to BSE in vitro, where methionine homozygosity shows greater susceptibility to conversion with some CWD samples (*11*). Barria et al. (*11*) found that humanized mouse-derived MM substrates showed some degree of conversion by white-tailed deer CWD prions by PMCA, whereas MV and VV substrates were resistant. All 3 genotypes, however, showed susceptibility to reindeer CWD prions. Those assays showed that, given the right circumstances, human PrP can be seeded by cervid CWD prions;

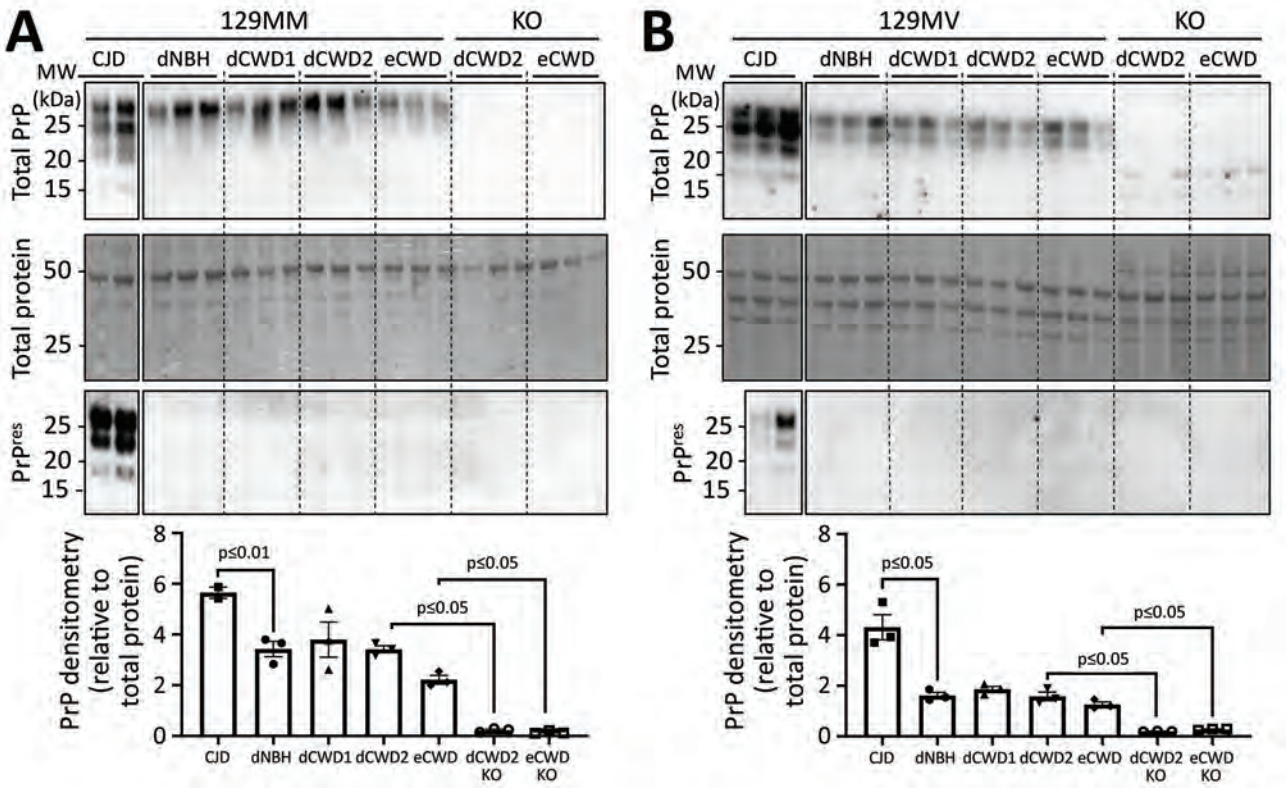

Figure 4. Western blot analysis of total PrP and PrP^{res} levels in representative organoids for sporadic CJD and CWD-exposed human cerebral organoids in study of lack of transmission of chronic wasting disease prions to 129mm (A) and129MV (B) human cerebral organoids. Matched KO organoids inoculated with dCWD2 or eCWD are shown for comparison. Densitometric analysis (shown in bottom panels) shows total PrP levels relative to total protein with each point representing an individual organoid; means and SDs are indicated. p values were calculated using Welch's t-test. Uncropped Western analyses are shown in Appendix Figure 3 (https://wwwnc.cdc.gov/EID/article/30/6/23-1568-App1.pdf). CJD, Creutzfeldt-Jakob disease; CWD, chronic wasting disease; dCWD1, whitetail deer CWD; dCWD2, mule deer CWD; dNBH, deer normal brain homogenate; eCWD, elk CWD; eNBH, elk normal brain homogenate; hNBH, human normal brain homogenate; KO, knockout; PrP, prion protein; PrP^{res}, protease-resistant prion protein.

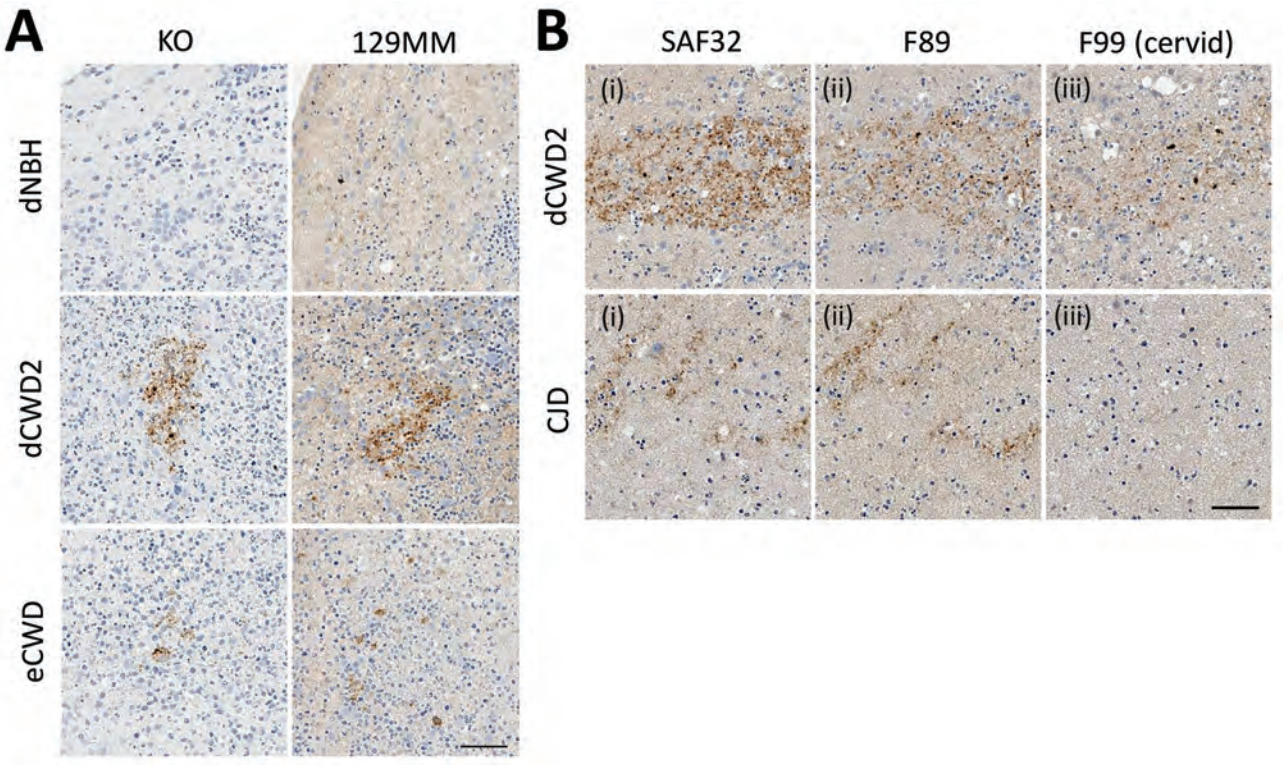

Figure 5. Prion protein (PrP) deposits in organoids. A) Deposits of PrP in 129MM and KO organoids detected with SAF32 antibody in study of lack of transmission of chronic wasting disease prions to human cerebral organoids. B) Prion deposition in sequential slices of representative 129MV organoids is detected by both SAF32 (i) and F89 (ii) total PrP antibodies in both CWD and CJD inoculated organoids. Cervid PrP-specific antibody F99 (iii) detects the same deposits in the just the CWD inoculated organoids, indicating that the deposits are of cervid origin (i.e., inocula) and not misfolded human PrP. Scale bars indicate 50 μm. CJD, Creutzfeldt-Jakob disease; CWD, chronic wasting disease; dCWD2, mule deer CWD; dNBH, deer normal brain homogenate; eCWD, elk CWD; KO, knockout.

however, they forced a reaction in a way that might not be representative of the genuine risk to humans from a more natural exposure. The lack of propagation in the organoid model supports the idea that other aspects of the PMCA reaction, such as the radicals formed by sonolysis (*35*), might be necessary to initiate the observed conversion.

A lack of transmission of CWD to the human cerebral organoid model supports the data found in macaques, where transmission did not produce prion disease (*21*,*22*,*29*). That finding is in clear contrast to BSE, in which the macaques infected with BSE prions succumbed to prion disease (*36*,*37*). BSE has also been demonstrated to infect humanized mice (*38*,*39*). Inoculation of humanized mice with CWD has been mostly unsuccessful in causing infection (*13*,*17*–*19*), but transmission of CWD to humanized mice was observed in 1 study (*20*). Those mice overexpressed (≈6-fold) human PrP with methionine at codon 129. Our cerebral organoids, which also express methionine at codon 129 (129MM and 129MV), are a model of completely human brain tissue with normal PrP expression levels. Thus, this finding suggests that the mouse background, possibly in combination with overexpression of human PrP, is a more favorable environment than human brain tissue for CWD infection to occur.

The organoid model, although the closest to human brain tissue currently available, has various limitations and does not reproduce all aspects of the human brain (*40*). Thus, hCOs might be lacking factors or cell types that would make the human brain more susceptible to CWD prions. Many more unknowns cannot be accounted for in this system. For example, we cannot exclude unknown susceptibility factors that could make a small population more vulnerable to infection, and we have not tested all cervid genotypes against all human genotypes. Likewise, the possibility remains that new strains of CWD with the capacity to cross the species barrier could emerge in the future. For now, our data suggest that such seeding of human PrP by cervid CWD prions is unlikely to occur or be sustained in human brain tissue.

In conclusion, experimental transmissions of 3 sources of CWD to 2 *PRNP* codon 129 genotypes of human cerebral organoids were unsuccessful.

Although we cannot rule out the possibility of CWD crossing into humans, our data suggest that a significant species barrier exists, even when human brain tissue is directly exposed to high-titer CWD brain homogenate for a prolonged period.

Acknowledgments

We thank Clayton Winkler, Arielle Hay, and Byron Caughey for critical reading of the manuscript.

This research was supported by the Intramural Research Program of the National Institutes of Health, National Institute of Allergy and Infectious Diseases.

About the Author

Dr. Groveman is a biologist in the Laboratory of Neurological Infections and Immunity at Rocky Mountain Laboratories, National Institute of Allergy and Infectious Diseases, National Institutes of Health. His primary research interests involve infectious diseases of animals and humans, particularly involving prions and prion-like proteins.

References

1. Benestad SL, Telling GC. Chronic wasting disease: an evolving prion disease of cervids. Handb Clin Neurol. 2018;153:135–51. https://doi.org/10.1016/B978-0-444-63945-5.00008-8
2. Kraus A, Groveman BR, Caughey B. Prions and the potential transmissibility of protein misfolding diseases. Annu Rev Microbiol. 2013;67:543–64. https://doi.org/10.1146/annurev-micro-092412-155735
3. Igel A, Fornara B, Rezaei H, Béringue V. Prion assemblies: structural heterogeneity, mechanisms of formation, and role in species barrier. Cell Tissue Res. 2023;392:149–66. https://doi.org/10.1007/s00441-022-03700-2
4. Lewis PA, Tattum MH, Jones S, Bhelt D, Batchelor M, Clarke AR, et al. Codon 129 polymorphism of the human prion protein influences the kinetics of amyloid formation. J Gen Virol. 2006;87:2443–9. https://doi.org/10.1099/vir.0.81630-0
5. Bishop M. Influence of the prion protein gene codon 129 genotype on the clinical and pathological phenotype of human prion disease, and transmission to transgenic mice. In: Collins SJ, Lawson VA, editors. The cellular and molecular biology of prion disease. Kerala (India): Research Signpost; 2011. p. 173–188.
6. Kaski D, Mead S, Hyare H, Cooper S, Jampana R, Overell J, et al. Variant CJD in an individual heterozygous for PRNP codon 129. Lancet. 2009;374:2128. https://doi.org/10.1016/S0140-6736(09)61568-3
7. Mok T, Jaunmuktane Z, Joiner S, Campbell T, Morgan C, Wakerley B, et al. Variant Creutzfeldt-Jakob disease in a patient with heterozygosity at PRNP codon 129. N Engl J Med. 2017;376:292–4. https://doi.org/10.1056/NEJMc1610003
8. Smith PG, Cousens SN, d' Huillard Aignaux JN, Ward HJT, Will RG. The epidemiology of variant Creutzfeldt-Jakob disease. Curr Top Microbiol Immunol. 2004;284:161–91. https://doi.org/10.1007/978-3-662-08441-0_7
9. Gill ON, Spencer Y, Richard-Loendt A, Kelly C, Dabaghian R, Boyes L, et al. Prevalent abnormal prion protein in human appendixes after bovine spongiform encephalopathy epizootic: large scale survey. BMJ. 2013;347(oct15 5):f5675. https://doi.org/10.1136/bmj.f5675
10. Gill ON, Spencer Y, Richard-Loendt A, Kelly C, Brown D, Sinka K, et al. Prevalence in Britain of abnormal prion protein in human appendices before and after exposure to the cattle BSE epizootic. Acta Neuropathol. 2020;139:965–76. https://doi.org/10.1007/s00401-020-02153-7
11. Barria MA, Libori A, Mitchell G, Head MW. Susceptibility of human prion protein to conversion by chronic wasting disease prions. Emerg Infect Dis. 2018;24:1482–9. https://doi.org/10.3201/eid2408.161888
12. Raymond GJ, Bossers A, Raymond LD, O'Rourke KI, McHolland LE, Bryant PK III, et al. Evidence of a molecular barrier limiting susceptibility of humans, cattle and sheep to chronic wasting disease. EMBO J. 2000;19:4425–30. https://doi.org/10.1093/emboj/19.17.4425
13. Kong Q, Huang S, Zou W, Vanegas D, Wang M, Wu D, et al. Chronic wasting disease of elk: transmissibility to humans examined by transgenic mouse models. J Neurosci. 2005;25:7944–9. https://doi.org/10.1523/JNEUROSCI.2467-05.2005
14. Sandberg MK, Al-Doujaily H, Sigurdson CJ, Glatzel M, O'Malley C, Powell C, et al. Chronic wasting disease prions are not transmissible to transgenic mice overexpressing human prion protein. J Gen Virol. 2010;91:2651–7. https://doi.org/10.1099/vir.0.024380-0
15. Tamgüney G, Giles K, Bouzamondo-Bernstein E, Bosque PJ, Miller MW, Safar J, et al. Transmission of elk and deer prions to transgenic mice. J Virol. 2006;80:9104–14. https://doi.org/10.1128/JVI.00098-06
16. Wilson R, Plinston C, Hunter N, Casalone C, Corona C, Tagliavini F, et al. Chronic wasting disease and atypical forms of bovine spongiform encephalopathy and scrapie are not transmissible to mice expressing wild-type levels of human prion protein. J Gen Virol. 2012;93:1624–9. https://doi.org/10.1099/vir.0.042507-0
17. Wadsworth JDF, Joiner S, Linehan JM, Jack K, Al-Doujaily H, Costa H, et al. Humanized transgenic mice are resistant to chronic wasting disease prions from Norwegian reindeer and moose. J Infect Dis. 2022;226:933–7. https://doi.org/10.1093/infdis/jiab033
18. Race B, Williams K, Chesebro B. Transmission studies of chronic wasting disease to transgenic mice overexpressing human prion protein using the RT-QuIC assay. Vet Res (Faisalabad). 2019;50:6. https://doi.org/10.1186/s13567-019-0626-2
19. Race B, Baune C, Williams K, Striebel JF, Hughson AG, Chesebro B. Second passage experiments of chronic wasting disease in transgenic mice overexpressing human prion protein. Vet Res (Faisalabad). 2022;53:111. https://doi.org/10.1186/s13567-022-01130-0
20. Hannaoui S, Zemlyankina I, Chang SC, Arifin MI, Béringue V, McKenzie D, et al. Transmission of cervid prions to humanized mice demonstrates the zoonotic potential of CWD. Acta Neuropathol. 2022;144:767–84. https://doi.org/10.1007/s00401-022-02482-9
21. Race B, Meade-White KD, Phillips K, Striebel J, Race R, Chesebro B. Chronic wasting disease agents in nonhuman primates. Emerg Infect Dis. 2014;20:833–7. https://doi.org/10.3201/eid2005.130778
22. Race B, Williams K, Orrú CD, Hughson AG, Lubke L, Chesebro B. Lack of transmission of chronic wasting

disease to cynomolgus macaques. J Virol. 2018;92:e00550–18. https://doi.org/10.1128/JVI.00550-18
23. Lasmézas CI, Deslys J-P, Demaimay R, Adjou KT, Lamoury F, Dormont D, et al. BSE transmission to macaques. Nature. 1996;381:743–4. https://doi.org/10.1038/381743a0
24. Groveman BR, Ferreira NC, Foliaki ST, Walters RO, Winkler CW, Race B, et al. Human cerebral organoids as a therapeutic drug screening model for Creutzfeldt-Jakob disease. Sci Rep. 2021;11:5165. https://doi.org/10.1038/s41598-021-84689-6
25. Groveman BR, Foliaki ST, Orru CD, Zanusso G, Carroll JA, Race B, et al. Sporadic Creutzfeldt-Jakob disease prion infection of human cerebral organoids. Acta Neuropathol Commun. 2019;7:90. https://doi.org/10.1186/s40478-019-0742-2
26. Foliaki ST, Schwarz B, Groveman BR, Walters RO, Ferreira NC, Orrù CD, et al. Neuronal excitatory-to-inhibitory balance is altered in cerebral organoid models of genetic neurological diseases. Mol Brain. 2021;14:156. https://doi.org/10.1186/s13041-021-00864-w
27. Lancaster MA, Knoblich JA. Generation of cerebral organoids from human pluripotent stem cells. Nat Protoc. 2014;9:2329–40. https://doi.org/10.1038/nprot.2014.158
28. Renner M, Lancaster MA, Bian S, Choi H, Ku T, Peer A, et al. Self-organized developmental patterning and differentiation in cerebral organoids. EMBO J. 2017;36:1316–29. https://doi.org/10.15252/embj.201694700
29. Race B, Meade-White KD, Miller MW, Barbian KD, Rubenstein R, LaFauci G, et al. Susceptibilities of nonhuman primates to chronic wasting disease. Emerg Infect Dis. 2009;15:1366–76. https://doi.org/10.3201/eid1509.090253
30. Féraudet C, Morel N, Simon S, Volland H, Frobert Y, Créminon C, et al. Screening of 145 anti-PrP monoclonal antibodies for their capacity to inhibit PrPSc replication in infected cells. J Biol Chem. 2005;280:11247–58. https://doi.org/10.1074/jbc.M407006200
31. O'Rourke KI, Baszler TV, Besser TE, Miller JM, Cutlip RC, Wells GAH, et al. Preclinical diagnosis of scrapie by immunohistochemistry of third eyelid lymphoid tissue. J Clin Microbiol. 2000;38:3254–9. https://doi.org/10.1128/JCM.38.9.3254-3259.2000
32. Groveman BR, Race B, Foliaki ST, Williams K, Hughson AG, Baune C, et al. Sporadic Creutzfeldt-Jakob disease infected human cerebral organoids retain the original human brain subtype features following transmission to humanized transgenic mice. Acta Neuropathol Commun. 2023;11:28. https://doi.org/10.1186/s40478-023-01512-1
33. Smith A, Groveman BR, Winkler C, Williams K, Walters R, Yuan J, et al. Stress and viral insults do not trigger E200K PrP conversion in human cerebral organoids. PLoS One. 2022;17:e0277051. https://doi.org/10.1371/journal.pone.0277051
34. Wang Z, Qin K, Camacho MV, Cali I, Yuan J, Shen P, et al. Generation of human chronic wasting disease in transgenic mice. Acta Neuropathol Commun. 2021;9:158. https://doi.org/10.1186/s40478-021-01262-y
35. Haigh CL, Drew SC. Cavitation during the protein misfolding cyclic amplification (PMCA) method—the trigger for de novo prion generation? Biochem Biophys Res Commun. 2015;461:494–500. https://doi.org/10.1016/j.bbrc.2015.04.048
36. Lasmézas CI, Deslys J-P, Demaimay R, Adjou KT, Lamoury F, Dormont D, et al. BSE transmission to macaques. Nature. 1996;381:743–4. https://doi.org/10.1038/381743a0
37. Montag J, Schulz-Schaeffer W, Schrod A, Hunsmann G, Motzkus D. Asynchronous onset of clinical disease in BSE-infected macaques. Emerg Infect Dis. 2013;19:1125–7. https://doi.org/10.3201/eid1907.120438
38. Espinosa JC, Comoy EE, Marin-Moreno A, Aguilar-Calvo P, Birling M-C, Pitarch JL, et al. Transgenic mouse models expressing human and macaque prion protein exhibit similar prion susceptibility on a strain-dependent manner. Sci Rep. 2019;9:15699. https://doi.org/10.1038/s41598-019-52155-z
39. Asante EA, Linehan JM, Desbruslais M, Joiner S, Gowland I, Wood AL, et al. BSE prions propagate as either variant CJD-like or sporadic CJD-like prion strains in transgenic mice expressing human prion protein. EMBO J. 2002;21:6358–66. https://doi.org/10.1093/emboj/cdf653
40. Walters RO, Haigh CL. Organoids for modeling prion diseases. Cell Tissue Res. 2023;392:97–111. https://doi.org/10.1007/s00441-022-03589-x

Address for correspondence: Cathryn Haigh, Laboratory of Neurological Infections and Immunity, National Institute of Allergy and Infectious Diseases, Division of Intramural Research, Rocky Mountain Laboratories, National Institutes of Health, 903 South 4th St, Hamilton, MT 59840, USA; email: cathryn.haigh@nih.gov

Introduction of New Dengue Virus Lineages of Multiple Serotypes after COVID-19 Pandemic, Nicaragua, 2022

Cristhiam Cerpas, Gerald Vásquez, Hanny Moreira, Jose G. Juarez, Josefina Coloma, Eva Harris [1], Shannon N. Bennett [1], Ángel Balmaseda[1]

Major dengue epidemics throughout Nicaragua's history have been dominated by 1 of 4 dengue virus serotypes (DENV-1–4). To examine serotypes during the dengue epidemic in Nicaragua in 2022, we performed real-time genomic surveillance in-country and documented cocirculation of all 4 serotypes. We observed a shift toward co-dominance of DENV-1 and DENV-4 over previously dominant DENV-2. By analyzing 135 new full-length DENV sequences, we found that introductions underlay the resurgence: DENV-1 clustered with viruses from Ecuador in 2014 rather than those previously seen in Nicaragua; DENV-3, which last circulated locally in 2014, grouped instead with Southeast Asia strains expanding into Florida and Cuba in 2022; and new DENV-4 strains clustered within a South America lineage spreading to Florida in 2022. In contrast, DENV-2 persisted from the formerly dominant Nicaragua clade. We posit that the resurgence emerged from travel after the COVID-19 pandemic and that the resultant intensifying hyperendemicity could affect future dengue immunity and severity.

Arthropodborne viruses are distinguished by alternating transmission between arthropod vectors and vertebrates. Some of the most clinically relevant arboviruses (e.g., dengue, Zika, and yellow fever) belong to the genus *Flavivirus*. Dengue virus (DENV) alone threatens more than half the world's population (*1*). DENV, transmitted by female *Aedes* mosquitoes, consists of 4 serotypes, DENV-1–4. Each serotype comprises 4–6 major lineages (genotypes), composed of various sublineages or clades (*2*). Clinical manifestations of infection may vary by DENV serotype, genotype, and clade (*3*–*6*); infection outcome (asymptomatic to potentially fatal disease) is also modulated by prior immunity. Knowledge of the complexities of DENV serotype, genotype, and specific lineage circulation is critical for improving public health responses to outbreaks.

Dengue epidemics cycle every 2–5 years in tropical and subtropical regions and are strongly influenced by season (*7*). In many countries, increasing human mobility, societal changes affecting human–mosquito contact, and challenges with vector control have all contributed to increased dengue epidemic activity and a change from nonendemic or hypoendemic patterns (noncontinuous transmission of a single serotype) to hyperendemic transmission patterns (multiple cocirculating serotypes) (*8*), resulting in increased interannual duration of transmission activity with fewer intervening years of little to no transmission.

DENV was first detected in Nicaragua in 1985 (*9*); since then, the 4 serotypes have periodically circulated in the country, albeit differing in relative and overall prevalence (*5*,*9*–*12*). Dengue has become a serious public health concern in Nicaragua because of its incidence and potential for severe and possibly fatal disease (*10*,*13*,*14*). We investigated the

Author affiliations: Sustainable Sciences Institute, Managua, Nicaragua (C. Cerpas, G. Vásquez, H. Moreira, J.G. Juarez, Á. Balmaseda); Laboratorio Nacional de Virologia, Centro Nacional de Diagnóstico y Referencia Ministerio de Salud, Managua (C. Cerpas, Á. Balmaseda); Division of Infectious Diseases and Vaccinology, School of Public Health, University of California Berkeley, Berkeley, California, USA (J. Coloma, E. Harris); California Academy of Sciences, San Francisco, California, USA (S.N. Bennett)

DOI: https://doi.org/10.3201/eid3006.231553

[1]These senior authors contributed equally to this article.

molecular and epidemiologic characteristics of the 2022 epidemic after air travel resumed and neighboring countries fully reopened their borders after the COVID-19 pandemic. We observed substantial cocirculation of all 4 DENV serotypes, including DENV-4 after a 30-year absence of epidemic transmission. We generated virus genome sequences in Nicaragua using a portable genomic approach, enabling a detailed description of DENV evolutionary histories and demonstrating the introduction of new clades of 3 serotypes (DENV-1, DENV-3, and DENV-4) and persistence of DENV-2.

Materials and Methods

Ethics Statement

Protocols for the collection and testing of samples were reviewed and approved by the institutional review board of the University of California, Berkeley (PDCS: 2010-09-2245; PDHS: 2010-06-1649; A2CARES: 2021-03-14191). They were also approved by the institutional review board of the Nicaraguan Ministry of Health (PDCS: CIRE 09/03/07/-008. Ver25; PDHS: CIRE 01/10/06-13. Ver. 18; A2CARES: CIRE 02/08/21-114 Ver. 4).

Study Population and Sample Collection

Samples were collected during June–December 2022 as part of 3 ongoing studies, the Nicaraguan Pediatric Dengue Cohort Study (PDCS), Pediatric Hospital-based Study (PDHS), and Asian-American Center for Arbovirus Research and Enhanced Surveillance (A2CARES) cohort study (part of the National Institutes of Health Centers for Research in Emerging Infectious Diseases Network), and through the National Dengue Surveillance Program of the Nicaraguan Ministry of Health (Appendix Table, https://wwwnc.cdc.gov/EID/article/30/6/23-1553-App1.pdf). Since 2004, the PDCS has been conducted within the Sócrates Flores Vivas Health Center catchment area in District 2 of Managua, with participants 2–17 years of age (*3*,*13*,*15*,*16*). The PDHS collects samples from patients with suspected dengue 6 months–14 years of age who receive medical attention in the Infectious Diseases Ward of the National Pediatric Reference Hospital in Managua (Hospital Infantil Manuel de Jesús Rivera) and who have received parent/guardian consent for the study (*17*). The A2CARES cohort study follows ≈2,000 persons 2–80 years of age in ≈1,000 households in District 3 of Managua.

We selected 3,171 suspected dengue cases for potential sequencing analysis, of which 1,353 were confirmed as DENV-positive with known serotype. To ensure a representative national distribution in the selection of samples for sequencing, we included 10 ±2% of the DENV-confirmed serotyped samples from each department that had adequate coverage for genomic analysis (n = 135), which included samples from the studies in Managua. We sequenced 49 DENV-1, 6 DENV-2, 38 DENV-3 and 42 DENV-4 samples that were positive by real-time reverse transcription PCR (rRT-PCR). To assess the relationships of the samples collected in 2022 to previously circulating strains from Nicaragua, we included 68 DENV-1, 62 DENV-2, and 51 DENV-3 previously published sequences (*5*,*10*,*18*).

RNA Extraction and RT-PCR

Serum or plasma collected during the acutephase (days 1–5 since symptom onset) from patients with suspected dengue was processed at the National Virology Laboratory (Centro Nacional de Diagnóstico y Referencia, Ministerio de Salud, Managua, Nicaragua). We extracted viral RNA by using the QIAmp viral RNA mini kit (QIAGEN, https://www.qiagen.com) according to manufacturer instructions and used it to perform a single-reaction multiplex rRT-PCR for detection of Zika virus, chikungunya virus, and DENV (*19*). We further analyzed DENV-positive samples to identify the infecting serotype by using a multiplex DENV rRT-PCR (*20*,*21*). We prioritized cycle threshold values <28 for genomic sequencing to ensure the presence of ample genetic material, which ultimately enhanced sequence quality, minimized contamination risk, and improved detection sensitivity. In >90% of cases, sequences included in genomic analysis had >60% genome coverage.

Library Preparation and Next-Generation Sequencing

We reverse transcribed sample RNA (8 µL) with 2 µL LunaScript RT SuperMix (New England Biolabs, Inc., https://www.neb.com) as follows: 25°C for 2 minutes, 55°C for 10 minutes, 95°C for 1 minute, and a 4°C hold. The PCR reaction mixture contained 13.75 µL of nuclease-free water, 1.5 µL of pool A and pool B primers, 5 µL of 5X Q5 reaction buffer, 2 µL of 2.5 mM dNTPs (Invitrogen, https://www.thermofisher.com), 0.25 µL of Q5 DNA polymerase, and 2.5 µL of sample cDNA (*22*,*23*). PCR amplification consisted of 98°C for 30 seconds, followed by 45 cycles of 98°C for 15 seconds and 65°C for 5 minutes, followed by a 12°C hold. We selected samples with a 900-bp band in the pool A and pool B mix for sequencing. Using 5 µL pooled PCR products (from pools A and B), we prepared the cDNA MinION library by using a native barcoding kit (NBD196; NgelabKampus, https://ngelabkampus.com) with a ligation sequencing kit

(LSK-109; Interprise, https://interpriseusa.com) at 30°C for 2 minutes and 80°C for 2 minutes according to manufacturer instructions. We cleaned up PCR products by using AmpureXP purification beads (Beckman Coulter Diagnostics, https://www.beckmancoulter.com) and loaded the DNA library onto a primed MinION flow cell R9.4 (FLO-MIN 106; Oxford Nanopore Technologies, https//nanoporetech.com).

Consensus Genomes

We extracted raw sequence reads by using filters for quality and trimmed adaptors by using Porechop version 0.2.3_seqan 2.1.1 (https://github.com/rrwick/Porechop) and assessed resulting sequence quality by using Nanoplot (*24*). We mapped raw reads by using Minimap2 v2.17-R941 (https://github.com/lh3/minimap2) against reference genomes from GenBank for DENV-1 (accession no. NC_001474), DENV-2 (accession no. NC_001474.2), DENV-3 (accession no. NC_001475.2), and DENV-4 (accession no. NC_002640.1) by using the pipeline at https://github.com/gvaleman/CONSENSO_D. We generated consensus sequences by using SAMtools version 1.7 (https://www.htslib.org/doc/1.7/samtools.html) with the default minimum depth coverage of 1 and confirmed the serotype by using Genome Detective Arbovirus Typing software version 4.1 (https://www.genomedetective.com) and BLAST (https://blast.ncbi.nlm.nih.gov). Mean depth coverage by serotype per SAMtools-depth tool was 221 for DENV-1, 68 for DENV-2, 516 for DENV-3, and 393 for DENV-4.

Phylogenetic Analyses

To increase the resolution of the genetic relatedness of the 2022 viruses in terms of genotype, country, and time of sample origin, we constructed alignments with initial broad coverage by using the National Center for Biotechnology Information Virus database (https://www.ncbi.nlm.nih.gov/labs/virus) by first subjecting sequences to BLAST and selecting the top 100 hits, followed by performing a directed search across regions and timescales represented in the database. Thus, we cast a broad net of potential related sequences. To reduce redundancy while maintaining representation (genotype, country, year) for final analysis, we aligned the large sample sets and reviewed them as initial RAxML (*25*) trees (Appendix Figures 1–4) before downsampling. We conducted sequence alignments with MAFFT version 7.4 (*26*) and manually reviewed them by using AliView version 1.28 (https://ormbunkar.se). We constructed maximum-likelihood phylogenetic trees for each serotype by using RAxML-HPC Blackbox version 8.2.12 and using a general time-reversible substitution model with bootstrap replicates determined automatically. We visualized the maximum-likelihood trees by using FigTree version 1.4.4 (http://tree.bio.ed.ac.uk) (data not shown). We performed Bayesian phylogenetic analysis by using BEAST version 1.10.4 (https://beast.community) and a Hasegawa-Kishino-Yano substitution model, a less parameterized model (2 substitution rates, for transitions and transversions) often used in place of the general time-reversible model above (6 substitution rates, for every base combination) to reduce computational burden. We also used a strict molecular clock and a Bayesian constant size coalescent tree. We ran the Markov chain Monte Carlo analysis for 100 million steps, taking samples every 5,000 steps, discarding the first 10% as burn-in. We assessed convergence with Tracer version 1.7.1 (http://tree.bio.ed.ac.uk) by using an effective sample size threshold >200. We assessed parameter estimate uncertainty by using 95% high probability density (HPD) intervals. Last, we generated maximum clade credibility (MCC) trees by using TreeAnnotator version 1.10 (https://beast.community) and visualized them with Figtree version 1.4.4.

Results

Dengue Epidemiology after the COVID-19 Pandemic

Dengue epidemics in Nicaragua typically occur every 2–3 years (Figure 1, panel A); a given serotype surges to epidemic proportions roughly every 10 years: a shift from DENV-3 in 1998 (*14*) to DENV-2 in 1999 (*3*,*13*,*27*) to DENV-1 in 2003 (*3*) and again to DENV-2 in 2007 (*5*), then another surge of DENV-3 in 2009–11 (*28*), DENV-1 in 2012–13 (*10*), DENV-2 in 2015 and 2019 (*11*,*18*), and the cocirculation of all 4 serotypes in 2022 (Figure 1, panels A, B). However, during 2015–2020, only DENV-2 was detected in patients, whereas large epidemics resulted from newly introduced arboviruses such as chikungunya and Zika, followed by SARS-CoV-2 (*29*–*31*). Although Nicaragua did not implement official lockdown measures in response to the COVID-19 pandemic, international and specifically airline travel was severely curtailed for at least 1 year, starting in May 2020 (*32*,*33*). Together, the prolonged dominance of DENV-2 and the limited movement of people during the pandemic created a window of opportunity for hyperendemic DENV transmission in 2022 because of the susceptibility of the population to other serotypes. Furthermore, the

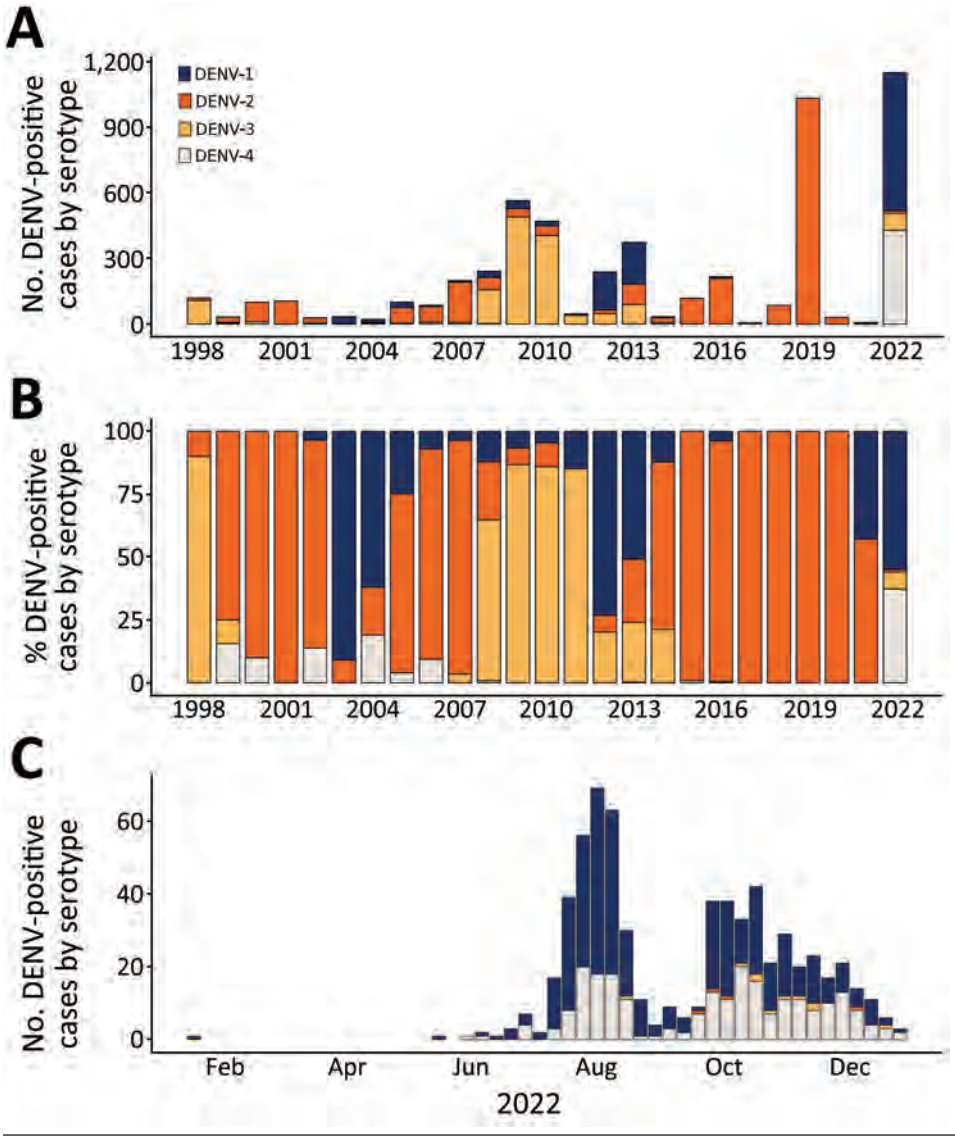

Figure 1. DENV serotypes 1–4 circulation in Nicaragua during 1998–2022. Data on dengue cases with serotype information available were obtained from the Nicaraguan Dengue Surveillance Program; many more cases were confirmed via serology that are not included here because the serotype is unknown. A) Total dengue cases by serotype and year. B) Percentage of circulating dengue cases by serotype and year. C) Case count of each serotype identified by real-time reverse transcription PCR over time during January–December 2022. DENV, dengue virus.

circulation of Zika in 2016 might have primed immunity to increase DENV-4 cases (*12*). The result was the cocirculation of all 4 serotypes in 2022 (Figure 1, panel C), associated with an ≈100-fold increase in reported dengue cases from the previous year.

DENV Genomic Surveillance during the 2022 Epidemic

Serum/plasma samples targeted for sequencing were collected through the PDCS (n = 57), PDHS (n = 13), A2CARES cohort study (n = 4), and the Nicaraguan epidemiologic surveillance system (n = 61) (Appendix Table) (*16*,*17*). A total of 135 sequences were generated by using newly established in-country sequencing capability based on the MinION platform and in-house bioinformatics and phylogenetics pipelines, markedly accelerating the time from clinical sample collection to pathogen sequencing from months to days.

DENV-1

We used 49 DENV-1 sequences from our study along with 81 publicly available sequences to build phylogenetic trees by using maximum-likelihood and Bayesian Marcov chain Monte Carlo methods to generate an MCC tree (Figure 2; Appendix Figure 1, showing the initial ML tree with 408 taxa). DENV-1 genomes recovered in 2022 all belong to genotype V (American/East African and Asian genotype), consistent with previous studies of DENV-1 in Nicaragua (*10*). However, the viruses from 2022 clustered into 2 distinct clades, DV1-NI-1 and DV1-NI-2. Most sequences clustered into DV1-NI-2, for which the closest relatives were Ecuador sequences from 2014, suggesting that DV1-NI-2 is derived from an introduction from South America into Nicaragua. The other clade, DV1-NI-1, is represented by only 4 sequences and is

associated with strains previously circulating in Nicaragua in 2013 and 2016. The date estimate of the time to most recent common ancestor (tMRCA) for DV1-NI-2 was 2013.7 (95% HPD 2012.8–2014.6) and for DV1-NI-1 was 1986.9 (95% HPD 1985–1989) (Figure 2). The genetic distance between DV1-NI-2 (2022) and DV1-NI-1 (2013 and 2016) is substantial, based on branch lengths relative to the rest of the phylogeny; mean rate is 0.04 substitutions per site (Appendix Figure 1). The introduction of the new clade, DV1-NI-2, and its cocirculation with the longer-standing Nicaragua-endemic clade, DV1-NI-1, represent increased DENV-1 genetic diversity circulating in Nicaragua in 2022.

DENV-2

We paired 6 DENV-2 sequences with 130 previously published genome sequences for phylogenetic analysis and tree building as previously described (MCC tree, Figure 3; Appendix Figure 2, showing the initial ML tree with 436 taxa). DENV-2 viruses circulating in Nicaragua in 2022 descended from DENV-2 present in Nicaragua since 2013 (clade DV2-NI-3B) and associated with epidemics in 2016 (*10*) and 2019, the latter marked by elevated numbers of cases, increased levels of disease severity, and accelerated rates of adaptive evolution (*18*). The estimated tMRCA of DV2-NI-3 was 2011.7 (95% HPD 2010.8–2012.4) (Figure 3). Globally, this DENV-2 lineage is a member of the Southeast Asian–American genotype IIIb, the only genotype circulating in Nicaragua since 1999 and in the region since the 1980s (*5*,*10*,*18*).

DENV-3

We combined the 38 DENV-3 sequences generated in this study with 93 published sequences to produce an MCC tree (Figure 4; Appendix Figure 3, showing the initial ML tree with 253 taxa). DENV-3 sequences from 2022 all fell within the Indian-subcontinent genotype III, the only genotype to have been detected in Nicaragua, first recorded in 1994 (*34*). Our prior studies had captured DENV-3 sequence evolution until 2014 (*10*,*28*) with an estimated tMRCA

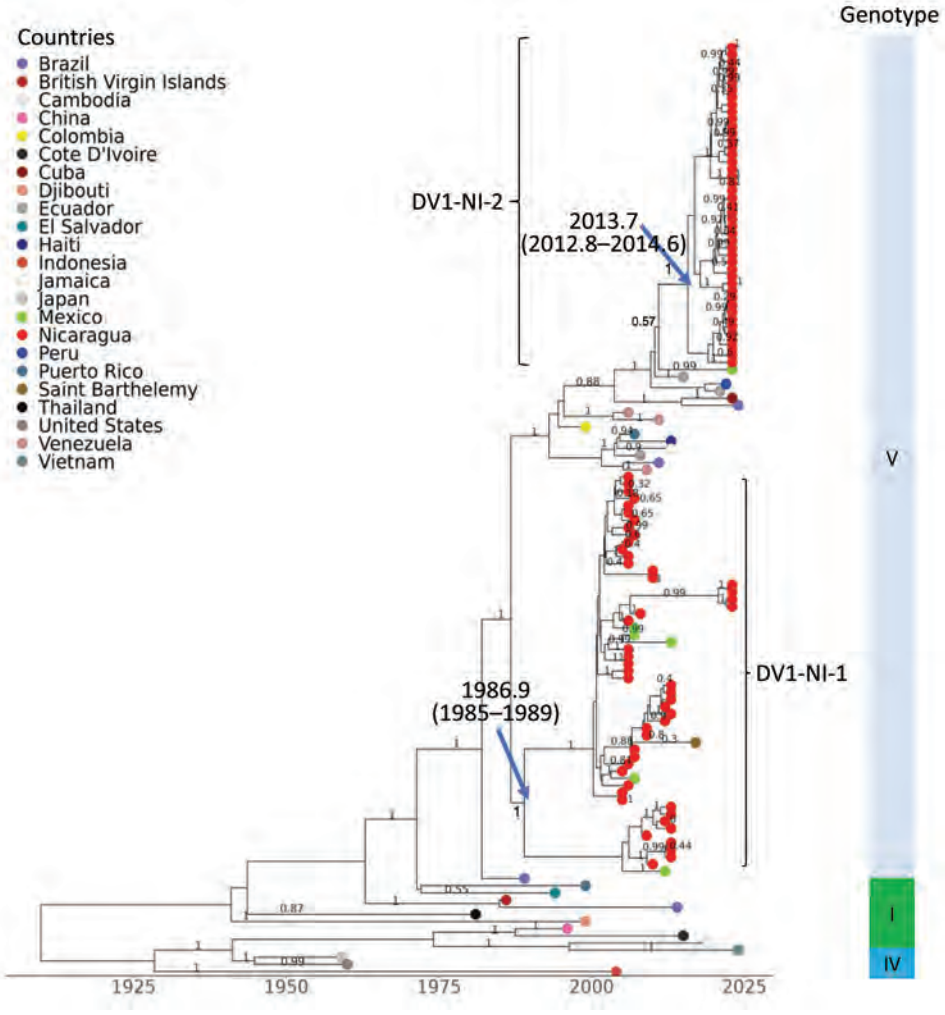

Figure 2. Dengue Virus (DENV) serotype 1 maximum clade credibility tree, generated from 130 DENV-1 nucleotide sequences, showing emergence over time. Sequences are labeled by country of sample origin, indicated by colored circles, and include Nicaragua sequences (red) and publicly available sequences. DENV-1 genotypes are identified in the vertical bar to the right. Two Nicaragua clades, DV1-NI-1 and DV1-NI-2, are indicated with square brackets. The time to most recent common ancestor (95% high probability density range) is indicated at the nodes leading to Nicaragua clades. Posterior node probabilities are indicated at major nodes.

of 2003.8 (95% HPD 2003.2–2004.5) (Figure 4), after which DENV-3 remained undetected until 2022. In 2013 and 2014, multiple lineages of DENV-3 were circulating (*10*), but none persisted; the DENV-3 viruses sequenced in 2022 cluster most closely with viruses reported from Puerto Rico (2022), Brazil (2023), Cuba (2023), the United States (Florida, 2023), and India (2018) (*35*) and have an estimated tMRCA of 2019.8 (95% HPD 2019.5–2020.2) (Figure 4). The basal sequences to this clade are from southern and Southeast Asia, suggesting that the clade was introduced recently (after 2018) into the region, including Nicaragua, replacing earlier strains of this serotype (*11*).

DENV-4

We combined 42 DENV-4 sequences with 73 publicly available sequences to generate an MCC tree (Figure 5; Appendix Figure 4, showing the initial ML tree with 168 taxa). DENV-4 has not been detected in dengue patients in Nicaragua since 2006. Our analysis places DENV-4 sequences within genotype II, Indonesia, with an estimated tMRCA of 2005.1 (95% HPD 2003.7–2006.5) (Figure 5). The sequences most closely related to the Nicaragua strains are from Mexico, El Salvador, and Florida (2021–2022). However, the clade includes basal sequences from Mexico (2010) and Nicaragua (1999), suggesting a regionally long-circulating lineage with not-infrequent exchange between countries since 1999 until 2022. From this information, we conclude that there is a regional reservoir and source of DENV-4 into Nicaragua.

Discussion

In 2022, genomic characterization of DENV in Nicaragua was conducted in real time during an ongoing epidemic. That approach revealed the considerable cocirculation of all 4 DENV serotypes, within the context of a particularly large epidemic in 2022. Phylogenetic analyses of the 2022 viruses enabled us to identify the introduction of new DENV strains (DENV-1,

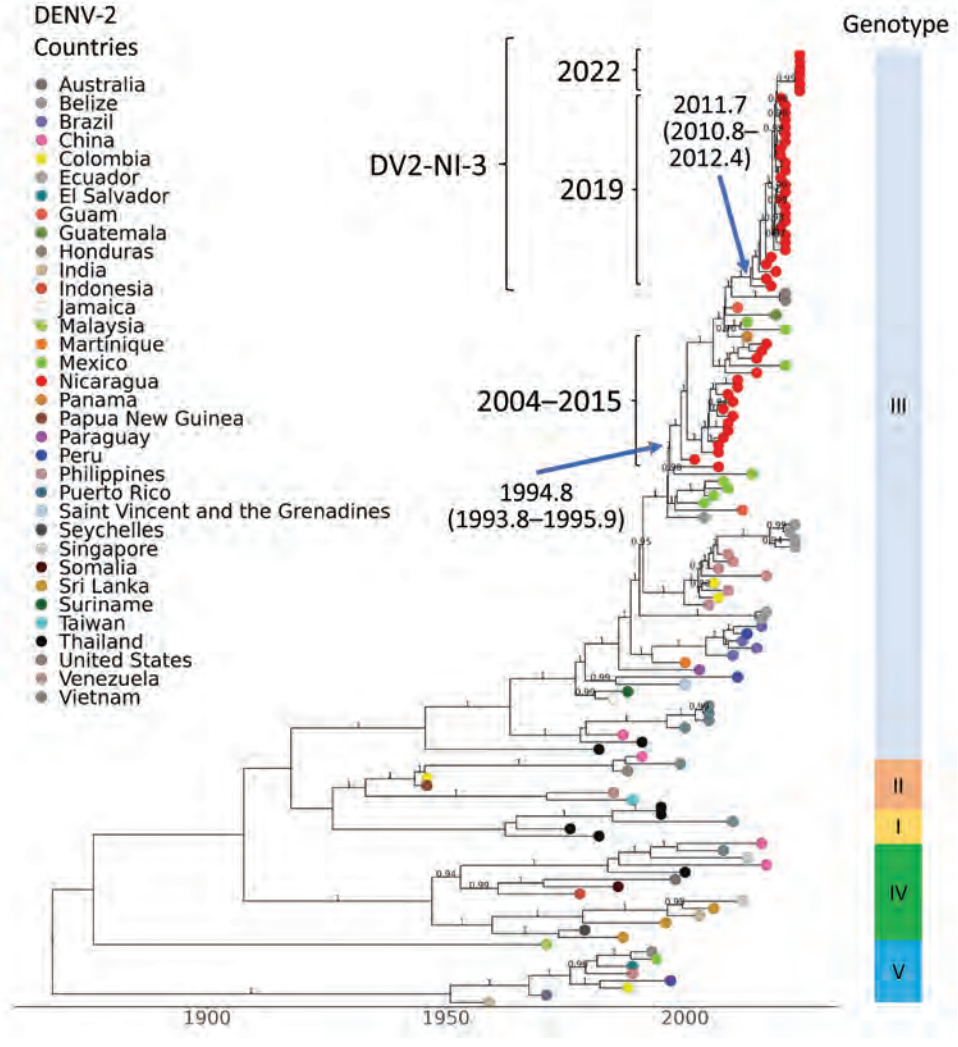

Figure 3. Time-scaled dengue virus (DENV) serotype 2 maximum clade credibility tree, generated from 136 DENV-2 nucleotide sequences, showing emergence over time. Sequences are labeled by country of sample origin, indicated by colored circles, and include Nicaragua sequences (red) and publicly available sequences, as indicated. Nicaragua clades are indicated with square brackets labeled by year(s) of detection, including the DV-NI-3 clade. The time to most recent common ancestor (95% high probability density) is indicated at the nodes leading to Nicaragua clades. Genotypes are identified by vertical bar to the right. Posterior node probabilities are indicated at major nodes.

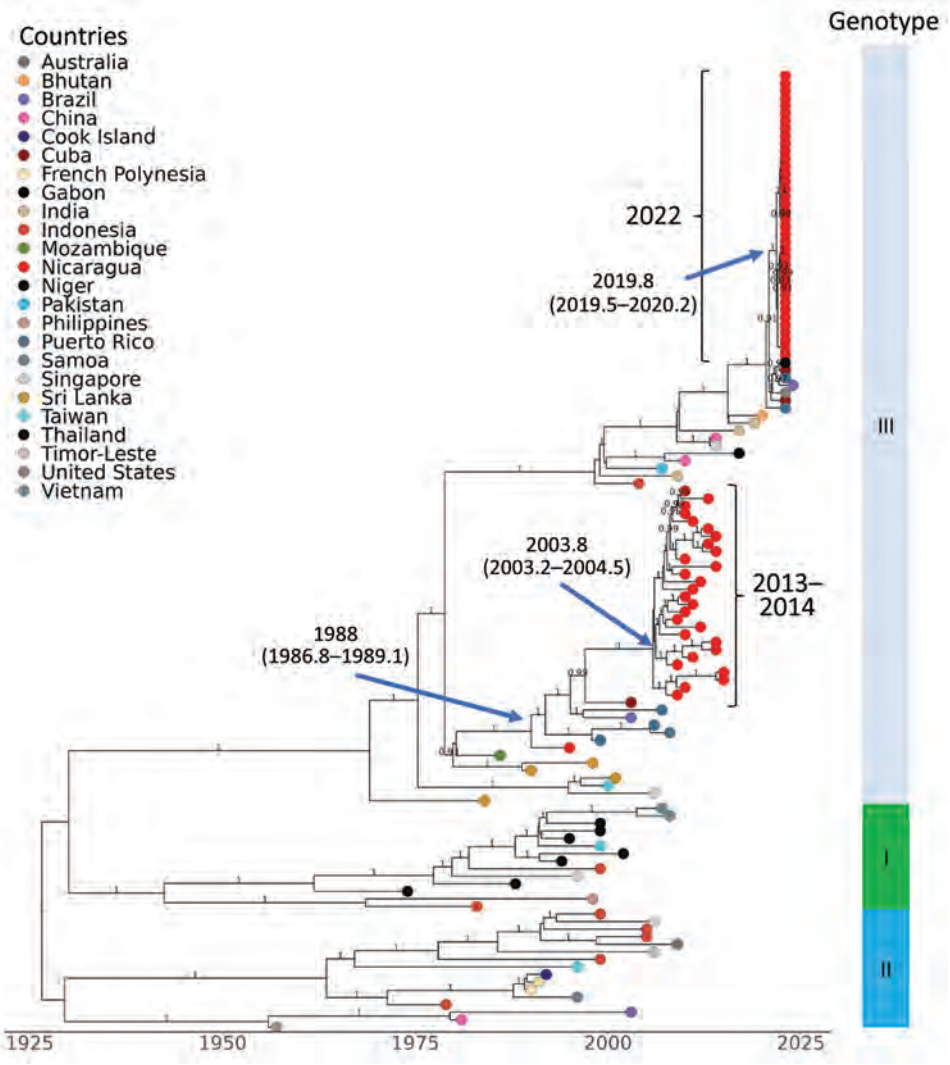

Figure 4. Dengue virus (DENV) serotype 3 maximum clade credibility tree, generated from 131 DENV-3 nucleotide sequences, showing emergence over time. Sequences are labeled by country of sample origin, indicated by colored circles, and include Nicaraguan sequences (red) and publicly available sequences, as indicated. Nicaragua clades are indicated with square brackets labeled by year(s) of detection. The estimated time to most recent common ancestor (95% high probability density) is indicated at the nodes leading to Nicaraguan clades. Genotypes are identified in the vertical bar to the right. Posterior node probabilities are indicated at major nodes.

DENV-3, DENV-4) from different regions of the Americas, although a small number of DENV-1 and DENV-2 viruses remained from previous periods of circulation in Nicaragua. We noted the resurgence of serotypes not seen since 2013 (DENV-1 and DENV-3) and the introduction of DENV-4, which had not circulated at epidemic levels since the early 1990s (*10*,*18*).

Because of the emergence of SARS-CoV-2 in 2019 and the subsequent COVID-19 pandemic, many countries closed their borders, restricted mobility, and implemented social distancing (*36*). Nicaragua was one of the few countries to use alternative approaches to shutdowns (i.e., travel restrictions and neighboring border closures). Vector control activities (e.g., residual indoor and spatial fumigation) were maintained. After 2 years of low dengue case incidence in 2020 and 2021, dengue cases in Nicaragua increased substantially during 2022, marked by the cocirculation of all 4 virus serotypes. We suggest that the marked dominant circulation of DENV-2 over the previous 7 years contributed strongly to the sudden rise of DENV-1, DENV-3, and DENV-4 cases in 2022 after new introductions (*11*,*18*,*37*). The absence of herd immunity to all serotypes except DENV-2, coupled with resumption of postpandemic international travel, increased the risk for establishment of new DENV strains in Nicaragua.

Of the 2022 dengue cases in Nicaragua sequenced in our study, 52% were caused by DENV-1, falling into 2 coexisting lineages within genotype V. Although a small number of sequences persisted from earlier 2012–2013 epidemics, 90% formed a new clade (DV1-NI-2) with genetic ties to DENV-1 in Ecuador, Colombia, and Venezuela. Gene flow has been previously reported among those countries (*38*,*39*) and might have been accelerated by post–COVID-19 border openings and regional increases in movement or displacement with South America (*40*), ultimately

leading to a turnover of the previous Nicaragua DENV-1 strains. Alternatively, the evolution of clades could represent undetected transmission of DENV-1 in the country over that period, which seems to be the case with DV1-NI-1. However, our results suggest that DV1-NI-2 was introduced after 2013. Pinpointing the exact source and potential influence of neighboring countries such as Costa Rica and Panama, with which Nicaragua shares close migratory ties, is limited because of the lack of public sequences from Central America during the study period.

Previous studies have detailed the clinical, epidemiologic, and immunologic pattern of DENV-2 within the Nicaragua population (*3*,*5*,*10*,*11*,*41*,*42*) (F. Narvaez et al., unpub. data, https://www.medrxiv.org/content/10.1101/2024.02.11.24302393v1). Emergence of the new, more fit, DV2-NI-2B clade (*5*,*43*) in an immunologically susceptible population during 2007–2008 was followed by further adapted DENV-2 lineages associated with outbreaks in 2015–2016 and 2019 (DV2-NI-3) (*10*,*18*). Our analysis confirmed that DENV-2 strains during 2022 descended from these previous strains, within the Southeast Asian–American genotype IIIb. Unlike the other serotypes, evolution of the DV2-NI-3 clade is consistent with a single introduction and subsequent local expansion, with no additional introductions or admixture from other regions, based on publicly available reference sequences. We believe that the recent decrease in DENV-2 cases within the population resulted from development of serotype-specific immunity from many years of almost exclusive apparent circulation of DENV-2. The low immunologic profile of the other serotypes contributed to a change in the disease trend of shifting dominance to serotypes other than DENV-2, as well as increased cases in 2022. Nevertheless, the recent introduction of the cosmopolitan DENV-2 genotype into Peru in 2019 (*44*) and Brazil in 2021 (*45*,*46*)

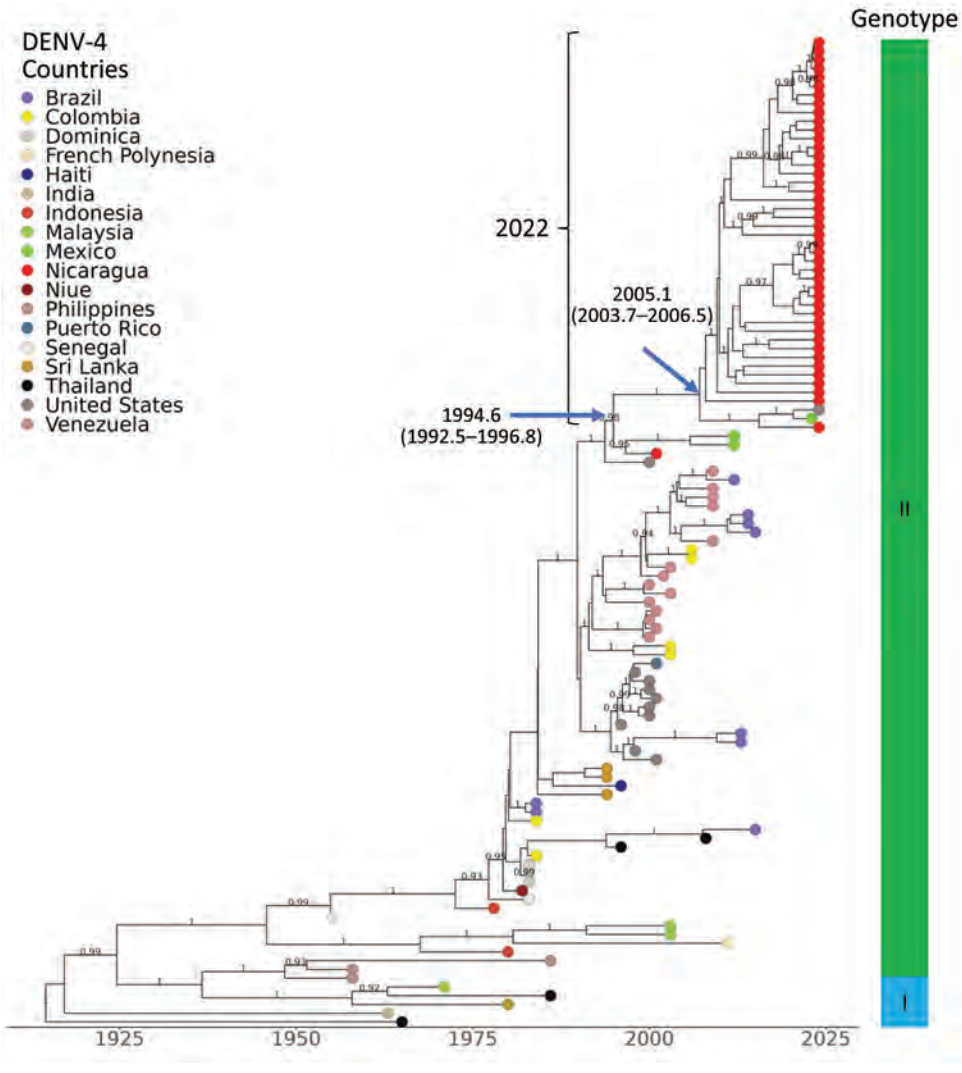

Figure 5. Dengue virus (DENV) serotype 4 maximum clade credibility tree, generated from 115 DENV-4 nucleotide sequences, showing emergence over time. Sequences are labeled by country of sample origin, indicated by colored circles, and include Nicaragua sequences (red) and publicly available sequences, as indicated. Nicaragua clades are indicated with square brackets labeled by year of detection. The time to most recent common ancestor (95% high probability density) is indicated at the nodes leading to Nicaragua clades. Genotypes are identified in the vertical bar to the right. Posterior node probabilities are indicated at major nodes.

poses a new risk for the country. As herd immunity for DENV-2 wanes with time, the introduction of a new genotype of DENV-2 associated with greater severity could increase both the incidence and severity of future cases. That possibility highlights the value of strong and continued genomic surveillance of DENV to determine in real time the genetic diversity and possible correlation with severity in future epidemics in Nicaragua.

Starting with the large 1994 dengue epidemic that was triggered by the initial introduction of DENV-3 into Nicaragua (*47*), DENV-3 has continued to cause epidemics (*14*,*28*). Dominating during 2008–2011, including a major epidemic in 2009–2010 (*28*), DENV-3 dropped noticeably in 2013–2014 (*10*). The 2013–2014 viruses were associated with earlier DENV-3 lineages circulating in Nicaragua (*10*), whereas our analysis reveals that 2022 DENV-3 strains, while still belonging to genotype III/Indian subcontinent, are part of a new, genetically distinct, monophyletic clade, replacing the previous variants. The clustering of the 2022 DENV-3 clade with viruses from India (2018), Puerto Rico (2022), and Brazil-Cuba-Florida (2023) implicates a recent introduction into the region, similar to DENV-1, possibly resulting from opened borders and increased international travel, and may represent an emerging epidemiologic situation of ongoing exchange between countries in the Caribbean, Central America, and South America.

In Nicaragua, DENV-4 caused epidemics in the early 1990s and has been virtually unreported since, with the exception of a few cases in 2006–2008, despite reports of DENV-4 circulation in South America in 2010 (*48*). In 2022, DENV-4 reemerged in Nicaragua, codominating the epidemic with DENV-1. That phenomenon could be attributed to low herd immunity resulting from limited DENV-4 circulation over the previous 30 years, coupled with increased cross-border and domestic movement leading to local virus transmission of what is considered the mildest of the 4 serotypes (*7*). DENV-4 sequences recovered in 2022 clustered with viruses from Florida, El Salvador, and Mexico collected in the same time frame, although the clade does have roots in Nicaragua (1999) as well as the region (e.g., Mexico 2010), suggesting resurgence of a long-standing lineage endemic to regions in Central America and the Caribbean.

We note limitations of this research in inferring chains of transmission within and across geographic regions, which would require systematic sampling of the populations in question—a resource-intensive undertaking involving the collaboration of epidemiologists, health services, and national virology laboratories. In the absence of comprehensive sampling, the issue of bias was addressed by random sampling for sequencing by the laboratory, stratified by geographic source within the country, without knowledge of the clinical status of the patient. We acknowledge that our phylogenetic inferences are biased by the sequence data available in the public domain, as with any phylogenetic analysis accessing publicly available sequences. Last, we did not assess the contribution of mosquito vectors to the transmission dynamics of dengue viruses. Nonetheless, our data offer valuable insights that will be beneficial for future research locally and regionally.

We report a new landscape of DENV transmission in Nicaragua, marked by the cocirculation of all 4 serotypes along with intensifying epidemic magnitude. Of the 4 DENV serotypes, 3 resurged after almost a decade or more of low to no case reports and coincide with the introduction of new lineages. We posit that the dengue hyperendemicity is the result of 2 windows of opportunity: a vacuum of herd immunity against DENV-1, DENV-3, and DENV-4 resulting from the prolonged dominance of DENV-2; and a surge of regional and international travel on the heels of COVID-19-induced country-level and worldwide mobility restrictions (*49*). The landscape of DENV transmission has been reset to include the active circulation of all 4 serotypes after the 2016 introduction of Zika virus, which is known to engender DENV cross-reactive immune responses with epidemiologic and clinical consequences (*11*,*12*). Our findings underscore the urgent need for public health interventions aimed at controlling the spread of dengue in Nicaragua and beyond, particularly in light of the increasing intensity of dengue epidemics and the potential for further transmission fueled by regional and international travel.

Acknowledgments

We are grateful to the study staff of the PDCS, PDHS, and A2CARES studies at the Sustainable Sciences Institute, National Virology Laboratory at the National Center for Diagnosis and Reference, Hospital Infantil Manuel de Jesús Rivera, Health Center Sócrates Flores Vivas, and Health Posts Camilo Ortega and Nejapa for their valuable contribution and assistance. We also extend our heartfelt thanks to our colleagues Paúl Cárdenas, Sully Márquez, Belén Prado, and Mateo Carvajal, who generously volunteered their time and effort to train Nicaraguan counterparts in sequencing and bioinformatics techniques that enabled our study to be conducted.

This work was supported by grants U01AI151788 (to E.H., J.C.) and P01AI106695 (to E.H.) from the National Institute of Allergy and Infectious Disease at the US National Institutes of Health.

The authors declare no conflicts of interest in this work. The funders had no role in the design, execution, interpretation, or reporting of the study.

About the Author

Mr. Cerpas has worked at the Sustainable Science Institute in Managua, Nicaragua, for over a decade. This manuscript formed the basis of his Master of Science degree in clinical biochemistry from the Universidad Nacional Autónoma de Nicaragua, León. His current research focuses on the genomic epidemiology and dynamics of viral diseases. He is also interested in studying how the immune system responds to dengue virus, Zika virus, and SARS-CoV-2 infections, as well as HIV drug-resistance mechanisms.

References

1. World Health Organization. Dengue and severe dengue [cited 2023 Oct 11]. https://www.who.int/news-room/fact-sheets/detail/dengue-and-severe-dengue
2. Holmes EC, Twiddy SS. The origin, emergence and evolutionary genetics of dengue virus. Infect Genet Evol. 2003;3:19–28. https://doi.org/10.1016/S1567-1348(03)00004-2
3. Balmaseda A, Hammond SN, Pérez L, Tellez Y, Saborío SI, Mercado JC, et al. Serotype-specific differences in clinical manifestations of dengue. Am J Trop Med Hyg. 2006;74:449–56. https://doi.org/10.4269/ajtmh.2006.74.449
4. Nisalak A, Endy TP, Nimmannitya S, Kalayanarooj S, Thisayakorn U, Scott RM, et al. Serotype-specific dengue virus circulation and dengue disease in Bangkok, Thailand from 1973 to 1999. Am J Trop Med Hyg. 2003;68:191–202. https://doi.org/10.4269/ajtmh.2003.68.191
5. OhAinle M, Balmaseda A, Macalalad AR, Tellez Y, Zody MC, Saborío S, et al. Dynamics of dengue disease severity determined by the interplay between viral genetics and serotype-specific immunity. Sci Transl Med. 2011;3:114ra128. https://doi.org/10.1126/scitranslmed.3003084
6. Vaughn DW, Green S, Kalayanarooj S, Innis BL, Nimmannitya S, Suntayakorn S, et al. Dengue viremia titer, antibody response pattern, and virus serotype correlate with disease severity. J Infect Dis. 2000;181:2–9. https://doi.org/10.1086/315215
7. Gubler DJ. Dengue and dengue hemorrhagic fever. Clin Microbiol Rev. 1998;11:480–96. https://doi.org/10.1128/CMR.11.3.480
8. Paz-Bailey G, Adams LE, Deen J, Anderson KB, Katzelnick LC. Dengue. Lancet. 2024;403:667–82. https://doi.org/10.1016/S0140-6736(23)02576-X
9. Kouri G, Valdéz M, Arguello L, Guzmán MG, Valdés L, Soler M, et al. [Dengue epidemic in Nicaragua, 1985] [in Spanish]. Rev Inst Med Trop São Paulo. 1991;33:365–71. https://doi.org/10.1590/S0036-46651991000500005
10. Edgerton SV, Thongsripong P, Wang C, Montaya M, Balmaseda A, Harris E, et al. Evolution and epidemiologic dynamics of dengue virus in Nicaragua during the emergence of chikungunya and Zika viruses. Infect Genet Evol. 2021;92:104680. https://doi.org/10.1016/j.meegid.2020.104680
11. Katzelnick LC, Narvaez C, Arguello S, Lopez Mercado B, Collado D, Ampie O, et al. Zika virus infection enhances future risk of severe dengue disease. Science. 2020;369:1123–8. https://doi.org/10.1126/science.abb6143
12. Zambrana JV, Hasund CM, Aogo RA, Bos S, Arguello S, Gonzalez K, et al. Primary exposure to Zika virus increases risk of symptomatic dengue virus infection with serotypes 2, 3, and 4 but not serotype 1. Sci Transl Med. 2024. In press.
13. Hammond SN, Balmaseda A, Pérez L, Tellez Y, Saborío SI, Mercado JC, et al. Differences in dengue severity in infants, children, and adults in a 3-year hospital-based study in Nicaragua. Am J Trop Med Hyg. 2005;73:1063–70. https://doi.org/10.4269/ajtmh.2005.73.1063
14. Harris E, Videa E, Pérez L, Sandoval E, Téllez Y, Pérez ML, et al. Clinical, epidemiologic, and virologic features of dengue in the 1998 epidemic in Nicaragua. Am J Trop Med Hyg. 2000;63:5–11. https://doi.org/10.4269/ajtmh.2000.63.5
15. Katzelnick LC, Gresh L, Halloran ME, Mercado JC, Kuan G, Gordon A, et al. Antibody-dependent enhancement of severe dengue disease in humans. Science. 2017;358:929–32. https://doi.org/10.1126/science.aan6836
16. Kuan G, Gordon A, Avilés W, Ortega O, Hammond SN, Elizondo D, et al. The Nicaraguan pediatric dengue cohort study: study design, methods, use of information technology, and extension to other infectious diseases. Am J Epidemiol. 2009;170:120–9. https://doi.org/10.1093/aje/kwp092
17. Narvaez F, Gutierrez G, Pérez MA, Elizondo D, Nuñez A, Balmaseda A, et al. Evaluation of the traditional and revised WHO classifications of Dengue disease severity. PLoS Negl Trop Dis. 2011;5:e1397. https://doi.org/10.1371/journal.pntd.0001397
18. Thongsripong P, Edgerton SV, Bos S, Saborío S, Kuan G, Balmaseda A, et al. Phylodynamics of dengue virus 2 in Nicaragua leading up to the 2019 epidemic reveals a role for lineage turnover. BMC Ecol Evol. 2023;23:58. https://doi.org/10.1186/s12862-023-02156-4
19. Waggoner JJ, Gresh L, Mohamed-Hadley A, Ballesteros G, Davila MJV, Tellez Y, et al. Single-reaction multiplex reverse transcription PCR for detection of Zika, chikungunya, and dengue viruses. Emerg Infect Dis. 2016;22:1295–7. https://doi.org/10.3201/eid2207.160326
20. Waggoner JJ, Abeynayake J, Sahoo MK, Gresh L, Tellez Y, Gonzalez K, et al. Single-reaction, multiplex, real-time rt-PCR for the detection, quantitation, and serotyping of dengue viruses. PLoS Negl Trop Dis. 2013;7:e2116. https://doi.org/10.1371/journal.pntd.0002116
21. Sarkar S, Bora I, Gupta P, Sapkal G, Shethi S, Kaur K, et al. Utility of CDC DENV1-4 real time PCR assay and trioplex assay for the diagnosis of dengue in patients with acute febrile illness. Virusdisease. 2023;34:365–72. https://doi.org/10.1007/s13337-023-00831-0
22. Vogels CBF, Hill V, Breban MI, Chaguza C, Paul LM, Sodeinde A, et al. DengueSeq: a pan-serotype whole genome amplicon sequencing protocol for dengue virus. BMC Genomics. 2024;25:433. https://doi.org/10.1186/s12864-024-10350-x
23. Quick J, Grubaugh ND, Pullan ST, Claro IM, Smith AD, Gangavarapu K, et al. Multiplex PCR method for MinION and Illumina sequencing of Zika and other virus genomes directly from clinical samples. Nat Protoc. 2017;12:1261–76. https://doi.org/10.1038/nprot.2017.066
24. De Coster W, D'Hert S, Schultz DT, Cruts M, Van Broeckhoven C. NanoPack: visualizing and processing

long-read sequencing data. Bioinformatics. 2018;34:2666–9. https://doi.org/10.1093/bioinformatics/bty149
25. Stamatakis A. RAxML version 8: a tool for phylogenetic analysis and post-analysis of large phylogenies. Bioinformatics. 2014;30:1312–3. https://doi.org/10.1093/bioinformatics/btu033
26. Katoh K, Misawa K, Kuma K, Miyata T. MAFFT: a novel method for rapid multiple sequence alignment based on fast Fourier transform. Nucleic Acids Res. 2002;30:3059–66. https://doi.org/10.1093/nar/gkf436
27. Balmaseda A, Sandoval E, Pérez L, Gutiérrez CM, Harris E. Application of molecular typing techniques in the 1998 dengue epidemic in Nicaragua. Am J Trop Med Hyg. 1999;61:893–7. https://doi.org/10.4269/ajtmh.1999.61.893
28. Gutierrez G, Standish K, Narvaez F, Perez MA, Saborio S, Elizondo D, et al. Unusual dengue virus 3 epidemic in Nicaragua, 2009. PLoS Negl Trop Dis. 2011;5:e1394. https://doi.org/10.1371/journal.pntd.0001394
29. Gordon A, Gresh L, Ojeda S, Chowell G, Gonzalez K, Sanchez N, et al. Differences in transmission and disease severity between 2 successive waves of chikungunya. Clin Infect Dis. 2018;67:1760–7. https://doi.org/10.1093/cid/ciy356
30. Zambrana JV, Bustos Carrillo F, Burger-Calderon R, Collado D, Sanchez N, Ojeda S, et al. Seroprevalence, risk factor, and spatial analyses of Zika virus infection after the 2016 epidemic in Managua, Nicaragua. Proc Natl Acad Sci U S A. 2018;115:9294–9. https://doi.org/10.1073/pnas.1804672115
31. Kubale J, Balmaseda A, Frutos AM, Sanchez N, Plazaola M, Ojeda S, et al. Association of SARS-CoV-2 seropositivity and symptomatic reinfection in children in Nicaragua. JAMA Netw Open. 2022;5:e2218794. https://doi.org/10.1001/jamanetworkopen.2022.18794
32. Agence France Presse. 2020. Aeropuerto de Managua reanuda vuelos tras cierre por covid-19 [cited 2023 Oct 27]. https://www.france24.com/es/20200919-aeropuerto-de-managua-reanuda-vuelos-tras-cierre-por-covid-19
33. Despacho 505. Aeropuerto de Nicaragua estará cerrado hasta junio. Despacho 505 [cited 2023 Oct 27]. https://www.despacho505.com/aeropuerto-de-nicaragua-estara-cerrado-hasta-junio
34. Messer WB, Gubler DJ, Harris E, Sivananthan K, de Silva AM. Emergence and global spread of a dengue serotype 3, subtype III virus. Emerg Infect Dis. 2003;9:800–9. https://doi.org/10.3201/eid0907.030038
35. Naveca FG, Santiago GA, Maito RM, Ribeiro Meneses CA, do Nascimento VA, de Souza VC, et al. Reemergence of dengue virus serotype 3, Brazil, 2023. Emerg Infect Dis. 2023;29:1482–4. https://doi.org/10.3201/eid2907.230595
36. Wilder-Smith A, Bar-Yam Y, Fisher D. Lockdown to contain COVID-19 is a window of opportunity to prevent the second wave. J Travel Med. 2020;27:taaa091 https://doi.org/10.1093/jtm/taaa091
37. Katzelnick LC, Coloma J, Harris E. Dengue: knowledge gaps, unmet needs, and research priorities. Lancet Infect Dis. 2017;17:e88–100. https://doi.org/10.1016/S1473-3099(16)30473-X
38. Márquez S, Lee G, Gutiérrez B, Bennett S, Coloma J, Eisenberg JNS, et al. Phylogenetic Analysis of transmission dynamics of dengue in large and small population centers, northern Ecuador. Emerg Infect Dis. 2023;29:888–97. https://doi.org/10.3201/eid2905.221226
39. Stewart-Ibarra AM, Ryan SJ, Kenneson A, King CA, Abbott M, Barbachano-Guerrero A, et al. The burden of dengue fever and chikungunya in southern coastal Ecuador: epidemiology, clinical presentation, and phylogenetics from the first two years of a prospective study. Am J Trop Med Hyg. 2018;98:1444–59. https://doi.org/10.4269/ajtmh.17-0762
40. United Nations High Commissioner for Refugees. Critical needs in the Americas [cited Oct 27]. https://reliefweb.int/report/venezuela-bolivarian-republic/critical-needs-americas-august-2023-enpt
41. Añez G, Morales-Betoulle ME, Rios M. Circulation of different lineages of dengue virus type 2 in Central America, their evolutionary time-scale and selection pressure analysis. PLoS One. 2011;6:e27459. https://doi.org/10.1371/journal.pone.0027459
42. Balmaseda A, Standish K, Mercado JC, Matute JC, Tellez Y, Saborío S, et al. Trends in patterns of dengue transmission over 4 years in a pediatric cohort study in Nicaragua. J Infect Dis. 2010;201:5–14. https://doi.org/10.1086/648592
43. Quiner CA, Parameswaran P, Ciota AT, Ehrbar DJ, Dodson BL, Schlesinger S, et al. Increased replicative fitness of a dengue virus 2 clade in native mosquitoes: potential contribution to a clade replacement event in Nicaragua. J Virol. 2014;88:13125–34. https://doi.org/10.1128/JVI.01822-14
44. García MP, Padilla C, Figueroa D, Manrique C, Cabezas C. Emergence of the Cosmopolitan genotype of dengue virus serotype 2 (DENV2) in Madre de Dios, Peru, 2019. [in Spanish]. Rev Peru Med Exp Salud Publica. 2022;39:126–8. https://doi.org/10.17843/rpmesp.2022.391.10861
45. Amorim MT, Hernández LHA, Naveca FG, Essashika Prazeres IT, Wanzeller ALM, Silva EVPD, et al. Emergence of a new strain of DENV-2 in South America: introduction of the cosmopolitan genotype through the Brazilian-Peruvian border. Trop Med Infect Dis. 2023;8:325. https://doi.org/10.3390/tropicalmed8060325
46. Giovanetti M, Pereira LA, Santiago GA, Fonseca V, Mendoza MPG, de Oliveira C, et al. Emergence of dengue virus serotype 2 cosmopolitan genotype, Brazil. Emerg Infect Dis. 2022;28:1725–7. https://doi.org/10.3201/eid2808.220550
47. Guzmán MG, Vázquez S, Martínez E, Álvarez M, Rodríguez R, Kourí G, et al. Dengue in Nicaragua, 1994: reintroduction of serotype 3 in the Americas. Rev Panam Salud Publica. 1997;1:193–9. https://doi.org/10.1590/S1020-49891997000300005
48. Ramos-Castañeda J, Barreto Dos Santos F, Martínez-Vega R, Galvão de Araujo JM, Joint G, Sarti E. Dengue in Latin America: systematic review of molecular epidemiological trends. PLoS Negl Trop Dis. 2017;11:e0005224. https://doi.org/10.1371/journal.pntd.0005224
49. UN World Tourism Organization Tourism Data Dashboard. Regional global tourism results [cited 2023 Mar 4]. https://www.unwto.org/es/datos-turismo/resultados-turisticos-globales-regionales

Address for correspondence: Eva Harris, Division of Infectious Diseases and Vaccinology, School of Public Health, University of California, Berkeley, 185 Li Ka Shing Center, 1951 Oxford St, Berkeley, CA 94720-3370, USA; email: eharris@berkeley.edu

Autochthonous *Plasmodium vivax* Infections, Florida, USA, 2023

Azhar Muneer,[1] Swamy R. Adapa,[1] Suzane Silbert, Kelly Scanlan, Harold Vore, Andrew Cannons, Andrea M. Morrison, Danielle Stanek, Carina Blackmore, John H. Adams, Kami Kim,[2] Rays H.Y. Jiang,[2] Liwang Cui[2]

During May–July 2023, a cluster of 7 patients at local hospitals in Florida, USA, received a diagnosis of *Plasmodium vivax* malaria. Whole-genome sequencing of the organism from 4 patients and phylogenetic analysis with worldwide representative *P. vivax* genomes indicated probable single parasite introduction from Central/South America.

Although commendable progress for combating malaria in endemic areas has been achieved and a dozen countries have been declared malaria-free since 2000 (*1*), increasing international travel has led to a rise in imported malaria cases, as well as sporadic cases of autochthonous malaria in non–malaria-endemic regions, especially those with competent vectors and favorable transmission conditions (*2*). In 2003 and 2023, two malaria outbreaks with local *Plasmodium vivax* transmission were reported in Florida (*3*,*4*). We examined the genomic characteristics, probable transmission dynamics, and likely origins of the 2023 *P. vivax* strains in Florida, demonstrating the role of genomic epidemiology in malaria control in non–malaria-endemic regions.

The Study

During May–July 2023, the Florida Department of Health received reports of a series of 7 cases of *P. vivax* malaria (*4*). The patients lacked risk factors for contracting malaria (e.g., recent histories of international travel, blood transfusion, or previous malaria), raising concerns for local mosquito transmission. All 7 patients were concentrated within a 4-mile radius, raising further concern about potential local transmission cycles. Pretreatment blood samples from 4 patients were collected on June 18, 20, 27, and July 12 (Appendix Figure 1, https://wwwnc.cdc.gov/EID/article/30/6/24-0336-App1.pdf). We used the anonymized remnant clinical samples collected for diagnosis purposes. Species-specific PCR of the samples (*5*) confirmed *P. vivax* infections (Figure 1). Three *Anopheles* mosquitoes collected in the affected region in June also tested positive for *P. vivax* (*4*).

To trace the origin of those *P. vivax* cases, we isolated DNA from 200 μL of whole blood from 4 patients by using a QIAamp DNA Blood Mini Kit (QIAGEN, https://www.qiagen.com). Recognizing the limited *P. vivax* DNA contaminated with overwhelming amounts of human DNA, we performed selective whole-genome amplification (sWGA) with *P. vivax*–specific primers (pvset1920) to enrich the *P. vivax* genome (*6*). Each 50-μL amplification reaction included 30 U of phi29 polymerase enzyme (New England Biolabs, https://www.neb.com), 1% bovine serum albumin, 2 mM of each of the 4 deoxynucleosides triphosphate, 3.5 μM of selective whole-genome amplification primers, and ≈70 ng of input DNA. Thermocycler conditions consisted of ramping down from 35°C to 30°C at a rate of 0.1°C per minute, 30°C for 16 hours, and 65°C for 10 minutes. The reaction product was purified with AMPure XP beads (Beckman-Coulter, https://www.beckmancoulter.com) and eluted in 50 μL Tris-EDTA buffer (pH 8). We obtained 10–12 μg of amplification product for each sample.

The sequencing libraries were prepared by using an Illumina DNA Prep Kit (https://www.illumina.com)

Author affiliations: University of South Florida Morsani College of Medicine, Tampa, Florida, USA (A. Muneer, K. Kim, L. Cui); University of South Florida School of Public Health, Tampa (S.R. Adapa, J.H. Adams, K. Kim, R.H.Y. Jiang); Tampa General Hospital, Tampa (S. Silbert, K. Kim); Sarasota Memorial Hospital, Sarasota, Florida, USA (K. Scanlan, H. Vore); Florida Department of Health Bureau of Public Health Laboratories, Tampa (A. Cannons); Florida Department of Health, Tallahassee, Florida, USA (A.M. Morrison, D. Stanek, C. Blackmore)

DOI: https://doi.org/10.3201/eid3006.240336

[1]These authors contributed equally to this article.

[2]These authors were co-principal investigators.

and were pooled and sequenced for 100 million reads at 150-bp paired-end reads mode on the Illumina Nextseq 2000 platform. After trimming adapters and removing low-quality reads (*7*), we aligned high-quality reads to the *P. vivax* PvP01 reference genome by using the BWA-MEM (Burroughs-Wheeler Aligner–maximum exact matches) algorithm (*8*). We compressed, sorted, and indexed the alignment files by using SAMtools version 1.11 (*9*). For the 4 samples, we mapped 3%, 16%, 29%, and 55% of total reads to the PvP01 genome (Table), resulting in 7–124-fold and ≈72% coverage of the PvP01 genome. We deposited sequence data in the National Center for Biotechnology Information BioProject database (https://www.ncbi.nlm.nih.gov; BioProject no. PRJNA1093439).

We performed variant calling by using the GATK HaplotypeCaller (https://gatk.broadinstitute.org). To retain only high-confidence variants, we applied stringent quality filtering criteria to the VCF (variant call format) files. Comparison with the PvP01 sequence identified 97,180 high-quality single-nucleotide polymorphisms (SNPs), of which 38,799 were shared among all 4 Florida *P. vivax* isolates.

Next, we calculated the within-host fixation index for each patient sample, which was >0.95, indicating monoclonal infections. Of note, 57,656 (≈60%) SNPs were shared among samples 2, 3, and 4, indicating their close genetic relationships. The level of genetic variation was similar to the limited variation found in meiosis of single crosses (*10*), suggesting a limited local transmission event, likely seeded by a single introduction into Florida.

We constructed phylogeny between the Florida *P. vivax* isolates and 53 selected genomes from a global collection of 1,041 isolates (MalariaGen Pv4) (*11*). We chose a dataset consisting of high-quality *P. vivax* genome sequences from all continents where *P. vivax* is endemic (Figure 2, panel A). We constructed phylogenetic trees by using IQtree version 2.2.0 (*12*) and the general time-reversible model with ascertainment bias corrrection or the general time-reversible model with proportion of invariable sites and gamma-distributed rate heterogeneity. We evaluated both models with 1,000 ultrafast bootstrap approximation replicates and Shimodaira-Hasegawa–like approximate likelihood ratio test iterations. We assigned the final phylogenetic tree on the basis of bootstrap support values, ensuring robust statistical support for the inferred relationships. To ensure the reliability of the phylogenetic models, we allowed both models to converge; convergence was assessed at 300 iterations. We visualized and annotated the generated tree file by using Interactive Tree Of Life v.6 (*13*). Phylogenetic analysis with genome-wide SNPs revealed continental *P. vivax* population division (Figure 2, panel B) as previously reported (*11*). The *P. vivax* isolates from Florida, showing a pairwise genome distance of <0.01, formed a tight cluster (Appendix Figure 2), suggesting that they were probably the progeny of a single parasite isolate. Those isolates formed a highly supported Central/South America cluster (Figure 1). In sum, the timeline of the 7 cases (*3,4*) and our phylogenomic analysis support the interpretation of a single, limited introduction event from Central/South America into Florida.

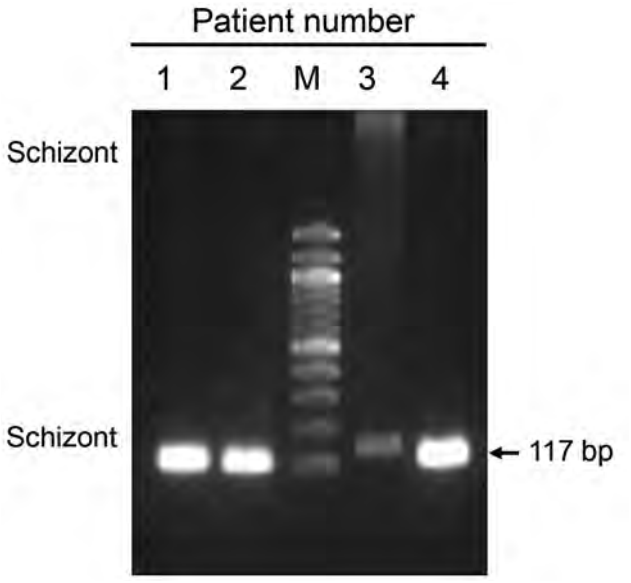

Figure 1. Identification of *Plasmodium vivax* infections in blood samples from malaria patients, Florida, USA, May–July 2023. Image shows 117-bp PCR products amplified from blood samples from 4 patients by using *P. vivax*–specific primers targeting the 18S rRNA gene. M, DNA ladder.

Conclusions

Each year in the United States, ≈2,000 cases of imported malaria are reported to the Centers for Disease

Table. Whole-genome sequencing of *Plasmodium vivax* isolates from 4 malaria patients, Florida, USA, May–July 2023*

Patient no.	Sample collection date	Total reads	Reads mapped to PvP01, no. (%)	Mean PvP01 coverage, × (%)
1	Jun 18	39,350,480	1,163,557 (3)	7.0 (72.3)
2	Jun 20	41,417,476	6,725,684 (16)	40.2 (72.3)
3	Jun 27	35,086,122	10,243,361 (29)	72.6 (72.3)
4	Jul 12	37,493,726	20,596,607 (55)	124.2 (72.3)

*PvP01, reference genome for *Plasmodium vivax*.

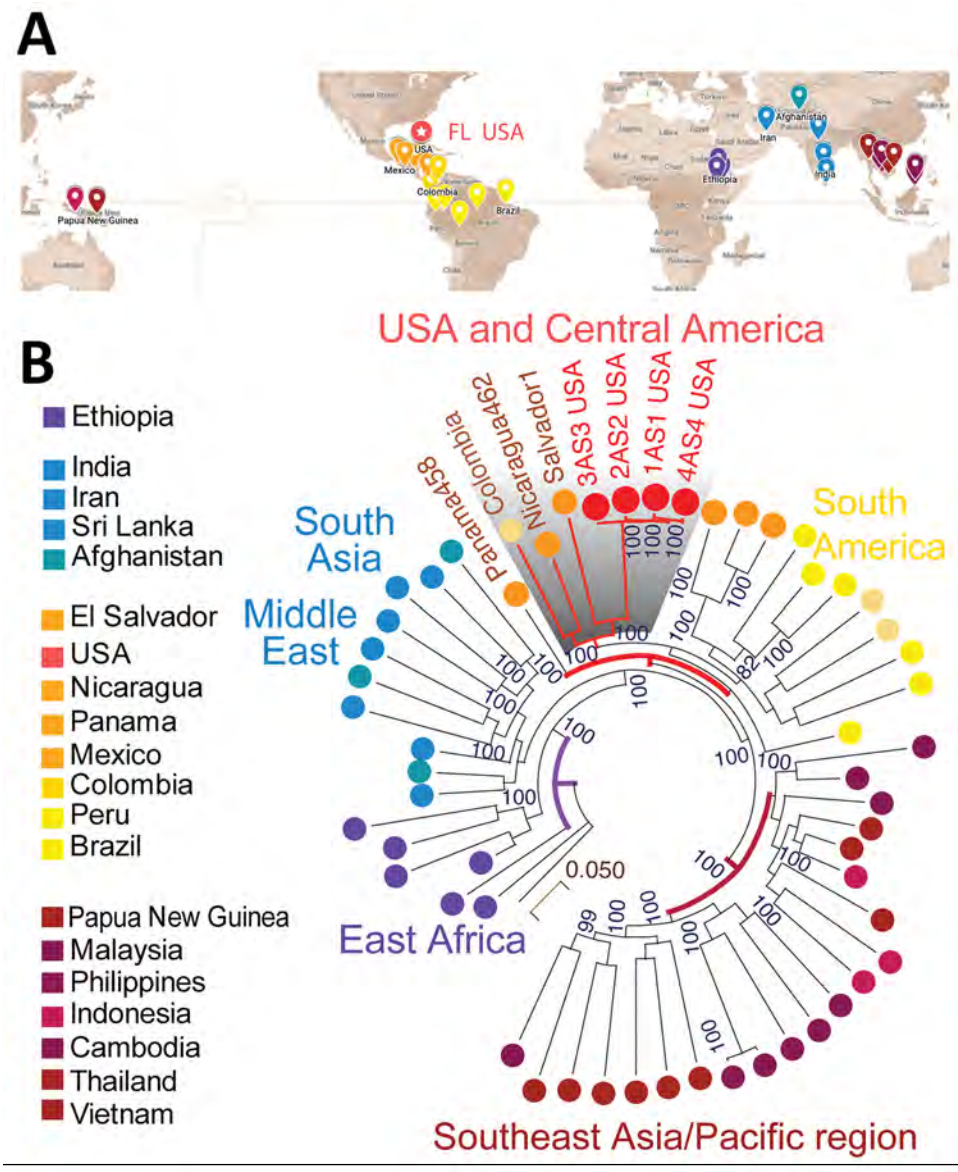

Figure 2. Phylogenetic analysis of *Plasmodium vivax* strains from blood samples from malaria patients, Florida, USA, May–July 2023, suggesting Central/South America origin. A) Geographic distribution of 53 high-quality global strains selected from >1,000 global *P. vivax* collections. B) Florida *P. vivax* strains clustering with Central/South America strains. The phylogenetic tree was constructed by using the maximum-likelihood method, and 1,000 bootstrap replications are shown next to the branches. The color coding of the geographic origin of the isolates matches the global map in panel A. The US and Central/South American cluster is shaded gray. The 4 Florida *P. vivax* strains are denoted as 1AS1, 2AS2, SAS3, and 4AS4. Scale bar indicates nucleotide substitutions per site.

Control and Prevention (*14*). Although most cases are caused by *P. falciparum* infections, the 2003 and 2023 autochthonous outbreaks in Florida were caused by *P. vivax* (*3*,*4*). Similarly, local outbreaks from introduced *P. vivax* in Greece (*2*) and the Republic of Korea (*15*) illustrate the high potential for imported *P. vivax* to establish sustained transmission, which may pose a substantial challenge for subsequent elimination. Although the risk for autochthonous malaria in the United States remains low, the potential threat of imported *P. vivax* setting off and establishing local transmission in areas with competent vectors and conducive environments is a public health concern.

The last mosquito-vectored *P. vivax* malaria outbreak in the United States was in 2003 in Palm Beach County, Florida, and involved a cluster of 7 cases (*3*) before the *P. vivax* genome sequence was available. Although microsatellites were used to identify their genetic relatedness, the genomic tools that we used offer unparalleled resolution of the genetic relatedness of parasite isolates of the 2023 malaria outbreak in Florida. The minimal genetic variations among the isolates indicate a single transmission chain. Phylogenetic clustering with *P. vivax* strains from Central/South America implies the travel-related import of the index isolate from that region. Of note, a case of imported *P. vivax* malaria with symptom onset April 20, 2023, was reported from the same area as the 7 *P. vivax* cases (*3*,*4*). We are unable to determine if the April case initiated local transmission because no remaining specimen was available for analysis.

In summary, our study underscores the usefulness and power of genomic tools in epidemiologic investigations. The established analytical pipeline will enable more streamlined and efficient genomic surveillance, provide health authorities with accurate information about the source of the infections, and enable communication of the risk to the public with solid scientific evidence. Given the rich genomic resources of worldwide *P. vivax* isolates, genomic surveillance will play a crucial role in tracking additional cases, detecting potential transmission chains, and identifying relapse. Although locally transmitted malaria in Florida has been successfully eliminated, ongoing surveillance, rapid responses, vigilance, and preparedness are still needed to prevent malaria reintroduction and local transmission.

Acknowledgments

We acknowledge the contribution of Min Zhang, the University of South Florida Genomics Program, and the USF Omics Hub for completion of this project. We thank Brian Raphael and Joel Barratt for helpful discussions and critical review of the manuscript.

The study is supported by grant no. U19AI089672 from the National Institute of Allergy and Infectious Diseases, National Insitutes of Health.

About the Author

Dr. Muneer is a postdoctoral scholar at the University of South Florida. His current focus is related to drug resistance in malaria parasites.

References

1. World Health Organization. World Malaria Report 2023. Geneva, Switzerland: The Organization; 2023.
2. Spanakos G, Snounou G, Pervanidou D, Alifrangis M, Rosanas-Urgell A, Baka A, et al.; MALWEST Project. Genetic spatiotemporal anatomy of *Plasmodium vivax* malaria episodes in Greece, 2009–2013. Emerg Infect Dis. 2018;24:541–8. https://doi.org/10.3201/eid2403.170605
3. Centers for Disease Control and Prevention. Local transmission of *Plasmodium vivax* malaria—Palm Beach County, Florida, 2003. MMWR Morb Mortal Wkly Rep. 2003;52:908–11.
4. Blackburn D, Drennon M, Broussard K, Morrison AM, Stanek D, Sarney E, et al. Outbreak of locally acquired mosquito-transmitted (autochthonous) malaria—Florida and Texas, May–July 2023. MMWR Morb Mortal Wkly Rep. 2023;72:973–8. https://doi.org/10.15585/mmwr.mm7236a1
5. Snounou G, Viriyakosol S, Zhu XP, Jarra W, Pinheiro L, do Rosario VE, et al. High sensitivity of detection of human malaria parasites by the use of nested polymerase chain reaction. Mol Biochem Parasitol. 1993;61:315–20. https://doi.org/10.1016/0166-6851(93)90077-B
6. Cowell AN, Loy DE, Sundararaman SA, Valdivia H, Fisch K, Lescano AG, et al. Selective whole-genome amplification is a robust method that enables scalable whole-genome sequencing of *Plasmodium vivax* from unprocessed clinical samples. mBio. 2017;8: e02257-16. https://doi.org/10.1128/mBio.02257-16
7. Andrews S. FastQC: a quality control tool for high throughput sequence data. Cambridge (UK): Babraham Bioinformatics, Babraham Institute; 2010.
8. Li H, Durbin R. Fast and accurate short read alignment with Burrows-Wheeler transform. Bioinformatics. 2009;25:1754–60. https://doi.org/10.1093/bioinformatics/btp324
9. Li H, Handsaker B, Wysoker A, Fennell T, Ruan J, Homer N, et al.; 1000 Genome Project Data Processing Subgroup. The sequence alignment/map format and SAMtools. Bioinformatics. 2009;25:2078–9. https://doi.org/10.1093/bioinformatics/btp352
10. Bright AT, Manary MJ, Tewhey R, Arango EM, Wang T, Schork NJ, et al. A high resolution case study of a patient with recurrent *Plasmodium vivax* infections shows that relapses were caused by meiotic siblings. PLoS Negl Trop Dis. 2014;8:e2882. https://doi.org/10.1371/journal.pntd.0002882
11. Adam I, Alam MS, Alemu S, Amaratunga C, Amato R, Andrianaranjaka V, et al.; MalariaGEN. An open dataset of *Plasmodium vivax* genome variation in 1,895 worldwide samples. Wellcome Open Res. 2022;7:136. https://doi.org/10.12688/wellcomeopenres.17795.1
12. Kalyaanamoorthy S, Minh BQ, Wong TKF, von Haeseler A, Jermiin LS. ModelFinder: fast model selection for accurate phylogenetic estimates. Nat Methods. 2017;14:587–9. https://doi.org/10.1038/nmeth.4285
13. Letunic I, Bork P. Interactive Tree Of Life (iTOL) v5: an online tool for phylogenetic tree display and annotation. Nucleic Acids Res. 2021;49(W1):W293–6. https://doi.org/10.1093/nar/gkab301
14. Mace KE, Lucchi NW, Tan KR. Malaria surveillance—United States, 2018. MMWR Surveill Summ. 2022;71:1–35. https://doi.org/10.15585/mmwr.ss7108a1
15. Bahk YY, Lee HW, Na BK, Kim J, Jin K, Hong YS, et al. Epidemiological characteristics of re-emerging vivax malaria in the Republic of Korea (1993–2017). Korean J Parasitol. 2018;56:531–43. https://doi.org/10.3347/kjp.2018.56.6.531

Address for correspondence: Liwang Cui, Division of Infectious Disease and International Medicine, Department of Internal Medicine, Morsani College of Medicine, University of South Florida, 3720 Spectrum Blvd, Ste 304, Tampa, FL 33612, USA; email: liwangcui@usf.edu

Evolution and Antigenic Differentiation of Avian Influenza A(H7N9) Virus, China

Yang Liu,[1] Yuhua Chen,[1] Zhiyi Yang, Yaozhong Lin, Siyuan Fu, Junhong Chen, Lingyu Xu, Tengfei Liu, Beibei Niu, Qiuhong Huang, Haixia Liu, Chaofeng Zheng, Ming Liao, Weixin Jia

We characterized the evolution and molecular characteristics of avian influenza A(H7N9) viruses isolated in China during 2021–2023. We systematically analyzed the 10-year evolution of the hemagglutinin gene to determine the evolutionary branch. Our results showed recent antigenic drift, providing crucial clues for updating the H7N9 vaccine and disease prevention and control.

From early 2013 through October 2017, a total of 5 outbreaks of avian influenza A(H7N9) virus infection occurred, resulting in 616 human deaths (1). In particular, the fifth wave of the epidemic saw a substantial increase in human fatalities. By late 2017, a total of 1,568 laboratory-confirmed cases of H7N9 virus infection in humans had been reported according to International Health Regulations guidelines (https://www.who.int/emergencies/disease-outbreak-news/item/26-october-2017-ah7n9-china-en). The rapid emergence, prevalence, and pandemic potential of H7N9 virus were suddenly of great concern. Since 2017, low-pathogenicity avian influenza H7N9 virus transformed into the highly pathogenic avian influenza (HPAI) A(H7N9) virus (*2*–*5*). In response, China initiated a large-scale vaccination program in the poultry industry, effectively limiting the H7N9 epidemic. Although no human H7N9 infections have been reported since February 2019, the virus is still circulating in poultry, particularly in laying hens, and remains a potential threat to poultry industry and public health (*6*–*8*). Furthermore, since 2017, the H7N9 virus has undergone multiple instances of antigenic drift to evade immune pressure from vaccines (*9*–*11*). We investigated the genetic evolution and antigenic differentiation of the H7N9 virus in China to provide information to better control the epidemic, ensure the safety of the poultry industry, and protect public health.

The Study

Through continuous monitoring of markets and breeding farms in several provinces, we successively isolated 23 H7N9 viruses. Using the sequences of those viruses and a reference sequence from the GISAID database (*12*), we conducted a phylogenetic analysis to study the evolution of H7N9 virus over the past decade (Figure 1).

We rooted the maximum-likelihood phylogenetic tree with A/Anhui/1/2013 and identified the branches as Group.y.0. During 2013–2017, the 5 low-pathogenicity avian influenza H7N9 virus waves formed Group.y.0–Group.y.2 branch. The first wave was mainly prevalent in the Yangtze River Delta. In 2014, the second wave spread to the Pearl River Delta and gradually expanded to all parts of the country in the subsequent 3 waves. Around 2017, or even as early as mid-2016, researchers successfully isolated an HPAI variant of H7N9 virus (*6*). That variant was found to contain alkaline amino acids inserted into the cleavage site of the hemagglutinin protein (*6*,*13*). The discovery of that variant in live poultry markets in Guangdong Province indicated an increased pathogenicity to poultry and potentially posed a greater threat to human health. We found that those HPAI H7N9 virus variants clustered within the Group.y.2.1 branch and its subordinate branch.

Author affiliations: South China Agricultural University, Guangzhou, China (Y. Liu, Z. Yang, Y. Lin, S. Fu, J. Chen, L. Xu, T. Liu, B. Niu, Q. Huang, M. Liao, W. Jia); Guangzhou Animal Health Inspection Institute, Guangzhou (Y. Chen); Guangdong Aib Polytechnic College, Guangzhou (H. Liu); Animal Husbandry and Veterinary Station, Urumqi, China (C. Zheng)

DOI: https://doi.org/10.3201/eid3006.230530

[1]These first authors contributed equally to this article.

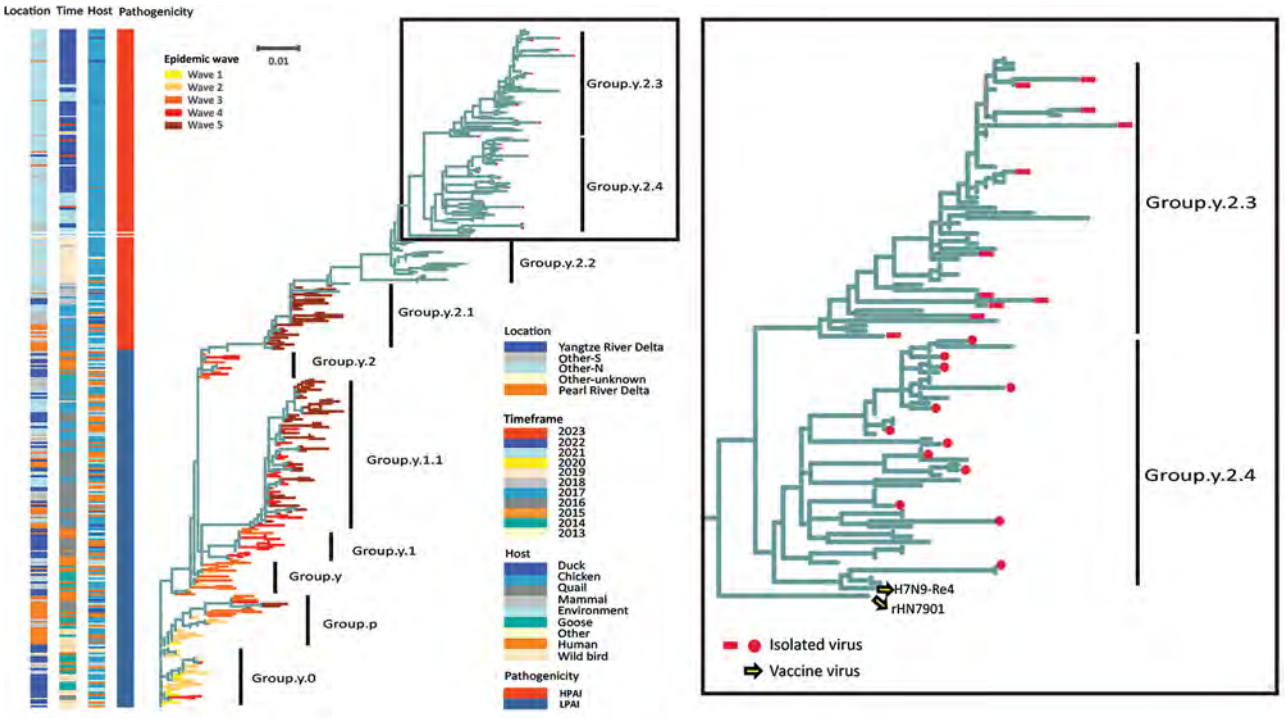

Figure 1. Phylogenetic analysis of evolution and antigenic differentiation of avian influenza A(H7N9) virus, China. Colors in columns at left show locations, timeframes, hosts, and pathogenicity of virus strains. The maximum-likelihood phylogenetic tree of the hemagglutinin gene depicts viruses corresponding to epidemic waves 1–5. Tree on right shows detail of Group.y.2.3 (red rectangles) and Group.y.2.4.4 (red circles) in comparison with vaccine strains. Scale bar indicates nucleotide substitutions per site. LPAI, low-pathogenicity avian influenza; HPAI, highly pathogenic avian influenza; Other-N, sites in the northern region; Other-S, sites in the southern region.

After implementation of a universal immunization program in 2017, the H7N9 virus outbreak was effectively controlled. However, some H7N9 viruses evolved to evade the vaccine. Those viruses continued to evolve and formed a new branch, Group.y.2.2, which is mainly found in northern China (Figure 1). Further investigation revealed that H7N9 virus is prevalent in the Bohai Rim region. Of note, we found no great differences in geographic, temporal, or host distribution between the 2 newly differentiated branches, Group.y.2.3 (A/Chicken/Hebei/1009/2020-like) and Group.y.2.4 (A/Chicken/Yunnan/1001/2021-like) (Figure 1). Those branches showed an average of 2.41% pairwise nucleotide distances between 2021 and 2023. That finding suggests that the evolutionary differences between those clades might not be influenced by geographic isolation, period, or host species, but rather by the adaptation of a new virus to natural selection. Positive selection pressure, which encourages mutations that contribute to the virus' adaptation to the environment, can play a role in viral evolution. Our analysis confirmed that an increase in positive selection pressure in H7N9 virus occurred at some sites after 2017 (Appendix Table 1, https://wwwnc.cdc.gov/EID/article/23-0530-App1.pdf).

To examine whether mutation and evolution of H7N9 viruses are a result of antigenic drift and discontinuous variation, we used serologic methods to assess the antigenicity of the more evolved viruses from different clades (Appendix Table 2). Using the H7-Re4 and rHN7901 vaccine viruses for comparison, we found a weak cross-reaction titer between the vaccine viruses and the epidemic viruses in Group.y.2.3 (Table). The antigenic map demonstrated that the Group.y.2.3 viruses were distantly located from the vaccine serum (Figure 2), implying a consistent antigenic drift and greater antigenic divergence from Group.y.2.4 viruses. However, the distance between the vaccine virus and certain Group.y.2.4 viruses was relatively close (Figure 2), suggesting minimal differences. Furthermore, some Group.y.2.4 viruses, including A/Chicken/BJ/732-1/2022 and A/Quail/HeN/621/2022, both originating from northern China, also exhibited antigenic drift.

Changes in antigenicity often are caused by accumulation of amino acid mutations in antigenic sites. Therefore, we compared virus sequences and observed that the cleavage sites were

Table. Hemagglutination inhibition titers of 23 H7N9 epidemic viruses and vaccine viruses in a study of evolution and antigenic differentiation of avian influenza A(H7N9) virus, China*

Group	Antigen	Antiserum, log_2					
		H7N9-Re4	rHN7901	229–2	257–3	320–1	363–4
Referent	H7N9-Re4	**10**	10	5	5	10	10
Referent	rHN7901	9	**10**	3	2	9	10
y.2.3	A/Chicken/HeB/229–2/2022	5	5	**10**	10	9	8
y.2.3	A/Chicken/HeB/257–3/2022	5	3	10	**10**	9	8
y.2.3	A/Quail/HeN/782–2/2022	4	4	10	9	8	6
y.2.3	A/Chicken/LN/976–3/2022	5	4	10	9	8	6
y.2.3	A/Duck/HeB/976–2/2022	5	4	10	9	7	5
y.2.3	A/Chicken/HeB/199–1/2022	7	5	10	10	9	8
y.2.3	A/Chicken/GX/J17/2022	7	7	10	10	8	9
y.2.3	A/Chicken/HeB/526/2022	6	5	8	8	7	7
y.2.3	A/Chicken/HeB/229–4/2022	6	6	10	10	9	8
y.2.3	A/Chicken/SX/B1323–1/2022	7	7	9	10	9	6
y.2.3	A/Chicken/SX/B22–2/2023	7	8	9	10	9	7
y.2.4	A/Chicken/HeB/363–4/2022	5	5	6	5	9	**10**
y.2.4	A/Chicken/HeB/320–1/2022	8	9	6	2	**10**	7
y.2.4	A/Quail/HeN/621/2022	5	3	3	4	6	6
y.2.4	A/Chicken/BJ/732–1/2022	5	5	5	3	6	9
y.2.4	A/Chicken/HuB/J15/2022	9	8	7	6	7	10
y.2.4	A/Chicken/BJ/470–6/2022	8	9	4	3	7	9
y.2.4	A/Chicken/SC/468–2/2022	8	8	6	5	8	10
y.2.4	A/Chicken/HeB/J94/2022	8	8	6	5	8	10
y.2.4	A/Chicken/YN/415–2/2022	9	9	8	6	8	9
y.2.4	A/Chicken/SD/1401–2/2021	7	7	6	4	8	9
y.2.4	A/Chicken/JSu/B14–3/2023	9	9	6	6	9	10
y.2.4	A/Chicken/HeB/B14–1/2023	10	10	6	6	9	9

*Bold text indicates the cross titers of sera with corresponding antigens. BJ, Beijing; GX, Guangxi; HeB, Hebei; HeN, Henan; HuB, Hubei; JS, Jiangsu; LN, Liaoning; SC, Sichuan; SD, Shandong; SX, Shanxi; YN, Yunnan.

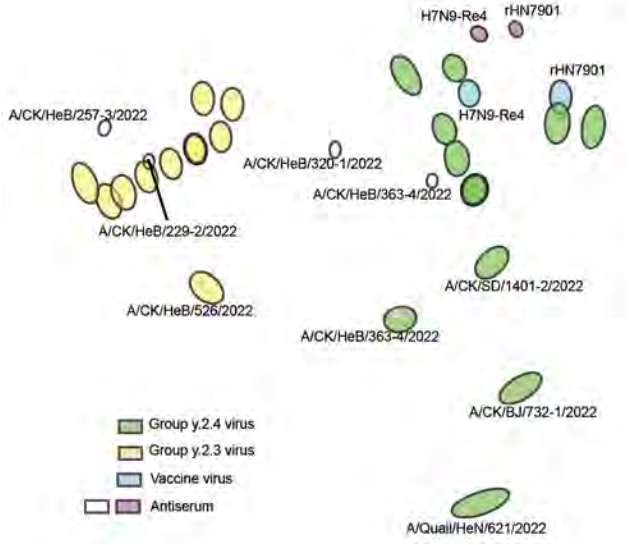

Figure 2. Antigenic map of avian influenza A(H7N9) virus, China, 2021–2023. The map was plotted using hemagglutinin inhibition assay results of 26 antigens (green, blue, and yellow dots), serum from 2 vaccine virus strains, H7N9-Re4 and rHN7901 (purple dots), and in-house designed serum of 4 circulating viruses (CK for chicken). The antigen map was constructed using the online website of the Antigenic Cartography Group, University of Cambridge (https://acmacs-web.antigenic-cartography.org). A/Chicken/HeB/257-3/2022 and A/Chicken/HeB/229-2/2022 belong to the Group.y.2.3 branch, whereas A/Chicken/HeB/320-1/2022 and A/Chicken/HeB/363-4/2022 belong to the Group.y.2.4 branch (indicated by white dots). The distance between the figures represents the antigen distance.

KRKRTAR↓GLF or KRKRIAR↓GLF, both of which exhibited the characteristics of HPAI viruses. However, we noted no substantial differences between Group.y.2.3 and Group.y.2.4 at positions 86, 129, 134, 141, 145, 148, 151, 159, 208, 284, and 319 of H7 (Appendix Table 3). Those findings demonstrated the high genetic diversity of the H7N9 virus. Except for position 208 in H7, all sites were antigenic sites, and positions 141, 145, and 148 were both antigenic sites and receptor-binding sites. For the Group.y.2.4 branch, we compared the hemagglutinin 1 peptide of the vaccine viruses against antigenically distant viruses A/Chicken/SD/1301-2/2022, A/Chicken/HeB/B363-4/2022, A/Chicken/BJ/B732-1/2022, and A/Quail/HeN/621/2022. We observed different amino acids that could affect H7N9 virus antigenicity (Appendix Table 4). Among the analyzed viruses, A/Quail/HeN/621/2022 exhibited the highest number of mutations compared with the vaccine viruses, followed by A/Chicken/BJ/B732-1/2022 and A/Chicken/HeB/B363-4/2022; A/Chicken/SD/1401-2/2022 displayed the fewest mutations. Moreover, the previously reported Q226L and G228S sites of H3 viruses (Appendix Table 5), which have the potential to enhance mammalian adaptation, remained unchanged in all H7N9 viruses. Those sites still showed a preference for avian receptors, except A/Quail/HeN/621/2022,

which mutated to P at position 160. All V125T H3 sites were replaced, indicating that the receptor-binding capacity and immune escape of the virus might be affected, making the virus more compatible with avian receptors (*14*,*15*).

Conclusions

This study explored the evolution and antigenic differentiation characteristics of H7N9 virus over the past decade through continuous monitoring and selection of representative sequences from all publicly available H7N9 virus sequences. However, our research still had certain limitations, and further investigation is needed to understand the relationship between the evolution of viruses under positive selection pressure and the underlying cause of antigenic variation.

In summary, influenza A viruses are highly prone to mutation and evolution, making the H7N9 virus epidemic more complex and challenging to control. This study offers vital insights into the genetic evolutionary branches and recent antigenic drift, providing crucial clues for updating the H7N9 vaccine seed virus and for disease prevention and control.

Acknowledgments

We appreciate the support of Guangzhou Animal Health Supervision Institute for our sampling work. We also gratefully acknowledge all data contributors, i.e., the Authors and their Originating laboratories responsible for obtaining the specimens, and their Submitting laboratories for generating the genetic sequence and metadata and sharing via the GISAID Initiative, on which this research is based.

In this study, we uploaded the hemagglutinin gene sequences of 23 H7N9 viruses isolates from 2021 to 2023. All sequencing data are available in the GISAID database (https://www.gisaid.org). (Accession number information is in Appendix Table 6.)

This work was supported by the Science and Technology Program of Guangdong Province (grant nos. 2022B1111010004 and 2021B1212030015), the China National Natural Science Foundation (grant no. 31972709), China Agriculture Research System of Ministry of Finance and Ministry of Agriculture and Rural Affairs (project no. CARS-41), China National Animal Disease Surveillance and Epidemiological Survey Program (2021–2025) (grant no. 202111), the Basic and Applied Basic Research Project of Guangzhou Basic Research Plan (grant no. 202102080576), and Guangdong Aib Polytechnic College Program (grant no. XJYB202105).

About the Authors

Dr. Liu is a postgraduate student at South China Agricultural University in Guangzhou, China. Her research interests are the epidemiology, pathogenesis, and control of major poultry diseases and zoonoses. Dr. Chen is a veterinarian at Guangzhou Animal Health Inspection Institute in Guangzhou, China. His research interests are animal disease prevention and control.

References

1. Wang X, Jiang H, Wu P, Uyeki TM, Feng L, Lai S, et al. Epidemiology of avian influenza A H7N9 virus in human beings across five epidemics in mainland China, 2013–17: an epidemiological study of laboratory-confirmed case series. Lancet Infect Dis. 2017;17:822–32. https://doi.org/10.1016/S1473-3099(17)30323-7
2. Ke C, Mok CKP, Zhu W, Zhou H, He J, Guan W, et al. Human infection with highly pathogenic avian influenza A(H7N9) virus, China. Emerg Infect Dis. 2017;23:1332–40. https://doi.org/10.3201/eid2308.170600
3. Yang L, Zhu W, Li X, Chen M, Wu J, Yu P, et al. Genesis and spread of newly emerged highly pathogenic H7N9 avian viruses in mainland China. J Virol. 2017;91:e01277-17. https://doi.org/10.1128/JVI.01277-17
4. Senne DA, Panigrahy B, Kawaoka Y, Pearson JE, Süss J, Lipkind M, et al. Survey of the hemagglutinin (HA) cleavage site sequence of H5 and H7 avian influenza viruses: amino acid sequence at the HA cleavage site as a marker of pathogenicity potential. Avian Dis. 1996;40:425–37. https://doi.org/10.2307/1592241
5. Qi W, Jia W, Liu D, Li J, Bi Y, Xie S, et al. Emergence and adaptation of a novel highly pathogenic H7N9 influenza virus in birds and humans from a 2013 human-infecting low-pathogenic ancestor. J Virol. 2018;92:e00921-17. https://doi.org/10.1128/JVI.00921-17
6. Gu J, Yan Y, Zeng Z, Wang W, Gao R, Hu J, et al. Characterization of two chicken origin highly pathogenic H7N9 viruses isolated in northern China. Vet Microbiol. 2022;268:109394. https://doi.org/10.1016/j.vetmic.2022.109394
7. Byrne AMP, Reid SM, Seekings AH, Núñez A, Obeso Prieto AB, Ridout S, et al. H7N7 avian influenza virus mutation from low to high pathogenicity on a layer chicken farm in the UK. Viruses. 2021;13:259. https://doi.org/10.3390/v13020259
8. Yin X, Deng G, Zeng X, Cui P, Hou Y, Liu Y, et al. Genetic and biological properties of H7N9 avian influenza viruses detected after application of the H7N9 poultry vaccine in China. PLoS Pathog. 2021;17:e1009561. https://doi.org/10.1371/journal.ppat.1009561
9. Wu Y, Hu J, Jin X, Li X, Wang J, Zhang M, et al. Accelerated evolution of H7N9 subtype influenza virus under vaccination pressure. Virol Sin. 2021;36:1124–32. https://doi.org/10.1007/s12250-021-00383-x
10. Chen J, Liu Z, Li K, Li X, Xu L, Zhang M, et al. Emergence of novel avian origin H7N9 viruses after introduction of H7-Re3 and rLN79 vaccine strains to China. Transbound Emerg Dis. 2022;69:213–20. https://doi.org/10.1111/tbed.14401
11. Jiang W, Hou G, Li J, Peng C, Wang S, Liu S, et al. Antigenic variant of highly pathogenic avian influenza A(H7N9) virus, China, 2019. Emerg Infect Dis. 2020;26:379–80. https://doi.org/10.3201/eid2602.191105

12. Khare S, Gurry C, Freitas L, Schultz MB, Bach G, Diallo A, et al. GISAID's role in pandemic response. China CDC Wkly. 2021;3:1049–51. https://doi.org/10.46234/ccdcw2021.255
13. Zhang F, Bi Y, Wang J, Wong G, Shi W, Hu F, et al. Human infections with recently-emerging highly pathogenic H7N9 avian influenza virus in China. J Infect. 2017;75:71–5. https://doi.org/10.1016/j.jinf.2017.04.001
14. Zhang J, Ye H, Li H, Ma K, Qiu W, Chen Y, et al. Evolution and antigenic drift of influenza A(H7N9) viruses, China, 2017–2019. Emerg Infect Dis. 2020;26:1906–11. https://doi.org/10.3201/eid2608.200244
15. Wu J, Ke C, Lau EHY, Song Y, Cheng KL, Zou L, et al. Influenza H5/H7 virus vaccination in poultry and reduction of zoonotic infections, Guangdong Province, China, 2017–18. Emerg Infect Dis. 2019;25:116–8. https://doi.org/10.3201/eid2501.181259

Address for correspondence: Weixin Jia or Ming Liao, College of Veterinary Medicine, South China Agricultural University, 483 Wushan Rd, Tianhe, Guangzhou, Guangdong 510642, China; email: jiaweixin@scau.edu.cn or mliao@scau.edu.cn

Concurrent Infection with Clade 2.3.4.4b Highly Pathogenic Avian Influenza H5N6 and H5N1 Viruses, South Korea, 2023

Gyeong-Beom Heo, Yong-Myung Kang, Se-Hee An, Yeongbu Kim, Ra Mi Cha, Yunyueng Jang, Eun-Kyoung Lee, Youn-Jeong Lee, Kwang-Nyeong Lee

Highly pathogenic avian influenza H5N6 and H5N1 viruses of clade 2.3.4.4b were simultaneously introduced into South Korea at the end of 2023. An outbreak at a broiler duck farm consisted of concurrent infection by both viruses. Sharing genetic information and international surveillance of such viruses in wild birds and poultry is critical.

Since clade 2.3.4.4 H5Nx highly pathogenic avian influenza (HPAI) viruses first emerged in East Asia in 2013–14, clade 2.3.4.4b has spread throughout Europe, Africa, and Middle East in 2016–17, causing ≥2,000 outbreaks in poultry and wild birds in >30 countries (*1*,*2*). Clade 2.3.4.4b H5N1 viruses were detected in Europe in late 2020; that clade became the predominant subtype in Europe in 2021 and spread throughout Asia and North America. By the end of 2023, H5N1 viruses of that clade had affected bird populations in most of the United States and spread to South America and Antarctica (*3*).

Since early 2014, South Korea has experienced epidemic outbreaks of different subtypes of this clade, including H5N8 in early 2014, 2016–17, and 2020–21; H5N6 in 2017–18; and H5N1 in 2021–22 and 2022–23 (*4*–*7*). All those outbreaks in poultry have occurred during the winter season, when migratory birds enter and stay on the Korean peninsula (*8*–*10*). No HPAI virus was detected during regular active surveillance of both wild birds and poultry during May–October 2023.

Author affiliation: Seoul National University, Seoul, South Korea (G.-B. Heo); Animal and Plant Quarantine Agency, Gimcheon, South Korea (G.-B. Heo, Y.-M. Kang, S.-H. An, Y. Kim, R.M. Cha, Y. Jang, E.-K. Lee, Y.-J. Lee, K.-N. Lee)

DOI: http://doi.org/10.3201/eid3006.240194

The first suspected case of HPAI in poultry in the 2023–24 winter season was reported in South Korea. Surprisingly, birds at that farm were found to be concurrently infected with H5N6 and H5N1 viruses of clade 2.3.4.4b. Subsequently, birds at poultry farms as well as wild birds were found to be infected with H5N6 or H5N1 viruses. Our study analyzed whole-genome sequences of the virus populations of pooled swab samples from the flocks at the farm that were infected with both H5N6 and H5N1 influenza viruses; we defined the farm as the index case. We compared those sequences with the sequences of viruses isolated from other affected farms and wild birds to determine the origins of the viruses and their relationships.

The Study

On December 3, 2023, a suspected HPAI infection that caused white diarrhea, reduced feed intake, and increased deaths was reported in 39-day-old broiler ducks at a broiler duck farm (D448) in Goheung, South Korea (Figure 1). We detected matrix and H5 genes in the clinical samples from this index farm by real-time reverse transcription PCR. We determined the deduced amino acid sequence of the HA cleavage site of the H5 genes to be PLREKRRKR/GLF, which indicated high pathogenicity. For the NA gene, we detected both N1 and N6 genes in some flocks at the farm, at which the flocks were separated in different houses. We analyzed co-infection status at that farm by using whole-genome sequences of avian influenza viruses obtained from pooled oropharyngeal swab samples of 20 live ducks from each of 11 flocks using the Nanopore (Oxford Nanopore, https://nanoporetech.com) amplicon sequencing method (Appendix, https://wwwnc.cdc.gov/EID/article/30/6/24-0194.App1.pdf).

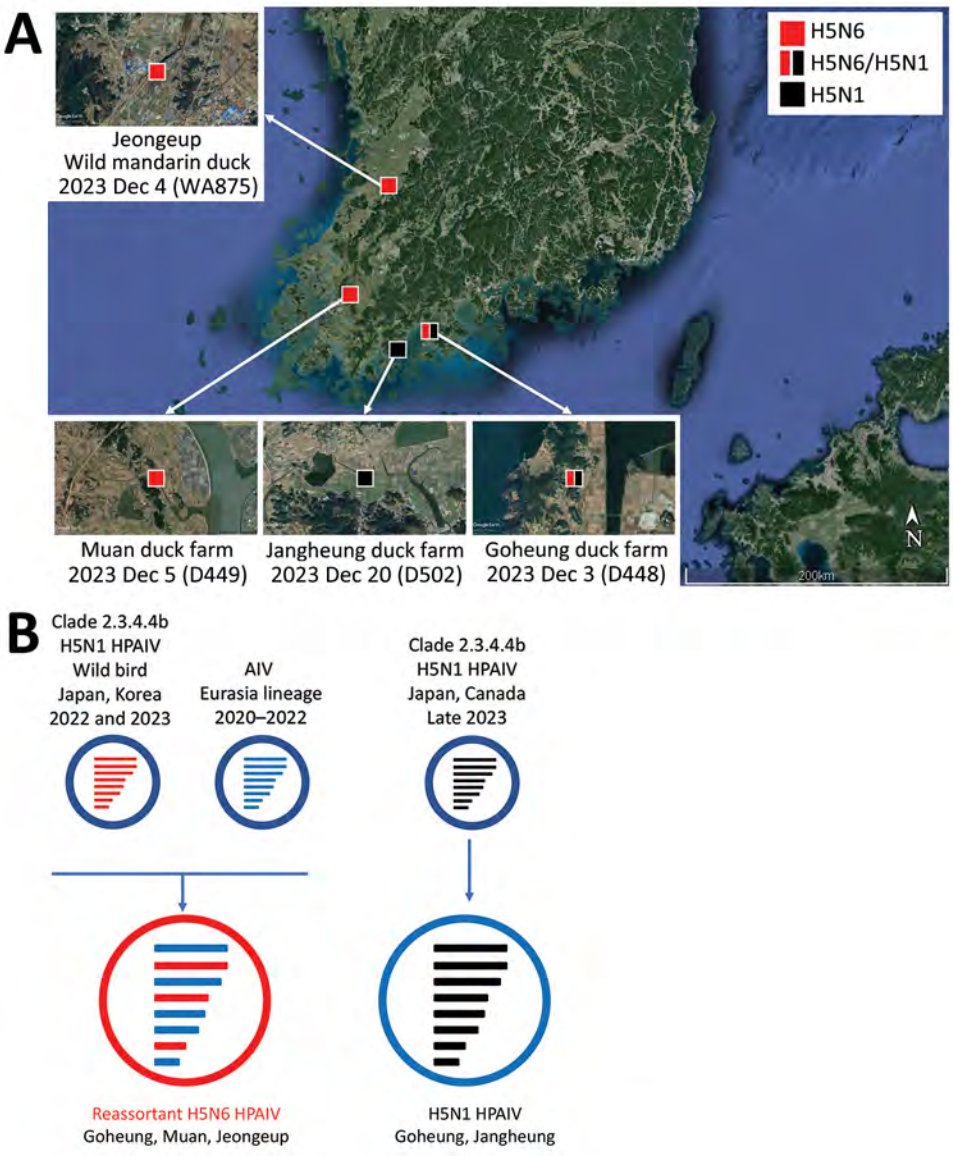

Figure 1. Locations of duck farms and of wild ducks infected with clade 2.3.4.4b HPAIV H5, South Korea, 2023, and their viral genotypes. A) Each square indicates the location of the infected farms or wild birds where the samples were collected. Red indicates H5N6 virus and black H5N1 virus. Satellite image is from Google Earth (https://earth.google.com). B) Genetic constellation of H5N6 and H5N1 viruses concurrently detected in December 2023. The bars represent 8 gene segments of the avian influenza virus in the following order (from top to bottom): polymerase basic 2, polymerase basic 1, polymerase acidic, hemagglutinin, nucleoprotein, neuraminidase, matrix, and nonstructural. The 8 genes of each virus are represented by colored bars, indicating presumed recent donors. HPAIV, highly pathogenic avian influenza virus.

We found that 3 flocks, numbers 1, 4, and 5, were co-infected with H5N6 and H5N1 viruses, whereas the other 8 flocks were infected with H5N6 virus only (Figure 2). Analysis of the average coverage at each gene segment as percentage composition showed that birds in flock 4 had more viral reads of H5N1, whereas flocks 1 and 5 had more reads of H5N6 (Figure 2, panel B). We observed the same co-infection pattern in pooled cloacal swabs of flock 4 (data not shown). Because all the swabs from flocks were pooled at sample collection, no clear evidence was found supporting infection with the 2 viruses in a single bird. Because this farm was located very close to the south sea and seawall lake and had a relatively low level of biosecurity, we considered this farm susceptible to virus introduction by migratory birds (Figure 1, panel A).

We detected HPAI H5N6 virus (WA875) in Jeollado province in an apparently healthy wild mandarin duck, which we captured and sampled on December 4, 2023, for the active wild bird surveillance program. Two additional broiler-duck farms in the same province were found to be infected with H5N6 (D449) and H5N1 (D502) virus on December 5 and December 20, 2023 (Figure 1, panel A). We assessed the genetic relationships among the HPAI viruses by determining and comparing the complete genome sequences of A/duck/Korea/D448-N6/2023(H5N6), A/duck/Korea/D448-N1/2023(H5N1), A/duck/Korea/D449/2023(H5N6),A/mandarin duck/Korea/WA875/2023(H5N6), and A/duck/Korea/D502/2023(H5N1). Their sequences have been deposited in GISAID (https://www.gisaid.org; accession nos.

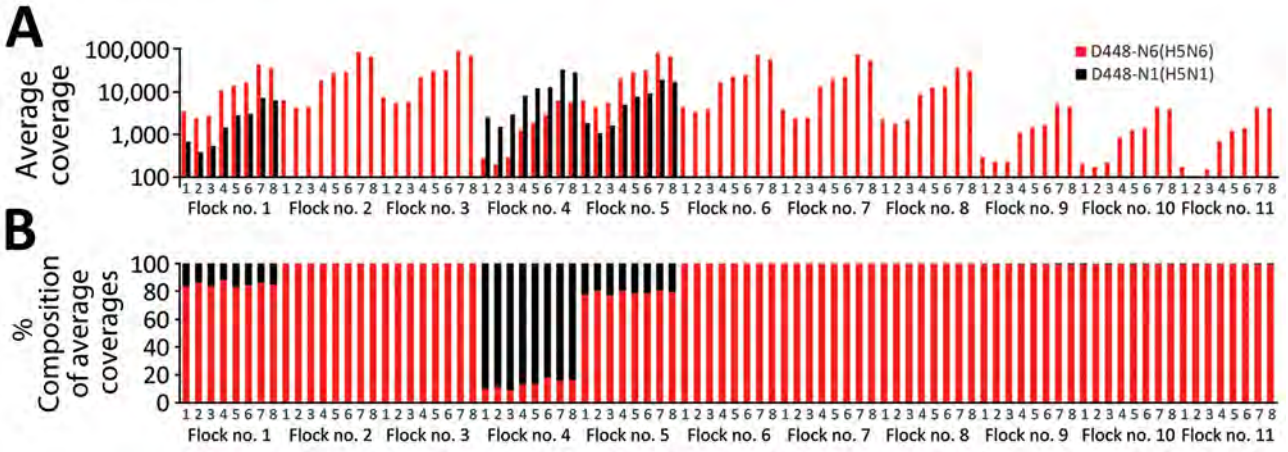

Figure 2. Co-infection status of birds at a broiler duck farm (D448) infected with clade 2.3.4.4b highly pathogenic avian influenza H5N6 and H5N1 viruses in South Korea, December 2023. Reference gene segments for mapping were designated as numbers 1–8; segment 1, polymerase basic 2; segment 2, polymerase basic 1; segment 3, polymerase acidic; segment 4, hemagglutinin; segment 5, nucleoprotein; segment 6, neuraminidase; segment 7, matrix; segment 8, nonstructural. A) Distribution of average coverages of the reads from each pooled oropharyngeal swab sample in the index farm, which had 11 flocks, mapped to the relevant reference viral genomes. Red bars indicate average mapping coverages of A/duck/Korea/D448-N6/2023(H5N6) to its reference gene segments and black bars indicate average mapping coverages of A/duck/Korea/D448-N1/2023(H5N1) to its reference gene segments. Three co-infected flocks (flocks 1, 4, and 5) had sufficient sequencing depth with >1,000-fold coverage of segments 4 (hemagglutinin) and 6 (neuraminidase). B) Distribution of percentage compositions of average coverages transformed from the average coverage values shown in panel A. Birds in flock 4 had more viral reads of H5N1 virus, whereas birds in flocks 1 and 5 had more reads of H5N6 virus. The other 8 flocks had the reads only mapped to H5N6 virus.

EPI_ISL_18819959–61, EPI_ISL_18819826, and EPI_ISL_18819797.

The H5N6 viruses, D448-N6, D449, and WA875, showed high nucleotide sequence identities in all 8 genes among them (>99.8%). The sequences of their polymerase basic (PB) 1, hemagglutinin (HA), and matrix (M) genes were very close (99.53%–99.83%) to the respective genes of clade 2.3.4.4b HPAI H5N1 viruses isolated from wild birds in Japan and South Korea in 2022–23. The 4 internal genes of the H5N6 viruses, PB2, polymerase acidic protein (PA), nucleoprotein (NP), and nonstructural protein (NS), were closely related to the respective genes found in the Eurasian low pathogenicity avian influenza (LPAI) viruses of diverse subtypes isolated from wild birds in 2020 and 2022. Their N6 genes appeared to be close to the poultry viruses isolated in East Asia in 2021 and 2022, although the nucleotide identities were relatively low (98.1%–98.62%) (Table 1). Of interest, the protein encoded by the N6 gene in the isolates from this study had a deletion of 12 aa residues at positions 58–69; this neuraminidase (NA) stalk deletion has been often observed in poultry-adapted viruses (*11*,*12*). From the avian influenza active surveillance program in South Korea during 2019–2023, N6 genes were detected only in LPAI viruses isolated from wild birds; we did not observe this NA stalk deletion among the analyzed viruses (data not shown).

Table 1. Nucleotide sequence identities of gene segments between reassortant clade 2.3.4.4b HPAI H5N6 virus from a duck farm in South Korea, 2023, compared with A/duck/Korea/D448-N6/2023(H5N6) virus and the closest referent in the GISAID database*

Gene	Virus	GISAID accession no.	% Identity	Sample date	LPIAI or HPAI H5 clade
PB2	A/mallard/South_Korea/20X-20/2021(H7N9)	EPI_ISL_6781375	98.73	2021 Jan 6	LPAI
PB1	A/large billed_crow/Kanagawa/1403C006/2023(H5N1)	EPI_ISL_17949961	99.69	2023 Mar 10	2.3.4.4b
PA	A/common_teal/Amur_region/92b/2020(H6N2)	EPI_ISL_1184535	99.58	2020 Sep 6	LPAI
HA	A/Mandarin_duck/Korea/WA496/2022(H5N1)	EPI_ISL_15647836	99.53	2022 Oct 10	2.3.4.4b
NP	A/gadwall/Novosibirsk_region/3407k/2020(H4N6)	EPI_ISL_1184520	98.8	2020 Aug 29	LPAI
NA	A/duck/Hunan/S40199/2021(H5N6)†	EPI_ISL_11208196	98.62	2021 Dec 1	2.3.4.4b
M	A/Mandarin_duck/Korea/WA496/2022(H5N1)	EPI_ISL_15647836	99.8	2022 Oct 10	2.3.4.4b
NS	A/Falcated_duck/South_Korea/JB42–30/2020(H9N2)	EPI_ISL_4072076	99.64	2020 Feb 19	LPAI

*One A/duck/Korea/D448-N6/2023(H5N6) isolate from a wild bird (WA875) and 2 isolates from poultry (D448-N6, D449) had high nucleotide identities among them in all 8 genes: PB2, >99.82%; PB1, >99.78%; PA, >99.86%; HA, >99.82%; NP, >99.87%; NA, >99.86%; M, >99.90%; NS, >99.88%. GISAID, https://www.gisaid.org; HA, hemagglutinin; HPAI, highly pathogenic avian influenza; LPAI, low pathogenicity avian influenza; M, matrix; N, nucleocapsid; NA, neuraminidase; NP, nucleoprotein; NS, nonstructural; PA, polymerase acidic; PB, polymerase basic.
†This virus was isolated from bird in poultry market, and all the other viruses compared were from wild birds.

Table 2. Nucleotide sequence identities of gene segments between the clade 2.3.4.4b HPAI H5N1 virus from a duck farm in South Korea, 2023, compared with A/duck/Korea/D448-N1/2023(H5N1) virus and the closest referent in the GISAID database*

Gene	Virus†	GISAID accession no.	% Identity	Sample date	H5 clade
PB2	A/large-billed_crow/Hokkaido/B067/2023(H5N1)	EPI_ISL_18591747	99.78	2023 Sep 23	2.3.4.4b
PB1	A/Eurasian_wigeon/Kagoshima/4611J002/2023(H5N1)	EPI_ISL_18603583	99.87	2023 Sep 12	2.3.4.4b
PA	A/goose/Magadan/2272–5/2022(H5N1)	EPI_ISL_18071580	99.81	2022 Oct 09	2.3.4.4b
HA	A/Eurasian_wigeon/Kagoshima/4611J002/2023(H5N1)	EPI_ISL_18603583	99.53	2023 Sep 12	2.3.4.4b
NP	A/large-billed_crow/Hokkaido/0103E088/2023(H5N1)	EPI_ISL_17950087	99.87	2023 Mar 30	2.3.4.4b
NA	A/canada_goose/BC/AIVPHL-371/2023(H5N1)	EPI_ISL_17051482	99.79	2023 Jan 16	2.3.4.4b
M	A/northern_pintail/Okayama/331A003/2023(H5N1)	EPI_ISL_18603584	99.9	2023 Sep 13	2.3.4.4b
NS	A/Barnacle_Goose/Netherlands/8/2022(H5N1)	EPI_ISL_10347219	99.76	2022 Jan 28	2.3.4.4b

*Two A/duck/Korea/D448-N1/2023(H5N1) isolates from poultry (D448-N1, D502) had high nucleotide identities between them in all 8 genes, PB2, 99.52%; PB1, 99.78%; PA, 99.72%; HA, 99.30%; NP, 99.73%; NA, 99.22%; M, 99.80%; NS, 99.05%. GISAID, https://www.gisaid.org; HA, hemagglutinin; HPAI, highly pathogenic avian influenza; M, matrix protein; N, nucleocapsid protein; NA, neuraminidase; NP, nucleoprotein; NS, nonstructural protein; PA, polymerase acidic protein; PB, polymerase basic protein.
†All the viruses compared were isolated from wild birds.

We found no HPAI H5N6 viruses showing nucleotide similarities >98.5% in all the 8 genes at once, to the new H5N6 isolates in the public databases. However, a wild bird isolate from Japan (A/peregrine falcon/Saga/4112A002/2023, EPI_ISL_18740267) that was collected on December 6, 2023, was almost identical to the H5N6 Korean viruses (T. Hiono, pers. comm., email, 2024 Jan 11), suggesting that these emerged viruses spread coincidently throughout this winter in East Asia.

The nucleotide sequences of the coding regions of 2 poultry H5N1 viruses, D448-N1 and D502, were very similar (>99.0%) and were very closely related to the sequences of clade 2.3.4.4b H5N1 viruses circulating in Japan and Canada in 2023 (Table 2; Appendix Figures 1–5,7–9). Those clade 2.3.4.4b HPAI H5N1 viruses of diverse genotypes have been prevalent in Europe and North America (*3*) and had been introduced into South Korea during the epidemics of 2021–22 and 2022–23 (*5*,*8*). We did not detect significant mutations related to mammal adaptation or antiviral resistance in the newly isolated H5N6 and H5N1 HPAI viruses.

Conclusions

This study describes the simultaneous introduction of H5N1 virus and a new reassortant H5N6 HPAI virus of clade 2.3.4.4b into South Korea in 2023. Better understanding of this spatial and genomic dynamic requires enhanced and timely sharing of genetic information and international surveillance of HPAI and LPAI viruses in wild birds and poultry.

Acknowledgments

We thank Jeong-Eui Lee, Byeong-Suk Jeon, and Chae-Rin Lee for excellent technical assistance. We also thank the Animal and Plant Quarantine Agency, Ministry of Agriculture, Food and Rural Affairs, and the regional office for Animal Disease Control, Livestock Health Control Association, for their efforts to control AIV. We thank Professor Takahiro Hiono of Hokkaido University of Japan for his prompt communications and colleagues worldwide for their laboratory contributions, made available through GISAID. We also thank the SDSC's CIPRES Science Gateway at the University of California-San Diego for computing resources.

This research was supported by a grant from the Animal and Plant Quarantine Agency(B-1543418-2023-23-01) of South Korea.

Author contributions: All authors have approved the final article.

About the Author

Dr. Heo is a researcher at Animal and Plant Quarantine Agency, South Korea. His research interests include surveillance of zoonotic viruses.

References

1. Napp S, Majó N, Sánchez-Gónzalez R, Vergara-Alert J. Emergence and spread of highly pathogenic avian influenza A(H5N8) in Europe in 2016–2017. Transbound Emerg Dis. 2018;65:1217–26. https://doi.org/10.1111/tbed.12861
2. Lee DH, Bertran K, Kwon JH, Swayne DE. Evolution, global spread, and pathogenicity of highly pathogenic avian influenza H5Nx clade 2.3.4.4. J Vet Sci. 2017;18(S1):269–80. https://doi.org/10.4142/jvs.2017.18.S1.269
3. Adlhoch C, Fusaro A, Gonzales JL, Kuiken T, Mirinavičiūtė G, Niqueux É, et al.; European Food Safety Authority; European Centre for Disease Prevention and Control; European Union Reference Laboratory for Avian Influenza. Avian influenza overview June–September 2023. EFSA J. 2023;21:e08328. https://doi.org/10.2903/j.efsa.2023.8328
4. Seo YR, Cho AY, Si YJ, Lee SI, Kim DJ, Jeong H, et al. Evolution and spread of highly pathogenic avian influenza A(H5N1) clade 2.3.4.4b virus in wild birds, South Korea, 2022–2023. Emerg Infect Dis. 2024;30:299–309. https://doi.org/10.3201/eid3002.231274
5. Kang YM, Heo GB, An SH, Lee YN, Cha RM, Cho HK, et al. Introduction of multiple novel high pathogenicity avian influenza (H5N1) virus of clade 2.3.4.4b into South Korea in 2022. Transbound Emerg Dis. 2023;2023:8339427. https://doi.org/10.1155/2023/8339427
6. Baek YG, Lee YN, Lee DH, Cheon SH, Kye SJ, Park YR, et al. A novel reassortant clade 2.3.4.4 highly pathogenic avian influenza H5N6 virus identified in South Korea in

2018. Infect Genet Evol. 2020;78:104056. https://doi.org/10.1016/j.meegid.2019.104056
7. Lee EK, Kang HM, Song BM, Lee YN, Heo GB, Lee HS, et al. Surveillance of avian influenza viruses in South Korea between 2012 and 2014. Virol J. 2017;14:54. https://doi.org/10.1186/s12985-017-0711-y
8. Sagong M, Lee YN, Song S, Cha RM, Lee EK, Kang YM, et al. Emergence of clade 2.3.4.4b novel reassortant H5N1 high pathogenicity avian influenza virus in South Korea during late 2021. Transbound Emerg Dis. 2022;69:e3255–60. https://doi.org/10.1111/tbed.14551
9. Lee YJ, Kang HM, Lee EK, Song BM, Jeong J, Kwon YK, et al. Novel reassortant influenza A(H5N8) viruses, South Korea, 2014. Emerg Infect Dis. 2014;20:1086–9. https://doi.org/10.3201/eid2006.140233
10. Nabeshima K, Takadate Y, Soda K, Hiono T, Isoda N, Sakoda Y, et al. Detection of H5N1 high pathogenicity avian influenza viruses in four raptors and two geese in Japan in the fall of 2022. Viruses. 2023;15:1865. https://doi.org/10.3390/v15091865
11. Li J, Zu Dohna H, Cardona CJ, Miller J, Carpenter TE. Emergence and genetic variation of neuraminidase stalk deletions in avian influenza viruses. PLoS One. 2011; 6:e14722. https://doi.org/10.1371/journal.pone.0014722
12. Yang L, Zhu W, Li X, Bo H, Zhang Y, Zou S, et al. Genesis and dissemination of highly pathogenic H5N6 avian influenza viruses. J Virol. 2017;91:e02199–16. https://doi.org/10.1128/JVI.02199-16

Address for correspondence: Kwang-Nyeong Lee, Avian Influenza Research and Diagnostic Division, Animal and Plant Quarantine Agency, 177 Hyeoksin 8-ro, Gimcheon-si, Gyeongsangbuk-do 39660, South Korea; email: leekwn@korea.kr

Emergence of Group B *Streptococcus* Disease in Pigs and Porcupines, Italy

Chiara Anna Garbarino,[1] Simone Bariselli,[1] Giovanni Pupillo, Patrizia Bassi, Andrea Luppi, Roberta Taddei, Alessandro Reggiani, Elisa Massella, Matteo Ricchi, Elena Carra,[2] Ruth N. Zadoks[2]

We describe group B *Streptococcus* linked to disease in farmed pigs and wild porcupines in Italy. Occurrence in pigs was attributed to transmission from nonpasteurized bovine milk whey. Antimicrobial-resistance profiles in isolates from porcupines suggest no common source of infection. Our findings expand the known host range for group B *Streptococcus* disease.

Streptococcus agalactiae (group B *Streptococcus* [GBS]) is a major pathogen of humans, cattle, aquatic species, and camels (*1*–*4*). GBS has been detected in pork but has not been associated with disease in pigs (*5*). Transmission between humans and animals may occur in multiple directions, and the organism's genome plasticity enables it to acquire accessory genome content that confers survival advantages in new niches, facilitating adaptation and onward transmission within new host species (*6*–*8*). We describe emergence of GBS as a cause of disease in domestic pigs (*Sus scrofa domesticus*) and wild porcupines (*Hystrix cristata*) in Italy.

The Study

In 2022, GBS was isolated during disease investigations on pig fattening farms in the provinces of Modena (farm 1, closed farming system with high biosecurity standards) and Reggio Emilia (farm 2, open farming system with low biosecurity standards), Emilia Romagna region, northern Italy (Figure 1; Appendix Table 1, https://wwwnc.cdc.gov/EID/article/30/6/23-1322-App1.pdf). The affected farms were ≈50 km apart and had no known links (e.g., through animals, feed, veterinarians, or workers). Neither farm had direct contact with dairy farms. Both farms used bovine milk whey as a feed ingredient in their pig fattening units. Farm 1 obtained whey from a single milk processing company, and farm 2 used multiple suppliers. Whey was used within 24 hours of receipt but was not heat treated at any stage.

In March 2022, farm 1 submitted the carcass of a pig found dead after 2 days of depression and anorexia to the Istituto Zooprofilattico Sperimentale della Lombardia e dell'Emilia Romagna (IZSLER; Brescia, Italy); no other animals in the group showed any signs of disease. On examination, we found lesions mainly in the lungs, liver, and heart, and histologic examination showed bacterial emboli containing GBS in lymphatic and pulmonary tissue (Figure 2). Farm 2 submitted samples from 1 pig in July 2022 and from 3 other pigs in December 2022, all having respiratory symptoms (coughs and dyspnea). On examination, we observed interstitial edema and multiple stages of pleuritis in the lungs and purulent catarrhal bronchopneumonia and mild fibrinous pericarditis in the pigs submitted in December. We isolated GBS from the lungs and lower airways of pigs from each submission (Appendix Table 1).

IZSLER also receives wildlife specimens from the Emilia Romagna region, where a regional wildlife surveillance plan has been in force since 2017, covering wild animals found dead or animal samples or carcasses from wildlife rescue centers. The plan covers numerous species, including porcupines, which are found in flat and hilly areas of the Emilia Romagna region and in many other regions of Italy. Porcupines mostly live in woods and areas with caves and

Author affiliations: Istituto Zooprofilattico Sperimentale della Lombardia e dell'Emilia Romagna, Brescia, Italy (C.A. Garbarino, S. Bariselli, G. Pupillo, P. Bassi, A. Luppi, R. Taddei, A. Reggiani, E. Massella, M. Ricchi, E. Carra); University of Sydney Faculty of Science, Sydney School of Veterinary Science, Camden, New South Wales, Australia (R.N. Zadoks)

DOI: https://doi.org/10.3201/eid3006.231322

[1]These first authors contributed equally to this article.

[2]These authors contributed equally to this article.

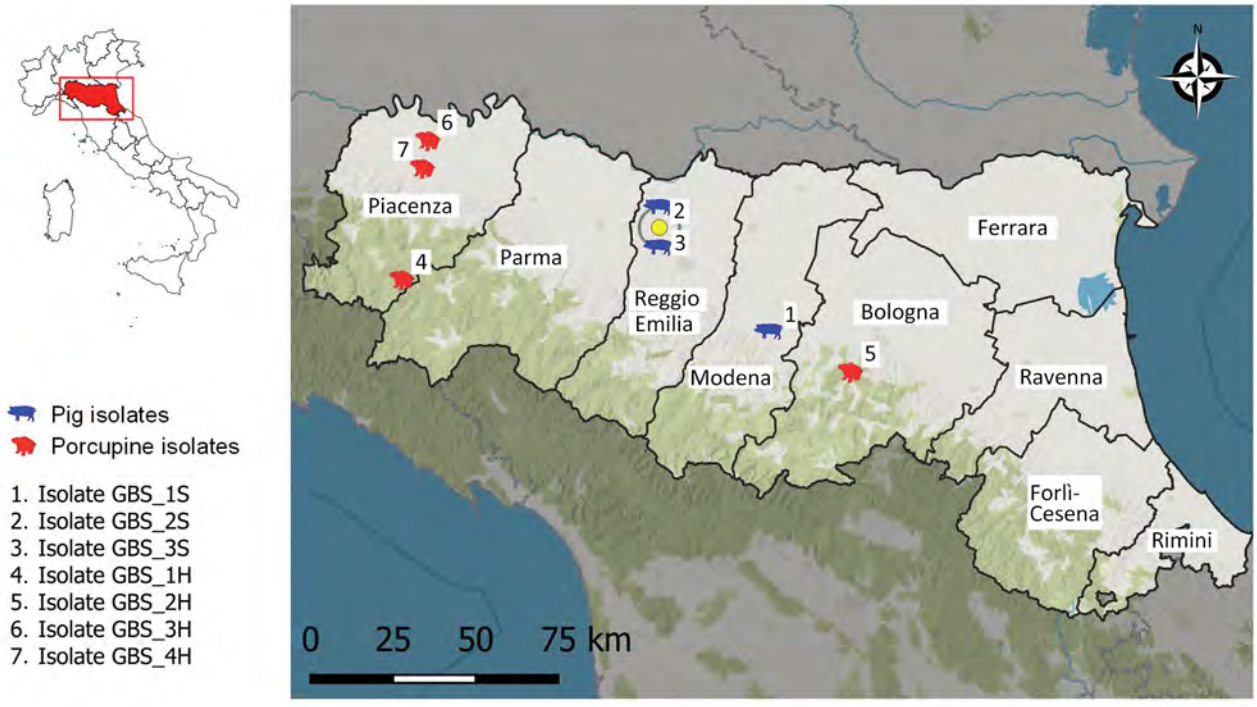

Figure 1. Geographic origin of group B *Streptococcus* bacterial isolates from pigs (*Sus scrofa*) and porcupines (*Hystrix cristata*) in Emilia Romagna region, northern Italy. Numbers indicate bacterial isolate for each diagnostic submission based on host and sequential number: GBS, group B *Streptococcus*; H, *H. cristata*; S, *S. scrofa*. Inset shows location of the region

bushes, but human interaction on farms or in gardens is possible. At the beginning of March 2023, a porcupine from San Gregorio of Ferriere, a Piacenza Province municipality located in the Apennine Mountains, was admitted to the Piacenza Rescue Centre (CRAS PC) with severe respiratory signs. CRAS PC collected a tracheal swab sample upon admission and submitted it to IZSLER with a request for bacteriologic culture and antimicrobial susceptibility testing to guide the animal's treatment. GBS was isolated in pure culture from the tracheal swab sample. The porcupine died within days, and the carcass was not submitted for necropsy. In March 2023, a young female porcupine was found dead in Sasso Marconi municipality, Bologna Province, and submitted to IZSLER. Necroscopic examination revealed numerous abscesses in the right lung and 1 inside the thoracic cavity. GBS was isolated from the abscesses in pure culture. In May and July 2023, two adult male porcupines were found in Piacenza Province, the first in Pittolo, a lowland municipality, and the second in Rivergaro. Both were submitted to CRAS PC and then to IZSLER. According to CRAS PC, the first porcupine was in poor condition and was euthanized at the rescue center; the second porcupine was found deceased. In both adult male porcupines, our necroscopic and bacteriologic analysis revealed hematomas and injuries consistent with multiple traumas, lung impairment with increased consistency and diffuse congestion, and the presence of GBS in pure culture in the lungs (Appendix Table 1).

We used the Sensititer (Thermo Fisher Scientific, https://www.thermofisher.com) for antimicrobial susceptibility testing of 1 isolate per diagnostic submission (Appendix Table 1) following Clinical and Laboratory Standards Institute guidelines (*9*). In the absence of specific breakpoints for GBS in pigs and

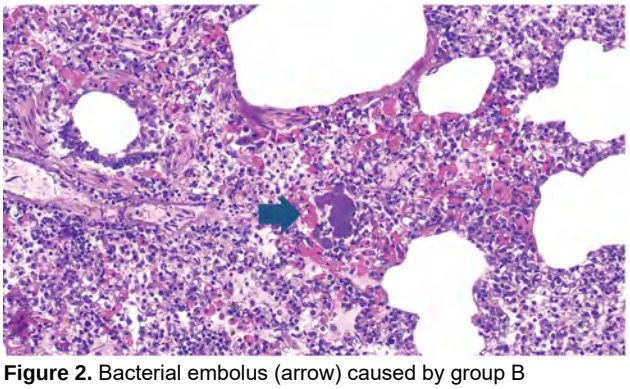

Figure 2. Bacterial embolus (arrow) caused by group B *Streptococcus* infection in a lung section of a pig (*Sus scrofa*) from a pig farm in the Modena Province, northern Italy. Group B *Streptococcus* was detected in the kidney, liver, and heart, indicating disseminated infection caused by septicemia. Hematoxylin–eosin staining; original magnification ×10.

porcupines, we used breakpoint values for *Streptococcus* in pigs (Appendix Table 2). The isolates from each of the 3 porcine submissions demonstrated resistance to erythromycin, tetracycline, and kanamycin (high level), whereas the 4 porcupine isolates were susceptible to most compounds, including kanamycin (Appendix Table 2). According to 7-gene multilocus sequence typing, the GBS isolates from each of the 7 diagnostic submissions belonged to sequence type (ST) 103 (*10*).

Conclusions

Detection of GBS in the tongue, tonsils, or intestines from pigs at slaughter has been reported previously without evidence of pathology (*5*,*11*). In this article, we describe GBS as a primary pathogen in pigs and porcupines on the basis of antemortem or postmortem evidence of respiratory disease because the GBS bacterial pathogen was isolated in pure culture from lung lesions and because the clinical and pathologic manifestations were consistent with GBS respiratory infection in humans, camels, and rabbits (*4*,*12*). For the porcupines, we speculate respiratory disease caused by GBS led to submission to the wildlife center either directly (sick porcupine) or indirectly, after sick animals were injured by traffic, which would explain the observed multiple traumas.

Human-to-animal transmission is possible for GBS (*3*,*7*). Such transmission seems unlikely in this case because the porcupines were positive for GBS before contact with the rescue centers. ST103 has also not been detected in the human population in the Emilia Romagna region (*13*). Introduction of GBS to the pig farms from raw milk whey is possible because ST103 is known to affect dairy herds in the Emilia Romagna region (*13*). Foodborne transmission of GBS has been documented previously (*6*,*14*). Source farms for the whey were not traced, but tracing could be attempted in future cases. The route of transmission to porcupines is unknown. Transmission from cattle to porcupines cannot be ruled out, possibly through dissemination of ST103 in bovine feces into the environment (*15*). Bovine ST103 isolates from the region, like the pig isolates in this study, are tetracycline-resistant and high level kanamycin-resistant (*13*). Isolates from the porcupines were fully susceptible, however, suggesting that an independent population of GBS might be present in the porcupine population.

Although a common exposure route was not identified and antimicrobial resistance profiles differed between GBS isolates from the 2 host species, all necropsied pigs and porcupines were infected with ST103. In Europe, ST103 has primarily been found in cattle, where it may have an environmental transmission cycle, in contrast to most other GBS strains that cause bovine mastitis (*7*,*15*). A single-locus variant of ST103 (ST651) was also the most common sequence type found in pig organs in Hong Kong (*10*). Our findings raise concerns about the ability of GBS ST103 and closely related sequence types to adapt to multiple host species and organs systems and highlights risks for future emergence in additional host species.

About the Authors

Dr. Garbarino is head of the Italian Reference Center for Paratuberculosis and works at the Experimental Zooprophylactic Institute of Lombardy in Emilia Romagna, Italy. Her interests include diagnostic service, research, and teaching with focus on animal infectious diseases. Dr. Bariselli works at the Experimental Zooprophylactic Institute of Lombardy and Emilia-Romagna, Italy. His main areas of interest are laboratory diagnostics and research in the field of infectious diseases of large animals and wildlife.

References

1. Bianchi-Jassir F, Paul P, To KN, Carreras-Abad C, Seale AC, Jauneikaite E, et al. Systematic review of group B streptococcal capsular types, sequence types and surface proteins as potential vaccine candidates. Vaccine. 2020;38:6682–94. https://doi.org/10.1016/j.vaccine.2020.08.052
2. Zadoks RN, Middleton JR, McDougall S, Katholm J, Schukken YH. Molecular epidemiology of mastitis pathogens of dairy cattle and comparative relevance to humans. J Mammary Gland Biol Neoplasia. 2011;16:357–72. https://doi.org/10.1007/s10911-011-9236-y
3. Delannoy CM, Crumlish M, Fontaine MC, Pollock J, Foster G, Dagleish MP, et al. Human *Streptococcus agalactiae* strains in aquatic mammals and fish. BMC Microbiol. 2013;13:41. https://doi.org/10.1186/1471-2180-13-41
4. Younan M, Bornstein S. Lancefield group B and C streptococci in East African camels (*Camelus dromedarius*). Vet Rec. 2007;160:330–5. https://doi.org/10.1136/vr.160.10.330
5. Sapugahawatte DN, Li C, Dharmaratne P, Zhu C, Yeoh YK, Yang J, et al. Prevalence and characteristics of *Streptococcus agalactiae* from freshwater fish and pork in Hong Kong wet markets. Antibiotics (Basel). 2022;11:397. https://doi.org/10.3390/antibiotics11030397
6. Barkham T, Zadoks RN, Azmai MNA, Baker S, Bich VTN, Chalker V, et al. One hypervirulent clone, sequence type 283, accounts for a large proportion of invasive *Streptococcus agalactiae* isolated from humans and diseased tilapia in Southeast Asia. PLoS Negl Trop Dis. 2019; 13:e0007421. https://doi.org/10.1371/journal.pntd.0007421
7. Crestani C, Forde TL, Lycett SJ, Holmes MA, Fasth C, Persson-Waller K, et al. The fall and rise of group B

Streptococcus in dairy cattle: reintroduction due to human-to-cattle host jumps? Microb Genom. 2021;7:000648. https://doi.org/10.1099/mgen.0.000648
8. Richards VP, Velsko IM, Alam MT, Zadoks RN, Manning SD, Pavinski Bitar PD, et al. Population gene introgression and high genome plasticity for the zoonotic pathogen *Streptococcus agalactiae*. Mol Biol Evol. 2019;36:2572–90. https://doi.org/10.1093/molbev/msz169
9. Clinical and Laboratory Standards Institute. Performance standards for antimicrobial susceptibility testing; twenty-fifth informational supplement (M100-S25). Wayne (PA): The Institute; 2015.
10. Jones N, Bohnsack JF, Takahashi S, Oliver KA, Chan MS, Kunst F, et al. Multilocus sequence typing system for group B *streptococcus*. J Clin Microbiol. 2003;41:2530–6. https://doi.org/10.1128/JCM.41.6.2530-2536.2003
11. O'Sullivan T, Friendship R, Blackwell T, Pearl D, McEwen B, Carman S, et al. Microbiological identification and analysis of swine tonsils collected from carcasses at slaughter. Can J Vet Res. 2011;75:106–11.
12. Ren SY, Geng Y, Wang KY, Zhou ZY, Liu XX, He M, et al. *Streptococcus agalactiae* infection in domestic rabbits, *Oryctolagus cuniculus*. Transbound Emerg Dis. 2014;61:e92–5. https://doi.org/10.1111/tbed.12073
13. Carra E, Russo S, Micheli A, Garbarino C, Ricchi M, Bergamini F, et al. Evidence of common isolates of *Streptococcus agalactiae* in bovines and humans in Emilia Romagna region (Northern Italy). Front Microbiol. 2021;12:673126. https://doi.org/10.3389/fmicb.2021.673126
14. Hetzel U, König A, Yildirim AO, Lämmler C, Kipar A. Septicaemia in emerald monitors (*Varanus prasinus* Schlegel 1839) caused by *Streptococcus agalactiae* acquired from mice. Vet Microbiol. 2003;95:283–93. https://doi.org/10.1016/S0378-1135(03)00184-6
15. Barsi F, Carra E, Ricchi M, Gnali G, Pisoni G, Russo S, et al. Circulation of *Streptococcus agalactiae* ST103 in a free stall Italian dairy farm. Appl Environ Microbiol. 2022;88:e0038322. https://doi.org/10.1128/aem.00383-22

Address for correspondence: Ruth N. Zadoks, Sydney School of Veterinary Science, Faculty of Science, University of Sydney, 425 Werombi Rd, Camden, NSW 2570, Australia; email: ruth.zadoks@sydney.edu.au

Molecular Identification of *Fonsecaea monophora*, Novel Agent of Fungal Brain Abscess

Sudesh Gourav, Gagandeep Singh, Mragnayani Pandey, Bhaskar Rana, Sonakshi Gupta, Himanshu Mishra, Immaculata Xess

A 3-year-old patient in India experiencing headaches and seizures was diagnosed with a fungal infection, initially misidentified as *Cladophialophora bantiana*. Follow-up sequencing identified the isolate to be *Fonsecaea monophora* fungus. This case demonstrates the use of molecular methods for the correct identification of *F. monophora*, an agent of fungal brain abscess.

A 3-year-old boy was admitted to the All India Institute of Medical Sciences, New Delhi, India, with headache for 3 weeks and 2 episodes of seizures. He had no history of fever, vomiting, or altered senses; no history suggestive of tuberculosis; and no predisposing conditions. Fundoscopic examination revealed bilateral papilledema. Magnetic resonance imaging of the brain showed multiple contrast enhancing lesions. Contrast enhanced computed tomography of chest and abdomen revealed well-defined nodules in the right lung and both lobes of the liver. Cerebrospinal fluid examination showed a glucose level of 51 mg/dL (reference range 40–70 mg/dL), protein level of 82 mg/dL (reference range 12–60 mg/dL), and leukocyte count of 45 cells/mm^3 (reference range 0–20 cells/mm^3) with 22% neutrophils. We found persistent eosinophilia (up to 31%) on sequential blood counts.

We conducted a potassium hydroxide-calcofluor white examination of the ultrasound-guided liver biopsy sample, which showed dematiaceous septate hyphae 3–6 μm in diameter. The hyphae showed bulbous dilatations at irregular intervals. Light microscopic examination also showed dematiaceous septate hyphae. A brain biopsy taken from the right parietal lesion showed similar dematiaceous septate hyphae on potassium hydroxide-calcofluor white examination. Histologic examination of both samples showed granulomatous inflammation with hyphae of dematiaceous fungi. We administered intravenous liposomal amphotericin B and voriconazole and continued treatment for 9 weeks.

We performed a fungal culture of the liver biopsy, but no growth was detected. The brain biopsy sample grew dark brown-black velvety colonies on sabouraud dextrose agar at both 25° and 37°C after 9 days of incubation. Lactophenol cotton blue mount showed septate brown hyphae with moderately long sparsely branched chains of smooth oval brown conidia (Figure 1). The organism was initially misidentified as *Cladophialophora bantiana* because of its known preponderance in cases of invasive fungal disease of the central nervous system (CNS).

We repeated brain imaging after the intravenous treatment course. Imaging showed the lesions had greatly reduced in size and number. We started the patient on an oral combination of flucytosine and voriconazole. After 8 weeks on the oral regimen, the patient's symptoms resolved, and imaging showed near-complete radiologic resolution of the lesions. We stopped antifungal treatment. We followed up with the patient after a year, and there was no recurrence.

We retrospectively performed molecular identification of the culture isolate from the brain biopsy sample. We ran conventional PCR on the extracted DNA targeting the internal transcribed spacer (ITS) region of the 18s rDNA. We conducted sequencing by using an ABI 3730XL automated sequencer (ThermoFisher Scientific, https://www.thermofisher.com).

We edited sequences by using Geneious Prime 2023.2.1 (Geneious, https://www.geneious.com). We conducted a basic local alignment search tool inquiry of the sequenced region in GenBank, resulting in 98.95% identity with *F. monophora* fungal strain

Author affiliation: All India Institute of Medical Sciences, New Delhi, India

DOI: https://doi.org/10.3201/eid3006.240077

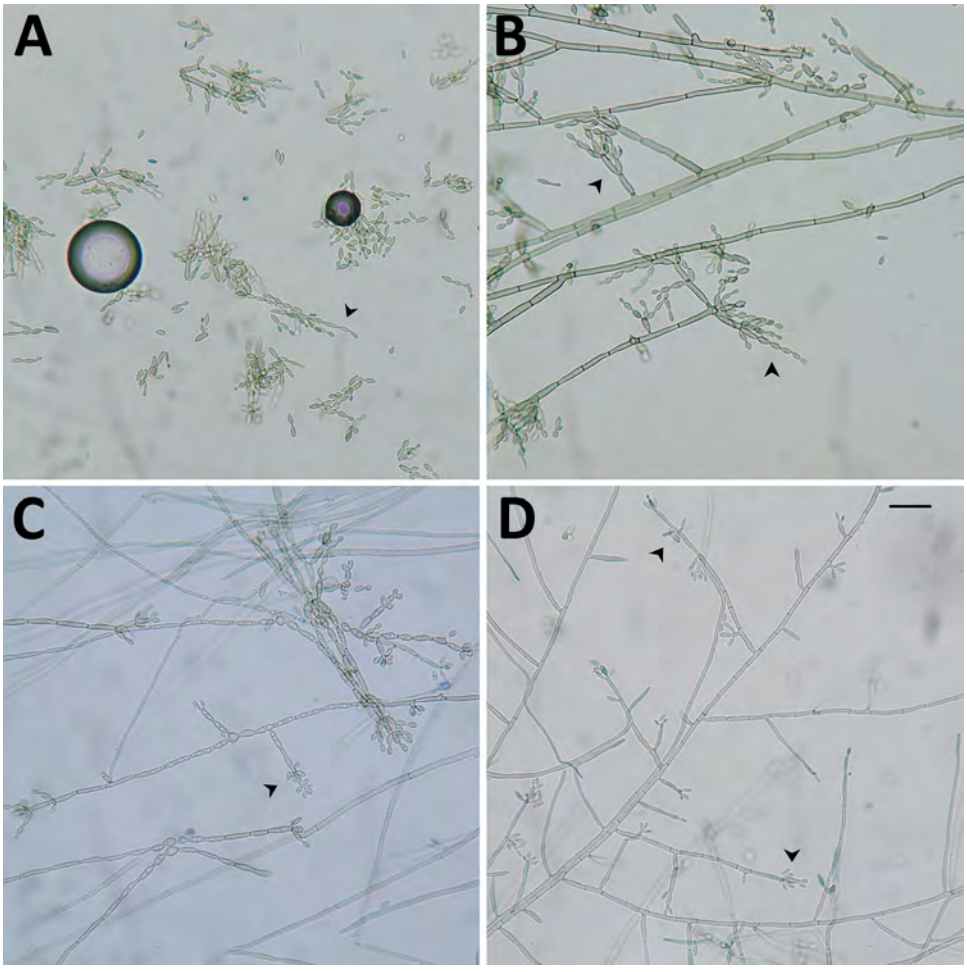

Figure 1. Lactophenol cotton blue mount of a culture from a brain biopsy sample from a 3-year-old patient in India with *Fonsecaea monophora* infection, showing dematiaceous septate hyphae with different types of conidiation (arrowheads). A) Multicelled sessile conidial chains resembling genus *Cladophialophora*, leading to the initial misidentification. B) *Fonsecaea*-type conidiation. C) *Rhinocladiella*-type conidiation. D) Asterisks of *Fonsecaea*-type conidiation.

CBS 269.37. We analyzed phylogenetically informative polymorphic sites in the ITS region of *Fonsecaea* spp. according to de Hoog et al. (*1*) and found 12 of 13 bases were identical with *F. monophora*, confirming the identification (GenBank accession no. OR773059) (Table).

We derived the phylogenetic relatedness of our isolate with selected global isolates of *Fonsecaea spp.* fungus by using MEGA version 11.0.13 software (MEGA, https://www.megasoftware.net). We aligned the sequences by using multiple sequence comparison by log-expectation algorithm, followed by phylogenetic model determination. We implemented the maximum-likelihood method with the Kimura 2 parameter model with 1,000 bootstrap replicates (Figure 2).

F. monophora was first described as a separate fungal species by de Hoog et al. (*1*) in 2004. The next year, Surash et al. (*2*) published a case report of *F. monophora* CNS invasion. They also reported 2 previous cases of *F. monophora* CNS invasion identified retrospectively with sequencing (*3*,*4*). Since then, 8 other case reports of *F. monophora* CNS invasion have been published (*5*–*12*) (Appendix Table, https://wwwnc.cdc.gov/EID/article/30/6/24-0077-App1.pdf). Many cases of brain abscesses caused by *F. pedrosoi* fungus have been described in literature. Although most of them were reported before *F. monophora* was

Table. Phylogenetically informative polymorphic sites in the ITS region of *Fonsecaea* spp., showing 12 of 13 bases from the isolate cultured from the brain biopsy of a 3-year-old patient were identical with *F. monophora* fungus*

	ITS 1 (206)								5.8s (169)	ITS 2 (152)			
Species	15	41	47	79	99	100	109	113	46	47	119	121	144
F. pedrosoi	C	C	A	T	C	T	T	A	C	G	T	T	T
F. monophora	T/–†	T	T	G	T	C	C	G	T	A	A	C	C
Study isolate	T	T	T	G	T	C	C	G	C	A	A	C	C

*ITS, internal transcribed spacer.
†Presence of thymine or deletion in position 15 of ITS 1 of *F. monophora*.

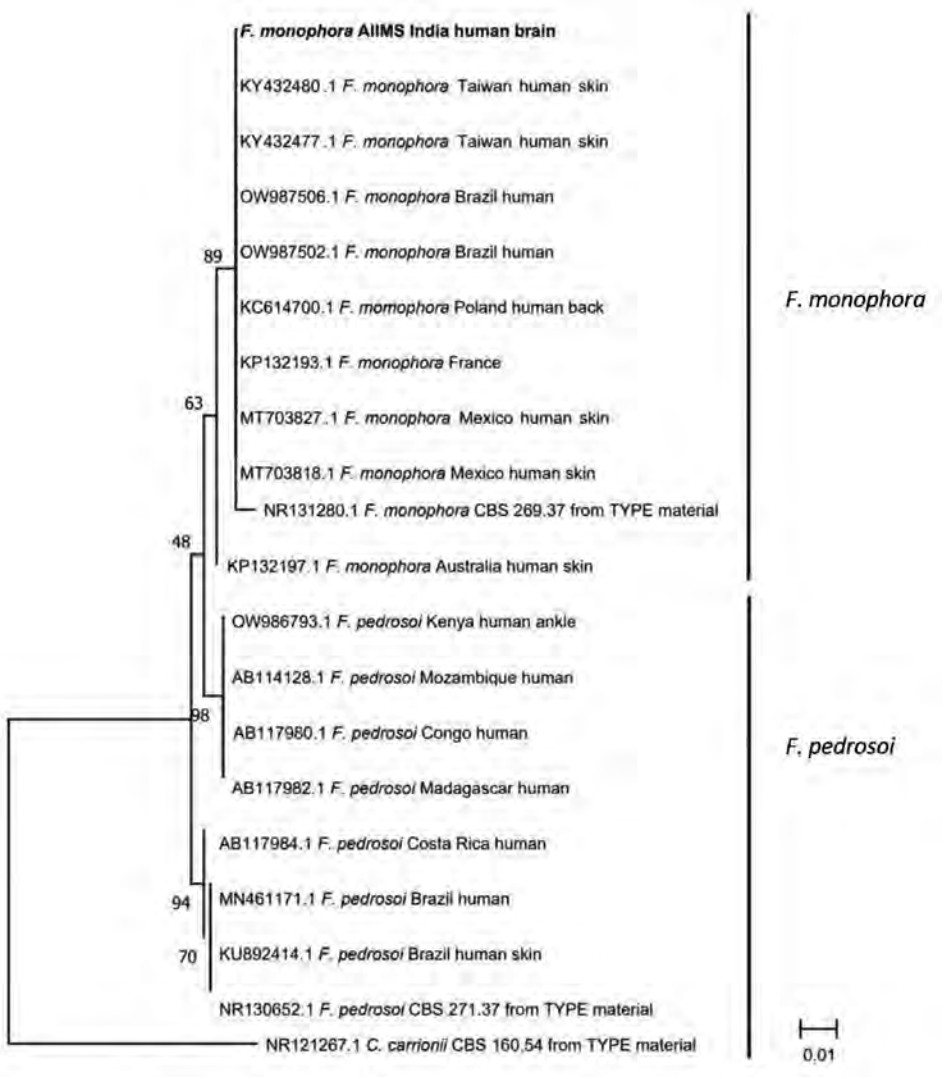

Figure 2. Phylogenetic relatedness of the isolate cultured from the brain biopsy sample from a 3-year-old patient in India with *Fonsecaea monophora* fungus infection (bold) compared with selected global isolates of *Fonsecaea* spp. Tree was derived by using the maximum-likelihood method with Kimura 2 parameter model and 1,000 bootstrap replicates implemented in MEGA 11.0.13 (MEGA, https://www.megasoftware.net).

established as a species in 2004, some have been described more recently. Of note, none of the cases in the literature have had identifications confirmed by molecular methods. Both *F. monophora* and *F. pedrosoi* are causative agents of human chromoblastomycosis. Although *F. pedrosoi* is usually associated with chromoblastomycosis, *F. monophora* is considered a more general opportunist. *F. monophora* is also more neurotropic (*1*). Because *F. monophora* cannot be reliably differentiated from *F. pedrosoi* on the basis of phenotypic methods, some cases attributed to *F. pedrosoi* may have been caused by *F. monophora*. Molecular methods are essential for definitive identification. A review of brain abscess cases caused by *F. pedrosoi* was provided by Madhugiri et al. (*13*).

We have reviewed only cases in which CNS involvement was seen with *F. monophora*. In the cases we reviewed, *F. monophora* was limited to the CNS, except for 1 case where there was also involvement of the left foot (*5*). Headache was the most common symptom experienced and was accompanied by focal neurologic deficits and symptoms of increased intracranial pressure in some cases. Patient symptoms usually occurred for weeks before care was sought. Three cases were associated with multiple lesions in the CNS discovered by radiologic examination (*2*,*4*,*5*). In all the cases, final identification was confirmed by sequencing the ITS region from 18s rDNA extracted from culture growth.

Antifungal-susceptibility testing was done in 7 cases. Most results showed low MICs for the commonly used antifungals. Three of them reported MICs of ≥2 μg/mL for amphotericin B (*8*,*9*,*11*). Two reports described higher MICs for flucytosine (*9*,*10*). Those MICs are like results obtained previously from 25 clinical isolates of *F. monophora* (*14*). In a separate study on 10 clinical isolates of *F. monophora*, terbinafine and voriconazole were the drugs with the best in vitro activity,

showing MICs <0.25 mg/L, whereas fluconazole, flucytosine, amphotericin B, caspofungin, and micafungin showed high MICs (*15*). Because voriconazole can penetrate the CNS well, it can be considered the drug of choice for CNS infections; amphotericin B monotherapy should be avoided. Terbinafine may also be considered in combination with voriconazole.

Six of the 11 patients we describe died. In 3 patients the immediate cause of death was not directly related to the fungal infection (*4*,*10*,*12*). Of the other 3 patients, surgical excision was not done in 2 (*3*,*9*). Of the 5 patients who survived, all were treated with surgical excision and various combinations of antifungals (*2*,*5*–*7*,*11*). All the patients improved greatly within weeks to months, and no recurrence of infection was reported after stopping antifungals. A combined approach with early surgical intervention and combination antifungals greatly improves outcome. Of note, serum (1,3)-β-D-glucan levels were elevated in 2 cases and decreased gradually with successful therapy (*6*,*11*). Thus (1,3)-β-D-glucan can be potentially used as a biomarker for follow-up.

Conclusions

This case and review emphasizes the importance of molecular methods for the definitive identification of *F. monophora*, a cause of fungal brain abscess that is increasingly being reported. All the published cases to date have used sequencing for final identification. Targeting the ITS region of 18s rDNA, the universal fungal barcode, is usually sufficient, and no additional foci need to be sequenced. Although the implication of *F. monophora* identification for patient management is not clear, patient management may be changed in the future once more data are available.

About the Author

Dr. Gourav is a senior resident in the Department of Microbiology, All India Institute of Medical Sciences, Ansari Nagar, New Delhi, with a research interest in clinical mycology.

References

1. De Hoog GS, Attili-Angelis D, Vicente VA, Van Den Ende AH, Queiroz-Telles F. Molecular ecology and pathogenic potential of *Fonsecaea species.* Med Mycol. 2004;42:405–16. https://doi.org/10.1080/13693780410001661464
2. Surash S, Tyagi A, De Hoog GS, Zeng JS, Barton RC, Hobson RP. Cerebral phaeohyphomycosis caused by *Fonsecaea monophora*. Med Mycol. 2005;43:465–72. https://doi.org/10.1080/13693780500220373
3. Lucasse C, Chardome J, Magis P. Cerebral mycosis from *Cladosporium trichoides* in a native of the Belgian Congo [in French]. Ann Soc Belg Med Trop (1920). 1954;34:475–8.
4. Nóbrega JP, Rosemberg S, Adami AM, Heins-Vaccari EM, Lacaz CS, de Brito T. *Fonsecaea pedrosoi* cerebral phaeohyphomycosis ("chromoblastomycosis"): first human culture-proven case reported in Brazil. Rev Inst Med Trop São Paulo. 2003;45:217–20. https://doi.org/10.1590/S0036-46652003000400008
5. Takei H, Goodman JC, Powell SZ. Cerebral phaeohyphomycosis caused by *Ladophialophora bantiana* and *Fonsecaea monophora*: report of three cases. Clin Neuropathol. 2007;26:21–7. https://doi.org/10.5414/NPP26021
6. Koo S, Klompas M, Marty FM. *Fonsecaea monophora* cerebral phaeohyphomycosis: case report of successful surgical excision and voriconazole treatment and review. Med Mycol. 2010;48:769–74. https://doi.org/10.3109/13693780903471081
7. Doymaz MZ, Seyithanoglu MF, Hakyemez İ, Gultepe BS, Cevik S, Aslan T. A case of cerebral phaeohyphomycosis caused by *Fonsecaea monophora*, a neurotropic dematiaceous fungus, and a review of the literature. Mycoses. 2015;58:187–92. https://doi.org/10.1111/myc.12290
8. Bagla P, Loeffelholz M, Blanton LS. Cerebral phaeohyphomycosis by *Fonsecaea monophora*: report in a patient with AIDS and a ring enhancing lesion. Med Mycol Case Rep. 2016;12:4–7. https://doi.org/10.1016/j.mmcr.2016.06.002
9. Varghese P, Jalal MJA, Ahmad S, Khan Z, Johny M, Mahadevan P, et al. Cerebral phaeohyphomycosis caused by *Fonsecaea monophora*: first report from India. Int J Surg Med. 2016;2:44–9. https://doi.org/10.5455/ijsm.neurosurgery01
10. Stokes W, Fuller J, Meier-Stephenson V, Remington L, Meatherall BL. Case report of cerebral phaeohyphomycosis caused by *Fonsecaea monophora.* Off J Assoc Med Microbiol Infect Dis Canada. 2017;2:86–92. https://doi.org/10.3138/jammi.2.1.013
11. Dobias R, Filip M, Vragova K, Dolinska D, Zavodna P, Dujka A, et al. Successful surgical excision of cerebral abscess caused by *Fonsecaea monophora* in an immunocompetent patient and review of literature. Folia Microbiol (Praha). 2019;64:383–8. https://doi.org/10.1007/s12223-018-0661-9
12. Helbig S, Thuermer A, Dengl M, Krukowski P, de With K. Cerebral abscess by *Fonsecaea monophora*—the first case reported in Germany. Open Forum Infect Dis. 2018;5:ofy129. https://doi.org/10.1093/ofid/ofy129
13. Madhugiri VS, Singh R, Vyavahare M, Vijayahari R, Sasidharan GM, Kuma VR, et al. Opportunistic *Fonsecaea pedrosoi* brain abscess in a patient with non-cirrhotic portal fibrosis-induced hypersplenism—a novel association. Br J Neurosurg. 2013;27:690–3. https://doi.org/10.3109/02688697.2013.771732
14. Najafzadeh MJ, Badali H, Illnait-Zaragozi MT, De Hoog GS, Meis JF. In vitro activities of eight antifungal drugs against 55 clinical isolates of *Fonsecaea* spp. Antimicrob Agents Chemother. 2010;54:1636–8. https://doi.org/10.1128/AAC.01655-09
15. Coelho RA, Brito-Santos F, Figueiredo-Carvalho MHG, Silva JVDS, Gutierrez-Galhardo MC, do Valle ACF, et al. Molecular identification and antifungal susceptibility profiles of clinical strains of *Fonsecaea* spp. isolated from patients with chromoblastomycosis in Rio de Janeiro, Brazil. PLoS Negl Trop Dis. 2018;12:e0006675. https://doi.org/10.1371/journal.pntd.0006675

Address for correspondence: Immaculata Xess, Department of Microbiology, All India Institute of Medical Sciences, Ansari Nagar, New Delhi 110029, India; email: immaxess@gmail.com

Human Passage of *Schistosoma incognitum*, Tamil Nadu, India, and Review of Autochthonous Schistosomiasis, South Asia

Sitara S.R. Ajjampur, Rajiv Sarkar, Richard S. Bradbury

A fecal survey in Tamil Nadu, India, revealed 2 persons passed schistosome eggs, later identified as *Schistosoma incognitum*, a parasite of pigs, dogs, and rats. We investigated those cases and reviewed autochthonous schistosomiasis cases from India and Nepal. Whether the 2 new cases represent true infection or spurious passage is undetermined.

In 1926, A.C. Chandler described "a new schistosome infection of man" based on the presence of distinctive terminal spined schistosome eggs from 2 human fecal samples collected in Krishnanagar, West Bengal, and Kalimpong, Sikkim, both in northeast India (*1*). Obtaining fecal samples directly from humans was difficult; thus, both specimens were collected from areas where humans regularly defecated, and the provenance of the specimens could not be confirmed (*1*). No subsequent human infections with that schistosome species, *Schistosoma incognitum*, were reported, and pigs, which are natural hosts, were prevalent in the areas where the samples were collected. Other researchers later considered those 2 infections likely were derived from misidentified pig feces (*2*). However, Chandler claimed in the original report that "from the nature of the stool there was no reasonable doubt that it was human stool" based upon its fresh collection from an area frequented by humans for defecation and the presence of *Trichuris* and *Ascaris* eggs in 1 of the stool samples and hookworm eggs in both samples (*1*). No further reports of *S. incognitum* in human stool were made after Chandler's initial findings. We report detection of *S. incognitum* from 2 persons in Tamil Nadu, India, and review autochthonous schistosomiasis cases from Nepal and India.

Author affiliations: Christian Medical College, Vellore, India (S.S.R. Ajjampur); Indian Institute of Public Health Shillong, Meghalaya, India (R. Sarkar); James Cook University, Townsville, Queensland, Australia (R.S. Bradbury)

DOI: https://doi.org/10.3201/eid3006.231641

The Study

In September 2016, as part of a community-based study on hookworm, stool surveys from ≈8,600 participants were conducted in 45 villages in Thiruvanamalai District, Tamil Nadu, India (*3*), an area that has high rates of open defecation. Participants provided written informed consent, and the study was reviewed and approved by the institutional review board of Christian Medical College, Vellore, India (approval no. 8264, 2023 March 27).

As part of that study, suspected schistosome eggs were seen in direct wet mounts (2–3 ova/slide) from fecal samples of 2 women, 50 and 35 years of age, who were from the same household. The eggs were 110–120 μm in length, suboval, flatter on one side, and bluntly rounded at the aspinous end and displayed a prominent asymmetric terminal spine (Figure 1). Motile miracidia were clearly visible within the eggs. The eggs were consistent with morphologic descriptions and illustrations of *S. incognitum* (*1*,*2*,*4*).

Both women were generally in good health. The older woman was co-infected with hookworm. Both women belonged to low socioeconomic strata, had no toilet access, and used water from a public tap for drinking and household use. Other infection risks were owning or exposure to animals, including dogs, pigs, and free roaming cattle and poultry, as well as handling animal manure daily. The women's house was located next to a stream that was used for open defecation. On re-evaluation in 2018, both women were in good health; stool sample examinations, complete blood counts, and liver function tests were

within normal ranges, and no *Schistosoma* ova were detected in stool samples. No treatment was given during either observation; the women were advised regarding good hygiene practices.

Those 2 cases likely represent spurious fecal passage of *S. incognitum* eggs after consumption of animal liver, food contaminated with animal feces, or other environmental ingestion. However, long-term or transient true infections cannot be excluded. Species identification relied on morphology of the passed eggs because molecular identification was not possible.

S. incognitum is a natural parasite of pigs, dogs, sheep, goats, and rodents in Asia (*2*,*4*,*5*). In ricefield rats (*Rattus argentiventer*), *S. incognitum* eggs invade the liver and cause hepatic granulomas; less commonly, ectopic egg granulomas can be found in the intestine, stomach, pancreas, or lungs (*5*). *Lymnaea luteola* water snails are the intermediate host (*4*,*6*,*7*).

Experimental infection of primates with *S. incognitum* is possible (*6*,*7*), indicating that human infection also might occur. In 1 experiment, 13 immunocompetent rhesus monkeys (*Macaca mulatta*) were percutaneously exposed to 1,000–2,500 cercariae (*6*). Fatal infection developed in 2 monkeys. At necropsy, 1 monkey harbored 100 mature *S. incognitum* flukes in the intrahepatic portal veins and 4 adult flukes (2 female and 2 male) in the mesenteric veins. Both viable and immature *S. incognitum* eggs were found in the liver but none in the intestinal wall or feces. The second deceased monkey was infected with 400 immature *S. incognitum* flukes in the intrahepatic vessels and 8 in the spleen. Another 4 infected monkeys had 1–6 immature *S. incognitum* flukes in the intrahepatic portal veins, and the other animals were refractory to infection, including 1 monkey exposed multiple times (*6*).

In another experiment, 10 immunocompetent rhesus monkeys were percutaneously exposed to 2,000–2,500 cercariae (*7*). Upon necropsy at 21–35 days postinfection, 2–114 adult *S. incognitum* flukes were recovered from the hepatointestinal circulation; 2 monkeys also had 2–3 adult flukes in the lungs. Four monkeys were euthanized at 45–100 days postinfection; 2 were infected with single immature *S. incognitum* flukes (*7*). That study did not state whether the animals were euthanized later because they did not show evidence of infection. Two other studies either found rhesus monkeys were refractory to or only capable of maintaining transient *S. incognitum* infections (*7*). Neither study reported *S. incognitum* eggs in feces from infected monkeys.

Our report on human passage of *S. incognitum* eggs and that by Chandler (*1*) are not the only reports of schistosomiasis from the subcontinent of India. Many convincing reports from India and Nepal document autochthonous schistosomiasis cases without a history of travel to endemic regions (*8*–*15*) (Figure 2). In India, in 1952, a large focus of genitourinary schistosomiasis, assigned to *S. haematobium*, was discovered in Gimvi Village, Ratnagiri District, Maharashtra (*8*). Of 1,200 village inhabitants, 250 cases were detected, a 21% overall prevalence (*8*). In 1956, *S. haematobium*–like eggs were reported in the feces of 3 people from New Delhi and 1 from Punjab, none with travel histories (*9*). Later, 30% of 3,000 inhabitants of Tirupparankundram Village, Madurai District, Madras, were found to be passing eggs resembling *S. haematobium* (*10*). A 1989 parasitologic survey of Dokur Village, Andhra Pradesh, found samples from 4 participants, 2 stool and 2 urine samples, contained eggs clearly resembling those of *S. haematobium* (*11*), but the 2 positive fecal samples were assumed to have been contaminated by urine during collection (*12*). No travel to *S. haematobium*–endemic regions was reported in those cases (*8*–*12*). Several other reports of schistosomiasis from India

Figure 1. *Schistosoma incognitum* egg identified in the feces of a woman from Tamil Nadu, India. Saline direct smear. Original magnification ×400; scale bar indicates 25 μm.

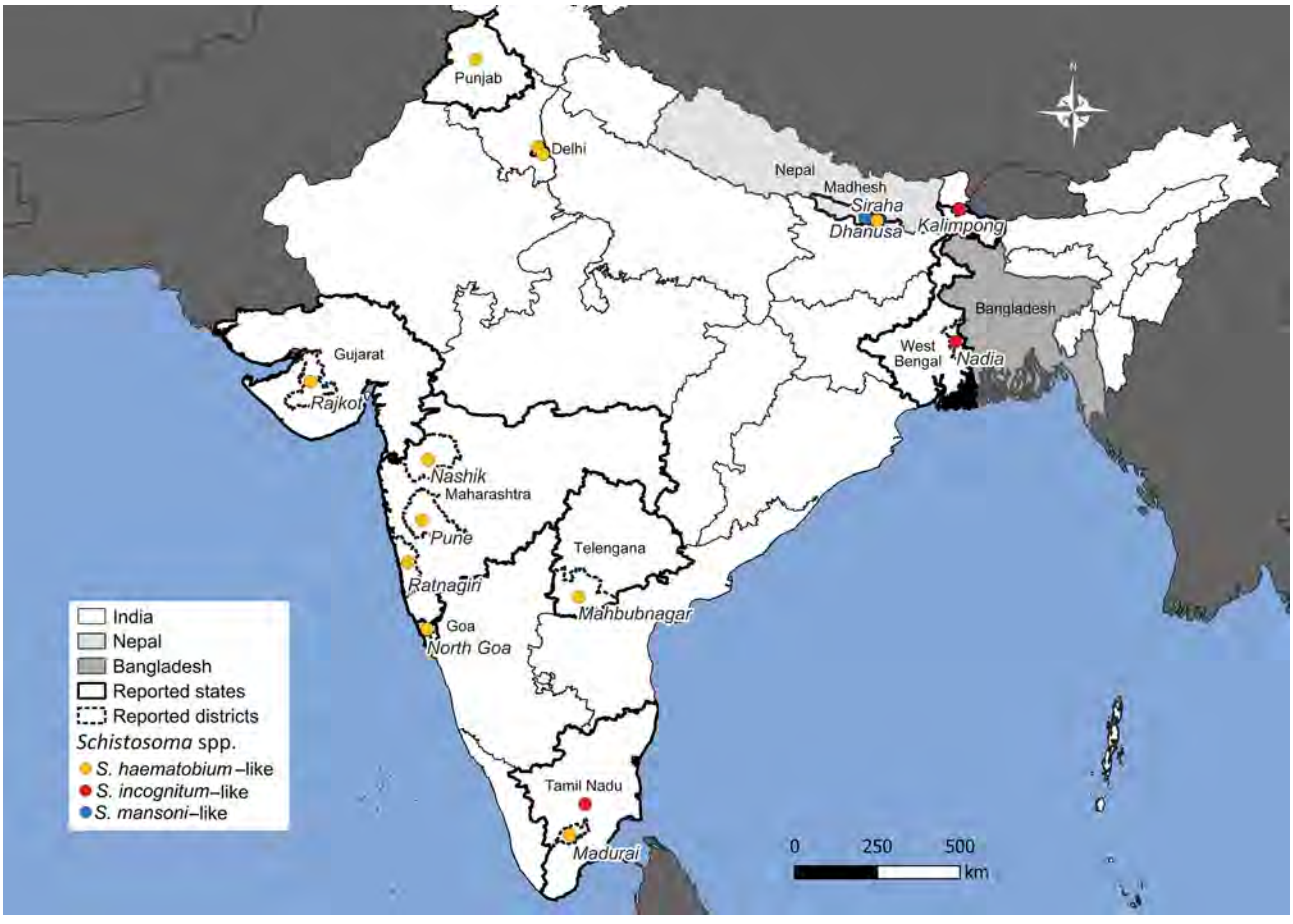

Figure 2. Geographic locations of *Schistosoma incognitum* passage from humans and autochthonous human schistosomiasis in India and Nepal. Map shows credible reports of urinary or fecal passage of schistosome eggs in India and Nepal from this study and others (*1*,*8*–*11*,*14*,*15*). Included patients had no reported travel history to known endemic areas. Where possible, state and district information are provided.

lack sufficient evidence or have travel histories to known endemic regions (*12*). Other reports clearly show artifacts mistaken for schistosome eggs (*13*).

Autochthonous schistosomiasis has also been reported from Nepal. In the late 1990s, eggs morphologically indistinguishable from *S. mansoni* were found in the feces of 3 persons from the Dhanusha district, none of whom had traveled outside of Nepal (*14*). A subsequent serologic survey using a *Schistosoma* antibody ELISA assay revealed a seroprevalence of 18.1% in 518 participants from 4 villages (*14*). In 2019, urinary passage of terminal spined schistosome eggs morphologically indistinguishable from *S. haematobium* was reported in a patient from the Siraha district of Nepal with no travel history outside of India and Nepal (*15*).

Conclusions

Whether reports of human schistosomiasis represent true *S. haematobium*, *S. mansoni*, and *S. incognitum* infections, hybrids of human and animal schistosomes, spurious passage of animal schistosome eggs, or hitherto unrecognized zoonotic schistosome infections remain unclear. Those reports also could represent minor transmission foci after local introduction of schistosomiasis to an area by a traveler or returning resident. We recommend further investigation of the many reports of human schistosomiasis in India and Nepal. Those investigations should include molecular typing and phylogenetic placement to taxonomically identify *Schistosoma* species and surveillance to determine species distribution in the region.

About the Author

Dr. Ajjampur is a professor of microbiology at The Wellcome Trust Research Laboratory, Christian Medical College, Vellore, India. Her research interests include the epidemiology, impact, and prevention of endemic enteric and parasitic infections.

References

1. Chandler AC. A new schistosome infection of man, with notes on other human fluke infections in India. Indian J Med Res. 1926;14:179–83.
2. Sinha PK, Srivastava HD. Studies on *Schistosoma incognitum* Chandler, 1926. I. On the synonymy and morphology of the blood-fluke. Parasitology. 1956;46:91–100. https://doi.org/10.1017/S0031182000026366
3. Ajjampur SSR, Kaliappan SP, Halliday KE, Palanisamy G, Farzana J, Manuel M, et al. Epidemiology of soil transmitted helminths and risk analysis of hookworm infections in the community: results from the DeWorm3 Trial in southern India. PLoS Negl Trop Dis. 2021;15:e0009338. https://doi.org/10.1371/journal.pntd.0009338
4. Agrawal MC. The schistosomes. In: Agrawal MC editor. Schistosomes and schistosomiasis in South Asia. New Delhi: Springer India; 2012. p. 7–50.
5. Carney WP, Brown RJ, Van Peenen PF, Purnomo, Ibrahim B, Koesharjono CR. *Schistosoma incognitum* from Cikurai, West Java, Indonesia. Int J Parasitol. 1977;7:361–6. https://doi.org/10.1016/0020-7519(77)90060-1
6. Dutt SC. On the susceptibility of *Macaca mulatta* to infection with *Schistosoma incognitum*. Curr Sci. 1965;34:49–51.
7. Das M, Agrawal MC. Experimental infection of rhesus monkeys with *Schistosoma incognitum* and *Orientobilharzia dattai*. Vet Parasitol. 1986;22:151–5. https://doi.org/10.1016/0304-4017(86)90018-X
8. Gadgil RK, Shah SN. Human schistosomiasis in India. Discovery of an endemic focus in the Bombay State. Indian J Med Sci. 1952;6:760–3.
9. Dhanda L. Infestation with ova morphologically resembling *Schistosoma haematobium*. J Indian Med Assoc. 1956;26:407–8.
10. Santhanakrishnan G, Sundarajajulu G. Human schistosemiasis in India: discovery of an endemic focus in the Madras State. Curr Sci. 1967;36:480–1.
11. Bidinger PD, Crompton DW. A possible focus of schistosomiasis in Andhra Pradesh, India. Trans R Soc Trop Med Hyg. 1989;83:526. https://doi.org/10.1016/0035-9203(89)90277-0
12. Kali A. Schistosome infections: an Indian perspective. J Clin Diagn Res. 2015;9:DE01–04.
13. Shrivastava KK, Arora MM. *Schistosoma haematobium* infection in Lahager, a village in Raipur District of Madhya Pradesh. Indian J Med Res. 1969;57:2016–7.
14. Sherchand JB, Ohara H, Sherchand S, Matsuda H. The suspected existence of *Schistosoma mansoni* in Dhanusha district, southern Nepal. Ann Trop Med Parasitol. 1999;93:273–8. https://doi.org/10.1080/00034983.1999.11813423
15. Sah R, Utzinger J, Neumayr A. Urogenital schistosomiasis in fisherman, Nepal, 2019. Emerg Infect Dis. 2020;26:1607–9. https://doi.org/10.3201/eid2607.191828

Address for correspondence: Richard S. Bradbury, School of Public Health and Tropical Medicine, College of Public Health, Medical and Veterinary Sciences, James Cook University, 1 James Cook Dr, Douglas, QLD 4811, Australia; email: richard.bradbury@jcu.edu.au

etymologia revisited

Enterocytozoon bieneusi

['entərə͵saitə'ʒu:ən bɪə'nəʊsɪ]

From the Greek *en'tĕr-ō-sī'tōn* (intestine), *kútos* (vessel, cell), and *zō'on* (animal), and the surname Bieneus, in memory of the first infected patient whose case was reported in Haiti during 1985. *Enterocytozoon bieneusi*, a member of the wide-ranging phylum Microsporidia, is the only species of this genus known to infect humans. Microsporidia are unicellular intracellular parasites closely related to fungi, although the nature of the relationship is not clear.

E. bieneusi, a spore-forming, obligate intracellular eukaryote, was discovered during the HIV/AIDS pandemic and is the main species responsible for intestinal microsporidiosis, a lethal disease before widespread use of antiretroviral therapies. More than 500 genotypes are described, which are divided into different host-specific or zoonotic groups. This pathogen is an emerging issue in solid organ transplantation, especially in renal transplant recipients.

Sources

1. Desportes I, Le Charpentier Y, Galian A, Bernard F, Cochand-Priollet B, Lavergne A, et al. Occurrence of a new microsporidan: *Enterocytozoon bieneusi* n.g., n. sp., in the enterocytes of a human patient with AIDS. J Protozool. 1985;32:250–4. https://doi.org/10.1111/j.1550-7408.1985.tb03046.x
2. Didier ES, Weiss LM. Microsporidiosis: not just in AIDS patients. Curr Opin Infect Dis. 2011;24:490–5. https://doi.org/10.1097/QCO.0b013e32834aa152
3. Han B, Weiss LM. Microsporidia: obligate intracellular pathogens within the fungal kingdom. Microbiol Spectr. 2017;5:97–113. https://doi.org/10.1128/microbiolspec.FUNK-0018-2016
4. Moniot M, Nourrisson C, Faure C, Delbac F, Favennec L, Dalle F, et al. Assessment of a multiplex PCR for the simultaneous diagnosis of intestinal cryptosporidiosis and microsporidiosis: epidemiologic report from a French prospective study. J Mol Diagn. 2021;23:417–23. https://doi.org/10.1016/j.jmoldx.2020.12.005

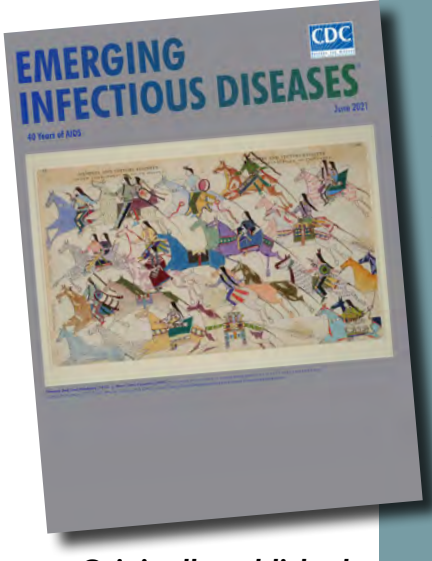

Originally published in June 2021

https://wwwnc.cdc.gov/eid/article/27/6/et-2706_article

Emerging Variants of Canine Enteric Coronavirus Associated with Outbreaks of Gastroenteric Disease

Edward Cunningham-Oakes,[1] Jack Pilgrim,[1] Alistair C. Darby, Charlotte Appleton, Chris Jewell, Barry Rowlingson, Carmen Tamayo Cuartero, Richard Newton, Fernando Sánchez-Vizcaíno, Ivo Salgueiro Fins, Bethaney Brant, Shirley Smith, Rebekah Penrice-Randal, Simon R. Clegg, Ashley P.E. Roberts, Stefan H. Millson, Gina L. Pinchbeck, P.-J.M. Noble, Alan D. Radford

A 2022 canine gastroenteritis outbreak in the United Kingdom was associated with circulation of a new canine enteric coronavirus closely related to a 2020 variant with an additional spike gene recombination. The variants are unrelated to canine enteric coronavirus–like viruses associated with human disease but represent a model for coronavirus population adaptation.

Recent spillover events by coronaviruses highlights the potential devastating effects of emergence into human populations (*1*). Subsequent evolution can create variants in response to natural and vaccine-induced immunity. Canine enteric coronavirus (CECoV) is an alphacoronavirus with a complex evolutionary history punctuated by recombination (*2*). Type I and II CECoVs were largely defined by serologic differences; type I CECoVs also contain an additional open reading frame (*3*). Recently, type IIb and IIc (also called type I/II) variants were defined on the basis of recombination in the N terminal domain of the spike protein between type IIa CECoVs and either transmissible gastroenteritis virus of pigs or type I CECoV (*2*).

CECoV is generally associated with mild endemic canine gastroenteritis, and only sporadic reports of severe disease occur. Severe disease is usually associated with co-infection with other pathogens, known as pantropic CECoV (*4*). In 2020, an outbreak of gastroenteric disease occurred in dogs in the United Kingdom and was associated with a nationally distributed variant of CECoV (*5*). In 2022, a similar outbreak was reported on social media and initially affected coastal regions of Yorkshire, UK. Speculation about etiologies included contact with dead marine animals.

The Study

We obtained electronic health data from the Small Animal Veterinary Surveillance Network (SAVSNET) (https://www.liverpool.ac.uk/savsnet). Veterinary data are collected passively by SAVSNET from ≈10% of veterinary practices in the United Kingdom, including a practitioner-recorded main presenting complaint (MPC). Laboratory data are collected passively by SAVSNET from participating diagnostic laboratories used by ≈60% of veterinary practices in the United Kingdom. We provided validated questionnaires to owners and veterinary surgeons to collect more detailed descriptive information. We recruited participants by using SAVSNET websites and social media.

We obtained canine fecal samples from 2 sources. We asked veterinary surgeons completing questionnaires to submit samples from dogs with vomiting, diarrhea, or both of unknown etiology. We also asked them to submit samples from control dogs. We additionally retrieved samples sent directly to IDEXX Laboratories (https://www.idexx.com) for testing for canine enteric pathogens after the completion of diagnostic testing (*6*). This study was approved by Liverpool University's Central Committee

Author affiliations: University of Liverpool, Liverpool, UK (E. Cunningham-Oakes, J. Pilgrim, A.C. Darby, I.S. Fins, B. Brant, S. Smith, R. Penrice-Randal, G.L. Pinchbeck, P.-J.M. Noble, A.D. Radford); Lancaster University, Lancaster, UK (C. Appleton, C. Jewell, B. Rowlingson); University of Bristol, Bristol, UK (C.T. Cuartero, F. Sánchez-Vizcaíno); University of Cambridge, Cambridge, UK (R. Newton); University of Lincoln, Lincoln, UK (S.R. Clegg, A.P.E. Roberts, S.H. Millson).

DOI: https://doi.org/10.3201/eid3006.231184

[1]These first authors contributed equally to this article.

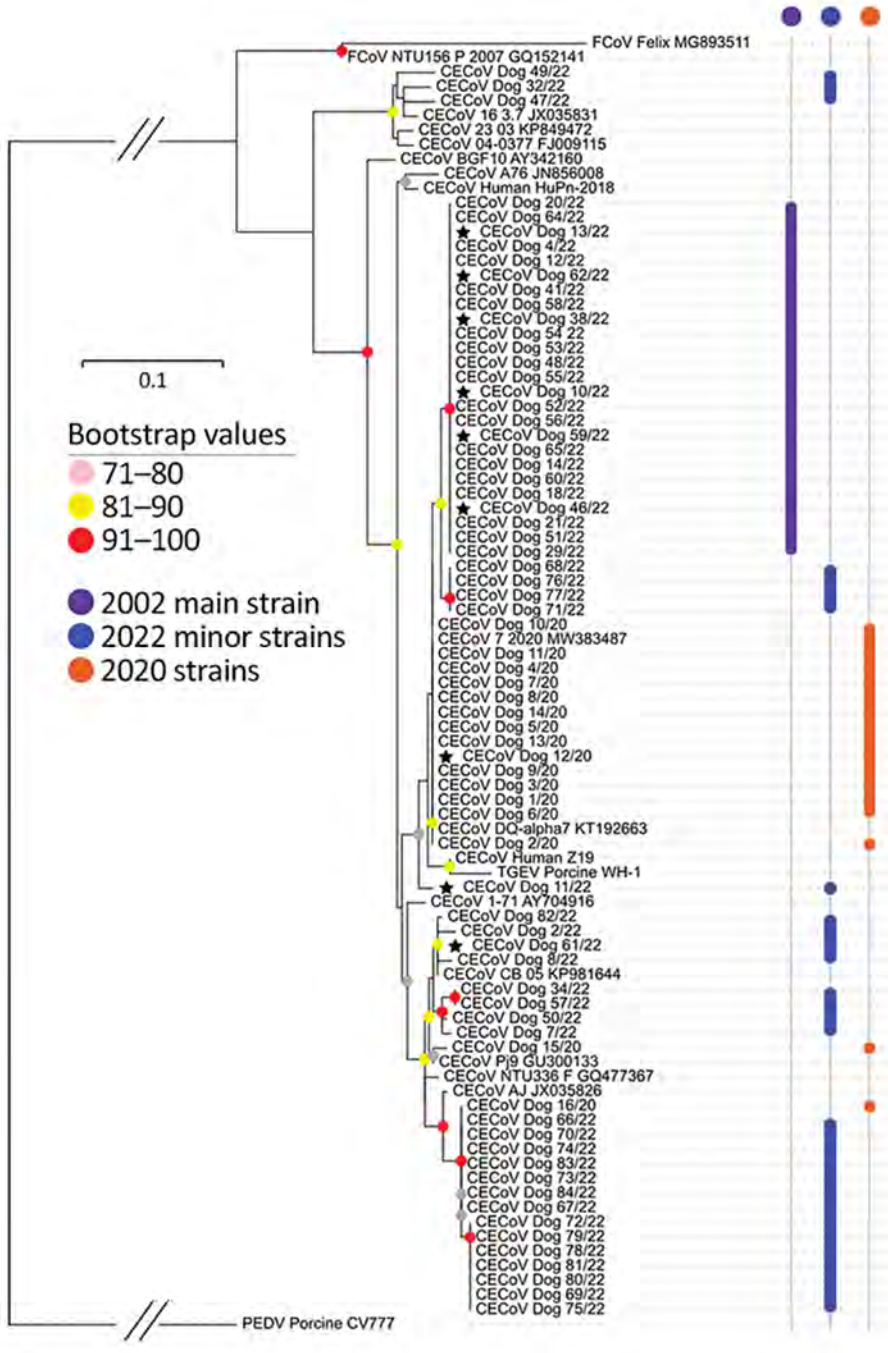

Figure 1. Maximum-likelihood tree of partial matrix gene (315-bp) sequences of canine enteric coronavirus recovered from infected canines, United Kingdom, 2020 and 2022. Sequences obtained from samples collected in 2022 are marked in purple (main strain) and blue (minor strains); stars indicate samples that were whole-genome sequenced as part of this study. Sequences obtained from 2020 are marked in orange. Scale bar indicates number of base differences per site.

(approval no. RETH00964) and Veterinary Research Ethics Committee (approval no. VREC922ab).

We modeled the weekly prevalence of gastroenteric MPC cases by using a logistic latent Gaussian process model, as done in previous studies (*5*), while adjusting for COVID-19–related disturbances in consult numbers. The modeling allowed us to capture the normal pattern of seasonal incidence in MPC cases; we considered the detection of high case prevalence as extreme relative to the model-based predictive distribution (Appendix, https://wwwnc.cdc.gov/EID/article/30/6/23-1184-App1.pdf).

We performed nucleic acid extraction, PCR, matrix gene sequencing, and analyses, as previously described (*5*). The diversity of sampled CECoVs required 2 approaches for whole-genome sequencing: initial sequence-independent single-primer amplification (SISPA) (*7*) and amplicon-tiling by using overlapping primers on the basis of SISPA-derived sequences (*8*) (Appendix).

We assessed recombination by visualizing whole genome alignments by using SimPlot++ 1.3 (https://github.com/Stephane-S/Simplot_PlusPlus). We aligned draft CECoV genomes and the nearest GenBank matches by using MAFFT (https://mafft.cbrc.jp/alignment/software). We identified regions of recombination by using Gubbins 2.3.4 (https://github.com/nickjcroucher/gubbins) and Phandango 1.3.0 (https://bivi.co/visualisation/phandango). We then masked those regions by using BEDTools 2.31.0 (https://bedtools.readthedocs.io/en/latest/index.html) and removed excessive gaps by using Gblocks 0.91b (https://gensoft.pasteur.fr/docs/gblocks/0.91b) before performing phylogenetic reconstruction with ModelFinder IQTree (http://www.iqtree.org/ModelFinder) and EvolView 3 (https://www.evolgenius.info).

The canine gastroenteric MPC was seasonal, peaking in January and February at 4%–5% of consultations. In Yorkshire, a 2-week period in 2022 exceeded 99% prediction intervals, consistent with an outbreak. Laboratory results showed CECoV diagnosis peaking each winter, with >20% of submitted samples positive (Appendix Figure 3). We received 28 questionnaire responses from veterinarians (20 cases, 8 controls) and 438 from owners (cases). The primary clinical signs were vomiting, diarrhea, and inappetence. Most cases lasted 3–7 days (7 [35.0%] of vet responses and 170 [38.8%] of owner responses). In co-habiting dogs, 108 (59.3%) were also unwell, suggesting possible transmission. Twenty-five percent of veterinary-reported cases and controls indicated a recent beach visit. All groups showed similar diet profiles.

We received 46 canine fecal samples from veterinary practices (45 cases, 1 control); 18 tested CECoV-positive. We obtained 87 samples from the diagnostic laboratory. We tested 27 and found that 19 were CECoV-positive, including 16 known CECoV-positive samples from the submitting laboratory. Matrix gene sequences for 36 of 37 amplicons were supplemented from a parallel study at the University of Lincoln. Phylogenetic analysis identified 1 main variant (25/55 sequences) (Figure 1) widely distributed across the United Kingdom (Appendix Figure 1); the remaining samples distributed into 14 minor variants.

Our use of SISPA recovered 4 genomes, and by using primers on the basis of the sequence for Dog10/22, our amplicon tiling resulted in 6 additional near full-length genomes. Sequences of the 2022 major variant were most closely related to the 2020 major variant (Dog7/20) over most of the genome (96% coverage and 97.08% identity), and the gap in coverage was associated with low 5′ spike gene similarity (Figure 2). The mismatched area was closely related to A76-type viruses, suggestive of a recombination event. A core genome phylogeny excluding recombinant regions identified by Gubbins confirmed that the main 2022 variant was highly homogenous, clustering most closely with the main 2020 variant (Appendix Figure 2). All 2022 CECoVs from the United Kingdom were distinct from serotype IIb strains (Appendix Figure 4), which were associated with human pneumonia (HuPn-2018 and CECoV-Z19). The main 2020 variant, although classified as part of serotype IIb, lacked amino acid changes typically associated with a respiratory tropism (Appendix Figure 5).

Conclusions

Our investigation showed a repeated winter rise in canine gastrointestinal disease nationally, which regionally exceeded normal seasonal prediction intervals and coincided with increased CECoV diagnoses. Questionnaire responses aided in refuting links to

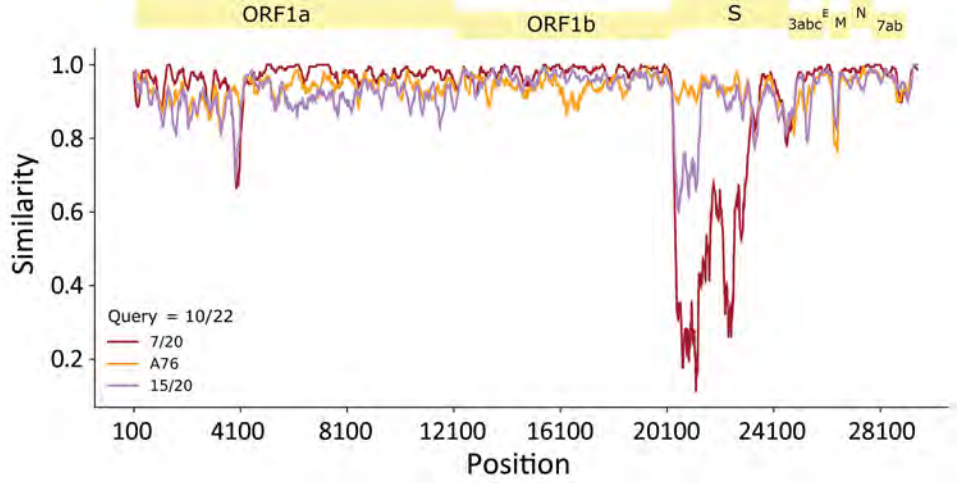

Figure 2. Viral sequences from 2022 identified from canine enteric coronavirus–infected canines in the United Kingdom, demonstrating a close relation to the 2020 major variant. The mismatched area was closely related to A76-type viruses, suggestive of a recombination event. Simplot analysis used the main variant observed in the 2022 United Kingdom outbreak (Dog 10/22) as a reference compared with the main (Dog 7/20) and minor (Dog 15/20) strains from the 2020 outbreak and the A76 strain. E, envelope; M, membrane; N, nucleocapsid; ORF, open reading frame; S, spike.

possible exposures to beaches and highlighted the severity and prolonged duration of many cases. Sequence analysis identified diverse variants of CECoV circulating in dogs in the United Kingdom during the 2022 sampling period, and 1 variant predominated. Whole-genome sequencing demonstrated that the predominant variant was closely related to a variant associated with a similar outbreak but had an additional spike gene recombination. We cannot formally link CECoV infection to disease; however, we suggest that because of the dominance of the 2022-sampled CECoV population by a single new variant, coupled with spike gene mutations likely to affect transmissibility or immunity (*2*), we may classify CECoV10/22 as a CECoV variant of interest in dogs (*9*).

Advances in sequencing technologies have enabled high-throughput and cost-effective methods to generate viral genomes for disease surveillance (*10*). Matrix gene PCR and SISPA of representative samples, followed by specific amplicon tiling, is an efficient strategy for surveillance in relatively resource-poor populations regardless of the affected species, where prior knowledge of circulating variants will likely be limited.

On the basis of resulting whole-genome sequences, our explanation for the origins of the predominant variant from 2022 is past co-infection with both a serotype I/II strain, such as an A76-type virus (*11*), and a virus like the major variant strain from 2020 (*2*). The complex mosaic nature of CECoV genomes suggests whole-genome sequencing is required for future surveillance. Because of the role of the spike protein in determining receptor binding, host affinity, immunoevasion, and severity of disease (*2*), the recombinant variants might behave differently from prototypical CECoV strains (*11*,*12*). Recent identification of CECoV variants in raccoon dogs (*Nyctereutes procyonoides*) from Wuhan, China, closely related to the major variant we identified in 2020 (*13*) and of CECoV-like viruses in humans (*14*,*15*) heightens the need for efficient surveillance of circulating CECoV variants in pet dogs and other domesticated species, wildlife, and humans.

Raw reads, annotated genomes, and matrix gene sequences can be found in the European Nucleotide Archive (Bioproject no. PRJEB55544). Primer schemes, reference genomes, pilot amplicon-tiling, and BugSeq results can be found at https://github.com/edwardcunningham-oakes/CECoV-outbreak-2022.

This publication was supported by Dogs Trust as part of SAVSNET Agile project to develop a methodology for efficient national canine health surveillance based on health data and bioinformatics. This work would not be possible without the generous participation of veterinary surgeries and diagnostic laboratories submitting data to SAVSNET.

Author contributions: SAVSNET database management (A.D.R., P.-J.M.N., B.B., and G.L.P.); project conception (A.D.R., P.-J.M.N., B.B., G.L.P., F.S.-V., C.J., and R.N.); field epidemiology (C.T.C., R.N., F.S.-V., and G.L.P.); statistical analysis (C.A., C.J., and B.R.); obtaining and sequencing the University of Liverpool samples (S.S. and I.S.F.); whole-genome sequencing and informatics (E.C.-O., J.P., A.C.D., S.S., A.D.R., R.P-R., and J.A.H.); obtaining and sequencing of the University of Lincoln samples (S.R.C., A.P.E.R., and S.H.M.).

About the Authors

Dr. Cunningham-Oakes is a postdoctoral research associate at the University of Liverpool. His primary research interests are the microbiome and the development of metagenomics and metatranscriptomics in the contexts of outbreak surveillance and pathogen evolution. Dr. Pilgrim is a postdoctoral research associate at the University of Liverpool in the Department of Evolution, Ecology and Behavior. His research interests include microbial ecology, vector-borne diseases, and virology.

References

1. Masood N, Malik SS, Raja MN, Mubarik S, Yu C. Unravelling the epidemiology, geographical distribution, and genomic evolution of potentially lethal coronaviruses (SARS, MERS, and SARS CoV-2). Front Cell Infect Microbiol. 2020;10:499. https://doi.org/10.3389/fcimb.2020.00499
2. Licitra BN, Duhamel GE, Whittaker GR. Canine enteric coronaviruses: emerging viral pathogens with distinct recombinant spike proteins. Viruses. 2014;6:3363–76. https://doi.org/10.3390/v6083363
3. Lorusso A, Decaro N, Schellen P, Rottier PJ, Buonavoglia C, Haijema BJ, et al. Gain, preservation, and loss of a group 1a coronavirus accessory glycoprotein. J Virol. 2008;82:10312–7. https://doi.org/10.1128/JVI.01031-08
4. Buonavoglia C, Decaro N, Martella V, Elia G, Campolo M, Desario C, et al. Canine coronavirus highly pathogenic for dogs. Emerg Infect Dis. 2006;12:492–4. https://doi.org/10.3201/eid1203.050839
5. Radford AD, Singleton DA, Jewell C, Appleton C, Rowlingson B, Hale AC, et al. Outbreak of severe vomiting in dogs associated with a canine enteric coronavirus, United Kingdom. Emerg Infect Dis. 2021;27:517–28. https://doi.org/10.3201/eid2702.202452
6. Smith SL, Afonso MM, Roberts L, Noble PM, Pinchbeck GL, Radford AD. A virtual biobank for companion animals: a parvovirus pilot study. Vet Rec. 2021;189:e556. https://doi.org/10.1002/vetr.556
7. Greninger AL, Naccache SN, Federman S, Yu G, Mbala P, Bres V, et al. Rapid metagenomic identification of viral pathogens in clinical samples by real-time nanopore sequencing analysis. Genome Med. 2015;7:99. https://doi.org/10.1186/s13073-015-0220-9

8. Quick J, Grubaugh ND, Pullan ST, Claro IM, Smith AD, Gangavarapu K, et al. Multiplex PCR method for MinION and Illumina sequencing of Zika and other virus genomes directly from clinical samples. Nat Protoc. 2017;12:1261–76. https://doi.org/10.1038/nprot.2017.066
9. World Health Organization. Tracking SARS-CoV-2 variants. [cited 2024 May 8] https://www.who.int/activities/tracking-SARS-CoV-2-variants
10. Vöhringer HS, Sanderson T, Sinnott M, De Maio N, Nguyen T, Goater R, et al.; The Wellcome Sanger Institute COVID-19 Surveillance Team; COVID-19 Genomics UK (COG-UK) Consortium. Genomic reconstruction of the SARS-CoV-2 epidemic in England. Nature. 2021;600:506–11. https://doi.org/10.1038/s41586-021-04069-y
11. Regan AD, Millet JK, Tse LP, Chillag Z, Rinaldi VD, Licitra BN, et al. Characterization of a recombinant canine coronavirus with a distinct receptor-binding (S1) domain. Virology. 2012;430:90–9. https://doi.org/10.1016/j.virol.2012.04.013
12. Hulswit RJ, de Haan CA, Bosch BJ. Coronavirus spike protein and tropism changes. Adv Virus Res. 2016;96:29-57.
13. Wang W, Tian JH, Chen X, Hu RX, Lin XD, Pei YY, et al. Coronaviruses in wild animals sampled in and around Wuhan at the beginning of COVID-19 emergence. Virus Evol. 2022;8:veac046.
14. Vlasova AN, Diaz A, Damtie D, Xiu L, Toh TH, Lee JS, et al. Novel canine coronavirus isolated from a hospitalized patient with pneumonia in East Malaysia. Clin Infect Dis. 2022;74:446–54. https://doi.org/10.1093/cid/ciab456
15. Lednicky JA, Tagliamonte MS, White SK, Blohm GM, Alam MM, Iovine NM, et al. Isolation of a novel recombinant canine coronavirus from a visitor to Haiti: further evidence of transmission of coronaviruses of zoonotic origin to humans. Clin Infect Dis. 2022;75:e1184-e1187.

Address for correspondence: Alan D. Radford, University of Liverpool, Chester High Road, Wirral, CH64 7TE, UK; email: alanrad@liverpool.ac.uk

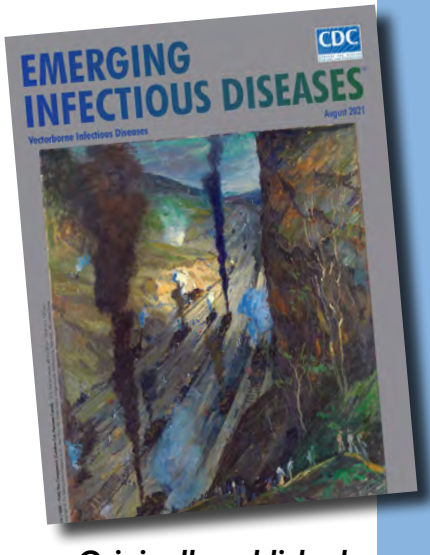

Originally published in August 2021

etymologia revisited

Culex quinquefasciatus
['kyo͞o leks 'kwinkwə fa she 'ah tus]

In 1823, the American entomologist Thomas Say described *Culex* (Latin for "gnat") *quinquefasciatus*, which he collected along the Mississippi River. Originally written as "C. 5-fasciatus," the name refers to 5 ("quinque") black, broad, transverse bands ("fasciatus" or "fasciae") on the mosquito's dorsal abdomen. The name remains despite later revelations of more than 5 fasciae, thanks to improved microscopy. Although quinquefasciatus is the official scientific name, there are at least 5 synonymous names for this species.

Say described this species as "exceedingly numerous and troublesome." "Quinx" are among the world's most abundant peridomestic mosquitoes, earning the nickname "southern house mosquito." *Cx. quinquefasciatus* is found throughout subtropical and tropical areas worldwide, except for exceedingly dry or cold regions. This mosquito is a principal vector of many pathogens, transmitting the phlebovirus Rift Valley fever virus and the 2 flaviviruses St. Louis encephalitis virus and West Nile virus, in addition to filarial worms and avian malarial parasites.

Sources

1. Belkin J. *Quinquefasciatus* or *Fatigans* for the tropical (Southern) house mosquito (Diptera: Culicidae). Proc Entomol Soc Wash. 1977;79:45–52.
2. Farajollahi A, Fonseca DM, Kramer LD, Marm Kilpatrick A. "Bird biting" mosquitoes and human disease: a review of the role of *Culex pipiens* complex mosquitoes in epidemiology. Infect Genet Evol. 2011;11:1577–85. https://doi.org/10.1016/j.meegid.2011.08.013
3. Harrison BA, Byrd BD, Sither CB, Whitt PB. The Mosquitoes of the Mid-Atlantic Region: An Identification Guide. Cullowhee (NC): Western Carolina University; 2016.
4. Say T. Descriptions of dipterous insects of the United States. Journal of the Academy of Natural Sciences. 1823;3:9–54.
5 University of Florida, Department of Entomology and Nematology. Featured creatures. [cited 2021 Mar 3]. http://entnemdept.ufl.edu/creatures/aquatic/southern_house_mosquito.htm

https://wwwnc.cdc.gov/eid/article/27/8/et-2708_article

Choanephora infundibulifera Rhinosinusitis in Man with Acute Lymphoblastic Leukemia, Tennessee, USA

Anita Max, Heather L. Glasgow, Teresa C.B. Santiago, Ashley Holland, Hiroto Inaba, Connie F. Cañete-Gibas, Nathan P. Wiederhold, Randall T. Hayden, Elisabeth E. Adderson

Choanephora infundibulifera is a member of the Mucorales order of fungi. The species is associated with plants as a saprophyte or parasite and may be responsible for spoilage or disease but is an uncommon cause of human infection. We describe *C. infundibulifera* rhinosinusitis in a young man with leukemia in Tennessee, USA.

An 18-year-old man visited St. Jude Children Research Hospital in Memphis, Tennessee, USA, with systemic symptoms and lymphadenopathy and received a diagnosis of early T-cell precursor acute lymphoblastic leukemia. Induction chemotherapy was complicated by rhinosinusitis linked to species of *Alternaria* and *Curvularia* and presumed fungal pneumonia. The man's treatment consisted of debridement of his nasal and sinus passages and administration of liposomal amphotericin B, followed by oral posaconazole for 5 months. Thereafter, posaconazole secondary prophylaxis was prescribed during severe neutropenia.

The man's leukemia relapsed 6 months after his original diagnosis, and he received treatment that included cyclophosphamide, vincristine, doxorubicin, methotrexate, cytarabine, dexamethasone, dasatinib, and venetoclax. At 4 months postrelapse, while receiving posaconazole prophylaxis (300 mg orally 2×/d), the patient sought medical treatment for acute right facial pain and a black eschar on his anterior nasal septum. His leukocyte count was 0.16 × 10^3 cells/mm^3 (normal 4.5 to 11.0 x 10^3 cells/mm^3), and his absolute neutrophil count was 20 cells/mm^3 (normal 1,500 to 8,000 cells/mm^3). Measurement of his serum posaconazole trough concentration revealed a level of 1.4 μg/mL (desired concentration ≥0.7 μg/mL). Computed tomography of the sinuses showed evidence of rhinosinusitis (Figure 1, panel A). A magnetic resonance imaging scan revealed soft tissue swelling, right nodularity and irregular nasal septal mucosal thinning, sinus mucosal thickening, and enhancing right jugular lymph nodes. Computed tomography of the chest yielded unremarkable results. The patient used smokeless chewing tobacco and electronic cigarettes but had an otherwise unremarkable exposure history.

The patient underwent nasal endoscopy and debridement (Figure 1, panel B). Hematoxylin and eosin–stained sections from a biopsy of the right nasal septum revealed necrotic tissue with numerous hyaline fungal elements with a wide. ribbon-like appearance, further highlighted by Gomori methenamine-silver staining (Figure 1, panels C–F). Technicians isolated coagulase-negative *Staphylococcus* and *Enterococcus faecium* from bacterial cultures but considered those elements contaminants. We obtained 2 isolates from a fungal culture, identifying 1 microscopically, on lactophenol cotton blue stain, as a *Curvularia* species. Further testing by matrix-assisted laser desorption/ionization time-of-flight mass spectrometry (Vitek MS V3.2; bioMérieux, https://www.biomerieux.com) revealed the isolate to be *Curvularia lunata*. We determined the other isolate to be *Choanephora infundibulifera* by phenotypic characterization (Figure 2) and BLAST searches (https://blast.ncbi.nlm.nih.gov) using sequences

Author affiliations: St. Jude Children's Research Hospital, Memphis, Tennessee, USA (A. Max, H.L. Glasgow, T.C.B. Santiago, A. Holland, H. Inaba, E.E. Adderson); University of Tennessee Health Sciences Center, Memphis (H. Inaba, E.E. Adderson); University of Texas Health Science Center, San Antonio, Texas, USA (C.F. Cañete-Gibas, N.P. Wiederhold)

DOI: http://doi.org/10.3201/eid3006.230794

of the nuclear ribosomal internal transcribed spacer region (GenBank accession no. OR643928) and the D1 and D2 domains of the 28S rRNA gene (GenBank accession no. OR643927). BLAST search results matched with reference strains as follows: internal transcribed spacer region, *C. infundibulifera* CBS 153.51 99.46%, *C. infundibulifera* KUS-F27535 99.49%; D1 and D2 domains of the 28S rRNA gene, *C. infundibulifera* CBS 153.51 100%, *C. infundibulifera* KUS-F27535 100% (*1*–*3*). We determined MICs for amphotericin B (≤0.3 μg/mL), micafungin (>8 μg/mL), voriconazole (>16 μg/mL), posaconazole (1 μg/mL), and isavuconazole (>16 μg/mL) per the Clinical and Laboratory Standards Institute's broth microdilution method (*4*).

We initiated liposomal amphotericin B (5 mg/kg/d) as treatment and continued posaconazole. We directed the patient to receive 4 additional nasal and sinus debridements over 2 weeks, observing fungal elements in biopsies obtained from the first 3 operations. Cultures from all biopsies, however, were sterile. We transitioned the patient to amphotericin B (3×/wk) after 3 weeks and discontinued posaconazole 1 month thereafter. The patient's nasal pain and tenderness progressively improved. Otolaryngology evaluation 4 weeks after the onset of infection was unremarkable. Unfortunately, the patient died of refractory leukemia 4 months after the diagnosis of his fungal infection (14 months after leukemia diagnosis).

Conclusions

The Mucorales group consists of over 260 species in 55 genera that are ubiquitous in wet, organic environments. Approximately 40 species are clinically significant, causing invasive infection (mucormycosis) chiefly in persons with diabetes and immunocompromising conditions (*1*). The genus *Choanephora* (family *Choanephoraceae*) contains 2 species, *C. infundibulifera* and *C. cucurbitarum* (*5*). These species are saprophytes or parasites of plants that can promote spoilage and disease (*6*). *C. cucurbitarum*, the more commonly recognized species, causes wet blight, flower rot blight, and leaf blight, chiefly on summer squash and other cucurbits (*7*).

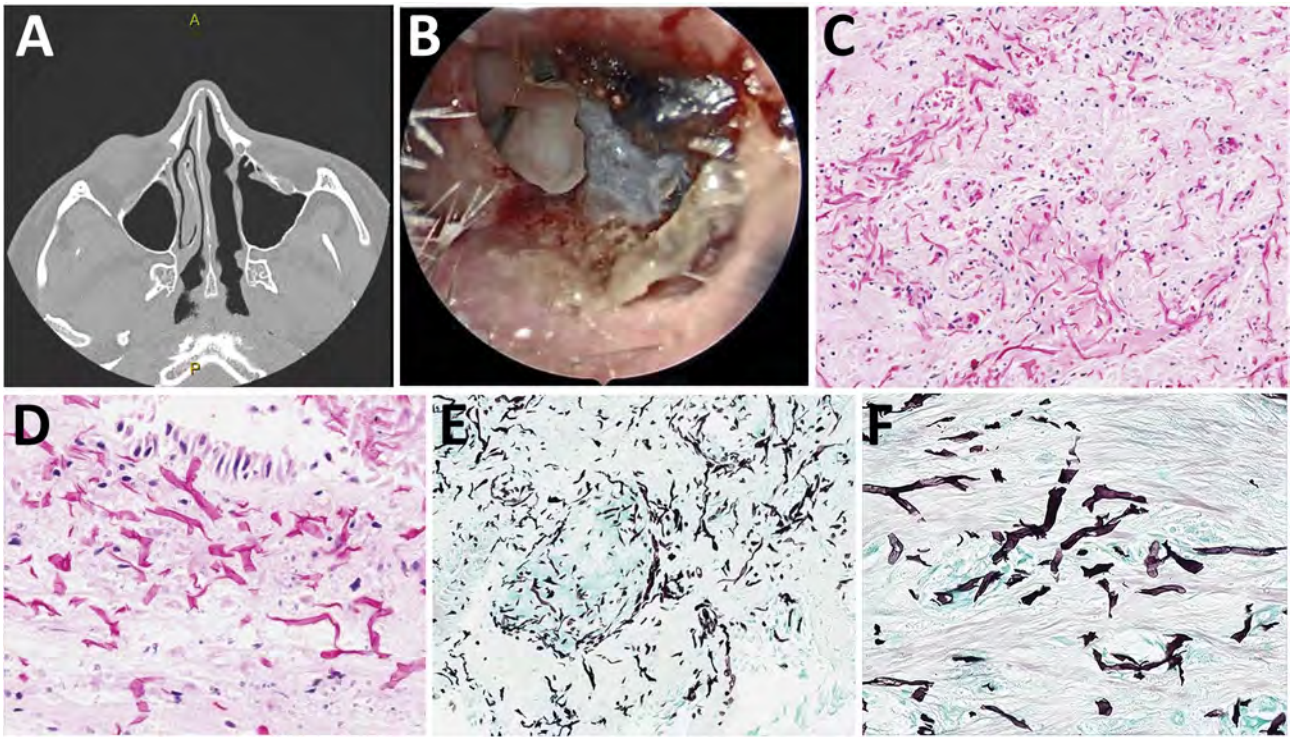

Figure 1. Computed tomography, endoscopic findings, and histomorphology of rhinosinusitis caused by *Choanephora infundibulifera* in a man with leukemia in Memphis, Tennessee, USA. A) Computed tomography shows new asymmetric swelling of the anterior nasal septum and irregularity of the right septum, edema of the inferior turbinates, and obstruction of the right frontal sinus outflow tract. A septal perforation, the sequela of the patient's previous fungal rhinosinusitis, was stable. B) Nasal endoscopy reveals necrosis of the anterior nasal septa. C, D) Necrotic sinonasal mucosa contains numerous hyaline (nonpigmented) fungal elements with broad (ribbon-like), thin-walled, nonseptated, and pleomorphic fungal hyphae. Hematoxylin and eosin stain; original magnification ×200 for panel C, ×400 for panel D. E, F) Gomori methenamine-silver stain highlights the fungal elements (in black). Original magnification ×200 for panel E, ×400 for panel F.

First described by Currey in 1873, *C. infundibulifera* infrequently causes plant disease but has been implicated in twig and leaf rot and blossom blight (*8*–*11*). On potato-carrot or potato dextrose agar, colonies grow rapidly at 25°C with abundant white, pale-yellow, or brown mycelia and sporangiophores, with sporangia arising from substrate mycelium or nonseptate, unbranched, hyaline aerial hyphae (*11*). Definitive identification is based on morphology and sequencing of the nuclear ribosomal internal transcribed spacer region and the D1 and D2 domains of the 28S rRNA gene.

In the patient we describe, *Curvularia* species was among those isolated from the initial nasal biopsy, but histopathologic features observed in multiple biopsies over 2 weeks suggested that this was not the predominant pathogen. The fungal elements we observed in the infected tissue were consistently suggestive of an infection caused by a species in the order of Mucorales rather than a species of *Curvularia*, a dematiaceous mold that is typically pigmented, with septate and often acutely branched hyphae. Furthermore, the patient's clinical course, with progressive tissue necrosis necessitating serial debridement to achieve a cure, was more consistent with the aggressive disease characteristic of a species in the order of Mucorales (*12*).

We could not determine a clear source of the patient's fungal infection. We noted that he had limited exposure to the outdoors in the weeks before his infection and no close contact with plants or soil. We did not obtain hospital and domiciliary environmental samples; however, we did determine that no additional cases of infection caused by *Choanephora* or *Curvularia* species were reported in the hospital proximate to the patient's illness.

The optimal treatment for infections caused by *Choanephora* species is unknown. The minimal inhibitory concentration correlation with treatment response in vivo is unknown, but the in vitro antifungal minimal inhibitory concentrations against this isolate suggest amphotericin B might have greater activity than posaconazole and isavuconazole, which are used to treat mucormycosis caused by other species. Consistent with the antifungal susceptibility results, our patient's infection developed while he was receiving secondary prophylaxis with posaconazole. Treatment with liposomal amphotericin, initially in combination with posaconazole and with adjunctive surgical debridement, led to clinical and microbiological resolution of his infection despite ongoing cancer therapy and neutropenia. This report of human nasal infection caused by a species of *Choanephora* serves as a reminder that emerging fungal pathogens continue to pose clinical challenges, especially in severely immunocompromised patients.

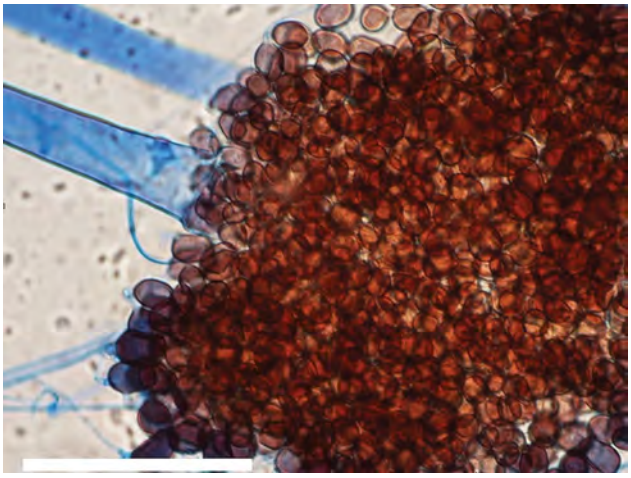

Figure 2. Microscopic morphology of *Choanephora infundibulifera* showing sporangiophore-bearing sporangiola and sporangiospores from a tape mount on banana leaf agar for 7 days at 25°C. Scale bar indicates 100 μm.

This work was reviewed by the St. Jude Children's Research Hospital Institutional Review Board.

Acknowledgments

We thank the staff of the St. Jude Children's Research Hospital Biomedical Library for their research assistance.

This work was supported by a National Cancer Institute Comprehensive Cancer Center Support Grant (P30CA021765) and the American Lebanese Syrian Associated Charities.

About the Author

Ms. Max is an advanced practice provider in the Department of Infectious Diseases, St. Jude Children's Research Hospital, Memphis, Tennessee. Her research interest is infections in immunocompromised hosts.

References

1. Walther G, Wagner L, Kurzai O. Updates on the taxonomy of Mucorales with an emphasis on clinically important taxa. J Fungi (Basel). 2019;5:106. https://doi.org/10.3390/jof5040106
2. Lee SH, Nguyen TTT, Lee HB. Isolation and characterization of two rare Mucoralean species with specific habitats. Mycobiology. 2018;46:205–14. https://doi.org/10.1080/12298093.2018.1509513
3. Yin H, Tian M, Peng Y, Qin N, Lü H, Ren L, et al. First report on *Choanephora cucurbitarum* causing Choanephora rot in Chenopodium plants and its sensitivity to fungicide. J Fungi (Basel). 2023;9:881. https://doi.org/10.3390/jof9090881

4. Clinical and Laboratory Standards Institute. Reference method for broth dilution antifungal susceptibility testing of filamentous fungi, 3rd edition (M38). Malvern (PA): Clinical and Laboratory Standards Institute; 2017 [cited 2023 Feb 27]. https://clsi.org/standards/products/microbiology/documents/m38
5. Kirk PM. A monograph of the Choanephoraceae. Kew (UK): Commonwealth Agricultural Bureaux; 1984.
6. Hoffmann K, Pawłowska J, Walther G, Wrzosek M, de Hoog GS, Benny GL, et al. The family structure of the Mucorales: a synoptic revision based on comprehensive multigene-genealogies. Persoonia. 2013;30:57–76. https://doi.org/10.3767/003158513X666259
7. Schuh M, Grabowski M. Choanephora rot. St. Paul (MN): University of Minnesota Extension; 2022 [cited 2023 Feb 27]. https://extension.umn.edu/disease-management/choanephora-rot
8. Subba Rao KV, Padgett GB, Berner DK, Berggren GT, Snow JP. Choanephora leaf blight of soybeans in Louisiana. Plant Dis. 1990;74:614. https://doi.org/10.1094/PD-74-0614B
9. Alfieri SA Jr, Langdon KR, Wehlburg C, Kimbrough JW. Index of plant diseases in Florida (revised). Bull 11. Tallahassee, FL: Florida Department of Agriculture, Division of Consumer Services; 1984 [cited 2023 Feb 27]. https://original-ufdc.uflib.ufl.edu/UF00002948/00001/1j
10. United States Department of Agriculture. Index of plant diseases in the United States. Washington: The Department of Agriculture, Agricultural Research Service; 1960.
11. Currey F. On a new genus in the order Mucedines. Bot J Linn Soc. 1873;13:333–4. https://doi.org/10.1111/j.1095-8339.1873.tb00100.x
12. Chang YC, Graf E, Green AM. Invasive *Curvularia* infection in pediatric patients with hematologic malignancy identified by fungal sequencing. J Pediatric Infect Dis Soc. 2019;8:87–91. https://doi.org/10.1093/jpids/piy092

Address for correspondence: Elisabeth Adderson, Department of Infectious Diseases, St. Jude Children's Research Hospital, Mailstop 320, 262 Danny Thomas Pl, Memphis, TN 38105, USA; email: elisabeth.adderson@stjude.org

etymologia revisited

Picobirnavirus [pi-ko-burr′nə-vi″rəs]

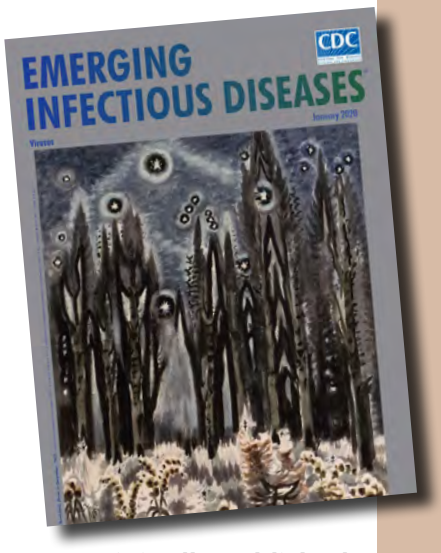

Originally published in January 2020

Picobirnavirus, the recently recognized sole genus in the family *Picobirnaviridae*, is a small (*Pico*, Spanish for small), bisegmented (*bi*, Latin for two), double-stranded RNA virus. Picobirnaviruses were initially considered to be birna-like viruses, and the name was derived from birnavirus (bisegmented RNA), but the virions are much smaller (diameter 35 nm vs. 65 nm).

Picobirnaviruses are reported in gastroenteric and respiratory infections. These infections were first described in humans and black-footed pigmy rice rats in 1988. Thereafter, these infections have been reported in feces and intestinal contents from a wide variety of mammals with or without diarrhea, and in birds and reptiles worldwide.

Sources

1. Delmas B, Attoui H, Ghosh S, Malik YS, Mundt E, Vakharia VN; ICTV Report Consortium. ICTV virus taxonomy profile: Picobirnaviridae. J Gen Virol. 2019;100:133–4. https://doi.org/10.1099/jgv.0.001186
2. Malik YS, Kumar N, Sharma K, Dhama K, Shabbir MZ, Ganesh B, et al. Epidemiology, phylogeny, and evolution of emerging enteric Picobirnaviruses of animal origin and their relationship to human strains. BioMed Res Int. 2014;2014:780752. https://doi org/10.1155/2014/780752
3. Pereira HG, Flewett TH, Candeias JA, Barth OM. A virus with a bisegmented double-stranded RNA genome in rat (*Oryzomys nigripes*) intestines. J Gen Virol. 1988;69:2749–54. https://doi.org/10.1099/0022-1317-69-11-2749
4. Smits SL, van Leeuwen M, Schapendonk CM, Schürch AC, Bodewes R, Haagmans BL, et al. Picobirnaviruses in the human respiratory tract. Emerg Infect Dis. 2012;18:1539–40. https://doi.org/10.3201/eid1809.120507

https://wwwnc.cdc.gov/eid/article/26/1/et-2601_article

Burkholderia semiarida as Cause of Recurrent Pulmonary Infection in Immunocompetent Patient, China

Dai Kuang,[1] Feng Liu,[1] Shen Tian,[1] Wei Liu, Anyang Li, Yujing Zhou, Huaping Huang, Qianfeng Xia

Burkholderia semiarida was previously identified solely as a plant pathogen within the *Burkholderia cepacia* complex. We present a case in China involving recurrent pneumonia attributed to *B. semiarida* infection. Of note, the infection manifested in an immunocompetent patient with no associated primary diseases and endured for >3 years.

Burkholderia semiarida has only been reported as a plant pathogen causing onion sour skin (*1*). The *Burkholderia* genus encompasses >120 bacterial species that are typically reported to inhabit soil and water environments (*2*). The *Burkholderia* species that are most frequently reported to cause infection in humans are *B. cenocepacia*, *B. mallei*, and *B. pseudomallei*. However, severe infections have been also caused by other species (*3*,*4*). We report a rare case of *B. semiarida* human infection: recurrent pneumonia in an immunocompetent patient. Ethics approval for this study, including the waiver of informed consent of the clinical strains and samples, was approved by the Ethics Committee of the First Affiliated Hospital of Hainan Medical University under approval no. 2023-KYL-219.

The Study

A 56-year-old woman was admitted to The First Affiliated Hospital of Hainan Medical University (Haikou, China) on February 23, 2022. She reported a 3-year history of recurrent cough, copious sputum production, and chest pain, which had worsened over the previous 5 days.

On August 18, 2020, the woman had been admitted to Hainan Traditional Chinese Medicine Hospital for a cough without obvious cause that was accompanied by white sticky sputum and right-sided chest pain that was aggravated by coughing. She did not have fever or hemoptysis. A computed tomography (CT) scan of the chest showed infiltrative lesions in the right lung (Figure, panel A). Initial laboratory workup revealed leukocyte count of 11.1×10^9/L with 8.11×10^9/L neutrophils. Symptoms resolved substantially after 10 days of treatment with ceftriaxone/tazobactam and levofloxacin.

The patient was readmitted to the hospital on November 3, 2020, with a recurrence of the symptoms previously described. Chest CT scans showed infiltrative lesions in both lungs and new lesions in the left upper and lower lobes. Results of routine blood tests were within normal limits, albeit with a slightly elevated hypersensitive C-reactive protein (6.64 mg/L) and erythrocyte sedimentation rate (29 mm/h). Metagenomic next-generation sequencing (mNGS) analysis of bronchoalveolar lavage fluid (BALF) suggested that the infection could have resulted from *B. cepacia*. The patient received a 10-day intravenous meropenem treatment, followed by 8 weeks of trimethoprim/sulfamethoxazole. A subsequent chest CT showed mild bronchiectasis in the right middle lobe and lower lingula segment of the left upper lobe, in addition to multiple lesions. *B. cenocepacia* infection was suspected, according to mNGS retesting on January 27, 2021. Thus, the ongoing trimethoprim/sulfamethoxazole treatment was extended to 24 weeks. CT chest scans on June 7, 2021, showed multiple lesions in both lungs that were substantially resorbed, whereas new lesions emerged in right middle lobes (Figure, panel B). Treatment was then changed to minocycline for another 4 weeks. The patient returned to the hospital on July 20, 2021, because of recurrent right-sided

Author affiliations: NHC Key Laboratory of Tropical Disease Control, School of Tropical Medicine, Hainan Medical University, Haikou, China (D. Kuang, S. Tian, W. Liu, A. Li, Y. Zhou, Q. Xia); The First Affiliated Hospital of Hainan Medical University, Haikou (F. Liu, H. Huang)

DOI: https://doi.org/10.3201/eid3006.231676

[1]These authors contributed equally to this article and share first authorship.

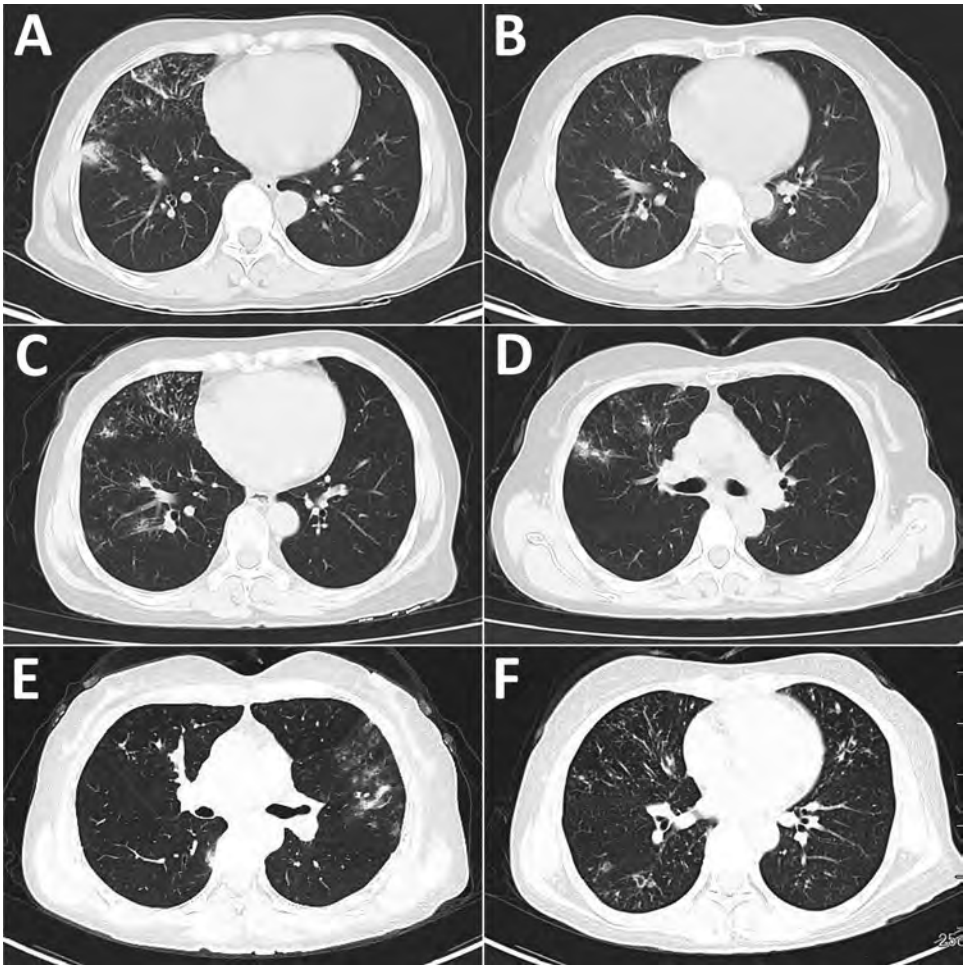

Figure. Computed tomography scans of the chest at different stages of disease in immunocompetent patient with recurrent pulmonary infection caused by *Burkholderia semiarida*, China. A) Infiltrative lesions in the right lung in August 2020; B) multiple infiltrative lesions in both lungs substantially resorbed in June 2021; C) multiple infiltrative lesions of both lungs, predominantly in the right lung, in February 2022; D) bronchiectasis with scattered multiple lesions in both lungs and increased exudative lesions in the right upper lung in May 2022; E) lesions in the right lung more resorbed than before and multiple emerging lesions in the left lung in August 2022; F) lesions in the left lung more absorbed than before, with multiple emerging foci in the right lung in March 2023.

chest pain. Chest CT showed more serious lesions in both lungs, and BALF culture suggested *B. cenocepacia* infection. The isolates were sensitive to ceftazidime, meropenem, trimethoprim/sulfamethoxazole, minocycline, and levofloxacin. Treatment was then adjusted to intravenous meropenem and 20 weeks of amoxicillin/clavulanate potassium.

On February 20, 2022, the previous symptoms recurred, accompanied by hemoptysis. Chest CT scan revealed multiple infiltrative lesions, predominantly in the right lung (Figure, panel C). The patient's personal and family medical history were unremarkable. Physical examination showed normal temperature, coarse breath sounds, moist rales, and no enlargement of superficial lymph nodes, lower extremity swelling, or heart and abdominal abnormalities. Results of tests of complete blood count, C-reactive protein, procalcitonin, and liver and kidney function were within reference ranges. Tests for tumor markers and extractable nuclear antigen were negative. Peripheral blood T lymphocyte subsets, natural killer cells, B lymphocytes, serum immunoglobulins, and complement levels were all within reference ranges. Gram staining demonstrated the agents as gram-negative rods or cocci. Tests for mycobacteria and fungi were negative.

After a week of intravenous imipenem/cilastatin treatment, the patient was discharged with improved symptoms. Outpatient therapy included oral nemonoxacin and amoxicillin/clavulanate, along with acetylcysteine and subcutaneous thymopentin. A follow-up chest CT in May 2022 revealed mild bronchiectasis and multiple lesions in both lungs, including increased exudative lesions in the right upper lung (Figure, panel D). Subsequently, the therapy was adjusted to moxifloxacin and doxycycline. Chest CT scan in August indicated better absorption of right lung lesions but new infections in the left lung (Figure, panel E). The therapy was then adjusted to oral ciprofloxacin with doxycycline. The mNGS conducted in October indicated the possibility of *B. anthina* infection. Chest CT scan in March 2023 showed improved left lung lesions but new infection foci in the right lung (Figure, panel F). At the time of this

article, the patient was still receiving conservative outpatient treatment.

BALF samples were sent to Hainan Medical University for bacterial isolation and characterization. The suspected bacteria showed typical morphologic characteristics of *B. cepacia* complex species (Appendix Figure 1, https://wwwnc.cdc.gov/EID/article/30/6/23-1676-App1.pdf). Susceptibility tests showed sensitivity to ceftazidime, meropenem, and trimethoprim/sulfamethoxazole, intermediate resistance to minocycline, and resistance to levofloxacin. Whole-genome sequencing indicated 3 circular chromosomes and 1 plasmid with guanine-cytosine content of 66.89% (National Center for Biotechnology Information Bioproject accession no. PRJNA1028481). The values of digital DNA-DNA hybridization (*5*) and average nucleotide identity (*6*) were used to compare the representative genomes of *Burkholderia* genus in the National Center for Biotechnology Information Reference Sequence database. Pairwise comparison showed that digital DNA-DNA hybridization and average nucleotide identity values between our strain with representative genome of *B. semiarida* CCRMBC171 (accession no. GCF_029268915.1) were 88.8% and 98.6%, which are above the threshold of 70% and 95%–96% used for bacterial species delineation (*6*,*7*) (Appendix Figure 2). Thus, although misidentification can occur using mNGS to distinguish *B. semiarida* from other *Burkholderia* species, we can conclude that the recurrent pulmonary infection was caused by *B. semiarida*.

Conclusions

We present a rare case of pulmonary infection caused by *B. semiarida* in a 56-year-old immunocompetent woman. The early clinical manifestations were cough, sputum production, and chest pain. Hemoptysis and moist crackles in the lungs emerged late in the course of disease. The inflammatory markers and immune indicators suggest the patient had normal immune function. Chest CT scans indicated inflammation alternated in both lungs for >3 years. Mild local bronchiectasis occurred repeatedly at multiple sites on both sides. Persistent infections usually result in high levels of illness and death (*8*). Thus, a long period of follow-up after hospitalization should be used to assess the outcome of therapy in infections caused by *B. semiarida*.

The choice of antimicrobial therapy is usually made on the basis of in vitro susceptibility. In our case, the infection failed to respond to prolonged antibiotic therapy using common medications despite apparent drug susceptibility. Of note, the strain exhibited a decreasing susceptibility to minocycline and levofloxacin as the disease endured and progressed. This observation suggests that the frequency of antibiotic use might drive rapid evolutionary adaptation of resistance as previously described (*9*,*10*). This case report highlights that patients who have persistent respiratory symptoms who do not respond to initial treatment might be candidates for closer assessment for *Burkholderia* infection.

In summary, we present the clinical features of a patient with *B. semiarida* infection. Key aspects of this case were the occurrence of infection in an immunocompetent patient with no related primary diseases, that inflammation alternated in both lungs and persisted for >3 years, and that the infection did not appear to respond to in vitro active antimicrobial medications. Our case report alerts *B. semiarida* as a stubborn pathogen in persistent pulmonary infection and highlights the importance of extended follow-up care to assess the outcome of antimicrobial therapy in *Burkholderia* infections.

Acknowledgments

We thank Okugbe Ebiotubo Ohore for English language editing and the patient for her participation in this study. We also thank the technological support of mNGS from Vision Medicals Co., Ltd (Guangzhou, China).

Because testing was conducted at different institutions and considerations related to data privacy, we only have access to the raw data from the third round of mNGS testing. The obtained sequencing data of mNGS were submitted to the National Center for Biotechnology Information Bioproject database under accession no. PRJNA1075918.

This study was funded under the National Natural Science Foundation of China (82000011 and 82370018) and supported by Hainan Province Clinical Medical Center.

About the Author

Dr. Kuang is an associate researcher in the National Health Commission Key Laboratory of Tropical Disease Control, School of Tropical Medicine, Hainan Medical University. His primary research interests are emerging and reemerging infectious diseases and the mechanisms of antibiotic resistance and pathogenicity of bacteria.

References

1. Velez LS, Aburjaile FF, Farias ARG, Baia ADB, Oliveira WJ, Silva AMF, et al. *Burkholderia semiarida* sp. nov. and *Burkholderia sola* sp. nov., two novel *B. cepacia* complex species causing onion sour skin. Syst Appl Microbiol. 2023; 46:126415. https://doi.org/10.1016/j.syapm.2023.126415

2. Parte AC. LPSN—list of prokaryotic names with standing in nomenclature (bacterio.net), 20 years on. Int J Syst Evol Microbiol. 2018;68:1825–9. https://doi.org/10.1099/ijsem.0.002786
3. Meumann EM, Limmathurotsakul D, Dunachie SJ, Wiersinga WJ, Currie BJ. *Burkholderia pseudomallei* and melioidosis. Nat Rev Microbiol. 2024;22:155–69. https://doi.org/10.1038/s41579-023-00972-5
4. Sfeir MM. *Burkholderia cepacia* complex infections: more complex than the bacterium name suggest. J Infect. 2018;77:166–70. https://doi.org/10.1016/j.jinf.2018.07.006
5. Lee I, Ouk Kim Y, Park SC, Chun J. OrthoANI: an improved algorithm and software for calculating average nucleotide identity. Int J Syst Evol Microbiol. 2016;66:1100–3. https://doi.org/10.1099/ijsem.0.000760
6. Meier-Kolthoff JP, Göker M. TYGS is an automated high-throughput platform for state-of-the-art genome-based taxonomy. Nat Commun. 2019;10:2182. https://doi.org/10.1038/s41467-019-10210-3
7. Goris J, Konstantinidis KT, Klappenbach JA, Coenye T, Vandamme P, Tiedje JM. DNA-DNA hybridization values and their relationship to whole-genome sequence similarities. Int J Syst Evol Microbiol. 2007;57:81–91. https://doi.org/10.1099/ijs.0.64483-0
8. Fisher RA, Gollan B, Helaine S. Persistent bacterial infections and persister cells. Nat Rev Microbiol. 2017;15:453–64. https://doi.org/10.1038/nrmicro.2017.42
9. Levin-Reisman I, Ronin I, Gefen O, Braniss I, Shoresh N, Balaban NQ. Antibiotic tolerance facilitates the evolution of resistance. Science. 2017;355:826–30. https://doi.org/10.1126/science.aaj2191
10. Van den Bergh B, Michiels JE, Wenseleers T, Windels EM, Boer PV, Kestemont D, et al. Frequency of antibiotic application drives rapid evolutionary adaptation of *Escherichia coli* persistence. Nat Microbiol. 2016;1:16020. https://doi.org/10.1038/nmicrobiol.2016.20

Address for correspondence: Huaping Huang, The First Affiliated Hospital of Hainan Medical University, 31 Longhua Rd, Haikou, Hainan 570102, China; email: huapinghuang153@163.com; Qianfeng Xia, NHC Key Laboratory of Tropical Disease Control, School of Tropical Medicine, Hainan Medical University, 3 Xueyuan Rd, Haikou, Hainan 570102, China; email: xiaqianfeng@hainmc.edu.cn

SARS-CoV-2 in Captive Nonhuman Primates, Spain, 2020–2023

David Cano-Terriza, Adrián Beato-Benítez, Leira Fernández-Bastit, Joaquim Segalés, Júlia Vergara-Alert, Eva Martínez-Nevado, Andrea Carretero, Dietmar Crailsheim, Pilar Soriano, Javier Planas, Mario Torro, Ignacio García-Bocanegra

We conducted a serologic and molecular study to assess exposure of captive nonhuman primates (NHPs) to SARS-CoV-2 in Spain during the 2020–2023 COVID-19 pandemic. We found limited exposure of NHPs to SARS-CoV-2. Biosafety measures must be strictly maintained to avoid SARS-CoV-2 reverse-zoonotic transmission in the human–NHP interface.

COVID-19 caused by SARS-CoV-2 is an emerging respiratory disease that likely originated from wildlife in late 2019 (*1*). Although the main driver of SARS-CoV-2 spread is human-to-human transmission, several wild and domestic mammals are susceptible to SARS-CoV-2 infection; natural infections have been reported in 29 nonhuman animal species (*2*).

Nonhuman primates (NHPs) are among the most susceptible taxonomic groups to SARS-CoV-2 infection (*3*) and are suitable animal models to evaluate SARS-CoV-2 pathogenesis (*4*). Natural infections with clinical outcomes have been reported in both captive and free-living NHPs worldwide (*2*,*5*–*8*). Because active surveillance of SARS-CoV-2 has not been conducted in NHPs, we assessed SARS-CoV-2 circulation among NHPs housed in zoos and rescue centers in Spain, where NHPs can be found in proximity to humans.

Author affiliations: Universidad de Córdoba, Córdoba, Spain (D. Cano-Terriza, A. Beato-Benítez, I. García-Bocanegra); CIBERINFEC ISCIII, Madrid, Spain (D. Cano-Terriza, I. García-Bocanegra); Universitat Autònoma de Barcelona, Barcelona, Spain (L. Fernández-Bastit, J. Segalés, J. Vergara-Alert); Zoo Aquarium de Madrid, Madrid (E. Martínez-Nevado); Centro de Rescate de Primates RAINFER/Fundación Chimpatía, Madrid (A. Carretero); Fundació Mona, Girona, Spain (D. Crailsheim); Río Safari Elche, Alicante, Spain (P. Soriano); Oasis Wildlife Fuerteventura, La Lajita, Canary Islands, Spain (J. Planas); Terra Natura Benidorm, Benidorm, Spain (M. Torro)

DOI: https://doi.org/10.3201/eid3006.231247

The Study

During January 2020–March 2023, we collected serum samples from 127 different NHPs belonging to 30 species housed in 17 zoos and NHP rescue centers in Spain. The number of sampled animals represented ≈40% of the total census of those species in the selected zoos and rescue centers. We collected 16 serum samples in 2020, 76 in 2021, 28 in 2022, and 7 in 2023 (Table; Figure 1). In addition, we collected 186 fresh fecal samples during February–May 2022 within the same zoos and NHPs rescue centers, which comprised 39 samples collected from animals housed in individual facilities and 147 pooled samples from the floors of facilities with >1 animal (1 pool per facility and species) belonging to 64 different NHP species (Appendix Table, https://wwwnc.cdc.gov/EID/article/30/6/23-1247-App1.pdf). The study did not require additional blood extractions because we obtained all serum samples from serum banks or from NHPs that had medical check-ups or surgical interventions during the study period.

We tested all serum samples for antibodies against SARS-CoV-2 nucleocapsid (N) and spike (S) proteins by using 2 commercial multispecies ELISAs (ID Screen SARS-CoV-2 Double Antigen and NeutraLISA SARS-CoV-2; Euroimmun, https://www.euroimmun.com) according to the manufacturer's instructions. We analyzed ELISA-positive serum samples further by using a virus neutralization test (VNT) as previously described (*9*). In brief, we preincubated 100 SARS-CoV-2 (B.1 lineage) 50% tissue culture infectious doses with 2-fold serial dilutions (1:20 to 1:10,240) of heat-inactivated serum samples in Nunc 96-well cell culture plates (Thermo Fisher Scientific, https://www.thermofisher.com) for 30 minutes at 37°C. Then, we added the virus-serum mixtures onto Vero cells (ATCC, https://www.atcc.org) and read results after 72 hours by using the Cell Titer Glo kit (Promega, https://www.promega.com).

Table. Distribution of serum samples in study of SARS-CoV-2 in captive nonhuman primates in Spain, 2020–2023*

NHP family and species	No. positive/total†	Zoos and rescue centers‡																
		A	B	C	D	E	F	G	H	I	J	K	L	M	N	O	P	Q
Callitrichidae																		
Callithrix geoffroyi	0/1	0	0	0	0	0	0	0	0	0	0	0	0	0	0	0	0	1
Callithrix jacchus	0/3	0	0	0	0	0	0	0	0	0	0	0	0	0	0	0	0	3
Leonthopithecus rosalia	0/1	0	0	0	0	0	0	0	0	0	1	0	0	0	0	0	0	0
Mico argentatus	0/2	0	0	0	0	0	0	0	0	0	0	0	0	0	0	0	0	2
Saguinus oedipus	0/2	0	0	0	0	1	0	0	0	0	0	0	0	0	0	0	0	1
Subtotal	0/9	0	0	0	0	1	0	0	0	0	1	0	0	0	0	0	0	7
Cebidae																		
Sapajus apella	0/1	0	0	0	0	0	0	0	0	0	1	0	0	0	0	0	0	0
Subtotal	0/1	0	0	0	0	0	0	0	0	0	1	0	0	0	0	0	0	0
Cercopithecidae																		
Cercocebus atys lunulatus	0/6	0	0	0	0	0	0	0	0	0	0	0	0	0	0	4	2	0
Cercopithecus mitis	0/1	0	0	0	0	1	0	0	0	0	0	0	0	0	0	0	0	0
Cercopithecus neglectus	0/3	0	0	0	0	0	0	0	0	0	0	0	2	0	0	1	0	0
Colobus guereza	0/1	0	0	0	0	0	0	0	0	0	0	0	0	0	1	0	0	0
Lophocebus aterrimus	0/1	0	0	0	0	0	0	0	0	0	0	1	0	0	0	0	0	0
Macaca sylvanus	0/11	0	0	0	0	3	0	0	0	0	0	0	0	0	5	3	0	0
Macaca tonkeana	0/1	0	0	0	0	1	0	0	0	0	0	0	0	0	0	0	0	0
Mandrillus leucophaeus	0/1	0	0	0	0	0	0	0	1	0	0	0	0	0	0	0	0	0
Mandrillus sphinx	0/1	0	0	0	1	0	0	0	0	0	0	0	0	0	0	0	0	0
Miopithecus ogouensis	0/2	0	0	0	0	0	0	0	0	0	0	0	0	2	0	0	0	0
Papio cynocephalus	0/1	0	0	0	1	0	0	0	0	0	0	0	0	0	0	0	0	0
Subtotal	0/29	0	0	0	2	5	0	0	1	0	0	1	2	2	6	8	2	0
Hominidae																		
Gorilla gorilla gorilla	2/3	0	0	1	**2**	0	0	0	0	0	0	0	0	0	0	0	0	0
Pan troglodytes	0/4	0	0	0	0	0	0	0	0	0	0	4	0	0	0	0	0	0
Pan troglodytes ellioti	0/1	0	0	0	0	0	0	1	0	0	0	0	0	0	0	0	0	0
Pan troglodytes troglodytes	0/3	0	0	0	1	0	0	2	0	0	0	0	0	0	0	0	0	0
Pan troglodytes verus	0/1	0	0	0	0	0	0	1	0	0	0	0	0	0	0	0	0	0
Pan troglodytes verus/troglodytes	0/4	0	0	0	0	0	0	4	0	0	0	0	0	0	0	0	0	0
Pongo pygmaeus	0/6	0	0	0	1	1	0	0	0	0	0	2	0	2	0	0	0	0
Subtotal	2/22	0	0	1	4	1	0	8	0	0	0	6	0	2	0	0	0	0
Hylobatidae																		
Hylobates lar	0/3	0	0	0	1	0	0	0	0	0	1	0	0	0	1	0	0	0
Hylobates syndactylus	0/1	0	0	0	0	0	0	0	0	0	1	0	0	0	0	0	0	0
Subtotal	0/4	0	0	0	1	0	0	0	0	0	2	0	0	0	1	0	0	0
Lemuridae																		
Eulemur macaco	0/3	0	0	0	0	0	0	0	0	0	0	0	0	3	0	0	0	0
Lemur catta	0/38	0	0	0	0	6	2	0	0	17	0	4	0	5	0	0	4	0
Varecia rubra	0/1	0	0	0	0	0	0	0	0	0	0	0	0	1	0	0	0	0
Varecia variegata	0/20	0	0	0	0	0	0	0	0	17	0	0	0	2	0	0	0	1
Subtotal	0/62	0	0	0	0	6	2	0	0	34	0	4	0	11	0	0	4	1
Grand total	2/127	0	0	1	7	13	2	8	1	34	4	11	2	15	7	8	6	8

*Sampling was conducted during January 2020–March 2023. Numbers indicate the number of NHP species tested for SARS-Co-V-2 at each zoo or rescue center. Bold number indicates the 2 SARS-CoV-2–seropositive gorillas identified at zoo D. NHP, nonhuman primate.
†Number of SARS-CoV-2–seropositive animals per the total number of animals tested at each zoo or rescue center.
‡Serum samples were obtained from zoos or rescue centers represented by letters A–Q. Locations of the zoos and rescue centers are shown in Figure 1.

We normalized values and calculated VNT_{50} (the reciprocal dilution inhibiting 50% of Vero cell infection) by plotting and fitting the log of serum dilution versus normalized response in Prism 8.4.3 (Graphpad, https://www.graphpad.com). We performed VNTs in duplicate for each sample.

We tested fecal samples for SARS-CoV-2 RNA by using quantitative reverse transcription PCR. We extracted RNA from feces by using the IndiSpin QIAcube HT Pathogen Kit (Indical Biosciences, https://www.indical.com) according to the manufacturer's instructions. We detected SARS-CoV-2 RNA by using a previously published method (*10*) that had minor modifications adapting it to the Applied Biosystems AgPath-ID One-Step RT-PCR Kit (Thermo Fisher Scientific). We performed PCR amplification by using an Applied Biosystems 7500 Fast Real-Time PCR System (Thermo Fisher Scientific) and considered samples with a cycle threshold value of <40 to be positive for SARS-CoV-2 RNA.

We confirmed SARS-CoV-2 antibodies in 2/127 (1.6% [95% CI 0.0%–3.7%]) tested animals by both

ELISA and VNT. The seropositive animals were 2 western lowland gorillas (*Gorilla gorilla gorilla*) designated as G1 and G2. VNT_{50} titers were 1:131.4 for G1 and 1:191.9 for G2 serum samples (Figure 2).

G1 and G2 were adult female gorillas sampled at zoo D within the same enclosure (Table; Figure 1). G1 arrived at zoo D from a UK zoo on March 4, 2020, after a favorable medical evaluation. During April 7–10, zookeepers reported that G1 was exhibiting a dry cough. A serum sample was collected from G1 on April 24, 2020, during a clinical intervention after an aggression was suffered by another gorilla from the same group. Previous studies of NHPs experimentally infected with SARS-CoV-2 reported clinical signs within the first week after infection (*4*,*11*). Therefore, the exposure of G1 to SARS-CoV-2 most likely occurred during the first wave of the COVID-19 pandemic in Spain (February–June 2020), when the zoo was closed to the public because of lockdown efforts to curb coronavirus cases. G2 was sampled on November 4, 2022, and did not show previous clinical signs compatible with SARS-CoV-2 infection. The 4 group members that shared the same facilities with the 2 seropositive gorillas could not be sampled, but they did not show any indications of disease at that time.

Previous cases of natural SARS-CoV-2 infections have been described in gorillas; the animals experienced asymptomatic or mild illness, involving coughing, congestion, nasal discharge, loss of appetite, and tiredness that did not require medical interventions and resolved within a few days (*5*,*6*,*8*,*12*). In those previous cases, intraspecific transmission among animals from the same facilities was suggested.

Despite the rigorous biosafety protocols used when working with NHPs (e.g., using disinfection mats, masks, gloves, and hand disinfectants and changing overalls), the zoo staff was the most plausible source of transmission to the gorilla troop, which has been suggested for previous outbreaks

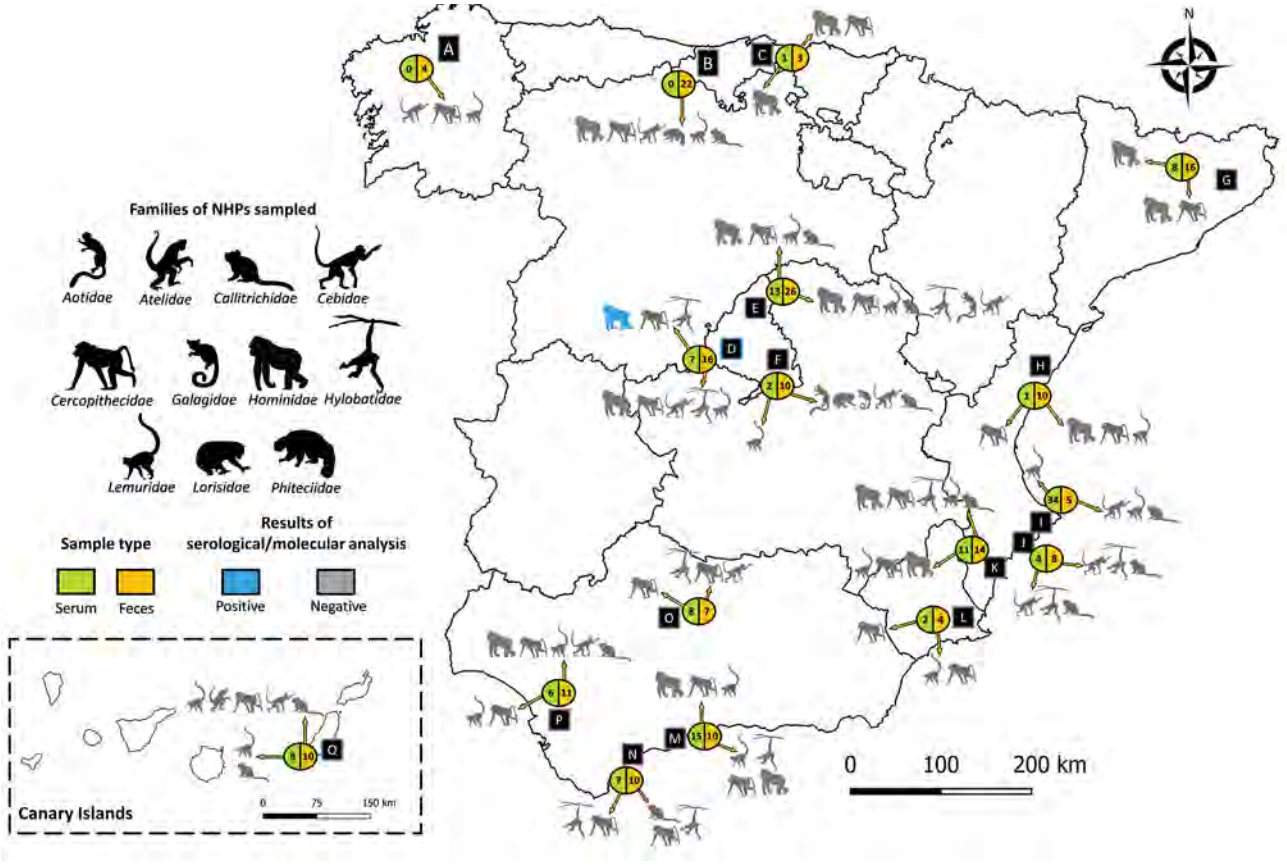

Figure 1. Geographic distribution of captive NHPs sampled in study of SARS-CoV-2 in Spain, 2020–2023. Serum and fecal samples were collected from different NHP species at 17 zoos and NHPs rescue centers (letters A–Q) in Spain during January 2020–March 2023. Inset indicates the specimens collected in the Canary Islands, Spain. Animal images indicate the families of NHPs examined. Blue image indicates the 2 gorillas that were SARS-CoV-2 seropositive. Circles show the total numbers of serum or fecal samples analyzed at each zoo or rescue center. Arrows indicate which NHP families underwent serum or fecal sample testing for SARS-CoV-2. NHP, nonhuman primate.

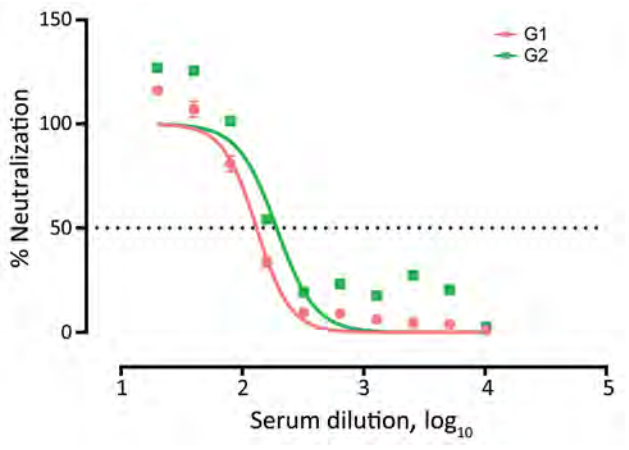

Figure 2. Virus neutralization tests conducted for 2 SARS-CoV-2–seropositive gorillas in study of captive nonhuman primates, Spain, 2020–2023. Serum samples from 2 gorillas tested positive for SARS-CoV-2 antibodies by ELISA. Virus neutralization tests were performed; 50% neutralizing antibody titers were 1:131.4 for G1 and 1:191.9 for G2 serum samples. G1, gorilla 1; G2, gorilla 2.

reported in zoos (*6*,*8*). Nevertheless, exposure of G1 to SARS-CoV-2 at the zoo of origin or during transport, as well as intraspecific transmission, cannot be ruled out.

Fecal shedding of SARS-CoV-2 peaks during the symptomatic period and can persist 1–35 days after onset of clinical signs in humans (*13*,*14*). Similarly, a study of rhesus macaques (*Macaca mulatta*) experimentally infected with SARS-CoV-2 reported that rectal swab samples tested positive for RNA up to 27 days after infection (*15*). In our study, SARS-CoV-2 RNA was not detected in any of the 186 fecal samples tested (Appendix Table), including those obtained at the facility housing G1 and G2. Considering the time of fecal sampling and the virus excretion period in primate species (≈1 month), our findings indicate an absence of virus circulation during this temporal window. Discrepancies between serologic and molecular results in the 2 seropositive gorillas could be explained by differences in antibody persistence, which ranged from 3 to >9 months in experimentally immunized NHPs (Appendix references *16*,*17*), and by differences in virus RNA excretion in feces, as well as sampling times (April 2020 and November 2022 for serum samples and February 2022 for fecal samples).

The first limitation of this study is that the spatial distribution of sampling was not homogeneous. Approximately 60% of the tested serum samples were from 4 of the sampled centers. Second, serum samples could not be longitudinally analyzed. Because antibodies decay over time (Appendix references *16*,*17*), SARS-CoV-2 exposure before the sampling period cannot be ruled out. Further longitudinal studies would be of great interest to better understand the temporal dynamics of SARS-CoV-2 in NHPs.

Conclusions

Our findings indicate a limited SARS-CoV-2 exposure in captive NHPs populations in zoos and NHPs rescue centers in Spain during the 2020–2023 COVID-19 pandemic period. G1 only exhibited mild symptoms, and G2 exhibited no symptoms, highlighting the importance of conducting active screening and surveillance testing to reduce the potential emergence of unidentified reservoirs and virus evolution. Considering the potential health risk and threat to the conservation of NHP species, the possibility of the emergence of new reservoirs, and the opportunities for virus evolution, vaccination of captive animals and the proper use of biosafety measures and personal protective equipment are critical to prevent future reverse-zoonotic transmission of SARS-CoV-2.

Acknowledgments

We thank Bioparc Fuengirola, Bioparc Valencia, Centro de Conservación Zoo Córdoba, Faunia, Marcelle Naturaleza, MundoMar Benidorm, Parque de la Naturaleza de Cabárceno, Selwo Aventura, Terra Natura Murcia, Zoo de Santillana del Mar, and Centro de Conservación de la Biodiversidad Zoobotánico Jerez-Alberto Durán for providing the valuable samples.

This research was partially supported by the Innovation and Transfer Plan of the University of Cordoba and CIBER, Consorcio Centro de Investigación Biomédica en Red (CB2021/13/00083), Instituto de Salud Carlos III, Ministerio de Ciencia e Innovación and Unión Europea–NextGenerationEU. A.B.-B. is a PhD. candidate supported by the Andalusian System of Knowledge.

About the Author

Dr. Cano-Terriza is an assistant professor in the Department of Veterinary Medicine at the University of Cordoba. His research interests focus on the epidemiology of emerging and reemerging zoonotic diseases.

References

1. Zhou P, Yang XL, Wang XG, Hu B, Zhang L, Zhang W, et al. A pneumonia outbreak associated with a new coronavirus of probable bat origin. Nature. 2020;579:270–3. https://doi.org/10.1038/s41586-020-2012-7
2. World Organisation for Animal Health. SARS-CoV-2 in animals—situation report 22. 2023 [cited 2023 July 1] https://www.woah.org/app/uploads/2023/07/sars-cov-2-situation-report-22.pdf

3. Melin AD, Janiak MC, Marrone F 3rd, Arora PS, Higham JP. Comparative ACE2 variation and primate COVID-19 risk. Commun Biol. 2020;3:641. https://doi.org/10.1038/s42003-020-01370-w
4. Meekins DA, Gaudreault NN, Richt JA. Natural and experimental SARS-CoV-2 infection in domestic and wild animals. Viruses. 2021;13:1993. https://doi.org/10.3390/v13101993
5. Gibbons A. Captive gorillas test positive for coronavirus. Scienceinsider. January 12, 2021 [cited 2023 May 23]. https://www.science.org/content/article/captive-gorillas-test-positive-coronavirus
6. Nagy A, Stará M, Vodička R, Černíková L, Jiřincová H, Křivda V, et al. Reverse-zoonotic transmission of SARS-CoV-2 lineage alpha (B.1.1.7) to great apes and exotic felids in a zoo in the Czech Republic. Arch Virol. 2022;167:1681–5. https://doi.org/10.1007/s00705-022-05469-9
7. Pereira AH, Vasconcelos AL, Silva VL, Nogueira BS, Silva AC, Pacheco RC, et al. Natural SARS-CoV-2 infection in a free-ranging black-tailed marmoset (*Mico melanurus*) from an urban area in mid-west Brazil. J Comp Pathol. 2022;194:22–7. https://doi.org/10.1016/j.jcpa.2022.03.005
8. Dusseldorp F, Bruins-van-Sonsbeek LGR, Buskermolen M, Niphuis H, Dirven M, Whelan J, et al. SARS-CoV-2 in lions, gorillas and zookeepers in the Rotterdam Zoo, the Netherlands, a One Health investigation, November 2021. Euro Surveill. 2023;28:2200741. https://doi.org/10.2807/1560-7917.ES.2023.28.28.2200741
9. Fernández-Bastit L, Rodon J, Pradenas E, Marfil S, Trinité B, Parera M, et al. First detection of SARS-CoV-2 Delta (B.1.617.2) variant of concern in a dog with clinical signs in Spain. Viruses. 2021;13:2526. https://doi.org/10.3390/v13122526
10. Corman VM, Landt O, Kaiser M, Molenkamp R, Meijer A, Chu DK, et al. Detection of 2019 novel coronavirus (2019-nCoV) by real-time RT-PCR. Euro Surveill. 2020;25:2000045. https://doi.org/10.2807/1560-7917.ES.2020.25.3.2000045
11. Yuan L, Tang Q, Zhu H, Guan Y, Cheng T, Xia N. SARS-CoV-2 infection and disease outcomes in non-human primate models: advances and implications. Emerg Microbes Infect. 2021;10:1881–9. https://doi.org/10.1080/22221751.2021.1976598
12. Zoo Atlanta. Update on gorilla population—Sept 17. September 17, 2021 [cited 2023 Jun 23]. https://zooatlanta.org/update-on-gorilla-population-sept-17
13. Jones DL, Baluja MQ, Graham DW, Corbishley A, McDonald JE, Malham SK, et al. Shedding of SARS-CoV-2 in feces and urine and its potential role in person-to-person transmission and the environment-based spread of COVID-19. Sci Total Environ. 2020;749:141364. https://doi.org/10.1016/j.scitotenv.2020.141364
14. Ma X, Su L, Zhang Y, Zhang X, Gai Z, Zhang Z. Do children need a longer time to shed SARS-CoV-2 in stool than adults? J Microbiol Immunol Infect. 2020;53:373–6. https://doi.org/10.1016/j.jmii.2020.03.010
15. Zheng H, Li H, Guo L, Liang Y, Li J, Wang X, et al. Virulence and pathogenesis of SARS-CoV-2 infection in rhesus macaques: a nonhuman primate model of COVID-19 progression. PLoS Pathog. 2020;16:e1008949. https://doi.org/10.1371/journal.ppat.1008949

Address for correspondence: David Cano-Terriza, Departamento de Sanidad Animal, Campus universitario de Rabanales, Carretera Madrid Km 396, Universidad de Córdoba, Cordoba 14014, Spain; email: v82cated@uco.es

Zoonotic *Ancylostoma ceylanicum* Infection in Coyotes from Guanacaste Conservation Area, Costa Rica, 2021

Patsy A. Zendejas-Heredia, Joby Robleto-Quesada, Alberto Solano, Alicia Rojas, Vito Colella

Ancylostoma ceylanicum is the second most common hookworm infecting humans in the Asia-Pacific region. Recent reports suggest presence of the parasite in the Americas. We report *A. ceylanicum* infections in coyotes from the Guanacaste Conservation Area, Costa Rica. Our findings call for active surveillance in humans and animals.

The zoonotic hookworm *Ancylostoma ceylanicum* infects canids, felids, and humans in tropical regions of the world (*1*,*2*). Heavy infections may cause iron-deficiency anemia and bloody diarrhea as a result of ≈0.03 mL/worm/day blood loss caused by repeated blood meals taken from the intestines of infected persons by the parasites (*2*,*3*). Across the Asia-Pacific region, domestic and wild animals and humans, especially children and women of childbearing age, are at high risk for illness from infection with the parasite (*2*). The pooled proportion of *A. ceylanicum* hookworm–infected persons within the Asia Pacific is 12%, making it the second most common hookworm infecting humans in that region (*4*). However, the extent of its geographic distribution in the Americas and the range of animals this hookworm can infect are unknown.

In studies dating to 1922, adult hookworms, later identified as *A. ceylanicum*, were recovered from human cadavers from Brazil and, in 1976, from animals necropsied in Suriname, suggesting that the parasite might have been present in the Americas more than a century ago (*2*). However, except for those cases, research on *A. ceylanicum* hookworms in the Americas has remained neglected for a long time; that prolonged absence in research might be attributable to use of traditional microscopy techniques for hookworm diagnosis in the region (*2*). Those techniques are unable to differentiate hookworms at the species level, thereby limiting more detailed information on their distribution. More recently, applying molecular techniques has increased identification of regions endemic for *A. ceylanicum* hookworms (*2*). For example, in 1 recent study, samples from patients in Ecuador initially screened for hookworms in 2000 were reexamined, and *A. ceylanicum* hookworms were molecularly identified (*5*). In addition, *A. ceylanicum* hookworms have been reported in France in a migrant from Colombia and a traveler returning from French Guiana (*6*); in Germany, the parasite was reported in a child from Colombia (*7*). Furthermore, in 2022, endemicity of *A. ceylanicum* hookworms was molecularly confirmed in dogs in Grenada, West Indies (*8*). Despite the discovery of *A. ceylanicum* hookworms in wildlife elsewhere, initially in a civet cat native to Sri Lanka and subsequently in Asia in golden cats and leopards and in dingoes in Australia (*9*), no studies have reported infections in wildlife in the Americas.

The Study

This project was approved by the National System of Conserved Areas of Costa Rica (R-SINAC-ACG-003-2021). Costa Rica is in Central America within the equatorial tropical region. Among its 5 million residents, 766,000 are school-age children. Coyotes (*Canis latrans*) live around national parks and are widely distributed across the plains,

Author affiliations: University of Melbourne, Parkville, Victoria, Australia (P.A. Zendejas-Heredia, V. Colella); Centro de Investigación en Enfermedades Tropicales, University of Costa Rica, San José, Costa Rica (J. Robleto Quesada, A. Solano, A. Rojas); Universidad de Costa Rica, Montes de Oca, San José (A. Solano, A. Rojas).

DOI: https://doi.org/10.3201/eid3006.231618

mountains, forests, and tropics. To investigate the prevalence of hookworm and threadworm infections among coyotes, during May–October 2021, we collected and tested coyote scat from the Central Conservation Area in central and the Guanacaste Conservation Area in northwestern Costa Rica (*10*). To confirm coyotes were the origin of the collected fecal samples, we cross-referenced data from a separate study conducted on the same samples that employed restriction fragment-length polymorphism–based methods and metabarcoding analyses of the vertebrate 12S ribosomal RNA gene (*11*).

We extracted genomic DNA from fecal samples (n = 111) using the QIAamp PowerFecal Pro DNA Kit (QIAGEN, https://www.qiagen.com) according to manufacturer instructions and added an extra initial bead-beating step. We performed 2 TaqMan (Thermo Fisher Scientific; https://www.thermofisher.com) probe–based real-time quantitative PCRs in duplicate to detect all present canine hookworm species (*A. ceylanicum*, *A. caninum*, *A. braziliense*, and *Uncinaria stenocephala*) and *Strongyloides* spp. threadworms, as described elsewhere (*10*,*12*). We subjected samples positive for *A. ceylanicum* to molecular characterization of a partial region of the *cox*1 gene (*13*). We downloaded nucleotide *cox*1 sequences from dogs, humans, and cats from GenBank to assess the phylogenetic relationship among *Ancylostoma* spp. parasites and hosts.

We used MEGA11 (https://www.megasoftware.net) for aligning sequences and determining the best-fit substitution model. We conducted phylogenetic analyses using MrBayes version 3.2.7a (https://nbisweden.github.io/MrBayes/download.html) for Bayesian and RAxML version 8.2.12 (https://github.com/stamatak/standard-RAxML) for maximum-likelihood inference. We annotated the resulting phylogenic tree using TreeViewer version 1.17.6 (https://treeviewer.org) and constructed a haplotype network using PopArt (https://github.com/jessicawleigh/popart).

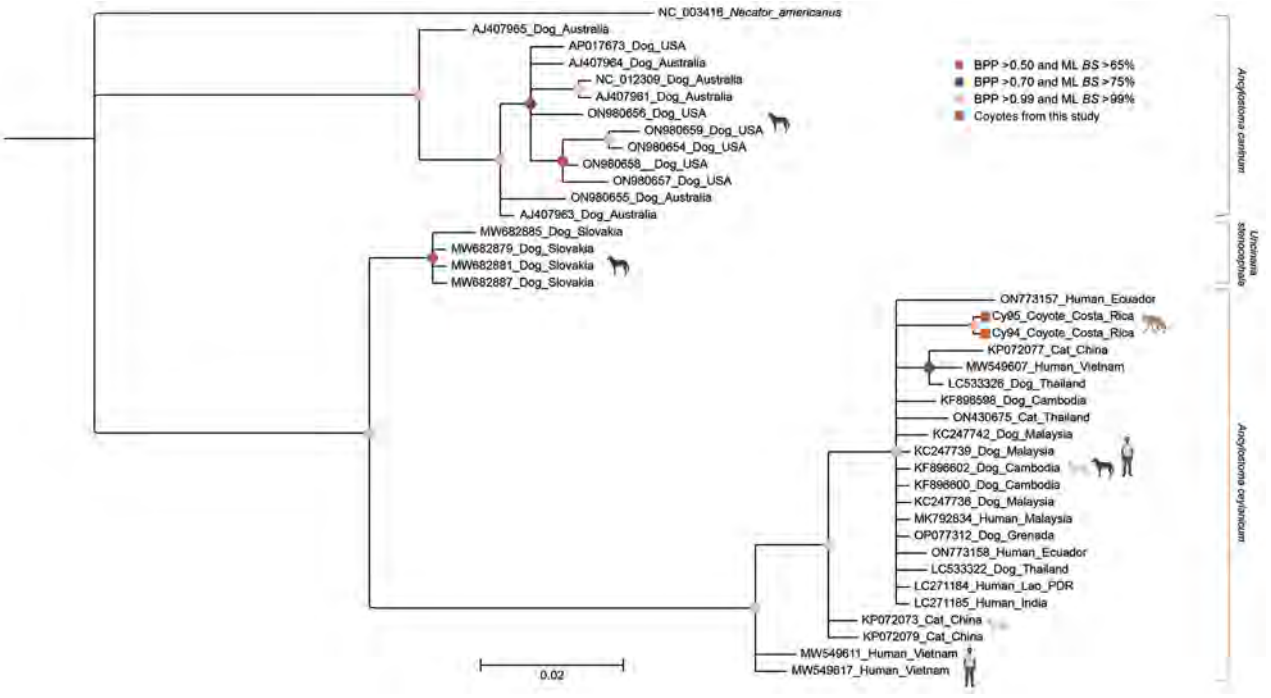

Figure 1. Phylogeny of *Ancylostoma ceylanicum* hookworms from coyotes in from Guanacaste Conservation Area, Costa Rica, 2021, and reference sequences. Gene tree shows a partial region of the mitochondrial *cox*1 gene for the hookworms *A. caninum*, *A. ceylanicum*, and *Uncinaria stenocephala*. Phylogenetic analyses were conducted using Bayesian inference in MrBayes v3.2.7a, employing the Hasegawa-Kishino-Yano substitution model with 4 gamma-distributed categories. Four independent Markov chains ran for 1,000,000 Markov chain Monte Carlo generations, with tree sampling occurring every 200 generations. The initial 25% of generated trees was considered burn-in, while the remaining trees were used to derive consensus trees. The analysis proceeded until the potential scale reduction factor approached 1, and the average SD of split frequencies was <0.01. For maximum-likelihood analysis, we used the rapid bootstrapping option with 10,000 iterations based on the Akaike information criterion. To root the tree, we included the human hookworm *Necator americanus* (GenBank NC_003416). Circles on nodes indicate BPP and ML *BS* percentages. Taxon names are annotated with GenBank accession numbers, host, and country of origin. Scale bar indicates the mean number of nucleotide substitutions per site. BPP, Bayesian posterior probability; ML *BS*, maximum-likelihood bootstrap support.

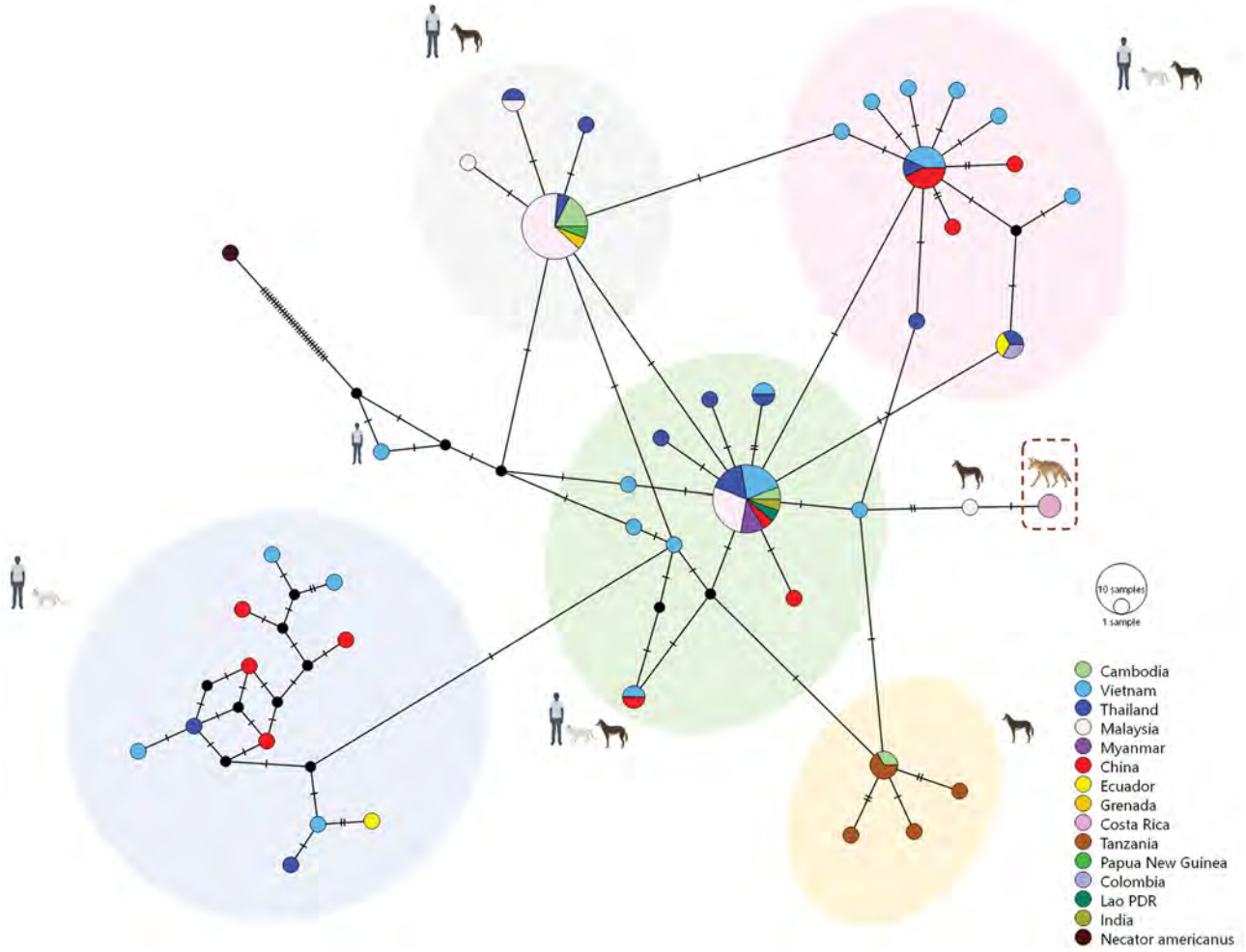

Figure 2. Median joining haplotype network showing global *Ancylostoma ceylanicum* sequences for cats, humans, and dogs and coyotes from Guanacaste Conservation Area, Costa Rica, 2021 (dashed box). Each circle represents a haplotype; circle size is proportional to the number of animals and persons with that haplotype, with the proportion found in each country indicated by color. A hatch mark across a line represents a mutation step between haplotypes. The legend illustrates color-coded haplotypes corresponding to each country. In addition, icons representing humans, dogs, cats, and coyotes are juxtaposed with each haplotype cluster to indicate host origins.

Of the 111 samples collected, 103 had sufficient feces for successfully extracting DNA, determined by amplifying a housekeeping gene of canids as DNA extraction control. Of those 103 samples, 59 (57.3%, 95% CI 46.6%–62.2%) harbored ≥1 zoonotic hookworms; *A. caninum* accounted for most infections (53.4%; 95% CI 43.3%–63.3%), followed by *U. stenocephala* (4.7%, 95% CI 1.5%–10.7%), and *A. ceylanicum* (2.8%, 95% CI 0.56%–8.05%). *Strongyloides* spp. threadworms were found in 3.8% (95% CI 1.04%–9.3%) of coyotes.

We obtained a 289-bp amplicon showing 99.6%–100% nucleotide identity with *A. ceylanicum* sequences from 2 positive *A. ceylanicum* samples (GenBank accession numbers OR801542 and OR801543). We determined phylogeny from 40 sequences that included *A. ceylanicum* sequences from dogs, cats, and humans, and *U. stenocephala* and *A. caninum* sequences from dogs. Phylogenetic analyses enabled separation of *A. ceylanicum* nucleotide sequences from coyote samples from Costa Rica from *A. caninum* and *U. stenocephala* sequences (Figure 1). Upon examining the median joining network of global *A. ceylanicum* sequences, we identified 5 distinct clusters, 4 of which were shared between domestic animals and humans and only 1 with dogs. We observed no clear population structure among countries represented by an admixture of haplotypes. *A. ceylanicum* haplotype from coyotes was unique but separated by only a few mutational steps from those from dogs and humans, and from zoonotic clusters (Figure 2).

Conclusions

We report zoonotic hookworm infections in coyotes from Costa Rica. Our data provide further evidence of the endemicity and local transmission of *A. ceylanicum* hookworm in the Americas and show that coyotes might play a role in transmitting this parasite to other animals. Even though coyotes are widely distributed across North and Central America and are established reservoirs of other zoonotic hookworms, such as *A. caninum* and *U. stenocephala* (*14*), their role as hosts of *A. ceylanicum* hookworm remains unexplored. Furthermore, detection of *A. ceylanicum* hookworms in wildlife poses questions about the parasite's possible role as a disease agent in endangered animals, such as jaguars, giant anteaters, and Baird's tapir, that live in sympatry in the Guanacaste Conservation Area (*15*).

Costa Rica has effectively controlled soil-transmitted helminths in humans, and residents no longer require preventive chemotherapy. However, the Pan American Health Organization still recommends continuous monitoring and evaluation to maintain control of soil-transmitted helminths (*15*). Although eliminating the need for preventive chemotherapy constituted a great milestone, doing so leaves untreated persons vulnerable to infection with zoonotic helminths, including *A. ceylanicum*. We therefore advocate for increased surveillance of *A. ceylanicum* hookworm in domestic animals, wildlife, and humans in the Americas to monitor and prevent transmission of zoonotic hookworms. Expanded surveillance is crucial considering active transmission of *A. ceylanicum* hookworm in humans has been reported in Ecuador, another country listed by the Pan American Health Organization as no longer requiring preventive chemotherapy (*5*,*15*). In-depth population genetics studies are needed to assess whether increases in the reports of *A. ceylanicum* hookworms in the Americas are attributable to recent human and animal migration from areas where the parasite is highly endemic. More robust epidemiologic data on *A. ceylanicum* infection in domestic animals and humans would help public health agencies assess the extent of local transmission in Costa Rica and other regions of the Americas and the role of animals in transmitting the parasite to humans.

Acknowledgments

We acknowledge Kevin Lloyd, Víctor Montalvo, Carolina Sáenz, Juan Carlos Cruz, and park rangers from the Central Conservation Area and Guanacaste Conservation Area for their collaboration in collecting fecal samples of coyotes.

About the Author

Ms. Zendejas-Heredia is a PhD candidate at the University of Melbourne, Australia. Her research focuses on understanding the transmission dynamics of zoonotic soil-transmitted helminths.

References

1. Smout FA, Skerratt LF, Butler JRA, Johnson CN, Congdon BC, Thompson RCA. The hookworm *Ancylostoma ceylanicum*: an emerging public health risk in Australian tropical rainforests and indigenous communities. One Health. 2017;3:66–9. https://doi.org/10.1016/j.onehlt.2017.04.002
2. Traub RJ, Zendejas-Heredia PA, Massetti L, Colella V. Zoonotic hookworms of dogs and cats—lessons from the past to inform current knowledge and future directions of research. Int J Parasitol. 2021;51:1233–41. https://doi.org/10.1016/j.ijpara.2021.10.005
3. Areekul S, Saenghirun C, Ukoskit K. Studies on the pathogenicity of *Ancylostoma ceylanicum*. I. Blood loss in experimental dogs. Southeast Asian J Trop Med Public Health. 1975;6:235–40.
4. Clements ACA, Addis Alene K. Global distribution of human hookworm species and differences in their morbidity effects: a systematic review. Lancet Microbe. 2022;3:e72–9. https://doi.org/10.1016/S2666-5247(21)00181-6
5. Sears WJ, Cardenas J, Kubofcik J, Nutman TB, Cooper PJ. Zoonotic *Ancylostoma ceylanicum* hookworm infections, Ecuador. Emerg Infect Dis. 2022;28:1867–9. https://doi.org/10.3201/eid2809.220248
6. Gerber V, Le Govic Y, Ramade C, Chemla C, Hamane S, Desoubeaux G, et al. *Ancylostoma ceylanicum* as the second most frequent hookworm species isolated in France in travellers returning from tropical areas. J Travel Med. 2021;28:28. https://doi.org/10.1093/jtm/taab014
7. Poppert S, Heideking M, Agostini H, Fritzenwanker M, Wüppenhorst N, Muntau B, et al. Diffuse unilateral subacute neuroretinitis caused by *Ancylostoma* hookworm. Emerg Infect Dis. 2017;23:343–4. https://doi.org/10.3201/eid2302.142064
8. Zendejas-Heredia PA, Colella V, Macpherson MLA, Sylvester W, Gasser RB, Macpherson CNL, et al. *Ancylostoma ceylanicum* hookworms in dogs, Grenada, West Indies. Emerg Infect Dis. 2022;28:1870–2. https://doi.org/10.3201/eid2809.220634
9. Smout FA, Thompson RCA, Skerratt LF. First report of *Ancylostoma ceylanicum* in wild canids. Int J Parasitol Parasites Wildl. 2013;2:173–7. https://doi.org/10.1016/j.ijppaw.2013.04.003
10. Massetti L, Colella V, Zendejas PA, Ng-Nguyen D, Harriott L, Marwedel L, et al. High-throughput multiplex qPCRs for the surveillance of zoonotic species of canine hookworms. PLoS Negl Trop Dis. 2020;14:e0008392. https://doi.org/10.1371/journal.pntd.0008392
11. Alfaro-Segura P, Robleto-Quesada J, Montenegro-Hidalgo VM, Molina-Mora JA, Baneth G, Verocai GG, et al. Elucidating *Spirocerca lupi* spread in the Americas by using phylogenetic and phylogeographic analyses. Front Parasitol. 2023;2:1249593.
12. Verweij JJ, Canales M, Polman K, Ziem J, Brienen EA, Polderman AM, et al. Molecular diagnosis of *Strongyloides stercoralis* in faecal samples using real-time PCR. Trans

R Soc Trop Med Hyg. 2009;103:342–6. https://doi.org/10.1016/j.trstmh.2008.12.001
13. Inpankaew T, Schär F, Dalsgaard A, Khieu V, Chimnoi W, Chhoun C, et al. High prevalence of *Ancylostoma ceylanicum* hookworm infections in humans, Cambodia, 2012. Emerg Infect Dis. 2014;20:976–82. https://doi.org/10.3201/eid2006.131770
14. Seguel M, Gottdenker N. The diversity and impact of hookworm infections in wildlife. Int J Parasitol Parasites Wildl. 2017;6:177–94. https://doi.org/10.1016/j.ijppaw.2017.03.007
15. Gyorkos T, Nicholls R, Montresor A, Luciañez A, Casapia M, St-Denis K, et al. Eliminating morbidity caused by neglected tropical diseases by 2030. Rev Panam Salud Publica. 2023;47:e16. https://doi.org/10.26633/RPSP.2023.16

Address for correspondence: Vito Colella, University of Melbourne, Melbourne Veterinary School, Parkville, VIC 3052, Australia; email: vito.colella@unimelb.edu.au

Encephalitozoon cuniculi Microsporidia in Cerebrospinal Fluid from Immunocompetent Patients, Czech Republic

Bohumil Sak, Katka Mansfeldová, Klára Brdíčková, Petra Gottliebová, Elka Nyčová, Nikola Holubová, Jana Fenclová, Marta Kicia, Żaneta Zajączkowska, Martin Kváč

We retrospectively analyzed of 211 frozen cerebrospinal fluid samples from immunocompetent persons in the Czech Republic and detected 6 *Encephalitozoon cuniculi*–positive samples. Microsporidiosis is generally underestimated and patients are not usually tested for microsporidia, but latent infection in immunodeficient and immunocompetent patients can cause serious complications if not detected and treated.

Microsporidia are obligate intracellular parasites of invertebrate and vertebrate hosts and are considered to be a sister group to fungi (*1*). Of the 1,300 species in >200 genera that have been described (*2*), *Encephalitozoon cuniculi*, especially genotypes I and II, is the most common in humans (*3*,*4*).

Although the digestive tract represents a port of entry, *Encephalitozoon* infections can occur in almost every organ system and can cause various diseases (*4*). Encephalitozoonosis is a serious problem in immunodeficient hosts, including HIV-positive patients and patients on immunosuppressive treatments. In immunocompetent persons, microsporidial infections are predominantly chronic and asymptomatic (*5*).

Recent studies have described engagement of macrophages, or other immune cells involved in the development of inflammation, serving as vehicles and transporting microsporidia toward target tissues outside the intestines (*6*,*7*). Microsporidia are often overlooked in clinical samples because diagnosis is problematic, but hidden infections can cause tremendous multisystem damage and various nonspecific pathologies, and few effective treatments are available (*8*). We evaluated the incidence of generally neglected *Encephalitozoon* spp. in immunocompetent patients by retrospectively analyzing previously collected cerebrospinal fluid (CSF) samples.

Author affiliations: Biology Centre of the Czech Academy of Sciences, České Budějovice, Czech Republic (B. Sak, N. Holubová, J. Fenclová, M. Kváč); University of South Bohemia, České Budějovice (K. Mansfeldová, J. Fenclová, M. Kváč); Bulovka Hospital, Prague, Czech Republic (K. Brdíčková, P. Gottliebová, E. Nyčová); Wroclaw Medical University, Wroclaw, Poland (M. Kicia, Ż. Zajączkowska)

DOI: https://doi.org/10.3201/eid3006.231585

The Study

Bulovka Hospital, Prague, Czech Republic, provided 211 CSF samples that had been deep frozen at −80°C. CSF samples were collected from immunocompetent patients; the only other patient data reported were the year of birth and sex. We obtained total DNA from sediments obtained from thawed CSF together with extraction negative control in each series, as previously described (*6*). We used the same methods to isolate control DNA from purified *E. intestinalis* spores. The study was conducted beyond the routine screening of existing unused specimens and focused on potential detection of microsporidia in CSF recovered from immunocompetent patients hospitalized at 1 hospital. Because the study was performed using anonymized samples with no intervention tract, patient consent was not required.

We used an *Encephalitozoon* spp.–specific nested PCR to amplify the internal transcribed spacer region (*9*,*10*). We included DNA of *E. intestinalis* microsporidia as a PCR-positive control and ultrapure water as a negative control and evaluated PCR products by gel electrophoresis.

We quantified DNA from PCR-positive samples by using reverse transcription PCR to amplify a 268-bp region of the 16S rRNA gene of *E. cuniculi* (*10*). Each run included unspiked specimens and diluent

Table. Characteristics of patients in a study of *Encephalitozoon cuniculi* in cerebrospinal fluid from immunocompetent patients, Czech Republic

Sex	Total no. sampled	Median age (range)	*E. cuniculi*–positive patients		Sample testing results	
			Patient no.	Age, y	Nested PCR genotype	RT-PCR quantification/mL (Ct)
M	115	34.0 (4–81)	56	63	*E. cuniculi* II	3.0×10^1 (39)
F	96	33.5 (2–80)	54	13	*E. cuniculi* II	5.7×10^1 (38)
			139	45	*E. cuniculi* II	1.1×10^2 (36)
			185	48	*E. cuniculi* II	5.1×10^2 (35)
			194	75	*E. cuniculi* II	3.0×10^1 (38)
			197	32	*E. cuniculi* II	1.0×10^1 (39)
Total	211	34.0 (2–81)				

blanks. We considered results positive when the fluorescence signal crossed the baseline at ≤43 cycles. We used a standard curve to calculate the total number of spores in 1 mL of each sample.

We used the QIAquick Gel Extraction Kit (QIAGEN, https://www.qiagen.com) to purify PCR amplicons of the internal transcribed spacer region and submitted amplicons to SEQme (https://www.seqme.eu) for sequencing in both directions. We manually edited nucleotide sequences by using the ChromasPro 2.1.4 program (Technelysium, https://technelysium.com.au) and used MAFFT version 7 (http://mafft.cbrc.jp) to align sequences with reference GenBank submissions. We also microscopically examined PCR-positive samples. We air dried a drop of CSF, fixed it with methanol, and stained with standard Calcofluor M2R (Sigma-Aldrich, https://www.sigmaaldrich.com) (*11*).

Of 211 CSF samples examined, 115 were from male patients and 96 from female patients. The median patient age was 34.0 (range 2–81) years (Table). Among all samples, 6 were positive for microsporidia DNA, 0.9% (1/115) of samples from male and 5.2% (5/96) of samples from female patients. The age of positive patients ranged from 13 to 75 years (median 45.5 years). The spore concentration in samples was 30–500 spores/mL.

Sequence analyses revealed 100% identity to *E. cuniculi* genotype II (GenBank accession no. MF062430) in all positive samples (Table; Figure 1). Microscopic analysis of Calcofluor M2R–stained smears confirmed the presence of spores (1–2 spores per slide) in samples obtained from 2 patients, nos. 139 and 185, who had the highest *Encephalitozoon* DNA burden (Figure 2). The other 4 patients were microscopically negative.

Conclusions

Although microsporidiosis is mainly detected in immunodeficient patients, data from the literature

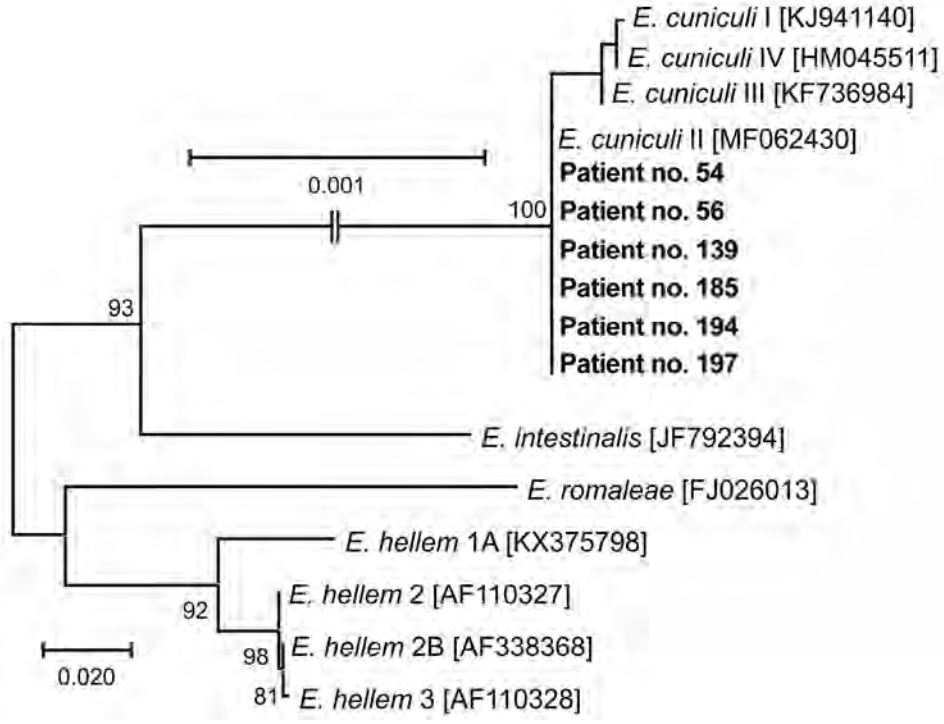

Figure 1. Phylogenetic analysis of *Encephalitozoon cuniculi* genotypes recovered from cerebrospinal fluid of immunocompetent patients, Czech Republic. Bold indicates sequences obtained in this study, identified by patient number. Sequences for comparisons were obtained from GenBank; accession numbers are in brackets. Tree was constructed by using the maximum-likelihood method. Partial sequences of 16S rRNA gene, the entire internal transcribed spacer region, and a partial sequence of 5.8S rRNA gene were inferred by using neighbor-joining analyses, and relationships were computed by using the Tamura 3-parameter method with gamma distribution and parametric bootstrap analysis of 1,000 replicates in MEGA X software (MEGA, https://www.megasoftware.net). Scale bar indicates nucleotide substitutions per site.

imply that otherwise healthy persons also are at risk (*12*,*13*). Those data indicate that apparently healthy persons could be infected without any clinical signs, and the risk increases with age (*12*). Whether microsporidial infection potentially leads to a deterioration in health that could be life-threatening in the event of a decline in immunity has not been determined (*12*,*14*,*15*).

The fecal–oral route is generally accepted as the most common transmission route because the spores are passed in the urine or feces of infected patients, then mostly contaminate water sources. Moreover, possible foodborne transmission, including through fresh vegetables and fruits, milk, cheese, and fermented meat products, has been reported (*13*). Besides those transmission routes, respiratory tract infection suggests airborne transmission by contaminated aerosols (*13*).

Microsporidia are small intracellular fungi capable of causing widespread infections within a few days, despite their lack of active motility and limited spreading possibilities (*14*). The exact spreading mechanism is still unknown; however, the possible connection between activation of proinflammatory cellular immune response and targeted transport of microsporidia toward inflammation site has been proposed on the basis of clinical and experimental data (*6*,*7*,*11*).

In this study, we detected microsporidia DNA in 3% of tested CSF samples from 211 patients of one hospital. The molecular data were supported by microscopy in 2 patients who had the highest spore loads. Although the other 4 PCR-positive patients tested microscopically negative, those results could be caused by limited sensitivity of microscopy in low burden samples, rather than laboratory contamination. Because we obtained uniform results from specific patients using both PCR and quantitative PCR, contamination is unlikely. Moreover, we can exclude laboratory contamination because the same trained personnel took the samples and ran PCRs under sterile conditions. In addition, PCR diagnostic laboratory is structurally divided into separate areas that adhere to the 1-direction workflow, and all negative controls used in sample processing were negative.

Our results for microsporidia detection indicate an increasing prevalence of latent microsporidiosis with patient age, which is consistent with the results of previous studies (*12*). Moreover, the presence of microsporidia in CSF represents a potentially serious condition; unfortunately, we cannot infer any association with the clinical condition of the patients because we did not have patient histories or reasons for collecting CSF samples. However, we can assume a possible link between the patients' health issues and the presence of microsporidia in CSF, similar to those found in another study (*15*). That study reported a case of a paralyzed patient with a right frontal lobe abscess containing *E. cuniculi* genotype I; the patient was successfully treated following appropriate treatment regimen.

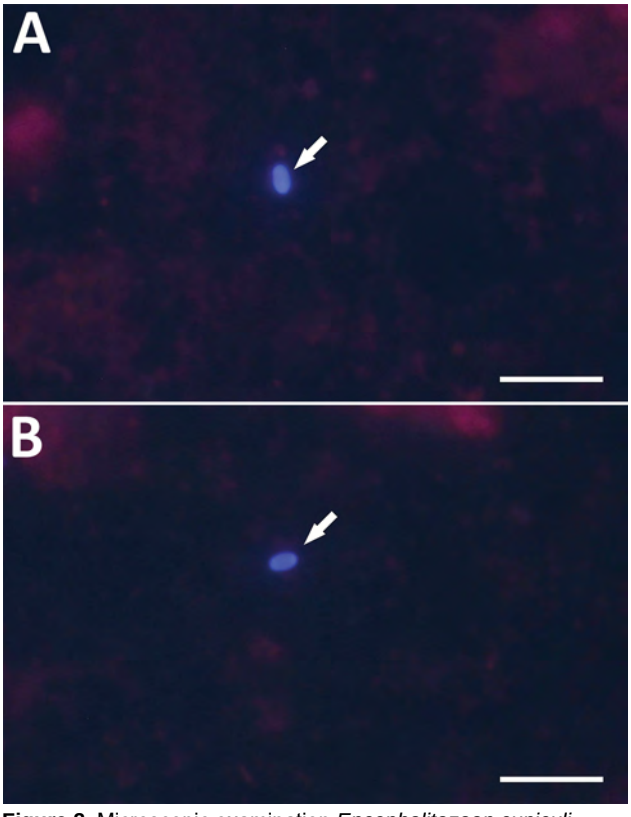

Figure 2. Microscopic examination *Encephalitozoon cuniculi*–positive cerebrospinal fluid from immunocompetent patients, Czech Republic. Microsporidial spores (arrows) were stained with Calcofluor M2R and viewed in 490 nm. A) Patient no. 139; B) patient no. 185. Scale bar indicates 10 μm.

In conclusion, disseminated latent microsporidiosis can cause several serious diseases with nonspecific symptoms and ambiguous etiology that can be life-threating or fatal if misdiagnosed and left untreated. We encourage increased awareness of latent microsporidiosis and development of targeted screening that enables timely treatment.

This work was supported by grants from the Grant Agency of the Czech Republic (nos. 20-10706S, 23-06571S) and National Science Centre, Poland (no. 2020/39/O/NZ6/02313). The funders had no role in study design, data collection and analysis, decision to publish, or preparation of the manuscript.

About the Author

Dr. Sak is a research scientist at Biology Centre CAS, České Budějovice, Czech Republic. His research interests include detection of parasites, such as microsporidia, including diagnostics, isolation, in vitro cultivation, experimental infections, and morphological and molecular characterization.

References

1. Keeling PJ, Doolittle WF. Alpha-tubulin from early-diverging eukaryotic lineages and the evolution of the tubulin family. Mol Biol Evol. 1996;13:1297–305. https://doi.org/10.1093/oxfordjournals.molbev.a025576
2. Cali A, Becnel JJ, Takvorian PM. Microsporidia. In: Archibald JM, Simpson AGB, Slamovits CH, editors. Handbook of the protists. Cham (Switzerland): Springer; 2017. p. 1559–618.
3. Didier ES. Microsporidiosis: an emerging and opportunistic infection in humans and animals. Acta Trop. 2005;94:61–76. https://doi.org/10.1016/j.actatropica.2005.01.010
4. Didier ES, Weiss LM. Microsporidiosis: not just in AIDS patients. Curr Opin Infect Dis. 2011;24:490–5. https://doi.org/10.1097/QCO.0b013e32834aa152
5. Weber R, Bryan RT, Schwartz DA, Owen RL. Human microsporidial infections. Clin Microbiol Rev. 1994;7:426–61. https://doi.org/10.1128/CMR.7.4.426
6. Brdíčková K, Sak B, Holubová N, Květoňová D, Hlásková L, Kicia M, et al. *Encephalitozoon cuniculi* genotype II concentrates in inflammation foci. J Inflamm Res. 2020;13:583–93. https://doi.org/10.2147/JIR.S271628
7. Sak B, Holubová N, Květoňová D, Hlásková L, Tinavská J, Kicia M, et al. Comparison of the concentration of *Encephalitozoon cuniculi* genotypes I and III in inflammatory foci under experimental conditions. J Inflamm Res. 2022;15:2721–30. https://doi.org/10.2147/JIR.S363509
8. Lallo MA, da Costa LF, de Castro JM. Effect of three drugs against *Encephalitozoon cuniculi* infection in immunosuppressed mice. Antimicrob Agents Chemother. 2013;57:3067–71. https://doi.org/10.1128/AAC.00157-13
9. Katzwinkel-Wladarsch S, Lieb M, Heise W, Löscher T, Rinder H. Direct amplification and species determination of microsporidian DNA from stool specimens. Trop Med Int Health. 1996;1:373–8. https://doi.org/10.1046/j.1365-3156.1996.d01-51.x
10. Wolk DM, Schneider SK, Wengenack NL, Sloan LM, Rosenblatt JE. Real-time PCR method for detection of *Encephalitozoon intestinalis* from stool specimens. J Clin Microbiol. 2002;40:3922–8. https://doi.org/10.1128/JCM.40.11.3922-3928.2002
11. Kicia M, Wesolowska M, Kopacz Z, Kvác M, Sak B, Sokulska M, et al. Disseminated infection of *Encephalitozoon cuniculi* associated with osteolysis of hip periprosthetic tissue. Clin Infect Dis. 2018;67:1228–34. https://doi.org/10.1093/cid/ciy256
12. Sak B, Kváč M, Kučerová Z, Květoňová D, Saková K. Latent microsporidial infection in immunocompetent individuals—a longitudinal study. PLoS Negl Trop Dis. 2011;5:e1162. https://doi.org/10.1371/journal.pntd.0001162
13. Sak B, Kváč M. Chronic infections in mammals due to microsporidia. In: Weiss LM, Reinke AW, editors. Microsporidia: current advances in biology. Cham (Switzerland): Springer Experientia Supplementum; 2022. p. 319–71.
14. Kotková M, Sak B, Květoňová D, Kváč M. Latent microsporidiosis caused by *Encephalitozoon cuniculi* in immunocompetent hosts: a murine model demonstrating the ineffectiveness of the immune system and treatment with albendazole. PLoS One. 2013;8:e60941. https://doi.org/10.1371/journal.pone.0060941
15. Ditrich O, Chrdle A, Sak B, Chmelík V, Kubále J, Dyková I, et al. *Encephalitozoon cuniculi* genotype I as a causative agent of brain abscess in an immunocompetent patient. J Clin Microbiol. 2011;49:2769–71. https://doi.org/10.1128/JCM.00620-11

Address for correspondence: Bohumil Sak, Institute of Parasitology, Biology Centre of the Czech Academy of Sciences, Branišovská 31, 37005 České Budějovice, Czech Republic; email: casio@paru.cas.cz

Infection- and Vaccine-Induced SARS-CoV-2 Seroprevalence, Japan, 2023

Ryo Kinoshita,[1] Sho Miyamoto,[1] Shoko Sakuraba, Jun Sugihara, Motoi Suzuki, Tadaki Suzuki,[2] Daisuke Yoneoka[2]

We assessed SARS-CoV-2 seroprevalence in Japan during July–August 2023, with a focus on 2 key age groups, 0–15 and ≥80 years. We estimated overall seroprevalence of 45.3% for nucleocapsid antibodies and 95.4% for spike antibodies and found notable maternally derived spike antibodies in infants 6–11 months of age (90.0%).

Before the Omicron variant emerged, <5% of Japan's population had experienced SARS-CoV-2 infection (*1*), but ≈34 million (27%) COVID-19 cases were reported by May 7, 2023 (*2*). The mandatory reporting of all cases burdened the healthcare system, prompting Japan to adopt a sentinel surveillance approach starting May 8, 2023. Sentinel surveillance may restrict representativeness because of its limited coverage population and overlooks persons with mild or no symptoms because they often remain undiagnosed. Persons ≥6 months of age have been recommended to receive COVID-19 vaccines in Japan, where mRNA vaccines (Pfizer-BioNTech, https://www.pfizer.com; Moderna, https://www.modernatx.com) are predominantly used. Seroepidemiologic surveys can aid in understanding ascertainment rate and assessing the real-time prevalence of antibodies resulting from both natural infection and vaccination (*3*).

Since 2020, Japan's Ministry of Health, Labour, and Welfare has conducted 6 rounds of seroepidemiologic surveys among residents (survey 1) (*1*,*4*) and 4 rounds among blood donors (survey 2) (*4*,*5*). Survey 1 analyzed both nucleocapsid (N) and spike (S) antibody seroprevalence through random samples of participating residents (≥20 years of age), whereas survey 2 focused solely on N antibody seroprevalence among blood donors (16–69 years of age). Those surveys revealed that older and at-risk age groups exhibit lower infection rates and higher vaccination rates as well as a relatively lower seroprevalence before Omicron emergence compared with the United Kingdom and United States (*5*). However, the surveys excluded infants, children, and the elderly. To complement the previous surveys, our study aimed to assess SARS-CoV-2 seroprevalence among outpatients, focusing on 2 key age groups (*6*–*8*): the younger generation (0–15 years) and the older generation (≥80 years).

The Study

We used residual blood samples from local clinics collected across 22 prefectures in Japan during July 22–August 21, 2023, to investigate SARS-CoV-2 antibody seroprevalence across persons 0 to 101 years of age. This study, conducted in accordance with the Act on the Prevention of Infectious Diseases and Medical Care for Patients with Infectious Diseases (*9*), did not require a formal ethics review or participant consent.

From various private testing companies offering testing services for nonbed clinics across regions, 1 was chosen to closely mirror Japan's population density and age distribution. We conducted random sampling from the collected pool of residual specimens among 11 age groups (0–4, 5–9, 10–14, 15–19, 20–29, 30–39, 40–49, 50–59, 60–69, 70–79, and ≥80 years) until 385 specimens were sampled per age group, assuming a 50% (±5%) seroprevalence, with a 5% α-error. We measured N antibodies by using Elecsys

Author affiliations: National Institute of Infectious Diseases, Tokyo, Japan (R. Kinoshita, S. Miyamoto, M. Suzuki, T. Suzuki, D. Yoneoka), Ministry of Health, Labour, and Welfare, Tokyo (S. Sakuraba, J. Sugihara)

DOI: https://doi.org/10.3201/eid3006.231454

[1]These first authors contributed equally to this article.

[2]These senior authors contributed equally to this article.

Anti-SARS-CoV-2 (Roche, https://www.roche.com) and S antibodies by using Elecsys Anti-SARS-CoV-2 S (Roche). We used a cutoff index of 1.0 U/mL to determine the presence of N antibodies and 0.8 U/mL to determine the presence S antibodies, as determined by the manufacturer. We assumed S antibody concentrations measured ≤0.4 U/mL to be 0.2 U/mL. We also collected data on age, sex, and prefecture. To adjust for each prefecture's age and sex distribution, we used weighted tabulation on the basis of the October 2022 baseline population (*10*). We computed 95% CIs by using the binomial exact method.

We analyzed 4,235 blood samples; median age of participants was 34.0 (SD ±27.5) years, and the male-to-female ratio was 0.82 (Appendix, https://wwwnc.cdc.gov/EID/article/30/6/23-1454-App1.pdf). The seroprevalence of N antibodies was 45.3% (95% CI 43.7%–46.8%) and for S antibodies was 95.4% (95% CI 94.7%–96.0%). The age-stratified weighted seroprevalence of N antibodies indicated higher seroprevalences in younger age groups (68.0% [95% CI 64.7%–71.1%] in persons 5–29 years of age) and lower seroprevalences in older age groups (25.7% [95% CI 21.1%–30.7%] in persons ≥80 years of age) (Figure 1, panel A). Age-stratified weighted seroprevalence of S antibodies was 96.2% (95% CI 95.5%–96.8%) for persons ≥5 years of age and 71.0% (95% CI 61.5%–79.4%) for persons 0–4 years of age.

We measured S antibody concentrations categorized by N antibody seroprevalence status (Figure 2). For persons 6–11 months of age, the estimated weighted median S antibody concentration among N antibody–negative participants was 1.75 U/mL (interquartile range [IQR] 1.14–2.44 U/mL) and among N antibody–positive participants was 2.01 U/mL (IQR 1.77–2.57 U/mL). For persons 1–4 years of age, the estimated weighted median S antibody concentrations among N antibody–negative participants was –0.70 U/mL (IQR -0.70–-0.07 U/mL) and among N antibody–positive participants was 1.98 U/mL (IQR 1.70–2.63 U/mL) (Figure 2, panel A). Overall, for persons ≥10 years of age, the S antibody concentrations tended to be higher because of immunity from natural infection and vaccination. Antibody concentrations in persons ≤4 years of age (Figure 2, panel B) suggest the presence of maternally derived immunity; among persons 6–9 months of age, we observed similar S antibody concentrations regardless of N antibody status, whereas we observed a gradual decline in median S antibody concentrations among N antibody-seronegative persons >10 months of age.

Conclusions

This survey revealed SARS-CoV-2 seroprevalence across various age groups in Japan, with a specific focus on persons 0–15 and ≥80 years of age, who were not covered in previous surveys. Consistent with prior surveys (surveys 1 and 2), we observed higher N antibody seroprevalence in younger age groups compared with older age groups. Although N antibody

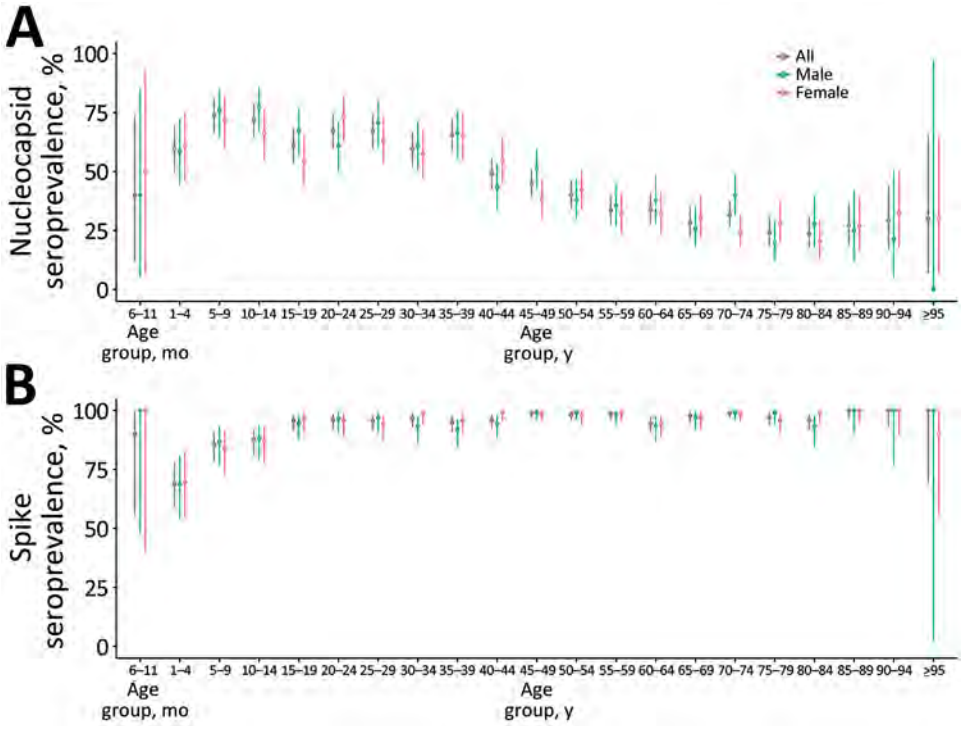

Figure 1. Age-stratified weighted seroprevalence of nucleocapsid and spike SARS-Cov-2 antibodies in Japan, 2023. A) Weighted seroprevalence of nucleocapsid antibodies by sex and age group. B) Weighted seroprevalence of spike antibodies by sex and age group.

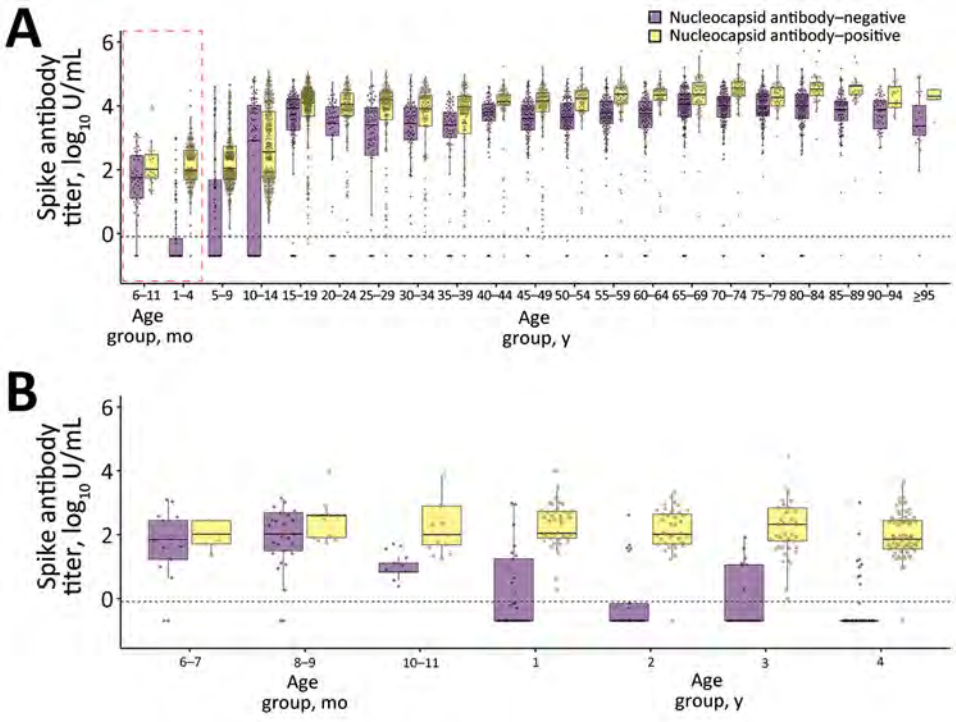

Figure 2. Age-stratified weighted concentrations of spike SARS-Cov-2 antibody stratified by nucleocapsid SARS-Cov-2 antibody seroprevalence in Japan, 2023. A) Spike antibody concentrations stratified by nucleocapsid antibody seroprevalence in persons 6 months to >95 years of age. Red dashed box represents the age group analyzed in panel B. B) Spike antibody concentrations stratified by nucleocapsid antibody seroprevalence in persons 6 months to 4 years of age. Horizonal lines within boxes indicate the median, box tops and bottoms indicate the 75th percentile and 25th percentile, and whiskers extend to 1.5 times the interquartile range (IQR) from 25th percentile and 75th percentile. Dotted horizontal lines represent the cutoff index of 0.8 U/mL. Box plots are weighted with respect to the demography of Japan.

seroprevalence is low among older populations, the vaccination coverage among persons ≥65 years of age during the survey period ranged from 91.5% to 92.8% for the first to third doses, which is higher than for the general vaccinated population (≥6 months of age) (68.7%–80.9% for the first to third doses) (*11*). Vaccination coverage for children 5–11 years of age was low; of only 24.1% had first, 23.4% had second, and 9.8% had third doses, and those 6 months–4 years of age had even lower coverage (2.9%–4.0% for the first to third doses) (*11*). Of note, S antibody seroprevalence is higher, especially among persons >10 years of age, because of immunity acquired from infection and vaccination. Therefore, the S antibody seroprevalence in Japan reflects most the younger population acquiring immunity from natural infection and the older population acquiring immunity from vaccination.

Despite low vaccination coverage among children, we observed a high S antibody seroprevalence among children 6–11 months of age at 90.0% (95% CI 55.5%–99.7%). Among the same age group, the N antibody seroprevalence was 40.0% (95% CI 12.2%–73.8%), raising speculation about the presence of maternally derived antibodies in infants. When stratified by N antibody seroprevalence, S antibody concentrations were notably high among N antibody-seronegative persons in the 6–11-months age group (Figure 2, panel B). Although the duration of immunity may vary depending on the mother's vaccination and infection status (*12*), and a longitudinal study is essential for better understanding, we observed a potential persistence of positive S antibodies until 10–11 months of age, followed by a decline to negative status by 1 year of age.

One limitation of our study is that, despite demographic adjustments using survey weights, biases from the selected clinics in 22 prefectures may not reflect the seroprevalence of the entire population of Japan. To understand the potential effect of selection bias, we are conducting additional surveys simultaneously from different sources. In addition, the proportion does consider the sensitivity or decline of N antibodies (*13*). However, we believe this effect is minimal when using the Roche assay, because only 2.1% of N antibody seroprevalence was reported in December 2021 (*1*) and the assay typically remains positive for ≈2 years (*14*,*15*). Furthermore, the absence of vaccination information for the sampled population hindered a comprehensive understanding of the effect of vaccination on S antibody levels.

Acknowledgments

We thank FALCO Biosystems Ltd. for analyzing the residual blood samples.

The survey was directly conducted and funded by the Ministry of Health, Labour, and Welfare of Japan. R.K. received funding from the Japan Society for the Promotion of Science KAKENHI (grant no. 21K17307) and Japan Agency for Medical Research and Development

(grant no. JP23fk0108685). D.Y. received funding from the Japan Science and Technology Agency PRESTO (grant no. JPMJPR21RC). T.S. received funding from the Ministry of Health, Labour, and Welfare of Japan (grant nos. 20HA2001 and 22HA2006).

The opinions expressed by authors contributing to this journal do not necessarily reflect the official position of the Ministry of Health, Labour, and Welfare of Japan, or the authors' affiliated institutions.

Author contribution: T.S., J.S., and S.S. coordinated the survey. R.K., S.M., and D.Y. analyzed the dataset and drafted the article. All the authors made critical revisions to the manuscript for important intellectual content and gave final approval of the manuscript.

About the Author

Dr. Kinoshita is a researcher at the Center for Surveillance, Immunization, and Epidemiologic Research, National Institute of Infectious Diseases, Tokyo, Japan. His primary research interests include infectious diseases epidemiology and modeling with a current focus on prevention of vaccine-preventable diseases.

References

1. Arashiro T, Arai S, Kinoshita R, Otani K, Miyamoto S, Yoneoka D, et al. National seroepidemiological study of COVID-19 after the initial rollout of vaccines: before and at the peak of the Omicron-dominant period in Japan. Influenza Other Respir Viruses. 2023;17:e13094. https://doi.org/10.1111/irv.13094
2. Ministry of Health, Labour, and Welfare of Japan. Health Center Real-time Information-sharing System (HER-SYS). 2023 [cited 2023 Oct 12]. https://www.mhlw.go.jp/stf/seisakunitsuite/bunya/0000121431_00129.html
3. Wiegand RE, Deng Y, Deng X, Lee A, Meyer WA III, Letovsky S, et al. Estimated SARS-CoV-2 antibody seroprevalence trends and relationship to reported case prevalence from a repeated, cross-sectional study in the 50 states and the District of Columbia, United States—October 25, 2020–February 26, 2022. Lancet Reg Health Am. 2023;18:100403. https://doi.org/10.1016/j.lana.2022.100403
4. Ministry of Health, Labour, and Welfare of Japan. Seroprevalence of SARS-CoV-2. 2023 [cited 2023 Oct 12]. https://www.mhlw.go.jp/stf/seisakunitsuite/bunya/0000121431_00132.html
5. Kinoshita R, Arashiro T, Kitamura N, Arai S, Takahashi K, Suzuki T, et al. Infection-induced SARS-CoV-2 seroprevalence among blood donors, Japan, 2022. Emerg Infect Dis. 2023;29:1868–71. https://doi.org/10.3201/eid2909.230365
6. Axfors C, Ioannidis JPA. Infection fatality rate of COVID-19 in community-dwelling elderly populations. Eur J Epidemiol. 2022;37:235–49.
7. Ahmed A, DeWitt ME, Dantuluri KL, Castri P, Buahin A, LaGarde WH, et al.; COVID-19 Community Research Partnership. Characterisation of infection-induced SARS-CoV-2 seroprevalence amongst children and adolescents in North Carolina. Epidemiol Infect. 2023;151:e63. https://doi.org/10.1017/S0950268823000481
8. Clarke KEN, Kim Y, Jones J, Lee A, Deng Y, Nycz E, et al. Pediatric infection-induced SARS-CoV-2 seroprevalence increases and seroprevalence by type of clinical care—September 2021 to February 2022. J Infect Dis. 2023;227:364–70. https://doi.org/10.1093/infdis/jiac423
9. Government of Japan. Act on the prevention of infectious diseases and medical care for patients with infectious diseases. Act no. 114 of 1998. [cited 2024 Feb 20]. https://elaws.e-gov.go.jp/document?lawid=410AC0000000114
10. Gideon L. Handbook of survey methodology for the social sciences. New York: Springer; 2012.
11. Ministry of Health, Labour, and Welfare of Japan. About COVID-19 vaccination. 2023 [cited 2023 Oct 16]. https://www.mhlw.go.jp/content/10900000/001132657.pdf
12. Shook LL, Atyeo CG, Yonker LM, Fasano A, Gray KJ, Alter G, et al. Durability of anti-spike antibodies in infants after maternal COVID-19 vaccination or natural infection. JAMA. 2022;327:1087–9. https://doi.org/10.1001/jama.2022.1206
13. Navaratnam AMD, Shrotri M, Nguyen V, Braithwaite I, Beale S, Byrne TE, et al.; Virus Watch Collaborative. Nucleocapsid and spike antibody responses following virologically confirmed SARS-CoV-2 infection: an observational analysis in the Virus Watch community cohort. Int J Infect Dis. 2022;123:104–11. https://doi.org/10.1016/j.ijid.2022.07.053
14. Loesche M, Karlson EW, Talabi O, Zhou G, Boutin N, Atchley R, et al. Longitudinal SARS-CoV-2 nucleocapsid antibody kinetics, seroreversion, and implications for seroepidemiologic Studies. Emerg Infect Dis. 2022;28:1859–62. https://doi.org/10.3201/eid2809.220729
15. Swartz MD, DeSantis SM, Yaseen A, Brito FA, Valerio-Shewmaker MA, Messiah SE, et al. Antibody duration after infection from SARS-CoV-2 in the Texas Coronavirus Antibody Response Survey. J Infect Dis. 2023;227:193–201. https://doi.org/10.1093/infdis/jiac167

Address for correspondence: Daisuke Yoneoka or Tadaki Suzuki, National Institute of Infectious Diseases, 1-23-1 Toyama, Shinjuku-Ku, Tokyo 162-0052, Japan; email: yoneoka@niid.go.jp, tksuzuki@niid.go.jp

Antibodies to Influenza A(H5N1) Virus in Hunting Dogs Retrieving Wild Fowl, Washington, USA

Justin D. Brown, Adam Black, Katherine H. Haman, Diego G. Diel, Vickie E. Ramirez, Rachel S. Ziejka, Hannah T. Fenelon, Peter M. Rabinowitz, Lila Stevens, Rebecca Poulson, David E. Stallknecht

We detected antibodies to H5 and N1 subtype influenza A viruses in 4/194 (2%) dogs from Washington, USA, that hunted or engaged in hunt tests and training with wild birds. Historical data provided by dog owners showed seropositive dogs had high levels of exposure to waterfowl.

Since 1996, goose/Guangdong lineage H5 highly pathogenic influenza A viruses (HPIAV) have caused an unprecedented panzootic. In 2020, subclade 2.3.4.4b HPIAV H5N1 emerged and spread to multiple continents causing substantial death in poultry and wild birds. Recently, increased detection in mammals has stimulated concern that the virus might be adapting to mammal hosts.

Despite the prolonged global epizootic of HPIAV H5N1, reported infections in dogs have been rare. During an HPIAV H5N1 outbreak in Thailand, a fatal canine infection in 2004 associated with a dog eating a duck carcass was reported (*1*). A follow-up serosurvey of outwardly healthy stray dogs in Thailand detected HPIAV H5N1 antibodies in 25.4% (160/629) of sampled dogs (*2*). During April 2023, another fatal HPIAV H5N1 infection was identified in Ontario, Canada, in a dog that developed severe respiratory and systemic signs shortly after chewing on a dead wild goose (*3*). In experiments, beagles were susceptible to HPIAV H5N1 infections, during which some infected dogs excreted high concentrations of virus through the respiratory tract and experienced severe disease (*4*). In contrast, previous studies in beagles reported susceptibility to HPIAV H5N1 infection that manifested with moderate to no clinical signs (*5*,*6*). Existing field and experimental data collectively suggest dogs are susceptible to HPIAV H5N1 infection but clinical outcomes vary. However, infection appears to be restricted to dogs with high virus exposure. To investigate this further, we tested for antibodies to influenza A(H5N1) virus in bird hunting dogs, a category of dogs at high risk for contact with HPIAV H5N1–infected wild birds, and compared serologic results to reported hunting or training activities.

Dog owners completed a questionnaire providing details about their dogs' retrieving activities, canine influenza virus (CIV) vaccination status, and clinical history. Methods used in this research were approved by the Institutional Animal Care and Use Committee at Penn State University (#202302394).

The Study

During March–June 2023 in Washington, USA, we collected blood samples from 194 dogs identified by owners as having engaged in bird hunting or bird hunt tests and training over the previous 12 months (Figure). Waterfowl hunting season in Washington extends from mid-October through February; consequently, we collected samples 1–4 months after season closure. We collected blood from the jugular vein, immediately centrifuged it, and stored it at 4°C in the field, then stored serum at –20°C until testing was performed.

We screened serum samples for antibodies to influenza A virus (IAV) nucleoprotein using an

Author affiliations: Pennsylvania State University, University Park, Pennsylvania, USA (J.D. Brown, L. Stevens); Adam Black Veterinary Services, Anacortes, Washington, USA (A. Black); Washington Department of Fish and Wildlife, Olympia, Washington, USA (K.H. Haman); Cornell University College of Veterinary Medicine, Ithaca, New York, USA (D.G. Diel); University of Washington, Seattle, Washington, USA (V.E. Ramirez, R.S. Ziejka, H.T. Fenelon, P.M. Rabinowitz); University of Georgia College of Veterinary Medicine, Athens, Georgia, USA (R. Poulson, D.E. Stallknecht)

DOI: https://doi.org/10.3201/eid3006.231459

MultiS-Screen Ab blocking ELISA (bELISA; IDEXX, https://www.idexx.com), according to manufacturer instructions. We subsequently tested all bELISA-positive samples for antibodies to H5 using a hemagglutination inhibition (HI) assay and virus neutralization (VN), and to N1 with an enzyme-linked lectin assay (ELLA) using published protocols (*7*,*8*). In addition, we ran 11 bELISA-negative samples as negative field controls. In both the HI and VN assays, we used 2 reverse genetics antigens to detect antibodies to clade 2.3.4.4b H5 and North American H5 low pathogenic IAV. Antigens included IDCDC-RG71A containing Eurasia hemagglutinin (HA) and neuraminidase (NA) from A/Astrakhan/3212/2020(H5N8) on an A/Puerto Rico/8/1934(H1N1)(PR8) backbone and LP-RGBWT/TX that included North America HA and NA from A/blue-winged teal/AI12–4150/Texas/2012(H5N2) on a PR8 backbone. The HA of IDCDC-RG71A has a modified protease cleavage site consistent with a low pathogenic IAV phenotype. For the ELLA, we used A/ruddy turnstone/New Jersey/AI13-2948/2013(H10N1) as the antigen.

We used conservative positive threshold titers: H5 HI, >1:32; H5 VN, >1:20; and N1 ELLA, >1:80. We considered samples H5 seropositive if positive for H5 using HI assay or VN and N1 seropositive if positive for N1 using ELLA. We also tested all bELISA-positive serum samples for antibodies to H3N2 and H3N8 CIV by HI assay (positive threshold ≥1:8) (*9*). We calculated seroprevalence using R (*10*).

Most dogs retrieved waterfowl (86%), and many (69%) retrieved both waterfowl and upland game birds (Appendix Tables 1, 2, https://wwwnc.cdc.gov/EID/article/30/6/23-1459-App1.pdf). Dogs most commonly contacted dabbling ducks (81% of dogs), which are notable reservoirs for HPIAV H5N1. Dogs also frequently contacted birds from other categories considered high risk for HPIAV H5N1, including geese (32% of dogs) and diving ducks (23% of dogs) (Appendix Table 3). Most dogs had retrieved or trained multiple times during the previous 12

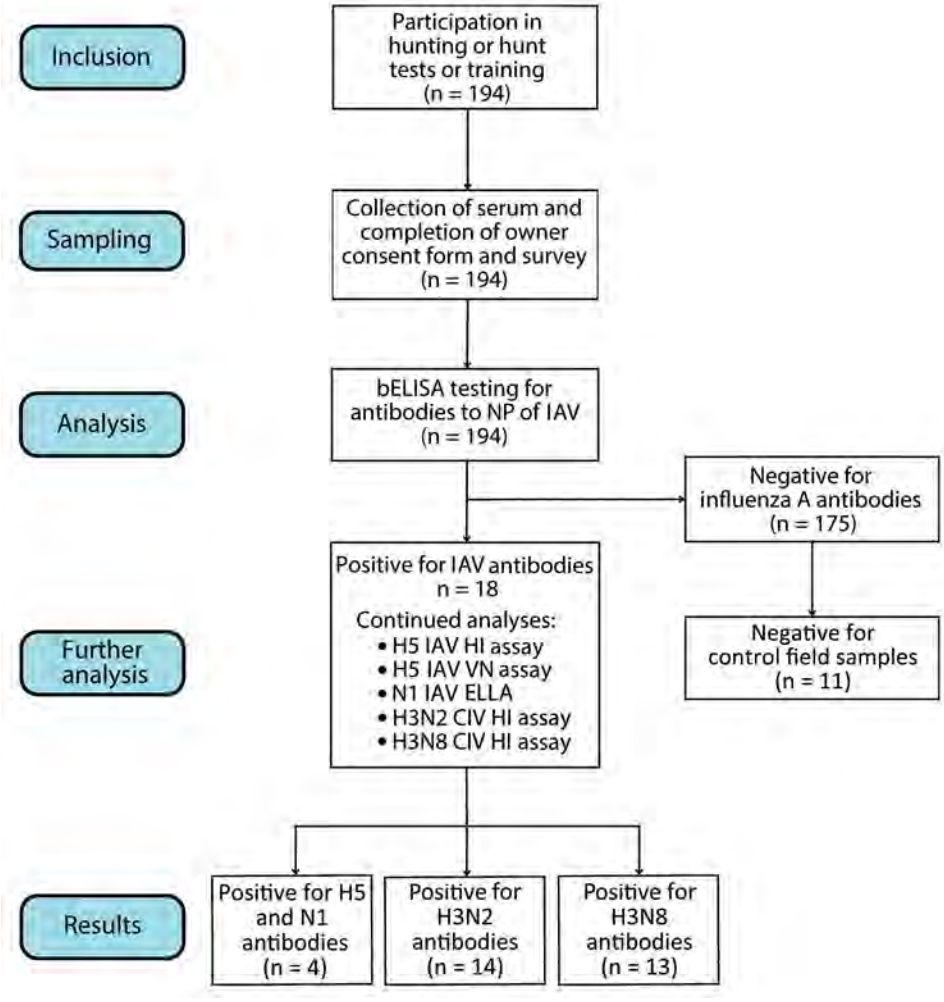

Figure. Flow diagram of participation in a serosurvey for antibodies to IAV in hunters and their hunting dogs, Washington, USA. CIV, canine influenza virus; ELLA, enzyme-linked lectin assay; HI, hemagglutination inhibition; IAV, influenza A virus; NP, nucleoprotein; VN, virus neutralization

Table. Data for individual hunting dogs that tested positive for antibodies to H5 and N1 influenza A virus, Washington, USA*

		Influenza A subtype-specific test results					
Dog ID	Mean S/N	HI rg BWT	HI rg AST H5 (titer)	VN rg AST H5	ELLA N1	HI-CIV H3N2	HI-CIV H3N8
HD23-21	0.275	Neg	+ (32)	–	+ (320)	+ (8)	–
HD23-30	0.345	Neg	–	+ (80)	+ (>2,560)	–	–
HD23-135	0.474	Neg	–	+ (40)	+ (>2,560)	–	–
HD23-139	0.375	Neg	+ (1:32)	+ (320)	+ (>1,280)	–	–

*Determined using AI MultiS-Screen AB blocking ELISA (IDEXX Laboratories, https://www.idexx.com), HI assay, virus neutralization, and ELLA. Positive threshold titers for the influenza A subtype-specific tests: H5 HI, >1:32; H5 VN, >1:20; N1 ELLA, >1:80; H3N2 and H3N8 CIV HI assay, ≥1:8. Negative antibody results based on the reported positive threshold titer for each assay. BWT, wild-type (wt) influenza B virus; CIV, canine influenza virus; ELLA, enzyme-linked lectin assay; HI, hemagglutination inhibition; ID, identifier; rg, reverse genetics; N1, A/ruddy turnstone/New Jersey/AI13–2948/2013(H10N1) antigen; rg AST, modified HA and NA antigen from A/Astrakhan/3212/2020(H5N8); rg BWT, HA and NA antigen from A/blue-winged teal/AI12-4150/Texas/2012(H5N2); S/N, ratio of sample to negative control absorbance values; VN, virus neutralization; –, negative antibody result.

months; 38% were reported to have been in the field during ≥15 hunts and 78% reported to have trained with live or dead birds ≥15 times (Appendix Table 2). Reportedly 11% of dogs retrieved dead or clinically ill waterfowl that showed no evidence of having been shot or hunted.

Antibodies to IAV were detected by bELISA in 18/194 (9.3%, 95% CI 5.6%–14.3%) dogs not displaying overt disease. Of the 18 bELISA-positive samples, 14 (77.8%, 95% CI 52.4%–93.6%) were seropositive for CIV H3N2 and 13 (72.2%, 95% CI 46.5%–90.3%) for CIV H3N8. The closeness of those results might have resulted from cross-reactivity between H3N2 and CIV H3N8. Of the 18 bELISA-positive dogs, 12 (66.7%, 95% CI 41.0%–86.7%) had reportedly been vaccinated for CIV. Four (22%, 95% CI 6.4%–47.6%) of the 18 were seropositive for H5 antibodies when tested using HI or VN and for N1 antibodies when tested using ELLA (Table). Two dogs were seropositive for H5 by HI and 3 dogs by VN, both using the IDCDC-RG71A antigen. No dogs had antibodies detectable above the positive threshold for H5 using the North America LP-RGBWT/TX antigen. Despite using an unmatched N1, all 4 H5-seropositive dogs tested positive for N1 antibodies using ELLA. Three of the H5- and N1-seropositive dogs had not been vaccinated for CIV and were negative for H3N2 and H3N8 antibodies. One H5- and N1-seropositive dog reportedly had been vaccinated in 2021 and had a low antibody titer to CIV H3N2 (1:8). All 11 bELISA-negative serum samples (i.e., negative controls) tested negative on HI and VN for antibodies to H5; however, 3 were seropositive for N1. The cause of the N1 seropositivity is unknown; however, serologic evidence of pandemic H1N1 infections in dogs has been previously reported, and additional testing is warranted (*11*).

Over the previous 12 months, all 4 H5- and N1-seropositive dogs reportedly had hunted waterfowl extensively in areas affected by H5N1 HPIAV outbreaks in wild waterfowl. Three H5- and N1-seropositive dogs reportedly had retrieved waterfowl that were either dead or had neurologic symptoms but that showed no evidence of having been shot or hunted. Two H5- and N1-seropositive dogs were from households that owned multiple hunting dogs included in this study; 1 seropositive dog was 1 of 2 dogs included in the study and the other was 1 of 3. None of the other tested dogs from those multidog households were seropositive for IAV.

Conclusions

We detected antibodies to H5 and N1 only in hunting dogs with high levels of bird hunting and waterfowl retrieval. Although that finding suggests transmission of HPIAV H5N1 from waterfowl to dogs can occur, low seroprevalence, lack of reported disease in seropositive dogs, and lack of evidence for dog-to-dog transmission among dogs sharing households collectively indicate that the subclade 2.3.4.4b HPIAV H5N1 strains that circulated in North America during 2022–2023 were poorly adapted to dogs. Those results suggest that effective risk communication with hunting dog owners could be an inexpensive and effective strategy to reduce the potential for spillover to dogs, and monitoring hunting dogs for IAV could be a useful addition to existing surveillance efforts.

Acknowledgments

We thank the sportsmen and sportswomen who collaborated on this project for allowing their dogs to be sampled for this research. We thank the Centers for Disease Control and Prevention and Daniel Perez, University of Georgia, for the reverse genetic H5 antigens used in this study.

This research was funded by Ducks Unlimited and a Pennsylvania State University College of Agricultural Sciences Undergraduate Research Grant. Laboratory work was also funded in part by the National Institute of Allergy and Infectious Diseases, National Institutes of Health, Department of Health and Human Services, under contract 75N93021C00016.

About the Author

Dr. Brown is an assistant teaching professor in the Department of Veterinary and Biomedical Sciences in the College of Agricultural Sciences at Pennsylvania State University. His research focuses on defining the impacts of infectious diseases on wildlife populations.

References

1. Songserm T, Amonsin A, Jam-on R, Sae-Heng N, Pariyothorn N, Payungporn S, et al. Fatal avian influenza A H5N1 in a dog. Emerg Infect Dis. 2006;12:1744–7. https://doi.org/10.3201/eid1211.060542
2. Butler D. Thai dogs carry bird-flu virus, but will they spread it? Nature. 2006;439:773. https://doi.org/10.1038/439773a
3. Canadian Food Inspection Agency. Domestic dog tests positive for avian influenza in Canada [cited 2023 Apr 24]. 2023. https://www.canada.ca/en/food-inspection-agency/news/2023/04/domestic-dog-tests-positive-for-avian-influenza-in-canada.html
4. Chen Y, Zhong G, Wang G, Deng G, Li Y, Shi J, et al. Dogs are highly susceptible to H5N1 avian influenza virus. Virology. 2010;405:15–9. https://doi.org/10.1016/j.virol.2010.05.024
5. Giese M, Harder TC, Teifke JP, Klopfleisch R, Breithaupt A, Mettenleiter TC, et al. Experimental infection and natural contact exposure of dogs with avian influenza virus (H5N1). Emerg Infect Dis. 2008;14:308–10. https://doi.org/10.3201/eid1402.070864
6. Maas R, Tacken M, Ruuls L, Koch G, van Rooij E, Stockhofe-Zurwieden N. Avian influenza (H5N1) susceptibility and receptors in dogs. Emerg Infect Dis. 2007;13:1219–21. https://doi.org/10.3201/eid1308.070393
7. Stallknecht DE, Fojtik A, Carter DL, Crum-Bradley JA, Perez DR, Poulson RL. Naturally acquired antibodies to influenza A virus in fall-migrating North American mallards. Vet Sci. 2022;9:214. https://doi.org/10.3390/vetsci9050214
8. Stallknecht DE, Kienzle-Dean C, Davis-Fields N, Jennelle CS, Bowman AS, Nolting JM, et al. Limited detection of antibodies to clade 2.3.4.4 A/goose Guandong/1/1996 lineage highly pathogenic H5 avian influenza virus in North American waterfowl. J Wildl Dis. 2020;56:47–57. https://doi.org/10.7589/2019-01-003
9. Anderson TC, Crawford PC, Katz JM, Dubovi EJ, Landolt G, Gibbs EPJ. Diagnostic performance of the canine influenza A virus subtype H3N8 hemagglutination inhibition assay. J Vet Diagn Invest. 2012;24:499–508. https://doi.org/10.1177/1040638712440992
10. Batra N, editor. The epidemiologist R handbook. Applied Epi; 2021. https://doi.org/10.5281/zenodo.4752646
11. Dundon WG, De Benedictis P, Viale E, Capua I. Serologic evidence of pandemic (H1N1) 2009 infection in dogs, Italy. Emerg Infect Dis. 2010;16:2019–21. https://doi.org/10.3201/eid1612.100514

Address for correspondence: Justin Brown, Pennsylvania State University, Department of Veterinary and Biomedical Sciences, 108D AVBS Bldg, University Park, PA 16802, USA; email: jdb56@psu.edu

Invasive Pulmonary Aspergillosis in Critically Ill Patients with Hantavirus Infection, Austria

Stefan Hatzl, Laura Scholz, Florian Posch, Philipp Eller, Alexander C. Reisinger, Martin Zacharias, Gregor Gorkiewicz, Martin Hoenigl, Ines Zollner-Schwetz, Robert Krause

We investigated a cohort of 370 patients in Austria with hantavirus infections (7.8% ICU admission rate) and detected 2 cases (cumulative incidence 7%) of invasive pulmonary aspergillosis; 1 patient died. Hantavirus-associated pulmonary aspergillosis may complicate the course of critically ill patients who have hemorrhagic fever with renal syndrome.

Hantaviruses are a large group of rodentborne single-stranded RNA viruses that cause clinical illness of varying severity in humans. Austria, and especially its southernmost federal states (Styria, Carinthia, and Burgenland), are endemic regions for the hantavirus puumala virus (PUUV), as well as for Dobrava/Belgrade virus (DOBV) in rare cases (*1*). Both hantavirus entities cause hemorrhagic fever with renal syndrome (HFRS); case-fatality rates of 0.1%–1% in PUUV patients and up to 12% in DOBV patients have been reported (*2*). HFRS is characterized by strong inflammation affecting vascular endothelial cells, leading to thrombocytopenia and potentially to disseminated intravascular coagulopathy. HFRS leads to renal failure of varying severity; half of patients develop respiratory symptoms. Hypoxia might lead to intensive care unit (ICU) admission for patients who need oxygen supply or organ support (*3*–*6*).

Invasive pulmonary aspergillosis (IPA) has been increasingly reported as a serious and potentially lethal complication in patients who require ICU treatment for severe influenza or COVID-19–associated acute respiratory failure. Although exact ICU admission rates and treatment characteristics (e.g., mechanical ventilation, hemodynamic shock) in the context of HFRS are lacking, hantaviruses have been shown to cause direct damage to the airway epithelium, potentially enabling aspergillus to invade tissue (*7*). We therefore speculated that there is a risk for invasive pulmonary aspergillosis (IPA) in critically ill patients with HFRS.

The Study

We performed a retrospective observational study, enrolling all consecutive adult patients with HFRS admitted to the ICU Medical University of Graz in Graz, Austria, during 2003–2023, and determined the rate of IPA. We screened all patients with clinical suspicion of HFRS and detection of PUUV or Hantaan virus (HTNV)/DOBV IgM by immunoassay (Reagena, https://www.reagena.com) (Appendix, https://wwwnc.cdc.gov/EID/article/30/6/23-1720.App1.pdf). All patient data were uniformly collected as described previously (*1*,*8*). The institutional review board of the Medical University of Graz approved the study (approval no. 33-329 ex 20/21), which we conducted in accordance with the Declaration of Helsinki (Version Fortaleza, 2013).

We classified the patients according to the European Confederation of Medical Mycology/International Society for Human & Animal Mycology consensus criteria for COVID-19–associated invasive pulmonary aspergillosis and influenza-associated pulmonary aspergillosis (*9*) by 2 infectious disease specialists who were blinded against the baseline characteristics. We performed all analyses using Stata version 16.1 (StataCorp., https://www.stata.com) and R version 4.0.5 (https://www.r-project.org). We reported continuous data as medians with 25th–75th percentiles; we summarized categorical data using

Author affiliations: Medical University of Graz, Graz, Austria (S. Hatzl, L. Scholz, F. Posch, P. Eller, A.C. Reisinger, M. Zacharias, G. Gorkiewicz, M. Hoenig, I. Zollner-Schwetz, R. Krause); BioTechMed-Graz, Graz (S. Hatzl, G. Gorkiewicz, M. Hoenigl, R. Krause)

DOI: http://doi.org/10.3201/eid3006.231720

absolute frequencies and percentages. We estimated median survival of the overall cohort by the reverse Kaplan–Meier method. We analyzed risks for development of hantavirus-associated pulmonary aspergillosis (HAPA) and death from any cause using competing risk cumulative incidence estimators.

Of 370 patients with HFRS, 29 (7.8%) were admitted to the ICU and therefore included in our study; median follow-up time was 4.3 years (Table 1). A total of 28/29 (96%) had PUUV-caused HFRS; 1 patient had DOBV-caused HFRS, confirmed by PCR. A total of 17/29 (59%) patients reported contact with rodents or rodent excreta. All patients had fever, 21/29 (72%) patients had headache and 13/29 (45%) had diarrhea. At ICU admission, the median sequential organ failure assessment (SOFA) score was 10 (7–15) and the median paO_2/FiO_2 ratio (Horowitz index) was 150 mm Hg (97–188 mm Hg). Almost all patients (27/29 [92%]) received oxygen supply upon ICU admission. A total of 19/29 (66%) patients received noninvasive ventilation support (Table 1). The remaining 9 patients received invasive mechanical ventilation; 3 received additional extracorporeal membrane oxygenation (ECMO). Hemodialysis was necessary in 19/29 (66%) patients. A total of 5 patients died during intensive care treatment, corresponding to a 10-day ICU survival of 86.2% (95% CI 67.3–94.5), 30-day ICU survival of 86.2% (67.3–94.5), and 90-day ICU survival of 82.7% (63.4%–92.4%). No patients died outside the ICU (Table 1; Appendix).

Table 1. Baseline characteristics of 29 hantavirus patients hospitalized in ICU, Graz, Austria*

Characteristic	Value
Age, y (range)	51 (44–65)
Sex	
F	5 (17)
M	24 (83)
BMI, kg/m^2 (range)	26.2 (24.1–28.1)
Known contact with rodents or rodent excreta	17 (59)
Signs and symptoms at diagnosis	
Headache	21 (72)
Eye pain	2 (7)
Fever ≥38.5°C (101.3°F)	29 (100)
Body temperature, °C (range)	39.5 (39.2–40.1)
Diarrhea	13 (45)
Abdominal pain	11 (38)
Kidney pain	3 (10)
Blurred vision	2 (8)
Time from first symptom to diagnosis, d	3 (1–4)
Median blood counts at diagnosis (range)	
Leukocytes, G/L	10.2 (6.9−14.7)
Neutrophils, G/L	8.2 (5.5−12.5)
Lymphocytes, G/L	0.7 (0.6–0.9)
Hemoglobin, g/dL	15.2 (11.4–17.5)
Platelets, G/L	58 (33–74)
Median laboratory results at diagnosis (range)	
Creatinine, mg/dL	4.2 (1.6–6.6)
eGFR, mL/min/l	16.3 (8.0–40.9)
Urea, mg/dL	117 (69−178)
C-reactive protein, mg/L	131 (95−176)
PCT, mg/L	8.5 (2.6−19.5)
Interleukin-6, pg/mL	151 (56–410)
Bilirubin, mg/dL	0.59 (0.5–0.8)
AST, U/L	46 (30–99)
ALT, U/L	46 (26–135)
LDH, U/L	390 (271–696)
Outcomes	
Proportion of HAPA	2 (6.9)
Deceased	5 (17)
Length of ICU stay, d (range)	4.5 (2.8−10.3)
Length of hospital stay, d (range)	13.0 (9.0–28.0)

*Values are no. (%) except as indicated. An expanded table is available online (https://wwwnc.cdc.gov/EID/article/30/06//23-1720-T1.htm). ALT, alanine aminotransferase; aPTT, activated prothrombin time; AST, aspartate aminotransferase; BMI, body mass index; COPD, chronic obstructive pulmonary disease; eGFR, estimated glomerular filtration rate; ICU, intensive care unit; LDH, lactate dehydrogenase.

We observed 2 cases of probable HAPA 2 days and 7 days after ICU admission with a total proportion of 6.9% (95% binomial exact CI 0.1–22.8) of patients during the ICU stay. One patient had PUUV and the other had DOBV infection. Their laboratory findings included positive bronchoalveolar lavage galactomannan >1.0 optical density index (2/2 patients), bronchoalveolar lavage culture growing *Aspergillus* species (2/2), and positive serum GM optical density >0.5 ODI (1/2), in addition to the other required parameters defining HAPA. Neither patient exhibited any notable concurrent conditions before ICU admission. Both patients received prednisolone, initiated after the first diagnostic test indicating pulmonary aspergillosis; daily dose was 1 mg/kg body weight for supportive treatment of acute respiratory failure (Table 2). The cumulative incidence of HAPA was 3.4% (95% CI 0.3–14.9) at 5 days, 7% (1.2–20.1) at 10 days, and 7% (1.2–20.1) at 90 days after ICU admission. After diagnosis of HAPA, we observed a 10-day ICU survival of 100%, 30-day survival of 100%, and 90-day survival of 50% (0.6%–91%) (Appendix).

Conclusions

We report invasive pulmonary aspergillosis as an infectious complication in critically ill patients with HFRS, without any classical risk factors for IPA. The 2 cases of HAPA observed in our study correspond to a cumulative incidence of invasive pulmonary aspergillosis of 7% in our ICU cohort, comprising 29 patients with HFRS. Of note, the corrected cumulative incidence rate including only patients with diagnostic tests for mold infections was 22.2% (95% CI 2.8%–60%).

During the COVID-19 pandemic and previous epidemic waves of influenza, secondary pulmonary mold infections and especially aspergillosis gained

Table 2. Characteristics of 2 patients with hantavirus pulmonary aspergillosis and mycological criteria, Graz, Austria*

Characteristic	Patient 1, DOBV infection	Patient 2, PUUV infection
EORTC risk factors	None	None
APACHE II score	36	26
Thoracic CT scan/radiograph	Bilateral dense infiltrates	Bilateral dense infiltrates
Steroids to treat pneumonia	Yes	Yes
Renal replacement therapy	Yes	Yes
Vasopressor	High-dose nordarenalin and vasopressin	High-dose nordarenalin and vasopressin
BAL *Aspergillus* culture	+	+
BAL *Aspergillus* qPCR	−	−
BAL galactomannan index	7,11	7,71
Serum *Aspergillus* qPCR	NA	NA
β-D-glucan, pg/mL	126	626
Serum galactomannan index	0.79	0.32
Mycologic criteria	4	3
Antifungal therapy	Voriconazole	Posaconazole
Outcome	Dead	Alive

*The table summarizes diagnostic and therapeutic characteristics of invasive pulmonary aspergillosis associated with hantavirus-disease. APACHE score, Acute Physiology and Chronic Health Evaluation score; BAL, bronchoalveolar lavage; CT, computed tomography; EORTC, European Organisation for Research and Treatment of Cancer; NA, not available; qPCR, quantitative PCR; +, positive; −, negative.

increasing attention (*9*–*11*). Previous studies investigating noninfluenza/non-COVID respiratory virus–associated invasive pulmonary aspergillosis nearly exclusively reported these co-infections in patients with well-known classical risk factors for IPA, mostly immunocompromised solid organ or hematopoietic stem cell transplant recipients (*12*–*14*). Those findings are in contrast with our findings for HFRS, in which neither of the 2 HAPA patients had underlying diseases predisposing to IPA or received immunosuppression before ICU admission. This fact is a major characteristic of HFRS patients who acquire their infections primarily during outdoor recreational activities or physical work in mouse-infested areas, thereby excluding almost all severely comorbid or immunocompromised persons (*2*). Therefore, we hypothesize that hantaviruses such as PUUV or DOBV may change the lung immune composition by viral pathogenic factors in a similar extent as COVID-19 or influenza to pave the way for *Aspergillus* infections.

The 2 patients of our cohort showed biomarkers indicative for IPA immediately after ICU admission. Therefore, if our findings are confirmed in larger studies, preemptive antifungal treatment or prophylaxis after ICU admission could be considered in intubated and mechanically ventilated hantavirus-infected patients. That possibility holds especially true for patients with acute respiratory failure requiring ECMO treatment or receiving corticosteroids, which both contribute to the risk for invasive mold infection (*11*,*15*).

This study's limitations include its retrospective design and nonstandardized investigation of respiratory samples. The incidence of HAPA might have been higher than reported here if we included only patients with more severe HFRS or if fungal biomarkers were incorporated into diagnoses in all cases. The incidence rates of invasive aspergillosis may also depend on environmental factors. Therefore, our results may probably differ from observations in other centers. Finally, the relatively small number of critically ill patients included here limited our ability to examine risk factors for HAPA; prospective multicenter studies are warranted. In the meantime, clinicians should remain aware that HAPA may complicate the course of illness in HFRS patients.

Author contributions: S.H. and R.K. designed the study. S.H. and R.K. collected clinical data. S.H. and F.P. performed the statistical analysis. S.H., M.H., I.Z., and R.K. analyzed results, S.H. and R.K. wrote the first draft of the manuscript. All authors reviewed the draft and approved the final version.

About the Author

Dr. Hatzl is an intensive care and hematology consultant at the Department of Internal Medicine at the Medical University of Graz, Austria. His primary research interests are emerging viral diseases and infectious diseases in critically ill and immunocompromised patients.

References

1. Hatzl S, Posch F, Linhofer M, Aberle S, Zollner-Schwetz I, Krammer F, et al. Poor prognosis for puumala virus infections predicted by lymphopenia and dyspnea. Emerg Infect Dis. 2023;29:1038–41. https://doi.org/10.3201/eid2905.221625
2. Avšič-Županc T, Saksida A, Korva M. Hantavirus infections. Clin Microbiol Infect. 2019;21:e6–16. https://doi.org/10.1111/1469-0691.12291
3. Koehler FC, Di Cristanziano V, Späth MR, Hoyer-Allo KJR, Wanken M, Müller RU, et al. The kidney in hantavirus infection—epidemiology, virology, pathophysiology, clinical presentation, diagnosis and management. Clin Kidney J. 2022;15:1231–52. https://doi.org/10.1093/ckj/sfac008

4. Riquelme R, Rioseco ML, Bastidas L, Trincado D, Riquelme M, Loyola H, et al. Hantavirus pulmonary syndrome, southern Chile, 1995–2012. Emerg Infect Dis. 2015;21:562–8. https://doi.org/10.3201/eid2104.141437
5. Du H, Li J, Jiang W, Yu H, Zhang Y, Wang J, et al. Clinical study of critical patients with hemorrhagic fever with renal syndrome complicated by acute respiratory distress syndrome. PLoS One. 2014;9:e89740. https://doi.org/10.1371/journal.pone.0089740
6. Rasmuson J, Lindqvist P, Sörensen K, Hedström M, Blomberg A, Ahlm C. Cardiopulmonary involvement in Puumala hantavirus infection. BMC Infect Dis. 2013;13:501. https://doi.org/10.1186/1471-2334-13-501
7. Rasmuson J, Pourazar J, Mohamed N, Lejon K, Evander M, Blomberg A, et al. Cytotoxic immune responses in the lungs correlate to disease severity in patients with hantavirus infection. Eur J Clin Microbiol Infect Dis. 2016;35:713–21. https://doi.org/10.1007/s10096-016-2592-1
8. Hatzl S, Reisinger AC, Posch F, Prattes J, Stradner M, Pilz S, et al. Antifungal prophylaxis for prevention of COVID-19–associated pulmonary aspergillosis in critically ill patients: an observational study. Crit Care. 2021;25:335–9. https://doi.org/10.1186/s13054-021-03753-9
9. Koehler P, Bassetti M, Chakrabarti A, Chen SCA, Colombo AL, Hoenigl M, et al.; European Confederation of Medical Mycology; International Society for Human Animal Mycology; Asia Fungal Working Group; INFOCUS LATAM/ISHAM Working Group; ISHAM Pan Africa Mycology Working Group; European Society for Clinical Microbiology; Infectious Diseases Fungal Infection Study Group; ESCMID Study Group for Infections in Critically Ill Patients; Interregional Association of Clinical Microbiology and Antimicrobial Chemotherapy; Medical Mycology Society of Nigeria; Medical Mycology Society of China Medicine Education Association; Infectious Diseases Working Party of the German Society for Haematology and Medical Oncology; Association of Medical Microbiology; Infectious Disease Canada. Defining and managing COVID-19–associated pulmonary aspergillosis: the 2020 ECMM/ISHAM consensus criteria for research and clinical guidance. Lancet Infect Dis. 2021;21:e149–62. https://doi.org/10.1016/S1473-3099(20)30847-1
10. Verweij PE, Rijnders BJA, Brüggemann RJM, Azoulay E, Bassetti M, Blot S, et al. Review of influenza-associated pulmonary aspergillosis in ICU patients and proposal for a case definition: an expert opinion. Intensive Care Med. 2020;46:1524–35. https://doi.org/10.1007/s00134-020-06091-6
11. Schauwvlieghe AFAD, Rijnders BJA, Philips N, Verwijs R, Vanderbeke L, Van Tienen C, et al.; Dutch-Belgian Mycosis Study Group. Invasive aspergillosis in patients admitted to the intensive care unit with severe influenza: a retrospective cohort study. Lancet Respir Med. 2018;6:782–92. https://doi.org/10.1016/S2213-2600(18)30274-1
12. Chang A, Musk M, Lavender M, Wrobel J, Yaw MC, Lawrence S, et al. Epidemiology of invasive fungal infections in lung transplant recipients in Western Australia. Transpl Infect Dis. 2019;21:e13085. https://doi.org/10.1111/tid.13085
13. Pappas PG, Alexander BD, Andes DR, Hadley S, Kauffman CA, Freifeld A, et al. Invasive fungal infections among organ transplant recipients: results of the Transplant-Associated Infection Surveillance Network (TRANSNET). Clin Infect Dis. 2010;50:1101–11. https://doi.org/10.1086/651262
14. Apostolopoulou A, Clancy CJ, Skeel A, Nguyen MH. Invasive pulmonary aspergillosis complicating noninfluenza respiratory viral infections in solid organ transplant recipients. Open Forum Infect Dis. 2021;8:ofab478.
15. Hatzl S, Kriegl L, Posch F, Schilcher G, Eller P, Reisinger A, et al. Early attainment of isavuconazole target concentration using an increased loading dose in critically ill patients with extracorporeal membrane oxygenation. J Antimicrob Chemother. 2023;78:2902–8. https://doi.org/10.1093/jac/dkad328

Address for correspondence: Robert Krause, Division of Infectious Diseases, Department of Internal Medicine, Medical University of Graz, Auenbruggerplatz 15, Austria; email: robert.krause@medunigraz.at

IMI-Type Carbapenemase-Producing *Enterobacter cloacae* Complex, France and Overseas Regions, 2012–2022

Cécile Emeraud, Delphine Girlich, Manon Deschamps, Inès Rezzoug, Aymeric Jacquemin, Agnès B. Jousset, Solène Lecolant, Lucy Locher, Aurélien Birer, Thierry Naas, Rémy A. Bonnin, Laurent Dortet

We characterized a collection of IMI-like–producing *Enterobacter* spp. isolates (n = 112) in France. The main clone corresponded to IMI-1–producing sequence type 820 *E. cloacae* subspecies *cloacae* that was involved in an outbreak. Clinicians should be aware of potential antimicrobial resistance among these bacteria.

The *Enterobacter cloacae* complex (ECC) is highly diverse; its many species and subspecies can be distinguished by using phenotypic methods or matrix-assisted laser desorption/ionization time-of-flight mass spectrometry. Whole-genome sequencing enables the precise determination of the bacterial species inside this complex; 22 species, including 6 subspecies, have been assigned to the ECC. IMI and NmcA, which are Ambler class A carbapenemases conferring antimicrobial resistance, are typically associated with the ECC (*1*), but they are rarely reported in other bacterial species (*2*,*3*) despite a worldwide distribution.

A total of 24 NmcA/IMI-type variants have been identified in accordance with the Beta-Lactamase DataBase (http://www.bldb.eu) (*4*). The $bla_{\text{IMI/NmcA}}$ genes can be either chromosome or plasmid encoded; bla_{NmcA}, $bla_{\text{IMI-1}}$, $bla_{\text{IMI-4}}$ and $bla_{\text{IMI-9}}$ have been described as chromosome encoded (*5*–*7*). The chromosome-encoded $bla_{\text{IMI/NmcA}}$ genes are usually described into XerC/XerD recombinase-dependent integrative mobile elements (IMEX) called *Eclo*IMEX elements. For all IMI producers, the genetic features showed an integration of *Eclo*IMEX structures at the same position between *setB* and *yeiP* genes. For chromosomal variant, the bla_{IMI} gene were mostly identified in *E. cloacae* subsp. *cloacae* as *E. bugandensis* or *E. ludwigii* strains (*6*,*8*,*9*). In contrast, the plasmid-encoded genes (such as $bla_{\text{IMI-2}}$ or $bla_{\text{IMI-6}}$) were mostly identified on a IncFII(Yp)-type plasmid in *E. asburiae* isolates (*3*,*6*,*10*). We characterized a large collection of IMI/NmcA producers collected in France.

The Study

We included all nonduplicate IMI-producing and NmcA-producing isolates showing antimicrobial resistance received at the French National Reference Center for Antimicrobial resistance (F-NRC) during 2012–2022 (n = 112) (Appendix 1 Table 1, https://wwwnc.cdc.gov/EID/article/30/6/23-1525-App1.xlsx). Mass spectrometry showed that all strains belonged to the ECC. Since 2014, each year, 3–20 IMI/NmcA producers were identified, representing 0.03%–0.91% of all carbapenemase-producing Enterobacterales analyzed at F-NRC. No IMI/NmcA producers were found before 2014. (Appendix 2 Figure 1, https://wwwnc.cdc.gov/EID/article/30/6/23-1525-App2.pdf).

Author affiliations: INSERM, Université Paris-Saclay, Le Kremlin-Bicêtre, France (C. Emeraud, D. Girlich, M. Deschamps, I. Rezzoug, A. Jacquemin, A.B. Jousset, T. Naas, R.A. Bonnin, L. Dortet); Associated French National Reference Center for Antibiotic Resistance: Carbapenemase-Producing Enterobacteriaceae, Le Kremlin-Bicêtre (C. Emeraud, D. Girlich, I. Rezzoug, A.B. Jousset, T. Naas, R.A. Bonnin, L. Dortet); Bicêtre Hospital, Assistance Publique-Hôpitaux de Paris, Le Kremlin-Bicêtre (C. Emeraud, I. Rezzoug, A.B. Jousset, S. Lecolant, L. Locher, T. Naas, L. Dortet); Microbes, Intestin, Inflammation et Susceptibilité de l'Hôte (M2iSH), INRAE (Institut national de recherche pour l'agriculture, l'alimentation et l'environnement), Clermont-Ferrand, France (A. Birer); Associated French National Reference Center for Antibiotic Resistance, CHU Gabriel-Montpied, Clermont-Ferrand (A. Birer)

DOI: http://doi.org/10.3201/eid3006.231525

Disc diffusion antimicrobial susceptibility testing revealed resistance to third-generation cephalosporins for 1 strain (257D9, overexpression of *ampC* confirmed with CLOXA agar) of the 112 tested. We determined MICs for last-resort antibiotics against highly resistant bacteria on 30 IMI/NmcA producers belonging to several sequence types (STs) (Appendix 1 Table 2). Relebactam restored imipenem activity for 67% of the strains and vaborbactam restored susceptibility to meropenem for all strains with lower MICs than imipenem/relebactam. Then, 37% of the tested strains were susceptible to colistin.

We performed WGS on the 112 IMI-/NmcA producers and identified 74 IMI-1 producers (Appendix 2 Figures 1, 2). Of those, 44 IMI-1-producing ECC were involved in an outbreak in Mayotte and La Réunion islands.

We confirmed ECC species identification using average nucleotide identity (ANI) calculation (Appendix 1 Table 3; Appendix 3, https://wwwnc.cdc.gov/EID/article/30/6/23-1525-App3.xlsx). *E. cloacae* subsp. cloacae was the most prevalent species (n = 56 [50.0%]) (Figure). Multilocus sequence typing (MLST) assigned 42 known unique STs for 105 strains. The 7 remaining isolates belonged to new or undetermined STs. Major STs (≥4 isolates) were ST820 (n = 45), ST250 (n = 5), ST657 (n = 5), ST1516 (n = 4), and ST1517 (n = 4) (Figure). Of note, 44 of the ST820 strains corresponded to the strain isolated in the Mayotte/La Réunion outbreak; the last IMI-1 *E. cloacae* subsp. *cloacae* of ST820, 193I8, was isolated in Paris and was not clonally related to the outbreak strains. That strain exposed >1,200 single-nucleotide polymorphisms (SNPs) corresponding with the other IMI-1 ECC ST820 isolates from Mayotte or La Réunion.

Genes encoding NmcA, IMI-1, IMI-4, IMI-12, and IMI-13 were localized on the chromosome, whereas those coding for IMI-2, IMI-6, IMI-17, IMI-19, IMI-25, IMI-26 and IMI-27 were carried on plasmids. We characterized genetic environments of $bla_{\text{IMI/NmcA}}$ genes using Illumina (https://illumina.com) and MinION long-read (Oxford Nanopore, https://nanoporetech.com) sequencing. All chromosome-encoded $bla_{\text{IMI/NmcA}}$ genes were located into a *Eclo*-IMEX-type genetic element (Appendix 2 Figure 4, panel A), except $bla_{\text{IMI-13}}$, which possessed a distinct genetic environment (Appendix 2 Figure 4, panel B). We detected already-characterized *Eclo*IMEX-type and 6 new variants, named *Eclo*IMEX-11–16 (Appendix 2 Figure 4, panel A). Those *Eclo*IMEX elements were ≈15–≈39.4-kb long, possessed a highly

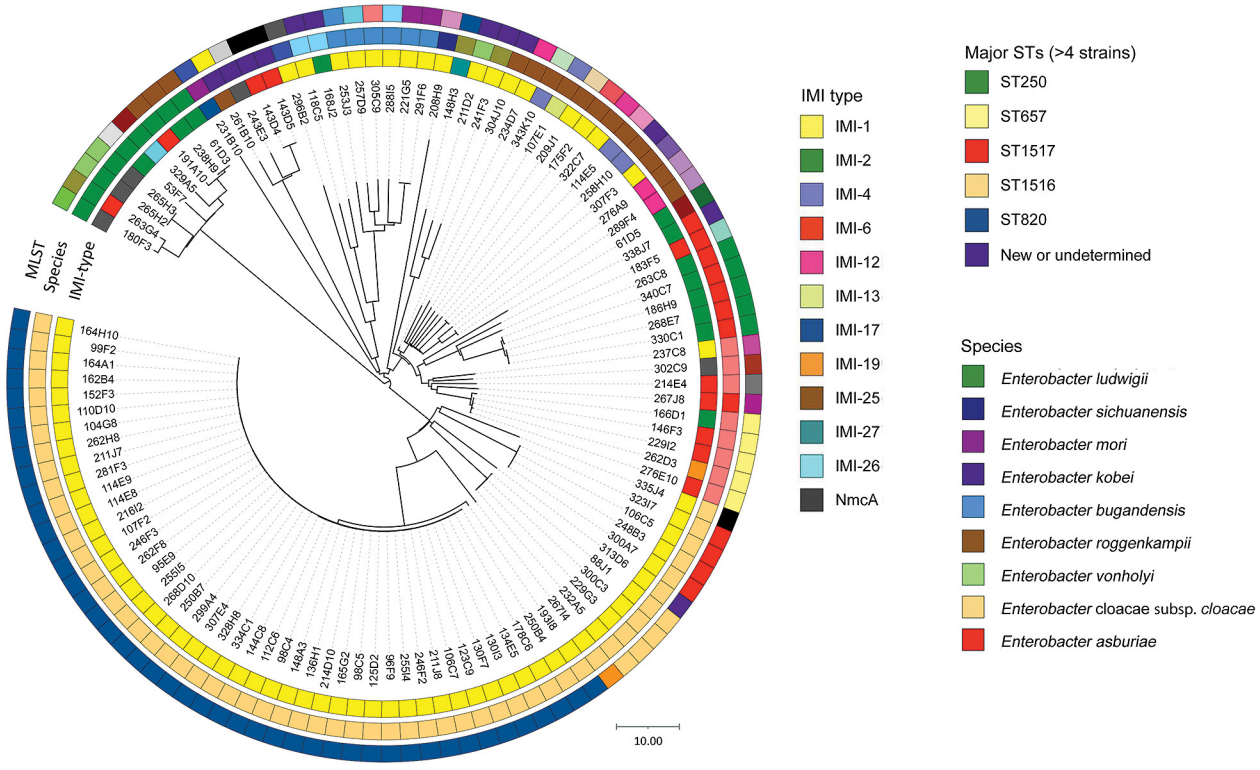

Figure. Phylogenetic relationship and global characterization of 112 IMI-producing *E. cloacae* complex received by the French National Reference Center, France, 2012–2022. The phylogenetic tree was built with a single-nucleotide polymorphism analysis approach from whole-genome sequencing data. MLST, multilocus sequence type; ST, sequence type.

conserved 5′ region, and were inserted between *setB* and *yieP* genes. We observed a strong correlation between bla_{NmcA} and *Eclo*IMEX-1. In contrast, we identified bla_{IMI-1} on 9 different *Eclo*IMEX elements. We saw no correlation between the *Enterobacter* species and the type of *Eclo*IMEX. The bla_{IMI-13} gene was inserted in the chromosome between genes encoding a hypothetical protein and an Inovirus-type Gp2 protein. We identified several complete or partially deleted insertion sequences (IS) close to bla_{IMI-13} (Appendix 2 Figure 4, panel B); however, the mechanism of bla_{IMI-13} acquisition is unclear.

All bla_{IMI-6} genes were carried on a IncFII(Yb)-type plasmid (160–200 kb) (Appendix 1 Table 4). Similarly, bla_{IMI-2} genes were carried on a IncFII(Yp)-type plasmid for 75% (8/12) of the IMI-2 producers. The plasmidic replicase was not identified in the 4 remaining IMI-2 producers. The long-read sequencing performed on strains producing new IMI variants enabled a more precise identification of plasmid type and size (Appendix 1 Table 4). The close genetic environments of the bla_{IMI} genes included several IS that differed according to the bla_{IMI} variants (Appendix 2 Figure 3). Conjugation experiments performed in *E. coli* J53 used as recipient strain confirmed those plasmids were conjugative except the 1 carrying bla_{IMI-17}.

We built an SNP matrix for the 44 IMI-1 *E. cloacae* subsp. *cloacae* ST820 isolates involved in the Mayotte/La Réunion outbreak to confirm their clonality. Those strains were closely related (1–62 SNPs between 2 isolates). We also performed a Bayesian analysis to estimate the date of the most recent ancestor and the evolutionary rate of that population. We estimated the evolutionary rate of the clone to 3.94×10^{-7} substitutions per site and per year (95% highest posterior density [HPD], $2.50–5.33 \times 10^{-7}$), corresponding to 1.63 SNPs per genome per year (95% HPD 1.04–2.21 SNPs). The common ancestor of the 44 IMI-1–producing *E. cloacae* subsp. *cloacae* ST820 isolates has an estimated date of 1994.7 (95% HPD 1990.8–2000.2) (Appendix 2 Figure 5).

Conclusions

Consistent with previous findings (*6*,*9*), our collection of IMI producers included uncommon species of ECC, such as *E. cloacae* subsp. *cloacae*, a rarely described species; IMI-1, IMI-2 and IMI-6 were the most prevalent variants. We identified no isolates of *E. hormaechei*, the most prevalent carbapenemase-producing ECC species (*11*,*12*).

Genetic environments and plasmid types of IMI-2 producers identified in this study were similar to those previously described (*2*,*3*,*13*); IncFII(Yp)-type plasmids were most common. The close genetic environment of bla_{IMI-2} observed in our isolates has been reported on a plasmid identified in *E. coli* (*2*). The genetic environment of bla_{IMI-6} was previously reported in an *E. cloacae* isolate described by Boyd et al. (*6*). Regarding the chromosome-encoded IMI and NmcA variants (n = 85), we described a variety of *Eclo*IMEX elements (n = 11) including 6 novel elements; that the same *Eclo*IMEX could be identified in different ECC species suggests that XerC/D recombinases enable the mobility of these $bla_{IMI-/NmcA}$–carrying *Eclo*IMEX structures specifically between ECC species. Finally, the evolution rate of the IMI-1–producing *E. cloacae* subsp. *cloacae* ST820 clone (1.63 SNPs/genome/year) is similar to the 0.5–3 SNPs/year for a genome reported for a population of multidrug-resistant ECC in the United Kingdom (*14*) and the 2.5–3 SNPs/year for a genome identified for ST171 and ST78 carbapenem-resistant ECC (*15*).

In conclusion, in IMI/NmcA producers in France, we observed a large diversity of ECC species, STs, genetic supports, and genetic environments. Future work should elucidate why *E. cloacae* subsp. *cloacae* is highly prevalent among IMI producers; why $bla_{IMI/NmcA}$-carrying plasmids were almost always found alone in IMI-producing isolates that always do not carry any other resistance genes; and whether *Eclo*IMEX genetic elements are mobilizable. Clinicians should remain aware of potential antimicrobial resistance among ECC species.

About the Author

Dr. Emeraud is assistant professor at the INSERM. Her main field of research interest includes epidemiology, genetics, and biochemistry of β-lactamases in Gram negatives.

References

1. Rasmussen BA, Bush K, Keeney D, Yang Y, Hare R, O'Gara C, et al. Characterization of IMI-1 beta-lactamase, a class A carbapenem-hydrolyzing enzyme from *Enterobacter cloacae*. Antimicrob Agents Chemother. 1996;40:2080–6. https://doi.org/10.1128/AAC.40.9.2080
2. Zhang F, Wang X, Xie L, Zheng Q, Guo X, Han L, et al. A novel transposon, Tn6306, mediates the spread of bla_{IMI} in Enterobacteriaceae in hospitals. Int J Infect Dis. 2017;65:22–6. https://doi.org/10.1016/j.ijid.2017.09.014
3. Hopkins KL, Findlay J, Doumith M, Mather B, Meunier D, D'Arcy S, et al. IMI-2 carbapenemase in a clinical *Klebsiella variicola* isolated in the UK. J Antimicrob Chemother. 2017;72:2129–31. https://doi.org/10.1093/jac/dkx103
4. Naas T, Oueslati S, Bonnin RA, Dabos ML, Zavala A, Dortet L, et al. Beta-lactamase database (BLDB)—structure and function. J Enzyme Inhib Med Chem. 2017;32:917–9. https://doi.org/10.1080/14756366.2017.1344235

5. Antonelli A, D'Andrea MM, Di Pilato V, Viaggi B, Torricelli F, Rossolini GM. Characterization of a novel putative Xer-dependent integrative mobile element carrying the bla_{NMC-A} carbapenemase gene, inserted into the chromosome of members of the *Enterobacter cloacae* complex. Antimicrob Agents Chemother. 2015;59:6620–4. https://doi.org/10.1128/AAC.01452-15
6. Boyd DA, Mataseje LF, Davidson R, Delport JA, Fuller J, Hoang L, et al. *Enterobacter cloacae* complex isolates harboring bla_{NMC-A} or bla_{IMI}-type class A carbapenemase genes on novel chromosomal integrative elements and plasmids. Antimicrob Agents Chemother. 2017;61:e02578-16. https://doi.org/10.1128/AAC.02578-16
7. Koh TH, Rahman NBA, Teo JWP, La MV, Periaswamy B, Chen SL. Putative integrative mobile elements that exploit the Xer recombination machinery carrying bla_{IMI}-type carbapenemase genes in *Enterobacter cloacae* complex isolates in Singapore. Antimicrob Agents Chemother. 2017;62:e01542–17.
8. Miltgen G, Bonnin RA, Avril C, Benoit-Cattin T, Martak D, Leclaire A, et al. Outbreak of IMI-1 carbapenemase-producing colistin-resistant *Enterobacter cloacae* on the French island of Mayotte (Indian Ocean). Int J Antimicrob Agents. 2018;52:416–20. https://doi.org/10.1016/j.ijantimicag.2018.05.015
9. Octavia S, Koh TH, Ng OT, Marimuthu K, Venkatachalam I, Lin RTP, et al. Genomic study of bla_{IMI}-positive *Enterobacter cloacae* complex in Singapore over a five-year study period. Antimicrob Agents Chemother. 2020;64:e00510-20. https://doi.org/10.1128/AAC.00510-20
10. Rotova V, Papagiannitsis CC, Chudejova K, Medvecky M, Skalova A, Adamkova V, et al. First description of the emergence of *Enterobacter asburiae* producing IMI-2 carbapenemase in the Czech Republic. J Glob Antimicrob Resist. 2017;11:98–9. https://doi.org/10.1016/j.jgar.2017.10.001
11. Peirano G, Matsumura Y, Adams MD, Bradford P, Motyl M, Chen L, et al. Genomic epidemiology of global carbapenemase-producing *Enterobacter* spp., 2008–2014. Emerg Infect Dis. 2018;24:1010–9. https://doi.org/10.3201/eid2406.171648
12. Emeraud C, Petit C, Gauthier L, Bonnin RA, Naas T, Dortet L. Emergence of VIM-producing *Enterobacter cloacae* complex in France between 2015 and 2018. J Antimicrob Chemother. 2022;77:944–51.
13. Rojo-Bezares B, Martín C, López M, Torres C, Sáenz Y. First detection of bla_{IMI-2} gene in a clinical *Escherichia coli* strain. Antimicrob Agents Chemother. 2012;56:1146–7. https://doi.org/10.1128/AAC.05478-11
14. Moradigaravand D, Reuter S, Martin V, Peacock SJ, Parkhill J. The dissemination of multidrug-resistant *Enterobacter cloacae* throughout the UK and Ireland. Nat Microbiol. 2016;1:16173. https://doi.org/10.1038/nmicrobiol.2016.173
15. Gomez-Simmonds A, Annavajhala MK, Wang Z, Macesic N, Hu Y, Giddins MJ, et al. Genomic and geographic context for the evolution of high-risk carbapenem-resistant *Enterobacter cloacae* complex clones ST171 and ST78. MBio. 2018;9:e00542–18. https://doi.org/10.1128/mBio.00542-18

Address for correspondence: Cécile Emeraud, Service de Bactériologie-Hygiène, Hôpital de Bicêtre, 78 rue du Général Leclerc, 94275 Le Kremlin-Bicêtre CEDEX, France; email: cecile.emeraud@aphp.fr

Evaluating Humoral Immunity Elicited by XBB.1.5 Monovalent COVID-19 Vaccine

Xammy Huu Nguyenla, Timothy A. Bates, Mila Trank-Greene, Mastura Wahedi, Fikadu G. Tafesse, Marcel E. Curlin

Authors affiliation: Oregon Health and Science University, Portland, Oregon, USA

DOI: https://doi.org/10.3201/eid3006.240051

Because novel SARS-CoV-2 variants continue to emerge, immunogenicity of XBB.1.5 monovalent vaccines against live clinical isolates needs to be evaluated. We report boosting of IgG (2.1×), IgA (1.5×), and total IgG/A/M (1.7×) targeting the spike receptor-binding domain and neutralizing titers against WA1 (2.2×), XBB.1.5 (7.4×), EG.5.1 (10.5×), and JN.1 (4.7×) variants.

A monovalent COVID-19 vaccine containing the XBB.1.5 variant SARS-CoV-2 spike protein was approved in September 2023, but uptake has been hesitant (*1*). Evaluating the immunogenicity of variant-adapted vaccines could inspire trust in COVID-19 immunization, especially as neutralization-evading variants such as JN.1 emerge. Studies have demonstrated induction of antibodies capable of neutralizing variant spike proteins (*2*–*4*), but those studies used pseudo-typed virus that recombinantly expressed variant spike proteins, not true SARS-CoV-2. We evaluated immunogenicity of XBB.1.5 vaccination in humans by using live SARS-CoV-2 clinical isolates to capture the biology of virus neutralization.

During October–November 2023, we recruited healthcare workers at Oregon Health and Science University (OHSU) in Portland, Oregon, USA. We collected paired serum samples from participants: 1 on the day XBB.1.5 monovalent booster vaccine (Moderna, https://www.modernatx.com) was administered, and 1 ≈21 days after vaccination. To identify recent infection, we used ELISA to detect nucleocapsid antibodies. We used 50% ELISA effective concentrations to determine IgG, IgA, IgM, and total IgG/A/M titers against the ancestral spike receptor binding domain (RBD) (Appendix, https://wwwnc.cdc.gov/EID/article/30/6/24-0051-App1.pdf). We determined SARS-CoV-2 neutralizing antibody titers by using 50% focus reduction neutralization tests against the ancestral (wild-type) strain and XBB.1.5, EG.5.1, and JN.1 variants (Figure, panel A). We used restricted effect maximum-likelihood model or repeated analysis of variance measures with Šídák's multiple comparison tests to calculate p values and considered $p<0.05$ statistically significant. The OHSU institutional review board approved this study, and participants provided written informed consent.

We enrolled 55 participants, 37 (67%) female and 18 (33%) male; mean age was 53 years. Eleven (20%) preboost samples and 15 (27%) postboost samples were positive for nucleocapsid antibodies. We included those samples to demonstrate generalized boosting in a population with heterogenous exposure history; however, removing those participants from analysis resulted in similar antibody induction by XBB.1.5 vaccination (Appendix Figure, panels A, B). The XBB.1.5 vaccine boosted total serum spike RBD–specific IgG/A/M; after boosting, geometric mean titers (GMT) rose 1.7-fold from 293 (95% CI 195–442) to 174 (95% CI 124–244) ($p<0.0001$). IgG isotypes demonstrated a greater increase than IgA isotypes (IgG postboost GMT 267 [95% CI 196–363], preboost GMT 130 [95% CI 95.7–176], a 2.1-fold change [$p<0.0001$]; IgA postboost GMT 96.1 [95% CI 74.6–124], preboost GMT 62.8 [95% CI 50.3–78.3], a 1.5-fold change [$p = 0.0002$]). The reason for this difference is unclear. IgM isotypes trended toward a slight increase, likely because IgM is short-lived; postboost GMT was 76.6 (95% CI 57.6–102) versus preboost GMT 57.1 (95% CI 44.5–73.2), a 1.3-fold change ($p = 0.1548$) (Figure, panel B). Of note, the XBB.1.5 vaccine boosted neutralizing titers against the wild-type strain; postboost GMT was 11,905 (95% CI 8,454–16,766) versus preboost GMT 5,518 (95% CI 3,899–7,809), a 2.1-fold change ($p<0.0001$). The vaccine also boosted neutralizing titers against the vaccine-matched XBB.1.5 variant; postboost GMT was 838 (95% CI 548–1,281) versus preboost GMT 114 (95% CI 80.9–162), a 7.4-fold change ($p<0.0001$). In addition, the vaccine boosted neutralizing titers against EG.5.1 by 10.5 fold (postboost GMT 824 [95% CI 518–1,311] vs. preboost GMT 78.3 [95% CI 55.0–112]; ($p<0.0001$), and the JN.1 variant by 4.7 fold (postboost GMT 361 [95% CI 270–483] vs. preboost GMT 77.6 [95% CI 60.7–99.2]; $p<0.0001$) (Figure, panel C).

To assess changes in the proportion of serum antibodies with neutralizing capacity, we divided the serum neutralizing titer against each variant by the total IgG/A/M titer to produce a neutralizing potency index (NPI). The NPI against wild-type strain was unchanged by XBB.1.5 monovalent vaccination. That finding is likely explained by preexisting neutralizing immunity that is dominated by responses against ancestral epitopes. However,

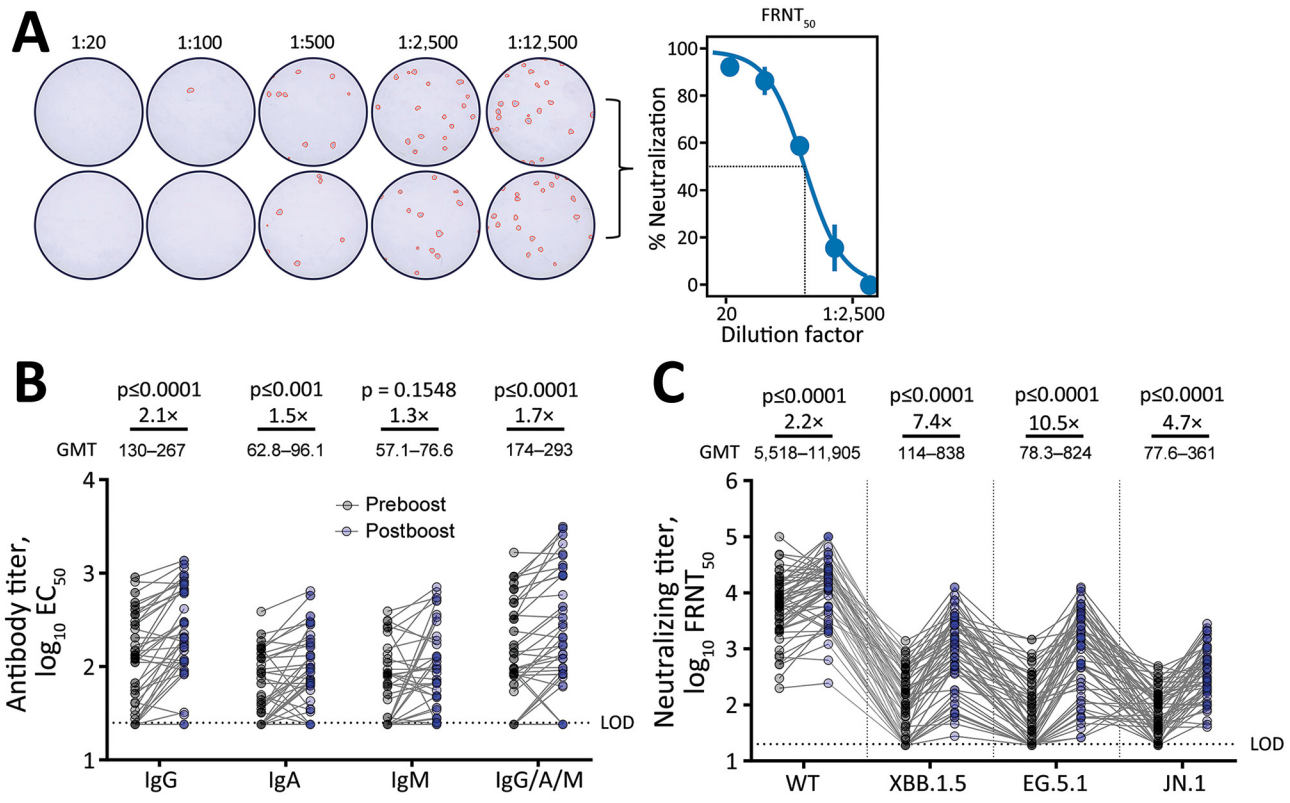

Figure. SARS-CoV-2 antibody titers in an evaluation of humoral immunity elicited by XBB.1.5 monovalent COVID-19 vaccine. A) Duplicate wells infected with live SARS-CoV-2 virus at serially diluted titers. OD was measured at 492 nm using a CLARIOstar plate reader (BMG LABTECH, https://www.bmglabtech.com). Wells were stained and counted to create representative $FRNT_{50}$ curve at right. B) Preboost and postboost serum antibody isotype titers against spike RBD. C) Neutralizing titers against live ancestral (WT) SARS-CoV-2 and variants. GMT for each bar was calculated in Prism (GraphPad Software Inc., https://www.graphpad.com). All individual data points are displayed as filled circles. Boost ratios were calculated by dividing the post-XBB.1.5 vaccination GMT (postboost) by pre-vaccination GMT (preboost). Reported p values were calculated using restricted effect maximum-likelihood model (B) or 1-way repeated measures analysis of variance (C) with Šídák's multiple comparisons tests. EC_{50}, 50% ELISA effective concentration; $FRNT_{50}$, 50% focus reduction neutralization; GMT, geometric mean titer; LOD, lower limit of detection; OD, optical density; WT, wild-type.

the XBB.1.5 vaccine elicited an NPI increase against XBB.1.5, EG.5.1, and JN.1 variants (Appendix Figure, panel C).

Our results demonstrated that, before vaccination, persons have low titers of antibodies capable of neutralizing XBB.1.5, EG.5.1, and JN.1, and that the XBB.1.5 monovalent vaccine increases the capacity of serum antibodies to neutralize contemporary variants. IgG, IgA, and total IgG/A/M titers were boosted, which likely includes expansion of a nonneutralizing compartment may influence disease severity and longer-term protection through Fc effector functions (*5*). Indeed, the XBB.1.5 monovalent vaccine was reported to reduce risk for COVID-19 hospitalization by 76.1% in Denmark (*6*). In the United States, an analysis of 2 vaccine effectiveness data networks estimated 52% (95% CI 47%–57%) and 43% (27%–56%) vaccine effectiveness against hospitalization (*7*).

In summary, these data provide direct evidence for immunogenicity of XBB.1.5 monovalent vaccines against SARS-CoV-2 variants and supports public health recommendations to stay current with adapted COVID-19 vaccines. Neutralizing antibodies were boosted against the wild-type, vaccine-matched, and emergent strains, suggesting that updated vaccines enhance protection against infection by historic and novel variants.

This article was preprinted at https://www.medrxiv.org/content/10.1101/2024.03.25.24304857v1.

Acknowledgments

We thank the many participants in this study for their generous contributions. We also gratefully acknowledge the efforts of the entire Oregon Health and Science University COVID-19 serology study team.

This work was funded in part by National Institutes of Health (grant no. R01AI141549 to F.G.T.).

About the Author

Mr. Nguyenla is an MD/PhD candidate at Oregon Health and Science University in Portland, Oregon, USA. His main research interest is humoral responses to COVID-19 vaccines.

References

1. Centers for Disease Control and Prevention. COVID-19 vaccine uptake and CDC's commitment to vaccine equity [cited 2024 Jan 10]. https://www.cdc.gov/respiratory-viruses/whats-new/vaccine-equity.html
2. Stankov MV, Hoffmann M, Gutierrez Jauregui R, Cossmann A, Morillas Ramos G, Graalmann T, et al. Humoral and cellular immune responses following BNT162b2 XBB.1.5 vaccination. Lancet Infect Dis. 2024;24:e1–3. https://doi.org/10.1016/S1473-3099(23)00690-4
3. Patel N, Trost JF, Guebre-Xabier M, Zhou H, Norton J, Jiang D, et al. XBB.1.5 spike protein COVID-19 vaccine induces broadly neutralizing and cellular immune responses against EG.5.1 and emerging XBB variants. Sci Rep. 2023;13:19176. https://doi.org/10.1038/s41598-023-46025-y
4. Wang Q, Guo Y, Bowen A, Mellis IA, Valdez R, Gherasim C, et al. XBB.1.5 monovalent mRNA vaccine booster elicits robust neutralizing antibodies against XBB subvariants and JN.1. Cell Host Microbe. 2024;32:315–321.e3. https://doi.org/10.1016/j.chom.2024.01.014
5. Chakraborty S, Gonzalez JC, Sievers BL, Mallajosyula V, Chakraborty S, Dubey M, et al. Early non-neutralizing, afucosylated antibody responses are associated with COVID-19 severity. Sci Transl Med. 2022;14:eabm7853. https://doi.org/10.1126/scitranslmed.abm7853
6. Hansen CH, Moustsen-Helms IR, Rasmussen M, Søborg B, Ullum H, Valentiner-Branth P. Short-term effectiveness of the XBB.1.5 updated COVID-19 vaccine against hospitalisation in Denmark: a national cohort study. Lancet Infect Dis. 2024;14:e73–4. https://doi.org/10.1016/S1473-3099(23)00746-6
7. DeCuir J, Payne AB, Self WH, Rowley EAK, Dascomb K, DeSilva MB, et al.; CDC COVID-19 Vaccine Effectiveness Collaborators. Interim effectiveness of updated 2023–2024 (monovalent XBB.1.5) COVID-19 vaccines against COVID-19–associated emergency department and urgent care encounters and hospitalization among immunocompetent adults aged ≥18 years—VISION and IVY networks, September 2023–January 2024. MMWR Morb Mortal Wkly Rep. 2024;73:180–8. https://doi.org/10.15585/mmwr.mm7308a5

Address for correspondence: Fikadu G. Tafesse or Marcel E. Curlin, Oregon Health and Science University, 3181 SW Sam Jackson Park Rd, Portland, OR 97239, USA; email: tafesse@ohsu.edu or curlin@ohsu.edu

Novel Avian Influenza A(H5N6) Virus in Wild Birds, South Korea, 2023

Andrew Yong Cho,[1] Young-Jae Si,[1] Dong-Ju Kim,[1] Ye-Ram Seo, Dong-Yeop Lee, Daehun Kim, Dongbin Lee, Yaemoon Son, Hyesung Jeong, Chang-Seon Song, Dong-Hun Lee

Author affiliations: Wildlife Health Laboratory, Seoul, South Korea (A.Y. Cho, Y.-R. Seo, D.-Y. Lee, D.-H. Lee); Avian Disease Laboratory, Seoul (A.Y. Cho, Y.-R. Seo, C.-S. Song); National Institute of Wildlife Disease Control and Prevention, Gwangju, South Korea (Y.-J. Si, D.-J. Kim, D. Kim, D. Lee, Y. Son, H. Jeong); Konkuk University Zoonotic Disease Research Center, Seoul (C.-S. Song, D.-H. Lee)

DOI: https://doi.org/10.3201/eid3006.240192

We isolated novel reassortant avian influenza A(H5N6) viruses containing genes from clade 2.3.4.4b H5N1 virus and low pathogenicity avian influenza viruses in carcasses of whooper swans and bean geese in South Korea during December 2023. Neuraminidase gene was from a clade 2.3.4.4b H5N6 virus infecting poultry and humans in China.

Infection caused by highly pathogenic avian influenza viruses (HPAIVs) have caused major economic losses in the poultry industry and pose a serious threat to public health. The A/goose/Guangdong/1/1996 (gs/GD) lineage of H5 HPAIV emerged in China in 1996 and diverged into 10 genetically independent hemagglutinin (HA) clades (0–9) and subclades (*1*). The gs/GD lineage of H5 HPAIV has caused outbreaks worldwide, infecting a range of wildlife, poultry, and humans (*1*). Clade 2.3.4.4 H5Nx HPAIV containing multiple neuraminidase (NA) subtypes (*2*) has dominated outbreaks worldwide from 2014 onwards and further divided into subclades 2.3.4.4a–h (*3*). Currently, clade 2.3.4.4b H5N1 HPAIV is predominant globally after causing outbreaks in Europe in the fall of 2020 and in Africa, the Americas, Asia, and Antarctica (*4*–*7*).

During October 2022–March 2023, a total of 16 different genotypes of H5N1 2.3.4.4b HPAIV caused outbreaks in South Korea, including 174 cases in wild birds (*8*). Based on the available surveillance data, no new virus incursions have occurred in South Korea during summer and fall 2023. National surveillance

[1]These authors contributed equally to this article.

Table. Nucleotide sequence identities between gene segments of novel clade 2.3.4.4b highly pathogenic avian influenza A(H5N6) virus isolate A/whooper_swan/Korea/23WC075/2023 from South Korea and nearest top 3 homologs in the GISAID EpiFlu database*

Gene	Top 3 query	Accession no.	Nucleotide identity	% Identity
PB2	A/peregrine falcon/Saga/4112A002/2023 (A/H5N6) segment 1 (PB2)	EPI2898974	2280/2280	100.00
	A/environment/chongqing/1795/2023 (A/H9N2) segment 1 (PB2)	EPI2841012	2271/2280	99.61
	A/environment/Kagoshima/KU-I6/2021 (H4N6) (A/H4N6) segment 1 (PB2)	EPI2553141	2253/2280	98.82
PB1	A/peregrine falcon/Saga/4112A002/2023 (A/H5N6) segment 2 (PB1)	EPI2898975	2273/2274	99.96
	A/egret/Korea/22WC394/2023 (A/H5N1) segment 2 (PB1)	EPI2743089	2271/2274	99.87
	A/common buzzard/Korea/22WC336/2023 (A/H5N1) segment 2 (PB1)	EPI2742993	2271/2274	99.87
PA	A/peregrine falcon/Saga/4112A002/2023 (A/H5N6) segment 3 (PA)	EPI2898976	2150/2151	99.95
	A/common teal/Amur region/92b/2020 (A/H6N2) segment 3 (PA)	EPI1849993	2142/2151	99.58
	A/mallard/Russia Primorje/94T/2020 (A/H1N1) segment 3 (PA)	EPI1849961	2141/2151	99.54
HA	A/peregrine falcon/Saga/4112A002/2023 (A/H5N6) segment 4 (HA)	EPI2898977	1700/1704	99.77
	A/environment/Kagoshima/KU-G4/2022 (H5N1) (A/H5N1) segment 4 (HA)	EPI2789597	1697/1704	99.59
	A/environment/Kagoshima/KU-D4/2022 (H5N1) (A/H5N1) segment 4 (HA)	EPI2789589	1697/1704	99.59
NP	A/peregrine falcon/Saga/4112A002/2023 (A/H5N6) segment 5 (NP)	EPI2898978	1496/1497	99.93
	A/gadwall/Novosibirsk region/3407k/2020 (A/H4N6) segment 5 (NP)	EPI1849870	1479/1497	98.80
	A/mallard/Novosibirsk region/3286k/2020 (A/H4N6) segment 5 (NP)	EPI1849878	1478/1497	98.73
NA	A/peregrine falcon/Saga/4112A002/2023 (A/H5N6) segment 6 (NA)	EPI2898979	1377/1380	99.78
	A/duck/Hunan/S40199/2021(H5N6) (A/H5N6) segment 6 (NA)	EPI1997201	1360/1380	98.55
	A/Changsha/1/2022 (A/H5N6) segment 6 (NA)	EPI2287050	1359/1380	98.48
M	A/peregrine falcon/Saga/4112A002/2023 (A/H5N6) segment 7 (MP)	EPI2898980	982/982	100.00
	A/northern pintail/Kagoshima/KU-64/2022 (H5N1) (A/H5N1) segment 7 (MP)	EPI2794001	980/982	99.80
	A/environment/Kagoshima/KU-B4/2022 (H5N1) (A/H5N1) segment 7 (MP)	EPI2789385	980/982	99.80
NS	A/peregrine falcon/Saga/4112A002/2023 (A/H5N6) segment 8 (NS)	EPI2898981	837/838	99.88
	A/bean goose/Korea/KNU-10/2022 (A/H10N7) segment 8 (NS)	EPI2873490	836/838	99.76
	A/bean goose/Korea/KNU-14/2022 (A/H6N1) segment 8 (NS)	EPI2873460	836/838	99.76

*GISAID, https://www.gisaid.org; HA, hemagglutinin; P, matrix; NA, neuraminidase; NP, nucleoprotein; NS, nonstructural; PA, polymerase acidic; PB, polymerase basic.

for HPAIV began in South Korea in the fall of 2023. We isolated 3 H5N6 HPAIVs from wild bird carcasses found in South Korea during December 2023 (A/whooper swan/Korea/23WC075/2023[H5N6], A/whooper swan/Korea/23WC116/2023[H5N6], and A/bean goose/Korea/23WC111/2023[H5N6]) (AppendixTable1,https://wwwnc.cdc.gov/EID/article/30/6/24-0192-App1.pdf). We conducted next-generation sequencing of the isolates and shared complete genome sequences publicly. We conducted comparative phylogenetic analysis to infer the origin and evolution of the viruses.

All H5N6 isolates were identified as HPAIVs based on the presence of multiple basic amino acids at the HA proteolytic cleavage site (REKRRKR/GLF). BLAST inquiries of the GISAID database (https://www.gisaid.org) indicated all 8 genes shared the highest nucleotide sequence identity (99.77%–100%) with a clade 2.3.4.4b H5N6 virus identified from a peregrine falcon in 2023 in Japan (A/peregrine falcon/Saga/4112A002/2023[H5N6]), harboring the same genome constellation as the H5N6 viruses in South Korea (Table). The HA gene clustered with the major genotype a of the H5N1 clade 2.3.4.4b HPAIV that circulated during 2022–2023 in South Korea (*8*). The NA gene of H5N6 virus clustered with H5N6 HPAIV from China, previously isolated in poultry and humans in 2018, but other internal genes were genetically distinct. Polymerase basic 1 and matrix protein genes also clustered with 2022–2023 H5N1 HPAIVs from South Korea. Polymerase basic 2, polymerase acidic, nucleoprotein, and nonstructural genes clustered with low-pathogenicity avian influenza viruses in Eurasia (Appendix Figure 2).

Estimated time to most recent common ancestor (tMRCA) of each gene of the H5N6 viruses and the A/peregrine falcon/Saga/4112A002/2023(H5N6) ranged from February through November 2023 (Figure; Appendix Table 2). On the basis of overlap between the 95% highest posterior density intervals of tMRCA, we assume the novel reassortant H5N6 viruses emerged around August–October 2023 and were introduced into Japan and South Korea. Maximum clade credibility tree of the NA gene revealed the wild bird H5N6 viruses from Japan and South Korea shared a common ancestor with the human infection case of H5N6 virus (A/Changsha/1/2022) from China. Since 2014, a total of 90 human cases of H5N6 infection have been reported in China;w most infections were reported after 2021 (*9*; https://iris.who.int/handle/10665/375483). The tMRCA of the wild bird H5N6 viruses from Japan and Korea and the human infection H5N6 virus from China is estimated to be June 12, 2022 (95% highest posterior density December 7, 2021–November 10, 2022)

(Figure; Appendix Table 2). The ancestral H5N6 HPAIV circulating in China potentially donated the NA gene to the clade 2.3.4.4b H5N1 virus in late 2022. The N6 gene of current and ancestral H5N6 HPAIV possessed a stalk deletion potentially acquired during the circulation of viruses in domestic poultry (*10*).

The H5N6 viruses possessed molecular markers T188, V210, Q222, and G224 in HA, which are associated with binding affinity to α-2,3 sialic acid receptors. We observed S133A and T156A mutations in HA, known to be associated with increased binding to α-2,6 sialic acid receptors. We observed L89V in polymerase basic 2, but not Q591K, E627K, and D701N. We also observed D622G in polymerase basic 1, N30D and I43M in matrix 1, and P42S in nonstructural protein 1, which are associated with increased virulence in mice (*10*).

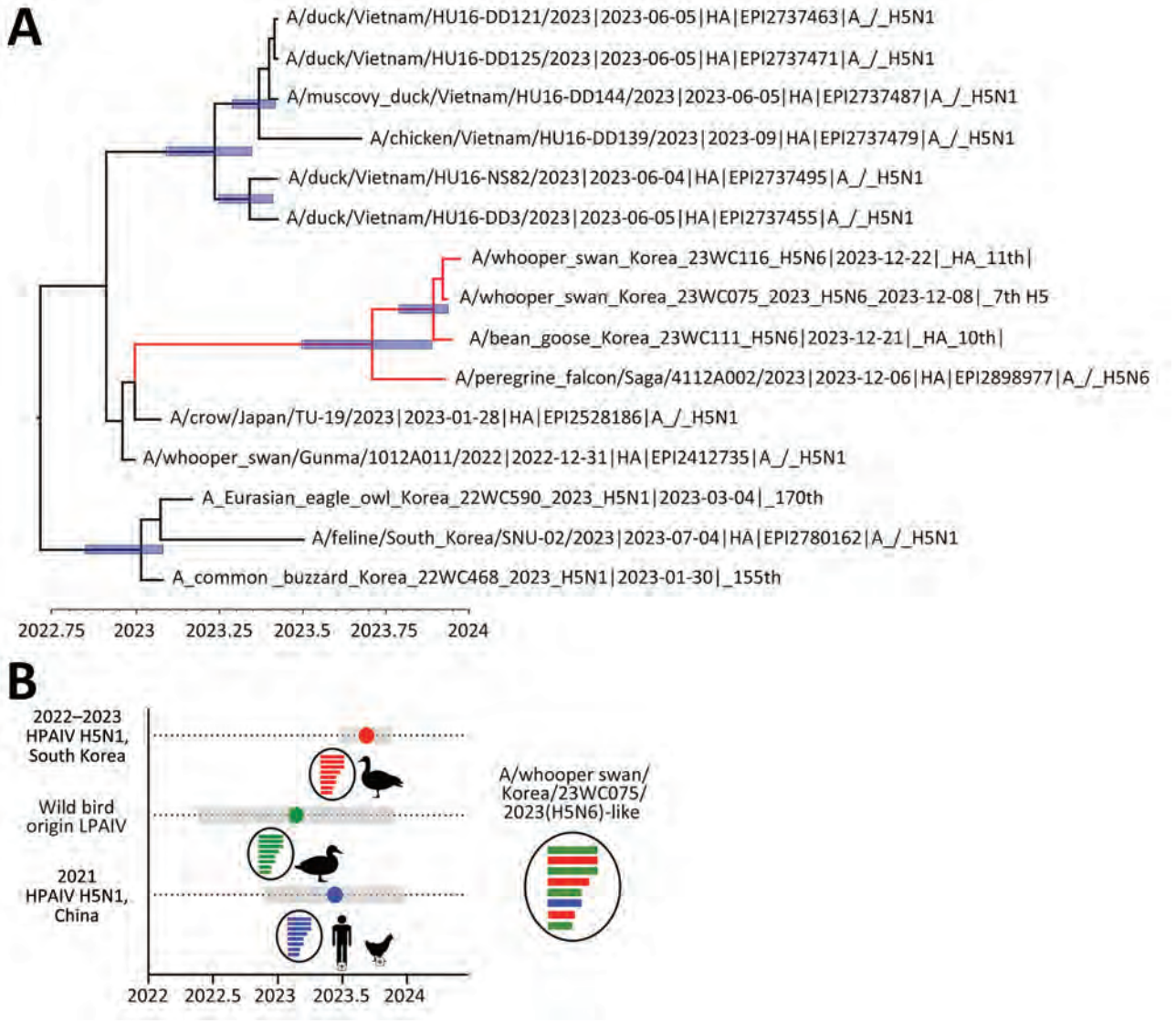

Figure. Exploration of most common ancestors for novel reassortant highly pathogenic avian influenza A(H5N6) clade 2.3.4.4 b isolates recovered from wild birds, South Korea. A) Maximum clade credibility tree of viruses found in the carcasses of whooper swans and bean geese in South Korea, December 2023. Tree was constructed using the hemagglutinin gene of the H5N6 viruses. Red indicates H5N6 isolates from South Korea and Japan. The timescale is shown on the horizontal axis in decimal years. Node bars represent 95% highest posterior density of the heights. Accession numbers beginning with EPI indicate isolates from the GISAID database (https://www.gisaid.org). B) Temporal schematic of the reassortant genome constellation of the novel reassortant H5N6 viruses from South Korea. Gene segments originating from H5N1 HPAIVs (red), LPAIVs (green), and H5N6 (blue) HPAIVs are indicated. Shade bars represent 95% highest posterior density range of time to most recent common ancestor. Circles represent the mean time to most recent common ancestor. HPAIV, highly pathogenic avian influenza virus; LPAIV, low-pathogenicity avian influenza viruses.

Previous reports suggest the genomes of clade 2.3.4.4b are evolving through frequent genome reassortments, forming transient and diverse genome constellations change with no apparent pattern of gene segment association (*8*). Detection of H5N6 HPAIVs from wild birds in South Korea and Japan during the 2023–24 wintering season and our phylogenetic analysis suggest H5N6 HPAIVs most likely descended from clade 2.3.4.4b H5N1 viruses circulating during 2022–2023, evolved from reassortment with other low-pathogenicity avian influenza viruses and HPAIVs, and were introduced into South Korea and Japan by wild birds during the fall migration season. Enhanced genomic surveillance of HPAIVs in wild birds is needed for early detection and monitoring of further evolution and spread of viruses.

This research was financially supported by a grant from National Institute of Wildlife Disease Control and Prevention (NIWDC) (grant no. 2023-016) and the Ministry of Environment, Republic of Korea.

The datasets in this study can be found in online repositories. The names of repositories and accession numbers are available through the GISAID (https://www.gisaid.org) EpiFlu database (accession nos. EPI2976997–EPI2977029).

About the Author

Mr. Cho is a PhD candidate at the College of Veterinary Medicine, Konkuk University. His research interests include molecular epidemiology and development of vaccines against avian diseases.

References

1. Wan XF. Lessons from emergence of A/goose/Guangdong/1996-like H5N1 highly pathogenic avian influenza viruses and recent influenza surveillance efforts in southern China. Zoonoses Public Health. 2012;59(Suppl 2):32–42. https://doi.org/10.1111/j.1863-2378.2012.01497.x
2. Lee DH, Bertran K, Kwon JH, Swayne DE. Evolution, global spread, and pathogenicity of highly pathogenic avian influenza H5Nx clade 2.3.4.4. J Vet Sci. 2017;18(S1):269–80. https://doi.org/10.4142/jvs.2017.18.S1.269
3. World Health Organization. Antigenic and genetic characteristics of zoonotic influenza A viruses and development of candidate vaccine viruses for pandemic preparedness. Wkly Epidemiol Rec. 2020;95:525–39 [cited 2024 Feb 4] https://www.who.int/publications/journals/weekly-epidemiological-record
4. Bevins SN, Shriner SA, Cumbee JC Jr, Dilione KE, Douglass KE, Ellis JW, et al. Intercontinental movement of highly pathogenic avian influenza A(H5N1) clade 2.3.4.4 virus to the United States, 2021. Emerg Infect Dis. 2022;28:1006–11. https://doi.org/10.3201/eid2805.220318
5. Baek YG, Lee YN, Lee DH, Shin JI, Lee JH, Chung DH, et al. Multiple reassortants of H5N8 clade 2.3.4.4b highly pathogenic avian influenza viruses detected in South Korea during the winter of 2020–2021. Viruses. 2021;13:490. https://doi.org/10.3390/v13030490
6. Wu H, Peng X, Xu L, Jin C, Cheng L, Lu X, et al. Novel reassortant influenza A(H5N8) viruses in domestic ducks, eastern China. Emerg Infect Dis. 2014;20:1315–8. https://doi.org/10.3201/eid2008.140339
7. European Food Safety Authority, European Centre for Disease Prevention and Control, European Union Reference Laboratory for Avian Influenza, Fusaro A, Gonzales JL, Kuiken T, et al. Avian influenza overview December 2023–March 2024. EFSA J. 2024;22:e8754.
8. Seo Y-R, Cho AY, Si Y-J, Lee S-I, Kim D-J, Jeong H, et al. Evolution and spread of highly pathogenic avian influenza A(H5N1) clade 2.3.4.4b virus in wild birds, South Korea, 2022–2023. Emerg Infect Dis. 2024;30:299–309. https://doi.org/10.3201/eid3002.231274
9. Huang P, Sun L, Li J, Wu Q, Rezaei N, Jiang S, et al. Potential cross-species transmission of highly pathogenic avian influenza H5 subtype (HPAI H5) viruses to humans calls for the development of H5-specific and universal influenza vaccines. Cell Discov. 2023;9:58. https://doi.org/10.1038/s41421-023-00571-x
10. Suttie A, Deng YM, Greenhill AR, Dussart P, Horwood PF, Karlsson EA. Inventory of molecular markers affecting biological characteristics of avian influenza A viruses. Virus Genes. 2019;55:739–68. https://doi.org/10.1007/s11262-019-01700-z

Address for correspondence: Dong-Hun Lee, Wildlife Health Laboratory, Konkuk University, 120 Neungdong-ro, Gwangjin-gu, Seoul, 05029, South Korea; email: donghunlee@konkuk.ac.kr

Sporadic Occurrence of Ensitrelvir-Resistant SARS-CoV-2, Japan

Akihiro Doi,[1] Masayuki Ota, Masumichi Saito, Shutoku Matsuyama

Author affiliation: National Institute of Infectious Diseases, Tokyo, Japan

DOI: https://doi.org/10.3201/eid3006.240023

Using the GISAID EpiCoV database, we identified 256 COVID-19 patients in Japan during March 31–December 31, 2023, who had mutations in the SARS-CoV-2 nonstructural protein 5 conferring ensitrelvir resistance. Ongoing genomic surveillance is required to monitor emergence of SARS-CoV-2 mutations that are resistant to anticoronaviral drugs.

Ensitrelvir fumaric acid (hereafter ensitrelvir) is a drug that inhibits the 3-chymotrypsin-like protease of SARS-CoV-2, also known as nonstructural protein 5 (NSP5), thereby inhibiting virus replication (*1*–*3*). Ensitrelvir was first approved for use in Japan on November 22, 2022. After drug approval, ensitrelvir was prescribed widely after March 2023 by many internal medicine clinics throughout Japan for COVID-19 treatment; indeed, 227,216 doses have been distributed in Japan since March 31, 2023 (*4*). However, in other countries, ensitrelvir prescriptions have been limited to clinical trials. To track emergence of SARS-CoV-2 mutations conferring resistance to ensitrelvir, we searched the GISAID EpiCoV database (https://www.gisaid.org), which contains virus genome sequences collected from COVID-19 patients worldwide.

We counted the number of SARS-CoV-2 cases that had NSP5 amino acid substitutions conferring ensitrelvir resistance (*5*–*8*) from March 31, 2023, the date ensitrelvir was first prescribed by general internal medicine clinics, through December 31, 2023 (Table). Although the occurrence of some NSP5 amino acid substitutions showed a regional bias, most were not associated with ensitrelvir prescription. For example, of the 77 sequences harboring the M46I amino acid substitution in NSP5 observed in the United States, 66 were identified in specimens collected during the same period in May 2023, suggesting an association with a cluster that likely arose from a sporadic occurrence. However, the M49L amino acid substitution in NSP5, which confers ensitrelvir resistance without attenuating virus infection both in vitro and in vivo (*5*), was observed in 256/49,414 (0.55%) virus sequences from Japan. By comparison, the M49L substitution was observed in 277/845,796 (0.03%) virus sequences deposited globally in the GISAID database; therefore, 92.4% of the deposited M49L mutant sequences of NSP5 were from Japan. The M49L substitution is caused by transversion of adenine at position 10199 within the SARS-CoV-2 NSP5 coding sequence to either cytosine or uracil. Of the 277 sequences with the M49L amino acid substitution, 89 (32.1%) had g.10199A>C, and 188 (67.9%) had g.10199A>U nucleotide mutations. Only 2 sequences had g.10199A>G transitions despite transitions generally occurring more frequently than transversions, which indicates ensitrelvir exerts high selective pressure on SARS-CoV-2 in COVID-19 patients. The number of virus sequences with M49L substitutions began to increase in June, peaked in September, and then decreased in November of 2023, a pattern corresponding to the number of COVID-19 cases observed throughout Japan during that period (Figure). In Japan, the monthly occurrence rate of ensitrelvir-resistant SARS-CoV-2 infections was significantly higher during the 9 months after initiating widespread ensitrelvir prescriptions than during the preceding period (Appendix Figure 1, https://wwwnc.cdc.gov/EID/article/30/6/24-0023-App1.pdf).

We constructed a phylogenetic tree as described previously (*9*). We downloaded whole-genome sequences from 277 SARS-CoV-2 mutants collected globally during March 31–December 31, 2023, and constructed the tree by using Nextstrain (https://www.nextstrain.org) and 570 reference genomes (Appendix Figure 2). Single sporadic occurrences of ensitrelvir-resistant mutants that were not linked to each other in the phylogenetic tree were counted if only 1 case occurred in a clade or if 1 case occurred ≥2 segments downstream of different branches from other cases belonging to the same clade, as described previously (*9*). Sporadic occurrence of g.10199A>C was detected 24 times and g.10199A>U was detected 22 times.

Although SARS-CoV-2 g.10199A>C and g.10199A>U mutations were detected nationwide in Japan, they were more frequent in populated metropolitan areas (Appendix Figure 3). Sporadic occurrence of mutants not linked to human-to-human virus transmission within a prefecture was defined as detection of 1 genome with either the g.10199A>C or g.10199A>U mutation or defined as detection of 1 mutant genome collected >1 month apart from others. We considered ≥105 genome mutations, 46 with g.10199A>C and 59 with g.10199A>U, to be sporadic

[1]Current affiliation: ACEL Inc., Kanagawa, Japan.

Table. Number of mutations in NSP5 causing ensitrelvir resistance during March 31–December 31, 2023, in study of sporadic occurrence of ensitrelvir-resistant SARS-CoV-2, Japan*

Amino acid substitutions‡	No. cases from GISAID database†					
	Globally	Japan	China	United States	Europe	Others
T45I	25	0	1	4	15 (60.0)	5
D48Y	0	0	0	0	0	0
M49I	90	6	0	77 (85.6)	5	2
M49L	277	256 (92.4)	2	15	0	4
M49T	1	0	0	0	0	1
M49V	1	0	0	1	0	0
L50F	85	6	2	31	26	20
P52L	4	2	0	0	0	2
Y54C	0	0	0	0	0	0
S144A	4	2	0	0	1	1
E166A	1	1	0	0	0	0
E166V	23	0	1	4	10	8
L167F	0	0	0	0	0	0
P168del	4	0	0	0	0	4
A173T	23	0	1	6	11	5
A173V	23	2	0	6	3	12 (52.2)
Q192R	2	0	0	0	1	1

*Numbers in parentheses are percentages of total global cases (if a particular mutation was found in >10 cases and was responsible for >50% of global cases). del, deletion; NSP5, nonstructural protein 5.
†Sequences were extracted from the GISAID EpiCoV database (https://www.gisaid.org).
‡Amino acid substitutions in NSP5 that trigger emergence of ensitrelvir-resistant SARS-CoV-2 (*5*–*8*).

occurrences (Appendix Figure 3), suggesting that ensitrelvir-resistant SARS-CoV-2 emerges frequently in Japan.

In conclusion, COVID-19 patients in Japan are usually prescribed ensitrelvir immediately after receiving positive results from a rapid immunochromatographic SARS-CoV-2 test. The Japan Ministry of Health, Labour and Welfare has conducted surveillance by using next-generation sequencing to enable rapid detection of drug-resistant SARS-CoV-2 (*10*). We examined the occurrence of ensitrelvir-resistant SARS-CoV-2 after widespread ensitrelvir prescription in Japan. Replication of those ensitrelvir-resistant mutant viruses in individual patients is thought to be driven predominantly by selective pressure exerted by the drug, leading to sporadic occurrence. The decreased occurrence of ensitrelvir-resistant SARS-CoV-2 after October 1, 2023, might be because patients are required to pay a portion of their medical costs, which could thereby decrease the number of ensitrelvir prescriptions. Increasing use of ensitrelvir worldwide will likely increase the frequency of mutations in SARS-CoV-2 causing ensitrelvir resistance. Ongoing genome surveillance using next-generation sequencing is required to monitor emergence of SARS-CoV-2 mutants that are resistant to anticoronaviral drugs.

Acknowledgments

We thank Yuriko Tomita for helpful suggestions and all researchers in the COVID-19 Genomic Surveillance Network in Japan for their continuing analysis and uploading of high-quality sequence data.

This study was supported by a Health and Labour Sciences Research grant (no. 21HA2003).

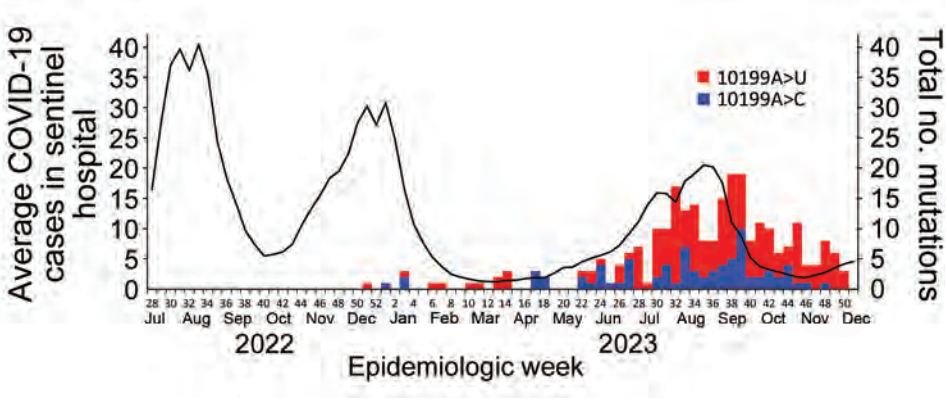

Figure. Sporadic occurrence of ensitrelvir-resistant SARS-CoV-2 mutants during December 2022–December 2023 in Japan. Solid line indicates the average number of COVID-19 cases. Weekly numbers of SARS-CoV-2 sequences harboring g.10199A>U and g.10199A>C mutations within nonstructural protein 5 were extracted from the GISAID EpiCoV database (https://www.gisaid.org). Number of mutations were aligned on the same time axis as the weekly average number of COVID-19 patients identified at ≈5,000 sentinel hospitals organized by the Japan Ministry of Health, Labor and Welfare. Scales for the y-axes differ substantially to underscore patterns but do not permit direct comparisons.

About the Author

Dr. Doi was a researcher at the Japan National Institute of Infectious Diseases in Tokyo during this work. His research interests focus on the mechanisms underlying emergence of drug-resistant viruses.

References

1. Sasaki M, Tabata K, Kishimoto M, Itakura Y, Kobayashi H, Ariizumi T, et al. S-217622, a SARS-CoV-2 main protease inhibitor, decreases viral load and ameliorates COVID-19 severity in hamsters. Sci Transl Med. 2023;15:eabq4064. https://doi.org/10.1126/scitranslmed.abq4064
2. Kuroda T, Nobori H, Fukao K, Baba K, Matsumoto K, Yoshida S, et al. Efficacy comparison of 3CL protease inhibitors ensitrelvir and nirmatrelvir against SARS-CoV-2 in vitro and in vivo. J Antimicrob Chemother. 2023;78:946–52. https://doi.org/10.1093/jac/dkad027
3. Noske GD, de Souza Silva E, de Godoy MO, Dolci I, Fernandes RS, Guido RVC, et al. Structural basis of nirmatrelvir and ensitrelvir activity against naturally occurring polymorphisms of the SARS-CoV-2 main protease. J Biol Chem. 2023;299:103004. https://doi.org/10.1016/j.jbc.2023.103004
4. Japan Ministry of Health, Labour and Welfare. Usage of drugs for the treatment of novel coronavirus infections [cited 2023 Dec 31]. https://www.mhlw.go.jp/stf/seisakunitsuite/bunya/0000121431_00324.html
5. Kiso M, Yamayoshi S, Iida S, Furusawa Y, Hirata Y, Uraki R, et al. In vitro and in vivo characterization of SARS-CoV-2 resistance to ensitrelvir. Nat Commun. 2023;14:4231. https://doi.org/10.1038/s41467-023-40018-1
6. Moghadasi SA, Heilmann E, Khalil AM, Nnabuife C, Kearns FL, Ye C, et al. Transmissible SARS-CoV-2 variants with resistance to clinical protease inhibitors. Sci Adv. 2023;9:eade8778. https://doi.org/10.1126/sciadv.ade8778
7. Jochmans D, Liu C, Donckers K, Stoycheva A, Boland S, Stevens SK, et al. The substitutions L50F, E166A, and L167F in SARS-CoV-2 3CLpro are selected by a protease inhibitor in vitro and confer resistance to nirmatrelvir. mBio. 2023; 14:e0281522. PubMed https://doi.org/10.1128/mbio.02815-22
8. Flynn JM, Huang QYJ, Zvornicanin SN, Schneider-Nachum G, Shaqra AM, Yilmaz NK, et al. Systematic analyses of the resistance potential of drugs targeting SARS-CoV-2 main protease. ACS Infect Dis. 2023;9:1372–86. https://doi.org/10.1021/acsinfecdis.3c00125
9. Doi A, Tomita Y, Okura H, Matsuyama S. Frequent occurrence of mutations in nsp3 and nsp4 of SARS-CoV-2, presumably caused by the inhaled asthma drug ciclesonide. PNAS Nexus. 2022;1:pgac197. PubMed https://doi.org/10.1093/pnasnexus/pgac197
10. Japan National Institute of Infectious Diseases. Amino acid substitutions due to viral genomic mutations that may affect the efficacy of therapeutic drugs against the new coronavirus (SARS-CoV-2) (4th edition) [cited 2023 Dec 31]. https://www.niid.go.jp/niid/ja/2019-ncov/2624-flu/12170-sars-cov-2-mutation-v4.html

Address for correspondence: Shutoku Matsuyama, Research Center for Influenza and Respiratory Viruses, National Institute of Infectious Diseases, Murayama Branch, 4-7-1 Gakuen, Musashi-Murayama, Tokyo 208-0011, Japan; email: matuyama@niid.go.jp

Foodborne Disease Outbreaks Linked to Foods Eligible for Irradiation, United States, 2009–2020

Marta Zlotnick, Taylor Eisenstein, Misha Park Robyn, Katherine E. Marshall

Author affiliations: Oak Ridge Institute for Science and Education, Oak Ridge, Tennessee, USA (M. Zlotnick); Centers for Disease Control and Prevention, Atlanta, Georgia, USA (M. Zlotnick, T. Eisenstein, M.P. Robyn, K.E. Marshall)

DOI: https://doi.org/10.3201/eid3006.230922

Food irradiation can reduce foodborne illnesses but is rarely used in the United States. We determined whether outbreaks related to *Campylobacter*, *Salmonella*, *Escherichia coli*, and *Listeria monocytogenes* were linked to irradiation-eligible foods. Of 482 outbreaks, 155 (32.2%) were linked to an irradiation-eligible food, none of which were known to be irradiated.

Food irradiation has been studied globally for decades and is a safe, effective means of reducing foodborne illness–causing pathogens, sterilizing insects, delaying ripening or sprouting, and extending shelf life (*1*,*2*). The US Food and Drug Administration has approved various foods for irradiation, including meat, poultry, fresh shell eggs, and spices (*2*) (Appendix Table, https://wwwnc.cdc.gov/EID/article/30/6/23-0922-App1.pdf). However, irradiation has not been widely adopted in the United States because of large fixed costs and the perception of consumer unwillingness to purchase irradiated food (*3*). Estimates of the amount of irradiated food available in the United States are scarce, but as of 2010, approximately one third of spices consumed and <0.1% of imported fruit, vegetables, and meats were irradiated (*3*).

Campylobacter, *Salmonella*, *Escherichia coli*, and *Listeria monocytogenes* are among the most common bacterial foodborne pathogens causing illnesses, hospitalizations, and death in the United States (*4*) and can be neutralized by irradiation at sufficient doses (*5*). We identified outbreaks caused by these pathogens and linked to irradiation-eligible foods; then, we determined whether any of the foods had been irradiated.

In the United States, the Foodborne Disease Outbreak Surveillance System (FDOSS) collects information from state, local, and territorial health departments about foodborne disease outbreaks. The National Outbreak Reporting System, launched in

2009, reports information gathered by FDOSS, including food processing methods such as shredding, pasteurizing, or irradiation. We searched for foodborne disease outbreaks reported and finalized through FDOSS and the National Outbreak Reporting System as of February 4, 2022, for which the date of first illness onset occurred during 2009–2020 and a confirmed pathogen was *Campylobacter*, *Salmonella*, *E. coli*, or *Listeria monocytogenes.* A foodborne disease outbreak was defined as ≥2 illnesses linked to a common exposure with evidence suggesting a food source. FDOSS variables we examined included method of processing, food vehicle, Interagency Food Safety Analytics Collaboration (IFSAC) food category, and the number of estimated primary illnesses, hospitalizations, and deaths. We grouped outbreaks by IFSAC category and irradiation approval status (eligible, some foods eligible, not yet eligible, or undetermined) (Appendix Table). We conducted a literature review to identify outbreaks not captured through FDOSS. We obtained foods approved for irradiation for pathogen reduction and approval years from the Code of Federal Regulations 21 Part 179 (Appendix Table).

In FDOSS, we identified 2,153 foodborne outbreaks during 2009–2020 caused by *Campylobacter*, *Salmonella*, *E. coli*, or *Listeria monocytogenes*. Of those, 482 (22.4%) included information regarding processing methods other than unknown or a missing value; none had irradiation listed as a processing method. Of the 482 outbreaks, 155 (32.2%) were linked to a food eligible for irradiation when the onset of the first reported illness occurred; those outbreaks resulted in 3,512 illnesses, 463 hospitalizations, and 10 deaths (Appendix Table). The most common sources were chicken (52 outbreaks), beef (31), and eggs (29), comprising 72% (112/155) of outbreaks linked to irradiation-eligible foods.

During our literature search, we identified 1 outbreak linked to food that might have included an irradiated ingredient. During 2009–2010, *Salmonella enterica* serotype Montevideo was found in imported pepper used in ready-to-eat salami (*6*). Some of the manufacturer's pepper was reportedly irradiated, but some was not. Whether the implicated product contained irradiated pepper is unclear. Irradiation was not reported as a processing method for the outbreak in FDOSS. After consultation with the Centers for Disease Control and Prevention outbreak investigation team, we determined there was insufficient evidence to link that outbreak to irradiated pepper.

The illnesses, hospitalizations, and deaths associated with outbreaks linked to irradiation-eligible foods might have been prevented or reduced had these foods been irradiated. Irradiation has repeatedly been proposed as a strategy to reduce foodborne disease outbreaks (*5*,*7*,*8*). Irradiation typically eliminates a large proportion of pathogenic microorganisms. The efficacy of irradiation depends on factors like temperature and water content (*9*). Food may become contaminated after irradiation. Irradiation can be a useful tool in improving food safety complementary to existing food safety practices. Consumer demand for irradiated foods may be increased through education (*10*).

The first limitation of our study is that IFSAC food categories do not always correspond to food groups approved for irradiation by the US Food and Drug Administration (Appendix Table); therefore, misclassification of irradiation approval status might have occurred for some foods. Reporting of outbreaks to FDOSS is voluntary, and processing method information was frequently missing, so irradiation might have been underreported or unrecognized by public health partners because of limited knowledge of irradiation or unfamiliarity with labeling. For outbreaks with multiple etiologies including a pathogen other than the 4 of interest, irradiation might not have reduced those pathogens.

We identified 155 *Campylobacter*, *Salmonella*, *E. coli*, or *Listeria monocytogenes* outbreaks with a known method of processing that were linked to irradiation-eligible foods during 2009–2020; none of the implicated foods were reported as irradiated. These results suggest that some outbreaks could be prevented or mitigated through irradiation. Prioritizing food irradiation efforts, particularly for chicken, beef, and eggs, could substantially reduce outbreaks and illnesses.

Acknowledgments

We thank Michelle Canning, Laura Gieraltowski, Lane Highbarger, and Jacqueline Roshelli Baker for their assistance.

This project was supported in part by an appointment to the Research Participation Program at the Centers for Disease Control and Prevention administered by the Oak Ridge Institute for Science and Education through an interagency agreement between the US Department of Energy and the Centers for Disease Control and Prevention.

About the Author

Dr. Zlotnick is an Oak Ridge Institute for Science and Education Fellow at the Centers for Disease Control and Prevention, Atlanta. Her work focuses on the prevention of zoonotic disease originating in food or animal contact.

References

1. High-dose irradiation: wholesomeness of food irradiated with doses above 10 kGy. Report of a joint FAO/IAEA/WHO study group. World Health Organ Tech Rep Ser. 1999;890:i–vi, 1–197.
2. Food and Drug Administration. Food irradiation: what you need to know. 2022 [cited 2022 Jun 23]. https://www.fda.gov/food/buy-store-serve-safe-food/food-irradiation-what-you-need-know
3. Ferrier P. Irradiation of produce imports: small inroads, big obstacles. 2011 [cited 2022 June 27]. https://www.ers.usda.gov/amber-waves/2011/june/irradiation-of-produce-imports
4. Scallan E, Hoekstra RM, Angulo FJ, Tauxe RV, Widdowson MA, Roy SL, et al. Foodborne illness acquired in the United States—major pathogens. Emerg Infect Dis. 2011;17:7–15. https://doi.org/10.3201/eid1701.P11101
5. Tauxe RV. Food safety and irradiation: protecting the public from foodborne infections. Emerg Infect Dis. 2001;7(Suppl):516–21. https://doi.org/10.3201/eid0707.017706
6. Gieraltowski L, Julian E, Pringle J, Macdonald K, Quilliam D, Marsden-Haug N, et al. Nationwide outbreak of *Salmonella* Montevideo infections associated with contaminated imported black and red pepper: warehouse membership cards provide critical clues to identify the source. Epidemiol Infect. 2013;141:1244–52. https://doi.org/10.1017/S0950268812001859
7. Osterholm MT, Norgan AP. The role of irradiation in food safety. N Engl J Med. 2004;350:1898–901. https://doi.org/10.1056/NEJMsb032657
8. Gunther NW IV, Abdul-Wakeel A, Scullen OJ, Sommers C. The evaluation of gamma irradiation and cold storage for the reduction of *Campylobacter jejuni* in chicken livers. Food Microbiol. 2019;82:249–53. https://doi.org/10.1016/j.fm.2019.02.014
9. World Health Organization. Safety and nutritional adequacy of irradiated food. Geneva: World Health Organization; 1994 [cited 2022 Nov 16]. https://iris.who.int/handle/10665/39463
10. Ablan M, Low MSF, Marshall KE, Devchand R, Koehler L, Hume H, et al. Focus groups exploring U.S. adults' knowledge, attitudes, and practices related to irradiation as a food safety intervention, 2021. Food Prot Trends. 2023;43:448–56.

Address for correspondence: Marta Zlotnick, Centers for Disease Control and Prevention, 1600 Clifton Rd NE, Mailstop H24-11, Atlanta, GA 30329-4018, USA; email: sst8@cdc.gov

Effect of Myxoma Virus Species Jump on Iberian Hare Populations

Beatriz Cardoso, Ignacio García-Bocanegra, João Queirós, Javier Fernández-López, Paulo C. Alves, Pelayo Acevedo

Author affiliations: Centro de Investigação em Biodiversidade e Recursos Genéticos, Vairão, Portugal (B. Cardoso, J. Queirós, P.C. Alves); Faculdade de Ciências da Universidade do Porto, Oporto, Portugal (B. Cardoso, J. Queirós, P.C. Alves); Estação Biológica de Mértola, Mértola, Portugal (B. Cardoso, J. Queirós, P.C. Alves); Instituto de Investigación en Recursos Cinegéticos, Ciudad Real, Spain (B. Cardoso, P. Acevedo); University of Córdoba, Cordoba, Spain (I. García-Bocanegra); Centre d'Ecologie Fonctionnelle et Evolutive, Montpellier, France (J. Fernández-López); Universidad Complutense de Madrid, Madrid, Spain (J. Fernández-López)

DOI: https://doi.org/10.3201/eid3006.231280

The myxoma virus species jump from European rabbits (*Oryctolagus cuniculus*) to Iberian hares (*Lepus granatensis*) has raised concerns. We assess the decline suffered by Iberian hare populations on the Iberian Peninsula and discuss the association between the effect of myxomatosis and the average abundance index, which we estimated by using hunting bags.

In July 2018, after 60 years of endemic circulation in European wild rabbits (*Oryctolagus cuniculus*), myxoma virus (MYXV) jumped to the Iberian hare (*Lepus granatensis*) (*1*). This species jump resulted from the emergence of a recombinant strain of MYXV, named ha-MYXV, containing a 2.8-kb insertion derived from an unknown poxvirus (*2*,*3*). Outbreak notifications rapidly spread across the Iberian Peninsula, resulting in an estimated mean mortality rate of 55.4% (median 70%) in hares (*4*). Concerns were raised about the effect of myxomatosis on the Iberian hare populations (*4*). We investigated those concerns and determined how myxomatosis affected Iberian hares by evaluating hare abundance indexes before and after the emergence of ha-MYXV.

We used hunting bag data to approximate population abundance (*5*). We collected information on hunting yields from hunting grounds in Portugal and the most affected regions of Spain, Andalusia, and Castilla-La Mancha during the hunting seasons (October–February) spanning from 2007–08 to 2020–21. Our study period includes 11 seasons before ha-MYXV emergence (premyxomatosis), from 2007–08 to 2017–18,

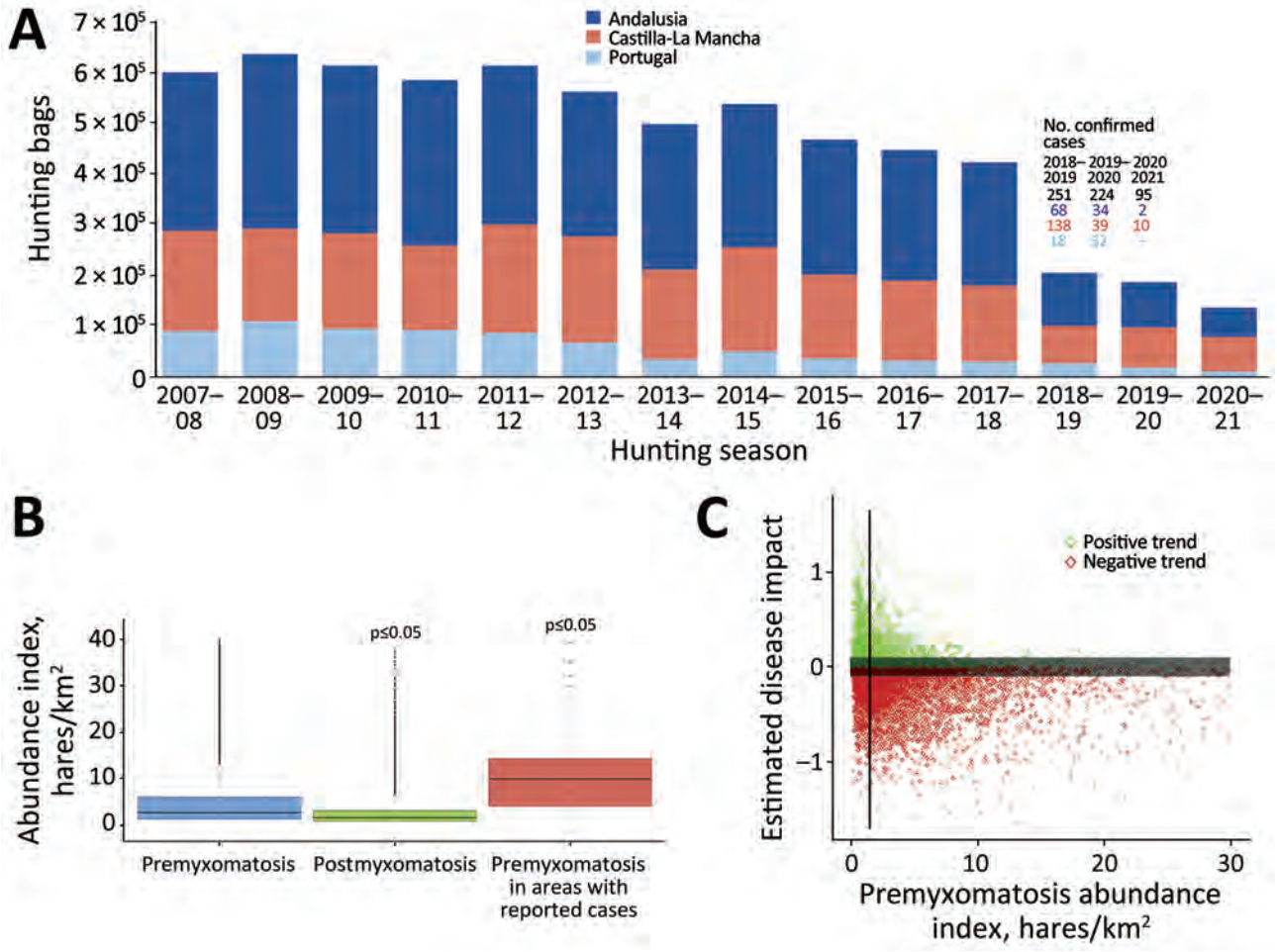

Figure. Evidence of the effect of myxomatosis outbreaks on Iberian hare (*Lepus granatensis*) populations and the link to the abundance index, in the Iberian Peninsula, after the initial species jump in 2018. A) Temporal evolution of the hunting yields from 2007–08 to 2020–21, along with the number of confirmed myxomatosis cases per hunting season, in the studied regions. B) Comparison between the average overall abundance index (hunted hares/km^2) in the premyxomatosis period versus the abundance index estimated for the postmyxomatosis period and the average overall abundance index versus the premyxomatosis period in hunting areas with reported outbreaks. C) Correlation between the estimated effect of myxomatosis (calculated as the difference between global and pre-myxomatosis trends) and the pre-myxomatosis hare abundance index. The vertical line represents the premyxomatosis abundance index threshold (1.5 hunted hares/km^2) from which most populations were negatively affected by disease. The dark gray buffer zone (trend values between −0.1 and 0.1) comprises hunting grounds excluded to account for the uncertainty of a trend proximate to zero.

and 3 after (postmyxomatosis), from 2018–19 until 2020–21. For each hunting ground and season, we estimated the abundance index as the number of hares hunted per square kilometer. We used analysis of variance tests to evaluate the differences between abundance indexes. We gathered data on myxomatosis outbreaks from nationwide passive surveillance efforts conducted after the first case reports. We used the coefficient (−1 to 1) obtained from the linear regression between hunting yields and hunting seasons to compute population trends (*6*) for the study period and the premyxomatosis period. Because the postmyxomatosis period was too short to estimate population trends accurately, we calculated the disease effect as the difference between the global and the premyxomatosis trends. We estimated the threshold of premyxomatosis abundance index from which >50% of populations were negatively affected by the disease.

We found a reduction of 77.2% in hares hunted during the study period (Figure 1, panel A). In the decade preceding the first myxomatosis outbreak, a smooth negative population trend was noted (https://www.intechopen.com/chapters/71640), with a mean annual reduction of 3.2% and a total decline of 29.6% in the number of hunted Iberian hares (Figure 1, panel A). Coinciding with the emergence of ha-MYXV, the highest annual decline of 51.5% occurred from 2017–18 to 2018–19 (Figure 1, panel A). This decrease was 57.1% in Andalusia and 50.9% in Castilla-La

Mancha. In Portugal, the decrease was only 10.0% but increased to 30.9% in the following hunting season (2019–20). This abrupt population decline could result from the rapid spread of ha-MYXV in the Iberian Peninsula (*4*). The number of hunted hares remained low after 2018, which is not suggestive of a postmyxomatosis recovery (Figure 1, panel A). Nevertheless, the evolution of hare population trends needs to be monitored over a longer period for more accurate inferences.

We found significant differences ($p \leq 0.05$) between the mean abundance indexes in the premyxomatosis versus postmyxomatosis periods, demonstrating further evidence of the myxomatosis-related decrease in hare populations (Figure 1, panel B). Areas with confirmed cases showed higher premyxomatosis abundance indexes compared with the overall average in the same period (Figure 1, panel B). We found concordant results when investigating the association between the premyxomatosis hare abundance index and the estimated disease effect. We found that, above a threshold of abundance index, the estimated disease effect is likely negative (Figure 1, panel C). Lower abundances may act as a barrier to virus dispersal, limiting the effect of myxomatosis, as previously described in wild rabbits (*7*). Of note, the abundance index threshold estimated for the study area is low (1.5 hares hunted/km^2) (Figure 1, panel C), meaning most hunting grounds have surpassing abundance indexes (76.4% in Spain and 51.0% in Portugal). This finding suggests ha-MYXV is highly effective in establishing itself in Iberian hare populations. The comparatively lower abundance indexes in Portugal may explain the lesser effect of myxomatosis in the Iberian Peninsula region.

The future evolution of myxomatosis in Iberian hare populations is uncertain, and concerns remain if myxomatosis will mimic the evolution documented in European wild rabbits. Hare populations were already in decline during the decade before the first myxomatosis outbreak. Information on hare population status was and still is scarce. To ensure the future sustainability of Iberian hares, long-term and holistic conservation, management, and monitoring programs are needed, especially when worldwide viral emergence events have become increasingly more frequent in lagomorph species over the past decade (*8*,*9*). The conservation status of the Iberian hare across its distribution range should be continuously monitored and reassessed as needed. Our results indicate the decline suffered by Iberian hare populations in the past few years can be linked to the emergence of ha-MYXV.

Acknowledgments

We thank Emídio Santos and the Regional Government of Andalusia for their collaboration.

This research was funded in part from a research grant provided by the Spanish Ministry of Science and Innovation (project LagoHealth; reference no. PID2019-111080RB-C21). This research was partially funded by the Sub-modality 2.4. "UCOLIDERA" of the "Enrique Aguilar Benítez de Lugo" Research Plan of the University of Cordoba and CIBER-Consorcio Centro de Investigación Biomédica en Red (grant no. CB 2021), Instituto de Salud Carlos III, Ministerio de Ciencia e Innovación and Unión Europea-Next Generation EU. B.C. was funded by the Fundação para a Ciência e Tecnologia, FCT (grant no. 2020.04872.BD). J.F.-L. was funded by the Margarita Salas grant from the European Union, NextGenerationEU, through Complutense University.

About the author:

Ms. Cardoso is a PhD candidate developing her doctoral research project at the Research Centre in Biodiversity and Genetic Resources, and the Spanish Game and Wildlife Research Institute at the University of Castilla-La Mancha. Her research interests focus on the epidemiology of myxomatosis and other lagomorph diseases, as well as their impact on the hosts' populations.

References

1. García-Bocanegra I, Camacho-Sillero L, Risalde MA, Dalton KP, Caballero-Gómez J, Agüero M, et al. First outbreak of myxomatosis in Iberian hares (*Lepus granatensis*). Transbound Emerg Dis. 2019;66:2204–8. https://doi.org/10.1111/tbed.13289
2. Águeda-Pinto A, Lemos de Matos A, Abrantes M, Kraberger S, Risalde MA, Gortázar C, et al. Genetic characterization of a recombinant myxoma virus in the iberian hare (*Lepus granatensis*). Viruses. 2019;11:1–16. https://doi.org/10.3390/v11060530
3. Dalton KP, Martín JM, Nicieza I, Podadera A, de Llano D, Casais R, et al. Myxoma virus jumps species to the Iberian hare. Transbound Emerg Dis. 2019;66:2218–26. https://doi.org/10.1111/tbed.13296
4. García-Bocanegra I, Camacho-Sillero L, Caballero-Gómez J, Agüero M, Gómez-Guillamón F, Manuel Ruiz-Casas J, et al. Monitoring of emerging myxoma virus epidemics in Iberian hares (*Lepus granatensis*) in Spain, 2018–2020. Transbound Emerg Dis. 2021;68:1275–82. https://doi.org/10.1111/tbed.13781
5. Imperio S, Ferrante M, Grignetti A, Santini G, Focardi S. Investigating population dynamics in ungulates: do hunting statistics make up a good index of population abundance? Wildl Biol. 2010;16:205–14. https://doi.org/10.2981/08-051
6. Williams D, Acevedo P, Gortázar C, Escudero MA, Labarta JL, Marco J, et al. Hunting for answers: rabbit (*Oryctolagus cuniculus*) population trends in northeastern Spain. Eur J Wildl Res. 2007;53:19–28. https://doi.org/10.1007/s10344-006-0056-0

7. Villafuerte R, Castro F, Ramírez E, Cotilla I, Parra F, Delibes-Mateos M, et al. Large-scale assessment of myxomatosis prevalence in European wild rabbits (*Oryctolagus cuniculus*) 60 years after first outbreak in Spain. Res Vet Sci. 2017;114:281–6. https://doi.org/10.1016/j.rvsc.2017.05.014
8. Asin J, Nyaoke AC, Moore JD, Gonzalez-Astudillo V, Clifford DL, Lantz EL, et al. Outbreak of rabbit hemorrhagic disease virus 2 in the southwestern United States: first detections in southern California. J Vet Diagn Invest. 2021;33:728–31. https://doi.org/10.1177/10406387211006353
9. Velarde R, Abrantes J, Lopes AM, Estruch J, Côrte-Real JV, Esteves PJ, et al. Spillover event of recombinant *Lagovirus europaeus*/GI.2 into the Iberian hare (*Lepus granatensis*) in Spain. Transbound Emerg Dis. 2021;68:3187–93. https://doi.org/10.1111/tbed.14264

Address for correspondence: Pelayo Acevedo, Instituto de Investigación en Recursos Cinegético, Ronda de Toledo, s/n, 13071 Ciudad Real, Spain; email: pacevedo@irec.csic.es

Characterization of Cetacean Morbillivirus in Humpback Whales, Brazil

Derek B. de Amorim, Laura J. de Camargo, Paula R. Ribeiro, Renata da F. Budaszewski, Jean Carlo O. Menegatt, Milena C. Paz, Lucas T. de Castro, Paula R. Almeida, Juliana C. Olegário, Cláudio W. Canal, Luciana Sonne

Author affiliations: Universidade Federal do Rio Grande do Sul, Imbé, Brazil (D.B. de Amorim); Universidade Federal do Rio Grande do Sul, Porto Alegre, Brazil (L.J. Camargo, P.R. Ribeiro, R.F. Budaszewski, J.C.O. Menegatt, M.C. Paz, L.T. de Castro, J.C. Olegário, C.W. Canal, L. Sonne); Universidade FEEVALE–Campus II, Novo Hamburgo, Brazil (P.R. Almeida)

DOI: http://doi.org/10.3201/eid3006.231769

Cetacean morbillivirus is an etiologic agent associated with strandings of live and dead cetacean species occurring sporadically or as epizootics worldwide. We report 2 cases of cetacean morbillivirus in humpback whales (*Megaptera novaeangliae*) in Brazil and describe the anatomopathological, immunohistochemical, and molecular characterization findings in the specimens.

The humpback whale (*Megaptera novaeangliae*) is a mysticete with a cosmopolitan distribution, including Brazil (*1*). Morbillivirus in cetaceans first occurred in 1988 in Europe. Since then, various strains of cetacean morbillivirus (CeMV) have been associated with strandings of live and dead cetaceans worldwide (*2*).

Two humpback whale specimens (MN1, MN2) stranded alive in southern Brazil in 2022 (Table; Appendix Figure 1, https://wwwnc.cdc.gov/EID/article/30/6/23-1769-App1.pdf). Because of deteriorated health, the whales were euthanized. In both cases, anesthetic protocols were performed by intramuscular infusion, followed by intracardiac administration of potassium chloride.

We performed necropsies immediately after euthanasia, fixed organ samples in 10% formalin for histologic analysis, and froze samples at −20°C for molecular analysis. To determine the presence of morbillivirus, we obtained samples of cerebrum, cerebellum, lung, lymph node, and urinary bladder and applied immunohistochemistry techniques by using anti–canine distemper virus (monoclonal, 1:400; VMRD, Inc., https://vmrd.com) as described (*3*). We also examined organ samples by reverse transcription PCR, subjecting cerebrum, cerebellum, lungs, and lymph nodes to RNA extraction by using TRIzol LS Reagent (Thermo Fisher Scientific Inc., https://www.thermofisher.com) according to manufacturer instructions. We performed complementary DNA synthesis by using GoScript Reverse Transcriptase (Promega, https://www.promega.com) and semi-nested PCR for detecting the L gene of paramyxoviruses by using GoTaq DNA polymerase (Promega) (*4*). We performed conventional PCR to detect the P gene, according to a published protocol (*5*). We purified positive reactions with the PureLink PCR purification kit (Thermo Fisher Scientific) and determined sequences by using the Sanger method (ABI PRISM 3100 genetic analyzer, Big-Dye Terminator v.3.1 Cycle Sequencing Kit; Thermo Fisher Scientific). We assembled sequences by using Geneious Prime version 2022.2.1 (Dotmatics, https://www.dotmatics.com) and analyzed them through BLASTn (https://blast.ncbi.nlm.nih.gov). For phylogenetic analysis, we retrieved sequences from GenBank and aligned using ClustalW with MEGA version 11 software (https://www.megasoftware.net). Finally, we analyzed sequences through the maximum-likelihood method.

MN1 was a juvenile male, 9.4 meters in length, with a poor body condition score. MN2 was a juvenile male, 11 meters in length, with a regular body condition score. Our microscopic investigations revealed

Table. Stranding data from 2 humpback whale specimens in southern Brazil, 2022*

Stranding data	MN1	MN2
Stranding date	September 14, 2022	October 5, 2022
Stranding location	Mostardas, RS	Jaguaruna, SC
Geographic coordinates	30°49′34.4″S, 50°33′59.2″W	28°45′48.6″S, 49°07′38.9″W
Carcass condition	Fresh	Fresh

*MN, *Megaptera novaeangliae*; RS, Rio Grande do Sul State; SC, Santa Catarina state.

findings primarily related to the central nervous system (CNS) (Figure, panels A, B; Appendix Table), as well as moderate lymphoid depletion in mesenteric and mediastinal lymph nodes in both specimens. Immunohistochemistry revealed discrete positive immunostaining in MN1 and marked positive immunostaining in MN2 for morbillivirus in astrocytes, neuronal cell bodies, and axons (Figure, panels C, D). In conducting reverse transcription PCR for MN1, we noted that the CNS tested positive for the L gene. Sequencing provided a 411-bp sequence (GenBank accession no. PP025976) that exhibited high similarity with the sequence of *Sotalia guianensis* morbillivirus (GD-CeMV; accession no. MG845553.1), showing 99.03% identity and 100% coverage (Appendix Figure 2, panel A). We saw different RT-PCR results in MN2, where all examined organs tested positive for the P gene but negative for the L gene. We obtained a 303-bp sequence of the P gene (GenBank accession no. PP549531), which exhibited 100% identity and 100% coverage with the reference GD-CeMV sequence (*6*) (Appendix Figure 2, panel B).

There are reports of CeMV in various cetaceans, but few reports for mysticetes (*2*). Morbillivirus has been identified in fin whales (*Balaenoptera physalus*) and is associated with death and strandings. The main findings included CNS lesions and lymphoid depletion (*7*). In odontocetes, the main findings reported for GD-CeMV infection are CNS lesions and pneumonia (*6*). Our study observed alterations in the CNS (Appendix Table) and moderate lymphoid depletion in lymph nodes. The first record of GD-CeMV occurred in Brazil in 2014 in a Guiana dolphin (*Sotalia guianensis*) (*2*,*6*). A highly similar sequence was also found in respiratory samples from healthy humpback whale using real-time RT-PCR (*8*). A retrospective study identified GD-CeMV in southern right whales (*Eubalaena australis*) (*9*).

For MN1, we were able to amplify a fragment of the morbillivirus L gene through seminested PCR, which we confirmed by sequencing, but not for the P

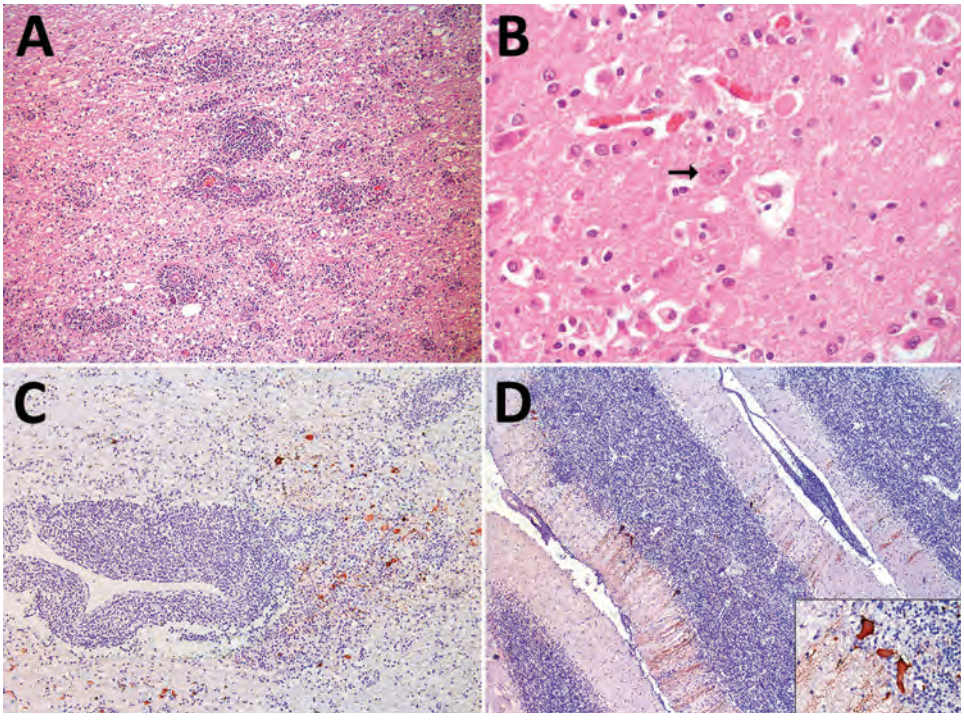

Figure. Microscopic findings of cetacean morbillivirus infection in 2 humpback whales in southern Brazil, 2022 (*Megaptera novaeangliae*). A) Cerebral cortex from whale MN2,. Note the pronounced perivascular cuffs composed of lymphocytes and plasma cells, moderate gliosis, and discreet vacuolization of the white matter. Hematoxylin and eosin stain; original magnification ×200. B) Cerebral cortex from whale. Eosinophilic intracytoplasmic inclusion body in a neuronal cell (arrow). Hematoxylin and eosin stain; original magnification ×400. C) Cerebral cortex from whale MN2. Neurons and astrocytes show severe, multifocal, cytoplasmic immunostaining with a marked perivascular lymphoplasmacytic cuff. Immunohistochemistry anti-canine distemper virus, morbillivirus; original magnification ×100. D) Cerebellum from MN2. Purkinje cells exhibit pronounced, multifocal, cytoplasmic immunostaining. Inset: Intense and granular immunostaining is observed in the cell body, in the dendrites of Purkinje cells, and occasionally in granule cells. Immunohistochemistry anti-canine distemper virus, morbillivirus; original magnification ×400.

gene. For MN2, we could not amplify the L gene but did amplify the P gene using conventional PCR. Both L and P gene sequences are closely related to a similar sequence from a study conducted in 2018, in which not all tested cetaceans were positive for both genes (L and P) (*6*), supporting our findings. The humpback whale southwest Atlantic population follows its route between Antarctica and the Abrolhos Bank (northeast Brazil), which is distant from the southern coast of Brazil (*1*). Strandings in off-route areas and reduced body scores suggest a weak condition of the specimens (*1*,*2*,*6*,*7*), a theory supported by our findings.

Our findings for the 2 humpback whales we evaluated, combined with those from other CeMV-related studies, indicate that a highly related cluster of strains (GD-CeMV) is circulating in the southwestern Atlantic (*6*,*8*,*9*), as demonstrated by previous phylogeography (*10*). Considering the prior analysis of the partial P gene, CeMV strains are not restricted to specific regions because cetaceans are migratory and strains are not host specific (*10*). Our findings of nonsuppurative meningoencephalitis in these whales, caused by CeMV that shows similarity to GD-CeMV, provide evidence of this viral threat to these and other cetaceans.

Acknowledgments

The authors express their gratitude to the teams from Área de Proteção Ambiental da Baleia Franca–Imbituba/SC, Associação R3 Animal, Projeto de Monitoramento Praia da Bacia de Santos from Santa Catarina, Parque Nacional da Lagoa do Peixe, Patrulha Ambiental (PATRAM), Municipality of Mostardas, Universidade do Extremo Sul Catarinense (UNESC), Educamar, and all the participants in the necropsies of the whales.

About the Author

Dr. de Amorim works at the Federal University of Rio Grande do Sul, Brazil. His areas of interest include biology, pathology, and medicine of wild animals, mainly marine animals.

References

1. Bamford CCG, Jackson JA, Kennedy AK, Trathan PN, Staniland IJ, Andriolo A, et al. Humpback whale (Megaptera novaeangliae) distribution and movements in the vicinity of South Georgia and the South Sandwich Islands Marine Protected Area. Deep Sea Research Part II: Topical Studies in Oceanography. 2022;198:1–16. https://doi.org/10.1016/j.dsr2.2022.105074
2. Van Bressem MF, Duignan PJ, Banyard A, Barbieri M, Colegrove KM, de Guise S, et al. Cetacean morbillivirus: Current knowledge and future directions. Viruses. 2014;6: 5145–81.
3. Slaviero M, Ehlers LP, De Lorenzo C, Zafalon-Silva B, Driemeier D, Pavarini SP, et al. Anatomopathological and immunohistochemical apects of distemper virus in crab-eating-foxes and pampa-foxes. Acta Sci Vet. 2019;47. https://doi.org/10.22456/1679-9216.90120
4. Tong S, Chern SWW, Li Y, Pallansch MA, Anderson LJ. Sensitive and broadly reactive reverse transcription-PCR assays to detect novel paramyxoviruses. J Clin Microbiol. 2008;46:2652–8. https://doi.org/10.1128/JCM.00192-08
5. Barrett T, Visser IK, Mamaev L, Goatley L, van Bressem MF, Osterhaust AD. Dolphin and porpoise morbilliviruses are genetically distinct from phocine distemper virus. Virology. 1993;193:1010–2. PMID: 8460473 https://doi.org/10.1006/viro.1993.1217
6. Groch KR, Santos-Neto EB, Díaz-Delgado J, Ikeda JMP, Carvalho RR, Oliveira RB, et al. Guiana dolphin unusual mortality event and link to cetacean morbillivirus, Brazil. Emerg Infect Dis. 2018;24:1349–54. https://doi.org/10.3201/eid2407.180139
7. Jo WK, Grilo ML, Wohlsein P, Andersen-Ranberg EU, Hansen MS, Kinze CC, et al. Dolphin morbillivirus in a fin whale (*Balaenoptera physalus*) in Denmark, 2016. J Wildl Dis. 2017;53:921–4. PMID: 28513327
8. Groch KR, Blazquez DNH, Marcondes MCC, Santos J, Colosio A, Díaz Delgado J, et al. Cetacean morbillivirus in humpback whales' exhaled breath. Transbound Emerg Dis. 2021;68:1736–43. https://doi.org/10.1111/tbed.13883
9. Groch KR, Groch KR, Kolesnikovas CKM, de Castilho PV, Moreira LMP, Barros CRMB, et al. Cetacean morbillivirus in Southern right whales, Brazil. Transbound Emerg Dis. 2019;66:606–10. https://doi.org/10.1111/tbed.13048
10. Jo WK, Kruppa J, Habierski A, van de Bildt M, Mazzariol S, Di Guardo G, et al. Evolutionary evidence for multi-host transmission of cetacean morbillivirus. Emerg Microbes Infect. 2018;7:201. https://doi.org/10.1038/s41426-018-0207-x

Address for correspondence: Derek Blaese de Amorim. Centro de Estudos Costeiros, Limunológicos e Marinhos (CECLIMAR/UFRGS). Av. Tramandaí, 976, Centro, Imbé, RS, Brazil; email: derek@ufrgs.br

Outbreak of Natural Severe Fever with Thrombocytopenia Syndrome Virus Infection in Farmed Minks, China

Ying Wang,[1] Mingfa Yang,[1] Hong Zhou, Chuansong Quan, Hongtao Kang

Author affiliations: Harbin Veterinary Research Institute, Chinese Academy of Agricultural Sciences, Harbin, China (Y. Wang, M. Yang, H. Kang); Shandong First Medical University and Shandong Academy of Medical Sciences, Taian, China (H. Zhou, C. Quan)

DOI: https://doi.org/10.3201/eid3006.240283

We isolated severe fever with thrombocytopenia syndrome virus (SFTSV) from farmed minks in China, providing evidence of natural SFTSV infection in farmed minks. Our findings support the potential role of farmed minks in maintaining SFTSV and are helpful for the development of public health interventions to reduce human infection.

Severe fever with thrombocytopenia syndrome (SFTS) is an emerging disease caused by a novel tickborne bunyavirus, SFTS virus (SFTSV), which was first identified in China in 2009 (*1*). Outside of China, SFTS was subsequently reported in South Korea, Japan, Vietnam, Myanmar, and Pakistan and now poses a global health problem (*2*–*6*). SFTSV is an enveloped virus belonging to the genus *Bandavirus*, family *Phenuiviridae*, order *Bunyavirales*. The virus has 3 single-stranded negative-sense RNA segments, large (L), medium (M), and small (S) (*1*). The *Haemaphysalis longicornis* tick is widely considered to be the primary transmission vector (*7*), but the natural animal hosts of SFTSV remain uncertain. Despite the high seroprevalence observed in various domestic animals in SFTSV-endemic regions, such as goats, cattle, dogs, pigs, chickens, and rodents, many of those animals do not show notable symptoms. Those infections were plausibly a result of SFTSV transmission from infected ticks (*8*).

We describe an outbreak of SFTS on a mink farm situated in Shandong, China. During late May through early July, 2022, >1,500 minks on this farm exhibited symptoms such as vomiting, diarrhea, and, in a small number, limb convulsions. Most minks exhibiting clinical manifestations died of the disease (Figure 1, panel A). Clinical manifestations included loose stools, mesenteric lymph node enlargement, and hyperemia (Figure 1, panels B and C), consistent with typical enteritis symptoms. Treatment with multiple antibiotics was not effective, and mink enteritis virus infection was ruled out through testing with a colloidal gold immunochromatographic assay. Intestinal tissue samples from minks with diarrhea (n = 10) were collected and forwarded to the Harbin Veterinary Research Institute, Chinese Academy of Agricultural Sciences, Harbin, China, for testing.

To identify the causative pathogen, we tested tissue samples for mink enteritis virus, Aleutian mink disease virus, carnivore rotavirus, carnivore coronavirus, and SFTSV. Among those, only tests for SFTSV were positive; cycle threshold (Ct) values were 18–22 (positive samples Ct<36) using SFTSV-specific primers (*9*). We obtained the SFTSV isolate from the intestinal tissue samples through a series of blind passages. We visualized virus particles by negative staining and transmission electron microscopy analysis following a discontinuous sucrose gradient purification. Virus particles presented the typical morphology of bunyavirus, as enveloped spherical particles with an average diameter of 100 nm (Figure 1, panel D). We then used immunofluorescence assays to analyze SFTSV nucleoprotein expression in Vero cells. We observed the green fluorescence by using an inverted fluorescence microscope. The results showed that SFTSV nucleoprotein expression was detected in Vero cells (Figure 1, panels E and F). Those results together confirmed the isolate, named SD01/China/2022, was SFTSV.

To obtain the complete genome of the SFTSV SD01/China/2022 isolate, we performed metagenomic next-generation sequencing to the sequence the RNA of the full-length genome. In brief, we constructed RNA sequencing libraries using the MGIEasy mRNA Library Prep Kit (BGI, https://www.bgi.com). Subsequently, we generated paired-end reads (100 bp) of the RNA libraries on the BGISEQ-500RS sequencing platform (BGI). We determined the complete genomes of SD01/China/2022, submitted to GenBank (accession nos. PP066883–5), and compared them with previously reported SFTSV strains. Phylogenetic analysis suggested that the L, M, and S gene segments of SD01/China/2022 all descended from C3; the L and M gene segments were genetically closest to the SFTSV strains HB2016-003 *Homo sapiens*/Hubei/China/2016 and the S gene segment was closest to the SFTSV strains SDLZDog01/2011 dog/China/2011 and SDPLP01/2011 *Homo sapiens*/

[1]These authors contributed equally to this article.

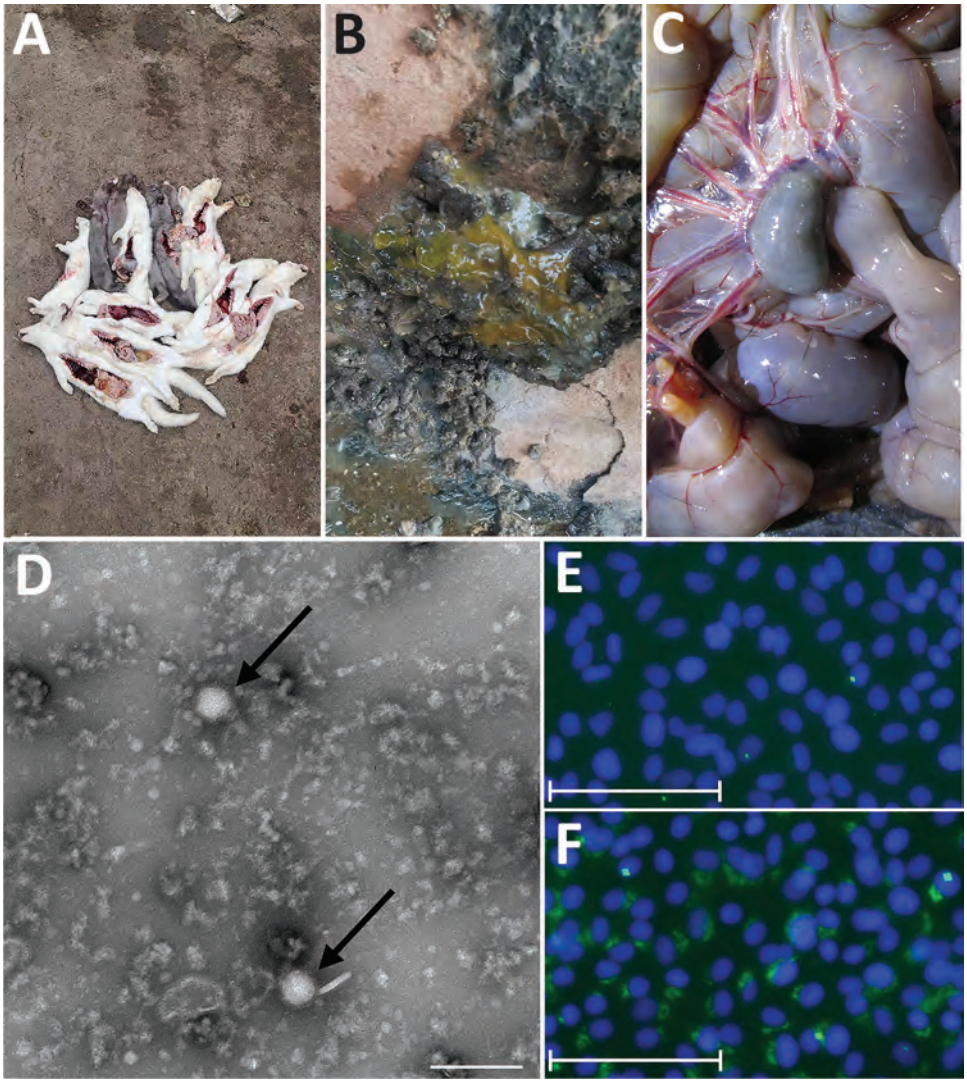

Figure 1. Clinical manifestations, TEM analysis, and immunofluorescence assay findings in outbreak of natural severe fever with thrombocytopenia syndrome virus (SFTSV) infection in farmed minks, China. A–C) Clinical manifestations were death (A), loose stools (B), and enlargement and hyperemia of the mesenteric lymph nodes (C). D) Virus detection by TEM analysis showed typical enveloped virions (arrows). Scale bar indicates 200 nm. E, F) Immunofluorescent pictures of Vero cells infected with SFTSV SD01/China/2022 isolate. Differences between the blank control (E) and green fluorescence (F) indicates SFTSV particles in the monolayer of Vero cells. Scale bars in panels E and F indicate 75 μm.

China/2011 (Figure 2, panels A–C, https://wwwnc.cdc.gov/EID/article/30/6/24-0283-F2.htm).

Previous research has shown the presence of antibodies to the nucleoprotein of SFTSV in farmed minks and suggested that minks were infected with SFTSV in China (*10*). In this study, we successfully isolated and identified an SFTSV isolate, named SD01/China/2022, in farmed minks in China. The symptoms of farmed minks in this case were consistent with SFTS symptoms, such as gastrointestinal disorders and central nervous system manifestations, which proved the occurrence of natural SFTSV infection–related fatalities in this population. Our findings reveal the threat of SFTS to the fur animal–breeding industry. Of note, phylogenetic analysis of the isolate indicated high homology with SFTSV strains in humans, suggesting that the viruses generally infected both humans and minks, further supporting the potential role of farm minks in maintaining SFTSV. Farmed minks have potential for direct contact with humans and might serve as crucial amplifying hosts in the transmission of SFTSV. Further analysis of SFTSV infection in other captive fur animals, such as raccoon dogs and foxes, will be required to determine other key reservoirs for SFTSV. We recommend a focus on the registration of mink exposure for humans with SFTS-like illnesses, as well as increased measures to reduce SFTSV exposure risk.

This study was supported by the National Natural Science Foundation of China (no. 32370164) and Central Public-interest Scientific Institution Basal Research Fund (no. 1610302022009).

About the Author

Ms. Wang is a PhD candidate at Harbin Veterinary Research Institute, Chinese Academy of Agricultural

Sciences, Harbin, China. Her primary research interests focus on the host–pathogen interactions of tickborne viruses. Dr. Yang is a research associate at Harbin Veterinary Research Institute, Chinese Academy of Agricultural Sciences, Harbin, China. His research interests focus on phylogeny, virology, and molecular epidemiology, especially for tickborne viruses.

References

1. Yu XJ, Liang MF, Zhang SY, Liu Y, Li JD, Sun YL, et al. Fever with thrombocytopenia associated with a novel bunyavirus in China. N Engl J Med. 2011;364:1523–32. https://doi.org/10.1056/NEJMoa1010095
2. Kim KH, Yi J, Kim G, Choi SJ, Jun KI, Kim NH, et al. Severe fever with thrombocytopenia syndrome, South Korea, 2012. Emerg Infect Dis. 2013;19:1892–4. https://doi.org/10.3201/eid1911.130792
3. Lin TL, Ou SC, Maeda K, Shimoda H, Chan JP, Tu WC, et al. The first discovery of severe fever with thrombocytopenia syndrome virus in Taiwan. Emerg Microbes Infect. 2020;9:148–51. https://doi.org/10.1080/22221751.2019.1710436
4. Takahashi T, Maeda K, Suzuki T, Ishido A, Shigeoka T, Tominaga T, et al. The first identification and retrospective study of Severe Fever with Thrombocytopenia Syndrome in Japan. J Infect Dis. 2014;209:816–27. https://doi.org/10.1093/infdis/jit603
5. Tran XC, Yun Y, Van An L, Kim SH, Thao NTP, Man PKC, et al. Endemic severe fever with thrombocytopenia syndrome, Vietnam. Emerg Infect Dis. 2019;25:1029–31. https://doi.org/10.3201/eid2505.181463
6. Zohaib A, Zhang J, Saqib M, Athar MA, Hussain MH, Chen J, et al.; Sajjad-Ur-Rahman. Serologic evidence of severe fever with thrombocytopenia syndrome virus and related viruses in Pakistan. Emerg Infect Dis. 2020;26:1513–6. https://doi.org/10.3201/eid2607.190611
7. Zhuang L, Sun Y, Cui XM, Tang F, Hu JG, Wang LY, et al. Transmission of severe fever with thrombocytopenia syndrome virus by *Haemaphysalis longicornis* ticks, China. Emerg Infect Dis. 2018;24:868–71. https://doi.org/10.3201/eid2405.151435
8. Niu G, Li J, Liang M, Jiang X, Jiang M, Yin H, et al. Severe fever with thrombocytopenia syndrome virus among domesticated animals, China. Emerg Infect Dis. 2013;19:756–63. https://doi.org/10.3201/eid1905.120245
9. Yu ZY, Yang MF, Ma YY, Kang HT, Jiang Q, Liu JS, et al. Establishment and application of real-time fluorescent quantitative RT-PCR for the detection of SFTSV [in Chinese]. Chinese Veterinary Science. 2022;52:292–7.
10. Wang GS, Wang JB, Tian FL, Zhang HJ, Yin FF, Xu C, et al. Severe fever with thrombocytopenia syndrome virus infection in minks in China. Vector Borne Zoonotic Dis. 2017;17:596–8. https://doi.org/10.1089/vbz.2017.2115

Address for correspondence: Hongtao Kang, Harbin Veterinary Research Institute, Chinese Academy of Agricultural Sciences, No. 678 Haping Rd, Harbin 150000, China; email: kanghongtao@caas.cn; Chuansong Quan, Shandong First Medical University and Shandong Academy of Medical Sciences, No. 2 Yingsheng East Rd, Taian 271000, China; email: emergy_2008@126.com

Nontuberculous Mycobacteria and Laboratory Surveillance, Virginia, USA

Isaac See, Kelly A. Jackson, Rebecca Byram, Nadege Charles Toney, Cheri Grigg, Shelley S. Magill

Author affiliation: Centers for Disease Control and Prevention, Atlanta, Georgia, USA

DOI: https://doi.org/10.3201/eid3006.240431

To the Editor: We read with interest the recent article by Mullen et al. (*1*) that describes associations between *Mycobacterium avium* complex and *Mycobacterium abscessus* pulmonary disease prevalence and environmental exposures and risk factors. We applaud the innovation of efforts in states to better characterize nontuberculous mycobacteria (NTM) epidemiology.

In the discussion section of the article, the authors reference a publication describing results from a surveillance pilot for pulmonary and extrapulmonary NTM conducted by the Centers for Disease Control and Prevention (CDC) Emerging Infections Program's Healthcare-Associated Infections–Community Interface Activity (*2*). The authors state, "Our study differed from that [CDC] study in multiple ways. Of note, we included data from a state in the southeastern United States, a region not represented in the CDC surveillance data, and gathered comprehensive surveillance data for the entire state from statewide laboratories rather than individual sentinel laboratories" (*1*). Although none of the sites in the CDC surveillance pilot conducted statewide surveillance for pulmonary NTM, we wish to clarify that the surveillance was active and also population-based (i.e., surveillance for isolation of NTM among all residents of certain counties) and was not a surveillance based on sentinel laboratories. Of note, in 2024 we have also recently expanded the geographic scope of Healthcare-Associated Infections–Community Interface Activity's active, laboratory- and population-based NTM infection surveillance (including pulmonary NTM surveillance) to include Georgia as one of our surveillance sites. This addition will improve the surveillance program by adding representation from the southeastern United States.

References

1. Mullen B, Houpt ER, Colston J, Becker L, Johnson S, Young L, et al. Geographic variation and environmental predictors of nontuberculous mycobacteria in laboratory surveillance, Virginia, USA, 2021-2023. Emerg Infect Dis. 2024;30:548–54. https://doi.org/10.3201/eid3003.231162
2. Grigg C, Jackson KA, Barter D, Czaja CA, Johnston H, Lynfield R, et al. Epidemiology of pulmonary and extrapulmonary nontuberculous mycobacteria infections at 4 US emerging infections program sites: a 6-month pilot. Clin Infect Dis. 2023;77:629–37. https://doi.org/10.1093/cid/ciad214

Address for correspondence: Isaac See, Centers for Disease Control and Prevention, 1600 Clifton Rd NE, Mailstop H16-3, Atlanta, GA 30329-4018, USA; email: isee@cdc.gov

Antimicrobial Stewardship in Non-Traditional Settings

Shira Doron, Maureen Campion, editors; Springer Nature Switzerland AG, Cham, Switzerland, 2023; ISBNs: 978-3-031-21709-8; 978-3-031-21710-7 (eBook) Pages: 221; Price: US$169.99

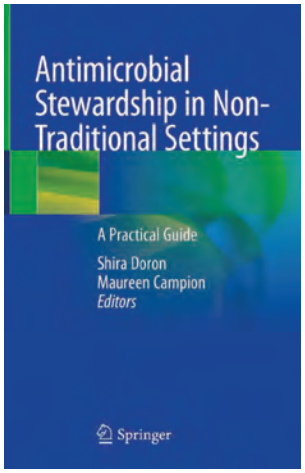

In 2014, the US Centers for Disease Control and Prevention launched a new set of core elements for acute-care hospitals to implement key strategies in antimicrobial stewardship (AS). Over the following years, those guidelines were gradually expanded to include outpatient spaces and long-term care facilities. However, uptake in these areas has remained sluggish in the United States, in part due to limited resource allocation, lack of supporting evidence, and competing healthcare priorities. Antimicrobial Stewardship in Non-Traditional Settings offers a timely and comprehensive examination of AS implementation strategies and potential pitfalls, emphasizing the importance and feasibility of AS beyond the confines of acute-care settings.

The book begins by highlighting the evolution of AS initiatives. Each subsequent chapter focuses on a distinct setting (e.g., long-term care facilities, ambulatory surgery centers, veterinary practices) or population (immunocompromised patients, pediatrics). The authors provide targeted strategies and practical recommendations for initiating AS programs and address the unique challenges encountered in each environment.

The discussion of antimicrobial resistance in long-term care facilities in the United States provides perhaps the clearest picture of how guidance from the CDC and other professional societies can be applied. Implementing such guidelines in other settings remains a less precise practice, and it is in discussion of these settings that the book truly shines. For instance, in discussing outpatient clinics and emergency departments, the authors perceptively note predominant barriers to effective AS to be improper documentation, challenges in formulating local antibiograms, and inadequate standardization of antibiotic use across facilities. The authors propose several solutions: use of rapid diagnostics, implementation of AS-friendly order-sets, and inclusion of multidisciplinary teams to strengthen early recognition and intervention.

In chapter 5, the authors describe how ambulatory surgery centers, often the more lucrative divisions within healthcare facilities, have increased incentives to reduce antimicrobial resistance and associated postsurgical complications. They propose that initiatives set forth in such well-funded facilities (e.g., standardized approaches for wound classification, decolonization practices) offer a unique template for implementing similar AS initiatives in less-resourced areas, such as small-access hospitals and veterinary practices.

In the last chapters of the book, the authors discuss an imbalance regarding the specific niche populations on which AS programs are focused nationwide, noting that patients in intensive care units are among the groups most targeted. Conversely, immunocompromised and pediatric patients remain understudied and underserved. The authors draw examples from outside the United States to support potential solutions for immunocompromised patients, but those suggestions are somewhat limited in the absence of evidence-based best practices.

Antimicrobial Stewardship in Non-Traditional Settings offers a comprehensive and insightful exploration of AS implementation beyond acute-care settings and serves as a call-to-arms for medical and scientific communities tasked with exploring AS solutions for settings and niche populations most in need of such guidance. This book serves as a valuable resource for healthcare professionals striving to combat antimicrobial resistance, providing them with targeted strategies for diverse healthcare environments. The book's breadth of coverage and practical recommendations make it an indispensable tool for advancing AS initiatives across various settings.

This work was funded in part by the National Institute of Allergy and Infectious Diseases Division of Intramural Research, National Institutes of Health, Bethesda, Maryland.

Nehal Hashem, Christina Yek

Author affiliation: National Institutes of Health, Bethesda, Maryland, USA

DOI: http://doi.org/10.3201/eid3006.240255

Address for correspondence: Christina Yek, NIAID International Center of Excellence in Research Cambodia, 1 Christopher Howes (St 96), Phnom Penh, Cambodia; email: christina.yek@nih.gov

EID Introduces New Article Category for Letters from the Emerging Infections Network

Emerging Infectious Diseases announces that it is now accepting submissions of articles in a new category, Letters from the Emerging Infections Network. The Emerging Infections Network (EIN) is a nationwide United States–based sentinel network of infectious disease physicians and related healthcare professionals that is funded by a 1995 cooperative agreement between the Infectious Disease Society of American and the Centers for Disease Control and Prevention (*1*).

According to its website, the specific goals of the EIN are to do the following (*2*):

- detect new or unusual clinical events;
- identify cases during outbreak investigations;
- gather information about clinical aspects of emerging infectious diseases;
- help connect members to the CDC and other public health investigators;
- develop new methods for gathering epidemiological and clinical information.

Background

The overarching goal of the EIN is to assist with surveillance for emerging infectious diseases and related phenomena by collecting relevant clinically oriented observations to complement other surveillance systems. The 2 major EIN-related activities revolve around an actively moderated listserv and the distribution of regular queries or 2 quick queries of EIN members. EIN members and CDC investigators suggest query topics. Before queries are distributed, they require approval from EIN staff, the EIN Executive Committee, and CDC program officers.

Regular queries are broadly focused on emerging infections or related phenomena and typically revolve around topics on diagnosis, treatment, quality, safety or about health policy. Regular queries are sent to eligible members 4–5 times per year by email. They typically include up to 10–12 questions and are distributed via email directly to EIN members with a clinical practice. Two reminders are sent to nonresponding members approximately 1 week apart. The known denominator of recipients allows regular queries to include member database information including practice location and characteristics and physician years of practice; data are aggregated and reported in such way that no patients, providers, or practice sites are identified.

Quick queries are very short polls (4–5 questions per topic) specifically designed to take a "pulse" and rapidly aggregate member experiences, opinions, or approaches regarding an emerging infectious disease or related phenomena. They can also be used for initial case finding to build future case series. Quick queries are distributed via the EIN listserv. Thus, unlike regular queries which are sent directly to individual members, there is no stable denominator. Therefore, no specific practice or location data are available unless such information is requested in a quick query question. These queries are designed to collect very preliminary data from clinical infectious diseases practitioners that is otherwise difficult to do using alternative approaches.

Information about Letters from the Emerging Infections Network

Letters from the Emerging Infections Network are short form articles that broadly focus on emerging infections or related phenomena and typically revolve around topics on diagnosis, treatment, quality, safety or about health policy.

Note that only members of the Emerging Infections Network, described previously, may submit articles in this category.

The following submission requirements, which are found in EID's Author Instructions and Quick Guide to Article Information, apply to these articles.

- Text maximum of 800 words.
- Unstructured 50-word abstract.
- Maximum of 2 figures or tables, total, e.g., 1 figure and 1 table; 2 figures and no tables; 2 tables and no figures.
- Maximum of 10 references.
- Include the EID Author Checklist with each submission.

For questions or more information, contact EID at eideditor@cdc.gov.

References

1. Pillai SK, Beekmann SE, Santibanez S, Polgreen PM. The Infectious Diseases Society of America Emerging Infections Network: bridging the gap between clinical infectious diseases and public health. Clin Infect Dis. 2014 Apr;58(7):991-6. http://doi.org/10.1093/cid/cit932.
2. Emerging Infections Network. About the Emerging Infections Network [cited 2024 May 13]. https://ein.idsociety.org/#

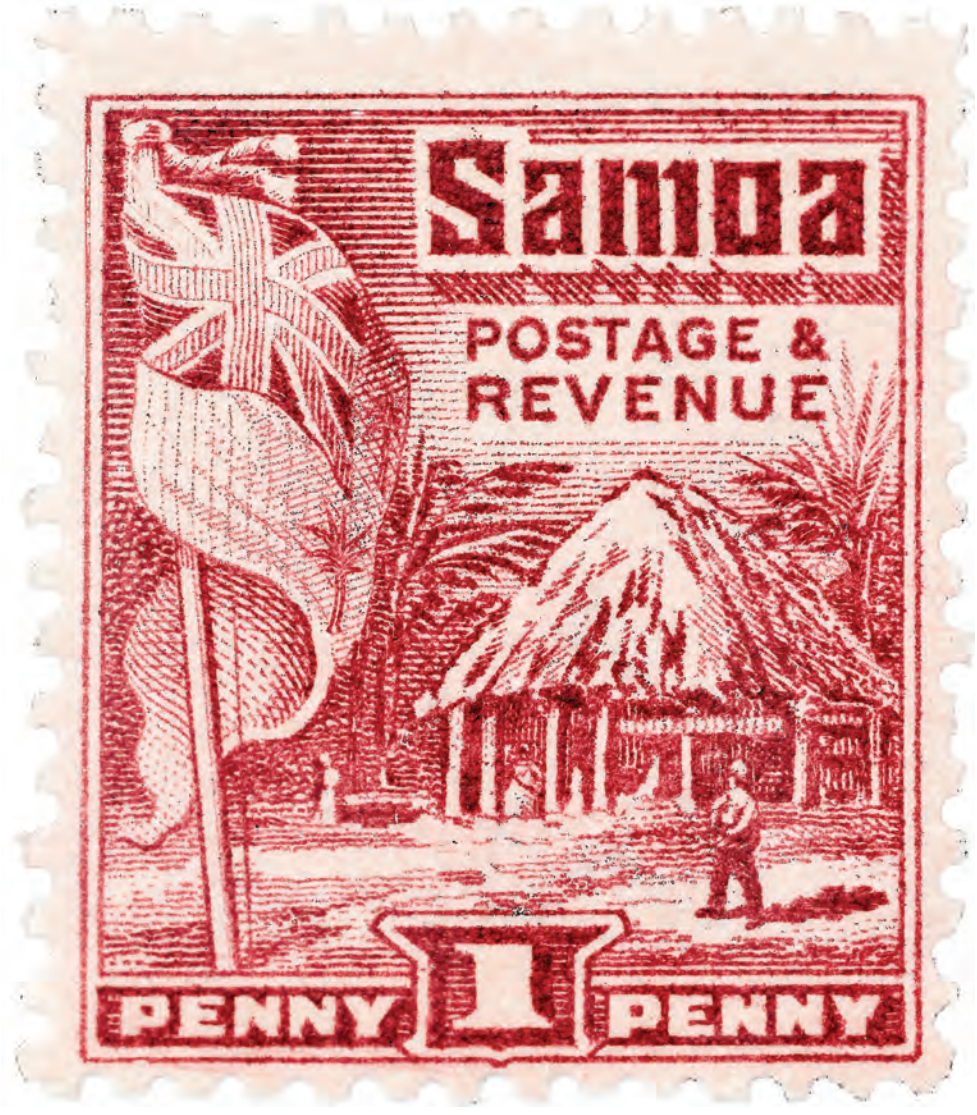

J. Potts (details unknown), engraver for Bradbury, Wilkinson & Co. Printer. Fluttering flag and Samoan house on stamp with designation "Samoa," by civil administration of the mandated territory of Western Samoa, 1921. Printed by the Government Printing Office, Wellington, New Zealand. Private collection, Atlanta, Georgia. Photography by Will Breedlove.

Architecture that Might Have Contributed to Disease Prevention

Terence Chorba

The Samoan Islands constitute a volcanic archipelago covering 1,170 square miles of the central South Pacific Ocean in the mid-Western part of the Polynesian triangle. The Islands are divided into 2 administrative jurisdictions—the Independent State of Samoa in the west and American Samoa in the east—separated by approximately 40 miles of water. Evidence of human occupation dates back 3 millennia, but European exploration to the islands was first documented in the mid-18th century. In December 1899, the Samoan archipelago was formally partitioned into a German colony (German Samoa) in the west and a US territory (American Samoa) in the east. During World War I, New Zealand forces overtook the

Author affiliation: Centers for Disease Control and Prevention, Atlanta, Georgia, USA

DOI: https://doi.org/10.3201/eid3006.AC3006

western islands, and in 1920, German interests were formally surrendered to New Zealand, which granted political independence to the western jurisdiction in 1962. In addition to English, the indigenous Polynesian people of 2 jurisdictions share a common Polynesian language, Samoan; in both jurisdictions, most Samoans are exclusively of Samoan ancestry.

As for many other Pacific Island jurisdictions, prevalence rates for adult-onset diabetes among the inhabitants of the Samoan Islands are among the highest in the world. In 2013, population-based surveys in the Independent State of Samoa found that, among adults (25–64 years of age), burdens of type 2 diabetes (commonly assessed in untreated persons as hemoglobin A1C ≥6.5% or fasting blood sugar ≥126 mg/dL) were 19.6% among men and 19.5% among women. Many observational cohort studies of persons with latent tuberculosis infection (LTBI) have found a higher risk for tuberculosis (TB) disease—generally 3-fold— among those with diabetes than among those with normal blood sugar levels. In most other Pacific Island jurisdictions where rates of type 2 diabetes are high, rates of TB are also high. For example, in the Federated States of Micronesia, TB incidence rates (cases/100,000 population) of 73.7 were reported in 2020 and 62.8 in 2021. By contrast, the World Bank lists the Independent State of Samoa as a low TB incidence jurisdiction with a reported TB incidence rate of 6.8 in 2021, comparable to that of New Zealand. In American Samoa, similarly low TB incidence rates of 6.8 were reported in 2020 and 8.6 in 2021. Although reasons to account for the disparity in TB incidence between the Samoan and the other Pacific Island populations may be matters of speculation, the architectural structure on the Samoan stamp on the cover of this month's journal may be in part responsible.

Among the shared cultural features of the Samoan peoples is the basic design of a house, or fale (pronounced fah-leh), the Samoan word referring to houses of any size, including traditional housing structures, workplaces, and meetinghouses. Although found elsewhere in Polynesia as well, the architecture of the fale is a source of great pride to Samoans and is a characteristic art form often featured in representations of Samoan life and culture. A traditional fale has an oval shape; a domed roof supported by breadfruit, coconut, or poumuli wood posts; and no permanent or structural walls (Figures 1, 2). Roll-down screens or weather blinds, called pola, are often fashioned and hung between the external wooden posts to afford some shelter and privacy, over a raised stone floor. Before the arrival of the European powers and availability of imported materials, metal and structural walls were not used in fale construction, in which beams and posts would be fastened together and plaited coconut fiber rope would be used for lashing. Roofing on top of a domed framework was thatch made of leaves of lau (taro), coconut, or sugar cane. This author would like to advance the theory that, although all modern-day houses in the 2 Samoas are constructed with walls, the fale has, in part, played a positive role in reducing the spread of TB infection in the Samoan population.

Throughout the world, almost all TB transmission results from a person inhaling droplet nuclei containing *Mycobacterium tuberculosis*, the dehydrated residua of larger respiratory droplets generated by persons with pulmonary or laryngeal TB infection who are coughing, sneezing, or otherwise aerosolizing the infecting bacterium. The odds of inhaling such particles are a function of how long the particles can remain suspended in the ambient air and follow room currents. After *M. tuberculosis* organisms strike surfaces, it is very difficult for them to re-aerosolize from droplet nuclei as respirable particles. A leading contributor to increased pulmonary infections in temperate climates during winter and in tropical climates during rainy seasons is the increased time that most people spend indoors, putatively sharing airspace with others who already are infected and infectious.

One outstanding meteorologic feature of the Samoan Islands is the often-present wind; Southeast trade winds bring clouds and rain throughout the

Figure 1. A late 19th-century artist's depiction of a standard fale, showing roll-down screens or weather blinds, called pola.

Figure 2. An early 20th-century photograph of a fale, a thatched pavilion without walls.

year. In Western Samoa, the highest average wind speeds are 11.9 miles/hour from June through October, and the lowest average wind speeds are 9.7 miles/hour in March. Unlike the common rectangular domiciliary and institutional structures found in other Pacific Island groups and introduced to the Samoan Islands by the Europeans in the 19th century, often with airtight or insulated building shells, the traditional fale both lacking walls and being buffeted consistently by wind would provide housing space that was naturally ventilated and cooled. Such structures would also not provide an environment conducive to person-to-person spread of respiratory particles. If this has been the case among Samoan populations for centuries, one would expect modern-day LTBI prevalence and TB disease incidence to be low and TB transmission to be rare among Samoans relative to other Pacific Island peoples. Unfortunately, due to lack of medical care access and lack of diagnostics, no systematically gathered rates of TB infection or disease are available for the Pacific Island populations from the first half of the 20th century. Recent World Health Organization estimates for the many Pacific Island jurisdictions show a wide range of TB incidence, no doubt the results of a multiplicity of factors; however, few Pacific Island jurisdictions report low TB incidence rates comparable to those of the Samoas (e.g., Tonga and the Cook Islands, both of which have near omnipresent wind similar to that in the Samoas and traditionally have had open and airy domestic architecture made of bamboo, wood, and palm fronds, with walls often omitted to enable easy passage of the trade winds in an extremely humid environment). Although systematic assessments of the LTBI burden among the population in American Samoa or in the Independent State of Samoa have not been published, the incidence of active TB disease reported in both jurisdictions is consistently low by any standard, but especially for a Pacific Island population.

The combination of trade winds and relatively wall-less domestic architecture has been by no means the sole contributor to the lower rates of TB in the Samoas compared with Pacific Island groups elsewhere in Polynesia and in Micronesia and Melanesia, which have differing environmental conditions, demographics, and traditional architecture that more customarily had a greater presence of walls. However, in the Samoas, the relatively constant trade winds and the basic traditional architectural form of the fale might have significantly contributed to the low burden of TB observed in their populations today.

Bibliography

1. Centers for Disease Control and Prevention. Reported tuberculosis in the United States, 2020 [cited 2024 Apr 24]. https://www.cdc.gov/tb/statistics/reports/2020/state_local_data.htm
2. Centers for Disease Control and Prevention. Reported tuberculosis in the United States, 2021 [cited 2024 Apr 24]. https://www.cdc.gov/tb/statistics/reports/2021/state_local_data.htm
3. Fennelly KP, Jones-López EC. Quantity and quality of inhaled dose predicts immunopathology in tuberculosis. Front Immunol. 2015;6:313. https://doi.org/10.3389/fimmu.2015.00313
4. Green RC, Leach HM. New information for the Ferry berth site, Mulifanua, Western Samoa. J Polyn Soc. 1989;98:319–30.
5. LaMonica LC, McGarvey ST, Rivara AC, Sweetman CA, Naseri T, Reupena MS, et al. Cascades of diabetes and hypertension care in Samoa: identifying gaps in the diagnosis, treatment, and control continuum—a cross-sectional study. The Lancet Regional Health–Western Pacific. 2022;18:100313. https://doi.org/10.1016/j.lanwpc.2021.100313
6. Stanley D. Moon Handbooks: South Pacific, 8th edition. Berkeley (CA): Avalon Travel Publishing; 2004.
7. UNESCO Office for the Pacific States (Western Samoa). The Samoan fale [cited 2024 Apr 24]. https://unesdoc.unesco.org/ark:/48223/pf000013989
8. van Crevel R, Critchley JA. The interaction of diabetes and tuberculosis: translating research to policy and practice. Trop Med Infect Dis. 2021;6:8. https://doi.org/10.3390/tropicalmed6010008
9. Weatherspark.com. Climate and average weather year-round in Samoa [cited 2024 Apr 24]. https://weatherspark.com/y/150290/Average-Weather-in-Samoa-Year-Round
10. World Bank. Samoa, Tuberculosis, 2021. Samoa tuberculosis—data, chart [cited 2024 Apr 24]. https://www.theglobaleconomy.com/Samoa/Tuberculosis
11. Yanagawa M, Morishita F, Oh KH, Rahevar K, Islam TA, Yadav S. Epidemiology of tuberculosis in the Pacific island countries and areas, 2000-2020. Western Pac Surveill Response J. 2023;14:1–12. https://doi.org/10.5365/wpsar.2023.14.1.996

Address for correspondence: Terence Chorba, Centers for Disease Control and Prevention, 1600 Clifton Rd NE, Mailstop H24-4, Atlanta, GA 30329-4018, USA; email: tlc2@cdc.gov

EMERGING INFECTIOUS DISEASES®

Upcoming Issue: Vectors • July 2024

- Looking Beyond the Lens of Crimean-Congo Hemorrhagic Fever in Africa
- Highly Pathogenic Avian Influenza A(H5N1) Clade 2.3.4.4b Virus Infection in Domestic Dairy Cattle and Cats, United States, 2024
- Phylogeographic Analysis of *Mycobacterium kansasii* Isolates from Patients with *M. kansasii* Lung Disease in Industrialized City, Taiwan
- *Borrelia miyamotoi*–associated Acute Meningoencephalitis, Minnesota, United States
- Treatment Outcomes for Tuberculosis Infection and Disease Among Persons Deprived of Liberty, Uganda, 2020
- Evidence of *Orientia* Genus Endemicity among Severe Infectious Disease Cohorts, Uganda
- Orthohantavirus in Misiones Province, Northeastern Argentina
- *Wuchereria bancrofti* Lymphatic Filariasis, Barrancabermeja, Colombia, 2023
- Alongshan Virus Infection in *Rangifer tarandus* Reindeers, Northeastern China
- Vaccine Effectiveness against SARS-CoV-2 among Household Contacts during Omicron BA.2–Dominant Period, Japan
- Body Louse Pathogen Surveillance Among Persons Experiencing Homelessness, Winnipeg, Canada, 2020–2021
- *Pasteurella bettyae* Infections in Men Who Have Sex With Men, France
- *Plasmodium vivax* Infections among Immigrants from China Traveling to the United States
- Emergence of Indigenous Dengue Fever, Niger, October 2023
- Germ Theory: Medical Pioneers in Infectious Diseases, 2nd Edition

Complete list of articles in the July issue at https://wwwnc.cdc.gov/eid/#issue-310

Earning CME Credit

To obtain credit, you should first read the journal article. After reading the article, you should be able to answer the following, related, multiple-choice questions. To complete the questions (with a minimum 75% passing score) and earn continuing medical education (CME) credit, please go to http://www.medscape.org/journal/eid. Credit cannot be obtained for tests completed on paper, although you may use the worksheet below to keep a record of your answers.

You must be a registered user on http://www.medscape.org. If you are not registered on http://www.medscape.org, please click on the "Register" link on the right hand side of the website.

Only one answer is correct for each question. Once you successfully answer all post-test questions, you will be able to view and/or print your certificate. For questions regarding this activity, contact the accredited provider, CME@medscape.net. For technical assistance, contact CME@medscape.net. American Medical Association's Physician's Recognition Award (AMA PRA) credits are accepted in the US as evidence of participation in CME activities. For further information on this award, please go to https://www.ama-assn.org. The AMA has determined that physicians not licensed in the US who participate in this CME activity are eligible for *AMA PRA Category 1 Credits*™. Through agreements that the AMA has made with agencies in some countries, AMA PRA credit may be acceptable as evidence of participation in CME activities. If you are not licensed in the US, please complete the questions online, print the AMA PRA CME credit certificate, and present it to your national medical association for review.

Article Title

Carbapenem-Resistant and Extended-Spectrum β-Lactamase–Producing Enterobacterales in Children, United States, 2016–2020

CME Questions

1. In the current study by Grome and colleagues, which was the most common organism implicated in cases of carbapenem-resistant Enterobacterales (CRE)?

A. *Escherichia coli*
B. *Escherichia cloacae*
C. *Klebsiella pneumoniae*
D. *Klebsiella aerogenes*

2. Which was the most common organism implicated in cases of ESBL-E in the current study?

A. *E. coli*
B. *E. cloacae*
C. *K. pneumoniae*
D. *K. aerogenes*

3. Which age group of children and adolescents in the current study experienced the highest incidence rates of CRE and ESBL-E?

A. Age <1 year
B. Ages 1 year to <5 years
C. Ages 5 years to <10 years
D. Age ≥10 years

4. Which of the following statements reflects characteristics of CRE and ESBL-E in the current study?

A. Most cases were hospital-acquired
B. Incidence rates were similar among female and male persons
C. >80% of cases were from urine isolates
D. Cases of ESBL-E were more likely to involve hospitalization and indwelling devices vs CRE

Emerging Infectious Diseases
Photo Quiz Articles

Volume 14, Number 9
September 2008

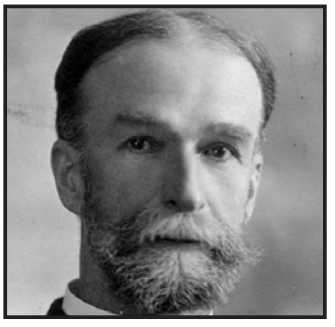

Volume 14, Number 12
December 2008

Volume 15, Number 9
September 2009

Volume 15, Number 10
October 2009

Volume 16, Number 6
June 2010

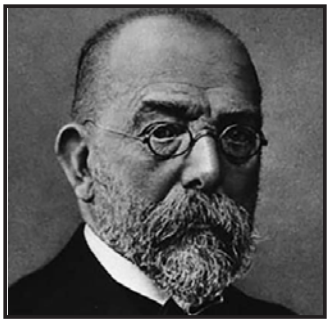

Volume 17, Number 3
March 2011

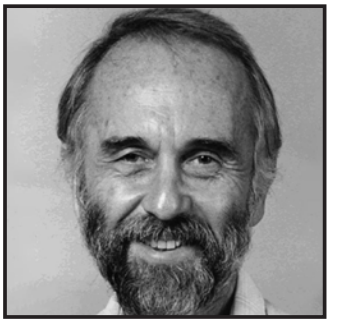

Volume 17, Number 12
December 2011

Volume 19, Number 4
April 2013

Volume 20, Number 5
May 2014

Volume 21, Number 9
September 2015

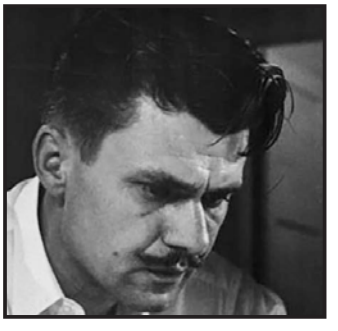

Volume 22, Number 8
August 2016

Volume 28, Number 3
March 2022

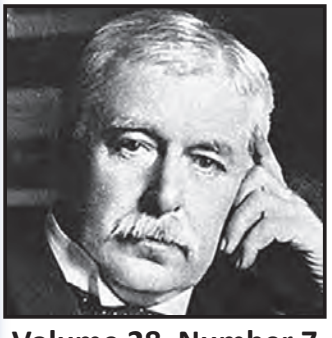

Volume 28, Number 7
July 2022

Click on the link below to read about the people behind the science.

https://bit.ly/3LN02tr

See requirements for submitting a photo quiz to EID.

https://bit.ly/3VUPqfj

EID Journal